20 April 2007 | S10

Science

Germ Cells

AAAS

Standardize!

SCIENCE @ WORK

With Sigma, standardize your proteomics research

Introducing the **Universal Proteomics Standard Set**, the first commercially available proteomics standard; developed in collaboration with the Association of Biomolecular Resource Facilities Proteomics Standards Research Group:

- Validate analytical method development
- Calibrate or troubleshoot methods and instrumentation
- Benchmark data among labs

To learn more visit: sigma.com/ups

sigma.com

Accelerating Customers' Success through Leadership in **Life Science**, **High Technology** and **Service**

SIGMA-ALDRICH CORPORATION • BOX 14508 • ST. LOUIS • MISSOURI 63178 • USA

SIGMA®

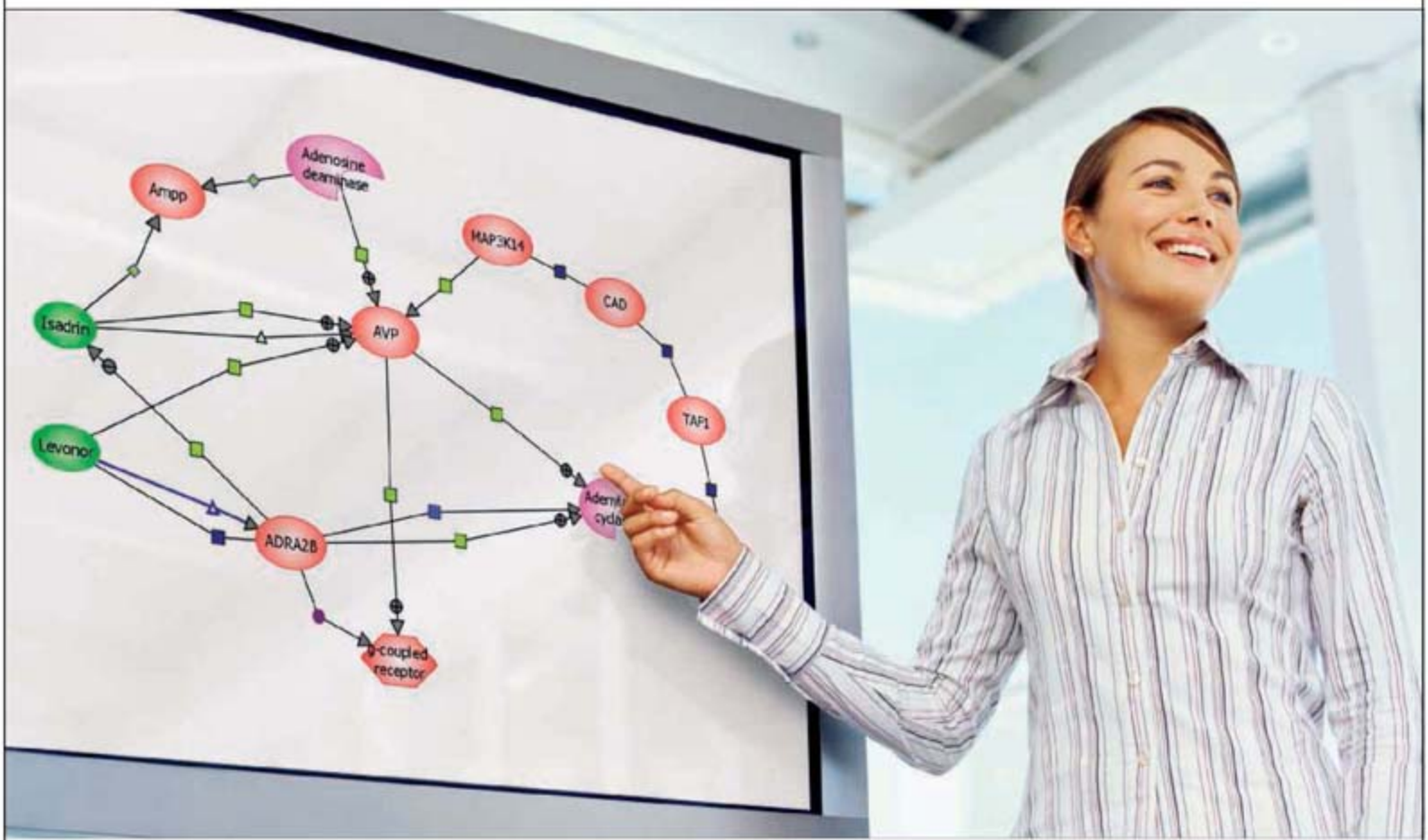

Connect the Dots.

PathwayArchitect® Software from Stratagene—make finding relationships simple.

Our next-generation PathwayArchitect® Software is designed for the life scientist who needs to obtain facts about a disease-relevant biological pathway as well as understand the statistically relevant relationships in their system and integrate complex numerical data. The guided workflow within the software takes you through the steps of searching for your pathway of interest. You can also build a pathway based on a list of genes and utilize the software to integrate and analyze your numerical data.

- **Pathway database expands target discovery**
- **Uncover new biological relationships**
- **Visualize your expression data as pathways**

TRY IT FREE TODAY!

Download a trial version today at www.stratagene.com/softwaresolutions.

Need More Information? Give Us A Call:

Stratagene US and Canada
Order: 800-424-5444 x3
Technical Service: 800-894-1304 x2

Stratagene Europe
Order: 00800-7000-7000
Technical Service: 00800-7400-7400

Stratagene Japan K.K.
Order: 3-5821-8077
Technical Service: 3-5821-8076

www.stratagene.com

Visit www.stratagene.com/softwaresolutions for complete details about our PathwayArchitect® Software and information about Academic, multiple year, and multiple user licensing options.

Our ArrayAssist® and PathwayArchitect® product suites are powered by the award-winning avadis™ technology and are co-developed with Strand Life Sciences.

ArrayAssist® and PathwayArchitect® are registered trademarks of Stratagene in the United States.

avadis™ is a trademark of Strand Life Sciences.

GeneChip® is a registered trademark of Affymetrix.

GeneChip Compatible

Strand Life Sciences

STRATAGENE

you've got **better** things to do...

better consistency

better purification

better results

Introducing
Personal Automation™

Meet Maxwell

Maxwell® 16 gives you consistent purification results — processing up to 16 samples in 30 minutes. It's Personal Automation™, right at your lab bench. DNA, RNA or protein purification, your choice. Finally reagents, instrumentation, service and support from one reliable source. You'd better visit: **www.MeetMaxwell.com**

Promega

GE Healthcare

Bringing protein analysis to life with Ettan DIGE and Amersham ECL

When it comes to life sciences, GE Healthcare is setting the standard. Tens of thousands of scientists worldwide rely on our products and proven expertise in protein analysis and detection every day. But we're never content to stand still. We're constantly striving for innovations that boost accuracy and deliver quantitative data.

The result is new fluorescence platforms like the Ettan™ DIGE Imager and Amersham ECL Plex™ for quantitative protein analysis.

By continually developing technology that can turn your scientific ideas into reality, we're bringing science to life and helping to transform drug discovery and healthcare.

We call it Protein Analysis Re-imagined.

Discover the full power of Ettan DIGE and the Amersham ECL™ family of Western blotting systems.

www.gehealthcare.com/protein_analysis

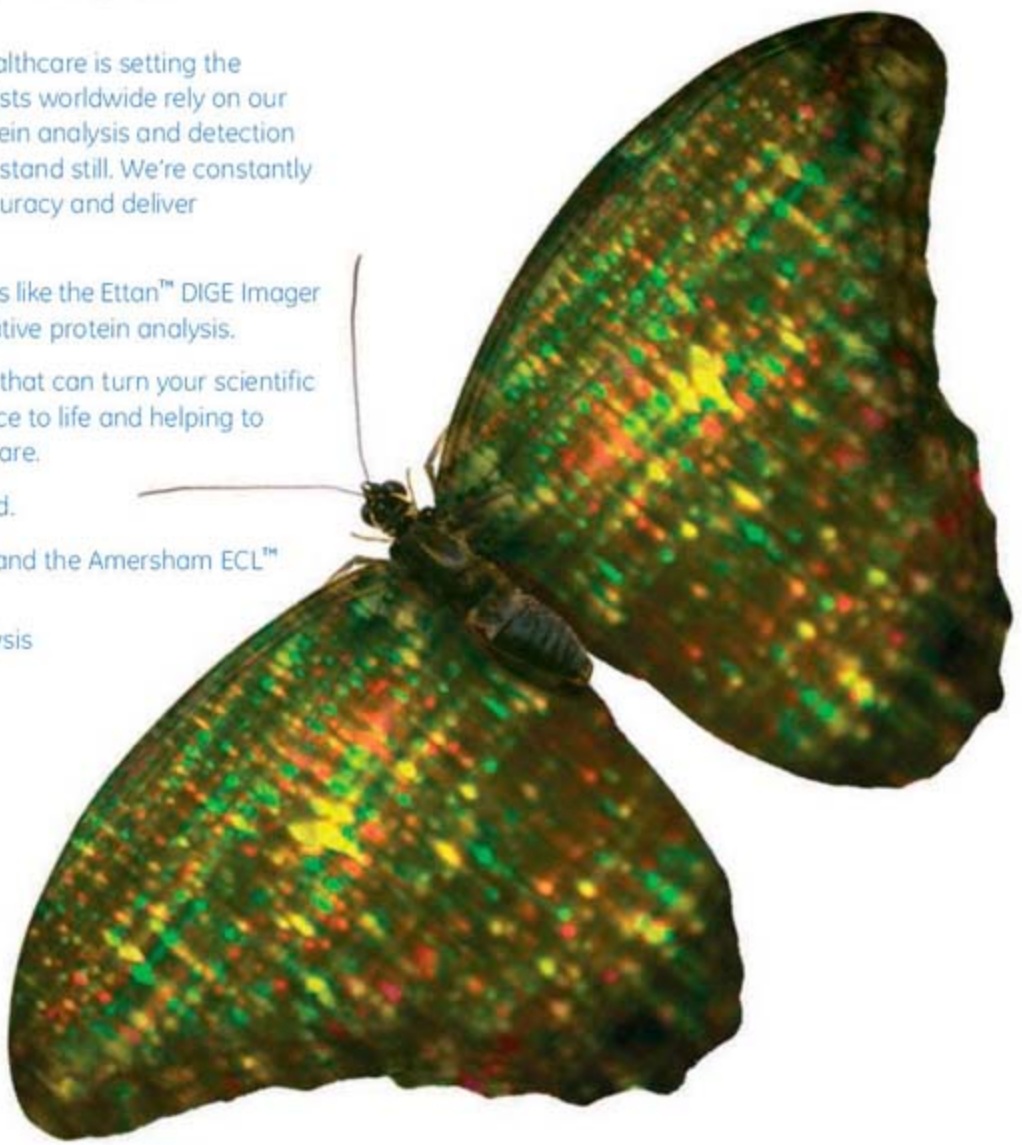

imagination at work

GE Healthcare Bio-Sciences AB, a General Electric Company.
Björkgatan 30, 751 84 Uppsala, Sweden.

GE08-06

Volume 316, Issue 5823

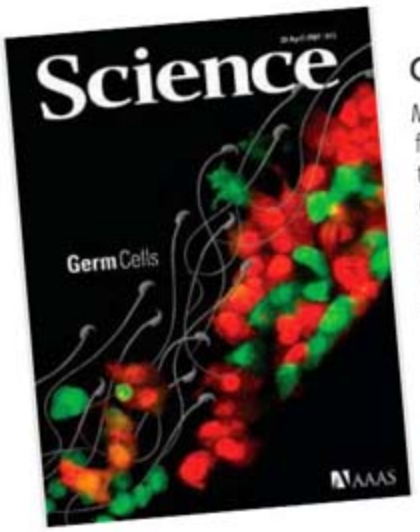

COVER

Male germline stem cells (red and green) from mice produce spermatozoa after transplantation to the seminiferous tubules of recipient mice. See the special section on germ cells beginning on page 387.

Photo illustration: J. Hayden, RBP, H. Kubota, and R. L. Brinster

>> Editorial p. 339; for related online content, see page 333 or go to www.sciencemag.org/sciext/germcells/

DEPARTMENTS

EDITORIAL

SPECIAL SECTION

Germ Cells

INTRODUCTION

NEWS

REVIEWS

NEWS OF THE WEEK

NEWS FOCUS

CONTENTS continued >>

QIAcube — pure efficiency

New

Winner of the New Product Award (NPA) Designation of the Association for Laboratory Automation (ALA) 2007

reddot design award winner 2007

reddot design award
product design 2007

- Eliminate manual processing steps
- Continue to use trusted QIAGEN spin-column kits
- Free up your time with affordable, automated sample preparation
- Purify DNA, RNA, or proteins from up to 12 samples per run
- Standardize your results and increase your productivity

Contact QIAGEN today or visit www.qiagen.com/MyQIAcube .

QIAGEN®

Sample & Assay Technologies

Science

SCIENCE EXPRESS

www.sciencexpress.org

DEVELOPMENTAL BIOLOGY

Blastocyst Axis Is Specified Independently of Early Cell Lineage But Aligns with the ZP Shape
Y. Kurotaki, K. Hatta, K. Nakao, Y. Nabeshima, T. Fujimori
Time-lapse imaging shows that the axis of the mouse embryo is not specified intrinsically but is influenced by the shape of the overlying zona pellucida.
10.1126/science.1138591

PLANETARY SCIENCE

Regolith Migration and Sorting on Asteroid Itokawa
H. Miyamoto et al.
Processes at work on asteroid Itokawa are documented in detailed pictures from the Hayabusa spacecraft, showing evidence of sorting due to shaking and convection.
10.1126/science.1134390

PLANT SCIENCE

Hd3a Protein Is a Mobile Flowering Signal in Rice
S. Tamaki, S. Matsuo, H. L. Wong, S. Yokoi, K. Shimamoto
10.1126/science.1141753

FT Protein Movement Contributes to Long-Distance Signaling in Floral Induction of *Arabidopsis*
L. Corbesier et al.
The protein products of the genes Hd3a in rice and FT in *Arabidopsis* are the elusive florigen signals that move from leaf to shoot to induce flowering.
>> News story p. 350
10.1126/science.1141752

MOLECULAR BIOLOGY

Developmentally Regulated piRNA Clusters Implicate MILI in Transposon Control
A. A. Aravin, R. Sachidanandam, A. Girard, K. Fejes-Toth, G. J. Hannon
A small class of RNA found only in the germline helps to suppress transposons—parasitic DNA elements—in mice, as they do in *Drosophila*.
10.1126/science.1142612

LETTERS

BOOKS *ET AL.*

POLICY FORUM

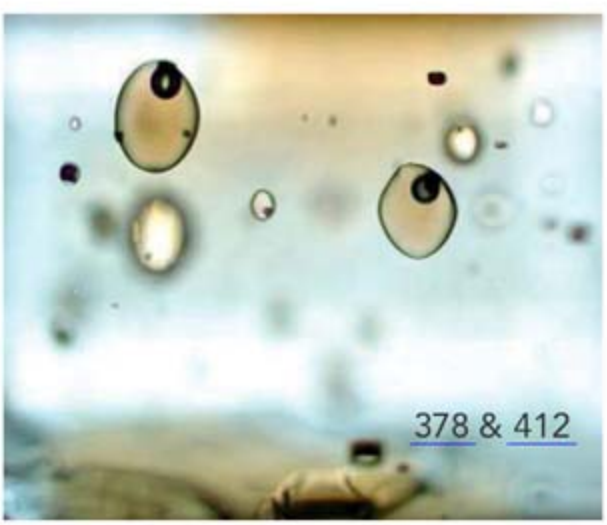

PERSPECTIVES

TECHNICAL COMMENT ABSTRACT

EVOLUTION

BREVIA

DEVELOPMENTAL BIOLOGY

RESEARCH ARTICLES

GEOCHEMISTRY

CONTENTS continued >>

Science

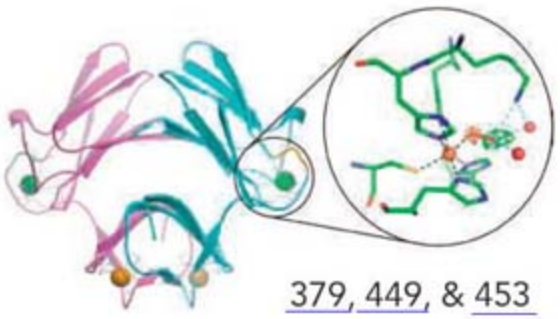

RESEARCH ARTICLES *CONTINUED...*

REPORTS

AAAS
ADVANCING SCIENCE, SERVING SOCIETY

SCIENCE (ISSN 0036-8075) is published weekly on Friday, except the last week in December, by the American Association for the Advancement of Science, 1200 New York Avenue, NW, Washington, DC 20005. Periodicals Mail postage (publication No. 484460) paid at Washington, DC, and additional mailing offices. Domestic individual membership and subscription (51 issues): $142 ($74 allocated to subscription). Domestic institutional subscription (51 issues): $710; Foreign postage extra: Mexico, Caribbean (surface mail) $55; other countries (air assist delivery) $85. First class, airmail, student, and emeritus rates on request. Canadian rates with GST available upon request, GST #1254 88122. Publications Mail Agreement Number 1069624. **Printed in the U.S.A.**

Change of address: Allow 4 weeks, giving old and new addresses and 8-digit account number. **Postmaster:** Send change of address to AAAS, P.O. Box 96178, Washington, DC 20090–6178. **Single-copy sales:** $10.00 current issue, $15.00 back issue prepaid includes surface postage; bulk rates on request. The identification code for *Science* is 0036-8075. *Science* is indexed in the *Reader's Guide to Periodical Literature* and in several specialized indexes.

CONTENTS continued >>

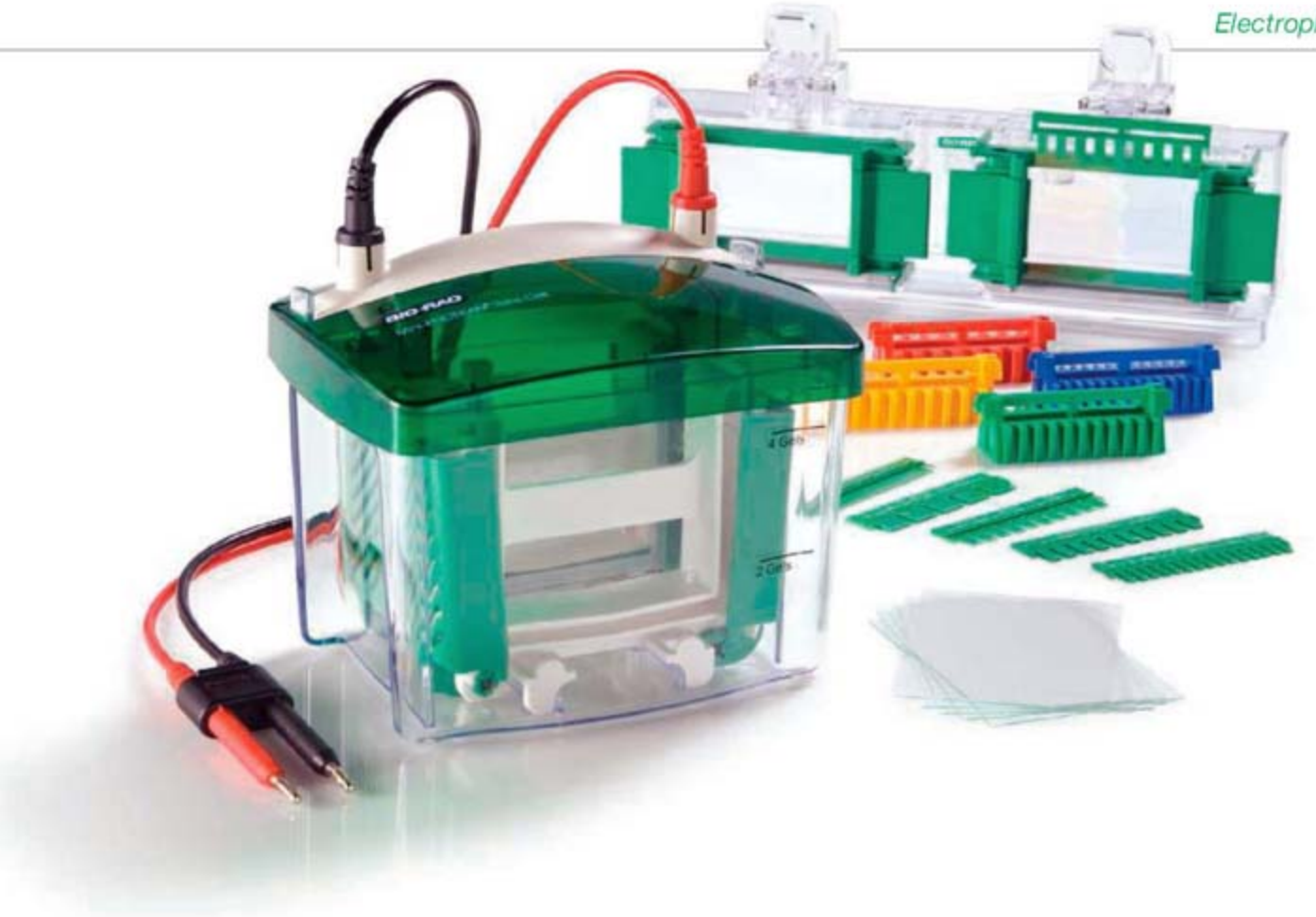

An old friend — with some new tricks.

For over 20 years, the Bio-Rad Mini-PROTEAN® system has set the standard for excellence in protein electrophoresis. Now the best mini electrophoresis system is even better — introducing the Mini-PROTEAN® Tetra cell system.

The new Mini-PROTEAN Tetra system offers:

- Ability to run up to 4 mini gels
- Easier assembly
- Virtually leak-free hand casting and running
- Ability to run either handcast or precast gels

For more information, visit us on the Web at **www.bio-rad.com/ad/miniproteantetra/**

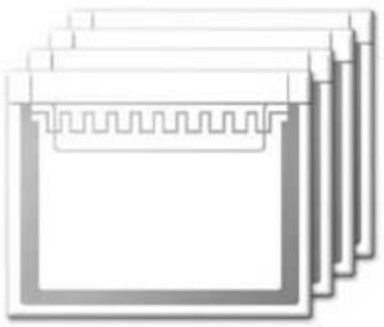

Double your throughput with the Mini-PROTEAN Tetra cell system.

Visit us on the Web at **discover.bio-rad.com**
Call toll free at 1-800-4BIORAD (1-800-424-6723);
outside the US, contact your local sales office.

BIO-RAD

SCIENCENOW

www.sciencenow.org DAILY NEWS COVERAGE

Bringing Sex Back
After millions of years of celibacy, soil mites launch a sexual revolution.

No Twisting Out of Newton's Law
New experiment confirms force-acceleration connection for tiniest shoves.

Chimps Are Champs of Genetic Changes
Natural selection acted more heavily on chimpanzee genome than human genome.

Growing pollen tube.

SPECIAL SECTION

Germ Cells

SCIENCE'S STKE

www.stke.org SIGNAL TRANSDUCTION KNOWLEDGE ENVIRONMENT

EDITORIAL GUIDE: Focus Issue—From Egg to Egg—Cell Signaling in Germ Cells
E. M. Adler and N. R. Gough
Signals from the surrounding tissues control survival and migration of germ cells.

PERSPECTIVE: What Is Left Behind—Quality Control in Germ Cell Migration
B. Boldajipour and E. Raz
Drosophila and mouse use different molecules but similar mechanisms to guide migration of primordial germ cells and eliminate those that fail to migrate.

PERSPECTIVE: Pollen-Pistil Signaling in Self-Incompatible Poppy—Does It Allow More Efficient Resource Allocation in the Pistil?
B. McClure
Destruction of incompatible pollen tubes may leave more resources available for supporting the growth of compatible ones.

>> *Germ Cells section p. 387*

Wilfredo Colón with RPI students.

SCIENCE CAREERS

www.sciencecareers.org CAREER RESOURCES FOR SCIENTISTS

MISCINET: Profile—Wilfredo Colón
A. Sasso
A biochemist at RPI welcomes minorities into his department and research lab.

GLOBAL: Mind Matters—Culture Shock
I. S. Levine
Knowing what's ahead can make adjusting to a new culture easier.

US: Tooling Up—'Culturing' Your Marketable Skills
D. Jensen
Some career skills need to be developed before employers can recognize and rely on them.

SCIENCEPODCAST

Tune in to the 20 April *Science* Podcast to hear about NIH's budget crunch, the influence of temperature on sex determination in reptiles, domestication of marine species, and more.
www.sciencemag.org/about/podcast.dtl

CREDIT (SCIENCE CAREERS): COURTESY RPI

Separate individual or institutional subscriptions to these products may be required for full-text access.

T4 DNA Ligase from New England Biolabs

WHEN YOU NEED LIGASE, TURN TO THE INDUSTRY STANDARD

New England Biolabs is dedicated to providing our customers with guaranteed enzyme performance. Our recombinant T4 DNA Ligase is the most extensively used ligase for cloning experiments. It is available at exceptional value, and an even greater value when purchased in large quantities for high throughput technologies. For cohesive, blunt, simple or complex reactions, make T4 DNA Ligase from NEB your first choice.

- **T4 DNA Ligase*** (R)
  - **Regular Concentration** — **M0202S/L**
    For standard cloning reactions
  - **High Concentration** — **M0202T/M**
    For large or difficult constructs
- **Quick Ligation™ Kit*** (R) — **M2200S/L**
  For ligation of cohesive or blunt-end DNA fragments in 5 minutes at room temperature. See our website for more details.

(R) = Recombinant
*NEB ligase products are BSA-free

Advantages:

- Quality – Highly pure enzyme with no lot-to-lot variation
- Convenience – Choose original T4 DNA Ligase or the Quick Ligation Kit to meet the demands of a variety of reaction conditions
- Flexibility – Active at room temperature or 16°C, reaction times run from 5 minutes to overnight
- Robustness – Active in a variety of reaction buffers

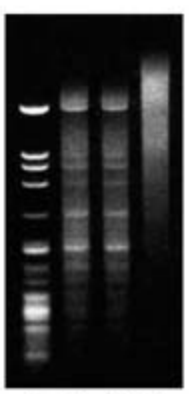

Ligation of blunt-ended HaeIII fragments of Lambda DNA using various amounts of T4 DNA Ligase (400,000 cohesive end units/ml) in a 20 µl reaction volume. Reactions were incubated for 30 minutes at 16°C.

Ligation of HindIII fragments (4-base overhang) of Lambda DNA using 1 cohesive end unit (1µl of 1:400 dilution) of T4 DNA Ligase. Reactions were incubated at 25°C.

For more information and our international distribution network, please visit www.neb.com
New England Biolabs, Inc. is an ISO 9001 certified company

New England Biolabs Inc. 240 County Road, Ipswich, MA 01938 USA 1-800-NEB-LABS Tel. (978) 927-5054 Fax (978) 921-1350 info@neb.com
Canada Tel. (800) 387-1095 info@ca.neb.com • **China** Tel. 010-82378266 beijing@neb-china.com • **Germany** Tel. 0800/246 5227 info@de.neb.com
Japan Tel. +81 (0)3 5669 6191 info@neb-japan.com • **UK** Tel. (0800) 318486 info@uk.neb.com

NEW ENGLAND BioLabs® Inc.
the leader in enzyme technology

EDITED BY STELLA HURTLEY AND PHIL SZUROMI

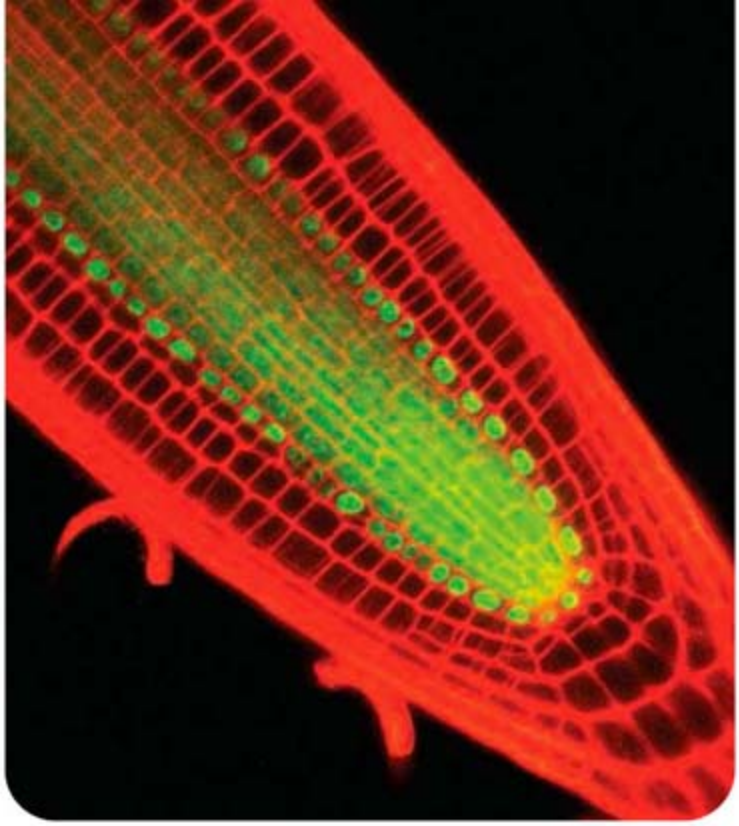

<< That's Far Enough

In the developing root tip of *Arabidopsis*, the transcription factor SHORTROOT (SHR) moves from cell to cell. However, the cells that are the target of this mobile transcription signal form a layer that is only one cell thick. **Cui *et al.*** (p. 421; see the Perspective by **Dolan**) now elucidate the interactions that send the mobile signal just so far, and no further. When SHR moves to the adjacent layer of cells, it meets its mate, the SCARECROW (SCR) protein, to which it binds. Together, SHR and SCR move to the nucleus and regulate transcription of the SCR gene. An excess of SCR protein scavenges the peripatetic SHR, and with more SCR available on demand, SHR and its developmental signal cannot move out any further than that first cell layer.

Mantle Melt Mixing

The heterogeneity of the convecting mantle is a result of recycling of oceanic and some continental crust within it. **Sobolev *et al.*** (p. 412, published online 29 March; see the Perspective by **Herzberg**) have developed a method for separating out the recycled crust components in basalts by combining measurements of a variety of elements, including Ni, Ca, Co, Mn, Cr, and Al. They amassed a large sample of olivine phenocrysts collected from basalts from mid-ocean ridges, ocean islands, and large igneous provinces. Ion microprobe analyses were carried out for 17,000 grains from 232 samples. By analyzing their compositions jointly, variations were seen for the different basalt types that can be ascribed to crustal mixing. Recycled material is detected in almost all melting environments, and its contribution to the melt can be related to potential temperature and the thickness of the lithosphere.

Measuring More Than Saturn's Rotation

Saturn's true inner rotation rate is hard to determine because the gas giant planet is swathed in thick layers of clouds that rotate more slowly. One measure that has been used is the modulation of intense radio emission (Saturn kilometric radiation) caused by the rotation of the planet's magnetic dipole. However, some changes in timing are seen that suggest there are slippages in the rotation of the plasma surrounding Saturn that may also modulate the radio signals. **Gurnett *et al.*** (p. 442, published online 22 March; see the Perspective by **Bagenal**) show that most of the variation occurs at particular longitudes and near the orbit of the moon Enceladus, where vapor is also being injected. The authors propose that twin convection cells are set up on either side of the plasma disk that funnel ions preferentially in one direction, which increases the electron density and radio emission at one longitude.

Cuprate Contortion

Advances in both x-ray and electron-diffraction technology have offered an increasingly detailed view of the sudden structural changes that solids can undergo upon optical excitation. Using electron diffraction with picosecond time resolution, **Gedik *et al.*** (p. 425) uncover a previously unappreciated light-induced expansion in a cuprate ceramic (a superconductor below 32 kelvin). Specifically, a pulse of 800-nanometer wavelength photons above a certain threshold intensity induces a discrete lattice expansion along the *c*-axis within tens of picoseconds; the solid then recontracts on a 10-fold slower time scale. The expansion scales linearly with photon fluence, which is consistent with a preliminary model of the transient geometry that attributes repulsive interactions to photoinduced oxide-to-copper charge transfer.

Bending Visible Light Backward

Artificial materials, or metamaterials, with tunable electric and magnetic responses can give rise to a negative index of refraction, in which electromagnetic radiation is bent in the opposite direction from that expected for natural materials. Other effects such as perfect lensing and cloaking have also been demonstrated at longer wavelengths. **Lezec *et al.*** (p. 430, published online 22 March) now demonstrate negative refractive index in the visible regime, providing the potential of practical devices, such as superlenses, for this important wavelength regime.

Beating Creep in the Heat

Heat engines are usually more efficient when they operate at higher temperatures, but materials properties, particularly creep strength, tend to degrade at extended elevated temperatures. Nickel-based superalloys can overcome this problem but are too expensive for widespread use. Some steels have sufficient creep strength, but their protective chromium oxide layers do not have sufficient oxidative resistance at high temperatures. Aluminum oxide provides better oxidative resistance, but at high Al content, steel forms a weaker ferrite phase. **Yamamoto *et al.*** (p. 433) show that by eliminating titanium and

Continued on page 337

CREDITS (TOP TO BOTTOM): HONGCHANG CUI; GEDIK *ET AL.*

Not using ExoSAP-IT? Your loss.

No Sample Loss with ExoSAP-IT®

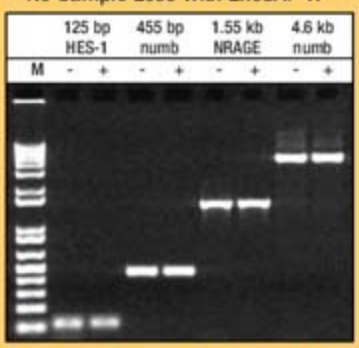

Untreated (-) and ExoSAP-IT treated (+) PCR products were analyzed by gel electrophoresis. A variety of PCR products of different lengths may be treated with ExoSAP-IT, with no sample loss.

Stop losing time and samples. ExoSAP-IT® offers quick, one step PCR clean-up with 100% recovery of both short and long PCR products.

ExoSAP-IT

- Utilizes Exonuclease I to degrade leftover primers & Shrimp Alkaline Phosphatase to degrade unused dNTPs
- One easy step – just add ExoSAP-IT, incubate, & heat inactivate
- Directly use treated sample for sequencing, SNP analysis, etc.

Benefits

- Rapid PCR clean-up – 15 min to treat, 15 min to inactivate
- No sample loss – PCR products are treated & then used directly in the next application
- No tedious columns involved – more free time
- Solution-based clean-up – completely scaleable for manual or automated use

For more information on ExoSAP-IT®, PN 78200
call 800.321.9322 or visit www.usbweb.com/exosapit
In Europe: +49(0)76 33 - 933 40 0 or visit www.usbweb.de/exosapit

usb
Fueling Innovation in Life Science

Continued from page 335

vanadium from the steel alloy, and using only niobium to form the carbide precipitates, a lower fraction of Al can be used and will form a protective scale. Thus, a high-temperature, lower-cost, creep-resistant steel alloy can be formed.

Lightweight Cleaver

The facility with which most transition metals can cleave H_2 has been attributed to a primary donation of electrons from hydrogen to metal, coupled with a secondary donation in the opposite direction. **Frey *et al.*** (p. 439) show that a similar process promotes H_2 addition to an electron-rich alkyl(amino)carbene. Like a transition metal, the stable singlet carbene has both an electron pair and vacant orbital, but calculations suggest that the primary process is nucleophilic electron donation from carbene to hydrogen. This nucleophilic mechanism also allows the carbene to cleave the N–H bond of ammonia, a much rarer reaction at electrophilic metal centers.

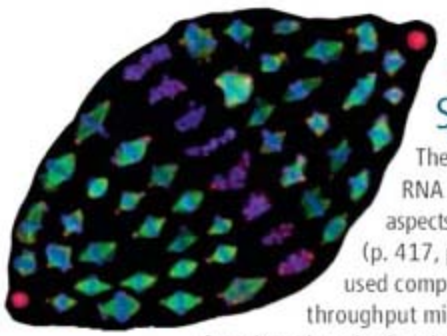

CREDIT: GOSHIMA *ET AL.*

Color-Coded Mitotic Spindle Assembly

The ability to screen the whole genome within *Drosophila* cells with RNA interference technology provides the opportunity to examine aspects of intracellular processes in unprecedented detail. **Goshima *et al.*** (p. 417, published online 5 April) present a whole-genome screen that used computational analysis to aid the phenotypic screening of high-throughput microscopy images to look for proteins involved in mitotic spindle function. The mitotic spindle represents the most complex intracellular structure to be screened to date, and the automated screening technology and detailed phenotypic analyses provide insight into how spindle microtubules are generated and how centrosomes are positioned.

Insight into Autism's Heritability

Although twin studies have shown that autism is "the most highly heritable" of all neuropsychiatric disorders, the majority of cases have no family history of autism, for reasons that are not understood. Linkage and association studies have not unambiguously identified strong gene candidates, which suggests that heritable risk factors for autism are complex. Rather than looking at patterns of inheritance (the focus of traditional genetic approaches), **Sebat *et al.*** (p. 445, published online 15 March) have looked for the occurrence of spontaneous variation in copy number by microarray comparative genomic hybridization. They found a 10-fold increase in the frequency of copy number variants in individuals with autism relative to controls. The chromosomal changes were in small regions and included changes in single genes.

Just Enough Oxygen Activation

Many iron-containing enzymes activate O_2 and harness the oxidizing power of the reactive oxo-ferryl species, whereas others protect the cell from activated oxygen. Two crystallography studies provide insight into the mechanisms of both O_2 activation and deactivation (see the Perspective by **Wilmot**). **Kovaleva and Lipscomb** (p. 453) report the structures of superoxo, alkylperoxo, and bound-product intermediates in the O_2 activation and insertion reaction of an extradiol ring-cleaving dioxygenase. Together, these structures define the major chemical steps of the dioxygenase mechanism. **Katona *et al.*** (p. 449) trapped iron peroxide intermediates in superoxide reductase and suggest how this enzyme forms the reaction product, H_2O_2, rather than producing reactive oxo-ferryl intermediates.

The Winners Recall Memories

Electrophysiological and cellular imaging studies show that only a portion of neurons are involved in a given memory. Why is one neuron, rather than its neighbor, included in a particular memory? **Han *et al.*** (p. 457) found that neurons in the lateral amygdala that contain the highest levels of function of the transcription factor CREB at the time of the encoding of an auditory fear memory are those that preferentially express the activity-regulated gene *Arc* after the recall of the memory. Thus, neurons compete during memory formation, and CREB helps to determine the winners.

Looking for solid ground in the ever-changing landscape of science & technology policy and budget issues?

Join the nation's top S&T experts at the 32nd Annual AAAS Forum on Science & Technology Policy
3–4 May 2007 • Washington DC
International Trade Center in the Ronald Reagan Building

The AAAS Forum on Science and Technology Policy provides a setting for discussion and debate about the federal budget and other policy issues facing the science, engineering, and higher education communities. Initiated in 1976 as the AAAS R&D Colloquium with about 100 participants, the Forum has emerged as the major public meeting in the U.S. devoted to science and technology policy issues. It annually draws upwards of 500 of the nation's top S&T policy experts.

- Get a full analysis of the President's federal R&D funding proposals.
- Have an opportunity to meet directly with key S&T policymakers.
- Learn how the changes in Congress are affecting S&T policy issues.
- Network with colleagues, including top decisionmakers in science and technology policy from all sectors.
- Learn about broader national and international developments that will affect strategic planning in universities, industries, and government.
- Registrants will receive, at the Forum, *AAAS Report XXXII: Research and Development, FY 2008,* a comprehensive analysis of the proposals for the FY 2008 budget, prepared by AAAS and a group of its affiliated scientific, engineering, and higher education associations.

For more complete details on the program, hotel registration and on-line registration, please visit the website: **www.aaas.org/forum**.

www.aaas.org/forum

AAAS
ADVANCING SCIENCE, SERVING SOCIETY

Anne McLaren is at the Wellcome Trust/Cancer Research UK Gurdon Institute, Cambridge, UK.

Free-Range Eggs?

HUMAN EGGS ARE IN SHORT SUPPLY, BUT MUCH IN DEMAND. MANY INFERTILE WOMEN need donated eggs if they are to bear children. Researchers need eggs for somatic-cell nuclear transfer (SCNT) to try to develop stem cell lines. If SCNT-derived stem cells could be made from patients suffering from devastating conditions such as motor neuron disease, they could provide unlimited material for molecular and biochemical analyses and clues for future therapy. But where can all these eggs come from to make these stem cells? And what about the reverse situation: making human eggs from stem cells?

The United Kingdom allows women undergoing in vitro fertilization to donate eggs for either clinical or research use, in exchange for further treatment. "Altruistic" donation is also permitted, in spite of possible health risks, with monetary compensation. The United States allows women to sell eggs for clinical use as well. Still, there is much debate about the ethics. For research use, cow or rabbit eggs have been used as carriers of human nuclei, because any stem cell lines derived from these would be essentially human. But in most countries, these cytoplasmic hybrids ("cybrids") are controversial. Earlier this month, a UK parliamentary committee said that restrictions on cybrids proposed by the Human Fertilization and Embryology Authority (HFEA) would delay important research on diseases. The HFEA plans to consult the public about such research this month and decide on its policy in September.

As far as making eggs from embryonic stem (ES) cells, we've known for more than 20 years that mouse stem cells mixed with embryo cells (chimeras) produce mice with functional gametes. Why then was it such a surprise when in 2003 and 2004, three groups reported deriving eggs and sperm from mouse ES cells in vitro rather than from chimeric embryos? After all, many other tissues could be derived from ES cells. Once the successful isolation of human ES cells had been reported in 1998, attention focused on their potential therapeutic value, and mouse modelers began seeking ways of inducing ES cells in vitro to make neural tissue, heart muscle, cartilage, and so forth.

But it is still not clear whether the reported stem cell–derived gametes are functional. Until this is firmly demonstrated, they should at best be referred to as "egglike" and "spermlike," but never as "artificial" or "synthetic" gametes. What would be needed for "egglike" to become "egg" or at least "ES cell–derived egg"? The cell must undergo normal cell division to produce haploid eggs. It must form a normal blastocyst, either parthenogenetically or after fertilization. It should reprogram a somatic cell nucleus to the same extent as an ovarian egg. And genes that are normally imprinted during oogenesis should show an appropriate pattern of chemical modification. Probably, ES cell–derived eggs could be generated from both female and male ES cell lines, but could ES cell–derived sperm be made from female ES cell lines? Ultimately, animal studies will need to show that ES cell–derived eggs can give rise to normal fertile progeny.

All this implies much further research, requiring human and mouse ES cells. Already, primordial germ cells have been detected in a human ES cell line. There will be ethical implications, including the wording of the consent document given to embryo donors. But even without reprogram a somatic cell nucleus to the same extent as an ovarian egg. And genes that are normally imprinted during oogenesis should show an appropriate pattern of chemical modification. Probably, ES cell–derived eggs could be generated from both female and male ES cell lines, but could ES cell–derived sperm be made from female ES cell lines? Ultimately, animal studies will need to show that ES cell–derived eggs can give rise to normal fertile progeny.

All this implies much further research, requiring human and mouse ES cells. Already, primordial germ cells have been detected in a human ES cell line. There will be ethical implications, including the wording of the consent document given to embryo donors. But even without full validation, human ES cell–derived eggs could have many research uses, such as making SCNT-derived stem cells, thus reducing the ethically problematic demand for donated human eggs for research.

Looking into the future, if ES cell–derived gametes are conclusively shown to be safe and effective in animal reproduction, the first pressure for the clinical use of human ES cell–derived gametes will be from those wanting donated eggs for in vitro fertilization. If human ES cell lines from SCNT-derived embryos could by then be made, irretrievably infertile people might be able to have children that are genetically their own without recourse to reproductive cloning, and safety will be the major ethical consideration. In the meantime, the long waiting list of women needing donated eggs to have babies demands that scientists wanting such eggs for stem cell research act with great restraint.

– Anne McLaren

10.1126/science.1142267

CREDIT: JOHNNY EGGITT/AFP/GETTY

www.roche-applied-science.com

LightCycler® 480 Real-Time PCR System and Universal ProbeLibrary

Let Your Gene Expression Analysis Take Off!

Are you looking for innovative solutions to streamline your qPCR workflow? Count on the powerful combination of the **LightCycler® 480 System** and **Universal ProbeLibrary** to meet your goals.

Maximize throughput: Obtain highly accurate qPCR data in less than 40 minutes with the LightCycler® 480 Instrument.

Increase efficiency: Rapidly design gene expression assays for virtually any organism and perform qPCR analysis without optimization.

Reduce costs: Perform dual-color assays in volumes as small as 5 µl with the Universal ProbeLibrary Probes and Reference Gene Sets.

Learn more about our powerful, optimized solutions for gene expression analysis and take advantage of special offers: visit ***www.roche-applied-science.com/geafly***

For general laboratory use. Not for use in diagnostic procedures.

Roche Diagnostics

Roche Diagnostics GmbH
Roche Applied Science
68298 Mannheim
Germany

EDITED BY GILBERT CHIN AND JAKE YESTON

CHEMISTRY

Sorting Out Lead Levels

The toxicity of lead has prompted significant concern over the presence of the heavy metal in various sources of drinking water. However, measuring the relatively low concentrations at issue can be an analytical challenge, particularly because of the need to avoid contamination of the vessels and apparatus. As a result, there have been conflicting reports of the lead concentrations measured in bottled waters.

Shotyk and Krachler have applied clean-room procedures and high-sensitivity detection technology—developed to gauge the nanogram-per-liter concentrations of lead present in polar ice—to the measurement of lead levels in a sample of 125 commercially available bottled waters from across the world. For comparison, they also assayed artesian flow sources in southern Ontario, Canada. In all cases, the measured concentrations were several orders of magnitude below the 10 μg/liter level considered hazardous. However, glass bottles appeared to leach lead over time, with concentrations roughly doubling (from ~100 to ~200 ng/liter) in water stored in them over a 6-month period. Concentrations measured in plastic bottles were generally much lower, and ranged from <1 to 761 ng/liter with a median of 8.5 ng/liter. The artesian sources exhibited a median lead concentration of 5.1 ng/liter in a much narrower range. — JSY

Environ. Sci. Technol. **41**, 10.1021/es062964h (2007).

PSYCHOLOGY

Bridging System and Individual

Equal opportunity is not, of course, quite the same thing as equal outcome, as an examination of even a small number of individuals will confirm. Inequalities abound—whether of wealth, educational achievement, or employment history—and can be the source of emotional distress, especially among the advantaged, when they are perceived as having gained these unfairly. Wakslak *et al.* show how adoption of a justification for inequality (that success is the product of effort and ability) alleviates three facets of emotional distress and then assess which of these mediates enervated support for redistributive social policies. They find that existential guilt and depressed mood (both of which are inwardly directed) were not primary motivations behind attitudes on redistribution but that an other-regarding moral outrage was. — GJC

Psychol. Sci. **18**, 267 (2007).

CELL BIOLOGY/MICROBIOLOGY

Subversions and Transformations

Epithelial cells are polarized, with their apical surface oriented toward the lumen of an organ and their basolateral side facing the blood. Layers of epithelial cells play an important and essential role in keeping the outside out and the inside in. Helping them to achieve this are the so-called tight junctions, which link neighboring cells and resist any intercellular infiltration of macromolecules. Kierbel *et al.* have studied how the pathogenic bacterium *Pseudomonas aeruginosa* (a major contributor to nosocomial infections) manages to invade epithelia, despite having a preference for binding to the basolateral surfaces of epithelial cells. Most of the invading bacteria will, in fact, be confronted by an apical surface when they attempt to colonize a new host. The authors find that the bacterium actually induces the remodeling of a small portion of the apical membrane into a basolateral-like protrusion. *P. aeruginosa* binds to epithelial monolayers and recruits phosphatidylinositol 3-kinase (PI3K). The PI3K generates phosphatidylinositol 3,4,5-trisphosphate (PIP3), which attracts actin filaments and the delivery of basolateral membrane proteins. The invading bacteria then become engulfed by the transplanted patch of basolateral membrane and thus succeed in breaching the barrier defenses of the epithelium. — SMH

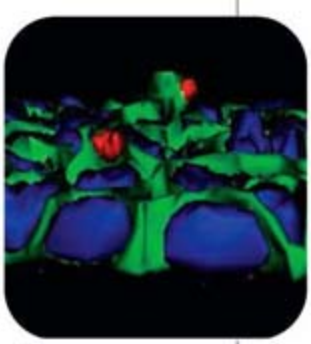

Bacteria (red) recruit PIP3 (green) at the apical side of an epithelial cell layer (blue).

J. Cell Biol. **177**, 21 (2007).

CHEMISTRY

Pampered by PAAMPSA

The promise of polymer electronics depends in part on the development of stable conductive materials that can be inexpensively processed. One material that has been extensively studied is polyaniline (PANI), which when doped with acids becomes conductive but has limited solubility in common solvents. An alternative is to polymerize the aniline onto a polymer acid template that provides the acid doping, may enhance the PANI crystallinity, and may also provide excess pendant groups to enhance solubility. Yoo *et al.* explored the strongly acidic poly(2-acrylamido-2-methyl-1-propanesulfonic acid) (PAAMPSA) as a template material. For the highest-molecular-weight PAAMPSA studied, the conductivity was high even though the acid doping was found to be incomplete. The best results (1.1 S/cm) were obtained for the lowest-molecular-weight template. ^{15}N solid-state nuclear magnetic resonance spectroscopy suggested that the

Continued on page 343

CREDITS (TOP TO BOTTOM): WILLIAM SHOTYK; KIERBEL *ET AL.*, *J. CELL BIOL.* **177**, 21 (2007)

“Combining live imaging with high resolution electron microscopy is a real challenge.”

“With the introduction of Green Fluorescent Protein (GFP) technology, cell biology and life sciences in general have entered a whole new exciting era of research. [...] In some instances however, the resolution of the light microscope is the limiting factor in answering our scientific questions. In these cases, the higher resolution of the electron microscope is essential. Combining both light and electron microscopy is my field of interest. By performing so-called Correlative Light Electron Microscopy (CLEM) experiments one has the advantage of live cell imaging in the confocal microscope and afterwards have high resolution results from the transmission electron microscope of the same cell. The Leica EM RTS was specifically developed to be used in such experiments in conjunction with EM PACT2. It provides a high time resolution between the light and electron microscope, allowing excellent preservation of the ultrastructure close to the natural state, an essential prerequisite for electron microscopy. It allows us to decide upon the exact moment of interest and study that particular event at high resolution.”

Dr. Paul Verkade, Max Planck Institute for Molecular Cell Biology and Genetics, Dresden, Germany
Dr. Verkade works with the Leica EM PACT2 & RTS High Pressure Freezer.

www.leica-microsystems.com

Leica

MICROSYSTEMS

Continued from page 341

enhanced conductivity in these systems stemmed from a nitrogen environment in which the protonated amines can delocalize charge along the PANI-PAAMPSA backbone, an effect not seen in other polymer acid–doped systems. — MSL

J. Mater. Chem. **17**, 1268 (2007).

CLIMATE SCIENCE

Backdrop for the Future

One of the most frequently invoked potential effects of global warming is an abrupt change in precipitation patterns. In order to assess the onset of such a change, it is necessary to have baseline knowledge of the variability of precipitation in the past. Narisma *et al.* have analyzed the record of global rainfall for the 20th century in order to establish the spatial and temporal distributions of abrupt decreases in rainfall over that period. They find that about 30 regional instances of large, sudden decreases in precipitation have occurred over the past 100 years, all of which deviated from the climatological norm by at least 10% and lasted for 10 years or more. The authors also observe that these sudden decreases in rainfall occurred mostly in arid and semi-arid regions, which is consistent with the results of climate modeling studies, and they suggest that this finding could be a consequence of a strong positive feedback between vegetation and climate. — HJS

Geophys. Res. Lett. **34**, L06710 (2007).

MATERIALS SCIENCE

Simply Hexagonal Stacks

When nanoparticles pack into colloidal crystals, they usually adopt a hexagonally close-packed (hcp) structure in which two layers stack in an ABAB sequence, even though hard-sphere models favor a face-centered cubic (fcc) structure in which three layers stack ABCABC. Talapin *et al.* found that when they grew superlattices on carbon substrates of more polar, nearly spherical, semiconducting PbS, PbSe, or γ-Fe_2O_3 nanoparticles that were also somewhat larger (>7 nm in diameter), the layers did not stack in threefold hollow sites but rather directly on top of the underlying nanoparticle in a simple hexagonal (sh) lattice. Transmission electron microscopy images were analyzed to show that the stacking was not simply a projection plane of an fcc lattice. The authors calculated total electrostatic and dispersive energies for different lattices and attribute the stability of the sh superlattices to interactions of nonlocal dipoles between individual nanoparticles and with the underlying substrate, favoring the more open sh packing arrangement. — PDS

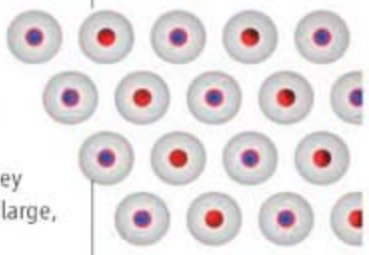

Dipole ordering in sh lattice.

Nano Lett. **7**, 10.1021/nl070058c (2007).

CREDIT: TALAPIN *ET AL.*, *NANO LETT.* 7, 10.1021/NL070058C (2007)

Science STKE AAAS

www.stke.org

<< Sigmoid Overrules Hyperbolic

Many cell-surface proteins, such as growth factor receptors, are glycosylated on asparagines residues as they transit the biosynthetic pathway. Proteins with more richly branched N-glycans will display more poly-*N*-acetyllactosamine and thus bind more tightly to galectins, which are lattice-forming cell-surface proteins. Interaction with galectin appears to hinder receptor endocytosis; the longer residence time supports a greater capacity for signal transduction via these receptors. The synthesis of glycan branches requires an intermediate produced by the enzyme *N*-acetylglucosaminyltransferase V (Mgat5), whose substrate is UDP-*N*-acetylglucosamine (GlcNAc), which is a product of the hexosamine pathway.

Lau *et al.* found that adding GlcNAc to *Mgat5*$^{-/-}$ cells increased the interaction of epidermal growth factor receptors (EGFRs) and transforming growth factor–β receptors (TGFβRs) with galectin. Surprisingly, EGFR (with eight N-glycosylation sites) showed a hyberbolic increase in response (phosphorylation of its downstream effector ERK), whereas TGFβR (with only one or two glycosylation sites) showed a sigmoid or switchlike increase in response (nuclear translocation of its downstream effector Smad) when the *Mgat5*$^{-/-}$ cells were supplemented with increasing concentrations of GlcNAc. Based on these observations, they built a mathematical model that described the dependence of cell-surface growth-regulating receptor abundance on glycosylation state and on metabolic flux through the hexosamine pathway. Receptors that promote proliferation generally have higher numbers of glycosylation sites than those that promote growth arrest and differentiation, which keeps the surface number of the latter relatively low until high concentrations of GlcNAc become available. — NRG

Cell **129**, 123 (2007).

www.sciencemag.org

Science

1200 New York Avenue, NW
Washington, DC 20005
Editorial: 202-326-6550, FAX 202-289-7562
News: 202-326-6581, FAX 202-371-9227

Bateman House, 82-88 Hills Road
Cambridge, UK CB2 1LQ
+44 (0) 1223 326500, FAX +44 (0) 1223 326501

Subscription Services For change of address, missing issues, new orders and renewals, and payment questions: 866-434-AAAS (2227) or 202-326-6417, FAX 202-842-1065. Mailing addresses: AAAS, P.O. Box 96178, Washington, DC 20090-6178 or AAAS Member Services, 1200 New York Avenue, NW, Washington, DC 20005

Institutional Site Licenses please call 202-326-6755 for any questions or information

Reprints: Author Inquiries 800-635-7181
Commercial Inquiries 803-359-4578

Permissions 202-326-7074, FAX 202-682-0816

Member Benefits Bookstore: AAAS/BarnesandNoble.com bookstore www.aaas.org/bn; Car purchase discount: Subaru VIP Program 202-326-6417; Credit Card: MBNA 800-847-7378; Car Rentals: Hertz 800-654-2200 CDP#343457, Dollar 800-800-4000 #AA1115; AAAS Travels: Betchart Expeditions 800-252-4910; Life Insurance: Seabury & Smith 800-424-9883; Other Benefits: AAAS Member Services 202-326-6417 or www.aaasmember.org.

science_editors@aaas.org	(for general editorial queries)
science_letters@aaas.org	(for queries about letters)
science_reviews@aaas.org	(for returning manuscript reviews)
science_bookrevs@aaas.org	(for book review queries)

Published by the American Association for the Advancement of Science (AAAS), *Science* serves its readers as a forum for the presentation and discussion of important issues related to the advancement of science, including the presentation of minority or conflicting points of view, rather than by publishing only material on which a consensus has been reached. Accordingly, all articles published in *Science*—including editorials, news and comment, and book reviews—are signed and reflect the individual views of the authors and not official points of view adopted by the AAAS or the institutions with which the authors are affiliated.

AAAS was founded in 1848 and incorporated in 1874. Its mission is to advance science and innovation throughout the world for the benefit of all people. The goals of the association are to: foster communication among scientists, engineers and the public; enhance international cooperation in science and its applications; promote the responsible conduct and use of science and technology; foster education in science and technology for everyone; enhance the science and technology workforce and infrastructure; increase public understanding and appreciation of science and technology; and strengthen support for the science and technology enterprise.

Information for Authors

See pages 120 and 121 of the 5 January 2007 issue or access www.sciencemag.org/feature/contribinfo/home.shtml

EDITOR-IN-CHIEF **Donald Kennedy**
EXECUTIVE EDITOR **Monica M. Bradford**
DEPUTY EDITORS **R. Brooks Hanson, Barbara R. Jasny, Katrina L. Kelner**
NEWS EDITOR **Colin Norman**

Editorial Supervisory Senior Editor Phillip D. Szuromi; **Senior Editor/Perspectives** Lisa D. Chong; **Senior Editors** Gilbert J. Chin, Pamela J. Hines, Paula A. Kiberstis (Boston), Marc S. Lavine (Toronto), Beverly A. Purnell, L. Bryan Ray, Guy Riddihough, H. Jesse Smith, Valda Vinson, David Voss; **Associate Editors** Jake S. Yeston, Laura M. Zahn; **Online Editor** Stewart Wills; **Associate Online Editor** Tara S. Marathe; **Book Review Editor** Sherman J. Suter; **Associate Letters Editor** Etta Kavanagh; **Editorial Manager** Cara Tate; **Senior Copy Editors** Jeffrey E. Cook, Cynthia Howe, Harry Jach, Barbara P. Ordway, Jennifer Sills, Trista Wagoner; **Copy Editors** Lauren Kmec, Peter Mooreside; **Editorial Coordinators** Carolyn Kyle, Beverly Shields; **Publications Assistants** Ramatoulaye Diop, Chris Filiatreau, Joi S. Granger, Jeffrey Hearn, Lisa Johnson, Scott Miller, Jerry Richardson, Brian White, Anita Wynn; **Editorial Assistants** Maris M. Bish, Emily Guise, Patricia M. Moore, Jennifer A. Seibert; **Executive Assistant** Sylvia S. Kihara; **Administrative Support** Maryrose Police

News Senior Correspondent Jean Marx; **Deputy News Editors** Robert Coontz, Eliot Marshall, Jeffrey Mervis, Leslie Roberts; **Contributing Editors** Elizabeth Culotta, Polly Shulman; **News Writers** Yudhijit Bhattacharjee, Adrian Cho, Jennifer Couzin, David Grimm, Constance Holden, Jocelyn Kaiser, Richard A. Kerr, Eli Kintisch, Andrew Lawler (New England), Greg Miller, Elizabeth Pennisi, Robert F. Service (Pacific NW), Erik Stokstad; **Intern** John Simpson; **Contributing Correspondents** Barry A. Cipra, Jon Cohen (San Diego, CA), Daniel Ferber, Ann Gibbons, Robert Irion, Mitch Leslie, Charles C. Mann, Evelyn Strauss, Gary Taubes; **Copy Editors** Linda B. Felaco, Rachel Curran, Sean Richardson; **Administrative Support** Scherraine Mack, Fannie Groom; **Bureaus** Berkeley, CA: 510-652-0302, FAX 510-652-1867, New England: 207-549-7755, San Diego, CA: 760-942-3252, FAX 760-942-4979, Pacific Northwest: 503-963-1940

Production Director James Landry; **Senior Manager** Wendy K. Shank; **Assistant Manager** Rebecca Doshi; **Senior Specialists** Jay Covert, Chris Redwood; **Specialist** Steve Forrester; **Preflight Director** David M. Tompkins; **Manager** Marcus Spiegler; **Specialist** Jessie Mudjitaba

Art Director Kelly Buckheit Krause; **Associate Art Director** Aaron Morales; **Illustrators** Chris Bickel, Katharine Sutliff; **Senior Art Associates** Holly Bishop, Laura Creveling, Preston Huey; **Associates** Nayomi Kevitiyagala, Jessica Newfield; **Photo Editor** Leslie Blizard

***Science* International**

Europe (science@science-int.co.uk) **Editorial: International Managing Editor** Andrew M. Sugden; **Senior Editor/Perspectives** Julia Fahrenkamp-Uppenbrink; **Senior Editors** Caroline Ash (Geneva: +41 (0) 222 346 3106), Stella M. Hurtley, Ian S. Osborne, Stephen J. Simpson, Peter Stern; **Associate Editor** Joanne Baker **Editorial Support** Alice Whaley; Deborah Dennison **Administrative Support** Janet Clements, Jill White; **News: Europe News Editor** John Travis; **Deputy News Editor** Daniel Clery; **Correspondent** Gretchen Vogel (Berlin: +49 (0) 30 2809 3902, FAX +49 (0) 30 2809 8365); **Contributing Correspondents** Michael Balter (Paris), Martin Enserink (Amsterdam and Paris), John Bohannon (Vienna); **Intern** Krista Zala

Asia Japan Office: Asca Corporation, Eiko Ishioka, Fusako Tamura, 1-8-13, Hirano-cho, Chuo-ku, Osaka-shi, Osaka, 541-0046 Japan; +81 (0) 6 6202 6272, FAX +81 (0) 6 6202 6271; asca@os.gulf.or.jp; **Asia News Editor** Richard Stone +66 2 662 5818 (rstone@aaas.org); **Contributing Correspondents** Dennis Normile (Japan: +81 (0) 3 3391 0630, FAX 81 (0) 3 5936 3531; dnormile@gol.com); Hao Xin (China: + 86 (0) 10 6307 4439 or 6307 3676, FAX +86 (0) 10 6307 4358; cindyhao@gmail.com); Pallava Bagla (South Asia: +91 (0) 11 2271 2896; pbagla@vsnl.com)

Africa Robert Koenig (contributing correspondent, rob.koenig@gmail.com)

EXECUTIVE PUBLISHER **Alan I. Leshner**
PUBLISHER **Beth Rosner**

Fulfillment & Membership Services (membership@aaas.org) **Director** Marlene Zendell; **Manager** Waylon Butler; **Systems Specialist** Andrew Vargo; **Customer Service Supervisor** Pat Butler; **Specialists** Laurie Baker, Tamara Alfson, Karena Smith, Vicki Linton, Latoya Casteel; **Circulation Associate** Christopher Refice; **Data Entry Supervisor** Cynthia Johnson; **Specialists** Tomeka Diggs, Tarrika Hill, Erin Layne

Business Operations and Administration Director Deborah Rivera-Wienhold; **Business Manager** Randy Yi; **Senior Business Analyst** Lisa Donovan; **Business Analyst** Jessica Tierney; **Financial Analysts** Michael LoBue, Farida Yeasmin; **Rights and Permissions: Administrator** Emilie David; **Associate** Elizabeth Sandler; **Marketing Director** John Meyers; **Marketing Managers** Darryl Walter, Allison Pritchard; **Marketing Associates** Julianne Wielga, Mary Ellen Crowley, Catherine Featherston, Alison Chandler, Lauren Lamoureux; **International Marketing Manager** Wendy Sturley; **Marketing Executive** Jennifer Reeves; **Marketing/Member Services Executive** Linda Rusk; **Japan Sales** Jason Hannaford; **Site License Sales Director** Tom Ryan; **Sales and Customer Service** Mehan Dossani, Kiki Forsythe, Catherine Holland, Wendy Wise; **Electronic Media: Manager** Lizabeth Harman; **Project Manager** Trista Snyder; **Assistant Manager** Lisa Stanford **Production Associates** Nichele Johnston, Kimberly Oster

Advertising Director Worldwide Ad Sales Bill Moran

Product (science_advertising@aaas.org); **Midwest** Rick Bongiovanni: 330-405-7080, FAX 330-405-7081 • **West Coast/W. Canada** Teola Young: 650-964-2266 **East Coast/E. Canada** Christopher Breslin: 443-512-0330, FAX 443-512-0331 • **UK/Europe/Asia** Julie Skeet: +44 (0) 1223-326-524, FAX +44 (0) 1223-325-532 **Japan** Mashy Yoshikawa: +81 (0) 33235 5961, FAX +81 (0) 33235 5852 **Traffic Manager** Carol Maddox; **Sales Coordinator** Deiandra Simms

Commercial Editor Sean Sanders: 202-326-6430

Classified (advertise@sciencecareers.org); **U.S.: Recruitment Sales Manager** Ian King: 202-326-6528, FAX 202-289-6742; **U.S./Industry:** Darrell Bryant: 202-326-6533; **Midwest/Canada:** Daryl Anderson: 202-326-6543; **Northeast:** Allison Millar: 202-326-6572; **Southeast:** Fernando Junco: 202-326-6740; **West:** Katie Putney: 202-326-6577; **Sales Coordinators** Erika Bryant, Rohan Edmonson, Shirley Young; **International: Sales Manager** Tracy Holmes: +44 (0) 1223 326525, FAX +44 (0) 1223 326532; **Sales** Christina Harrison, Svitlana Barnes; **Sales Assistant** Louise Moore; **Japan:** Jason Hannaford: +81 (0) 52 757 5360, FAX +81 (0) 52 757 5361; **Advertising Production Operations Manager** Deborah Tompkins; **Associates** Christine Hall, Amy Hardcastle; **Publications Assistants** Robert Buck, Mary Lagnaoui

AAAS Board of Directors **Retiring President, Chair** John P. Holdren; **President** David Baltimore; **President-Elect** James J. McCarthy; **Treasurer** David E. Shaw; **Chief Executive Officer** Alan I. Leshner; **Board** John E. Dowling, Lynn W. Enquist, Susan M. Fitzpatrick, Alice Gast, Linda P. B. Katehi, Cherry A. Murray, Thomas D. Pollard, Kathryn D. Sullivan

AAAS
ADVANCING SCIENCE, SERVING SOCIETY

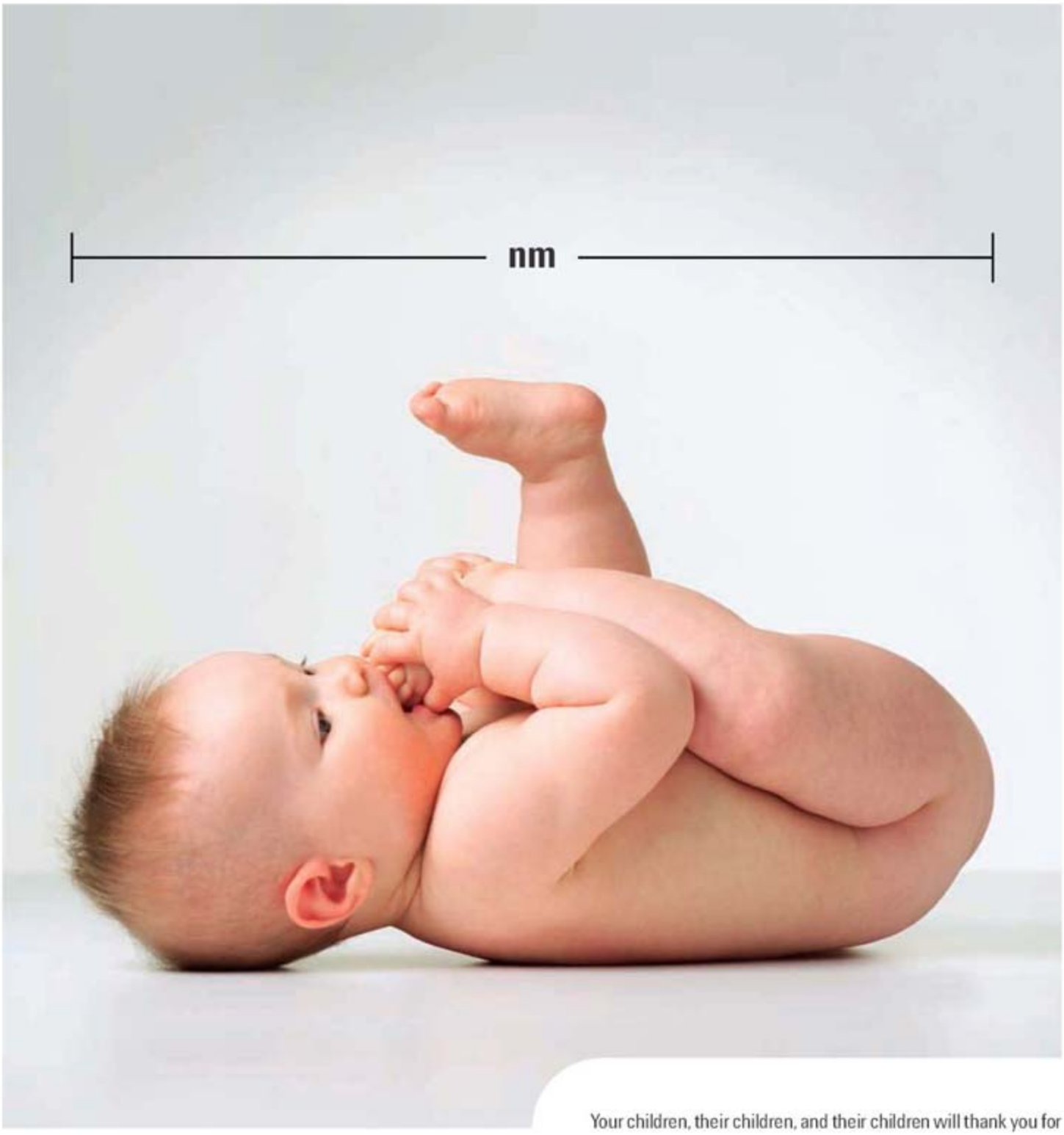

Your children, their children, and their children will thank you for the work you do in nanotechnology today. Agilent instruments for electronics, bioanalysis, chemical analysis, and microscopy make it possible for you to explore, be novel, and be first.

www.agilent.com/find/nanotechnology

Agilent Technologies

Chemistry's Constant Companion™

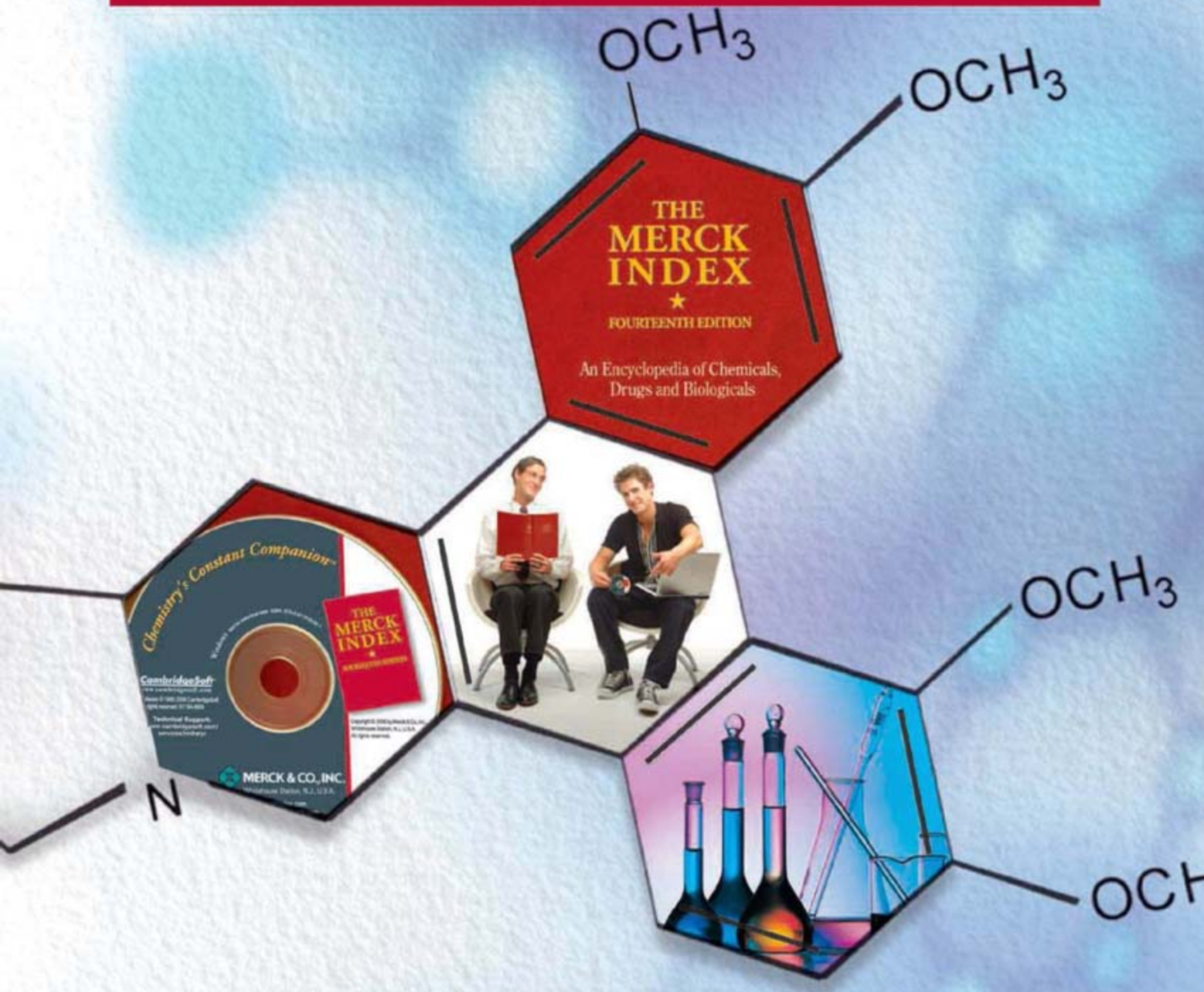

Just Published– Over 25,000 copies sold!

- NEW 14th Edition book comes with a text searchable CD
- Plus free 1-year personal subscription to CambridgeSoft's Internet Edition
- Monographs, tables and organic name reactions extensively revised

Order your copy today at www.merckindex.com or call toll-free at 877-438-6643

Where patients come first MERCK

Crying Wolf?

South Korea's cloning reputation is still not out of the woods: Seoul National University (SNU) announced on 9 April that it will investigate a paper on wolf cloning following complaints that some data are inaccurate. And the journal *Cloning and Stem Cells*, which published the paper in March, took it off the Web on 11 April.

Two cloned wolves—the first of their kind—were introduced to the world on 26 March by researchers at SNU led by Byung-Cheon Lee and Nam-Sik Shin. Snuwolf and Snuwolffy, endangered gray wolf females born in October 2005, were produced by the same team that came up with Snuppy, the world's first cloned dog, using the same methods.

Shortly after the paper appeared, members of BRICs, a scientists' Web forum, claimed that Lee manipulated statistics to exaggerate the success rate of the cloning and that a table on DNA sequence analysis contained errors. Lee admitted to miscalculations at a press conference but said they were unintentional. The university has submitted for outside analysis blood and cell samples from all parties in the exercise: the two wolves, a dog that supplied enucleated eggs, and the wolf whose DNA was inserted into the eggs. Results are expected soon.

Modeling Mecca's Crowds

THE ANNUAL PILGRIMAGE, or haj, to Mecca in Saudi Arabia offers one of the world's greatest challenges in crowd control. The millions in attendance create a volatile environment in which pilgrims have been trampled to death performing a ceremony on the Jamarat Bridge in Mina, where they hurl stones at pillars representing the devil. In January 2006, more than 360 people were killed in a stampede near the bridge. Haj officials have since instituted new safety rules and enlarged the bridge; they have also sought advice from experts in traffic and crowd flow.

One of these experts is Dirk Helbing, a physicist at the Technical University of Dresden in Germany, who was asked to suggest safe routes for crowd movements. Last week, he reported on this work at a physics conference at the University of Leicester, U.K. He and co-workers analyzed videotapes of the 2006 disaster, observing how thick crowds of people, like high-density flows of fluids, can turn "turbulent," causing groups to move erratically. When this happens, people fall and get trampled. Helbing described how it is possible to identify changes in crowd behavior in advance of the turbulence and thus pinpoint danger spots.

The changes have apparently been effective: At the latest haj, from 29 December to 1 January, there were no major incidents.

NET WATCH

Postdoc See, Postdoc Do

Short of a personal tutor who's willing to devote weeks or months to your training, a video might be the best way to learn the subtleties of a lab procedure. This pair of sites can help biologists find or swap video how-to's.

At the *Journal of Visualized Experiments*,* you'll find step-by-step demonstrations of more than 30 lab techniques, including how to isolate blood-forming stem cells or extract embryos from a mouse uterus. Launched last winter by former postdoc Moshe Pritsker and computer scientist Nikita Bernstein, the site features videos shot by professionals and vetted by scientists.

For a YouTube-style site on subjects such as genetics and bioinformatics, go to the new LabAction† from grad student Siddharth Singh of Devi Ahilya University in India. Although it has only a handful of clips so far, it aims to be fun as well as educational, with a category set aside for amusing takes on campus life. >>

* www.jove.com
† www.labaction.com

Mistaken Identity

Until the mid-1800s, leeches were applied to treat ailments including headaches, stomach pain, obesity, fever, and even mental illness, after which their efficacy was seriously doubted.

Today, one species, *Hirudo medicinalis*, is a U.S. Food and Drug Administration (FDA)–cleared device that is widely used to help reattached scalps and fingers as they grow new blood vessels. Demand for the species is great, and so is the loss of its wetlands habitat in Europe. Most now come from leech "farms."

But it turns out many people have the wrong *Hirudo*. Mark Siddall, a systematist at the American Museum of Natural History in New York City, and colleagues compared DNA from various leeches. Commercially available creatures are actually *H. verbana*, they reported online 10 April in the *Proceedings of the Royal Society B*. Siddall explains that in the 1800s, taxonomists discerned no internal differences and lumped the two species as *H. medicinalis*. But, he says, from the genetic evidence "it's unfathomable that they are the same species by any measure." Brijitte Latrille, of the French leech supplier Ricarimpex, says both work the same magic and "I see no problem" in asking FDA to add *H. verbana* to its approved leech list.

CREDITS (TOP TO BOTTOM): KAMRAN JEBREILI/AP; LEE JIN-MAN/AP; ANDREI UTEVSKY

EDITED BY YUDHIJIT BHATTACHARJEE

On Campus

CRIME BUSTERS. Last spring, computer scientist Michael Black gave the 16 undergraduate and graduate students in his computer vision class at Brown University a real-life problem to work on: an unsolved murder. Their research helped narrow the search for a suspect, and on 19 April, Black and his class received a commendation from the Henrico County, Virginia, police. Although the culprit is still at large, Black's class extracted useful information about the crime from blurry and distorted video taken by two surveillance cameras.

"I've never had a class this motivated," says Black, who learned about the case from a colleague the Henrico police had contacted for help. The class used a variety of methods to clean up the video, which shows the victim getting into the suspect's car outside a convenience store. Black says the students developed algorithms "that went beyond the current state of the art" for determining the real-life dimensions of objects in the scene. Their analysis suggested that the car was a Toyota Camry, vintage 1992 to 1994, and that the driver was on the short side, about 170 centimeters.

"We have a suspect now," says Investigator Andrew Stromberg of the Henrico County police. "He's wanted for another crime, and we're trying to catch him and ask him where he was that night."

IN THE NEWS

HECK OF A FIELD TRIP. A French sociologist returned to Paris on 13 April after having been held in Iran for more than 2 months for allegedly entering a forbidden military zone. Stéphane Dudoignon, an expert on Central Asia and Islam at the National Center for Scientific Research in Paris, was arrested on 30 January after taking pictures of a religious procession in Sistan-Baluchestan, a province bordering Afghanistan and Pakistan that's home to a sizable Sunni minority and has been the scene of recent antigovernment violence.

Dudoignon was released shortly after his arrest and was not charged, but Iranian authorities held his passport. He lived with his Iranian wife's family in Tehran until the government sent him home.

Dudoignon said in an interview in *Le Figaro* a week before his return that his research on Iran's Sunni community may be over. "The next time you want to come to Iran," he said an Iranian official told him, "it will be to see your in-laws—and nothing else."

POLITICS

BANISHING THE COLLEGE. Computer scientist John Koza of Stanford University in Palo Alto, California, a pioneer of "genetic programming," made his mark in the wider world by inventing the scratch-off lottery ticket. Last week, Maryland became the first state to endorse Koza's latest idea: overriding the electoral college that chooses U.S. presidents.

Koza first took an interest in elections in 1966 as a grad student, selling a board game based on the electoral college. That system, which aggregates the popular vote into state-based "electoral votes" and awards each state bloc to the candidate who wins the most votes in the state, can elect a president who may not have won the most votes in the nation. In 2000, Al Gore became the fourth presidential candidate to win the popular vote but lose the election.

In 2004, Koza—who views the current system as unfair—teamed up with the nonprofit FairVote to lobby state legislatures to allocate their electoral votes to the national winner of the popular vote. The scheme would go into effect only if enough states sign on, at which point the electoral college would become meaningless. Last week, Maryland's governor signed a law adopting the proposal, which is under consideration in 40 other states. Koza is optimistic that the movement will now take off: "The biggest single question we've gotten has been who else has done this."

Movers >>

EASTWARD BOUND. In its bid to become a major research hub, Singapore has nabbed yet another high-profile Western scientist. Earlier this month, Swedish biochemist Bertil Andersson gave up the post of chief executive of the European Science Foundation (ESF) to become provost at Nanyang Technological University. Andersson, 58, who has served as rector of Linköping University in Sweden and as chair of the Nobel Committee for Chemistry, says he wanted to "be part of the scientific explosion happening in Asia." He found Nanyang, which has 25,000 students and one of the largest engineering schools in the world, appealing because of its growing investment in facilities and Singapore's rising R&D budget.

As provost, a new position one rung beneath the president, Andersson will be in charge of all academic programs. "But my main mission is to build up top-level research efforts," he says. Andersson's successor at ESF is John Marks, who has served as ESF's director of science and strategy since 2004.

Got a tip for this page? E-mail people@aaas.org

CREDITS (TOP TO BOTTOM): JOHN ABROMOWSKI/BROWN UNIVERSITY; ERIC SLOMANSON/SLOMOPHOTOS.COM; NANYANG TECHNOLOGICAL UNIVERSITY

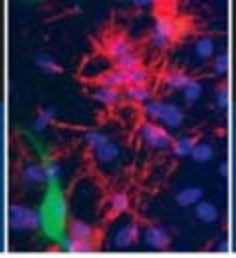

Astrocytes implicated in ALS 353

Tussle over Iraq death data 355

PLANT SCIENCE

Long-Sought Plant Flowering Signal Unmasked, Again

As elusive as the top quark, the signal that tells plants to flower has befuddled plant biologists for more than a century with many false leads to its identity. Two years ago, researchers created quite a stir with data indicating that this signal was messenger RNA (mRNA) that traveled from the so-called *flowering locus T* (*FT*) gene in plant leaves to the growth tip where flowering takes place. But those authors are now retracting that finding (p. 367). Instead, two new reports, published online by *Science* this week (www.sciencemag.org/cgi/content/abstract/1141752 and www.sciencemag.org/cgi/content/abstract/1141753), have fingered the FT protein itself.

"This is something we have been waiting for a long time," says J. A. D. Zeevaart, an emeritus plant physiologist at Michigan State University in East Lansing. "These two papers will be classics in the field for years to come," adds Philip Wigge, a plant biologist at the John Innes Centre in Norwich, U.K. Others, however, think the evidence is not yet conclusive. "They haven't taken the story any further," says William Lucas, a plant cell biologist at the University of California, Davis.

This story has its roots in a 1930s study by Russian plant physiologist Mikhail Chailakhyan. Based on grafting experiments, Chailakhyan proposed that when leaves sense the appropriate day length, they send a mobile signal called florigen to the plant's growing tip to initiate flowering. But promising leads led to dead ends, and "florigen [became] the pariah of botany, [akin to] Big Foot or intelligent extraterrestrial life," says Brian Ayre, a plant biologist at the University of North Texas in Denton.

In the past decade, researchers armed with molecular tools for manipulating genes and visualizing proteins in live tissue have revived the quest. They pinned down the *FT* gene, the leaf protein that turns *FT* on, and a flowering gene that the FT protein controls. Then, in 2005, Tao Huang, a postdoc at the Swedish University of Agricultural Sciences in Umeå, and his colleagues proposed that mRNA was the mobile signal in *Arabidopsis*, as they saw mRNA from *FT* build up in both the leaf and the growing tip. They concluded that FT mRNA was produced in the leaf and traveled to the growing tip, where it was translated into the FT protein, which then kicked off flowering (*Science*, 9 September 2005, p. 1694). This report seemed "an enormously exciting breakthrough," recalls Colin Turnbull, a plant biologist at Imperial College in Wye, U.K.

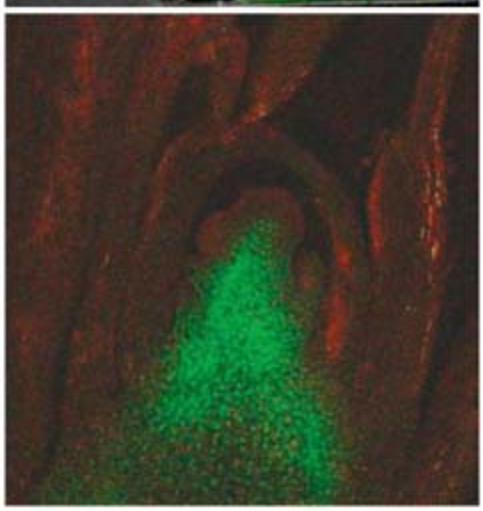

Peripatetic protein. In *Arabidopsis* (*top*), a leaf protein moves from a flowering graft into a nonflowering mutant, causing a stem and blossoms to form. In rice (*bottom*), the equivalent protein (green) shows up in the shoot apical meristem.

But it has not held up. In the 18 April 2006 *Proceedings of the National Academy of Sciences*, Eliezer Lifschitz of Technion Israel Institute of Technology in Haifa reported no sign of mRNA from the *FT*-equivalent gene in the flowering shoots of tomatoes. And in their retraction notice, Huang's collaborators report that their initial analysis excluded some data and gave extra weight to other data. When they redid the experiments, "we could not detect movement of the transgenic FT mRNA," says Ove Nillson, in whose lab Huang did this work. Huang, now at Xiamen University in China, has not agreed to the retraction.

Turnbull and George Coupland of the Max Planck Institute for Plant Breeding Research in Cologne, Germany, working with *Arabidopsis*, and another team studying rice, have now proposed that the mobile signal is the FT protein itself rather than mRNA.

In rice, the equivalent of the *FT* gene is called *Hd3a*. Ko Shimamoto of the Nara Institute of Science and Technology in Japan, his student Shojiro Tamaki, and their colleagues first measured Hd3a mRNA in various tissues. They found that in rice grown with short days (rice requires short days to develop flowers), the mRNA increased in leaves but was present only in very low amounts in the shoot apical meristem, the growing tip. Next, they made a transgenic rice strain by joining the gene for green fluorescent protein (GFP) with that for *Hd3a*, which made any Hd3a protein visible under a confocal laser scanning microscope. They saw the protein in the vascular tissue of the leaf and the upper stem as well as in the core of the growing tip.

They then attached promoters to the combination *GFP/Hd3a* gene that caused the genes to turn on in the leaf but not in the growing tip. Flowering still occurred, they report. "The only way [FT] could get there was if it moved," explains Zeevaart.

Like Shimamoto, Coupland and Turnbull focused on the FT protein and used GFP to track its fate, this time in *Arabidopsis*. Laurent Corbesier, a postdoc in Coupland's lab, added the fused *FT/GFP* gene to a mutant *Arabidopsis* strain that lacked the *FT* gene. They observed the protein first in the vascular tissue of the stem, and 4 days later, at the base of the growing tip.

In another experiment, the team grafted plants carrying the fused gene to mutant ▶

CREDITS (TOP TO BOTTOM): COLIN TURNBULL; S. TAMAKI AND K. SHIMAMOTO

Hard times for NIH grantees
356

Natural selection in Tibet
364

plants that could not make FT at all. The FT/GFP protein, but no mRNA, moved across the graft junction and through the mutant plant, they report.

Finally, when they attached two *GFP* genes to the *FT* gene, the resulting protein was too big to travel beyond the leaf—and in those plants, no flowers formed. Thus, the researchers could rule out both RNA and the existence of a signal activated by FT.

"The evidence is convincing, especially the grafting experiments," says Ayre. And, strengthening the case, several other researchers are preparing to publish similar results.

But not everyone agrees. Lifschitz calls the evidence in both reports "circumstantial." He, Nilsson, and Miguel Blázquez of the Polytechnic University of Valencia, Spain, point out that neither group tested whether GFP moves through the plant on its own accord. And Lucas doesn't think the authors adequately demonstrated that FT gets into the growing tip from the leaf. For example, in *Arabidopsis*, one leaf promoter used turns on genes elsewhere in the plant, so it could have turned on *FT* outside the leaf, Lucas points out. Even Ayre is still cautious. "Florigen has a long history of disappointing people," he says. "We're getting there, but the race is intense, and we need to keep cool heads."

–ELIZABETH PENNISI

OIL RESOURCES

The Looming Oil Crisis Could Arrive Uncomfortably Soon

The world's production of oil will peak, everyone agrees. Sometime in the coming decades, the amazing machinery of oil production that doubled world oil output every decade for a century will sputter. Output will stop rising, even as demand continues to grow. The question is when.

Forecasts of peak oil production have ranged from Thanksgiving weekend 2005 to somewhere beyond 2050. But at the annual meeting of the American Association of Petroleum Geologists (AAPG) in Long Beach, California, early this month, the latest answer emerged: World oil production could stop growing as early as 2020—too soon to avoid a crisis—or it could hold off until 2040. "The peak in world oil production is not imminent," oil information analyst Richard Nehring of Nehring Associates in Colorado Springs, Colorado, said at the meeting, but it is "nevertheless foreseeable."

Predictions of the timing of peak oil have been all over the map (*Science*, 18 November 2005, p. 1106). So-called peakists favor gauging future production by judging how much oil Earth still holds and how much has already been produced. They come up with a peak in the next few years, certainly before 2020. At the other extreme, major oil companies draw on in-house expertise about how much oil remains and how fast it will be produced. They see no end to rising production as far out as they look, usually not beyond 2030.

Nehring took a different tack, in two ways. First, he conducted an informal survey of experts by organizing a meeting, a prestigious Hedberg Conference, under the auspices of AAPG last November and inviting 75 experts from 19 countries to consider the world's oil resources. There he pressed them for their best estimates of everything from how much oil might be left to discover to how much might be wrung from existing oil fields and how much might come from unconventional sources such as Canadian tar sands.

From the meeting's discussions, Nehring came up with low, medium, and high estimates of all the oil likely ever to be produced. But as he said at the meeting, the ultimate resource is not the only constraint. Politics and social unrest can limit how fast those resources can be exploited, as is happening today in Venezuela, Iraq, and Nigeria. And technological challenges, as in the still-icebound Arctic, can slow extraction as well.

So for his second innovation, Nehring created three scenarios with successively higher peaks beginning in 2020, 2030, and 2040. He then compared the amount of effort it would take to achieve each scenario with the world oil industry's past performance. "The only scenario we're quite sure of is the low one" producing a 2020 peak, he says. Conference participants were confident that at least the low estimate of ultimate oil resource is actually out there, he says. And the world oil industry has managed to add the needed production capacity as fast as a 2020 peak would require.

Holding the peak off until 2040, however, would require both a high—and much less certain—total oil resource and adding more production each year than ever before, despite having already produced the world's most easily extractable oil. "We can't behave now like we're going to have the high scenario," Nehring concludes.

Nehring is getting some attention but not many converts. "Richard did a good service in holding this Hedberg Conference," says oil assessment specialist Donald Gautier of the U.S. Geological Survey in Menlo Park, California. But there's so much uncertainty, Gautier says, from when Arctic ice might melt out of the way to when needed new technology can be developed, that predicting the peak may not be worthwhile. A decade or so could tell.

–RICHARD A. KERR

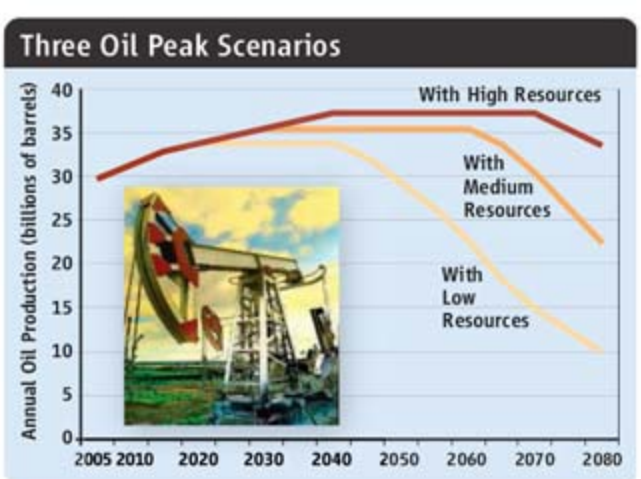

Sooner or later. The less oil left to be pumped from the ground, the earlier world production reaches a peak. In a new analysis, only the earliest, low-resource peak looks reliable.

CREDITS: (SOURCE) RICHARD NEHRING; (IMAGE) PHOTOS.COM

NEUROSCIENCE

Astrocytes Secrete Substance That Kills Motor Neurons in ALS

Astrocytes—among the glial, or "support," cells in the central nervous system—may be the primary culprit in the death of motor neurons in at least some cases of amyotrophic lateral sclerosis (ALS), researchers at Harvard and Columbia universities report. The new findings underscore the power of research with embryonic stem (ES) cells to elucidate basic disease processes, the researchers say.

ALS is an untreatable disease that progressively kills motor neurons. For years, scientists have debated whether the motor neurons themselves are defective, or whether some external factor kills them. Two papers, published online on 15 April in *Nature Neuroscience*, present new evidence that in some ALS sufferers—those with a mutant gene for superoxide dismutase (*SOD1*)—the astrocytes emit a toxin that selectively kills motor neurons. ALS researcher Jeffrey Rothstein of Johns Hopkins University in Baltimore, Maryland, says the papers "add weight to a growing body of data that has suggested that astrocytes contribute to ALS." Roughly 10% of ALS cases are familial, with the rest being labeled "sporadic." *SOD1*, the only gene that's so far been linked to the disease, is mutated in about 25% of familial cases.

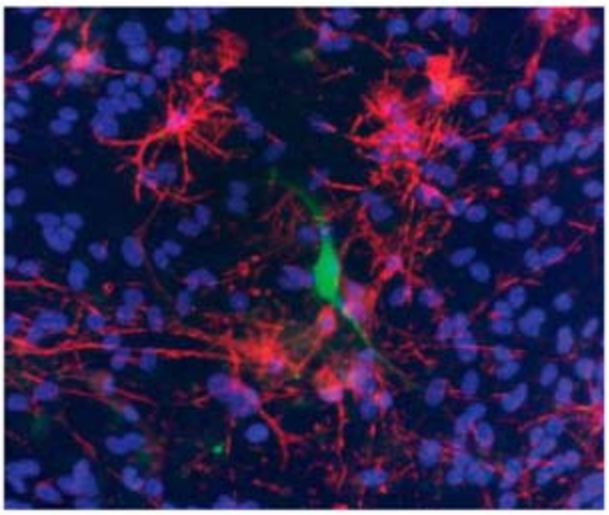

Bad neighborhood. Astrocytes (red) threaten motor neurons (green) in culture with mutant *SOD1* gene.

CREDIT: REPRINTED BY PERMISSION FROM MACMILLAN PUBLISHERS LTD., F. P. DI GIORGIO *ET AL.*, *NATURE NEUROSCIENCE* (15 APRIL 2007 ONLINE EDITION)

In the latest work, a Harvard group led by Kevin Eggan generated ES cells from the blastocysts of mice bred to express the normal human *SOD1* gene and from mice with the mutant *SOD1* gene. The scientists then coaxed the ES cells to become motor neurons and did some mixing and matching, cultivating the motor neurons and astrocytes with and without the mutation. They found that even normal neurons did badly in the presence of astrocytes with the *SOD1* mutation, showing a 50% decrease over 14 days. Reversing the conditions, they found that when mutant motor neurons were surrounded by normal astrocytes, their losses were much less severe.

Eggan says the work "really validates this song we've been singing: If you can make ES cell lines carrying the genes, you can study diseases in a much more sophisticated way." He plans to do the work with human ES cell populations containing the DNA from ALS patients.

The Columbia team, headed by biologist Serge Przedborski, took the findings a step further by demonstrating that astrocytes are solely responsible for this particular toxin, and that they only target motor neurons. They found that growing motor neurons in a culture in which astrocytes had been grown produced the same deadly results as exposing them to astrocytes directly. Przedborski says that points to a toxic substance emitted by the glial cells. The team ruled out both SOD1 and glutamate—a major troublemaker in brain disease also implicated in ALS—as the toxic substance.

Steven Goldman, a stem cell researcher at the University of Rochester Medical Center in New York, says the research provides a "very valuable model" for this particular type of ALS. "These are potentially quite exciting papers for introducing new avenues for research," says Goldman. He says identifying the agents being released by astrocytes, and ultimately seeing "whether this type of mechanism is limited to the SOD1 model," may help unlock the mysteries of sporadic types of ALS as well.

The Columbia group plans to define the basic characteristics of the poison and then use that knowledge to screen for new drugs. "For a disease in need of drugs like few others, that would be great," says Eggan.

–CONSTANCE HOLDEN

Texan Mishap Not Reported

Texas A&M University (TAMU) in College Station has admitted to running afoul of federal bioterror rules after an employee last year contracted brucellosis, an animal disease that's high on the list of potential bioterror weapons. In a statement to the Centers for Disease Control and Prevention (CDC) in Atlanta, Georgia, made last week, the university acknowledged that it should have notified CDC a year ago about the incident, which came to light through a freedom-of-information request from the Sunshine Project, a watchdog group in Austin, Texas. A CDC investigation begun this week could result in fines and loss of federal funding.

The researcher was diagnosed with brucellosis in April 2006 after cleaning an aerosol chamber containing *Brucella* bacteria in a biosafety level 3 lab in February. TAMU says the researcher recovered after treatment with antibiotics. There are a few hundred U.S. cases of brucellosis each year, but human-to-human transmission of the pathogen is extremely rare. Sunshine Project Director Edward Hammond says the government needs to devise a system to actively track such accidents.

–MARTIN ENSERINK

NIMR Eyes a Bigger Site

LONDON—The upcoming availability of a 1.5-hectare site in central London could end the controversy over government plans to relocate the National Institute of Medical Research (NIMR) from its famous suburban campus in the Mill Hill area to a 0.4-hectare site in downtown London. Critics had complained that the planned site was so small it would limit NIMR's science (*Science*, 4 February 2005, p. 652). In a letter earlier this month to NIMR staff, Colin Blakemore, director of the Medical Research Council (MRC), said the agency was now considering with "enthusiasm" a larger site next to the British Public Library that another government agency plans to sell. It's also near research hospitals, fulfilling MRC's desire for a revamped NIMR to focus on translational research.

NIMR's Robin Lovell-Badge, a critic of the planned move, agrees that the location near the library is more promising but warns that its cost could still end up shrinking NIMR. "The devil is in the details," he says. Blakemore says that the new site has clear advantages, although he stresses that the original one, which used to house the National Temperance Hospital, is still acceptable. Blakemore says MRC's chances of getting the new site are unclear and so are its costs, but he hopes to have NIMR's future resolved before he steps down as MRC director in September.

–JOHN TRAVIS

PHYSICS

Colliding Clouds May Hone Physical Constants

A new spin on the atomic clock could yield some of the most precise measurements to date of fundamental physical constants—potentially providing crucial experimental tests of a number of "theories of everything." Four physicists at Pennsylvania State University (Penn State) in State College have built the prototype of a "quantum scattering interferometer"—a device capable of registering differences in the mass and other properties of atoms with unheard-of sensitivity. The experiment, described this week in *Nature*, could lead to more-accurate atomic clocks and help physicists study exotic states of matter such as Bose-Einstein condensates and degenerate Fermi gases, says Randall Hulet of Rice University in Houston, Texas. "It's a new high-precision tool for measuring the effects of [atomic] interactions," Hulet says.

The researchers start by cooling two clouds of cesium atoms to fractions of a microdegree above absolute zero. One cloud is then put into its lowest-energy state (called the ground state) and sent through a chamber where microwaves excite the atoms into a bizarre state called quantum superposition, in which the outer electron in each atom has a property called its spin pointed both upward and downward at the same time. One spin state harbors slightly more energy than the other does. (In atomic clocks, the frequency of light emitted when cesium atoms move between these two "hyperfine" states provides the standard for determining the length of a second.)

In the Penn State experiment, the researchers bring the two clouds together. As the atoms collide, the two hyperfine states of each cesium atom recoil differently, causing them to interfere with each other in a way that creates a time lag or phase shift between the two states. The collided atoms are sent through a microwave chamber a second time and then are sorted using laser pulses that tally the phase shifts. The results provide a detailed portrait of the collision (see figure). "If you really want to understand atom-atom interactions very precisely, this is the method," says Kurt Gibble of the Penn State team.

Mind the gap. Time lag caused by interference of specially prepared cesium atoms could boost studies of atomic collisions and physical constants.

In the future, the scientists hope to further fine-tune the experiment by using magnetic fields to coax the atoms into short-lived connections called Feshbach resonances, which resemble molecular bonds. Because the atoms interact over longer periods, researchers will be able to learn more about their properties. The resonances should enable physicists to apply atomic-clock accuracy both to studies of the collisions and to measurements of fundamental physical constants—such as the ratio of the mass of the electron to the mass of the proton. Some versions of string theory and other grand unification theories predict that such constants will vary slowly over time. If so, Gibble says, an ultrasensitive future version of the quantum scattering interferometer would be able to measure the variations over the span of years.

–MARK ANDERSON

Mark Anderson is a writer in Northampton, Massachusetts.

PSYCHOPHARMACOLOGY

Study Questions Antidepressant Risks

An analysis of 27 clinical trials of antidepressants in youngsters has found a negligible risk of suicidal thoughts and suicide attempts, with the treated groups showing 0.7% greater risk than participants given a placebo. The study comes more than 2 years after regulatory agencies worldwide warned doctors to take great care in prescribing the drugs to children and teenagers because they might increase "suicidality." Since then, controversy has grown over whether the risks have been exaggerated.

The authors of the new study, published this week in the *Journal of the American Medical Association* (*JAMA*), undertook their analysis after the U.S. Food and Drug Administration (FDA) slapped a "black box" warning on most antidepressant drugs in late 2004. But that warning didn't take account of the medications' benefits, says Jeffrey Bridge, an epidemiologist who studies teen suicide at Columbus Children's Research Institute in Ohio. With David Brent of Western Psychiatric Institute and Clinic in Pittsburgh, Pennsylvania, and their colleagues, the group set out to mimic FDA's approach while incorporating some new data and reported benefits of the drugs.

As FDA did, the *JAMA* authors examined trials of depression, obsessive-compulsive disorder, and other anxiety disorders, bringing together 5310 subjects. Disorder-specific analyses did not yield statistically significant results, but when all data were pooled, the authors found that those on medication had a small but statistically significant increased risk of suicidal thinking and behavior of 0.7%. This was less than the FDA-cited 2% risk. The authors also found that, in general, teenagers were helped by many of the drugs tested. Depressed children, as has been previously reported, were helped only by Prozac. "What this shows is that the overall bad effect is very small, and the overall good effect is much bigger," says Charles Nemeroff, chair of the department of psychiatry and behavioral sciences at Emory University in Atlanta, Georgia.

Like nearly all so-called meta-analyses, the *JAMA* study has its drawbacks, researchers agree. The trials it examined were not designed to assess suicidal behavior and excluded individuals who were suicidal.

Although these drugs may pose a risk to some, says Kelly Posner, a child psychiatry researcher at Columbia University who assisted FDA in its safety analysis, we already know that "untreated depression is what kills people." Posner and others are convinced that youth suicide data now emerging—a 14% increase in the United States in 2004 and a staggering 49% increase in the Netherlands—show what happens when antidepressant drug use declines.

–JENNIFER COUZIN

CREDIT: ADAPTED FROM GRAPHIC BY KURT GIBBLE/PENNSYLVANIA STATE UNIVERSITY

A war's toll. The release of study data hasn't calmed a debate over the number of violence-related deaths in Iraq.

CREDIT: HADI MIZBAN/AP PHOTO

EPIDEMIOLOGY

Iraq Mortality Study Authors Release Data, but Only to Some

The authors of a controversial study on conflict-related deaths in Iraq are seeking to diffuse criticism by releasing their raw data. But the move has hardly settled the debate. Critics say the authors have withheld key details needed to check the study. And some are outraged by the conditions set for who can have the data, including the requestor's "objectivity."

The paper, published in *The Lancet* last October by a U.S. and Iraqi team, estimated that 655,000 more people have died than normally would have since the March 2003 U.S. invasion—more than 10 times any official estimate. The authors got this result by extrapolating from mortality data collected through door-to-door surveys. Other academics have questioned aspects of the study, from whether the interviews could have been done as quickly as claimed, to whether the results were inflated by surveying only households near main streets vulnerable to bombs and shootings (*Science*, 20 October 2006, p. 396).

Lead author Gilbert Burnham's team at Johns Hopkins University in Baltimore, Maryland, had resisted calls to release the raw data, citing possible danger to the Iraqi interviewers and the survey participants. Earlier this month, however, Burnham and his team posted a note on their Web site saying they would release a data set stripped of information that might reveal identities—but only to qualified scientific groups. Such groups must have expertise in biostatistics and epidemiology, the note says, and must also be "without publicly stated views that would cause doubt about their objectivity in analyzing the data." The Hopkins team says several groups have received the data.

But at least one researcher has been turned down: Michael Spagat, an economist and expert on conflict studies at Royal Holloway, University of London, in Egham, who has been a proponent of the street-bias idea. Burnham, e-mailing from Jordan, declined to explain which criteria Spagat did not meet; co-author Les Roberts, now at Columbia University, says he wasn't involved in the decision but that Spagat "would not meet the criteria by multiple measures."

Spagat calls the policy "deeply flawed," adding, "If we do something dumb or non-objective with the data, qualified people should be able to expose our stupidity." The decision also puzzles David Kane, a fellow at the Harvard Institute for Quantitative Social Science who has received the data set even though he says he posted comments on a Web log last fall that raised the possibility of fraud. Denying some critics access "is ridiculous," Kane adds.

One epidemiologist apart from the fray agrees that the conditions are unusual: "I am wary of trying to limit access based on the predilections of those requesting it," says David Savitz of Mount Sinai School of Medicine in New York City. But Allen Wilcox, editor-in-chief of *Epidemiology*, defends the conditions set by the Hopkins group: "I can hardly blame [them] for being cautious in this case," says Wilcox, because the topic is so politically charged.

Others are concerned that the group's decision to withhold information such as main street names and the sampling protocol has made it impossible to detect street bias or other potential problems. More details on the interviews "are necessary if the authors are to lay to rest intimations of 'fabricated' data," says Madelyn Hicks, a psychiatrist and public health researcher at King's College London. Burnham says his group "envision[s] no additional release of materials." **–JOCELYN KAISER**

With reporting by John Bohannon.

SCIENCESCOPE

Human—Not Martian—Error Cited

Mars Global Surveyor (MGS) went silent last November after orbiting the planet for 10 years, not from old age but because of a software error. A NASA investigative board report has concluded that the mission operations team sent a software update months before to the wrong part of the spacecraft's computer memory, wreaking havoc on the spacecraft after Surveyor received a routine command. An antiquated onboard fault-protection system subsequently misinterpreted the situation, and within 2 hours Surveyor had died of insufficient battery recharging.

Like other NASA missions extended far beyond their promised design lifetime, MGS had suffered reductions in its operations budget and staffing. "We didn't find that any decrease directly caused the anomaly," said board chair Dolly Perkins of Goddard Space Flight Center in Greenbelt, Maryland. But she said, "It's beneficial to step back and see what risks from aging and changes in operations" might be developing. That lesson is being applied to all Mars missions as well as ones taking the better part of a decade to reach targets such as Mercury and Pluto. **–RICHARD A. KERR**

Sensor Move Deemed Sensible

NASA and the National Oceanic and Atmospheric Administration last week restored a key environmental sensor to a long-awaited satellite demonstration mission due to be launched in 2009. But researchers are giving the move only one thumb up: The agencies haven't decided whether to restore the sensor, called the Ozone Mapping and Profiler Suite Limb (OMPS-Limb), to six planned satellites that make up the troubled National Polar-Orbiting Operational Environmental Satellite System (NPOESS).

OMPS-Limb, which will provide ozone-distribution data for environmental and climate studies, was knocked off the NPOESS demo and the main satellites to save money (*Science*, 16 June 2006, p. 1580). But in a March letter to the White House, House Science and Technology Committee leadership pointed out that the sensor for the demo had already been built and that it wouldn't cost any more to fly it on the demo.

Remote-sensing expert Berrien Moore of the University of New Hampshire, Durham, applauded the restoration of OMPS-Limb but also wants it on the NPOESS flights "as an operational sensor." A House Science committee staffer says members will continue their push to make that happen.

–ELI KINTISCH

Boom and Bust

Biomedical facilities are expanding after a growth spurt in the NIH budget. Yet individual scientists say that it's harder than before to get their work funded

KURT SVOBODA KNEW FROM DAY ONE that science meant sacrifices: pulling long hours, sweating over the data, and starving his personal life for professional success. What the young assistant professor at Louisiana State University (LSU) in Baton Rouge didn't realize was that time spent on grant proposals, not groundbreaking experiments, would be the big stressor.

Svoboda, who turned 40 in January, wants to study how nicotine affects brain development in zebrafish, as a model of fetal exposure in women who smoke during pregnancy. Last summer, his tenure review was little more than a year away, but he had yet to secure an unspoken prerequisite: a federal grant. It wasn't for lack of trying. Since landing his job at LSU in 2002, Svoboda has been on a continuous hunt for money, five times submitting or resubmitting major applications, along with two smaller ones. Last summer, he was down to his third and final chance for approval of a revised R01, the National Institutes of Health's (NIH's) bread-and-butter grant. Without one, Svoboda suspected he would lose his job.

He and his two graduate students worked 12-hour days cranking out data they hoped would sway the reviewers. The final version of the application contained 27 data figures, Svoboda says. "I've never seen a person work so hard in my life," says Svoboda's LSU colleague, neurobiologist John Caprio.

From California to Louisiana to Massachusetts, thousands of biomedical researchers find themselves in a similar financial bind. This year will be the fourth in a row that the budget of NIH, the wealthiest research agency in the world, has not kept pace with biomedical inflation. The slowdown is one of the longest veteran scientists can recall.

Chance of being funded on the first try:

1998: 21%

2006: 8%

To make matters worse, there may not be much sympathy for these scientists on the outside. Biomedicine is considered rich and well-protected territory. Indeed, today's crunch comes after a heady 5 years of growth, as the NIH budget doubled between 1998 and 2003. But people on the inside know the money crunch is real. "You're almost in a different movie now," says Anthony Fauci, who heads the National Institute of Allergy and Infectious Diseases (NIAID), one of the largest of NIH's 27 institutes and centers. The percentage of research proposals funded by NIH has dropped from 32% in 2001 to a projected 21% this year. Funded grants are routinely cut by 10% or more.

Dozens of investigators interviewed by *Science*, along with six NIH institute directors and agency head Elias Zerhouni, describe a climate in which young scientists struggle to launch their careers and even the most senior are trimming their research projects. Harold Varmus, a Nobel Prize winner who led NIH from 1993 to 1999 and is now head of the Memorial Sloan-Kettering Cancer Center in New York City, has had his grant cut, although he won't say by how much.

Still, with a budget totaling $29.2 billion in 2007, NIH is hardly a pauper. What brought biomedical research to this place of financial anxiety? The doubling flooded NIH with billions more dollars over a rela-

CREDIT: JEFF MILLER/UNIVERSITY OF WISCONSIN, MADISON; SOURCE: NIH (R01-EQUIVALENT AWARD)

Rising expectations. Like many, the University of Wisconsin, Madison, is investing in the biosciences.

tively brief time. Whereas a private corporation might conserve some of this windfall, by law NIH must spend nearly all the money it receives the year it receives it. That provoked a massive expansion in biomedical research, and expectations of federal support surged to a level that could not be sustained when the budget stopped growing. The crash is hitting labs, careers, and the psyches of scientists with a vengeance.

The big bubble

Nine years ago, Congress set out to double the NIH budget and within 5 years sent it soaring from $13.7 billion to $27.1 billion. But everyone knew the golden days would not last. In October 2000, eight senior scientists and policymakers began meeting informally to discuss how to maintain the momentum. In 2002, the group published a commentary in *Science* presenting different budget models and their impacts on research priorities (*Science*, 24 May 2002, p. 1401). Its most pessimistic prediction modeled annual increases of 4%. Says David Korn, a former Stanford University dean now at the Association of American Medical Colleges (AAMC) in Washington, D.C., who helped bring the group together: "We didn't model increases below 4% a year because the tradeoffs and the sacrifices that would have been caused … were too difficult for us to deal with in the model."

At NIH, senior officials found that "no matter what, there will be pain after the doubling," says Zerhouni, who became NIH director in 2002. To soften the blow, in 2002 and 2003, NIH tried to accelerate the pace of one-time expenditures such as construction, to free up money for the following years. But even "in the worst scenarios, people really didn't think that the NIH budget would go below inflation," says Zerhouni, an outcome he attributes to the 9/11 attacks, the wars in Afghanistan and Iraq, and Hurricane Katrina.

Meanwhile, research institutions everywhere were breaking ground on new facilities and expanding their faculty. In a 2002 survey, AAMC found that new construction at medical schools had exploded: From 1990 to 1997, schools invested $2.2 billion in new construction, compared to $3.9 billion from 1998 to 2002. But that paled in comparison to what was to come: an expected $7.4 billion in new construction from 2002 to 2007. AAMC has not yet confirmed whether these plans were carried out.

Schools hired new faculty members to fill the buildings, expecting to recoup their investments from the NIH grants investigators would haul in. "Universities and their leadership did what I would have done too," says Zerhouni. "The government is indicating support for these activities," and the expansion was "exactly what Congress intended."

This appears to have helped drive more applicants to NIH. In 1998, fewer than 20,000 scientists sought research grants from the agency; in 2006, that number was more than 33,000, and according to NIH forecasts, the number of applicants is expected to top 35,000 in 2007. The number of applications has grown at an even faster clip, as scientists, concerned about their chance of getting funded, are submitting proposals more frequently. Because growth at medical schools lagged somewhat behind the doubling, many institutions are still expanding. At Sloan-Kettering, for example, officials only recently began filling a new building with scientists. They expect to increase their faculty by almost 50%, says Varmus.

But as requests for NIH money edged upward, NIH's resources began to drop. After a 16% increase in 2003, the final year of the doubling, NIH received a 3% boost in 2004, an abrupt reversal of fortune. Although the general rate of inflation in 2006 was 3.1%, according to the U.S. Department of Commerce, the cost of goods and services in biomedical research and development rose 4.5%. The number of competing grants NIH funded peaked in 2003 and has been dropping since. The declining value of NIH's dollars and rising demand were "a perfect double whammy," says Zerhouni.

Number of applications per applicant:

1998:	1.23
2006:	1.38

Yet the numbers fail to convey the gnawing unease and foreboding expressed by scientists across disciplines and at every stage of their careers. "The ripple effect here is amazing and paralyzing," says Steven Dowdy, a cancer biologist at the University of California, San Diego. At Brown University, molecular cell biologist Susan Gerbi, who helps oversee graduate training, canvassed 49 faculty members in eight departments recently, as she does every year, to see how many would take on a graduate student from next year's pack. "In the past, it was a majority," around 90% of those who responded, she says. "This year, only about 25% of the trainers said they would be interested … because they did not have a guarantee of funding for next fall."

"What's chilling" about the drought is that "we're getting into years 3 and 4 with no end in sight," says Edward Benz Jr., the president and CEO of Dana-Farber Cancer Institute in Boston. Many researchers noted that the pressures on the federal budget, including the war in Iraq, leave Congress little room to expand or even stabilize other programs.

Crunched for cash

Alan Schneyer, a 52-year-old reproductive endocrinologist who has spent his career at Massachusetts General Hospital in Boston, at first wasn't too concerned when his grant application failed to make the cut. Like Svoboda and all scientists applying for R01s, Schneyer is allowed to submit two revisions of an application in hopes of persuading reviewers to give a fundable score. Schneyer's work had recently taken an unexpected turn. After a decade of studying how two proteins affect reproduction, he had eliminated them in mice and hit upon a surprising

Grant Applicants to NIH, 1998–2007*

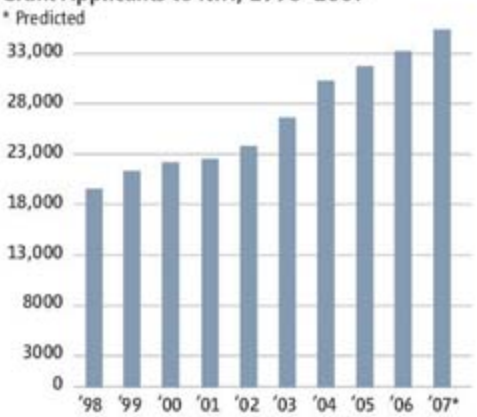

Percentage of Proposals Funded, 1998–2007*

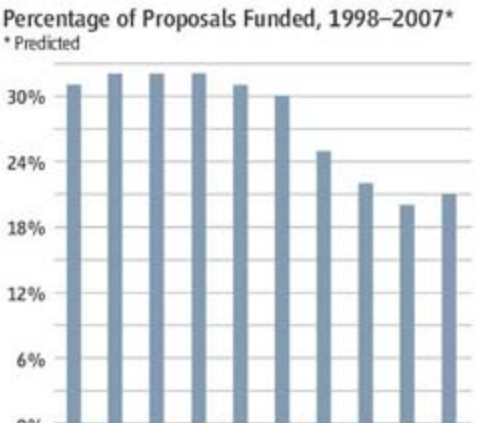

SOURCES (TOP TO BOTTOM): NIH; NIH OFFICE OF EXTRAMURAL RESEARCH

On the hunt. Submitting grant applications takes more and more time, says neurobiologist Kurt Svoboda.

result: The animals had superior glucose tolerance and an abundance of pancreatic cells that make insulin. "If you're trying to treat diabetes, this would be perfect," says Schneyer.

Schneyer says he went through a "several-years learning curve" transitioning into the diabetes field. In March, he learned that, on his third and last chance, he'd missed this year's funding cutoff by 3%.

After 3 years of trying for NIH grants and failing, including two unsuccessful attempts to renew a second R01, Schneyer's lab has shrunk from six people to one—he works there by himself. Although the National Institute of Diabetes and Digestive and Kidney Diseases may yet make an exception and fund him, he's not taking any chances. Next month, Schneyer will begin a job that doesn't rely as heavily on NIH money, working at Pioneer Valley Life Sciences Institute in Springfield, Massachusetts, and commuting from Boston 3 hours each day. "It's very real that you won't get a grant, even with an idea and 20 years of experience and a mouse that indicates treatment for diabetes," he says.

NIH officials say they're hearing from many scientists who, like Schneyer, can't keep their labs running. "I get phone calls from people saying, 'I'm letting my people go, what do I do now?' " says Michael Oberdorfer, a program director at the National Eye Institute. "I feel like I'm doing a lot of social work."

Compounding the problem is that most universities and medical institutions rely on NIH money for the bulk of scientists' salaries and overhead costs and are not set up to support faculty members long-term. Traditionally, "bridge funding" could tide researchers over for a few months. But now, more scientists than ever are having to resubmit grant applications, with a gap of 8 months or more in between each submission. At NIAID, the percentage of proposals funded on the first try has gone from 27% in 2001 to 11% in 2006.

Some schools are beefing up their bridge funding. Dana-Farber, for example, is setting aside $3 million to $4 million this year. Historically, the institute reserved $500,000 to $1 million "and almost never spent it," says Benz, Dana-Farber's CEO.

Even "the senior investigator is turning out to be a challenge for us to support," Benz continues. Funded grants are subject to cuts—24% on average at the National Cancer Institute (NCI), for example, and 18% at the National Institute on Aging. In each of the last 2 years, says Benz, two or three Dana-Farber labs have found themselves hundreds of thousands of dollars short of what they say they need to keep running

Chance of being funded on the first try in 2006:

First-time applicant	9%
Established investigator	7%

Peer Review Under Stress

With biomedical grant applications at an all-time high, competition is putting a strain on the system that picks the winners. After serving on recent study sections—as judging panels are known at the National Institutes of Health (NIH)—many researchers describe the stress and frustration of having to make arbitrary distinctions. "You're on the airplane flying home thinking 'We were really flipping coins on those last three grants,' " says Michael Mauk, a neuroscientist at the University of Texas, Austin, who chairs a study section on learning and memory. "The problem when pay lines get this low is that we're not cutting out the fat, we're cutting into the meat."

Although the system still works fairly well overall, says David Perkel, a neuroscientist at the University of Washington, Seattle, and a member of Mauk's study section, it doesn't have the resolution to precisely rank the top applications in a given pool. Yet as NIH pushes against a no-growth budget, small distinctions among the best proposals matter more and more. "It's possible to get to the top 20% and do it in a deliberative way," Perkel says. "But what I think is really problematic is subdividing that top fifth." For example, Perkel has seen what he calls "figure-skating effects." As in the Olympic finals, "the first skater never gets a 10" because the judges want to leave room for still-more-impressive performances, Perkel says. Similarly, in his study section, the best scores almost always come later in the meeting, Perkel says: "Because there's this score creep during the day, it introduces some inequities."

There's another unspoken rule, researchers say: grant applications being submitted for the third and final time often receive preferential treatment. (NIH only allows three tries.) Some reviewers admit to feeling torn between a desire to toss a lifeline to a vulnerable colleague and the obligation to score grant proposals strictly according to merit. "I think reviewers are very aware that there's a lot at stake here," says Michael Oberdorfer, a program director at the National Eye Institute. "You're talking about the survival of a lab." The success rates for bread-and-butter grants known as R01s tend to increase with each submission. Across NIH, the success rate (the number of funded grants divided by applications) in 2006 jumped from 8% for first-time R01 applications to 28% for second submissions and to 47% for third attempts. In 1998, in contrast, the difference between first and third application success rates was smaller: 21% and 41%.

Researchers want the best and brightest of their colleagues reviewing their grant proposals. But stocking study sections with well-qualified scientists has gotten harder recently. Grant applications to NIH are projected to increase 65% between 2002 and 2007, and in response to pleas from overloaded researchers, NIH has cut the number of proposals each reviewer is asked to review. As a result, the pool of reviewers has

CREDIT: EDDY PEREZ; SOURCE: NIH (R01-EQUIVALENT AWARD)

smoothly—money that Dana-Farber has kicked in. "The full impact hasn't been felt because institutions have provided a buffer, but the funds that provide for that buffer are disappearing," he says.

At Brown, Gerbi is running out of money and will submit her second shot at her R01 in July. In desperation, she's cast a wide net in her quest for funds, applying everywhere from disease foundations to the Department of Defense, and has about 10 grant applications pending inside and outside NIH. In the meantime, she says, the university offered her some money that will run out this summer—but only because she recently underwent treatment for breast cancer and an exception was made. If grant money doesn't come through within months, she says, she'll be closing the stock center she keeps of a rare fly species named *Sciara* and, in the worst case scenario, her lab as well.

Many scientists complain that the tough funding climate is exacerbated by an excessive focus at NIH on costly "big science," such as the Cancer Genome Atlas, which is using large-scale genetic sequencing to decipher the molecular basis of cancer and whose 3-year pilot phase is budgeted at $100 million. Projects like this one, many scientists say, are coming at the expense of grants that sustain individual labs and have been the source of much innovation over the years.

Zerhouni denies that R01s are a lower priority than they used to be. "I hear that just the way you do, but the numbers don't bear that out," he says. Still, centers have grown somewhat. In 1998, they made up 8% of the budget, compared with 10% in the 2008 budget request filed in February. The extramural grants budget devoted to R01s and other individual grants has dipped slightly, from 81% in 1998 to 78% in 2006. But it's not clear that this is compounding the troubles of individual researchers, says

Competing Grants Funded, 1998–2006

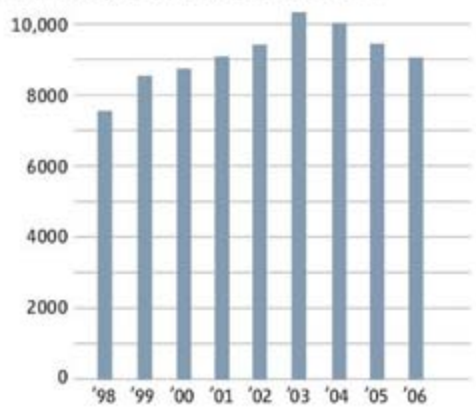

NCI Director John Niederhuber. Many big team initiatives at NCI, he says, are funding some of the same researchers who would be applying for R01s.

"It would be ridiculous to think we should be doing things today in 2007 exactly the way we did in 1970," says Niederhuber. "Science has changed tremendously."

A strain on the young

Nowhere does the funding gap seem wider than when looked at through the lens of age. "It's just about inconceivable for a brand-new investigator to get an NIH grant funded on their first submission these days," says David Sweatt, chair of the neurobiology department at the University of Alabama, Birmingham. Sweatt has hired three young scientists in the past year and worries about their future. "I see it as this dark shadow hanging over people who are just starting out their labs," he says. "They're having to spend so much time being anxious over funding, to the detriment of having time to think creatively about their research."

At Vanderbilt University in Nashville, Tennessee, pediatric infectious disease specialist John Williams recently learned that his first R01 application failed to make the cut on its second try. Although NIH institutes generally give new investigators a bonus by increasing the pay line—from 12% to 14% at NIAID, for example, or from 12% to 18% at NCI—that only helps if the grant isn't among the 40% or so that are set aside when they're "triaged" and left unscored by evaluators. This happened to Williams, who left a better-paying job as an emergency-room doctor and now studies a respiratory virus that strikes children. "We love science, and we want to do research," he says of physicians like himself, "but we have to eat." Williams, who has four children of his own, appreciates that NIH is nearly doubled in the past few years, and "the quality is not always there," concedes Antonio Scarpa, director of NIH's Center for Scientific Review (CSR), which coordinates the grant review process. Moreover, many top scientists, under pressure to keep their own labs productive, decline to serve on study sections.

The lack of experienced scientists on review panels is a long-standing issue that's been accentuated by the current funding squeeze, says Edward Kravitz, a neuroscientist at Harvard Medical School in Boston. He says he's the recent victim of what he claims was a poorly informed review. Although his group has published four papers in high-profile journals since November on the genetic basis of aggressive behavior in fruit flies, this month a proposal to continue this work was "triaged"—rejected without being discussed by the full study section. (CSR has long told study sections that about 50% of grant applications should be triaged to save time for discussing the best applications, but the rule has been more strictly enforced in the last year or two, Scarpa says.) "There's something very wrong here," says John Hildebrand, a neuroscientist at the University of Arizona in Tucson, who describes Kravitz's fly research as "utterly novel and creative."

Scarpa says CSR has several new initiatives to recruit qualified reviewers, including soliciting recommendations from scientific societies, tapping more researchers from outside the United States, and testing Web-based reviews that don't require researchers to travel to NIH headquarters in Bethesda, Maryland. Three senior scientists, members of the National Academy of Sciences, recently agreed to serve on such online study sections because they wouldn't have to travel from California, Scarpa says. He sees this as an encouraging sign. "The review is as good as the reviewers are," Scarpa says. "So that is one of our first priorities. **–G.M. AND J.C.**

SOURCE: NIH; CREDIT: MICHAEL LANG/CSR

Winnowing. Small distinctions loom large when grants are under review.

The 2007 Gairdner International Awards.

The Gairdner Foundation is pleased to announce the winners of the 2007 Gairdner International Awards.

The Gairdner Awards are amongst the most prestigious awards for outstanding discoveries in medical science. Each of the Gairdner Awardees will receive $30,000 and a statue, "La Coeur", at the awards ceremony held in Toronto October 25, 2007.

Since their beginning in 1957, 68 of 283 Gairdner Awardees have gone on to win the Nobel Prize in either Medicine or Chemistry. In the last five years alone, 9 of 11 Nobel Prizes in Medicine have gone to past Gairdner winners.

As part of its five-day National Program, October 22-26, 2007 current and past awardees will speak in 18 academic centres across Canada to faculty, medical and postgraduate students, senior high school students and the public. The Foundation will host a two-day Gairdner Symposium at the University of Toronto on 'Advances in the Understanding and Treatment and of Cancer'. Speakers include the 2007 awardees, as well as Sydney Brenner, John Dick, Brian Druker, Napoleone Ferrara, Robert Horvitz, Tak Mak, Richard Peto, Tom Hudson, and Robert Weinberg.

The 2007 Gairdner winners are:

C. David Allis, Ph.D.
Joy & Jack Fishman Professor
Head, Laboratory of Chromatin Biology
The Rockefeller University

"for the histone code."

Dr. Kim Nasmyth, Ph.D.
Whitley Chair
Department of Biochemistry
Oxford University

"for chromosome segregation in cell division."

Dennis Slamon, M.D., Ph.D.
Professor of Medicine, Chief of Hematology/ Oncology and Executive Vice Chair for Research for the Department of Medicine
UCLA

"for the development of Herceptin in breast cancer treatment."

Harry F. Noller, Ph.D.
Robert Louis Sinsheimer Professor of Molecular Biology
Director, Center for Molecular Biology of RNA
University of California, Santa Cruz

and

Thomas A. Steitz, Ph.D.
Sterling Professor of Molecular Biophysics & Biochemistry
Investigator, Howard Hughes Medical Institute
Yale University

"for the structure and function of the ribosome."


Dr. C. David Allis


Dr. Kim Nasmyth


Dr. Dennis Slamon

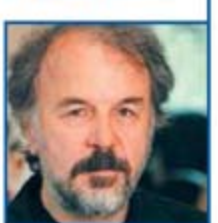
Dr. Harry F. Noller


Dr. Thomas A. Steitz

The Gairdner Foundation

www.gairdner.org

CIHR IRSC Canadian Institutes of Health Research / Instituts de recherche en santé du Canada

UNIVERSITY OF TORONTO

We would like to acknowledge the support of the University of Toronto for this announcement.

trying to help. But "the efforts being made don't seem to be very effective," he says.

As it happens, in 2006 first-time applicants actually had a better shot than established ones at scoring an R01 or equivalent grant on their first try: 9% compared to 7%, according to the NIH director's office. But NIH officials are increasingly worried about mid-career scientists, those seeking to renew their first or second grant. "That's probably where the pain is maximal," says Zerhouni. Last month, NIH announced the Director's Bridge Awards, promising up to $500,000 to tide over selected researchers for a year who just miss the funding cutoff. But such assistance is not the same as landing a grant, which is "a big element in the tenure decision," says Leonard Zwelling, vice president for research administration at M. D. Anderson Cancer Center in Houston, Texas.

Researchers early in their careers are eyeing the situation and wondering whether they should even try to ride it out. "We're losing some very talented people who are deciding that there's not enough stability here," says Thomas Insel, director of the National Institute of Mental Health.

One is Jerome Rekart, who was a postdoctoral fellow at the Massachusetts Institute of Technology (MIT) in Cambridge until he left last July for a teaching job at Rivier College, a liberal arts school in Nashua, New Hampshire. Concerns about funding were a major factor in his decision, Rekart says. Throughout his graduate school career and the first year of his postdoc at MIT, he'd seen mentors and respected scientists constantly fretting about their funding. "That was scary to me," he says.

Rekart's adviser, MIT neuroscientist Martha Constantine-Paton, says he came to her lab with outstanding recommendations and a number of publications. "This is not the kind of person you'd want to lose," she says.

NIH apparently felt the same way, awarding Rekart a training grant last year. By then he had already decided to move on, and he has no regrets. "I can control how well I teach," he says. "I don't have control over the NIH budget and how many pieces of the pie are available and whether or not I can get one."

While some senior scientists predict that a generation of younger ones will disappear, others reject such grim forecasts. "There is a sense of unease," says Varmus, but "I don't think we're losing young people outright yet."

Chilling. Biologist Susan Gerbi of Brown University worries about losing her stocks of *Sciara*, a rare fly.

Looking ahead

NIH officials are struggling, meanwhile, to keep the percentage of proposals funded from sinking even lower. But with 77% of the research budget tied up in ongoing projects, including grants that last several years, institute directors and Zerhouni say they have relatively little leverage. Many institutes have canceled or delayed programs, particularly costly clinical ones (*Science*, 2 March, p. 1202). At the National Heart, Lung, and Blood Institute, Director Elizabeth Nabel says she has put off funding a new hypertension trial, and at NIAID, Fauci says he freed up $15 million by delaying further development of an Ebola vaccine.

At the same time, "we can't not have any new initiatives," says Fauci. "Science moves in a way that you have to push it sometimes."

Today's anxiety appears to reflect what happens when funding patterns shift abruptly. "Once you've expanded the [research] capacity, what are you going to do?" asks Nabel. "You just can't turn off the spigot quickly and keep the engine running at full gear." Still, she adds, decisions about how to prioritize biomedical research "are really made at a societal level."

In hopes of influencing those decisions, scientists, convinced that an increase in NIH's budget will mark an improvement in their fortunes, are lobbying Congress heavily. Some are also considering alternative funding sources. "The real question to me," says Mary Hendrix, president and scientific director of Children's Memorial Research Center at Northwestern University in Chicago, Illinois, "is how to reconstitute the lost funding without relying on government support." Hendrix, one of the leadership group who met years ago to look beyond the NIH doubling, favors boosting public-private partnerships and working more closely with disease foundations. States, for example, are increasingly stepping in to finance human embryonic stem-cell research.

But ultimately, Congress will set the pace, and there are glimmers that next year's budget may reverse the years of flat funding. Although President George W. Bush has recommended cutting the 2008 NIH budget by about $500 million, Congress has suggested it may push the other way.

In February, Svoboda at LSU learned that on his third try, and to his great relief, his grant would win federal money. He scored in the 17th percentile and will be recommended for funding at the National Institute of Environmental Health Sciences.

As a result, Svoboda is feeling a lot more optimistic about his tenure review this fall, although the experience left him disillusioned. "It's wiped out my personal life," he says. "It's just been a brutal process." Now he has a few years before he'll need to compete for funding again.

–JENNIFER COUZIN AND GREG MILLER

Proposals Funded in 2006 By Institute

National Human Genome Research Institute	34%
National Institute of General Medical Sciences	26%
National Eye Institute	23%
National Institute of Environmental Health Sciences	22%
National Institute of Diabetes and Digestive and Kidney Diseases	21%
National Institute of Allergy and Infectious Diseases	21%
National Institute of Mental Health	20%
National Heart, Lung, and Blood Institute	20%
National Cancer Institute	19%
National Institute of Dental and Craniofacial Research	19%
National Institute of Neurological Disorders and Stroke	18%
National Institute on Aging	17%
National Institute of Child Health and Human Development	15%

CREDIT: FRANK MULLIN; SOURCE: NIH OFFICE OF EXTRAMURAL RESEARCH

Back on track? With the world still reeling from its 2003 boycott of the polio vaccine, the Nigerian state of Kano has resumed massive immunization campaigns.

INFECTIOUS DISEASE

Polio: No Cheap Way Out

Some experts have proposed abandoning efforts to eradicate the virus in favor of controlling it, but a new analysis says that could be more costly in the long run

Last year, several public health experts broached a heretical idea: Maybe it is time to give up on eradicating polio. Instead of trying to wipe out the disease, perhaps it makes more sense to settle for controlling it and use the money that would be saved for more pressing health problems, such as malaria or HIV/AIDS. The idea quickly gained advocates, but details of what a control strategy might entail—and what it would cost—have been lacking.

Now, researchers at Harvard School of Public Health in Boston have developed a mathematical model to explore the options. Specifically, they analyze almost a dozen control scenarios—from aggressive efforts to keep the number of polio cases very low to more minimal interventions that would accept a higher disease burden—and then examine the tradeoffs in terms of costs versus polio cases for each.

Eradication, assuming it is feasible, might yet cost billions to achieve. But it would still be cheaper than any control option—even those that would let cases soar to 200,000 a year—the team reports. "It is not intuitive. Control does not appear to offer any financial savings," says Kimberly Thompson of Harvard, who led the effort with postdoc Radboud J. Duintjer Tebbens. Their results were published online last week by *The Lancet*.

"Eradication is the best buy. It makes not just economic but humanitarian sense," says Bruce Aylward, who directs the global polio-eradication initiative from the World Health Organization (WHO) in Geneva, Switzerland, and is clearly delighted with the new analysis. Thompson's work is "a nail in the coffin for the idea that there is a cheap and painless way out."

Even critics of the campaign have been loath to throw in the towel. Polio is one of a very small number of diseases in the world that are even candidates for eradication, because it doesn't have an animal reservoir, and relatively cheap and effective vaccines are available. It's also hard to argue with the success of a program that has slashed cases 99%, from about 350,000 in 1988 to about 2000 in 2006.

But 20 years and $5 billion later, that last 1% remains elusive. After dropping to an all-time low of 483 in 2001, global cases have hovered around 1300 a year for the past 7 years, and polio retains a tenacious hold in four countries—India, Nigeria, Afghanistan, and Pakistan—from which it periodically erupts and reinfects polio-free countries. Between 2003 and 2006, the program spent $450 million battling outbreaks in 25 countries.

Most experts agree that eradication is technically feasible, given unlimited resources. But the program has been sidelined by budget shortfalls, rumors about vaccine safety, religious and political opposition, conflict, and the technical challenge of trying to vaccinate every child on the planet multiple times. As deadlines have come and gone, fatigue and a perception of diminishing returns have grown, and it has become increasingly tough to raise money. Right now, says Aylward, the program is facing its most critical funding shortfall ever.

Given these setbacks, it's not surprising that people are questioning whether eradication makes sense, concedes Stephen Cochi of the global immunization program at the U.S. Centers for Disease Control and Prevention (CDC) in Atlanta, Georgia. One of the most prominent calls for a reassessment came in an article in *Science* last year by Isao Arita, a veteran of both polio and smallpox eradication campaigns, and colleagues. "We believe the time has come for the global strategy for polio to be shifted from 'eradication' to 'effective control,' " they wrote (*Science*, 12 May 2006, p. 852).

Skeptical that a low-cost, low-case option existed, Thompson and Duintjer Tebbens set out to investigate, using funds from the Harvard Kids Risk Project; no support for this study came from WHO, CDC, or other partners in the eradication initiative, Thompson says.

First, they looked at what would happen if endemic countries were to scale back on immunization: To what extent, and how quickly, would polio cases rebound? They used a model that factors in variables such as the basic reproductive number of the virus, the level of population immunity, and outbreak risks, plugging in real-life data from Uttar Pradesh and Bihar, two states in northern India where polio transmission remains intense despite extensive vaccination.

The model confirmed what the experience of the past few years has shown, says Thompson: "If you back off, you will likely see huge outbreaks." Just a 10% decline in immunization intensity resulted in more than 5000 additional expected cases a year in these two Indian states alone.

Then they explored the tradeoffs of various control and eradication scenarios for the world's low-income countries, where the biggest burden of cases would likely occur. (Polio is not an issue in wealthy countries where routine vaccination rates are high.)

Control means, in essence, tolerating a certain number of polio cases a year, but there is no agreement on what an "acceptable" amount might be. Arita, for instance, had proposed keeping polio cases to fewer than 500 a year.

Thompson and Duintjer Tebbens decided

CREDIT: CHRIS HONDROS/GETTY IMAGES

Moderate Success for New Polio Vaccine

The first data from the field are in on a new weapon in the campaign to eradicate polio: monovalent oral poliovirus vaccine (mOPV), introduced in India in 2005 in the hope of stopping the most intransigent chains of transmission. The good news is that the vaccine seems to be three times more effective than the trivalent version that has been the mainstay of the polio eradication initiative. But the bad news is that even the new one is still a pretty blunt instrument.

Without question, Albert Sabin's OPV, a live vaccine made from three attenuated strains of poliovirus, has worked wonders, leading to the virtual disappearance of polio from all but a few corners of the world (see main text). The virus is hanging on in northern Nigeria, where an antivaccine boycott in 2003 led to a huge resurgence of cases. Along the rugged border of Pakistan and Afghanistan, insecurity and rumors are hampering vaccinators' access to children. In India, crowded, unhygienic conditions seem to be pushing the biological limits of vaccine.

It has long been known that OPV isn't as effective in poor tropical settings, where population density and inadequate sanitation combine to fuel viral transmission. But it wasn't clear exactly how bad things were until last year, when Nicholas Grassly of Imperial College London and colleagues reported a mere 11% efficacy per dose in the states of Uttar Pradesh and Bihar (*Science*, 17 November 2006, p. 1150). No wonder cases of polio are occurring there even in children who have received as many as 10 doses of OPV, Grassly says.

A 2006 outbreak in Uttar Pradesh provided a chance to assess the efficacy of the new vaccine on the ground. Grassly and colleagues scoured data from India's National Polio Surveillance Project to identify children who had developed type 1 poliomyelitis, with onset of paralysis between 1997 and 2006. Using admittedly indirect measures, they then compared how many doses of vaccine the 2076 cases and age-matched controls had received. They relied on parent recall, validated with government data on how many immunization rounds had been conducted in each area, and which vaccine, monovalent or trivalent, had been used. "It's not perfect," says Grassly of the methodology, "but it seems fairly reliable."

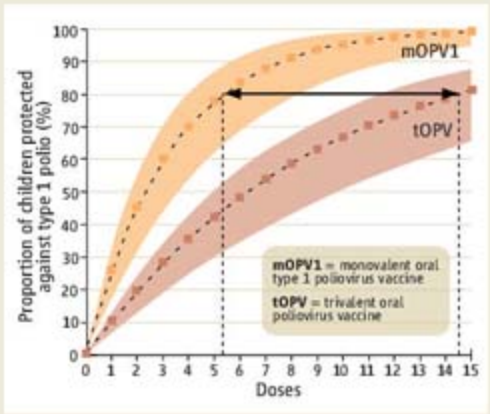

They found that the efficacy per dose of mOPV was 30%, three times that of tOPV in the same setting. "It is lower than you would expect and lower than you would like, but it is moving in the right direction," says Grassly, lead author on a study published online last week in *The Lancet*.

Paul Fine of the London School of Hygiene and Tropical Medicine agrees that the findings show that "mOPV is a better tool for type 1 polio. We would expect that." But is it good enough to stop transmission? "We don't know," says Fine. **–L.R.**

to start with a number that essentially reflects where we are today, about 1300 polio cases a year. We know what it takes to keep cases at that rate, says Thompson: about $680 million a year. About $400 million of that covers the costs of surveillance, routine polio immunization, and two rounds of supplemental immunization in all low-income countries. Another $280 million goes for four additional immunization rounds in endemic areas. Thompson and Duintjer Tebbens defined this option as "aggressive" or "very high" control. Playing it out over 20 years, as control efforts would continue indefinitely, led to a whopping cost of $10 billion.

They then fiddled with the variables to come up with less-aggressive control scenarios. Under the bare-bones option—routine immunization with no supplemental rounds and no outbreak response—global cases quickly soared to 200,000 per year. Something in the middle—say, two supplemental rounds every 3 years and a moderately aggressive emergency response—might keep cases to 46,000 a year and cost almost $8 billion over 20 years.

Control essentially means "low cost and high cases, or high cost and low cases, or something in between," says Thompson. She cautions that the numbers are projected values and should not be taken as gospel. "It's a big model. There are a lot of assumptions," she says. "All models can be criticized," concedes John Sterman, a fellow modeler at the Massachusetts Institute of Technology's Sloan School of Management in Cambridge. But this is "the best analysis out there. I don't know of any other analysis as detailed and carefully grounded in the data."

Hands down, the winner in terms of cases and costs is eradication, says Thompson. The team modeled four widely discussed "posteradication" options: stopping routine immunization after transmission of the wild virus has been halted, continuing immunization with oral poliovirus vaccine, continuing with OPV and supplemental rounds, and switching to the more expensive inactivated poliovirus vaccine. These scenarios ranged from roughly $80 million to $5.5 billion over 20 years, not including the cost to achieve eradication in the first place, which Aylward estimates could be another $2 billion.

Entrenched. The poliovirus continues to circulate in Uttar Pradesh, India, despite the highest vaccination rates in the world.

The bottom line, says CDC's Cochi, is "there is not a viable control option. It's an illusion that you can take your foot off the gas pedal and ease up and it will be much less costly and there won't be a huge resurgence." He adds that this analysis shows "we need to intensify efforts, not slack off. We need to get the money and commitment and finish."

The worst possible option, which looks something like what is happening today, is what Thompson calls "wavering commitment." As she describes it, when cases drop to low levels as they did in 2001, people may feel they are spending too much on polio and turn their attention elsewhere. Cases resurge, and the world rushes back in. "It's expensive, and we have more kids paralyzed," she says. "If we do it repeatedly, we pay more money than if we just finished it off." **–LESLIE ROBERTS**

CREDITS (TOP TO BOTTOM): ADAPTED FROM N. C. GRASSLY *ET AL.*, *THE LANCET* 369 (12 APRIL 2007); JEAN-MARC GIBOUX/GETTY IMAGES

MEETINGBRIEFS>>

AMERICAN ASSOCIATION OF PHYSICAL ANTHROPOLOGISTS | 28–31 MARCH | PHILADELPHIA, PENNSYLVANIA

European Skin Turned Pale Only Recently, Gene Suggests

Researchers have disagreed for decades about an issue that is only skin-deep: How quickly did the first modern humans who swept into Europe acquire pale skin? Now a new report on the evolution of a gene for skin color suggests that Europeans lightened up quite recently, perhaps only 6000 to 12,000 years ago. This contradicts a long-standing hypothesis that modern humans in Europe grew paler about 40,000 years ago, as soon as they migrated into northern latitudes. Under darker skies, pale skin absorbs more sunlight than dark skin, allowing ultraviolet rays to produce more vitamin D for bone growth and calcium absorption. "The [evolution of] light skin occurred long after the arrival of modern humans in Europe," molecular anthropologist Heather Norton of the University of Arizona, Tucson, said in her talk.

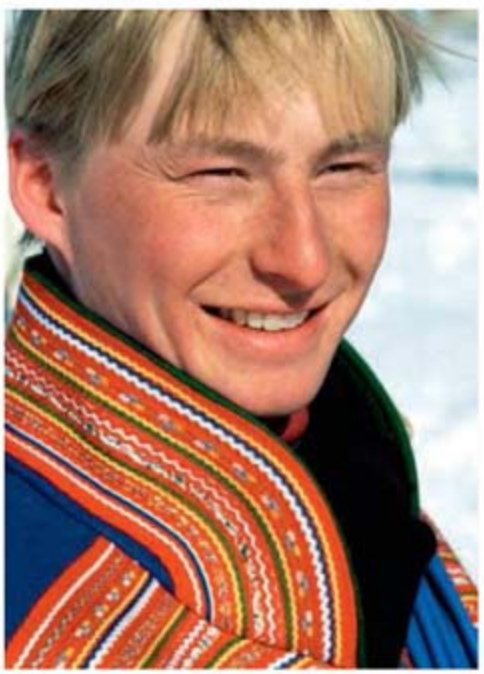

Lighten up. A gene for pale skin swept through Europeans relatively recently.

The genetic origin of the spectrum of human skin colors has been one of the big puzzles of biology. Researchers made a major breakthrough in 2005 by discovering a gene, *SLC24A5*, that apparently causes pale skin in many Europeans, but not in Asians. A team led by geneticist Keith Cheng of Pennsylvania State University (PSU) College of Medicine in Hershey found two variants of the gene that differed by just one amino acid. Nearly all Africans and East Asians had one allele, whereas 98% of the 120 Europeans they studied had the other (*Science*, 28 October 2005, p. 601).

Norton, who worked on the Cheng study as a graduate student, decided to find out when that mutation swept through Europeans. Working as a postdoc with geneticist Michael Hammer at the University of Arizona, she sequenced 9300 base pairs of DNA in the *SLC24A5* gene in 41 Europeans, Africans, Asians, and American Indians.

Using variations in the gene that did not cause paling, she calculated the background mutation rate of *SLC24A5* and thereby determined that 18,000 years had passed since the light-skin allele was fixed in Europeans. But the error margins were large, so she also analyzed variation in the DNA flanking the gene. She found that Europeans with the allele had a "striking lack of diversity" in this flanking DNA—a sign of very recent genetic change, because not enough time has passed for new mutations to arise. The data suggest that the selective sweep occurred 5300 to 6000 years ago, but given the imprecision of method, the real date could be as far back as 12,000 years ago, Norton said. She added that other, unknown, genes probably also cause paling in Europeans.

Either way, the implication is that our European ancestors were brown-skinned for tens of thousands of years—a suggestion made 30 years ago by Stanford University geneticist L. Luca Cavalli-Sforza. He argued that the early immigrants to Europe, who were hunter-gatherers, herders, and fishers, survived on ready-made sources of vitamin D in their diet. But when farming spread in the past 6000 years, he argued, Europeans had fewer sources of vitamin D in their food and needed to absorb more sunlight to produce the vitamin in their skin. Cultural factors such as heavier clothing might also have favored increased absorption of sunlight on the few exposed areas of skin, such as hands and faces, says paleoanthropologist Nina Jablonski of PSU in State College.

Such recent changes in skin color show that humans are still evolving, says molecular anthropologist Henry Harpending of the University of Utah, Salt Lake City: "We have all tacitly assumed for years that modern humans showed up 45,000 years ago and have not changed much since, while this and other work shows that we continue to change, often at a very fast rate."

Gorillas' Hidden History Revealed

Although gorillas are our closest living relatives other than chimpanzees, their evolution is something of a mystery. There are no fossils of gorillas and little DNA from wild ones. Now, a new study of nuclear DNA from the two species of wild gorillas offers a glimpse of their mysterious past and of how new species of primates arise.

Unlike their cousins the chimps, these shy herbivores turn out to have diverged slowly into two species, apparently taking the better part of a million years, according to a talk at the meeting by molecular anthropologist Linda Vigilant of the Max Planck Institute for Evolutionary Anthropology in Leipzig, Germany. "It shows us how little we've known about speciation in gorillas," says anthropological geneticist Anne Stone of Arizona State University in Tempe.

Previous studies of the paternally inherited Y chromosome from gorillas suggested that the two species—eastern gorillas and western gorillas—interbred until recently. But maternally inherited mitochondrial DNA suggested that they separated more than 1 million years ago. Nuclear DNA studies sampled too few individuals to clear up the confusion, says evolutionary biologist Michael Jensen-Seaman of Duquesne University in Pittsburgh, Pennsylvania.

Vigilant and her colleagues isolated DNA from the blood, liver, or feces of 18 of the 14,000 wild gorillas left on the planet, including three eastern gorillas from Uganda and the Congo; the western gorillas were chiefly from Cameroon. The team sequenced 14,000 base pairs of noncoding (and therefore presumably not under selection) nuclear

CREDIT: STAFFAN WIDSTRAND/CORBIS

Adapting to Tibet's Thin Air

Researchers seldom see Darwinian natural selection happening in living people. So physical anthropologist Cynthia Beall was delighted in 2004 when she discovered a trait that boosts the survival of some Tibetan children, apparently by raising the level of oxygen in their mothers' tissues—a crucial advantage during pregnancy 4 kilometers above sea level.

Now Beall has updated her study by exploring a possible mechanism for the adaptation and by documenting that the adaptation represents some of the strongest natural selection yet measured in humans. Her team is showing how a genetic trait can dramatically improve survival in real time, in living mothers and babies. "I love this work," says Mark Gladwin, chief of the vascular medicine branch of the National Heart, Lung, and Blood Institute in Bethesda, Maryland. "It shows you need a strong adaptive response to have children survive at high altitude."

Beall, of Case Western Reserve University in Cleveland, Ohio, and her colleagues have for a decade been gathering all sorts of family, biological, and fertility data from men, women, and children living in more than 900 households in 14 villages in Tibet. As part of the study, they also tracked the survival of children born to mothers who had high and low oxygen saturation in their blood (sciencenow.sciencemag.org/cgi/content/full/2004/916/4). Beall reported at the meeting that women with high levels of oxygen in their blood had more than twice as many surviving babies as had those with low oxygen levels—a ratio of 1:0.44. This is a startlingly strong selection pressure, she says—even stronger than that on the sickle cell gene, which protects against malaria and has a fitness ratio of 1:0.66.

But exactly how do these women manage to carry extra oxygen in their blood? They do not produce more hemoglobin the way Andeans living at high altitude do. One possibility is that the women with high oxygen have an adaptation that Beall is exploring independently in these same Tibetan villagers. She found that some villagers exhale extra nitric oxide in their breath, a sign of additional amounts of the gas in their blood. In those Tibetans, nitric oxide dilates the blood vessels so they can pump more blood and oxygen to organs and tissues, as measured by images of heart and lung blood vessels. The Tibetans can boost their blood volume—and so pump more oxygen to their tissues—without producing more hemoglobin or raising the blood pressure in their lungs. That's the reverse of what happens when mountaineers suffer from oxygen deficiency: The blood pressure in their lungs rises, the blood vessels constrict, and fluid builds up, suffocating the lungs.

The next step, says Beall, is to try to see whether these two lines of research meet. She wants to find the underlying gene behind the women's high-oxygen blood—and see whether it is related to genes that regulate levels of nitric oxide in the blood. She notes, however, that it's quite possible that the Tibetans have evolved more than one way to boost blood oxygen, and that these are independent adaptations. Gladwin suggests that Beall's team also measure nitric oxide and blood pressure in the lungs in pregnant women, who are under the most physiological stress at altitude and presumably would benefit most from this adaptation. "Study the pregnant women," he says, "because that's where you'll see evolution in action." **–A.G.**

On top of the world. Tibetans with oxygen-rich blood have more surviving children.

DNA from each gorilla. Disparities turned up at 79 different sites, similar to the genetic diversity in chimpanzees, but twice as high as in humans, who are remarkable for their lack of variation. "This shows us again how odd humans are," says Stone.

Vigilant's team used the number of genetic differences to calculate a mutation rate, which allowed them to date the timing of the initial speciation to about 900,000 to 1 million years ago. That's just when the two species of chimpanzees went their separate evolutionary ways, suggesting that changes in climate broke up the dense forests that are home to both chimps and gorillas.

Although chimpanzees sorted into two species rapidly, gorillas took much longer and continued to mate at low levels until 164,000 to 230,000 years ago, with males moving more than females, says Vigilant. That's surprising because today the two species live 1000 kilometers apart and most gorillas never venture far from home. "I find it amazing that gene flow persisted for hundreds of thousands of years," she says.

Her study offers a rare window on speciation in apes, which serves as "a model for understanding human evolution," says Jensen-Seaman. Until now, researchers have focused on the quick split between species of chimpanzees. In fact, says Jensen-Seaman, gorillas' "sloppy back-and-forth gene flow—a long, drawn-out process"—may be the norm.

–ANN GIBBONS

East met west. Eastern gorillas (*right*) bred with their western cousins until recently.

CREDITS (TOP TO BOTTOM): CYNTHIA BEALL AND MELVYN GOLDSTEIN; J. KALBITZ/MPI-EVA; M. M. ROBBINS/MPI-EVA

LETTERS

edited by Etta Kavanagh

Retraction

WE WISH TO RETRACT OUR RESEARCH ARTICLE "THE MRNA OF THE *ARABIDOPSIS* GENE *FT* MOVES from leaf to shoot apex and induces flowering" (*1*). After the first author (T.H.) left the Umeå Plant Science Centre for another position, analysis of his original data revealed several anomalies. It is apparent from these files that data from the real-time RT-PCR were analyzed incorrectly. Certain data points were removed, while other data points were given increased weight in the statistical analysis. When all the primary real-time RT-PCR data are subjected to correct statistical analysis, most of the reported significant differences between time points disappear. Because of this, we are retracting the paper in its entirety.

In new experiments, we have reproduced the floral induction caused by a heat-shock induction of *FT* in a single leaf, but we have failed to detect movement of the transgenic *FT* mRNA from leaf to shoot apex. We therefore retract the conclusion that *FT* mRNA is part of the floral inductive signal moving from leaf to shoot apex.

We deeply regret any scientific misconceptions that have resulted from the publication of these data.

The first author of the paper (T.H.) strongly objects to the retraction of the paper and has therefore declined to be an author of the retraction.

Our related *Science* Report on the *CO*/*FT* regulatory module in trees (*2*) is not affected by this Retraction. In this paper, T.H. was involved in the construction and analysis of the *PtCENL1* experiments reported in the Supporting Online Material. These data have been reevaluated and found to be correctly reported.

HENRIK BÖHLENIUS,[1] SVEN ERIKSSON,[1] FRANÇOIS PARCY,[2] OVE NILSSON[1]

[1]Umeå Plant Science Centre, Department of Forest Genetics and Plant Physiology, Swedish University of Agricultural Sciences, SE-90183 Umeå, Sweden. [2]Laboratoire de Physiologie Cellulaire Végétale, Département Réponse et Dynamique Cellulaires (DRDC/PCV), Unité Mixte de Recherche 5168 [(UMR) Joint Research Unit], Centre National de la Recherche Scientifique (CNRS), Commissariat à l'Energie Atomique (CEA), Institut National de la Recherche Agronomique (INRA), Université Joseph Fourier, 17 rue des Martyrs, batiment C2-38054, Grenoble Cedex 9, France.

References

1. T. Huang, H. Böhlenius, S.Eriksson, F. Parcy, O. Nilsson, *Science* **309**, 1694 (2005).
2. H. Böhlenius *et al.*, *Science* **312**, 1040 (2006).

A Thank You from Tulane University

IT HAS BEEN 19 MONTHS SINCE HURRICANE Katrina slammed into the Louisiana coastline, causing widespread destruction and prolonged flooding in New Orleans. Gulf Coast institutions continue to deal with the aftermath of the hurricane, but great progress has been made in reestablishing a vibrant competitive research community. At Tulane University, we have experienced a level of rebound and renewal beyond our expectations. I write to express gratitude to the academic community for the strong support that we received both during and after the storm. Many institutions advised us and hosted our research faculty, with a particularly large number located at Alliance of South Texas Health Sciences Centers institutions (Baylor College of Medicine, University of Texas Health Science Center at Houston, Texas A&M Health Science Center School of Medicine, University of Texas Medical Branch at Galveston).

We owe a special debt of gratitude to our colleagues at the National Institutes of Health (NIH) and the National Science Foundation (NSF) for their unwavering moral and fiscal support at our time of greatest need. Within days, communication was established with senior administrators at the NIH, including Director Elias Zerhouni and Deputy Director Norka Ruiz-Bravo, and at the NSF, Director Arden Bement and Deputy Director Kathie Olsen. Both agencies established points of contact and procedures to address our needs. Five senior NIH officials visited Tulane University and other severely affected institutions in March 2006 to assess the effectiveness of the NIH response. A site visit by Bement in April 2006 was also very meaningful, as were the many Katrina-related supplements provided to NIH and NSF grantees at affected institutions. Finally, we are very grateful to the U.S. Office of Science and Technology Policy and the Office of Management and Budget, which issued a Joint Announcement soon after the storm establishing special procedures for affected institutions, including extensions of application and reporting requirement deadlines.

"The swift and effective response of the academic community and government agencies made it possible to preserve much of the competitive research enterprise at Tulane and provided moral support for their colleagues in New Orleans."

—Levy

The swift and effective response of the academic community and government agencies made it possible to preserve much of the competitive research enterprise at Tulane and provided moral support for their colleagues in New Orleans.

LAURA S. LEVY

Professor of Microbiology and Immunology, Associate Senior Vice President for Research, Tulane University, New Orleans, LA 70112–2709, USA.

Astrobiology and Missions at NASA

IN HIS NEWS FOCUS ARTICLE "ASTROBIOLOGY fights for its life" (19 Jan., p. 318), A. Lawler describes NASA's astrobiology program as largely disconnected from its space-flight missions. But recent competitions paint a different picture. For example, Bruce Jakosky, the Principal Investigator (PI) of the Mars Atmosphere and Volatile Evolution mission (MAVEN), one of two candidates for the next Mars Scout, is also the PI of the NASA Astrobiology Institute's (NAI) University of Colorado team. MAVEN would study atmospheric gas escape from Mars to understand what effect atmospheric evolution has had on the planet's climate and habitability, placing that one piece of the puzzle into the larger context of the planet's biological potential. The NAI stimulates this kind of integrative thinking by bringing together broad, multidisciplinary groups of scientists who might not otherwise have the opportunity to work together and learn how to contribute to each other's research. MAVEN is an example of what can grow from this fertile ground.

The Mars Scout selections included two instrument development efforts for ESA's ExoMars mission, both of which are direct products of the NASA Astrobiology program. In addition, two PI instruments on the 2009 Mars Science Laboratory (MSL) received Astrobiology support to enable their selection for flight. NAI current and former PIs and Co-Investigators are centrally involved in operations and science analysis for the Mars Exploration Rovers, Spirit and Opportunity.

The NAI also contributes to future missions through Focus Groups that mobilize expertise from across the Institute and the wider scientific community. The Mars Focus Group began by playing a seminal role in restructuring the Mars Program after the loss of NASA missions launched in 1998. It accomplished this by organizing astrobiology community input to NASA's Mars Exploration Program Analysis Group (MEPAG). Two NAI PIs have served as MEPAG Chair. The NAI Europa and Titan Focus Groups have also provided input to mission planners studying those opportunities, and the Astronomy Focus Group has provided an analysis of the astrobiology potential of the James Webb Space Telescope. Rather than being disconnected from NASA flight opportunities, astrobiology objectives and the astrobiology community are repeatedly found at the heart of NASA's missions.

CARL B. PILCHER

Director, NASA Astrobiology Institute, NASA Ames Research Center, Moffett Field, CA 94035, USA.

Letters to the Editor

Letters (~300 words) discuss material published in *Science* in the previous 3 months or issues of general interest. They can be submitted through the Web (www.submit2science.org) or by regular mail (1200 New York Ave., NW, Washington, DC 20005, USA). Letters are not acknowledged upon receipt, nor are authors generally consulted before publication. Whether published in full or in part, letters are subject to editing for clarity and space.

Oocyte Donation for Stem Cell Research

THE NEWLY ISSUED INTERNATIONAL SOCIETY for Stem Cell Research (ISSCR) guidelines for human embryonic stem cell research (G. Q. Daley *et al.*, Policy Forum, 2 Feb., p. 603) include worthy goals and lofty language about truth and transparency in biomedical research, dissemination of research benefits "to humanity at large on just and reasonable terms," and discussion of enhancing the informed consent process for the procurement of tissues and gametes (*1*).

But the guidelines would in fact weaken important ethical standards that have already been established. We are particularly concerned about the recommendation that decisions about paying women for their eggs should be left to mostly local oversight committees.

This is a complex social and ethical question. Many who have examined the issue closely, including ourselves, have concluded that researchers should compensate women only for their direct expenses, to avoid inducing economically vulnerable women to accept the significant risks of egg retrieval when they would not otherwise be willing to do so. This perspective has been adopted as law in California and a number of countries, and it is recommended in the U.S. National Academies guidelines. In other words, the ISSCR is now suggesting that governments and agencies abdicate their role to protect the health and safety of women in favor of a patchwork of inconsistent and opaque decisions made by local committees.

Members of the ISSCR group justify weakening the rules on egg procurement by citing "cultural and political differences" (*2*). This is an unhelpful relativism that could all too easily endorse a kind of "tissue tourism," in which researchers arrange to obtain women's eggs wherever the rules are most lax.

This prospect, and emerging inconsistencies among standards for stem cell research, point to the need for binding rules to ensure that stem cell and other biotechnologies are developed and used in ways that truly support, rather than actually undermine, health and well-being.

MARCY DARNOVSKY[1] AND SUSAN BERKE FOGEL[2]

[1]Center for Genetics and Society, 436 14th Street, Suite 700, Oakland, CA 94612, USA. [2]Pro-Choice Alliance for Responsible Research, Los Angeles, CA 91401, USA.

References

1. See ISSCR guidelines at www.isscr.org/guidelines/index.htm.
2. A. Pearson, "New international guidelines for stem cell science," NewScientist.com news service, 1 Feb. 2007 (see www.newscientist.com/article.ns?id=dn11084&feedId=online-news_rss20).

AS EVIDENCED BY THE POLICY FORUM "THE ISSCR guidelines for human embryonic stem cell research" (G. Q. Daley *et al.*, 2 Feb., p. 603), countries with public policies on the donation of surplus embryos for stem cell research broadly agree on the need for a fully informed consent and the avoidance of conflicts of interest. Quality assurance, therapeutic purpose, transparency, confidentiality, traceability, and ethics review are also common ground. However, there is less agreement regarding the retrieval and use of human oocytes for stem cell research. The recently released ISSCR guidelines attempt to fill this gap, but, in an attempt to reach consensus, it resorted to a vague, unclarified prohibition of "undue inducement" regarding compensation of oocyte donors.

The use of financial incentives to obtain human oocytes to be used in stem cell research is a contentious issue. Are participating women vendors, providers, or donors? That depends on the type of compensation. Currently, there are five models of compensation: free market, pure gift, fixed compensation, minimum wage, and reimbursement of expenses. The free-market model is likely to prevail in the absence of sufficient debate and decision-making by governmental authorities around the world. Its obvious advantage is the high rate of recruitment given the increasing scarcity of access to human oocytes. Yet, this approach can result in commodification, undue inducement (if not coercion of the vulnerable), and commercialization. At the opposite extreme is an altruistic gift, which is likely to be rare, considering the invasive procedures involved and the unknown long-term health risks of ovarian hyperstimulation.

International debate is sorely lacking for the other three models. The fixed compensation model provides for a standardized amount irrespective of the financial costs to

Receive a free TaqMan® Low Density Array Upgrade and 20 Free TaqMan® Array cards*
Visit 7900HT.com to learn more.

Proven Performance in Labs Everywhere. Customized for Yours.

Applied Biosystems 7900HT Fast Real-Time PCR System Meets Your Changing Needs.

The gold standard in real-time PCR
Used by researchers all over the world and referenced in hundreds of journals, the Applied Biosystems 7900HT Fast Real-Time PCR System is the recognized gold standard in real-time PCR.

Interchangeable blocks
Configurable and highly flexible, the 7900HT Fast System offers user-interchangeable thermal cycling blocks, cycling times as low as 35 minutes and automated plate loading/unloading for higher throughput.

The world's largest collection of assays
Choose from over 2 million TaqMan® Gene Expression, Genotyping and miRNA Assays.

Easy, pre-loaded assays in a micro fluidic card format
For the ultimate in ease-of-use, order your assays pre-loaded in the 384-well TaqMan® Low Density Array.

To see how the 7900HT Fast System meets your changing research needs, visit www.7900HT.com

Applied Biosystems

* Receive a Low Density Array Upgrade and 20 Free TaqMan® Low Density Array cards with the purchase of an Applied Biosystems 7900HT Fast Real-Time PCR System. This offer cannot be combined with other promotions or discounts. Offer valid until March 31, 2006. Void where prohibited. This offer is for US customers only — International customers please inquire with your local sales office. Other restrictions may apply. All prices exclude any applicable delivery and/or local tax. Please contact your local Sales Representative for other details of this offer. http://www.7900HT.com

the donor, socioeconomic status (i.e., need), or time and inconvenience. This model prevents monetary inducements as a primary motivation and minimizes financial loss to the donors, but ignores individual expenses. Although arbitrary, it has the advantage of certainty and, in a societal sense, fairness. The minimum-wage approach takes into account the number of hours donated. In all likelihood, providing a minimum wage would result in a higher rate of payment than the fixed compensation model. Reimbursement of expenses seems to be a more individually tailored approach. This depends, however, on whether reimbursement is for inconvenience, time, pain, and discomfort, or is limited to actual receipted expenses such as travel, lodging, parking, meals, and daycare. There are limited incentives for donors and, in practice, the administrative proof required is burdensome. A narrower receipted expenses–only policy will in the long term further reduce the availability of these materials. This could result in commercial importation or a black market. Some would see the current "exceptional" case in the U.K. of egg donation for research in exchange for access to fertility treatment as a variation of the reimbursement model. This approach, however, is akin to providing access to drugs or treatments in clinical trials and does not parallel the healthy volunteer guidelines in international guidelines for biomedical research.

Perhaps a more equitable solution would be to develop a mixed model in which a standard amount of compensation would be determined by a competent authority, but would also include reimbursement for time and effort expended for procurement. Were such an approach to be adopted internationally, the additional issue of forum shopping (selecting a procurement site on the basis of the particular laws in effect there) may be lessened. The International Stem Cell Forum Ethics Working Party maintains that this approach respects altruism and solidarity. The amount will still largely remain a symbolic recognition of the true value of such participation in stem cell research. It provides a feasible solution to an issue that needs to be examined within the larger context of the participation in and ethical oversight of biomedical research.

FOR THE INTERNATIONAL STEM CELL FORUM ETHICS WORKING PARTY: BARTHA MARIA KNOPPERS,[1] MICHEL REVEL,[2] GENEVRA RICHARDSON,[3] JOSEF KURE,[4] SALLA LÖTJÖNEN,[5] ROSARIO ISASI,[1] ALEXANDRE MAURON,[6] JAN WAHLSTROM,[7] BRACHA RAGER,[8] PENG LEE HIN PENG[9]

[1]Centre de Recherche en Droit Public, Université de Montreal, Montreal, QC H3C 3J7, Canada. [2]Weizmann Institute of Science, Jerusalem, Israel. [3]School of Law, King's College London, London, UK. [4]University Centre of Bioethics, Masaryk University, Brno, Czech Republic. [5]National Advisory Board on Research Ethics, Helsinki, Finland. [6]Institut d'Éthique Biomédicale, University of Geneva, Geneva, Switzerland. [7]University of Gothenburg, Gothenburg, Sweden. [8]Ben Gurion University, Beer Sheva, Israel. [9]National Bioethics Committee, Singapore.

Response

DARNOVSKY AND FOGEL RAISE APPROPRIATE concerns that oocyte donation should not fall disproportionately on economically vulnerable women and that research guidelines should prohibit "tissue tourism." The ISSCR guidelines directly address these concerns. The introduction to section 11 ("Procurement of materials") clearly states: "Consistent with well-established principles of justice in human subject research, there must be a reasonable relationship between those from whom such materials are received and the populations most likely to benefit from the research," and section 11.5b reads: "There must be monitoring of recruitment practices to ensure that no vulnerable populations, for example, economically disadvantaged women, are disproportionately encouraged to participate as oocyte providers for research."

Furthermore, the guidelines articulate the core principle that there be a "rigorous review to ensure that reimbursement of direct expenses or financial considerations of any kind do not constitute an undue inducement." Research that is subject to a rigorous oversight process at the local, regional, or national level—as stipulated in the ISSCR guidelines—and conducted in accordance with these guiding principles will avoid the exploitation of women that is our shared concern.

The Letter from the Ethics Working Party (EWP) of the International Stem Cell Forum acknowledges that women should be free from "undue inducement" when making decisions regarding the donation of oocytes for research, and outlines a proposal that if approved through a rigorous process of review and subject to appropriate oversight would be consistent with ISSCR guidelines. The EWP Letter correctly highlights the difficulties in defining what constitutes allowable expenses and the need to guard against the disproportionate recruitment of economically disadvantaged women, and illustrates the complexity of the deliberations required to arrive at a reasonable policy for engaging women in research.

The ISSCR task force comprised scientists, ethicists, and legal experts from 14 countries. Despite the inevitable political, cultural, and religious differences that shape research policy internationally, our task force reached consensus on guiding principles for the conduct of human embryonic stem cell research. The ethical principles pertaining to oocyte donation are particularly challenging and continue to prompt debate and inquiry. The ISSCR guidelines encourage an open and ongoing dialogue concerning ethical procurement of human materials for stem cell research, and will be subject to review and refinement as more information becomes available.

GEORGE Q. DALEY

Chair, ISSCR Guidelines Task Force, and Children's Hospital, Boston, MA 02115, USA.

CORRECTIONS AND CLARIFICATIONS

News of the Week: "Mapping the 248-fold way" by D. Mackenzie (23 Mar., p. 1647). On page 1649, the story listed Hermann Nicolai's affiliation as the University of Potsdam. Nicolai is at the Max Planck Institute for Gravitational Physics (Albert Einstein Institute) in Potsdam.

Table of Contents: (2 Feb., p. 565). The one-sentence summary for the Report "Structural and regulatory genes required to make the gas dimethyl sulfide in bacteria" by J. D. Todd *et al.* was incorrect. It should read, "A bacteria gene is found that enables cleavage of DMSP to the volatile sulfur compound dimethyl sulfide (DMS) involved in cloud nucleation and hence reduction in global warming."

Books *et al.*: "Otherness—When killing is easy" by C. Ash (2 Feb., p. 601). The image on the far right is not John Burdon Sanderson Haldane, as identified in the caption, but is instead his father, John Scott Haldane.

TECHNICAL COMMENT ABSTRACT

COMMENT ON "Ongoing Adaptive Evolution of *ASPM*, a Brain Size Determinant in *Homo sapiens*"

Fuli Yu, R. Sean Hill, Stephen F. Schaffner, Pardis C. Sabeti, Eric T. Wang, Andre A. Mignault, Russell J. Ferland, Robert K. Moyzis, Christopher A. Walsh, David Reich

Mekel-Bobrov *et al.* (Reports, 9 September 2005, p. 1720) suggested that *ASPM*, a gene associated with microcephaly, underwent natural selection within the last 500 to 14,100 years. Their analyses based on comparison with computer simulations indicated that *ASPM* had an unusual pattern of variation. However, when we compare *ASPM* empirically to a large number of other loci, its variation is not unusual and does not support selection.

Full text at www.sciencemag.org/cgi/content/full/316/5823/370b

Now Available!
Custom panels in smaller, 10-card order sizes.

384 Wells. Preloaded for TaqMan® Performance.

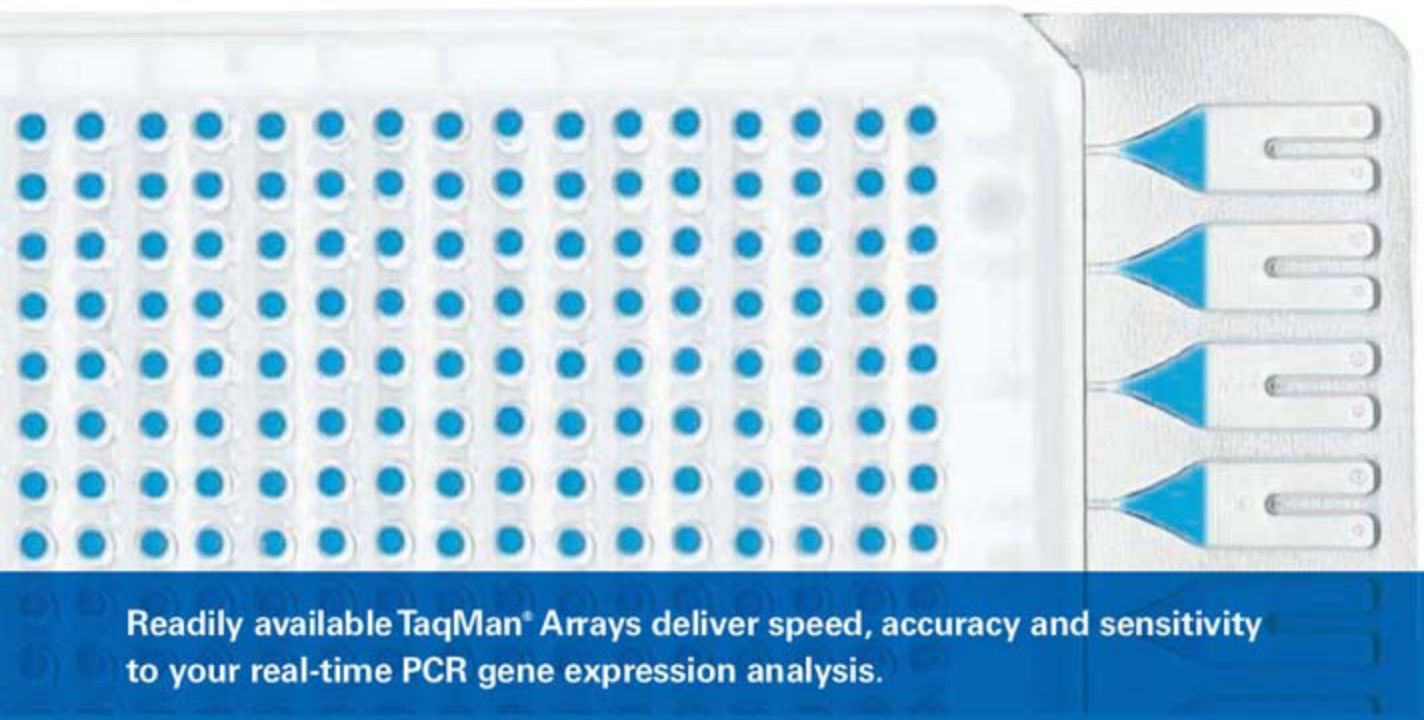

Readily available TaqMan® Arrays deliver speed, accuracy and sensitivity to your real-time PCR gene expression analysis.

TaqMan® Low Density Array Gene Signature Panels are readily available, expertly-designed, focused gene sets that don't require liquid handling robots or complex pipetting to use. Simply add your cDNA and TaqMan® Universal PCR Master Mix into the eight sample ports of this micro fluidic card and instantly run 384 real-time PCR reactions on the 7900HT Fast Real-Time PCR System. The Gene Signature Panels come pre-loaded with TaqMan® Gene Expression Assays, so you get the accuracy, reproducibility, and specificity that only TaqMan® Assays can provide. It's the fast and affordable way to validate microarray hits and screen pathways and biomarkers without the worry and difficulty associated with 96-well plates or individual tubes.

Order from the growing portfolio of TaqMan® Low Density Array Gene Signature Panels:

- Human or Mouse GPCR Panel
- Human or Mouse Immune Panel
- Human, Mouse, or Rat Endogenous Control Panel
- Human Protein Kinase Panel
- Human Apoptosis Panel
- Human ABC Transporter Panel

More panels will be available soon! Register to receive new Gene Signature Panel product announcements or suggest a panel of your own at tlda.appliedbiosystems.com

The perfect combination: the TaqMan Low Density Array and Applied Biosystems 7900HT Fast Real-Time PCR System.

Applied Biosystems

FOCUS ON CAREERS

Postdoc Scientists: Transferable Skills

UPCOMING FEATURES:

April 27 — Biotech and Pharma

May 11 — Focus on Diversity

IN THIS ISSUE:

For a postdoc today, lab bench experience and a good publication record may only get you so far. Developing skills beyond academia can help you to be competitive for a greater variety of jobs. Find out what you can do to improve your employment chances on page 471 of this issue.

Also available online at:
www.sciencecareers.org/businessfeatures

ScienceCareers.org
We know science
AAAS

DEVELOPMENTAL BIOLOGY

An Intelligent Primer

Nipam H. Patel

While most scientific disciplines have undergone remarkable advances in the past few decades, the field of developmental biology has seen truly astonishing progress. In her book *Coming to Life: How Genes Drive Development*, Christiane Nüsslein-Volhard offers a very accessible whirlwind tour of what modern developmental biology has taught us about the way in which a fertilized egg becomes a complex organism. In just under 150 pages, the reader is treated to a primer on genetics and molecular and cell biology; an overview of the development of the fruit fly *Drosophila melanogaster*; a summary of the general principles of vertebrate development; and, lastly, a concise presentation of some of the moral challenges that our advances have created. From a scientific perspective, Nüsslein-Volhard is eminently qualified for the task, having been at the forefront of the discipline for many years and sharing the 1995 Nobel Prize for Medicine. However, not all great scientists are endowed with the gift to communicate lucidly, especially in a way that is understandable to a layperson. This book succeeds because its brevity is matched by its clarity.

The field of developmental biology has its outstanding textbooks; the comprehensive standard of Scott Gilbert (*1*) and the elegantly organized volume of Lewis Wolpert and colleagues (*2*) immediately spring to mind. There have been, however, relatively few attempts to present the topic to a general audience. The recent popular work of Sean Carroll (*3*) merges developmental biology with evolution and natural history in an extremely appealing manner, but here Nüsslein-Volhard maintains an unwavering narrative designed to crystallize the key concepts and breakthroughs of developmental biology.

A sizable portion of the book focuses on the embryonic development of *Drosophila*, a logical choice given the author's long involvement in making this insect one of the premier model systems for developmental genetic analysis. We now know so much about the various steps of *Drosophila* pattern formation that even experts on the topic can become overwhelmed by the details, but in this book all that is stripped away and the reader is presented with the important principles that have emerged. The focus on distilling information comes across very prominently in the design of the book's figures—all 55 hand drawn by the author. Whereas multicolor confocal images, microarray data, and wiring diagrams of gene regulatory networks are ubiquitous in cutting-edge papers of the field, they are replaced here by elegant sketches in shades of gray and red that communicate all of the text's important points. The purpose of each figure is immediately obvious, and readers will never be stuck trying to decipher an illustration.

Coming to Life
How Genes Drive Development
by Christiane Nüsslein-Volhard
Kales Press, Carlsbad, CA, 2006. 180 pp. $29.95, C$42. ISBN 9780967007670.

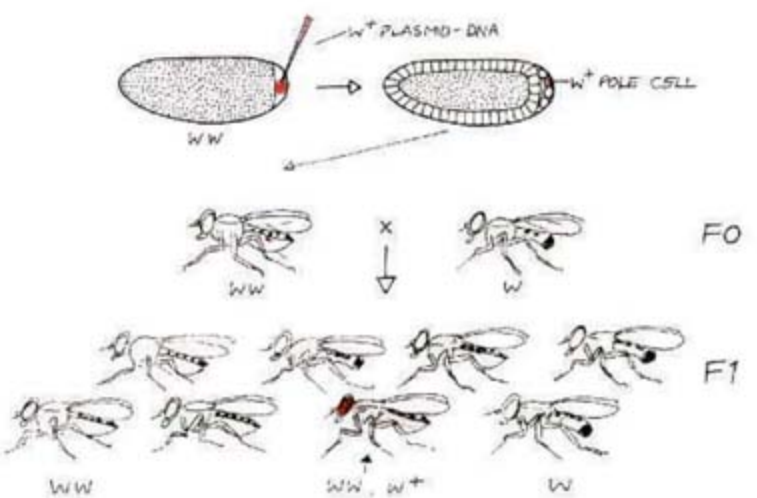

Simple and effective. The author's figures, such as this diagram of the production of transgenic *Drosophila*, help the reader to easily understand key concepts.

After going on to give a series of brief presentations that outline signaling pathways and the forces that drive morphogenesis, Nüsslein-Volhard then offers an overview of vertebrate development. Building on the foundation established in the chapters on *Drosophila*, she provides a succinct survey of the experimental approaches to and critical findings from frog, chick, mouse, and zebrafish development. Again, the simple illustrations help guide the reader through relatively complex topics. Most important, the direct relevance of all this research to understanding human development and health is made abundantly clear.

In places, the conciseness of the account may frustrate readers who are already well-versed in developmental biology given that the brevity sometimes leads to simplifications that are not accurate in all respects. Anyone who has had to give a public lecture on their area of expertise knows that such problems are almost unavoidable. Laypeople or scientists from outside the field of biology excited by this book, however, will undoubtedly pursue more detailed texts.

Some of the book's most interesting insights come from the author's forays in the final chapter, "Current Topics." There, Nüsslein-Volhard treats readers to brief discourses on matters such as cloning, designer babies, gene therapy, and human embryonic stem cells. Although her explanations of the complexity of the debates surrounding these issues will appeal to all, the author makes it clear that she holds unambiguous opinions in some of these controversies. For example, she provides an interesting summary of how laws regarding research on human embryonic stem cells vary among countries and points out the irony in this: "It seems morally questionable to profit from research performed in other countries, which is not permitted in one's own country, as is already happening in the case of IVF [in vitro fertilization]." By going to the effort of actually educating readers with *Coming to Life*, Nüsslein-Volhard can then make these sorts of statements in a way that appeals to her audience's intelligence. Such education of and respect for the public is vital to making progress on so many pressing issues that face society today.

References

1. S. F. Gilbert, *Developmental Biology* (Sinauer, Sunderland, MA, ed. 8, 2006).
2. L. Wolpert *et al.*, *Principles of Development* (Oxford Univ. Press, Oxford, ed. 3, 2007).
3. S. B. Carroll, *Endless Forms Most Beautiful: The New Science of Evo Devo and the Making of the Animal Kingdom* (Norton, New York, 2005); reviewed by D. Duboule, *Science* **308**, 955 (2005).

The reviewer is in the Department of Integrative Biology, the Department of Molecular Cell Biology, and the Howard Hughes Medical Institute, University of California, Berkeley, CA 94720–3140, USA. E-mail: nipam@uclink.berkeley.edu

10.1126/science.1130345

CREDIT: CHRISTIANE NÜSSLEIN-VOLHARD/FIG. 18 IN *COMING TO LIFE*

BIOETHICS

The Most Fragile of Newborns

Scott A. Lorch

To the uninitiated, the neonatal intensive care unit is a frightening place: rows of incubators; alarms and buzzers going off at irregular intervals, followed by the scurrying of nurses and doctors; and the quiet murmurs (and, sometimes, sobs) of families surrounding their tiny babies. But the neonatal intensive care unit is also a place of great hope and joy, as the newborns grow into babies capable of crying, eating, and smiling.

The trials of these infants, though, do not stop at the nursery's door. How these children affect both their families and society is the subject of Ruth Levy Guyer's *Baby at Risk: The Uncertain Legacies of Medical Miracles for Babies, Families, and Society*. Guyer (a science writer who teaches bioethics at Haverford College) uses conversations with neonatal professionals, parents of prematurely born infants, and medical ethicists to present what she hopes is a realistic picture of the survivors of neonatal intensive care. Ultimately, Guyer hopes that "the media will stop hyping 'miracle baby' stories and start reporting truthfully about the benefits and the burdens of neonatal intensive care and new reproductive technologies."

Each chapter uses the story of a premature infant or information from a medical professional to illustrate some key issues surrounding premature infants: long hospital stays, uncertain behavioral and developmental outcomes, and death. These stories lead the reader to think about the larger question: Who ultimately decides how to care for these newborns? Some of the stories are tragic—a six-year-old child born four months prematurely who eats via a feeding tube and whose family lives where "windows stay closed, even in summertime, because … [he] would think nothing of climbing out a window, no matter how high off the ground it is." Other stories reflect the magic of these children, such as 19-year-old twin college students who were delivered 3.5 months early and an 11-year-old child whose "bright eyes that her parents first saw on day eight are still probing, thoughtful, and expressive" even though she required heart-lung bypass at birth.

Although the book focuses on a very small segment of the population—those 1 to 2% of all births that occur at least three months prematurely and those children born with chromosomal or genetic defects—there is much to be learned from the care provided to these children, the outcomes of their birth, and popular media's treatment of them. Guyer points out that our political and financial policies send conflicting messages about the value and importance of these children. In several Western coun-

The reviewer is in the Division of Neonatology, Children's Hospital of Philadelphia, 34th Street and Civic Center Boulevard, Philadelphia, PA 19104, USA. E-mail: lorch@email.chop.edu

Baby at Risk
The Uncertain Legacies of Medical Miracles for Babies, Families, and Society

by Ruth Levy Guyer

Capital Books, Sterling, VA, 2006. 181 pp. $22.95. ISBN 9781933102269.

CREDIT: CORBIS

tries, there are regulations and laws that encourage aggressive treatment of the most fragile newborns around the time of birth. For example, Baby Doe regulations adopted during the Reagan Administration led to the display of posters that read "Discriminatory failure to feed and care for handicapped infants in this facility is prohibited by federal law." After these infants leave the neonatal intensive care unit, though, financial, educational, and medical support for families of these children are under the constant threat of cutbacks or elimination. Guyer endorses the conclusion of one commentator in the 2004 British Broadcasting Corporation documentary *When Miracle Baby Grows Up*, which she summarizes as "any country that is rich enough to afford neonatal intensive care also has the moral obligation to accept responsibility for the care of impaired children throughout their lives, but … none of them does."

Another question that the book raises, but cannot answer, is how society's understanding of the risks and ultimate benefits of health care ultimately contributes to the care and outcomes of these children. Media fascination with the "miracle child" may be a way to increase ratings or viewership, but it may also reflect the inherent belief among Western societies that medical technology can "cure anything." When a physician counsels a family that there is a 10% chance of a good outcome, how many families believe that their child will be that one baby out of ten? How many physicians or other health care professionals believe that this child will be different? We have not answered how the perspectives of the greater society factor into these very personal discussions between families and medical professionals, nor what the care of these children indicates about the fears of death and failure in our society. *Baby at Risk* should stimulate a discussion about difficult topics regarding a vulnerable portion of our population. For us, achieving a balance between risks and benefits, overtreatment and undertreatment, and reasonable hopes versus "miracles" will continue to be important as more and more children are born "at risk."

10.1126/science.1142263

ENVIRONMENT

The Burning Issue

David J. Lohman, David Bickford, Navjot S. Sodhi

Neither governments nor civil society have been able to mitigate the annual shroud of haze that blankets Southeast Asia.

The international community has failed repeatedly to prevent large-scale environmental catastrophes driven by perverse land-use practices in the tropics. Haze pollution in Southeast Asia is an example that has immediate and long-term negative consequences.

The use of fire to clear land is entrenched in many Southeast Asian cultures (*1*), and large commercial tree plantations—particularly in Indonesia and East Malaysia—have begun burning on an enormous scale (*2*). The resulting smoke, or "haze," from hundreds of simultaneous fires spreads across the region in the intermonsoonal dry season, lingering for weeks. Fires set to clear land may burn out of control, particularly during El Niño years, and consume large swaths of forest damaged by logging. These exact a high toll on this hotspot's biodiversity (*2, 3*). During the last El Niño in 1997–98, fires consumed over 8 million hectares on Borneo and Sumatra, blanketing more than 3 million km^2 and 70 million people in haze (*2, 4, 5*). Material damage estimates ranged from US$4.4 to $9.7 billion (*2, 4*) (see figure, above right); CO_2 and soot liberated from burning peat and biomass released an estimated 0.81 to 2.57 gigatons of carbon into the atmosphere (*6*). In addition to increasing hospital admissions throughout the region, unhealthy haze conditions increased mortality in Malaysia and lowered infant and fetal survival in Indonesia (*7, 8*).

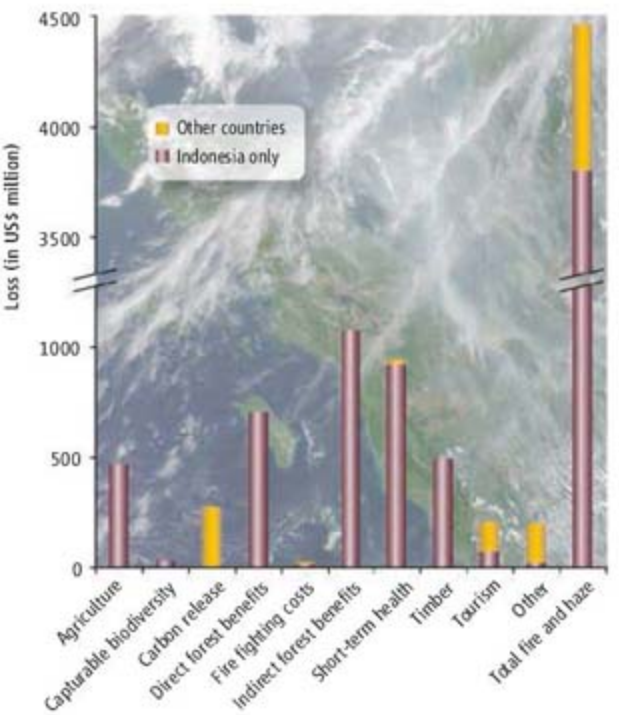

Effects of smoky haze. Estimated damage in Indonesia and other countries resulting from the haze episode exacerbated by the 1997–98 El Niño (*13*). The shroud of haze from July 2001 fires can be seen in the background satellite image.

Using fire to clear land has been illegal in Indonesia since 1995, and a zero-burning policy was ratified by the Association of Southeast Asian Nations (ASEAN) in 1999 (*4, 9*). Although many Malaysian plantations have stopped using fire (*4*), reappearing haze over Southeast Asia every year, including 2006, indicates that farmers throughout the region and plantations in Indonesia ignore the ban. Given the social and economic complexity of the annual haze problem, there will be no easy solution, but we highlight several priorities below.

Concentrate on "dirty fires." To minimize the greenhouse gases and pollution associated with fires, preventing and extinguishing "dirty fires" from peat and green vegetation, which release more CO_2 and soot than dried biomass, should get highest priority (*10*).

Coordinate fire-fighting efforts. The 1998 ASEAN Agreement on Transboundary Haze Pollution calls for establishing a coordinating center for battling haze, which has not been formally constituted because Indonesia has not yet ratified the agreement. Streamlining governmental procedures for handling fires may speed response.

Provide incentives to stop burning. Financial incentives could be provided to districts or villages that have policed themselves and have avoided burning during hazardous conditions. Stronger incentives for corporations that clear land for plantations, might include payment of up-front deposits or mandatory "no-fire insurance" (*10*).

Provide alternatives to burning. Fire will always be the cheapest method to clear land in the tropics. International aid agencies should focus on providing infrastructure and hardware needed to clear land without fire.

Teach environmental management. Efforts should be made to educate local farmers on the medical, environmental, and political ramifications of burning, along with alternate methods of land clearing. Volunteer organizations such as the U.S. Peace Corps could help stop fires on the ground and teach rural communities about alternatives to fire.

Neither the Indonesian government nor regional ASEAN pressure have been able to stop the haze (*10, 11*). Ongoing efforts by the Forest and Agriculture Organization of the United Nations (*9*), including a recent meeting on sustainable forest management and a workshop in Indonesia to train community-based fire managers, can address the problems at both governmental and community levels. In addition, the United Nations or the World Bank could help generate needed funds through debt-for-nature swap or carbon credit–offset funds.

Solutions to the haze problem are needed before the onset of the dry season in June, as 2007 may be another El Niño year (*12*). Lessons learned from this catastrophe may help ameliorate similar smoke-haze episodes in Amazonia, Africa, and other parts of Asia.

The authors are in the Department of Biological Sciences, National University of Singapore, Singapore 117543; e-mail: lohman@nus.edu.sg (D.J.L.) or dbsns@nus.edu.sg (N.S.S.)

References and Notes

1. G. G. Marten, Ed., *Traditional Agriculture in Southeast Asia: A Human Ecology Perspective* (Westview Press, Boulder, CO, 1986).
2. C. V. Barber, J. Schweithelm, *Trial by Fire: Forest Fire and Forestry Policy in Indonesia's Era of Crisis and Reform* (World Resources Institute, Washington, DC, 2000).
3. M. F. Kinnaird, T. G. O'Brien, *Conserv. Biol.* **12**, 954 (1998).
4. D. Glover, T. Jessup, Eds., *Indonesia's Fires and Haze: The Cost of Catastrophe* (International Development Research Center and the Institute of Southeast Asian Studies, Ottawa and Singapore, 1999).
5. J. Nichol, *Atmos. Environ.* **31**, 1209 (1997).
6. S. E. Page *et al.*, *Nature* **420**, 61 (2003).
7. S. Jayachandran, "Air quality and infant mortality during Indonesia's massive wildfires in 1997" (Tech. report no. 95, BREAD: Bureau for Research in Economic Analysis of Development, Cambridge, MA, 2005).
8. N. Sastry, *Demography* **39**, 1 (2002).
9. U.N. Food and Agriculture Organization (FAO), *Fire Management—Global Assessment 2006* (FAO, Rome, 2007).
10. N. Byron, *Agric. Ecosyst. Environ.* **104**, 57 (2004).
11. J. Nichol, *Atmos. Environ.* **32**, 3917 (1998).
12. Anonymous, "2007: Year of El Niño havoc?," *Straits Times*, 6 January 2007, p. 24.
13. T. P. Tomich, D. E. Thomas, M. van Noordwijk, *Agric. Ecosyst. Environ.* **104**, 229 (2004).

14. Grant R-154-000-270-112 from the Singapore Ministry of Education supported the authors.

Supporting Online Material
www.sciencemag.org/cgi/content/full/316/5823/376/DC1

10.1126/science.1140278

PHOTO CREDIT: JACQUMA DESCLOITRES, MODIS LAND RAPID RESPONSE TEAM

PLANT SCIENCE

SCARECROWs at the Border

The trapping of a diffusible regulatory protein by its binding partner is a central component in the development of a structure in plants that has the thickness of a single cell.

Liam Dolan

An important process during the development of multicellular organisms is the laying down of boundaries between groups of different cell types. The emergence of such borderlines usually requires cells on either side of the boundary to communicate with each other. In many organisms, these signals may be proteins that move from one cell group to another, eliciting responses that result in two distinct cell populations. In plants, a small number of proteins that control development move from the cytoplasm of one cell to that of neighboring cells. In a report on page 421 of this issue, Cui *et al.* (*1*) describe a mechanism that spatially restricts the movement of one such mobile protein between two adjacent groups of cells in plant roots. This may constitute a general means by which multicellular organisms control the formation of tissue boundaries.

In the plant *Arabidopsis thaliana*, SHORTROOT (SHR) is a GRAS family transcriptional regulator that only moves the distance of a single cell from its cell of origin (*2*). How is SHR movement restricted to this distance? It was previously shown that SHR protein is synthesized in the innermost tissue of the root, the stele, and moves to the adjacent endodermal tissue where a similar GRAS family transcription factor called SCARECROW (SCR) is expressed (*3*, *4*) (see the figure). Together, SHR and SCR positively regulate development of the endodermis and cortical tissue from a common set of stem cells. In addition, SHR moves from the stele into the endodermis to positively control SCR expression.

The model proposed by Cui *et al.* explains why SHR protein moves no farther than one cell layer. Once transported to an endodermal cell (by a currently unknown mechanism), SHR binds to SCR, forming a transcriptionally active complex that can no longer move from cell to cell. This complex, located in the nucleus, then positively regulates the production of more SCR, which in turn, traps any mobile SHR protein in the endodermal cell. This forms a positive feedback mechanism for SCR production in response to SHR transport. SHR therefore activates the production of its own trap, one cell layer away, a strategy that may account for the formation of a stele surrounded by a single layer of endodermis in the developing root.

Perhaps the most elegant part of this report is the test of this model. The authors genetically engineered plants with decreased expression of SCR (SCR-knockdown plants). Although the SCR-knockdown plants accumulate less of the SHR-trapping protein (SCR) relative to normal plants, they produce normal amounts of SHR. If SCR does indeed sequester SHR in the endodermis, then decreased amounts of SCR in the endodermal cells should be insufficient to bind all of the incoming SHR protein. Consequently, excess, nontrapped SHR could pass through this layer of endodermal cells and proceed to outer cells of the root, potentially triggering the development of another layer of endodermal cells. It was previously shown that ectopic expression of SHR induces the development of supernumerary endodermal layers (*3*). Indeed, Cui *et al.* found that plants with less SCR protein develop supernumerary layers of endodermis, consistent with the model that SCR restricts the mobility of SHR to a single layer of cells.

The proposed positive feedback loop that ensures sufficient SCR to trap SHR in the endodermal cell requires an initial developmental state in which there is a low background level of SCR expression in the endodermis, although there is no direct evidence for this yet. It also requires robust expression of SHR in the stele, which has been shown (*3*). The model of Cui *et al.* accounts for the stabilizing of these fields of expression with defined, constant boundaries and the development of a single layer of endodermis. The characterization of the signaling network that leads to these initial states of the two cell populations now needs to be fleshed out.

The Cui *et al.* results suggest that control of the direction and distance of movement of intercellular regulators is determined by the spatial distribution of their binding partners. It is therefore possible that the observed movement of other plant proteins, such as the transcriptional regulators CAPRICE (in the root epidermis) and KNOTTED/SHOOT MERISTEMLESS (in the shoot apical meristem) (*5*, *6*), is determined by the presence of a binding partner in the cell to which the regulator moves. In principle, the same mechanism could operate during animal development in which transcriptional regulators such as chick Engrailed2 move from cell to cell (*7*). Whereas chick Engrailed2 protein moves from the cell in which it is synthesized to its neighboring cell via a secretion and reuptake mechanism, it is unclear how plant proteins are moving from cell to cell.

Cui *et al.* also suggest that their proposed mechanism of endodermal boundary formation may be conserved through evolution, because the rice orthologs of SCR and SHR have similar expression patterns. The endoder-

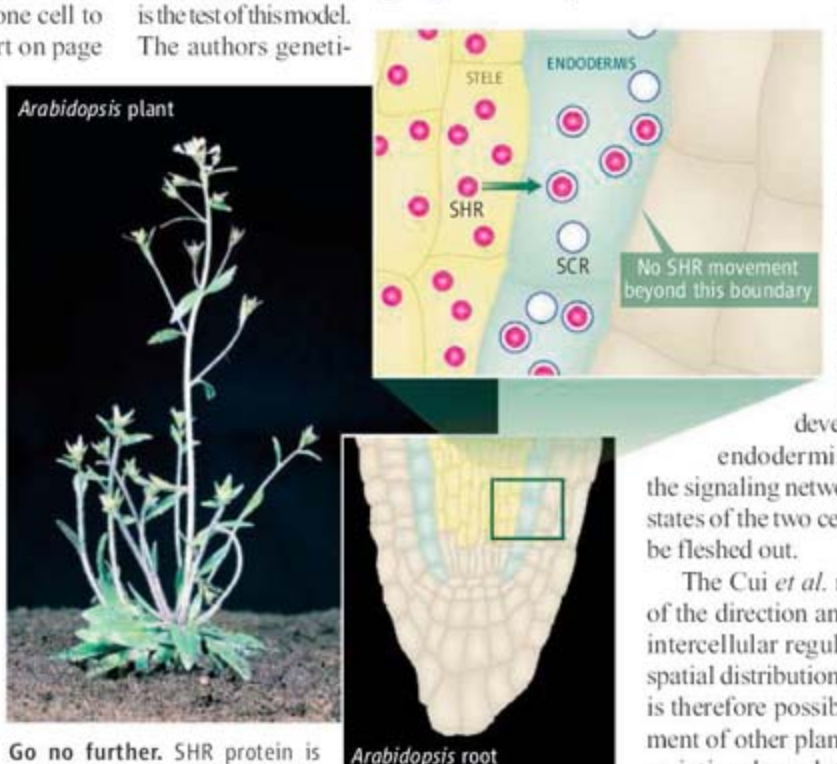

Go no further. SHR protein is synthesized in stele cells in plant (*Arabidopsis thaliana*) roots, and moves the distance of one cell where it binds to SCR protein. The complex remains trapped in these cells, triggers production of more SCR, and directs the cells to develop into a single layer of endodermis that surrounds the stele.

The author is in the Department of Cell and Developmental Biology, John Innes Centre, Norwich NR4 7UH, UK. E-mail: liam.dolan@bbsrc.ac.uk

mis of most land plants is uniseriate (comprising one layer), and if SHR and SCR orthologs control development in these species, this mechanism may have evolved early in the history of land plants. But there are some rare exceptions. For example, extant members of the Equisetales (horsetails), whose forebears were important species in Carboniferous forests 300 million years ago, have two layers of endodermis in some organs (*8*). These horsetails have apparently tinkered with their *SCR* and *SHR* genes to allow SHR to escape the clutches of SCR in the first endodermal layer, thus extending the endodermis to further layers.

Why is the structure of a single-layered endodermis so conserved across most land plants? Autotrophic plants rely on the uptake of nutrients and water from the soil, so tight spatial regulation of endodermal development reflects its significance. The endodermis is highly specialized in that intercellular spaces between the cells are sealed, prohibiting the free diffusion of water and ions through the interstices. If water and ions are to pass through this roadblock, they must do so in a regulated manner, via the cytoplasm of endodermal cells. This affords strict control over transport and may well have provided a survival advantage—the highest level of control over a specialized tissue of very limited size. If so, this discovery may explain the evolution of a tightly regulated developmental program in angiosperms (flowering plants) and also points to changes in developmental programs that may have occurred during the past 470 million years of land plant evolution.

References

1. H. Cui *et al. Science* **316**, 421 (2007).
2. Y. Helariutta *et al., Cell* **101**, 555 (2000).
3. K. Nakajima, G. Sena, T. Nawy, P. N. Benfey, *Nature* **413**, 307 (2001).
4. L. Di Laurenzio *et al., Cell* **86**, 423 (1996).
5. T. Wada *et al., Developmemt* **129**, 5409 (2002).
6. W. J. Lucas *et al., Science* **270**, 1980 (1995).
7. A. Maizel, O. Bensaude, A. Prochiantz, A. Joliot, *Development* **126**, 3183 (1999).
8. F. O. Bower, *Primitive Land Plants* (Macmillan, London, 1935).

10.1126/science.1142343

GEOCHEMISTRY

Food for a Volcanic Diet

Chemical analyses of lava can now reveal the nature of the rocks deep in the Earth that melted and rose to generate specific volcanoes.

Claude Herzberg

Volcanic eruptions have the power to reshape Earth's landscape, alter climate, and affect life. To understand how this works requires that we go deep into the Earth to learn exactly what kind of rock melts to produce magmas and the chemistry of this source rock. These are fundamental problems in geology, and they are also among the most difficult to understand. On page 412 in this issue, Sobolev *et al.* (*1*) describe a method for identifying some of these source rocks. We can think of them as food for volcanoes in the sense that they melt to provide the magmas that can erupt to the surface. To understand what Sobolev *et al.* have done and the ramifications that go beyond Earth science, we need to start with a refresher in geology.

Earth's mantle consists mostly of peridotite, a rock rich in the mineral olivine $(Mg,Fe)_2SiO_4$. When peridotite partially melts, the liquids collect to magmas that rise to the crust, give off gases like SO_2, CO_2, and H_2O, and solidify to basalt, a rock rich in the minerals clinopyroxene $[Ca(Mg,Fe)Si_2O_6]$ and plagioclase $[(Ca,Na)(Al_{1-2}Si_{2-3})O_8]$. Portions of these outer layers can be recycled back into the mantle at subduction zones and below thickened continents (see the figure). The recycled basaltic crust is transformed to a new rock called pyroxenite, so-called because it is rich in clinopyroxene. It may pile up on Earth's core, or be mixed back into the mantle with structures that have been described as marble cake (*2*), plum pudding (*3*), spaghetti (*4*), and gumbo (*5*) (see the figure). Volcanoes like those of Hawaii can melt from source rocks consisting of peridotite and/or pyroxenite from recycled crust. Sobolev *et al.* describe a method for identifying this rock based on the chemistry of lavas on volcanoes.

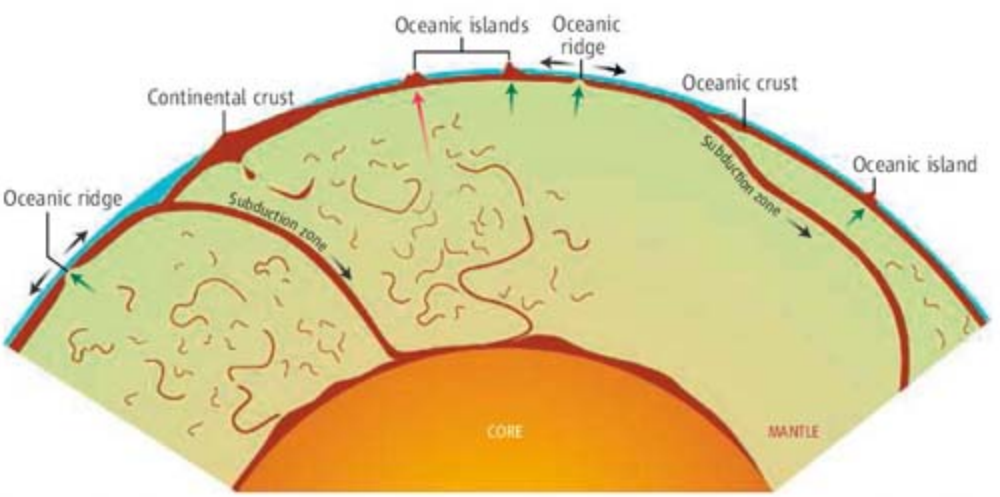

Models of Earth's crust and mantle. Oceanic crust (brown) is solidified liquid that forms by partial melting of mantle peridotite (green) at oceanic ridges; together with sediment, oceanic crust can be recycled back into the mantle at subduction zones (*2, 3, 6*). Continental crust (brown) forms at subduction zones and can be recycled when it thickens by delamination (*5, 15*). All crust (brown) is transformed to pyroxenite (brown) when recycled. Green arrow denotes melting peridotite. Red arrow denotes melting pyroxenite. Recycled crust may be distributed uniformly throughout the mantle, or it may be concentrated in certain hemispheres or depths. Crustal thickness is exaggerated for clarity, but ranges from ~6 to 40 km at the present time. Recycling is expected to reduce crust to dimensions ranging from micrometers to kilometers.

Sobolev *et al.* determined that many volcanoes melted from recycled crust, a conclusion that is not new (*6*). However, there has always been some ambiguity with past methods of identifying recycled crust based on the isotope and trace-element geochemistry of lavas at the surface. New interpretations suggest that many oceanic islands melted from mantle peridotite that had been modified by melts that flowed through it (*7, 8*), a process called metasomatism (*9*). Because it makes no difference to an atom of lanthanum, for example, whether it ends up concentrated in the crust or as metasomatized peridotite, using it as a tracer can be ambiguous and nonunique (*7, 8*).

A breakthrough came when Sobolev *et al.* (*10*) showed that the nickel contents of many

The author is in the Department of Geological Sciences, Rutgers University, Piscataway, NJ 08854, USA. E-mail: herzberg@rci.rutgers.edu

olivine crystals in Hawaiian lavas were higher than those expected from melts of peridotite, and they preferred to explain this with a recycled crust source instead. But a lingering ambiguity is that a high nickel content in olivine can also arise when peridotite is enriched in pyroxene by melt-rock reaction (*11*). Supporting evidence for the recycled-crust interpretation (*10*) comes from the calcium contents of the Hawaiian lavas, which are too low to be easily explained by melting peridotite (*12*). Nickel and calcium are therefore telling the same story. That is, the main shield-building lavas at Hawaii were melted from a pyroxenite source rock that required the involvement of recycled crust as proposed by Sobolev *et al.* (*10*). The authors go further in that they examine the problem that arises when nickel, calcium, and manganese are used, and they extend the analysis to a larger population of volcanoes. Their results, together with other recent studies (*7*, *8*, *11*), show that it is unlikely that a single rock type will be an appropriate source for all oceanic volcanoes. For example, recycled crust is an important source rock for the Hawaiian islands (*1*, *10*, *12*), whereas metasomatized peridotite is the source rock for the Cook islands (*7*). An outstanding question is whether peridotite sources become metasomatized by melted recycled crust (*13*) or in some other way (*7*, *8*).

Future studies might allow us to transform our picture from hypothetical models to actual three-dimensional views showing the size and distribution of recycled crust in the mantle. The implications go far beyond geology. For example, it may be no surprise that Sobolev *et al.* (*1*) identify pyroxenite as the rock that melted to produce the Siberian Traps. This was a magmatic flood on land so massive in scale that it triggered the largest mass extinction of life on Earth, some 250 million years ago (*14*). Although the exact causal links remain poorly understood in detail, one can reasonably imagine a different outcome if the mantle diet had less pyroxenite and more peridotite. Under these circumstances, less magma would have been produced and made available for eruptive flooding, and Earth's biosphere could have evolved along different pathways.

References

1. A. V. Sobolev *et al.*, *Science*, **316**, 412 (2007); published online 29 March 2007 (10.1126/science.1138113).
2. C. J. Allègre, D. L. Turcotte, *Nature* **323**, 123 (1986).
3. J. P. Morgan, W. J. Morgan, *Earth Planet. Sci. Lett.* **170**, 215 (1999).
4. W. Abouchami *et al.*, *Nature* **434**, 851 (2005).
5. D. L. Anderson, *New Theory of the Earth* (Cambridge Univ. Press, Cambridge, ed. 2, 2007).
6. A. W. Hofmann, W. M. White, *Earth Planet. Sci. Lett.* **57**, 421 (1982).
7. S. Pilet *et al.*, *Earth Planet. Sci. Lett.* **236**, 148 (2005).
8. Y. Niu, M. J. O'Hara, *J. Geophys. Res.* **108**, 2209 (2003).
9. J.-L. Bodinier *et al.*, *J. Petrol.* **45**, 1 (2004).
10. A. V. Sobolev *et al.*, *Nature* **434**, 590 (2005).
11. P. B. Kelemen *et al.*, *Earth Planet. Sci. Lett.* **164**, 387 (1998).
12. C. Herzberg, *Nature* **444**, 605 (2006).
13. R. Dasgupta *et al.*, *J. Petrol.* **47**, 647 (2006).
14. I. H. Campbell *et al.*, *Science* **258**, 1760 (1992).
15. C. Herzberg *et al.*, *Contrib. Mineral. Petrol.* **84**, 1 (1983).

Published online 29 March 2007;
10.1126/science.1141051
Include this information when citing this paper.

BIOCHEMISTRY

An Ancient and Intimate Partnership

Nonheme iron enzymes can catalyze a wide variety of chemical reactions. Two studies show how this versatility is achieved.

Carrie M. Wilmot

Before the evolution of photosynthesis ~3.5 billion years ago, Earth's atmosphere was reducing, and iron was mainly in its Fe(II) oxidation state. The abundant Fe(II) soaked up the early molecular oxygen generated by photosynthesis. Complex multicellular organisms could not evolve until substantial amounts of oxygen became available in Earth's atmosphere ~2 billion years ago. Then the tables were turned: Organisms used Fe(II) to access the oxidative power of molecular oxygen, thus dramatically increasing the efficiency of metabolic energy generation.

Two reports in this issue highlight the biological intimacy of the relation between Fe(II) and dioxygen. On page 453, Kovaleva and Lipscomb (*1*) show how an enzyme fine-tunes the properties of Fe(II) to activate O_2, thereby enabling the oxidation of aromatic diols in a four-electron metabolic process. However, the by-products of molecular oxygen reduction can be highly toxic and need to be removed rapidly. On page 449, Katona *et al.* (*2*) reveal details of how one enzyme helps to remove the most toxic by-product, superoxide, by reducing it to the less toxic hydrogen peroxide.

Kovaleva and Lipscomb report on the bacterial extradiol ring-cleaving dioxygenase, a key enzyme in the metabolic degradation of aromatic hydrocarbons introduced into soil by humans. The enzyme contains a mononuclear Fe(II) bound to two histidines and a carboxylate, a motif that has evolved several times in different enzymes that catalyze crucial chemistries in the synthesis of neurotransmitters, antibiotics, and plant hormones (*3*). The authors added an inefficient substrate (with a slow conversion rate) to the crystallized enzyme in an O_2-depleted atmosphere. By rapidly freezing the crystal, they were able to simultaneously trap three different steps in the catalyzed reaction. Iron acts as a conduit to enable electron density to move from the aromatic substrate to dioxygen. This transfer creates two reactive species: a superoxo and a substrate radical. The superoxo species is bound side-on to the iron, but the interaction is weak

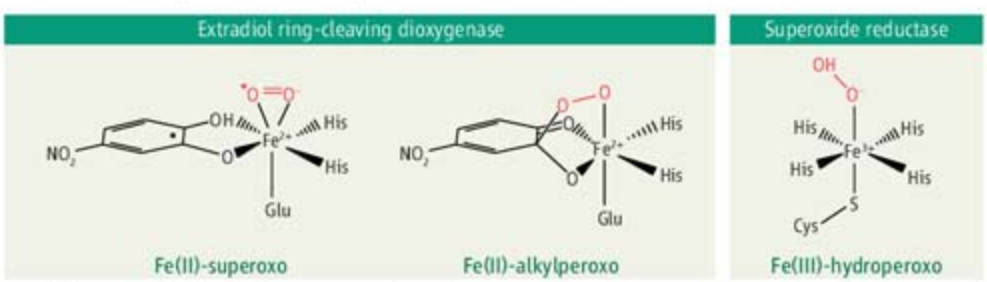

Iron-dioxygen relationships. Mononuclear nonheme iron enzymes can accommodate a diverse range of geometries with substrates and dioxygen, as illustrated here by the trapped catalytic intermediates in an extradiol ring-cleaving dioxygenase (**left** and **center**) reported by Kovaleva and Lipscomb and in superoxide reductase (**right**) reported by Katona *et al.*

The author is in the Department of Biochemistry, Molecular Biology and Biophysics, University of Minnesota, Minneapolis, MN 55455, USA. E-mail: wilmo004@umn.edu

because of steric crowding from the five other ligands to the metal (see the figure, left panel). In this arrangement, the superoxo is perfectly aligned to attack the substrate radical and form the alkylperoxo intermediate (see the figure, center panel). Interestingly, the only other crystal structure of dioxygen in complex with a mononuclear nonheme iron enzyme [a Rieske dioxygenase, with oxygen most likely as a Fe(III)-peroxo species] also has dioxygen bound side-on to the iron (*4*).

Katona *et al.* studied superoxide reductase, an enzyme that is found in a range of bacteria and archaea (*5*). Superoxide reductase converts superoxide ($O_2^{\bullet-}$) to hydrogen peroxide (H_2O_2) in a one-electron reduction. Reactive oxygen species, such as $O_2^{\bullet-}$, play a key role in human pathology and aging, and their destruction by enzymes such as superoxide reductase is therefore of great interest. Katona *et al.* freeze-trapped several peroxide conformations with Fe(III) in a crystal of an enzyme mutant that stabilizes the Fe(III)-peroxo. In contrast to the structures reported by Kovaleva *et al.*, the dioxygen is bound to the iron end-on configuration (see the figure, right panel).

The distinct names for the three oxidation states of dioxygen (molecular oxygen, superoxide, and peroxide) focus attention on electron transfer events, but sources and transfer of two protons are also required for the reduction from $O_2^{\bullet-}$ to H_2O_2. The protons can come from amino acids, cofactors, or water, and enzymes control the protonation steps in perfect synchrony with electron transfer. Although the iron-dioxygen structures presented by Katona *et al.* are all Fe(III)-peroxo species, they display three different end-on peroxide conformations through rotation on the Fe(III) pivot, thus linking the peroxide to water molecules and amino acids in the active site. The concerted movements of these players suggest possible proton transfer pathways, and this study represents the most complete insight into protonation through rotation to date [see the movie in (*2*)]. It should be noted that crystal structures of proteins are rarely at a high enough resolution to directly determine either oxidation or protonation states of chemical groups. These are indirectly inferred from geometries coupled with chemical knowledge, as in the study by Kovaleva and Lipscomb. In the study by Katona *et al.*, this uncertainty is removed through the use of Raman spectroscopy on the crystal, which directly confirms that only Fe(III)-peroxo species are present. Density functional theory calculations performed on the structures suggest that at least two are hydroperoxides, the singly protonated intermediate of peroxide during its conversion to product H_2O_2.

Crystal packing played a crucial role in trapping these various species. In both studies, the data used to generate all the intermediates came from a single crystal. In each case, there were four independent copies of the active site in the basic crystal building block, enabling four different images of the active site to be observed simultaneously. The different species in each study manifested themselves in structurally distinct active sites. The reason why different crystal packing environments stabilized different species is beyond the resolution of these data; subtle structural effects within the protein probably control the chemistry. The study by Katona *et al.* shows that the combination of high-resolution spectroscopic experiments (both in the crystal and in solution), computational methods, and crystal structures represents a potent toolbox that promises to unlock many secrets in chemical biology.

Together, the two studies provide stunning insights into the diverse structural relations that mononuclear nonheme iron enzymes can broker among oxygen, protein, solvent, and hydrocarbon substrates. The iron centers in these enzymes are much more flexible than those of their heme cousins, which are constrained by their porphyrin partners. This fact probably explains the great diversity of substrate chemistries that can be catalyzed by the nonheme enzymes.

The abundance of iron on Earth held back the development of complex life during the 1.5-billion-year rusting event that kept atmospheric oxygen levels low. It is interesting to wonder what life would be like at this point in geologic time if iron was less abundant and the evolution of complex multicellular organisms had started 1 billion years earlier. Would iron still have such a prominent role in the fabric of life? I believe it would. The chemical richness imparted by this versatile transition metal would be difficult to replace, and life would certainly be less interesting without it.

References and Notes

1. E. G. Kovaleva, J. D. Lipscomb, *Science* **316**, 453 (2007).
2. G. Katona *et al.*, *Science* **316**, 449 (2007).
3. K. D. Koehntop, J. P. Emerson, L. Que Jr., *J. Biol. Inorg. Chem.* **10**, 87 (2005).
4. A. Karlsson *et al.*, *Science* **299**, 1039 (2003).
5. V. Niviere, M. Fontecave, *J. Biol. Inorg. Chem.* **9**, 119 (2004).
6. Supported by NIH grant GM-66569.

10.1126/science.1141629

PLANETARY SCIENCE

A New Spin on Saturn's Rotation

Fran Bagenal

Modulations of radio emissions from Saturn that have been used to measure the rotation of the planet's interior now turn out to be caused by an external ring of plasma. The true internal rotation continues to be a mystery.

The rotation rate of a planet is among its most important properties. For solid planets, simple observation of the surface tells us how fast the object is spinning. On gas planets such as Saturn or Jupiter, however, the visible outer layers move differently from the interior. So how do we know how fast the interior of a gas planet is spinning? The usual trick is to measure the periodicity of radio emissions that are modulated by the planet's internal magnetic field. This method assumes that the magnetic field is tilted and that the dynamo region where the field is generated spins at a rate representative of the bulk of the planet. But on page 442 of this issue, Gurnett *et al.* (*1*) argue that recent data from NASA's Cassini spacecraft indicate that apparent changes in Saturn's spin could be caused by processes external to the planet. This raises new questions about how we are to measure and understand the rotation of the large gas planets.

Saturn first dumbfounded planetary theorists who study dynamo models by having a highly symmetric internal magnetic field. A field that is symmetric about the rotation axis violates a basic theorem of magnetic dynamos (*2*). The second puzzle came with the detection of a systematic rotational modulation of the radio emission similar to a flashing strobe, which should not occur in a symmetric magnetic field. Meanwhile, radio measurements have revealed that last year that Saturn's day has become about 6 to 8 mins longer—it is now roughly 10 hours and 47 min—since the 1980s when measured by the Voyager missions (*3*). And the spin rate seems to keep changing. In their new work, Gurnett *et al.* show how Saturn's radio emission, the magnetic field measured in the magnetosphere,

The author is at the University of Colorado, Boulder, CO 80309–0392, USA. E-mail: bagenal@colorado.edu

and the density of plasma trapped in the magnetic field are all modulated with the same drifting period. And the plasma produced by Saturn's moon Enceladus may hold the key to the puzzle of the radio emissions.

Cassini images of geysers on Saturn's small moon Enceladus (*4*) triggered great excitement, primarily because they implied that warm, potentially life-harboring water might lurk just below the icy surface. But to magnetospheric scientists, Enceladus' geysers evoked the volcanic plumes of Jupiter's moon Io. Io's plumes spew forth gases that are ionized at a rate of about a ton per second, forming a dense toroidal cloud of plasma trapped in Jupiter's strong magnetic field. The torus of plasma emanating from Enceladus is much weaker (at most a couple of hundred kilograms per second) than that of Io, with most of the gases remaining as neutral atoms or molecules (*5, 6*). Cassini observations show that the Enceladus plasma torus slowly spreads out to fill Saturn's magnetosphere.

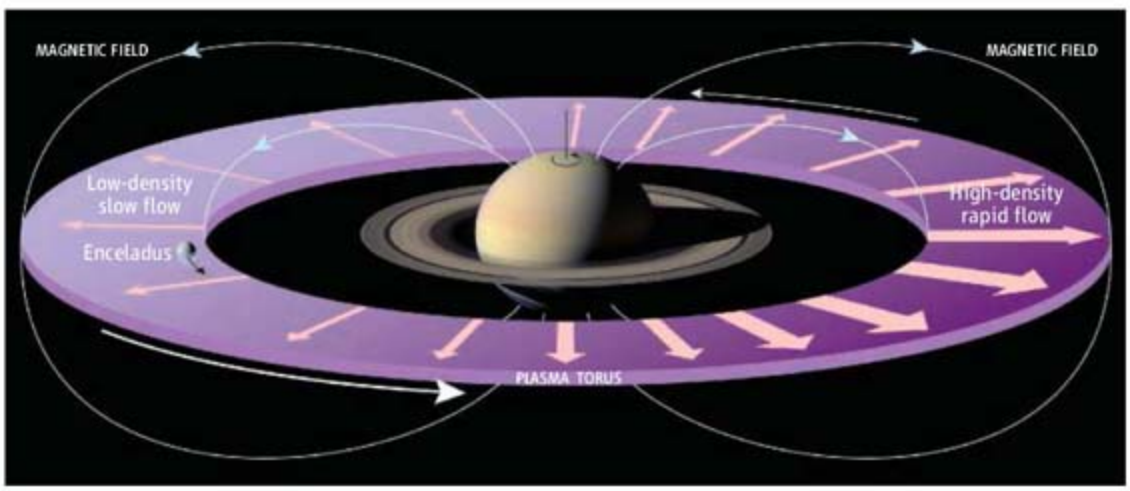

Plasma possibilities. Geysers on Saturn's moon Enceladus emit gases that form a plasma torus. The centrifugal instability that causes plasma outflow could be stronger on one side than the other. Gurnett *et al*. suggest that this asymmetric flow may rotate at a different rate than Saturn's interior.

Gurnett *et al*. argue that the process that transports plasma radially outwards could be stronger on one side of Saturn than the other (see the figure). They suggest that this circulation pattern also produces higher plasma densities in the region of stronger outflow. Gurnett *et al.* propose that plasma production stresses the electrodynamic coupling between the magnetosphere and the planet, causing the pattern of weaker/stronger outward flow to slowly slip in phase relative to Saturn's internal rotation.

Given the dynamic changes that occur in the external plasma structures around Saturn, an external explanation for Saturn's apparently erratic spin rate seems far more plausible than perturbations in the massive interior of the planet. Possibly the geysers on Enceladus are more active now than in the 1980s, or perhaps there are seasonal variations in the ionosphere (affecting the electrodynamic coupling) over Saturn's 29-year orbit.

The question remains: What causes the proposed asymmetric convection pattern? In the 1980s, researchers tried to explain variations in the Io plasma torus (*7*) by invoking a convection pattern that rotated with the planet. But evidence of such a flow pattern in the jovian magnetosphere remains elusive. Furthermore, recent modeling of the Io torus (*8*) suggests that high-energy electrons that make up a mere fraction of the total exert a huge effect on the plasma. Electrical currents that couple Io's plasma torus to the ionosphere may perturb these electrons. Such perturbations may then lead to asymmetric flows. Alternatively, a system of neutral winds in Jupiter's atmosphere could drag the ionosphere around, which then electrodynamically stirs up the magnetosphere.

Much more so than for Jupiter, the magnetosphere of Saturn is strongly dominated by neutral atoms and molecules. The number-density ratio of neutrals to ions is 10:1 in the Enceladus torus compared with 1:20 in the Io torus. This difference has recently been explained in terms of the much slower plasma speed (and hence lower energy of fresh plasma) flowing past Enceladus (at an orbital distance of ~4 saturnian radii) compared with the plasma flow past Io (at ~6 jovian radii) (*9*). Could small variations in high-energy electron population in the Enceladus torus be causing the dramatic changes in plasma density observed by Gurnett *et al*.? If so, large-scale convection patterns in the magnetosphere may not be necessary, just minor modulations in the electrical currents that flow along the magnetic field between the equatorial plasma disk and the planet's ionosphere, bringing small fluxes of ionizing high-energy electrons to the torus.

A fundamental issue is whether the magnetospheric observations, including the radio emissions, require the magnetic field emanating from the interior of Saturn to be asymmetric. Nearly 30 years ago, Stevenson suggested that strong shear motions in a conducting shell surrounding the dynamo might impose symmetry around the rotational axis (*10*). Southwood recently proposed that currents in the rings might cause a dipole tilt to be obscured (*11*). The fact that the rotational modulation of magnetospheric phenomena seems to be fairly constant with radial distance argues in favor of an external rather than an internal source. Yet localized magnetic anomalies (i.e., high-order multipoles) at high latitudes remain possible and may be affecting the currents that couple the magnetosphere to the planet.

As the mystery of Saturn's rotation thickens, the Cassini spacecraft migrates to orbits that reach higher latitudes and unexplored polar regions of the magnetosphere. If NASA extends funding for a few years beyond the mid-2008 end of the prime mission, Cassini can gather data over nearly one-quarter of Saturn's seasonal cycle. Magnetospheric physicists will have a grand time debating the meaning of the Cassini data. Meanwhile, the atmospheric dynamicists are trying to understand how the zonal jets in Saturn's banded atmosphere appear to change with seasonal variations in solar illumination (*12*). But before they can say how fast the winds are blowing relative to the interior of the planet, they must sit twiddling their thumbs and wait to be told the true rotation period of Saturn.

CREDIT: STEVE BARTLETT

References

1. D. A. Gurnett *et al*., *Science* **316**, 442 (2007).
2. T. G. Cowling, *Mon. Not. R. Astron. Soc.*, **94**, 39 (1934).
3. W. S. Kurth, A. Lecacheux, T. F. Averkamp, J. B. Groene, D. A. Gurnett, *Geophys. Res. Lett.* **34**, L02201, 10.1029/2006GL028336 (2007).
4. C. C. Porco *et al*., *Science* **311**, 1393 (2006).
5. M. K. Dougherty *et al*., *Science* **311**, 1406 (2006).
6. J. H. Waite, Jr. *et al*., *Science* **311**, 1419 (2006).
7. A. J. Dessler, R. R. Sandel, S. K. Atreya, *Planet. Space Sci.* **29**, 215 (1981).
8. A. Steffl, P. Delamere, F. Bagenal, *Icarus* **180**, 124 (2006).
9. P. Delamere, F. Bagenal, V. Dols, *J. Geophys. Res.*, 10.1029/2007GL029437 (2007).
10. D. J. Stevenson, *Science* **208**, 746 (1981).
11. D. J. Southwood, M. K. Dougherty, M. G. Kivelson, paper presented at the American Geophysical Union meeting, 11 to 15 December 2006, San Francisco, abstract P52A-08.
12. A. Sanchez-Lavega, *Science* **307**, 1223 (2005).

10.1126/science.1142329

ECOLOGY

Rapid Domestication of Marine Species

Domestication has had higher success rates in the sea relative to those seen in the long history of land species' domestication. The rise of aquaculture has global consequences.

Carlos M. Duarte, Nùria Marbà, Marianne Holmer

About 11,000 years ago, humans began to domesticate plants and animals (*1*–*3*). In the next 9000 years, hundreds of land species and a few aquatic species were domesticated. Since then, however, few land species have been domesticated. In contrast, the domestication of aquatic—particularly marine—species has grown exponentially. Aquaculture is emerging as a revolution in agriculture of global importance to humankind.

Domestication of wild species to produce food means that the breeding, care, and feeding of organisms are controlled by humans (*4*). By 2000 years ago, an estimated 90% of the species presently cultivated on land had been domesticated. Since the industrial revolution, the increase in the numbers of domesticated land plant and animal species has been modest (~3%) (see the figure).

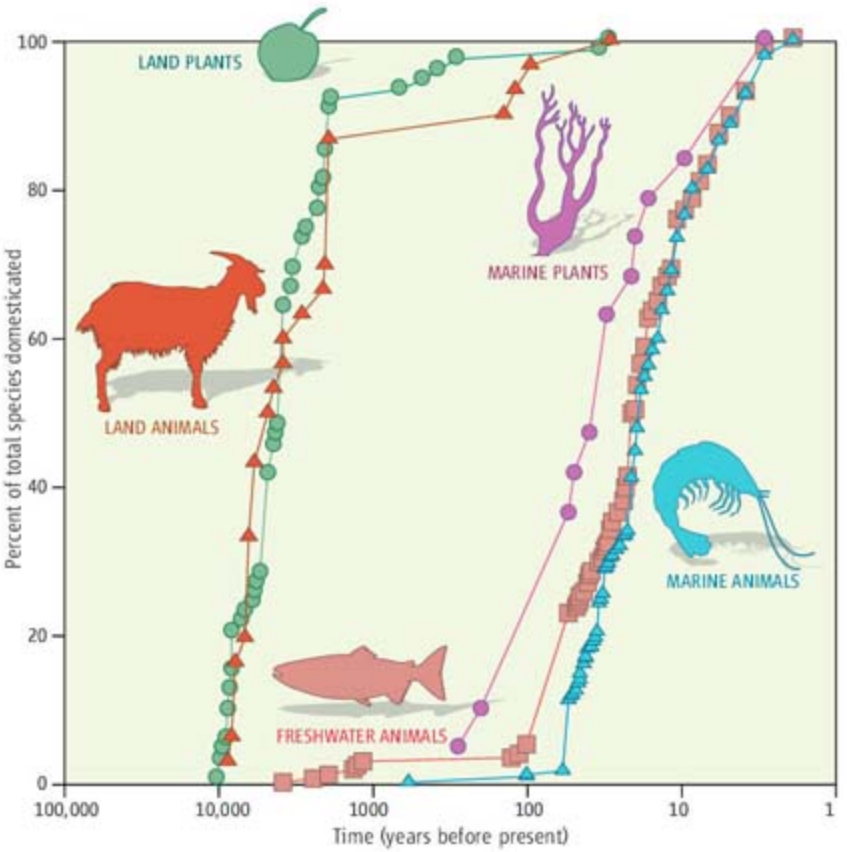

Land versus water. Most land species were domesticated earlier than aquatic species, but in the past 100 years, many more aquatic species than land species have been domesticated (*6*).

In contrast, the rise of aquaculture is a contemporary phenomenon (*5*). About 430 (97%) of the aquatic species presently in culture (see the table) have been domesticated since the start of the 20th century, and an estimated 106 aquatic species have been domesticated over the past decade (see the figure) (*6*). The number of aquatic species domesticated is still rising rapidly (see the figure) (*6*). Even allowing that the rates for early domesticates are estimates, aquatic domestication rates are ~100 times as fast as the rates of domestication of plant and animal species on land over the period when domestication was fastest (see the table) (*6*). Despite a vastly longer history, the domestication of land species has been less successful than that of marine species (*7*), particularly for animals: 0.08% of known land plant species and 0.0002% of known land animal species have been domesticated (*7*), compared with 0.17% of known marine plant species and 0.13% of known marine animal species. Effective genetic improvement programs for many aquaculture species (*8*) should be facilitated by their huge reproductive output and short generation times compared to those of domesticated land animals.

There are several reasons for this contrast between the success in the domestication of land and marine animal species. First, land domestication has drawn largely from mammals and birds, with few invertebrates (such as bees and snails) domesticated. In contrast, a diverse array of marine taxa—including mollusks, crustaceans, vertebrates, echinoderms, jellyfish, and worms—have been domesticated (*9*, *10*). Many more wild marine species are used as food [more than 3000 marine species compared to fewer than 200 land species (*9*, *11*, *12*)], providing further scope for future domestication.

Second, the greater diversity of life forms in the ocean compared to those on land provides a broader range of opportunities for domestication. The limited success in domesticating land animal species has been attributed to the paucity of suitable species: Many land plants are poisonous or toxic to humans, and many land animal species have slow growth and long life cycles, specialized diets, or adverse behavioral traits (*3*).

Third, aided by the rapid spread of technical and scientific knowledge, domestication of aquatic species is developing globally, whereas land species were domesticated in just a few regions (*1*–*3*). A similar global effort to domesticate additional land animal species is precluded by the paucity of candidate species and the lack of market demand.

The domestication of an aquatic species typically involves about a decade of scientific research (*13*). Current success in the domestication of aquatic species results from the 20th-century rise of knowledge on the basic biology of aquatic species and the lessons learned from past success and failure. The domestication of aquatic species also involves fewer risks than that of land animals, which took a large toll in human lives through diseases transferred from herds (*3*); no human pathogens of comparable virulence have yet emerged from aquaculture.

The stagnation in the world's fisheries and overexploitation of 20 to 30% of marine fish species (*11*) have provided additional impetus to domesticate marine species, just as overexploitation of land animals provided the impetus for the early domestication of land species (*2*). Aquaculture production has been growing at rates of ~7 to 8% per year (*5*), compensating

C. M. Duarte and N. Marbà are at IMEDEA (CSIC-UIB), Instituto Mediterráneo de Estudios Avanzados, 07190 Esporles, Mallorca, Spain. E-mail: carlosduarte@imedea.uib.es M. Holmer is in the Institute of Biology, University of Southern Denmark, 5230 Odense M, Denmark.

for the stagnation of fisheries, and is likely to become the main source of marine food for humans as demands continue to grow.

The broad range of domesticated marine species helps to integrate the production across trophic levels, thereby maximizing output while decreasing environmental impact (*14*). It also increases the range of marine habitats where aquaculture can be conducted, and diversifies food sources and generates a wide range of market prices for aquaculture products. However, aquaculture development also has negative consequences for the environment and biodiversity, including deterioration of coastal ecosystems by aquaculture effluents and impacts on wild species used as feed (*15*). The continuity of present rates of domestication and the capacity of aquaculture to meet the rising demands for seafood of a growing human population require that, by minimizing environmental impact, a sustainable model be achieved. Domestication should aim at closed production cycles, where feed is produced in the farm and the target organisms reproduce and grow from egg to adult in culture, reducing pressures on wild stocks.

The increase in aquaculture has global consequences, both as a food source and in terms of environmental implications. The development of aquaculture is bound to replace fisheries as animal husbandry replaced hunting on land. This should help release pressure on increasingly scarce freshwater resources used to produce food on land, and stimulate technological developments. These changes will modify employment and livelihood patterns of those involved in this industry. The growth in the domestication of marine biodiversity thus represents a fundamental change in the way humans relate to the oceans.

Global pace of species domestication

Species group	Number of species domesticated	Time since domestication (years before present)		Specific growth in the number of domesticated species (% year^{-1})
		50% species domesticated	90% species domesticated	
Land plants	250	4000	2000	0.026 (76)
Land animals	44	5000	146	0.014 (30)
Freshwater animals	180	22	4	3.4 (180)
Marine animals	250	19	4	3.3 (250)
Marine plants	19	32	<10	2.5 (19)

Rates of change. The numbers of presently domesticated species, the times by which 50% or 90% were domesticated, and the rates of domestication differ widely between land and aquatic species. In the last column, the specific growth in the number of domesticated species is defined as the percent increase in the number of species domesticated per year over the period of fastest domestication rates (*6*); the number of species for which domestication dates were available is given in parentheses.

References and Notes

1. D. Normile, *Science* **275**, 309 (1997).
2. A. M. Mannion, *Progr. Phys. Geogr.* **23**, 37 (1999).
3. J. Diamond, *Nature* **418**, 700 (2001).
4. E. B. Hale, in *The Behaviour of Domestic Animals*, E. S. E. Hafez, Ed. (Bailliere, Tindall and Cassell, London, 1969), pp. 22–42.
5. FAO, *State of World Aquaculture: 2006. FAO Fisheries Technical Paper. No. 500.* (UN Food and Agriculture Organization, Rome, 2006); see www.fao.org/fidefault.asp.
6. Materials and methods are available as supporting material on *Science* Online.
7. B. Groombridge, M. D. Jenkins, Eds., *Global Biodiversity: Earth's Living Resources in the 21st Century* (World Conservation, Cambridge, UK, 2000).
8. P. Sorgeloos, *World Aquaculture* **30**, 11 (1999).
9. FAO, *Fishstats. FAO Fishery Information, Data and Statistics Unit (FAO-FIDI). 2004—Collation, Analysis and Dissemination of Global and Regional Fishery Statistics. FI Programme Websites* (UN Food and Agriculture Organization, Rome, 2006); see www.fao.org/fi/default.asp.
10. P. J. W. Olive, *Hydrobiologia* **402**, 175 (1999).
11. FAO, *FAOSTAT-Agriculture* (UN Food and Agriculture Organization, Rome, 2006); see www.faostat.fao.org/default. aspx.
12. R. S. V. Pullin, in *Biodiversity, Science and Development: Toward a New Partnership*, F. Di Castri, T. Younes, Eds. (Cambridge Univ. Press, Cambridge, UK, 1996), pp. 409–423.
13. L. Curry Woods III, *Aquaculture* **202**, 343 (2001).
14. A. Neori *et al.*, *Aquaculture* **231**, 361 (2004).
15. R. L. Naylor *et al.*, *Science* **282**, 883 (1998).

16. Supported by the projects SAMI and MarBEF Network of Excellence, funded by the European Commission. We are indebted to Y. Olsen and D. Soto for insights and comments that have greatly improved this work, J. Guieu for help in compiling data, and S. Agusti and S. Zanuy for helpful suggestions.

Supporting Online Material
Materials and Methods
Table S1
References

10.1126/science.1138042

EVOLUTION

Aging and Sexual Conflict

Aging of male organisms and of their sperm reduces fertility and embryo viability, leading to evolutionary conflict between the sexes.

Rebecca Dean, Michael B. Bonsall, Tommaso Pizzari

In many human societies, men are becoming fathers increasingly late in life, and it is estimated that fertility problems experienced by one-third of couples can be attributed to male factors, including aging (*1*). Aging can affect male reproductive success through two processes, each with distinct evolutionary implications: the age of the male and the age of his sperm. Recent empirical studies demonstrate that both male aging and sperm aging may have a dramatic impact on fertility, embryo viability, and ultimately on the evolutionary conflict between sexual partners, known as sexual conflict.

Male fertilizing efficiency is especially important in species where females mate with multiple males and the ejaculates of different males compete for fertilization, a process called sperm competition. One recent study of the hide beetle (*Dermestes maculates*) (*2*) reveals that male aging may be an important determinant of the outcome of sperm competition. The study analyzed fertilization success in two scenarios: when the ejaculates of two males were inseminated into a female (sperm competition), and when the ejaculate of only one male was inseminated (absence of sperm competition). The study demonstrates that the fertilizing ability of an ejaculate peaks at an intermediate male age. Most young males copulated with females but only 36% of them had developed mature sperm, indicating that most young males were not sexually mature. Similarly, although all old males produced mature sperm, some of them failed to transfer sperm during mating (aspermic copulation). Males in their prime (intermediate age), on the other hand, never failed to inseminate a female. Moreover, in sperm competition, their ejaculates outcompeted those of old and young males in fertilizing the eggs of a female. These results confirm earlier work on this species showing that a female incurs

The authors are at the Edward Grey Institute, Department of Zoology, University of Oxford, Oxford OX1 3PS, UK. E-mail: tommaso.pizzari@zoo.ox.ac.uk

fertility costs when she mates with either a young or an old male (*3*).

This recent hide beetle study also indicates that the propensity of a female to mate with a particular male will depend on his age. The age-dependent risk of aspermic copulation and associated fertility costs thus favor female preference for partners of intermediate age to ensure fertilization. Similarly, we would expect a female to be more likely to re-mate after copulation with either a young or an old male. Whereas the ejaculates of intermediate-age males thrive in sperm competition, it would be particularly advantageous for young and old males, who produce less competitive ejaculates, to defend paternity by preventing females from re-mating with other males, thus imposing fertility costs on females. A cheap way to inhibit female propensity to re-mate may be precisely to perform aspermic copulations (*4*), which could explain why sperm-depleted young and old males still copulate with females. Therefore, the effect of male aging on fertilizing efficiency may be a critical factor underlying female partner choice and re-mating strategies. Ultimately, male aging sets the scene for evolutionary conflict over mating between two prospective partners.

In addition to male age effect on fertility rates, the impact of male age on gamete health also factors into reproductive costs. The DNA carried by sperm cells produced by old males may accumulate deleterious genetic mutations and thus cause developmental defects and reduced viability of the embryo. For instance, strong links have been revealed between male age and frequencies of sperm with DNA fragmentation and gene mutations associated with achondroplasia (*5*), a genetic disorder leading to drastically shortened bones. Therefore, in addition to fertility costs, inseminations by old males—when they do result in fertilization—may also reduce offspring quality, creating another source of conflict: sexual conflict over fertilization.

Damage to sperm DNA may also occur through sperm aging, independently of male aging. In several species, females store sperm over prolonged periods before fertilization, increasing the risk of sperm damage by such conditions as oxidation. For example, in kittiwakes (*Rissa tridactyla*), a colonial gull (see the figure), males face a low risk of sperm competition and copulate frequently with their social partner. Two weeks before a female starts ovulating, the pair is already copulating, and the female displays on average a 0.4 probability of ejecting an ejaculate shortly after copulation. The probability of a female ejecting the ejaculates of her partner declines linearly over successive days as ovulation approaches, suggesting that females may be biasing fertilization in favor of fresher ejaculates (*6*). Consistent with this idea, fertilization by sperm from early ejaculates (that is, from older sperm) results in hatching failure and reduced offspring quality (*6*, *7*). Similar female strategies occur in crickets (*Acheta domesticus*) and fruit flies (*Drosophila melanogaster*), where females appear to bias the outcome of sperm competition by preferentially using fresher inseminations (*8*, *9*).

Age matters. Sperm may suffer reduced fertilizing efficiency and high mutational load as a male ages. In addition, individual sperm cells age when stored for prolonged periods of time in the male before ejaculation and when stored in the female after insemination. This may reduce fertilizing efficiency and offspring fitness. Recent studies (*6*, *7*) in kittiwakes (shown) reveal that a female may be selected to bias fertilization in favor of more recent inseminations by her partner to reduce costs associated with fertilization by old sperm.

Sperm aging adds another source of sexual conflict over fertilization to that generated by sperm damage due to male aging. Fertilization by old sperm increases the reproductive success of the sperm donor but reduces the reproductive success of a female and the fitness of her offspring relative to fertilization by young sperm. These studies (*6*–*9*) therefore reveal that when current mating does not reduce the future reproductive success of a male (that is, mating is relatively cost-free), males are selected to re-mate with the same female to top up sperm reserves with fresh sperm. However, when male mating costs exceed a threshold, it is more advantageous for a male to inseminate new females rather than re-mate with the same female. Therefore, when the risk of sperm competition is sufficiently high and mating is costly for the male, males will impose fertilization by old sperm whereas females will be selected to avoid it.

Together, these recent studies highlight that distinct aging processes—at the organism and gamete levels—play critically different roles in sperm competition and lay out different battlegrounds for evolutionary conflict between the sexes. Reduction in fertilizing ability due to male aging is expected to influence female partner choice and generate sexual conflict over mating; reduction in offspring viability due to male and sperm aging, on the other hand, generates sexual conflicts over fertilization. Unraveling the mechanisms that underlie male aging and sperm aging not only provides a clearer picture of how reproductive strategies evolved, but may also help us to better manage male infertility problems in human societies.

References and Notes

1. V. Chow, A. P. Cheung, *J. Reprod. Med.* **51**, 149 (2006).
2. T. M. Jones, R. Featherston, D. B. B. P. Paris, M. A. Elgar, *Behav. Ecol.* **18**, 251 (2006).
3. T. M. Jones, M. A. Elgar, *Proc. R. Soc. London B* **271**, 1311 (2004).
4. H. Løvlie, C. K. Cornwallis, T. Pizzari, *Curr. Biol.* **15**, 1222 (2005).
5. A. J. Wyrobek *et al.*, *Proc. Natl. Acad. Sci. U.S.A.* **103**, 9601 (2006).
6. R. H. Wagner, F. Helfenstein, E. Danchin, *Proc. R. Soc. London B* **271**, S134 (2004).
7. J. White *et al.*, *J. Ornithol.* **147**, 88 (2006).
8. K. Reinhardt, M. T. Siva-Jothy, *Am. Nat.* **165**, 718 (2005).
9. R. R. Snook, D. J. Hosken, *Nature* **428**, 939 (2004).

10. The authors are supported by the Natural Environment Research Council. M.B.B. is also supported by the Royal Society.

10.1126/science.1142201

Fresh angles on the science of education

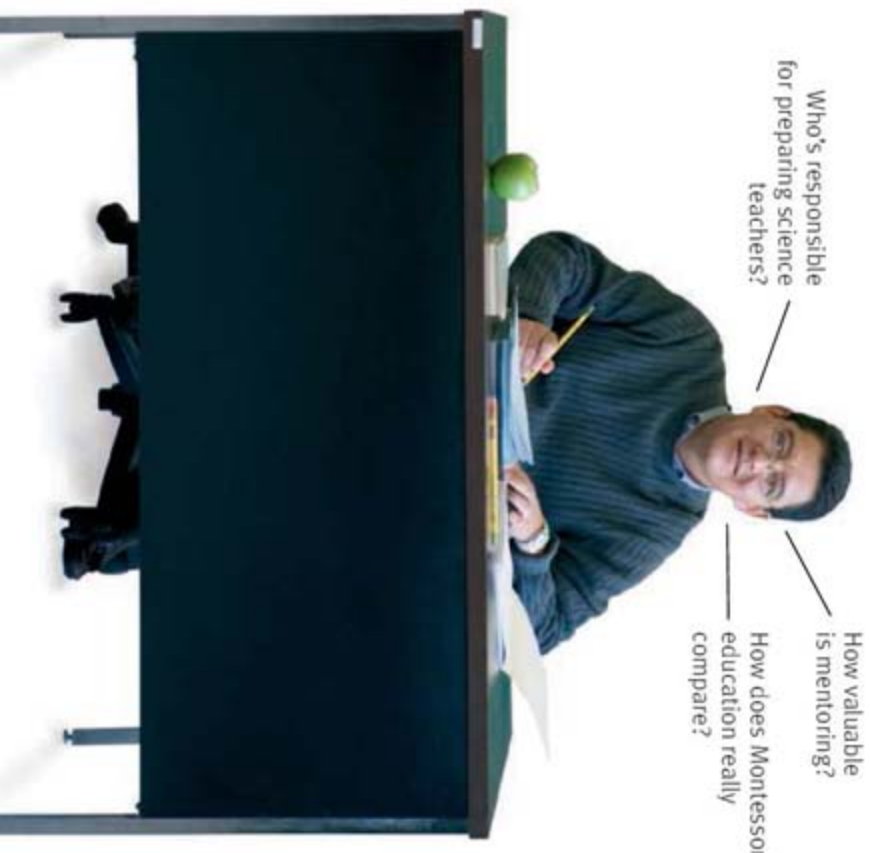

A wealth of knowledge

The *Science* Education Forum is a dynamic source of information and new ideas on every aspect of science education, as well as the science and policy of education. The forum is published in the last issue of every month and online, in collaboration with the Howard Hughes Medical Institute.

Keep up-to-date with the latest developments at: www.sciencemag.org/education

What's your perspective?
Do you have ideas or research you'd like to share in the *Science* Education Forum? We're now looking for thoughtful, concise submissions (around 2,000 words) for 2007. To submit your paper, go to: www.submit2science.org

Science

AAAS

AAAS
ADVANCING SCIENCE, SERVING SOCIETY

CONTACT US

To Join
1-866-434-AAAS (2227)
www.aaas.org/join

Customer Service
202-326-6417 phone
202-842-1065 fax
E-mail: membership@aaas.org

Annual Meeting
202-326-6450
E-mail: aaasmeeting@aaas.org
www.aaasmeeting.org

International Programs
202-326-6650
www.aaas.org/international

Project 2061
202-326-6666
www.project2061.org

Education & Human Resources
202-326-6470
ehrweb.aaas.org

Science and Policy Programs
202-326-6600
www.aaas.org/spp/

Media and Public Programs
202-326-6440
E-mail: media@aaas.org

***Science* Books & Films**
www.sbfonline.com

Fellowships
www.fellowships.aaas.org

EurekAlert
202-326-6716
E-mail: webmaster@eurekalert.org
www.eurekalert.org

www.aaas.org
American Association for the Advancement of Science
1200 New York Avenue, NW
Washington, DC 20005 USA

INTRODUCTION

The Transitioning Germ Line

GERMLINE CONSTANCY IS A MUST FOR SPECIES CONTINUITY, BUT THE LIFE OF THE germ cell itself is full of change. The trek to and from the germ line includes numerous transitions and decisions deftly choreographed for the gametes' unique ability in nature to develop into a complex animal and pass on genetic information. This special section highlights the transitioning germ line and otherwise expands on intriguing aspects of these cells of heredity.

In the early embryo, cells decide between becoming soma or germ line. Mechanisms protect germ cells from a somatic fate, just as somatic cells require insulation from the germline differentiation pathway. Strome and Lehmann (p. 392) outline activities in the fly and worm, such as transcriptional quiescence and inheritance of germ cell determinants, and Hayashi *et al.* (p. 394) tell of the murine system, invoking an inductive signal. Although model systems use different strategies, common themes exist.

A new class of molecules reportedly participates in germ cell development. Lin (p. 397) describes the generation and role of germline-specific small RNAs termed piRNAs. Functions as diverse as posttranscriptional regulation and epigenetic programming are suggested. Another epigenetic event—de novo DNA methylation—silences imprinted genes and repeat elements during vertebrate gametogenesis. Schaefer *et al.* (p. 398) detail this heritable silencing mechanism and its sexual dimorphism.

As the germ cell transitions to the mature form, more decisions are made: to enter mitosis or meiosis and to differentiate as sperm or egg, with possible linkage of these decisions as proposed by Kimble and Page (p. 400). Stem cell self-renewal versus differentiation in the *Drosophila* male and female germ lines is discussed by Fuller and Spradling (p. 402). Switching to vertebrate germline stem cells, Brinster (p. 404) reports methods for the recovery, culture, and transplantation of spermatogonial stem cells; and Daley (p. 409) summarizes advances in embryonic stem cell (ESC) differentiation to a germline fate: procedures with research and clinical applications but not without limitations. In an Editorial, McLaren (p. 339) takes the discussion further, highlighting ethical and social issues surrounding ESC-derived germ cells.

Changes continue as the oocyte transitions to the fertilized egg. Stitzel and Seydoux (p. 407) detail the oocyte-to-zygote transition, with associated alterations in protein synthesis, protein and RNA degradation, and organelle remodeling; and Schier (p. 406) discusses zygotic genome silencing and maternal messenger RNA degradation around the maternal-zygotic transition.

In News, Travis (p. 390) discusses "urbisexuality" with a biologist pondering the evolution of germ cell specification, and Leslie (p. 388) details how oocyte freezing has become more effective and acceptable despite questions about the long-term health of offspring. Finally, in *Science*'s STKE, McClure discusses how poppies reject self-pollen, and Boldajipour and Raz highlight similarities in *Drosophila* and mouse mechanisms involved in the migration of primordial germ cells and elimination of ectopic cells.

The articles here give but a sampling of exciting ongoing research on the seeds of life—themselves products of change. Advances bear fruit in understanding development and its underlying genetics, as well as infertility.

—BEVERLY A. PURNELL AND JOHN TRAVIS

Germ Cells

CONTENTS

See also related Editorial page 339; STKE material on page 333 or at www.sciencemag.org/sciext/germcells/

Science

Better cold? Freezing a human egg without damaging or killing it is tricky.

CREDIT: MICHAEL MARSLAND/YALE UNIVERSITY

NEWS

Melting Opposition to Frozen Eggs

Oocyte cryopreservation is starting to mature now that researchers have developed a faster, better way of freezing the vulnerable cells

UNDER THE HOT DESERT SUN IN PHOENIX, Arizona, something chilling is going on. Human eggs are slowly being iced down at what has been called the world's first bank offering frozen, donated eggs. For about $2500, Cryo Eggs International, the company running the bank, will sell an infertile woman an egg from one of its carefully screened donors. One egg won't be enough—women typically order six to eight to boost the odds of pregnancy—and the price doesn't include shipping in a liquid nitrogen–cooled container, which can run $200 for a U.S. address and around $1000 for delivery to Europe.

Some ethicists and physicians decry the selling of donated eggs because obtaining them from a woman involves hormone injections and a surgical procedure that can cause side effects. But Cryo Eggs's business plan is significant not because it raises new ethical issues—after all, women have been donating eggs for decades and even been getting paid—but because it signals that the practice of egg freezing has reached a new stage. And some say it's about time, given how unfair fertility is. A typical man has almost a lifetime to become a father, but a woman's reproductive prime lasts only a decade or so—and coincides with the critical time for getting an education and establishing a career.

Men facing cancer treatment that might render them sterile also have an advantage over women. They can freeze sperm for later use with in vitro fertilization (IVF)—some physicians even plan to store sperm stem cells from prepubescent boys scheduled for similar cancer therapy (See Brinster Review, p. 404).

But eggs have been difficult to freeze. As the largest cell in the human body, an egg brims with water that can form damaging ice crystals. "The problem with eggs is that they are sensitive to low temperature," says Juergen Liebermann, scientific director of the Fertility Centers of Illinois in Chicago.

However, recent technical refinements to egg freezing, also known as oocyte cryopreservation, may soon even out some of the reproductive inequalities between men and women. Although some scientists remain cautious about its effectiveness and safety, others argue that cryopreservation is ready for widespread use—not just to help cancer patients secure their fertility but also to give women more control over when they start families. The technology has already jumped beyond the realm of research. For the last 3 years, Extend Fertility, based in Woburn, Massachusetts, has marketed its services as an option for career-minded women who want to put aside oocytes to be thawed years or even decades later, when their jobs are secure or they've found the right partner. Cryo Eggs's donor bank opened the same year. Fertility clinics now offer elective egg storage.

Early frost

Oocyte cryopreservation sidesteps some of the practical and ethical pitfalls of IVF, says Jeffrey Boldt, an embryologist at Community Health Networks in Indianapolis, Indiana, who is also a partner in and scientific director of Cryo Eggs. For example, what to do with "spare" embryos that aren't implanted poses a dilemma, he says. Many couples are loath to discard them, and it's illegal to use them for federally funded research. Moreover, divorcing couples have fought for custody of frozen embryos in court, just as they would over children, notes clinical embryologist Michael Tucker of Georgia Reproductive Specialists in Atlanta. Fertility specialists in countries such as Italy and Germany face a different legal difficulty: Embryo freezing is forbidden.

Frozen oocytes obviate some of these concerns. For example, people may be less squeamish about tossing out a gamete than an embryo, Boldt says. And if spare oocytes are on ice, he adds, doctors shouldn't need to create as many embryos. Custody battles also shouldn't erupt, says Tucker: A woman's eggs are her own.

As welcome as egg-freezing is, the trick has been getting it to work. The first reports of pregnancies from thawed oocytes date back to 1986, just 3 years after the first birth from a frozen embryo. Although the use of frozen embryos created by IVF boomed, technical hurdles have largely excluded cryopreserved eggs from the clinic. Depending on who's counting, frozen oocytes account for a total of 300 to 600 babies worldwide, compared with the roughly 300,000 births from frozen embryos.

One reason for the slow acceptance of frozen oocytes in the 1980s and 1990s is that the IVF techniques then used were much less successful fertilizing thawed eggs than fresh ones. In addition to ice crystals, freezing an egg toughens the zona pellucida, the membrane around the egg that the sperm has to burrow through.

Another factor that gave people pause was concern about possible birth defects. Eggs are also susceptible to cold because a mature oocyte is stalled in the middle of meiosis, the

double division that parcels out the chromosomes to yield gametes. The chromosomes are hitched to the spindle, a network of microtubules that will help separate them if fertilization occurs. Even a slight drop below body temperature triggers a "chilling injury" to an egg, notes Stanley Leibo, a cryobiologist at the University of New Orleans in Louisiana. The spindle falls apart as the microtubules depolymerize. Although the structure reforms when temperatures rise, researchers haven't ruled out lasting damage from the disruption, such as abnormal numbers of chromosomes in the egg and rare birth defects.

Freezing saps sperm, too, killing about 50% of them, says reproductive endocrinologist Kutluk Oktay of Weill Medical College of Cornell University in New York City. But the prodigious numbers in a semen sample usually ensure that enough healthy ones survive thawing to permit fertilization, he says.

A shot in the egg for cryopreservation

The advance that revived egg freezing, says reproductive endocrinologist Richard Paulson of the University of Southern California (USC) in Los Angeles, was intracytoplasmic sperm injection (ICSI). The technique, which researchers first tested on frozen human oocytes in 1995, shoots the sperm through the cold-hardened zona pellucida directly into the egg. "I'm surprised they got any fertilizations at all without it," says Paulson. In 1997, Eleonora Porcu of the University of Bologna in Italy and colleagues reported the first birth from ICSI on a thawed oocyte.

A new technique for freezing eggs might produce just as large an impact as ICSI. Bathing eggs in cryoprotectant molecules such as propanediol, ethylene glycol, and sucrose can shelter the cells from ice damage but doesn't eliminate it. The solution, many scientists now say, is a method for superfast chilling known as vitrification.

The standard slow-freezing method—the technique Cryo Eggs uses with some modifications—entails gradually cooling the egg over about 90 minutes in a computer-controlled freezer. By contrast, fast-freezing involves dunking the egg into liquid nitrogen; it vitrifies, or transforms into a glassy material. The idea behind vitrification, says Leibo, is to "outrun chilling injury," freezing the egg before ice can crystallize.

Although only about 100 babies have been born from vitrified eggs, some researchers are already calling the method the future of oocyte cryopreservation. As Liebermann notes, recent statistics suggest that it boosts egg survival and fertilization over slow freezing, reducing the average number of oocytes required to produce a live birth from more than 50 to between 27 and 30.

Ready for prime time?

Hundreds of seemingly healthy babies around the world prove that oocyte cryopreservation works. But is it safe and efficient enough to become a standard part of assisted reproduction? In an analysis published last year in *Fertility and Sterility*, Oktay and colleagues pooled results of 26 studies on oocyte cryopreservation dating from 1997 to 2005, covering 97 children. Overall, slow-frozen eggs fell short of fresh ones on every measure, including fertilization rate and implantation rate. (There weren't enough data on vitrification to compare it to slow freezing, the researchers determined.) Porcu says that her experience is similar. About 3% to 4% of frozen eggs will yield a baby, versus 6% to 8% of fresh eggs, she says.

For many physicians and ethicists, the statistics back limited use of cryopreservation. Guidelines released by the American Society for Reproductive Medicine (ASRM) last fall regard the procedure as experimental and endorse it only for preserving fertility in women with cancer—as long as there's institutional review board supervision. An alternative that might enable women to retain their egg-producing capacity—freezing ovarian tissue and reimplanting it after treatment—is still for research only, the guidelines conclude. Moreover, ASRM advises against making elective egg freezing commercially available, citing the lack of long-term studies on babies' health. Oktay, who headed the ASRM committee, notes that freezing an egg effectively ages it 8 or 9 years. So unless a woman plans to wait longer than that to try to get pregnant, she is better off using her own fresh eggs.

Other fertility experts contend that the time is ripe for egg freezing, given the lack of alternatives. Although ethicists railed when Extend Fertility began advertising elective egg freezing to young women, the practice has spread, especially in the United States, where fertility clinics are un-regulated. How many facilities offer it now isn't certain, says Oktay. His clinic doesn't. But Paulson's USC clinic does. "I don't feel I can deny access to this technology" to well-informed patients, he says. The procedure "levels the field for men and women" reproductively.

Boldt also argues that the evidence backs the use of frozen eggs in fertility treatments for more than just cancer patients. "The technology is there to look at [egg banking] as a realistic option," he says. Boldt adds that frozen oocytes even offer advantages over fresh ones; the IVF procedure is simpler because the egg donor and recipient don't need to be reproductively synchronized.

Researchers agree on what's missing from our understanding of egg freezing: a clear picture of the health of the resulting children. Although some scientists have offered preliminary results for small numbers of children, no one has conducted a long-term, comprehensive study of babies born from defrosted eggs. That could soon change. Porcu and colleagues are working to create an Internet database in which clinicians can record information. The timing is apt. The oldest offspring are entering their reproductive years, so it will be possible to determine whether their fertility is normal. That research might tell us more about whether egg freezing deserves a warm reception.

–MITCH LESLIE

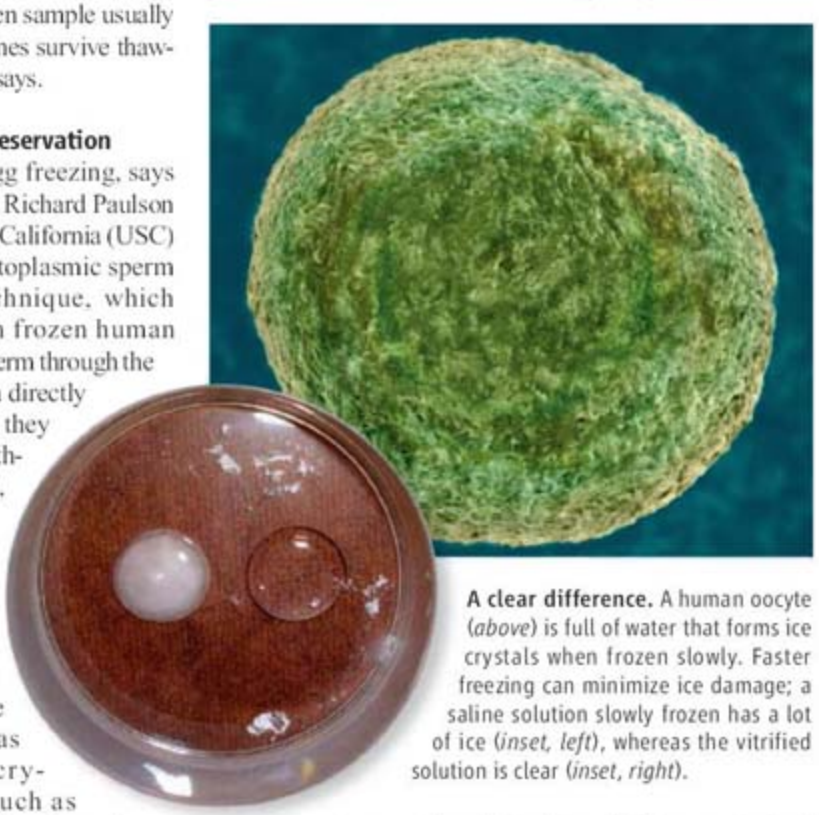

A clear difference. A human oocyte (*above*) is full of water that forms ice crystals when frozen slowly. Faster freezing can minimize ice damage; a saline solution slowly frozen has a lot of ice (*inset, left*), whereas the vitrified solution is clear (*inset, right*).

CREDITS (TOP TO BOTTOM): COPYRIGHT DENNIS KUNKEL MICROSCOPY INC.; JUERGEN LIEBERMANN

NEWS

A Close Look at Urbisexuality

A developmental biologist takes aim at understanding the evolutionary origins of eggs and sperm in our 600-million-year-old ancestor

For a creature no one has ever seen and never will see alive, Urbilateria generates a lot of passion. Scientists have vigorously debated whether it sported legs or antennae, whether it had a true heart, and whether its body was segmented. Such arguments may never be settled, however. Urbilateria is a hypothetical organism that lived 550 million to 800 million years ago and was the last common ancestor of a menagerie that includes mollusks, worms, flies, mice, and people.

Discussions of this mythical creature are more than just pub-fueled speculations at the end of a long day in the laboratory, say practitioners of evo-devo, a field that uses developmental biology to study evolution and vice versa. Although some animals have no anatomical symmetry (sponges) or display radial symmetry (corals and jellyfish), most animal phyla have bilateral symmetry, and Urbilateria would have been their forerunner. As such, Urbilateria offers a framework for thinking about how the current diversity of bilaterians emerged from the twists and turns of evolution.

In 2002, Cassandra Extavour, a postdoc in Michael Akam's laboratory at the University of Cambridge in the U.K., realized something was missing from all the musings on Urbilateria. "So much of evo-devo over the last 20 years centered on what Urbilateria looked like," says Extavour. "But no one [was] talking about how this animal reproduced."

So, in talks at the Society for Integrative and Comparative Biology annual meeting in January, and in book chapters in press, this developmental biologist has begun to discuss what she cleverly calls "urbisexuality." Her approach makes sense, says Adam Wilkins, editor of *Bioessays* and a geneticist who studies sex determination. "We'd like to know what the earliest bilateral animals looked like and acted like, and that includes their reproductive history."

The sex lives of these ancient creatures has eluded Extavour, but she has made progress understanding one of the more fundamental aspects of Urbilaterian reproduction: the origins of their sperm and egg. Her work "is original," says paleobiologist Douglas Erwin of the National Museum of Natural History in Washington, D.C., who has written considerably on the nature of Urbilateria. "It never dawned on me to consider these sorts of issues." Wilkins agrees: "As far as I know, this is the first serious attempt to look at their reproduction." Moreover, Extavour's contemplation of urbisexuality has led her to rethink the evolutionary connections between primordial germ cells, which ultimately make sperm and eggs, and the stem cells that give rise to other tissues.

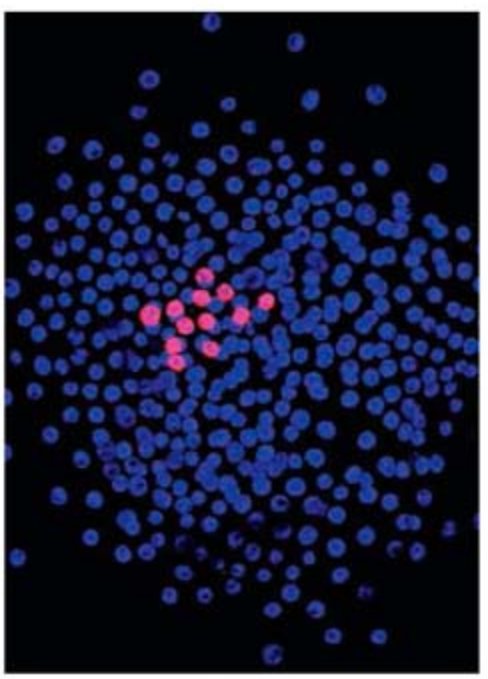

Future sperm or eggs. Antibodies to a protein called Vasa (pink) reveal the relatively few cells in this crustacean embryo destined to become germ cells.

CREDIT: C. G. EXTAVOUR

Humble beginnings

The sexiest questions about urbisexuality obviously concern Urbilateria's sex life. Was the ancient animal hermaphroditic? Or were the sexes of Urbilateria separate, and if so, did reproduction rely on external or internal fertilization? If the latter were the case, then Urbilateria's gonads would have been quite sophisticated.

Extavour considers the answers to such questions largely unknowable. Typically, evolutionary biologists piece together the lifestyle of a long-gone organism by scanning the modern tips of evolutionary trees for physical traits or developmental genetic networks shared by most of its descendents. Traits in common to a broad spectrum are likely ancestral. But so many reproductive strategies are strewn across every bilaterian phyla that the identification of an ancestral state is probably impossible. Both egg laying and vivipary, in which an embryo develops inside a parent, are seen across all clades, for example, so it's hard for researchers to tell which strategy evolved first.

Picking a more tractable question about urbisexuality, Extavour has concentrated on what got her thinking about Urbilateria in the first place: primordial germ cells. She notes that these germ-cell precursors compete with one another during development within arthropods. The primordial germ cells often arise in one portion of the embryo and migrate relatively long distances to what becomes a gonad; there they develop into sperm or eggs. But studies had shown that only some of the primordial germ cells win this race to the gonad; the latecomers vanish from the embryo's so-called germ line, its eggs or sperm. This example of survival of the fittest—or fastest—led Extavour to take a broader Darwinian look at primordial germ cells. "I started to think about the role of germ cells in evolution and began wondering how different animals make germ lines," she says.

Much has been written about when and why animals first evolved a germ line. Some researchers have even argued that the emergence of specialized reproductive cells distinct from other tissue—the soma—was a prerequisite for multicellular organisms. Extavour agrees with that thinking. So, assuming that a germ line predated Urbilateria, she asked how certain cells in an Urbilateria embryo ended up as the animal's germ cells, not a heart or a nerve cell.

Modern organisms typically use one of two methods to give germ cells their unique identity. By one route, preformation, part of an unfertilized egg's cytoplasm contains a distinctive mix of proteins, chemicals, and genetic instructions. This material is the so-called germplasm. As the egg divides and redivides, bits of germplasm wind up in some cells but not others. Inside those cells, it sets off a genetic cascade. Genes such as

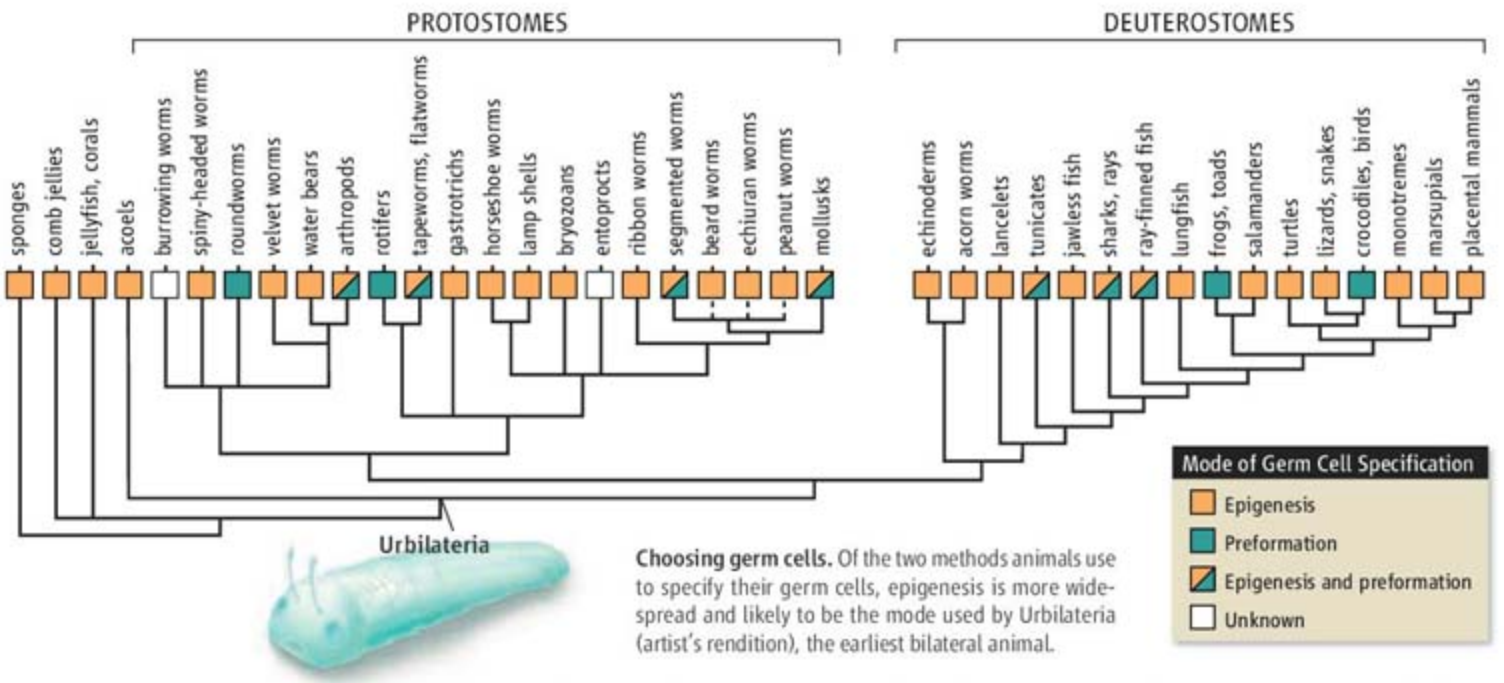

Choosing germ cells. Of the two methods animals use to specify their germ cells, epigenesis is more widespread and likely to be the mode used by Urbilateria (artist's rendition), the earliest bilateral animal.

vasa and *nanos* become active, for example, and help prepare those cells for a future as eggs or sperm. In animals relying on preformation, that germplasm is retained or restocked within new oocytes; thus, it is inherited from generation to generation.

Where there is no germplasm, epigenesis comes into play. All the cells in the embryo start out apparently equal. But as the embryo grows, certain cells release chemicals that force their neighbors to become the germ line. The question for Urbilateria: Do the cells that decide to become its primordial germ cells "inherit something or get an instruction?" asks Extavour.

The mouse relies on epigenesis: Certain embryonic cells release bone-morphogenic proteins that tell other cells to become germ cells. But the more primitive animals commonly studied in the lab—zebrafish, fruit flies, nematodes, frogs—all depend on germplasm to specify their germ cells, so biologists had assumed that preformation was the ancestral state. In a 2003 review of existing data on 28 animal phyla, however, Extavour and Akam found little cytological, cell lineage, or experimental data to indicate preformation in most species. They concluded that epigenesis was very widespread and that it probably arose first.

From stem cells to germ cells?

Extavour has continued to amass data supporting that surprise and has also developed a model of how preformation could have arisen in some of Urbilateria's descendents. In epigenesis, many of the molecules inside primordial germ cells that drive the cells' differentiation into sperm or eggs vanish once that job is done. Extavour thinks that at some point post-Urbilateria, a mutation occurred that allowed those factors to persist in an oocyte—voilà, preformation. It could have been a simple matter of keeping genes such as *vasa* and *nanos* turned on in oocytes instead of turning them off—so simple, in fact, that Extavour suspects this happened multiple times on different evolutionary branches. If that's true, she speculates, there are modern animals able to employ both modes of germ cell specification. Even so, their embryos likely rely on only one.

"Of all the evo-devo stories, Extavour's work is among the most interesting," says Helen White-Cooper of the University of Oxford, U.K., who studies germ-cell development in fruit flies. To strengthen her case, Extavour should try to confirm whether an animal known to rely upon preformation "might be able to use another mechanism if forced," White-Cooper suggests. Indeed, Extavour and collaborators are now doing just that.

Next, Extavour wants to understand evolutionary links between primordial germ cells and the somatic stem cells that give rise to all the nongermline tissues in an organism. The two cell types share many morphological features, and certain genes that guide somatic stem cell growth appear related to genes active in primordial germ cells. Also, at the most basic level, both classes of cells are close to immortal: They survive and divide for a long time without specializing.

Moreover, researchers have shown that the primordial germ cells of some species, including humans, can act as somatic stem cells, giving rise to more than just reproductive cells. And others are coaxing nongermline stem cells from early embryos to develop into sperm and eggs (*Science*, 23 September 2005, p. 1982).

Cell biologists have considered somatic stem cells to be developmental spinoffs of germ cells because of their similarities in gene expression and differentiation. Twisting that idea a bit, Extavour hypothesizes that germ cells arose as a subset of stem cells. She notes that primitive nonbilateral animals such as sponges and jellyfish maintain stem cells that can give rise to either new somatic cells or gametes. Because the stem cells of sponges and jellyfish are dispersed throughout their bodies, she suggests that Urbilateria's germ cells were similarly scattered. As scientists identify more genes that are active in both primordial germ cells and somatic stem cells and trace their history, Extavour hopes to confirm this evolutionary scenario.

Wilkins, who plans to collaborate with Extavour, calls her unconventional revision of the history of germ cells and stem cells a "big idea." And he thinks Extavour's investigations of urbisexuality will draw others to probe the evolution of germ cells and reproductive systems. The topic, Wilkins laughs, "will become, I can't resist saying, sexier to study." **–JOHN TRAVIS**

CREDIT: ADAPTED FROM C. G. EXTAVOUR AND M. AKAM, *DEVELOPMENT* 130 (2003). THE COMPANY OF BIOLOGISTS LIMITED

REVIEW

Germ Versus Soma Decisions: Lessons from Flies and Worms

Susan Strome[1]* and Ruth Lehmann[2]*

The early embryo is formed by the fusion of two germ cells that must generate not only all of the nonreproductive somatic cell types of its body but also the germ cells for the next generation. Therefore, embryo cells face a crucial decision: whether to develop as germ or soma. How is this fundamental decision made and germ cell fate maintained during development? Studies in the nematode worm *Caenorhabditis elegans* and fruit fly *Drosophila* identify some of the decision-making strategies, including segregation of a specialized germ plasm and global transcriptional regulation.

The *C. elegans* embryo separates the germ lineage from somatic lineages progressively, through a series of four asymmetric divisions (*1*). During each of those divisions, a specialized cytoplasm, or "germ plasm," is partitioned to one daughter cell, the P cell (Fig. 1). After the separation of the germ and soma is complete, the P_4 cell serves as the sole primordial germ cell (PGC). The germline fate of P_4 probably relies on both inheritance of germ plasm components and segregation of somatic differentiation factors away from the germ lineage. In *Drosophila*, the location of germ cells in the embryo is already established during oogenesis, when maternally synthesized germ plasm components assemble at only one pole of the oocyte (Fig. 1). During the initial stages of embryogenesis, the fly embryo divides by nuclear rather than cellular divisions. Those nuclei that enter the posterior germ plasm become PGCs (*2*).

Despite their different formation strategies, both worms and flies rely on the passage of specialized germ plasm from the oocyte to the future germ cells. Induction, an alternative mode of germ cell specification, operates in other organisms, including mice (*3*).

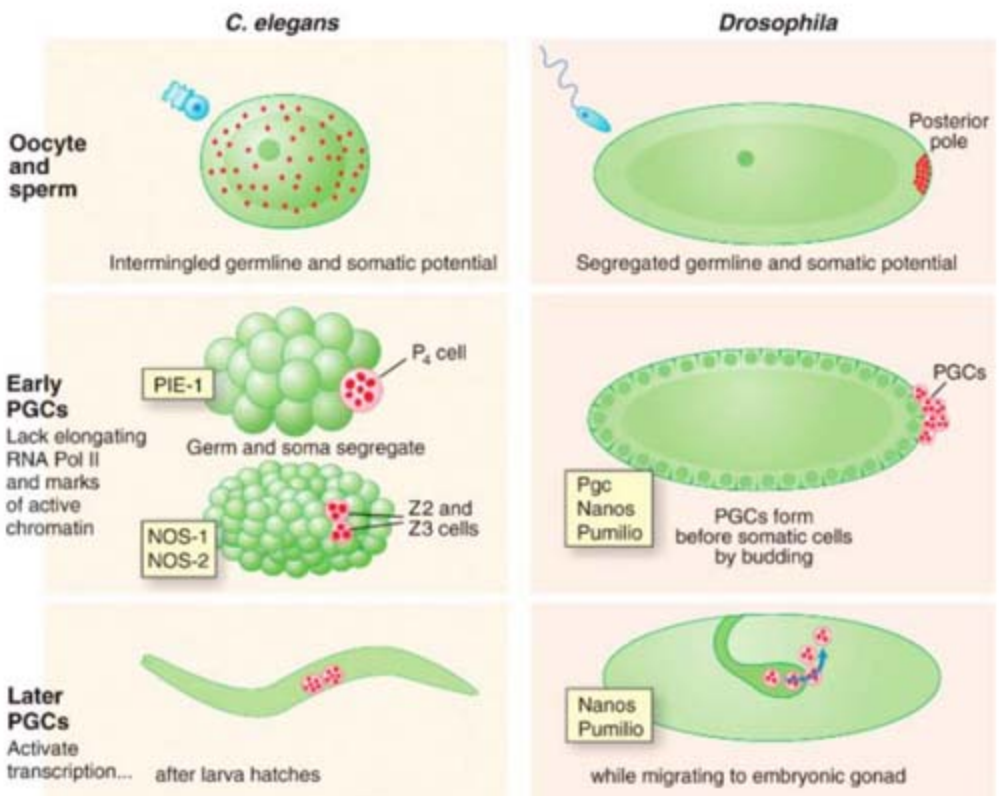

Fig. 1. Formation of PGCs and landmark stages in their development in *C. elegans* and *Drosophila*. Germ plasm is represented by red granules. Key regulators mentioned in the text are noted in yellow boxes. Blue arrow in final panel indicates direction of germ cell migration in *Drosophila*.

Newly Formed Germ Cells Are in a Transcriptionally Repressed State

A common feature of early germ cells in worms and flies is their transcriptional quiescence (Figs. 1 and 2). One likely role is to protect early germ cells from expressing somatic differentiation genes. Transcriptional quiescence is achieved through a repression program that regulates the core transcriptional machinery as well as chromatin states.

The earliest phase of repression is mediated at the level of transcription elongation in both organisms, as the germ line and soma are being separated from each other (*4*). Proteins involved in preventing RNA polymerase II (Pol II) elongation in germ cells have been identified in both organisms. The zinc finger protein PIE-1 is a key regulator in worms (*5*). In embryos that lack PIE-1 activity, newly formed germ cells contain elongating Pol II and produce mature mRNAs (*1*, *4*, *5*). In these mutants, the development of germ cells is similar to that of their somatic sister cells, and the embryos die. Mechanistically, PIE-1 apparently competes with the tail of Pol II for the enzymes that modify Pol II for elongation (*6*). In flies, the peptide Pgc and the translational repressors Nanos and Pumilio control transcriptional silencing (*4*, *7*–*9*). As in *pie-1* mutants, germ cells that lack either Pgc or Nanos activity show elongating Pol II activity and express genes characteristic of somatic cells (*7*, *8*, *10*) (Fig. 2, A, C, D, and F). These "transformed" cells either undergo apoptosis, a somatic cell death pathway, or adopt somatic cell fates (*10*). The mechanism (or mechanisms) by which Pgc and the Nanos and Pumilio translational repressors prevent elongation and the relationship between these regulators are unclear.

A chromatin-based phase of transcriptional repression kicks in soon after P_4 divides to generate the Z2 and Z3 cells, at the ~100-cell stage of worm embryogenesis, when PIE-1 disappears and PIE-1–mediated transcriptional repression ends (*11*). One indicator of this transition is the disappearance from Z2 and Z3 of histone modifications that are associated with transcriptional competence, such as methylation of lysine-4 of histone H3 (H3K4me). One key regulator of the transition is Nanos; H3K4me status is perturbed in Z2 and Z3 depleted of the two Nanos

[1]Department of Biology, Indiana University, Bloomington, IN 47405, USA. [2]Howard Hughes Medical Institute, Skirball Institute, Department of Cell Biology, New York University School of Medicine, New York, NY 10016, USA.

*To whom correspondence should be addressed. E-mail: sstrome@indiana.edu; lehmann@saturn.med.nyu.edu

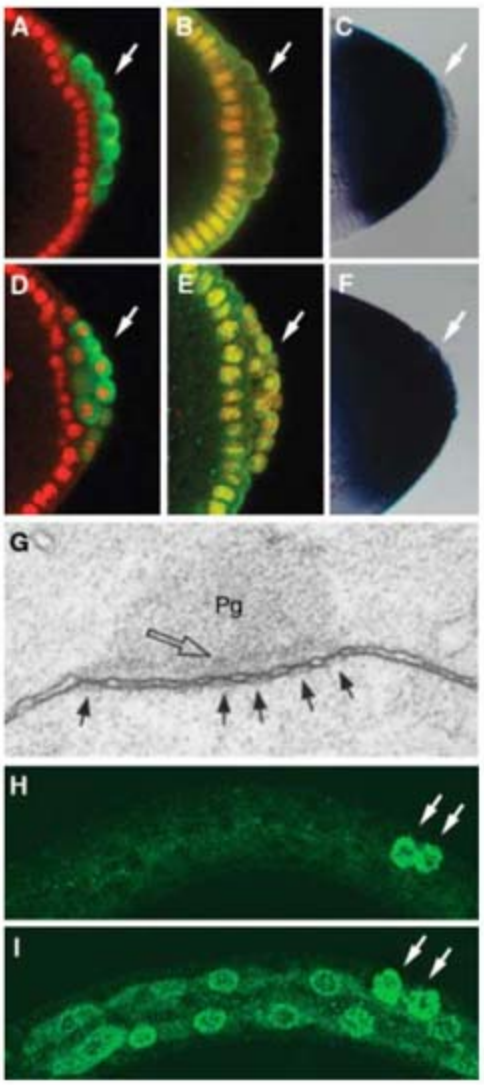

Fig. 2. Germ cell traits. (**A** to **F**) Posterior end of wild-type [(A) to (C)] and *pgc* mutant [(D) to (F)] *Drosophila* blastoderm embryos. The PGCs (arrows) contain the polar plasm component Vasa [green in (A) and (D)]. The somatic nuclei contain elongating RNA Pol II [red in (A), (B), (D), and (E)] and H3K4me [green in (B) and (E)] and produce *tailless* mRNA [blue in (C) and (F)]. In wild-type embryos [(A) to (C)], PGCs (white arrows) lack elongating RNA Pol II, H3K4me, and *tailless* mRNA. In *pgc* mutant embryos [(D) to (F)], PGCs (white arrows) contain those three markers. Overlap of green and red in (B) and (E) appears yellow. Images adapted from (*7*) with permission from Elsevier. (**G**) Electron micrograph of a P granule (electron-dense mass labeled Pg, containing internal electron-dense material marked by an open arrow) overlying five nuclear pores (black arrows) in the adult *C. elegans* germ line. Reprinted from (*17*) with permission from Elsevier. (**H**) Wild-type L1 *C. elegans* larva. P granules are restricted to the two PGCs Z2 and Z3 (arrows). (**I**) *mep-1* mutant L1 larva. P-granule markers (e.g., PGL-1) are ectopically expressed in somatic cells.

homologs NOS-1 and NOS-2 (*11*). In flies, H3K4me is absent from embryonic germ cells from the time they are born. This absence requires Pge and Nanos (*7*, *11*) (Fig. 2, B and E). Transcriptional activity and H3K4me appear as germ cells initiate their migration and Pge disappears (*11*).

Breakdown of the Germ Versus Soma Distinction

Both transcriptional quiescence and translational control protect germ cells from expressing somatic differentiation genes. Germ-to-soma transformations, which resemble teratomas in mammals, highlight the need for insulation of germline cells from conditions or signals that send them down a somatic differentiation pathway. In the adult worm, germ lines lacking the translational regulators GLD-1 and MEX-3 lose their germ granules and express markers characteristic of neurons and muscles (*12*). Conversely, somatic cells may require protection from conditions or signals that send them down a germline differentiation pathway. Loss of some of the *C. elegans* synMuv B chromatin regulators, such as LIN-35/Retinoblastoma and members of the nucleosome remodeling and histone deacetylase (NuRD) complex (e.g., MEP-1), causes somatic cells to display germline traits, such as germ granules and enhanced RNA interference (*13*, *14*) (Fig. 2, H and I). This ectopic expression of germline traits by somatic cells depends on the histone H3K36 methyltransferase MES-4 and the chromodomain protein MRG-1 (*13*–*15*). These chromatin regulators are known to be critical for germline development, but the mechanistic details in the soma are unclear.

Roles of Germ Granules

A distinctive feature of germ cells is possession of specialized germ plasm, which contains unique cytoplasmic organelles generically referred to as germ granules and specifically called polar granules in flies and P granules in worms (Fig. 2, G and H). Polar granules and P granules share some components, such as the RNA helicase Vasa in flies and the related germline helicases (GLHs) in worms, and they contain numerous species-specific proteins, such as Oskar in flies and PGL-1 in worms (*1*, *2*, *4*). Although the precise roles of these granules are still being worked out, it is clear that they are intimately associated with germline fate in all organisms, including those organisms that specify germ cells by inductive signals (*3*).

What roles do germ granules play? Studies in flies and worms suggest that a primary role is in handling RNA. Germ granules are rich in RNA and predicted RNA-binding proteins, and many RNAs and proteins are either specifically localized to or protected from degradation in these granules (*16*). The location of germ granules over nuclear pores positions them to encounter mRNAs during their transport from the nucleus and may contribute to control of mRNA translation and localization within the cytoplasm (*17*, *18*) (Fig. 2G). Functionally, germ granules may be related to P bodies. The latter have been shown in yeast and mammalian cells to participate in mRNA decay, RNA interference, and translation inhibition by microRNAs. Many P-body proteins are found in germ granules in worms and flies (*19*–*22*). Germ cells appear to be particularly dependent on RNA-based regulation and may benefit from consolidating RNA-processing machinery into large granular assemblies. Throughout the life cycle, however, germ granules are dynamic in morphology, composition, and RNA regulatory function. P body–like activities may thus be only one aspect that regulates germline fate.

Summary and Outlook

Flies and worms share several strategies to establish and maintain germ cells and protect them from somatic fates. Both systems segregate specialized germ plasm to the PGCs. The RNA-rich granules in germ plasm serve roles in localization, protection, and translation of mRNAs. Although mammalian germ cells are not specified by segregated germ plasm, they do contain germ plasm components. Transcriptional repression in early PGCs is a common theme to prevent PGCs from differentiating in the same way as their somatic neighbors, although the regulators—worm PIE-1, fly Pge, and mammalian Blimp1—differ between species (*3*). Studies across species promise to provide more mechanistic insights into how germ plasm and transcriptional regulation specify germ cells in the early embryo and protect germ cell fate throughout life.

References and Notes

1. S. Strome, in *WormBook*, The *C. elegans* Research Community, Ed. (WormBook, www.wormbook.org, 2005), 10.1895/wormbook.1.9.1.
2. A. C. Santos, R. Lehmann, *Curr. Biol.* **14**, R578 (2004).
3. K. Hayashi, S. M. Chuva de Sousa Lopes, M. A. Surani, *Science* **316**, 394 (2007).
4. G. Seydoux, R. E. Braun, *Cell* **127**, 891 (2006).
5. G. Seydoux, M. A. Dunn, *Development* **124**, 2191 (1997).
6. F. Zhang, M. Barboric, T. K. Blackwell, B. M. Peterlin, *Genes Dev.* **17**, 748 (2003).
7. R. G. Martinho, P. S. Kunwar, J. Casanova, R. Lehmann, *Curr. Biol.* **14**, 159 (2004).
8. G. Deshpande, G. Calhoun, T. M. Jinks, A. D. Polydorides, P. Schedl, *Mech. Dev.* **122**, 645 (2005).
9. M. Asaoka-Taguchi, M. Yamada, A. Nakamura, K. Hanyu, S. Kobayashi, *Nat. Cell Biol.* **1**, 431 (1999).
10. Y. Hayashi, M. Hayashi, S. Kobayashi, *Proc. Natl. Acad. Sci. U.S.A.* **101**, 10338 (2004).
11. C. E. Schaner, G. Deshpande, P. D. Schedl, W. G. Kelly, *Dev. Cell* **5**, 747 (2003).
12. R. Ciosk, M. DePalma, J. R. Priess, *Science* **311**, 851 (2006).
13. Y. Unhavaithaya *et al.*, *Cell* **111**, 991 (2002).
14. D. Wang *et al.*, *Nature* **436**, 593 (2005).
15. T. Takasaki *et al.*, *Development* **134**, 757 (2007).
16. W. Tadros, H. D. Lipshitz, *Dev. Dyn.* **232**, 593 (2005).
17. J. N. Pitt, J. A. Schisa, J. R. Priess, *Dev. Biol.* **219**, 315 (2000).
18. O. Hachet, A. Ephrussi, *Nature* **428**, 959 (2004).
19. P. R. Boag, A. Nakamura, T. K. Blackwell, *Development* **132**, 4975 (2005).
20. M. D. Lin, S. J. Fan, W. S. Hsu, T. B. Chou, *Dev. Cell* **10**, 601 (2006).
21. A. Nakamura, R. Amikura, K. Hanyu, S. Kobayashi, *Development* **128**, 3233 (2001).
22. H. B. Megosh, D. N. Cox, C. Campbell, H. Lin, *Curr. Biol.* **16**, 1884 (2006).
23. We thank our colleagues for discussions. Work in S.S.'s laboratory is supported by the NIH, and work in R.L.'s laboratory is supported by the NIH and the Howard Hughes Medical Institute.

10.1126/science.1140846

REVIEW

Germ Cell Specification in Mice

Katsuhiko Hayashi, Susana M. Chuva de Sousa Lopes, M. Azim Surani*

Specification of germ cells in mice occurs relatively late in embryonic development. It is initiated by signals that induce expression of Blimp1, a key regulator of the germ cell, in a few epiblast cells of early postimplantation embryos. Blimp1 represses the incipient somatic program in these cells and promotes progression toward the germ cell fate. Blimp1 may also have a role in the maintenance of early germ cell characteristics by ensuring their escape from the somatic fate as well as possible reversion to pluripotent stem cells.

Primordial germ cells (PGCs), the founder cells of the germ cell lineage, are usually established early during embryonic development. Specification of PGCs can occur either through the inheritance of germ cell determinants already present in the egg, as in *Caenorhabditis elegans* and *Drosophila*, or in response to inductive signals, as in mice and probably all mammals. In all instances however, germ cells are maintained by mechanisms that prevent them from differentiating into somatic cells.

The Stem Cell Model for PGC Specification in Mice

In *C. elegans* and *Drosophila*, founder PGCs are set aside at the outset from a totipotent zygote and prevented from differentiating into somatic cells by repression of the global transcriptional machinery (*1*). However, in mice, specification of PGCs is deferred until after implantation of blastocysts. The extraembryonic ectoderm (ExE) and visceral endoderm (VE), which surround the epiblast cells of the postimplantation egg cylinder, are the sources of signals that instruct a small number of epiblast cells to become PGCs; the rest of the cells commence differentiation into somatic tissues.

The rapidly dividing mouse epiblast cells are developmentally equivalent to the *Drosophila* egg (*2*). However, whereas in *Drosophila*, the determinants of somatic and germ cells are already segregated in specific regions of the oocyte, no such determinants exist in the mouse oocyte. Furthermore, PGCs originate from the proximal pluripotent epiblast cells that are already transcriptionally active and to some extent have embarked upon a somatic fate. Furthermore, pluripotent embryonic stem cells, which can be propagated indefinitely in vitro, can generate an infinite number of PGCs when returned to the blastocyst or when they otherwise receive specific signals to induce germ cell fate. We could therefore call this the stem cell model for PGC specification.

An elaborate transcriptional program that regulates PGC specification in mice prevents them from a continuing drift toward a somatic fate, and this is coupled with a chromatin-based mechanism that erases this trend, thereby resulting in reexpression of some key pluripotency-associated genes. At the same time, PGCs must acquire and maintain their lineage-specific characteristics. Recent advances are beginning to piece together the key steps that lead to PGC specification.

Origin of PGC Precursors from the Pluripotent Proximal Epiblast Cells

The pluripotent proximal epiblast cells respond to signals from the extraembryonic tissues and begin to express *fragilis/Ifitm3* as they acquire the ability to form PGCs, although only a small minority of them become germ cells in the end (*3*, *4*) (Fig. 1). Within these *fragilis*-positive cells, at embryonic day 6.25 (E6.25), about six cells in the prospective posterior proximal site of the embryo and directly in contact with the overlying ExE begin to show expression of *Blimp1/Prdm1*. Experiments tracing genetic lineage demonstrate that all of the *Blimp1*-expressing cells that originate in the proximal-posterior epiblast are the lineage-restricted PGC precursor cells (*5*).

There is further accretion of *Blimp1*-positive cells after this time. Lineage-tracing experiments had previously shown that some single cells in the proximal epiblast at E6.5 could give rise to both PGCs and extraembryonic mesoderm but never exclusively to PGCs (*6*). Furthermore, distal epiblast cells from E6.5 embryos when transplanted to the proximal-posterior region can contribute to the germ cell lineage, whereas proximal-posterior cells transplanted

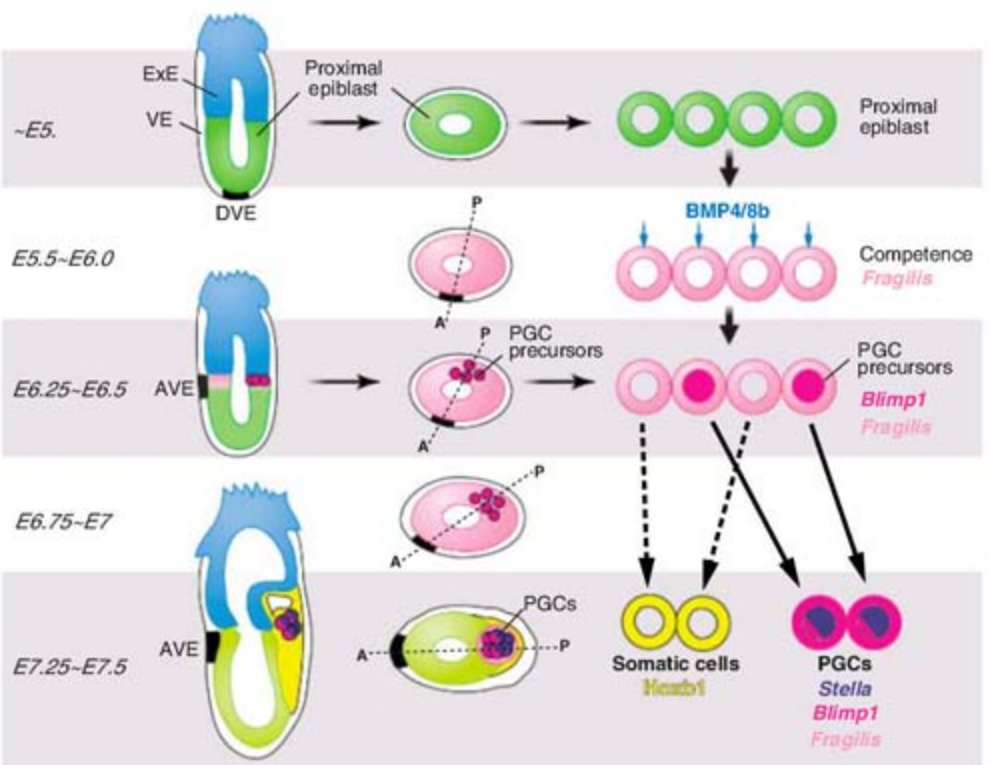

Fig. 1. Development of early postimplantation embryo from E5.0 to E7.5, depicting the formation of PGCs. The proximal epiblast cells respond to signals from the extraembryonic tissues, which induce expression of *fragilis* in the epiblast, and of *Blimp1* in the PGC precursor cells at one end of the short axis before gastrulation. After gastrulation, the PGC precursors locate to the posterior proximal region, where they undergo specification to form the founder population of *Stella*-positive PGCs.

Wellcome Trust Cancer Research UK Gurdon Institute, University of Cambridge, Tennis Court Road, Cambridge CB2 1QN, UK.

*To whom correspondence should be addressed. E-mail: as10021@mole.bio.cam.ac.uk

to the distal region of the epiblast can only give rise to somatic cells (*7*). These studies indicate the persistence of signals that can continually induce proximal-posterior epiblast cells at least up to E6.5 to commit to the PGC fate. Consistent with these findings, the number of *Blimp1*-expressing cells increases from about 6 to 16 between E6.25 and E6.5 (*5*). Taking into account the possibility that there is lengthening of the cell cycle time in the PGC precursors from 7 hours to about 16 hours, recruitment of additional precursors is necessary to account for about 40 Stella-positive founder PGCs that are finally observed at the posterior end of the primitive streak at E7.25 (*3*, *5*, *8*).

Signals for PGC Specification

Both the ExE and VE are essential for the acquisition of competence and PGC precursors but not for PGC specification itself (*9*, *10*). Bone morphogenetic protein 4 (BMP4), which is produced by ExE, is capable of inducing *fragilis/Ifitm3* expression (*3*). ExE and VE are also the sources of BMP8b and BMP2, respectively. Loss of any of these signaling molecules abrogates the competence to give rise to all or most of the PGCs (*11*–*13*). BMPs trigger serine phosphorylation of the transducer Smad1/5/8, which translocates into the nucleus with the common mediator, Smad4. Loss of Smad1 and Smad5 (but not Smad8) causes severe reduction in the numbers of PGCs (*14*–*16*), as does the conditional loss of Smad4 (*17*).

The *Bmp-Smad* gene dosage is critical for PGC specification. For example, in the *Bmp4*-heterozygous mutants, the number of PGCs is almost halved, which is also the case in the double heterozygous *Smad1* and *Smad5* (*18*). Indeed, the PGC precursors emerge from the most proximal layer of the epiblast, where the BMP-Smad signaling is strongly activated (Fig. 1).

The detection of *Blimp1*-positive PGC precursors at the posterior side of the early embryo indicates that the anterior-posterior (A-P) axis formation may play a role in determining their numbers and location. The anterior visceral endoderm (AVE) (*19*) produces Nodal and Wnt antagonists, thus restricting Nodal and Wnt3 signaling to the posterior side of the embryo, the site where the *Blimp1*-positive PGC precursors are detected. Notably, *Smad2*-mutant embryos, which disorder A-P axis formation and result in the expression of "posterior" genes, including *Nodal* and *Fgf8* in the entire epiblast, show many ectopic clusters of PGCs (*16*, *20*). It appears that an orchestration of growth factors, which may include Nodal and Fgf8, creates an environment for PGC precursors to be segregated from somatic cell lineages.

Blimp1: The Key Regulator of PGC Specification

A crucial part of PGC specification in many model organisms includes repression of the somatic program. In mice, a unique germ cell–specific transcriptional network seems to regulate PGC specification. Extensive analysis of gene expression profile in single cells shows the involvement of a molecular program during germ cell specification (*3*, *5*, *21*, *22*) (Fig. 2).

Among the genes identified so far, Blimp1 protein is a key transcriptional regulator that is partly responsible for repressing the somatic program in PGCs while allowing establishment of germ cell character in these cells (*5*, *23*). Blimp1 protein has a PR/SET domain, a proline-rich region, five C_2H_2 zinc fingers, and a C-terminal acidic domain.

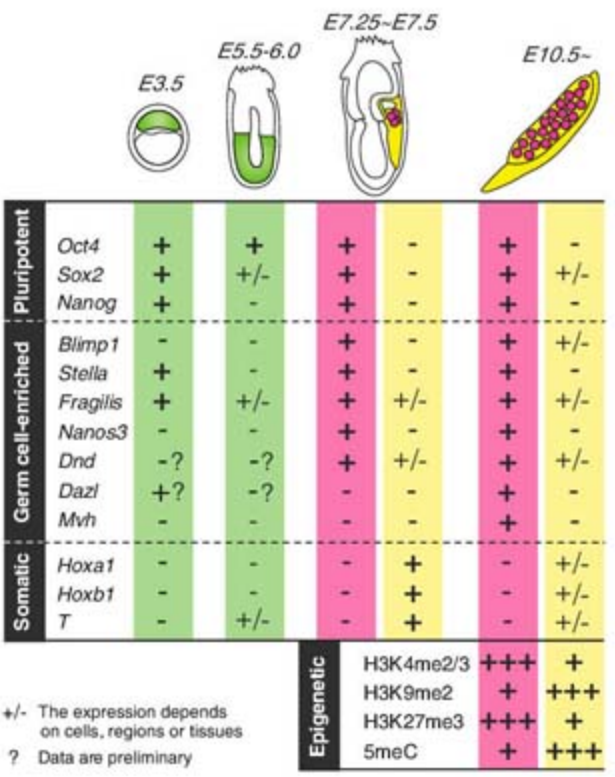

Fig. 2. A summary of PGC specification. Progressive changes in gene expression from the epiblast in early embryos (green) to PGCs (red) are indicated. Epigenetic differences between PGCs and somatic cells (yellow) are shown at E10.5. *Nanos3*, *Mvh*, *Dnd*, and *Dazl* are also germ cell–enriched genes. DNA methylation (5meC) is erased in imprinting control elements and gene-encoding regions after E10.5 (*33*).

Detailed analysis suggests that the PGC-competent proximal epiblast cells expressing *fragilis/Ifitm3* are initially destined for a somatic fate. Accordingly, early *Blimp1*-expressing cells at E6.75 originating in the proximal epiblast cells exhibit expression of *Hoxb1* as well as other mesodermal genes, including *T*, *Fgf8*, and *Snail* (*21*). These genes continue to be up-regulated in the neighboring mesodermal somatic tissues. However, they become repressed in the *Blimp1*-positive cells in an orderly manner along with the progression of PGC specification (*22*). The repression of somatic genes in PGCs is consistent with the phenomenon of repression of the somatic program observed in *C. elegans* and in *Drosophila*.

Coupled with the repression of mesodermal-specific genes, there is up-regulation of other genes, including *Sox2* (*5*, *22*). Another gene, *Nanog*, is also reexpressed in PGCs (*24*). Thus, among all the lineages that develop from the epiblast cells, only germ cells regain expression of pluripotency-associated genes during the course of their specification. There is also ex-

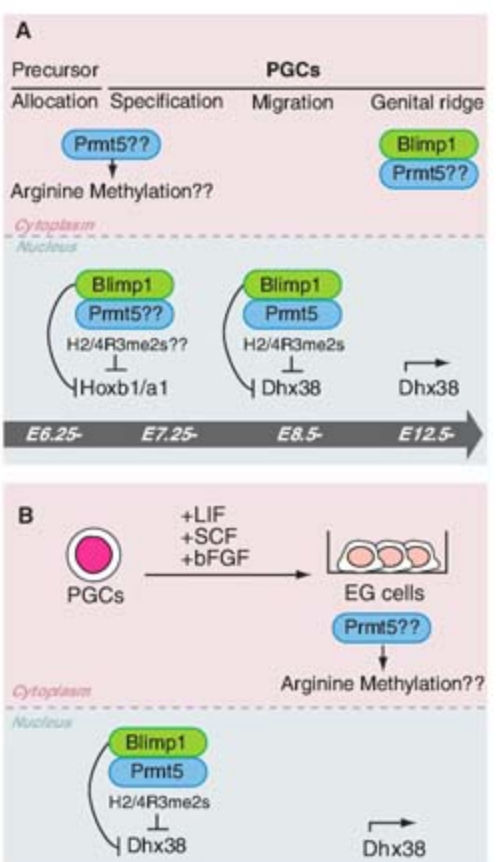

Fig. 3. (**A**) Potential role of Blimp1/Prmt5 complex in PGC specification until the migration of PGCs into the genital ridges, when the complex translocates from the nucleus to the cytoplasm. (**B**) The loss of Blimp1 during dedifferentiation of PGCs into pluripotent EG cells. Dhx38 is a target of Blimp1/Prmt5 complex.

pression of other unique genes in PGCs, including *Prdm14*, a gene that is closely related to *Blimp1/Prdm1*, which may also have a role in PGC specification (*22*).

The functional importance of Blimp1 in PGC specification became evident during the analysis of the *Blimp1*-mutant mouse embryos, which results in aberrant development of founder PGCs. In the absence of Blimp1, the mutant cells form a tight PGC-like cluster, but they cease to proliferate and they show little evidence for migration out of the cluster. They also show inconsistent repression of *Hoxb1*, which is a hallmark of PGC specification, while failing to show consistent up-regulation of *stella* and *Sox2*, as observed in normal PGC. Thus, Blimp1 plays a critical role in the establishment of the founder PGCs.

The Role of Prmt5 Arginine Methylase in PGC Specification

Recent studies have shown a previously unrecognized Blimp1/Prmt5 complex in germ cells. Prmt5 is an arginine-specific histone methyltransferase, which mediates symmetrical dimethylation of arginine-3 on histone H2A and/or H4 tails (H2Ame2s/H4R3me2s), which is detected in germ cells (*21*). A few targets of the Blimp1/Prmt5 complex have been identified in germ cells, including *Dhx38*. In PGCs, *Dhx38* is repressed and shows an H4R3me2s epigenetic mark until E12.5. Its expression at this time coincides with the translocation of Blimp1/Prmt5 from the nucleus to the cytoplasm at E11.5, after which the expression of pluripotency-associated genes also begins to be down-regulated. Thus, Blimp1/Prmt5 complex may play an essential role in maintaining the PGC lineage during the migration of the cells into the gonads (Fig. 3A).

Notably, recent studies in *Drosophila* indicate that a mutation in the Prmt5 homolog, *Capsuleen/dart5*, affects germ cell specification in females and development of spermatocytes in males (*25*, *26*). Both the formation of nuage in nurse cells and pole plasm integrity are affected in *Capsuleen/dart5* mutant flies. *Capsuleen/dart5* has the potential to methylate protein substrates, which have a role in the integrity of P granules in the germ cells of *C. elegans* (*27*). Both P granules and nuage are RNA rich and contain several proteins. In *Capsuleen/dart5* mutant flies, the localization of Tudor, an essential component of the pole plasm and nuage, is abolished.

It will be important to determine whether Prmt5 has a role earlier in the PGC precursors in mice, either through any cytoplasmic substrates or through its association with Blimp1 (Fig. 3A). It remains to be seen whether Tudor domain proteins, some of which are detected at the time of PGC specification (*28*), contribute to PGC specification in conjunction with Prmt5 or Blimp1/Prmt5 complex.

Postspecification Establishment of PGC Epigenetic Signature

An integral part of the PGC specification process includes substantial epigenetic modifications, which occur in the *stella*-positive PGCs. At E8.0, the level of H3K9me2 (an epigenetic mark associated with transcriptional repression) diminishes, whereas H3K27me3 (another repressive epigenetic mark associated with high levels of Ehz2) becomes prominent (*29*) (Fig. 2). These changes are followed by up-regulation of H3K4me2/3 (Fig. 2). The epigenetic marks H3K27me3 and H3K4me2/3 are notable as the facultative marks of gene loci that are repressed in pluripotent embryonic stem cells.

Germ Cells and Pluripotent Stem Cells: A Reversible Phenotype

PGCs undergo dedifferentiation into pluripotent embryonic germ (EG) cells when they are cultured with basic fibroblast growth factor (bFGF), leukemia inhibitory factor (LIF), and stem cell factor (SCF) (*30*–*32*). EG cells can only be derived from PGCs between E8.5 and E11.5 when H3K27me3 and H3K4me2/3 marks become prominent and when H3K9me2 is absent (*29*, *30*). At the same time, PGCs show expression of pluripotency-associated genes *Oct4*, *Sox2*, and *Nanog*. Blimp1 is down-regulated during the derivation of EG cells, whereas Prmt5 is detected not only in EG cells but also in all other pluripotent cells. The loss of Blimp1 may result in derepression of certain genes that maintain the germ cell lineage, such as *Dhx38* (Fig. 3B), a target of Blimp1/Prmt5 complex in PGCs until E11.5 (*21*). Reciprocally, ectopic expression of Blimp1 in pluripotent embryonic carcinoma (EC) cells leads to the repression of *Dhx38*. It will be of interest to determine whether the EC cells and indeed all pluripotent stem cells acquire aspects of the PGC character upon expression of Blimp1.

Outlook

Analysis of PGC specification in different organisms demonstrates both the differences and some common features of the mechanisms involved in their specification. An essential necessity for the germ line cycle is to prevent a loss of pluripotency and totipotency, which are lost from somatic cells as they begin to undergo differentiation.

An emerging theme in PGC specification is the potential role of the arginine methylase, Prmt5. In flies, it seems to have a role as a protein arginine methylase that acts on components of the germ plasm and helps to maintain its integrity through the involvement of Tudor. The role of Prmt5 in the mouse PGCs remains to be fully elucidated. It also seems that Blimp1 probably helps to direct Prmt5 to its targets, such as *Dhx38*, but a more comprehensive search for other targets is needed to unravel its role more fully in early PGCs. Further investigations will deepen our insights on the specification of germ cells, the most critical lineage in all species.

References and Notes

1. S. Strome, R. Lehmann, *Science* **316**, 392 (2007).
2. P. H. O'Farrell, J. Stumpff, T. T. Su, *Curr. Biol.* **14**, R35 (2004).
3. M. Saitou, S. C. Barton, M. A. Surani, *Nature* **418**, 293 (2002).
4. S. S. Tanaka, Y. Matsui, *Mech. Dev.* **119** (suppl. 1), S261 (2002).
5. Y. Ohinata *et al.*, *Nature* **436**, 207 (2005).
6. K. A. Lawson, W. J. Hage, *Ciba Found. Symp.* **182**, 68 (1994).
7. P. P. Tam, S. X. Zhou, *Dev. Biol.* **178**, 124 (1996).
8. A. McLaren, K. A. Lawson, *Differentiation* **73**, 435 (2005).
9. S. M. de Sousa Lopes *et al.*, *Genes Dev.* **18**, 1838 (2004).
10. T. Yoshimizu, M. Obinata, Y. Matsui, *Development* **128**, 481 (2001).
11. K. A. Lawson *et al.*, *Genes Dev.* **13**, 424 (1999).
12. Y. Ying, X. M. Liu, A. Marble, K. A. Lawson, G. Q. Zhao, *Mol. Endocrinol.* **14**, 1053 (2000).
13. Y. Ying, G. Q. Zhao, *Dev. Biol.* **232**, 484 (2001).
14. H. Chang, M. M. Matzuk, *Mech. Dev.* **104**, 61 (2001).
15. K. Hayashi *et al.*, *Mech. Dev.* **118**, 99 (2002).
16. K. D. Tremblay, N. R. Dunn, E. J. Robertson, *Development* **128**, 3609 (2001).
17. G. C. Chu, N. R. Dunn, D. C. Anderson, L. Oxburgh, E. J. Robertson, *Development* **131**, 3501 (2004).
18. S. J. Arnold, S. Maretto, A. Islam, E. K. Bikoff, E. J. Robertson, *Dev. Biol.* **296**, 104 (2006).
19. P. Q. Thomas, A. Brown, R. S. Beddington, *Development* **125**, 85 (1998).
20. W. R. Waldrip, E. K. Bikoff, P. A. Hoodless, J. L. Wrana, E. J. Robertson, *Cell* **92**, 797 (1998).
21. K. Ancelin *et al.*, *Nat. Cell Biol.* **8**, 623 (2006).
22. Y. Yabuta, K. Kurimoto, Y. Ohinata, Y. Seki, M. Saitou, *Biol. Reprod.* **75**, 705 (2006).
23. S. D. Vincent *et al.*, *Development* **132**, 1315 (2005).
24. S. Yamaguchi, H. Kimura, M. Tada, N. Nakatsuji, T. Tada, *Gene Expr. Patterns* **5**, 639 (2005).
25. J. Anne, R. Ollo, A. Ephrussi, B. M. Mechler, *Development* **134**, 137 (2007).
26. G. B. Gonsalvez, T. K. Rajendra, L. Tian, A. G. Matera, *Curr. Biol.* **16**, 1077 (2006).
27. S. A. Barbee, T. C. Evans, *Dev. Biol.* **291**, 132 (2006).
28. M. A. Surani, K. Hayashi, P. Hajkova, *Cell* **128**, 747 (2007).
29. Y. Seki *et al.*, *Dev. Biol.* **278**, 440 (2005).
30. G. Durcova-Hills, I. R. Adams, S. C. Barton, M. A. Surani, A. McLaren, *Stem Cells* **24**, 1441 (2006).
31. Y. Matsui, K. Zsebo, B. L. Hogan, *Cell* **70**, 841 (1992).
32. J. L. Resnick, L. S. Bixler, L. Cheng, P. J. Donovan, *Nature* **359**, 550 (1992).
33. P. Hajkova *et al.*, *Mech. Dev.* **117**, 15 (2002).

34. We thank M. Saitou for critical comments on the manuscript and the Wellcome Trust for a Programme Grant.

10.1126/science.1137545

REVIEW

piRNAs in the Germ Line

Haifan Lin

Small noncoding RNAs have emerged as potent regulators of gene expression at both transcriptional and posttranscriptional levels. Recently, a class of small RNAs that interact with Piwi proteins has been discovered in the mammalian germ line and *Drosophila*. These Piwi-interacting RNAs (piRNAs) represent a distinct small RNA pathway.

The importance of small noncoding RNAs as regulators of transcription, RNA stability, and translation is becoming increasingly evident (*1*). The recently discovered piRNAs differ from the known small interfering RNAs (siRNAs) or microRNAs (miRNAs) in several ways (*2*–*6*). First, piRNAs interact with the Piwi, but not the Argonaute (Ago), subfamily of the Piwi-Ago family proteins. Mouse Piwi (Miwi) is required for piRNA biogenesis and/or stability (*7*), whereas mouse Ago2 is required for the siRNA pathway. Second, piRNAs are 24 to 31 nucleotides (nt) instead of ~21 nt. Third, piRNAs consist of more than 50,000 different species, in contrast to several hundred species of miRNAs. Fourth, most piRNAs match to the genome in clusters of 20 to 90 kbs in a strand-specific manner, with each cluster likely representing a long single-stranded RNA precursor or, more often, two nonoverlapping and divergently transcribed precursors (Fig. 1A) (*2*). In contrast, siRNAs and miRNAs are derived from double-stranded and short-hairpin RNA precursors, respectively. Finally, some piRNAs might positively regulate mRNA stability and translation (see below), in contrast to the negative effect of the siRNAs and miRNAs.

In *Drosophila*, some piRNAs have been called repeat-associated siRNAs ("rasiRNAs") (*3*, *4*, *6*). However, unlike siRNAs, these rasiRNAs bind to Piwi, Aubergine (Aub), and Ago3—three Piwi subfamily proteins, but not to Ago subfamily proteins. Moreover, their production requires neither Dicer-1 nor Dicer-2, which generate miRNAs and siRNAs, respectively (*3*). Thus, by definition, these rasiRNAs are piRNAs.

How are piRNAs produced? They are likely produced from long single-stranded precursors by yet-to-be-identified endonucleases. In *Drosophila*, Piwi, Aub, and Ago3 could be such endonucleases because they have slicing activity (*4*, *6*). For some transposon-derived piRNAs in *Drosophila*, an additional "Ping-Pong" mechanism might be involved in accelerating their processing from precursors (*5*, *6*) (Fig. 1B). This is possible because the Aub- and Piwi-associated piRNAs match the antisense strand of DNA, showing a strong bias for a uracyl (U) at the 5′ ends; yet Ago3-associated piRNAs match the sense strand and complement Aub- and Piwi-associated piRNAs in their first 10 nucleotides, showing a conserved adenine (A) at position 10. Thus, the Ago3-piRNA complex might guide and cleave the 5′ ends of Aub- and Piwi-associated piRNAs, whereas the Aub-Piwi–piRNA complex might guide and cleave the 5′ ends of Ago3-associated piRNAs (Fig. 1B).

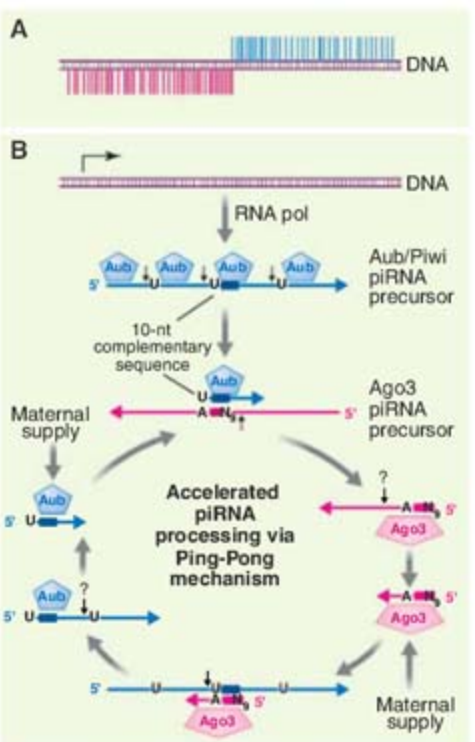

Fig. 1. (**A**) A bidirectional piRNA cluster. (**B**) A proposed piRNA biogenesis pathway. The resulting piRNA-protein complexes then regulate gene expression at the epigenetic or posttranscriptional levels (not shown). N_9, the 9th nucleotide from A_{10} in Ago3-piRNA; the question mark (?), other nuclease.

What are the roles of piRNAs in the germ line? The genomic distribution of piRNAs and the function of their Piwi proteins provide important clues to this question. Most piRNAs map to unique sites in the genome, including intergenic, intronic, and exonic sequences. For example, only 17 to 20% of mammalian piRNAs map to annotated repeats, including transposons and retrotransposons (*2*). Thus, piRNAs may have diverse functions from epigenetic programming and repressing transposition to posttranscriptional regulation. Each of these speculated roles is supported by the known function of their partner Piwi proteins. For instance, Piwi is an epigenetic regulator (*8*). It colocalizes with Polycomb group (PcG) proteins to cluster PcG response sequences in the genome (*9*). Thus, some PIWI-associated piRNAs may be involved in epigenetic regulation. In fact, gypsy piRNAs in *Drosophila* have been shown to down-regulate sense gypsy transcripts (*10*). In addition, Piwi prevents retrotransposon transposition in the testicular germ line (*11*), which suggests a second role of Piwi-associated piRNAs. Furthermore, Piwi and Aub appear to positively regulate translation in early *Drosophila* embryos (*12*, *13*). Similarly, Miwi promotes the stability (*14*) and, likely, translation of its target mRNAs (*15*). Thus, some piRNAs may have a third role in positively regulating translation and mRNA stability.

The discovery of piRNAs reveals a new dimension of gene regulation. Future studies on the biogenesis and the potentially diverse functions of piRNAs should substantially advance our understanding of gene regulation that defines the germ line.

Yale Stem Cell Center, Yale University School of Medicine, New Haven, CT 06510, USA. E-mail: haifan.lin@yale.edu

References

1. R. H. A. Plasterk, *Cell* **124**, 877 (2006).
2. V. N. Kim, *Genes Dev.* **20**, 1993 (2006).
3. V. V. Vagin *et al.*, *Science* **313**, 320 (2006).
4. K. Saito *et al.*, *Genes Dev.* **20**, 2214 (2006).
5. J. Brennecke *et al.*, *Cell* 7 March 2007 (10.1016/j.cell.2007.01.043), in press.
6. L. S. Gunawardane *et al.*, *Science* **315**, 1587 (2007).
7. S. T. Grivna, E. Beyret, Z. Wang, H. Lin, *Genes Dev.* **20**, 1709 (2006).
8. M. Pal-Bhadra *et al.*, *Science* **303**, 669 (2004).
9. C. Grimaud *et al.*, *Cell* **124**, 957 (2006).
10. A. Pelisson, E. Sarot, G. Payen-Groschene, A. Bucheton, *J. Virol.* **81**, 1951 (2007).
11. A. I. Kalmykova, M. S. Klenov, V. A. Gvozdev, *Nucleic Acids Res.* **33**, 2052 (2005).
12. H. B. Megosh, D. N. Cox, C. Campbell, H. Lin, *Curr. Biol.* **16**, 1884 (2006).
13. J. E. Wilson, J. E. Connell, P. M. Macdonald, *Development* **122**, 1631 (1996).
14. W. Deng, H. Lin, *Dev. Cell* **2**, 819 (2002).
15. S. T. Grivna, B. Pyhtila, H. Lin, *Proc. Natl. Acad. Sci. U.S.A.* **103**, 13415 (2006).

10.1126/science.1137543

REVIEW

Epigenetic Decisions in Mammalian Germ Cells

Christopher B. Schaefer,[1] Steen K. T. Ooi,[1] Timothy H. Bestor,[1] Déborah Bourc'his[2]*

Specific sequences are designated for de novo DNA methylation at CpG dinucleotides in mammalian germ cells. The result is the long-term transcriptional silencing of the methylated sequences, most of which are retrotransposons and CpG-rich sequences associated with imprinted genes. There is profound sexual dimorphism in both the nature of the sequences that undergo de novo methylation in germ cells and in the mechanism by which de novo methylation is regulated. The restriction of future gene expression by the imposition of heritable methylation patterns in germ cell genomes is characteristic of mammals but is rare in other taxa.

Genomic methylation patterns are largely erased during the proliferation and migration of primordial germ cells (PGCs) and reestablished in sex-specific patterns during spermatogenesis and oogenesis (*1*). Most de novo DNA methylation is directed to transposons and their remnants and to clustered repeats (primarily pericentric satellite DNA), with lesser amounts at single-copy sequences and the differentially methylated regions (DMRs) of imprinted loci (*2*). CpG islands associated with promoter regions of nonimprinted genes are mostly unmethylated (*3*). Loss of methylation, or a failure to establish methylation patterns, reanimates retrotransposons in germ and somatic cells and causes biallelic expression or repression of imprinted genes in embryonic tissues (*4*–*6*). Even minor disruption of methylation patterns can be lethal, and a broad range of developmental abnormalities is seen when specific genomic regions are abnormally methylated (*7*).

The DNMT3A/B and DNMT1 families of DNA cytosine-5 methyltransferases are responsible for the establishment and maintenance of methylation patterns, respectively, and are expressed in most dividing cell types (*2*). DNMT3L (DNMT3-like) is related in sequence to DNMT3A and DNMT3B but lacks enzymatic activity. It is expressed only in germ cells and only at the stages where de novo methylation occurs (*5*), and acts as a regulator of DNMT3A and DNMT3B (*8*). Most *Dnmt* genes contain sex-specific germline promoters that are activated at specific stages of gametogenesis (*9*–*11*). These promoters give rise to germ cell–specific transcripts that lead to the production of truncated forms of the proteins, or to untranslated mRNAs that may have regulatory properties (Fig. 1). The functional consequences of the alternative mRNAs and proteins are largely unknown. The oocyte-specific form of DNMT1 (DNMT1o) has a higher stability compared to the somatic form. It accumulates to very high levels in the cytoplasm of oocytes and persists in preimplantation embryos where it enters nuclei at the eight-cell stage to maintain imprinted methylation patterns (*12*).

DNMT3L-directed de novo methylation occurs in populations of nondividing cells in both male and female germ lines (Fig. 2). However, methylation acquisition is a premeiotic phenomenon in the male germ line, where it occurs in prenatal prospermatogonia, whereas methylation is acquired postmeiotically in the female germ line in growing oocytes that are arrested at the diplotene stage of meiosis I (*1*, *5*). Loss of DNMT3L results in very different phenotypes depending upon the sex examined. Deletion of *Dnmt3L* in female mice prevents establishment of maternal methylation imprints in oocytes without marked effects on retrotransposon methylation (*5*). The result is a maternal-effect lethal phenotype in which the heterozygous offspring of homozygous *Dnmt3L*-null females (which are of normal phenotype) show biallelic expression of genes that are normally maternally methylated and repressed. This leads to abnormal development of extraembryonic structures and death of the embryo before mid-gestation.

The *Dnmt3L*-null phenotype in male mice is markedly different. Male germ cells that lack DNMT3L show fulminating expression of retrotransposons of the LINE-1 (long interspersed elements) and IAP (intracisternal A particles) classes, severe asynapsis and nonhomologous synapsis at meiotic prophase, and eventual apoptosis of all germ cells before pachytene (*6*). Methylation patterns at the small number of paternally methylated DMRs are almost normal, but there is a failure to methylate retrotransposons. The DNMT3L protein appears to be essentially identical in both germ lines, but the timing of expression is markedly different in the two sexes, and the methylation phenotypes of *Dnmt3L*-null male and female germ cells are nearly mirror images. This implies that DNMT3L potentially interprets a preexisting mark that is established by other factors and located at different genomic regions in male premeiotic and female postmeiotic germ cells; the nature of the mark may be a particular posttranslational histone modification or set of modifications. This could explain how histone modifications (which have not been shown to be subject to long-term passive inheritance) might be converted into heritable patterns of DNA methylation that can impose long-term transcriptional silencing on the affected sequences.

The profound sexual dimorphism in the ontogeny of methylation patterns in male and female germ lines has a direct consequence on the genomic characteristics of the DMRs associated with paternally and maternally imprinted genes (*13*). De novo methylation occurs shortly before ovulation in growing oocytes, and methylation patterns are soon erased in the primordial germ cells of the next generation. CpG dinucleotides that are methylated in the germ line are rapidly mutated to TpG and CpA dinucleotides (*14*), and because female germline genomes are methylated for only a small number of cell divisions, the incidence of C→T mutations at methylated sites will be low. In the male germ line, the entire cohort of prospermatogonia undergo de novo methylation in the perinatal period, and spermatogonia must maintain methylation patterns for the large and variable number of mitotic divisions that precede entry into meiosis. This increases the load of C→T mutations, especially for the offspring of older males, and the mutational pressures have led to a low density of CpG dinucleotides in paternally methylated DMRs relative to maternal DMRs and to an underrepresentation of paternally methylated DMRs relative to maternally methylated DMRs. For unknown reasons, maternally methylated DMRs usually span the promoters of imprinted genes, whereas paternally methylated DMRs can be located many kilobases away from the affected genes.

Diversity in the nature of the sequences designated for de novo methylation (single-copy versus repeated sequences, clustered versus interspersed organization) makes it likely that multiple signals direct de novo methylation in germ cells, but the nature of those signals is unclear. RNA-directed DNA methylation (RdDM) is a candidate, and such a

[1]Department of Genetics and Development, College of Physicians and Surgeons of Columbia University, New York, NY 10032, USA. [2]INSERM U741 University Paris 7, 75251 Paris, Cedex 05, France.

*To whom correspondence should be addressed. Tour 43/44, 2ème étage 2 Place Jussieu, 75251 Paris, Cedex 05, France. E-mail: bourchis@ijm.jussieu.fr

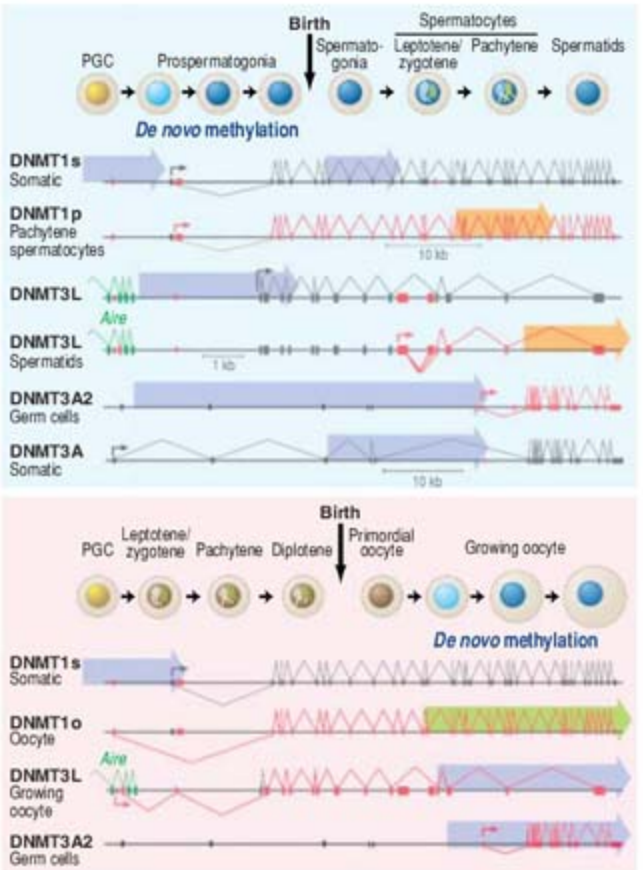

Fig. 1. Expression of germ cell–specific forms of Dnmt family members. Red indicates germ cell–specific exons and splice variants at left; approximate developmental timing of expression of each form is shown at right. DNMT1s and DNMT1o are active DNA methyltransferases; DNMT1p mRNA contains multiple stop codons in an alternative 5′ exon and is not translated. DNMT3L is expressed in both male and female germ cells but from different promoters, and a third alternative transcript, which cannot encode functional DNMT3L, is present in spermatids. De novo methylation occurs before birth in the entire cohort of prospermatogonia in males, but de novo methylation in females occurs before ovulation over the reproductive life span of the female. Also, de novo methylation occurs long before spermatogonia enter into meiosis in males, but de novo methylation occurs only after the crossing-over stage of meiosis I in females. PGC, primordial germ cell.

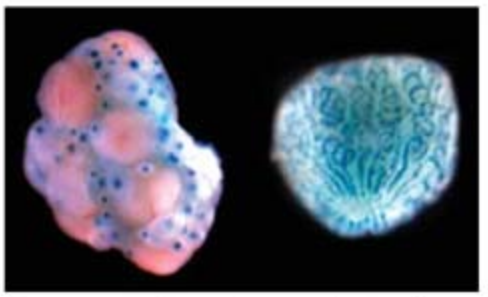

Fig. 2. Expression of *Dnmt3L* in female and male germ cells. A β-galactosidase–neomycin resistance marker was fused to the promoter of the endogenous *Dnmt3L* gene. Expression (blue) is seen in growing oocytes in the adult mouse ovary at left and in prospermatogonia (a nondividing precursor to spermatogonial stem cells) in the testis from a newborn mouse at right. Dnmt3L is expressed in testis from ~7 days before birth to ~3 days after birth.

pathway does exist in plants, where it is involved in transcriptional repression of transposons. However, an adaptive RNA interference (RNAi) response seems unlikely to exist in somatic mammalian cells where double-stranded RNA (dsRNA) provokes a general inhibition of translation via protein kinase RNA-activated (PKR) and the interferon response (*15*). Most organisms that use RNAi for both transcriptional and posttranscriptional silencing have a Dicer-like protein specific to each process [reviewed in (*16*)], which cleaves dsRNA to short 21- to 22-nucleotide dsRNAs that inhibit translation or induce degradation of homologous RNAs. Mammalian genomes encode only one Dicer protein, which localizes to the cytoplasm. Mammalian Dicer is most closely related to the *Drosophila melanogaster* Dicer-1, which is required for microRNA (miRNA) processing and not production of small interfering RNAs (siRNAs, which mediate the adaptive RNAi response). Loss of Dicer activity in mouse embryonic cell lines has a minimal effect on transposon methylation and activity, and siRNAs directed to transposable elements have not been identified (*17*). It appears that RNAi components in mammalian cells may be used exclusively for miRNA production under normal conditions and that DNA methylation in mammals may not require input from an RNA component. However, if an adaptive RNAi response does operate in mammals, it could be active only in germ cells, where the absence of an interferon response would allow for the use of a dsRNA-responsive mechanism (*18*). A germ cell–specific class of small RNAs has recently been identified, and their potential functions in the germ line are discussed elsewhere [reviewed in (*16*)]. They could provide evidence that RNA is implicated in sequence-specific de novo methylation in mammalian germ cells (*19*).

De novo methylation can be RNA independent. The ascomycete fungus *Neurospora crassa* genome senses and methylates repeated sequences just before meiosis in a process that is not affected by mutations in components of the RNAi pathway (*20*). The large majority of 5-methylcytosines in the mammalian genome is in dispersed and tandem repeats (*21*), and a repeat-sensing mechanism could operate in mammalian germ cells as well.

Errors in establishment or maintenance of germ cell methylation patterns can cause human diseases, as in some cases of the imprinting disorders Beckwith-Wiedeman, Angelmann, and Prader-Willi syndromes (*7*). High rates of discordance in monozygotic twins reported for psychiatric disorders may involve methylation abnormalities that arise in early development (germline mutations cannot explain the discordance), and the paternal-age effect in schizophrenia may involve errors in the maintenance of genomic methylation patterns during the many cell divisions that male germ cells must undergo as spermatogonia. Epigenetic errors during germ cell development are likely to contribute to many other disorders in which neither genetic nor environmental factors can account for all risk.

References and Notes

1. J. M. Trasler, *Reprod. Fertil. Dev.* **18**, 63 (2006).
2. M. G. Goll, T. H. Bestor, *Annu. Rev. Biochem.* **74**, 481 (2005).
3. R. A. Rollins *et al.*, *Genome Res.* **16**, 157 (2006).
4. E. Li, T. H. Bestor, R. Jaenisch, *Cell* **69**, 915 (1992).
5. D. Bourc'his, G.-L. Xu, C. S. Lin, B. Bollman, T. H. Bestor, *Science* **294**, 2536 (2001).
6. D. Bourc'his, T. H. Bestor, *Nature* **431**, 96 (2004).
7. K. D. Robertson, *Nat. Rev. Genet.* **6**, 597 (2005).
8. I. Suetake, F. Shinozaki, J. Miyagawa, H. Takeshima, S. Tajima, *J. Biol. Chem.* **279**, 27816 (2004).
9. C. Mertineit *et al.*, *Development* **125**, 889 (1998).
10. T. Chen, Y. Ueda, S. Xie, E. Li, *J. Biol. Chem.* **277**, 38746 (2002).
11. T. C. Shovlin *et al.*, *Hum. Reprod.* **22**, 457 (2007).
12. C. Y. Howell *et al.*, *Cell* **104**, 829 (2001).
13. D. Bourc'his, T. H. Bestor, *Cytogenet. Genome Res.* **113**, 36 (2006).
14. M. L. Gonzalgo, P. A. Jones, *Mutat. Res.* **386**, 107 (1997).
15. G. R. Stark, I. M. Kerr, B. R. Williams, R. H. Silverman, R. D. Schreiber, *Annu. Rev. Biochem.* **67**, 227 (1998).
16. H. Lin, *Science* **316**, 397 (2007).
17. C. Kanellopoulou *et al.*, *Genes Dev.* **19**, 489 (2005).
18. P. Stein, F. Zeng, H. Pan, R. M. Schultz, *Dev. Biol.* **286**, 464 (2005).
19. M. A. Carmell *et al.*, *Dev. Cell* 10.1016/j.devcel.2007.03.001 (28 March 2007).
20. M. Freitag *et al.*, *Science* **304**, 1939 (2004).
21. J. A. Yoder, C. P. Walsh, T. H. Bestor, *Trends Genet.* **13**, 335 (1997).
22. We thank S. La Salle and J. Trasler for helpful discussions. Supported by grants from the NIH (T.H.B.), a European Molecular Biology Organization long-term fellowship (S.K.T.O.), and a European Young Investigator Award and a grant from the Agence Nationale pour la Recherche (D.B.).

10.1126/science.1137544

REVIEW

The Mysteries of Sexual Identity: The Germ Cell's Perspective

Judith Kimble[1]* and David C. Page[2]

Animal germ cells differentiate as sperm or eggs, depending on their sex. Somatic signals tell germ cells whether they reside in a male or female body, but how do germ cells interpret those external cues to acquire their own sexual identity? A critical aspect of a germ cell's sexual puzzle is that the sperm/egg decision is closely linked to the cell-cycle decision between mitosis and meiosis. Molecular studies have begun to tease apart the regulators of both decisions, an essential step toward understanding the regulatory logic of this fundamental question of germ cell biology.

Germ cells confront two major cell-fate decisions as they move from an immature state into the world of sexuality. One decision is entry into a germline-specific cell cycle, called meiosis, and the other is commitment to differentiate as sperm or egg. During embryonic development, germ cells increase their total cell number using the standard mitotic cell cycle, and they use that same cell cycle in adults for stem cell maintenance. Then, as germ cells mature, they embark on the meiotic cell cycle, which reduces the number of chromosomes from the typical two sets to a single set in both sperm and eggs. Upon fertilization, two sets of chromosomes are restored and the next generation can be launched. Of particular importance for this review, the sperm/egg and mitosis/meiosis decisions are closely coupled, which stands out as a fundamental aspect of germ cell regulation that is only beginning to be understood.

Questions About Sexual Identity in Germ Cells

What directs a germ cell to differentiate as sperm or egg? One important and longstanding approach to this question has focused on how somatic tissues influence the sexual identity of germ cells. In mice, the question is usually rephrased to ask what somatic cues direct germ cells to transition from mitosis to meiosis; meiotic initiation is among the first signs of sexual dimorphism in the murine ovary (*1*). The molecular nature of somatic signaling depends on the organism: a variant hedgehog pathway in *Caenorhabditis elegans* (*2*), the JAK-STAT (Janus kinase–signal transducer and activator of transcription) pathway in *Drosophila* testes (*3*), and retinoic acid signaling in mice (*4*, *5*), for example. The common theme across these species is that the soma uses well-traveled molecular pathways to signal germ cells and influence their sexual identity.

In this review, we leave the soma and focus on what lies downstream of somatic signals to control germ cell sexual identity. A priori, the sperm/egg decision might be considered as distinct from the cell cycle decision between mitosis and meiosis, which takes place in both sexes. However, the timing of the mitosis/meiosis decision and features of meiosis itself (e.g., recombination and symmetry of divisions) are often sex-specific, suggesting a close relationship between the mitosis/meiosis and sperm/egg decisions. One must therefore ask three questions: (i) What molecular machinery inside germ cells directs their differentiation as sperm or egg? (ii) What molecular machinery governs the transition from mitosis to meiosis? and (iii) What is the relationship between regulators of the sperm/egg and mitosis/meiosis decisions? We consider two models. One idea is that the sperm/egg and mitosis/meiosis decisions are really one and the same (Fig. 1A). According to this model, a sex-specific regulator induces a sex-specific meiotic cell cycle and at the same time commits the germ cell to differentiation as sperm or egg. The other idea is that the two decisions are governed by distinct regulatory inputs (Fig. 1B). By this model, a gender-neutral mechanism governs entry into meiosis, but sex-specific regulators work in parallel to induce sex-specific aspects of meiosis and differentiation as sperm or egg. To distinguish between these two ideas, the molecular mechanisms controlling both mitosis/meiosis and sperm/egg decisions must be determined. That ultimate goal has not yet been reached for any organism, but progress has been made, and a molecular solution to this puzzle is on the horizon.

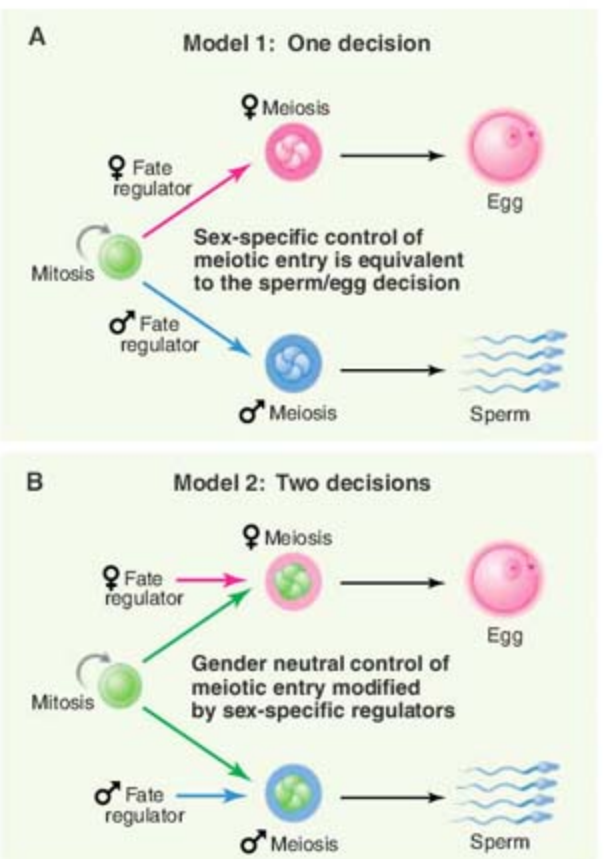

Fig. 1. Germ cell fate decisions. As germ cells mature, they enter meiosis and differentiate as sperm or egg. Germ cells are proposed to be uncommitted (green), female (fuschia), or male (blue).

Molecular Regulators of Germ Cell Fates

Our understanding of the mitosis/meiosis and sperm/egg decisions comes from studies in three model organisms—the nematode *C. elegans*, the fruit fly *Drosophila melanogaster*, and the mouse *Mus musculus*. We take a quick look at some of the key molecular regulators in the following order: regulators of mitosis, of entry into meiosis, and finally of differentiation as sperm or egg.

Germ cells are maintained in a state of undifferentiated mitotic divisions by sequence-specific RNA-binding proteins of the widely conserved PUF (Pumilio and FBF) family in both worms and flies (*6*–*8*). In mice, two PUF proteins, called Pum1 and Pum2, have been implicated in maintenance of germline stem cells, but that role has not yet been confirmed (*9*). In *C. elegans*, FBF keeps germ cells undifferentiated and dividing mitotically by the direct repression of specific mRNAs that encode regulators of both entry into the meiotic cell cycle and sexual identity (*8*, *10*). In flies, the mechanism is largely unknown.

[1]Howard Hughes Medical Institute, Department of Biochemistry, University of Wisconsin-Madison, Madison, WI 53706, USA. [2]Howard Hughes Medical Institute, Whitehead Institute, and Department of Biology, Massachusetts Institute of Technology, Cambridge, MA 02142, USA.

*To whom correspondence should be addressed. E-mail: jekimble@wisc.edu

Regulators that direct germ cells into the meiotic cell cycle have been found definitively in mice and nematodes. A novel cytoplasmic protein, called STRA8 (stimulated by retinoic acid-8), governs initiation of meiosis in embryonic mouse ovaries (*11*). In *C. elegans*, three broadly conserved cytoplasmic proteins accomplish this feat—two RNA-binding proteins (GLD-1/quaking and GLD-3/Bicaudal-C) and the catalytic subunit of an enzyme that adds adenosine residues to the 3′ end of mRNAs, a poly(A) polymerase called GLD-2 (*12*). A possible common theme is that the regulators are cytoplasmic, but without a better understanding of how STRA8 functions, it is premature to conclude a conserved mechanism.

Regulators of the sperm/egg decision have been identified in *C. elegans*. Most notable are FOG-1 (feminization of germ line) and FOG-3, which both reside at the end of a complex regulatory pathway controlling germ cell sex (*13*). FOG-1 is a homolog of the vertebrate CPEB (cytoplasmic polyadenylation element binding) translational regulator, and therefore is likely to control gene expression at a post-transcriptional level (*13*, *14*). FOG-3, on the other hand, bears an N-terminal motif typical of the poorly understood vertebrate Tob/BTG proteins; its molecular role in controlling germ cell sex remains uncharted territory (*15*). In animals lacking either FOG-1 or FOG-3, germ cells that normally differentiate as sperm are sexually transformed into oocytes. Therefore, both FOG-1 and FOG-3 promote the sperm fate at the expense of oogenesis.

The knowledge of molecules governing the sperm/egg decision in nematodes makes it possible to ask whether germ cells are irreversibly committed to their sexual identity. That question has been addressed by turning key regulators on or off at will, which is done using genetic tricks (e.g., RNA-mediated interference). The answer is that sexual identity is labile: adult females making eggs can be switched into spermatogenesis (*16*), and adult males producing sperm can be switched into oogenesis (*15*). Notably, germ cells adopt their sexual fate at about the same time they leave the mitotic cell cycle and enter meiosis (*17*). That temporal coincidence underscores the connection between the two decisions but says little about the underlying mechanism or logic of their relationship.

A prominent theme emerging from model organisms is the use of RNA regulatory proteins to control germ cell fates. Why RNA regulation is used for fate regulation in germ cells remains a matter for speculation. One idea is that differentiation of germ cells as sperm or egg is actually a transient phenomenon that must be reversed after fertilization. Regulation at the level of mRNA stability or translation might facilitate that reversal. Indeed, RNA regulators have also turned out to be critical for maintaining germ cell totipotency—the capacity to support differentiation of all cell fates in the next generation (*18*). How these RNA regulators interface with epigenetic regulation at the DNA level remains an open question and an interesting challenge for future studies.

A Molecular Link Between the Mitosis/Meiosis and Sperm/Egg Decisions

With specific regulators of the mitosis/meiosis and sperm/egg decisions in hand, one can begin to explore their molecular relationship. The initial identification of certain regulators of the mitosis/meiosis decision (e.g., GLD proteins) and others of the sperm/egg decision (e.g., FOG-1) lent support to model 2 (*10*–*13*). However, more in-depth studies revealed that the GLD and FOG regulators actually influence both decisions, revealing multiple molecular links between them (*13*). Most notable is FOG-1, which acts at the end of the pathway and is therefore likely to be one of its most important regulators. FOG-1 turns out to affect the two decisions in a dose-dependent manner, promoting mitosis at low levels but driving germ cells into the sperm fate at high levels (*10*). Is this FOG-1 duality a bizarre solution specific to nematodes, or the harbinger of a more universal phenomenon? In *Xenopus*, the FOG-1 homolog, called CPEB, promotes mitosis when present at a low level and progression through meiosis when more abundant (*19*). In *Drosophila*, the FOG-1 homolog, called Orb, has been implicated in controls of both entry into meiosis and germline sex determination (*20*). It is too early to conclude that this dual mechanism has been conserved, but the similarities are striking. Indeed, a molecular strategy in which a germline sexual regulator also promotes mitosis may explain the unusual tumors typical of putative germline sex determination genes in *Drosophila* (*21*), as well as having important implications for testicular cancers in mammals.

So, can we distinguish between the opposing models set forth earlier, one arguing that the mitosis/meiosis and sperm/egg decisions are the same and the other that they are different? In nematodes, the two decisions turn out to be governed by many of the same regulators, which could be argued to support model 1. But FOG-1 influences the two decisions by a dose-dependent mechanism, which could be interpreted as supporting model 2. Low FOG-1 and high FOG-1 might affect distinct mRNAs because of differences in binding affinity, or the two FOG-1 levels might affect the same mRNAs in different ways, for example, promoting translation at one level but inhibiting it at the other. A real understanding of the relationship between the two decisions requires identification of the targets of both FOG-1 and FOG-3 and a molecular explanation of how these two key regulators control their targets.

Remaining Questions and Puzzles

The intrinsic regulators of germ cell sex have long been a mystery, but insights drawn from work in model organisms have now opened a tantalizing crack in that large black box. Our first glimpse inside reveals some unexpected answers and a host of new questions. Will RNA regulation dominate the molecular strategy used to control germ cell fates? Or will transcriptional regulators, which have so far been elusive, prove to be the real key? Are PUF proteins universal regulators of germline stem cells? What about other germ cell fate regulators like the FOG and GLD proteins? Do their vertebrate homologs also control germ cell fates, or have they been co-opted for this task in nematodes by some quirk of evolution? And how do human germ cells fit into the picture? The answers to these basic questions of germ cell biology are now within experimental reach.

References

1. A. McLaren, D. Southee, *Dev. Biol.* **187**, 107 (1997).
2. D. Zarkower, in *WormBook*, *C. elegans* Research Community, Ed. (WormBook, www.wormbook.org, 2006), 10.1895/wormbook1.84.1.
3. M. Wawersik *et al.*, *Nature* **436**, 563 (2005).
4. J. Koubova *et al.*, *Proc. Natl. Acad. Sci. U.S.A.* **103**, 2474 (2006).
5. J. Bowles *et al.*, *Science* **312**, 596 (2006).
6. H. Lin, A. C. Spradling, *Development* **124**, 2463 (1997).
7. A. Forbes, R. Lehmann, *Development* **125**, 679 (1998).
8. S. L. Crittenden *et al.*, *Nature* **417**, 660 (2002).
9. E. Y. Xu, R. Chang, N. A. Salmon, R. A. Reijo Pera, *Mol. Reprod. Dev.*, E-pub ahead of print, 10.1002.mrd.20687 (2007).
10. B. E. Thompson *et al.*, *Development* **132**, 3471 (2005).
11. A. E. Baltus *et al.*, *Nat. Genet.* **38**, 1430 (2006).
12. J. Kimble, S. L. Crittenden, in *WormBook*, *C. elegans* Research Community, Ed. (WormBook, www.wormbook.org, 2005), 10.1895/wormbook.1.13.1.
13. R. Ellis, T. Schedl, in *WormBook*, *C. elegans* Research Community, Ed. (WormBook, www.wormbook.org, 2006), 10.1895/wormbook.1.82.1.
14. B. Thompson, M. Wickens, J. Kimble, in *Translational Control in Biology and Medicine*, M. B. Mathews, N. Sonenberg, J. W. B. Hershey, Eds. (Cold Spring Harbor Laboratory Press, Woodbury, NY, 2007).
15. P.-J. Chen, A. Singal, J. Kimble, R. E. Ellis, *Dev. Biol.* **217**, 77 (2000).
16. M. Otori, T. Karashima, M. Yamamoto, *Mol. Biol. Cell* **17**, 3147 (2006).
17. M. K. Barton, J. Kimble, *Genetics* **125**, 29 (1990).
18. R. Ciosk, M. DePalma, J. R. Priess, *Science* **311**, 851 (2006).
19. R. Mendez, J. D. Richter, *Nat. Rev. Mol. Cell Biol.* **2**, 521 (2001).
20. J.-R. Huynh, D. St Johnston, *Development* **127**, 2785 (2000).
21. B. Oliver, *Int. Rev. Cytol.* **219**, 1 (2002).

10.1126/science.1142109

REVIEW

Male and Female *Drosophila* Germline Stem Cells: Two Versions of Immortality

Margaret T. Fuller[1] and Allan C. Spradling[2]

Drosophila male and female germline stem cells (GSCs) are sustained by niches and regulatory pathways whose common principles serve as models for understanding mammalian stem cells. Despite striking cellular and genetic similarities that suggest a common evolutionary origin, however, male and female GSCs also display important differences. Comparing these two stem cells and their niches in detail is likely to reveal how a common heritage has been adapted to the differing requirements of male and female gamete production.

The germ line is emerging as one of the best models for studying the biology of adult stem cells in vivo. Many organisms produce sperm and eggs throughout their reproductive lives by classic high-throughput stem cell systems, although the active contribution of germline stem cells (GSCs) to oogenesis in adult mammals remains doubtful. Above all, GSCs fascinate as the ultimate manifestation of stemness: maintaining the only cell type capable of contributing to the next generation and thereby recapitulating a species' entire repertoire of cellular diversity.

A Tale of Two Niches

Drosophila GSCs are currently among the best-understood adult stem cells (*1*, *2*). A primary lesson from their study is the importance of the microenvironment (the stem cell niche) in regulating decisions between self-renewal and differentiation (*3*–*5*). The observation that self-renewal depends on short-range signals from a supporting niche can account for many properties of stem cell populations, including their ability to expand after transplantation to a stem cell–depleted host. Dependence on niches might also defend against cancer, capping stem cell numbers and preventing these potent undifferentiated precursors from self-renewing in the wrong location (*6*).

In males, the niche is limited to the space adjacent to a tightly packed plug of somatic hub cells at the testis tip, a region that is sufficient to accommodate 6 to 12 GSCs. In females, the niche is adjacent to four to seven cap cells and supports two to three GSCs (Fig. 1). In both sexes, GSCs are maintained by direct attachment to niche cells via adherens junctions and by receiving local signals that fail to stimulate germ cells located even one cell diameter away from the niche. Both niches also house somatic stem cells whose daughters enclose early germ cells. Internally, GSCs share other distinctive features, including the spectrosome: an aggregate of endoplasmic reticulum–like vesicles inherited asymmetrically during mitosis. Male and female GSC daughters, known as gonialblasts or cystoblasts, respectively, undergo synchronous incomplete divisions to generate analogous 16-cell germline cysts (Fig. 1, A and B). Also, many genes are required in common, including *piwi*, *bam*, *bgcn*, and *stet*. Despite these similarities, male and female GSC niches exhibit considerable differences.

Different Signals

The biggest known difference between the sexes is in the short-range signals used to specify GSC self-renewal. Female GSCs are strictly governed by bone morphogenetic protein (BMP) signaling from the niche, mediated by the ligands decapentaplegic and glass-bottomed boat (GBB) expressed in somatic niche cells (*1*). BMP signaling represses transcription of *bam* (*7*), a key differentiation regulator that is normally turned off in GSCs (Fig. 1C). Bam acts with its partner, benign gonial cell neoplasm (BGCN), a large DExH box protein, to drive GSC daughters that leave the niche to initiate differentiation by an unknown mechanism. The cell-fate switch may be stabilized by activation of *d-smurf*, an E3 ubiquitin ligase that blocks residual BMP signaling by promoting degradation of the SMAD *Medea* (*8*). Forced expression of BAM in GSCs flips the switch and causes GSCs to differentiate. Germ cell regulation by somatic BMP signals is probably an ancient mechanism (*1*, *9*); however, BAM and BGCN orthologs are unknown outside *Drosophila*.

The roles of BAM, BGCN, and BMP signaling are all substantially different in males, where BAM and BGCN function to end rather than initiate mitotic cyst divisions. BMP signal reception is still required to maintain GSCs and repress *bam* transcription, but GBB is expressed in cyst cells and the hub, and *bam* is repressed in gonialblasts as well as GSCs (Fig. 1D). BAM misexpression can be toxic to male GSCs, rather than just promoting differentiation, as it does in females (*10*).

The primary task of controlling GSC self-renewal in males is performed by a different signal, the cytokine-like ligand Unpaired (UPD) (*4*, *5*). UPD expressed by hub cells activates the Janus kinase–signal transducers and activators of transcription (JAK-STAT) pathway in GSCs to specify stem cell self-renewal. When a male GSC divides, the daughter retaining contact with the hub maintains stem cell identity, while the daughter displaced away experiences a weaker signal and initiates differentiation. In contrast, female GSCs have no autonomous requirement for JAK-STAT signaling (*1*, *11*). Thus, both male and female niches maintain GSCs and stimulate asymmetric division by limiting access to a local signal, but they rely on different signals for this function.

Sexual Differences in Orientation

For niches based on local signaling to reliably program asymmetric fate outcomes, one daughter cell must preferentially receive the signal after stem cell division. This is accomplished by oriented division: Normally, only one daughter cell remains in the niche. In both sexes, GSCs attach to niche cells via localized adherens junctions rich in E-cadherin (Fig. 1, C and D). Genetically disrupting the junctional components causes stem cell loss (*1*, *2*). The mechanism used to displace exactly one of the daughters from the niche differs between males and females, however. In males, anaphase-promoting complex 2 (APC2) colocalized with E-cadherin at the cortex where GSCs contact the hub (Fig. 1D) mediates a key polarity cue that orients the spindles of mitotic GSCs so that they lie perpendicular to the hub. There is no evidence that such a system acts in the female niche, where space limitations may constrain a daughter cell from exiting the niche. Male and female GSCs also differ in the location of the spectrosome, which may reflect as yet uncharacterized differences in centrosome behavior.

Centrosome positioning plays a key role in ensuring the correct spindle orientation in male GSCs (*2*, *12*). Early in interphase, the single GSC centrosome localizes near the cortex where it attaches to the hub (Fig. 1D). When the duplicated centrosomes separate, unusually early in G_2, one stays next to the hub, while the

[1]Departments of Developmental Biology and Genetics, Stanford University School of Medicine, Stanford, CA 94305, USA. [2]Department of Embryology and Howard Hughes Medical Institute (HHMI), Carnegie Institution of Washington, Baltimore, MD 21218, USA.

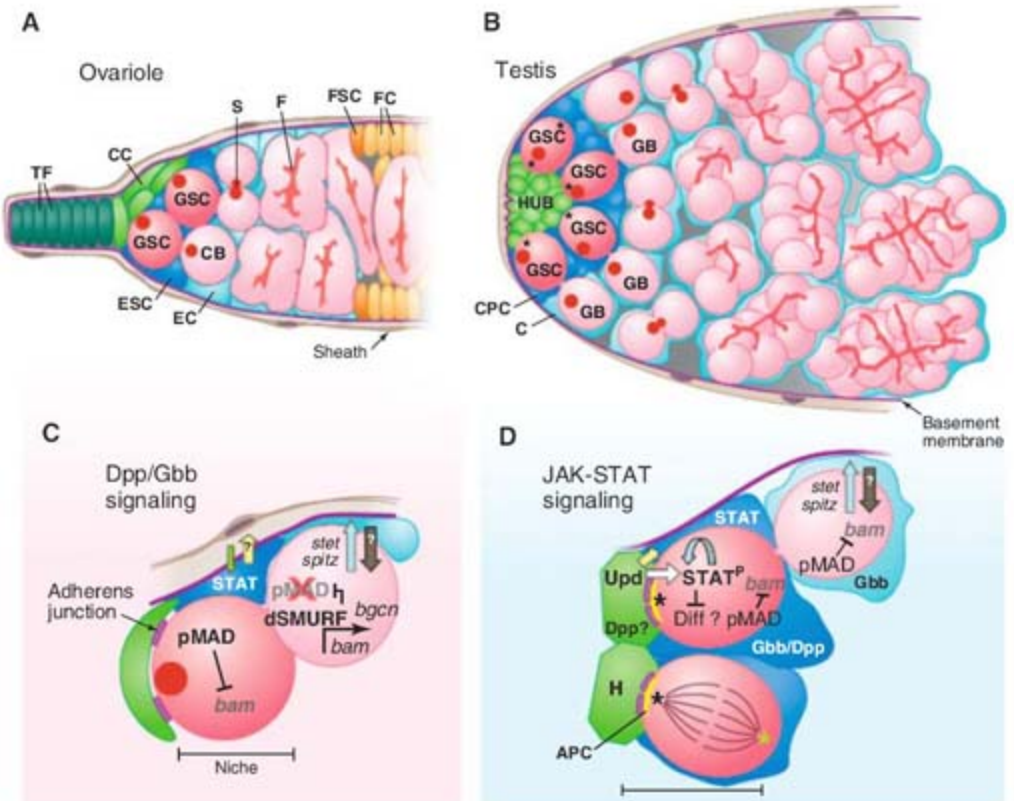

Fig. 1. Male and female germline and somatic stem cells in their gonadal niches. (**A**) Ovariole tip (16 per ovary) and (**B**) testis tip. Germ cells, dark pink (GSCs) and light pink (cysts); somatic cells, green, blue (ESCs or CPCs), turquoise, and yellow; spectrosome (S) and fusome (F), red. (A) Female. CB, cystoblast; TF, terminal filament; CC, cap cell; EC, escort cell; FSC, follicle stem cell; FC, follicle cell. (B) Male. GB, gonialblast; C, cyst cell; black asterisks, centrosomes. (**C** and **D**) Key regulatory pathways of the niche. (C) Female. BMP signaling maintains GSCs by repressing expression of *bam*. Activation of STAT maintains somatic escort stem cells. Dpp, decapentaplegic. (D) Male. Hub cells (H) express Upd, which activates STAT in GSCs. Yellow, localized APC2 and β-catenin; black asterisks, mother centrosomes; green asterisks, daughter centrosomes.

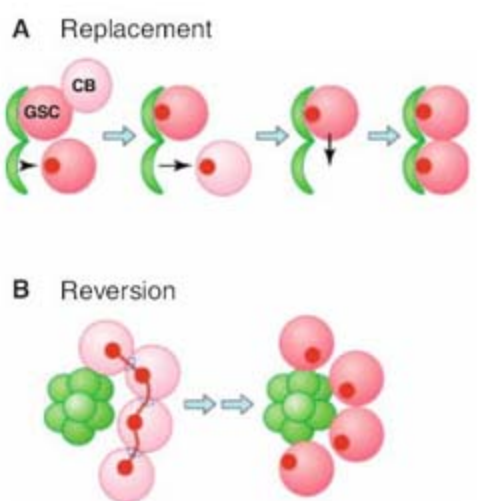

Fig. 2. Two modes for the replacement of lost stem cells. (**A**) Equal stem cell division. (**B**) Reversion of transit-amplifying cells in germline cysts. Dark pink, GSCs; light pink, differentiating transit-amplifying cell; green, somatic cells that provide the niche.

other migrates to the opposite side of the cell. The stereotyped position of the centrosomes reliably orients the mitotic spindle perpendicular to the interface with the hub. Perhaps because of its greater capacity to hold astral microtubules, the mother centrosome normally remains next to the hub and is retained by the GSC through many GSC generations (Fig. 1D) (*12*). It remains an interesting question whether preferential inheritance of the mother centrosome is important for stem cell fate or is a side effect of its tightly oriented divisional program.

Stem Cell Partnerships

Both male and female niches also maintain morphologically similar somatic stem cells interspersed among the GSCs (Fig. 1). Known as cyst progenitor cells (CPCs) in males or escort stem cells (ESCs) in females, both produce squamous nondividing daughters (cyst or escort cells) that enclose the GSC daughter destined for differentiation and persist to envelop its progeny (*2*, *11*). In the niche, thin processes from the CPCs or ESCs cover most GSC surfaces, isolating GSCs from each other but not from hub or cap cells. The close physical association of somatic and germline stem cells within a common niche probably facilitates their spatially coordinated production of differentiating daughters that must work together.

In both sexes, the proper interaction of germline and somatic cells to form cysts requires signals processed by the germline-specific *rhomboid*-class protease *STET* and received via the epidermal growth factor receptor in the adjacent cyst or escort cells (*13*), and the relationship between these germline and somatic partners in a cyst appears to be important for proper differentiation. JAK-STAT signaling plays a role in the female niche: ESCs require *Stat* to preserve niche function (*11*). Thus, although both male and female niches use BMP and JAK-STAT signaling, these signals play sex-specific roles, perhaps ultimately because of the very different functions carried out by *bam* in the two stem cell lineages.

Rules of Succession

Given their role as cellular reservoirs, it was surprising to learn that individual male and female GSCs turn over regularly (*1*, *2*). It is now clear that replacement GSCs for the affected niches can arise by at least two distinct mechanisms. New female GSCs are produced after GSC loss when a partner GSC divides parallel to the cap cells, causing both daughters to remain in the niche and become stem cells (*3*) (Fig. 2). The ability to undergo such symmetric divisions under the right circumstances has been postulated to explain the expansion in stem cell numbers observed after transplantation of mammalian GSCs into depleted seminiferous tubules (*14*). However, new GSCs can also arise from the reversion of transit-amplifying cells in germline cysts up to at least the eight-cell stage into fully functional stem cells (*15*, *16*) (Fig. 2). Reversion of differentiating cyst cells may normally be prevented by BAM, an insulating layer of escort or somatic cyst cells, or other factors. Symmetric division is the only mechanism that has been shown to replace female GSCs in adults. In contrast, there is no evidence at present for symmetric male GSC divisions. Furthermore, in mammalian testes, a breakdown of the youngest undifferentiated spermatogonial cysts is thought to replenish GSCs (*17*). Thus, male and female GSCs may employ different lines of succession when their reigning GSCs exit the niche.

Conclusion

Finer aspects of regulation that differ between male and female GSCs lie beneath common general features, such as adhesion to stromal cells and dependence on close range signals. We

can only speculate about the selective forces that may be responsible for these differences. The fact that there is only 1 niche per testis and 16 niches per ovary may explain the larger number of GSCs per niche in males. The more robust mechanism of spindle orientation in male GSCs may be a consequence of the larger niche. This, in turn, may cause a preferential use of cyst reversion rather than symmetric GSC division to generate replacement stem cells. Nonetheless, it is probably safe to expect that each stem cell type has become more or less specialized to the particular requirements of the cells it supports. Thus, while searching for the common laws of stem cells, we must continue to expect the unusual and even the unique.

References and Notes

1. L. Li, T. Xie, *Annu. Rev. Cell Dev. Biol.* **21**, 605 (2005).
2. Y. M. Yamashita, M. T. Fuller, D. L. Jones, *J. Cell Sci.* **118**, 665 (2005).
3. T. Xie, A. Spradling, *Science* **290**, 328 (2000).
4. A. A. Kiger, D. L. Jones, C. Schulz, M. B. Rogers, M. T. Fuller, *Science* **294**, 2542 (2001).
5. N. Tulina, E. Matunis, *Sciecne* **294**, 2546 (2001).
6. M. F. Clarke, M. T. Fuller, *Cell* **124**, 1111 (2006).
7. D. Chen, D. McKearin, *Curr. Biol.* **13**, 1786 (2003).
8. M. Casanueva, E. Ferguson, *Development* **131**, 1881 (2004).
9. L. Gilboa, R. Lehmann, *Curr. Biol.* **14**, 981 (2004).
10. C. Schulz *et al.*, *Genetics* **167**, 707 (2004).
11. E. Decotto, A. C. Spradling, *Dev. Cell* **9**, 501 (2005).
12. Y. M. Yamashita, A. P. Mahowald, J. R. Perlin, M. T. Fuller, *Science* **315**, 518 (2007).
13. C. Schulz, C. Wood, D. L. Jones, S. Tazuke, M. T. Fuller, *Development* **129**, 4523 (2002).
14. R. L. Brinster, *Science* **316**, 404 (2007).
15. T. Kai, A. Spradling, *Nature* **428**, 564 (2004).
16. C. Brawley, E. Matunis, *Science* **304**, 1331 (2004).
17. T. Nakagawa, Y. Nabeshima, S. Yoshida, *Dev. Cell* **12**, 195 (2007).

18. We gratefully acknowledge support from NIH (grants P01DK53074 and RO1GM61986) to M.T.F. and from the HHMI to A.C.S.

10.1126/science.1140861

REVIEW

Male Germline Stem Cells: From Mice to Men

Ralph L. Brinster

The production of functional male gametes is dependent on the continuous activity of germline stem cells. The availability of a transplantation assay system to unequivocally identify male germline stem cells has allowed their in vitro culture, cryopreservation, and genetic modification. Moreover, the system has enabled the identification of conditions and factors involved in stem cell self-renewal, the foundation of spermatogenesis, and the production of spermatozoa. The increased knowledge about these cells is also of great potential practical value, for example, for the possible cryopreservation of stem cells from boys undergoing treatment for cancer to safeguard their germ line.

Male germline stem cells, called spermatogonial stem cells (SSCs) in postnatal mammals, are the foundation of spermatogenesis (the process for spermatozoa production) and, together with oocytes from females, are essential for species continuity. SSCs reside on the basement membrane of the seminiferous tubule in the testis and are almost completely surrounded by somatic Sertoli cells, which form a microenvironment or niche. Within the niche, growth factors and extracellular signals regulate the fate decisions of SSCs either to self-renew or to form daughter cells that will begin the complex differentiation process of spermatogenesis, resulting in mature spermatozoa after about 35 days in the mouse and 64 days in the human (*1*, *2*). The timing of sequential steps in spermatogenesis is tightly regulated by genes of the germ cell, and Sertoli cells support the differentiation process.

The first step in spermatogenesis is the fate decision of an SSC to produce daughter cells committed to differentiation. There are no known unique biochemical or phenotypic markers for distinguishing SSCs from their initial daughters, called undifferentiated spermatogonia. This limitation has hampered studies on the biology of SSCs. However, in 1994 a spermatogonial stem cell assay was reported in mice that identified SSCs by their ability to generate a colony of spermatogenesis after transplantation to the seminiferous tubules of a recipient male. If a sufficient number of SSCs were transplanted, progeny displaying the donor haplotype were produced by the recipient (*3*). Subsequent studies showed that SSCs of all mammalian species examined (e.g., rat, rabbit, dog, pig, cow, baboon, and human) would colonize the seminiferous tubules of immunodeficient mice and generate colonies of stem cells and cells that appeared to be early differentiating daughter spermatogonia (*1*, *3*). These results indicate that signals in the stem cell and niche must have been highly conserved among mammalian species during the course of the 100 million years since the phylogenetic divergence of mice and humans. Moreover, unlike mature spermatozoa, which are difficult to cryopreserve and require species-specific procedures, SSCs from all of the species examined can be cryopreserved for long periods with common techniques used for somatic cells (*1*).

The availability of the transplantation assay made it possible to study SSCs in culture (*4*) and has led to the continuous replication of mouse SSCs in vitro (*5*). Glial cell line–derived neurotrophic factor (GDNF) was identified as a critical factor in vivo for the replication of spermatogonia (*6*). In vitro studies using serum-free culture medium demonstrated that GDNF is the primary growth factor supporting mouse SSC self-renewal (*7*). The development of culture methods has led to a wide range of studies on SSCs in vitro (*8*, *9*). GDNF binding and signaling occur through GDNF-family receptor α1 (GFRα1) and the Ret receptor on SSCs and undifferentiated spermatogonia. Although both GFRα1 and Ret are surface molecules, they have not been ideal for purifying SSCs from testes, resulting in, at best, a 1.75-fold enrichment (*10*, *11*). Selection with antibodies to thymus cell antigen 1, however, produces a 5- to 10-fold enrichment of SSCs, generating excellent cell populations for studies on SSCs (*10*, *12*).

In the presence of GDNF, SSCs grow on feeder cells as islands or clumps of cells. If GDNF is removed, the clump cells begin to grow in chains resembling the initial stages of stem cell differentiation, as seen in vivo (*2*, *12*–*15*). Thus, GDNF appears to be a primary regulator of the self-renewal versus differentiation fate decision for mouse and rat SSCs (*7*, *14*), and it is probably a conserved self-renewal signal for all mammalian SSCs (*7*, *14*, *15*). Similar to embryonic stem cells (ESCs), SSCs grow in vitro on feeder cells in islands or clumps, and they stain positive for *POU domain class 5 transcription factor 1* (*Oct 3/4*) and alkaline phosphatase (*7*). These observations suggested that SSCs might be pluripotent. However, whereas ESCs readily generate teratocarcinomas when transplanted in vivo, SSCs do not form tumors under similar conditions (*3*, *7*). Whether the normal adult SSC can be induced to become pluripotent remains controversial.

The availability of a functional transplantation assay and a culture system that allows long-term replication of SSCs made it possible to examine intracellular signals that influence self-renewal and differentiation in vitro in a rigorous manner that is not available for most adult stem cells (*16*). These studies demonstrated that *Oct 3/4* and *SRY–box-containing gene 2* (*Sox 2*), which regulate *Nanog*, are expressed in SSCs. However, *Nanog*, the key determinant of ESC self-renewal and pluripotency, is not expressed in SSCs (*16*). Therefore, the signaling mechanisms that maintain self-renewal in SSCs and ESCs are different. These studies also

Department of Animal Biology, School of Veterinary Medicine, University of Pennsylvania, Philadelphia, PA 19104, USA.

demonstrated that the expression of genes for three transcription factors, *B cell CLL/lymphoma 6 member B* (*Bcl6b*), *Ets-related molecule* (*Erm*), and *LIM homeobox 1* (*Lhx1*), is highly regulated by GDNF in vitro. Functional SSC transplantation assays confirmed the importance of *Bcl6b*, and it is therefore likely that *Erm* and *Lhx1* influence SSC self-renewal (*16*). *Erm* expression in Sertoli cells is also believed to affect niche function (*17*). Other studies indicate an important role in SSC self-renewal for *promyelocyte leukemia zinc-finger factor* (*Plzf*), *TATA-binding protein-associated factor 4b* (*TAF4b*), and perhaps *Nanos 2* (*NOS2*) (*18*–*20*), but GDNF does not regulate these genes (*16*). Therefore, the mechanism of their action is unclear.

Although the culture and transplantation systems have made it possible to study SSC self-renewal, the absence of similar systems for germ cell differentiation stages of spermatogenesis has complicated the examination of regulatory mechanisms for this process. Moreover, the intricate three-dimensional structural organization of spermatogenesis has compounded the problem. In addition to surrounding the stem cell to provide a regulatory niche, the Sertoli cell extends ~90 μm from the basement membrane to the lumen of the seminiferous tubule, contacting and surrounding germ cells in many stages of differentiation. Furthermore, an individual germ cell may associate with more than one Sertoli cell (*2*, *13*). Near the basement membrane are early stages of spermatogonia, including SSCs and undifferentiated spermatogonia. These cells are GDNF-responsive but do not display the c-Kit tyrosine kinase receptor on their surface (*7*, *8*). A critical step to initiate their conversion to differentiating spermatogonia is probably a signal to express c-*kit*. Then, the binding of the stem cell factor Kit ligand, from Sertoli cells to the c-Kit receptor, could initiate the remaining differentiation pathway. This step from undifferentiated to differentiating spermatogonia appears to be a critical regulatory point in spermatogenesis. The timing of subsequent steps in differentiation is controlled by germ cell genes (*1*). An exciting new area of spermatogenesis regulation involves small interfering RNAs, evolutionarily conserved molecules that inhibit gene expression and are present in germ cells throughout spermatogenesis (*21*).

The ability to recover, cryopreserve, culture, and transplant SSCs has stimulated new approaches to understanding the biology of these important cells. It has also provided an opportunity for practical and medical applications of SSCs and makes individual male germ lines potentially immortal. The continuous long-term increase in the number of SSCs in culture now allows for the introduction of genetic modifications through the germ line with methods developed for somatic cells and ESCs. Potentially, any genetic manipulation, including targeted gene knockout or correction, can be used in all mammalian species for which culture conditions are developed. However, in humans, clinical and ethical limitations will be critically important.

Stem cell recovery and cryopreservation may be applicable to all mammalian species and could be used to preserve the male germ line of valuable livestock animals, companion animals, and endangered species. Perhaps the most provocative and potentially valuable medical application of SSC research is for prepubertal boys undergoing chemotherapy or irradiation for cancer (*9*). In many cases, the SSCs are destroyed as a side effect of treatment, and the patient is left infertile. It is possible to obtain a testicular biopsy and cryopreserve a cell suspension produced from the biopsy. This cell suspension containing SSCs could then be transplanted back into the patient's testes at any age after treatment, potentially resulting in recolonization of the testes and spermatozoa production (Fig. 1). Development of culture techniques for human SSCs will facilitate this important medical application.

There are many possible future directions to pursue. Three particularly important areas include (i) the further definition of factors and signals that support self-renewal of SSCs, relative to those that initiate differentiation in order to provide a better understanding of this fate decision; (ii) the extension of the serum-free culture system to other species, including domestic animals, endangered species, and humans to confirm that self-renewal signals are conserved among mammals and for relevant applications; and (iii) the development of methods to allow in vitro differentiation of stem cells to provide mature spermatozoa, which would be enormously valuable in understanding the complex process of spermatogenesis and would have great practical use. These advances will dramatically expand the applications of SSCs.

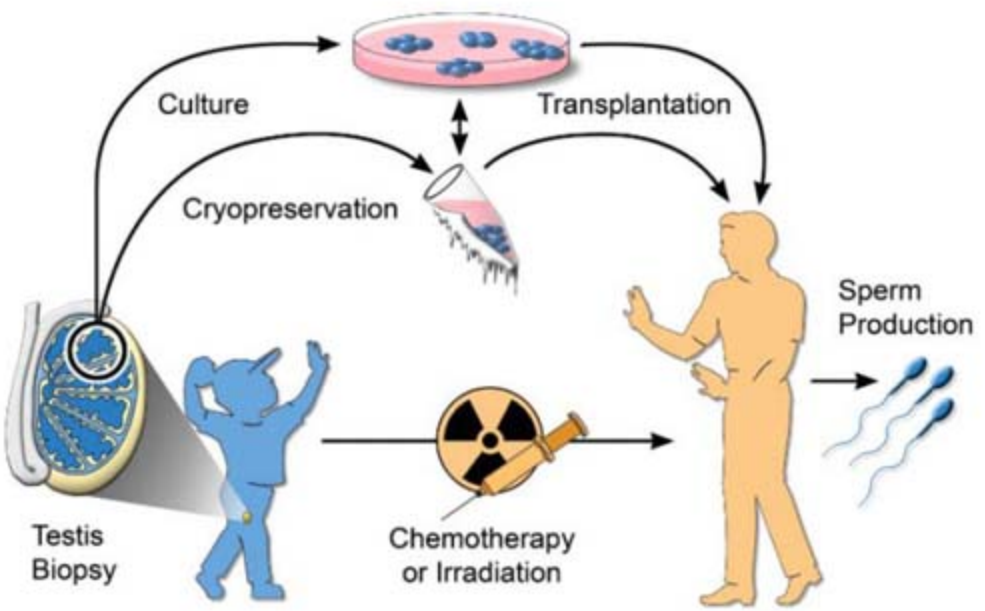

Fig. 1. Male germline stem cell preservation. Before treatment for cancer by chemotherapy or irradiation, a boy could undergo a testicular biopsy to recover stem cells. The stem cells could be cryopreserved or, after development of the necessary techniques, could be cultured. After treatment, the stem cells would be transplanted to the patient's testes for the production of spermatozoa.

References and Notes

1. R. L. Brinster, *Science* **296**, 2174 (2002).
2. L. D. Russell, R. A. Ettlin, A. P. Sinha Hikim, E. D. Clegg, in *Histological and Histopathological Evaluation of the Testis* (Cache River, Clearwater, FL, 1990). pp. 1–58.
3. R. L. Brinster, M. R. Avarbock, *Proc. Natl. Acad. Sci. U.S.A.* **91**, 11303 (1994).
4. M. Nagano, M. R. Avarbock, E. B. Leonida, C. J. Brinster, R. L. Brinster, *Tissue Cell* **30**, 389 (1998).
5. M. Kanatsu-Shinohara *et al.*, *Biol. Reprod.* **69**, 612 (2003).
6. X. Meng *et al.*, *Science* **287**, 1489 (2000).
7. H. Kubota, M. R. Avarbock, R. L. Brinster, *Proc. Natl. Acad. Sci. U.S.A.* **101**, 16489 (2004).
8. J. M. Oatley, R. L. Brinster, *Methods Enzymol.* **419**, 259 (2006).
9. H. Kubota, R. L. Brinster, *Nat. Clin. Pract. Endocrinol. Metab.* **2**, 99 (2006).
10. K. T. Ebata, X. Zhang, M. C. Nagano, *Mol. Reprod. Dev.* **72**, 171 (2005).
11. A. Buageaw *et al.*, *Biol. Reprod.* **73**, 1011 (2005).
12. H. Kubota, M. R. Avarbock, R. L. Brinster, *Biol. Reprod.* **71**, 722 (2004).
13. D. G. De Rooij, *Int. J. Exp. Pathol.* **79**, 67 (1998).
14. B.-Y. Ryu, H. Kubota, M. R. Avarbock, R. L. Brinster, *Proc. Natl. Acad. Sci. U.S.A.* **102**, 14302 (2005).
15. F. K. Hamra *et al.*, *Proc. Natl. Acad. Sci. U.S.A.* **102**, 17430 (2005).
16. J. M. Oatley, M. R. Avarbock, A. I. Teleranta, D. T. Fearon, R. L. Brinster, *Proc. Natl. Acad. Sci. U.S.A.* **103**, 9524 (2006).
17. C. Chen *et al.*, *Nature* **436**, 1030 (2005).
18. M. D. Wong, Z. Jin, T. Xie, *Annu. Rev. Genet.* **39**, 173 (2005).
19. A. E. Falender *et al.*, *Genes Dev.* **19**, 794 (2005).
20. A. Suzuki, M. Tsuda, Y. Saga, *Development* **134**, 77 (2007).
21. H. Lin, *Science* **316**, 397 (2007).
22. I thank R. Behringer, R. Davies, H. Kubota, J. Oatley, and J. Schmidt for valuable comments on and contributions to the manuscript; M. Avarbock, C. Freeman, R. Naroznowski, and C. Pope for assistance in experiments; J. Hayden for help with photography and figures; and the National Institute of Child Health and Human Development (grant HD044445) and the Robert J. Kleberg Jr. and Helen C. Kleberg Foundation for financial support.

10.1126/science.1137741

REVIEW

The Maternal-Zygotic Transition: Death and Birth of RNAs

Alexander F. Schier

Maternal gene products drive early development when the newly formed embryo is transcriptionally inactive. During the maternal-zygotic transition, embryonic transcription is initiated and many maternal RNAs are degraded. Multiple mechanisms regulate the birth of zygotic RNAs and the death of maternal RNAs. Genome activation appears to rely in part on the sequestration of transcriptional repressors by the exponentially increasing amount of DNA during cleavage divisions. Maternal RNA degradation is induced by the binding of proteins and microRNAs to the 3′ untranslated region of target RNAs.

To achieve the striking increase in cell number after fertilization, most animals devote their early development to rapid and synchronous cell cycles (*1*). Whereas the overall amount of cytoplasm in the embryo remains constant, the number of nuclei and the amount of DNA increase exponentially. During this period, mRNAs and proteins provided to the egg by the mother drive development. By contrast, the embryonic genome is transcriptionally activated only at later cell cycles. This transition from a maternal to a zygotic mode of development has been called the midblastula transition (*2*) or maternal-zygotic transition (MZT) (Fig. 1). It often coincides with cell cycle lengthening and the degradation of many maternal RNAs. Here I review our current understanding of the mechanisms that regulate the birth of zygotic RNAs and the death of maternal RNAs.

At least three mechanisms have been implicated in the silencing of the zygotic genome during early development: (i) chromatin-mediated repression, (ii) deficiencies in the transcription machinery, and (iii) transcriptional repression or abortion by rapid cell cycles. The first evidence for repressors was provided 25 years ago, when Newport and Kirschner reported that a premature increase in the number of nuclei or the amount of DNA resulted in premature initiation of cell cycle lengthening and zygotic transcription in *Xenopus* embryos (*2*, *3*). These results, and related studies in *Drosophila* and zebrafish, have suggested that the nucleo-cytoplasmic ratio and the titration of a transcriptional repressor by the exponentially increasing amount of genomic DNA determine the timing of MZT (the "excess repressor model"). The key factors that need to be titrated are still elusive, but it is conceivable that histones or other chromatin components maintain silencing until a critical amount of DNA is present (*4*, *5*). Gene-specific DNA methylation has also been implicated in repression. Depletion of the methyltransferase Dnmt1 or of Kaiso, a transcriptional repressor binding to methylated DNA, results in the premature activation of a subset of genes (*6*). These studies suggest that multiple chromatin-mediated mechanisms prevent zygotic genome activation.

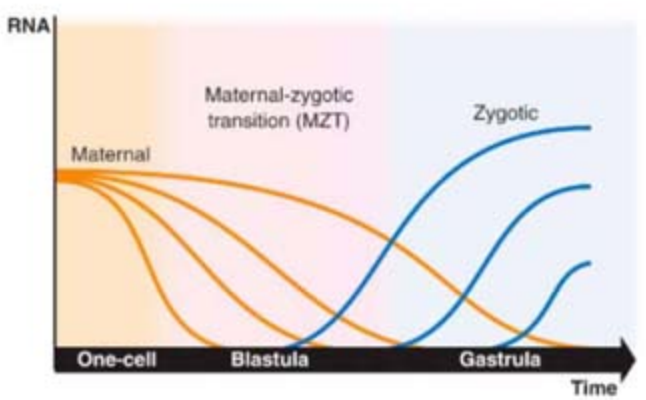

Fig. 1. The maternal-zygotic transition (MZT). Maternal RNAs are deposited by the mother into the egg and drive early development. These RNAs are degraded during different stages of embryogenesis, including blastula and gastrula stages. The embryonic genome is initially transcriptionally inactive until the MZT, when zygotic genes are starting to be transcribed.

A dearth or inactivation of components of the transcription machinery might be a second strategy for gene silencing before MZT (the "limited machinery model"). For example, premature expression of TATA-binding protein (TBP), a component of the transcriptional machinery, can induce premature activation of a subset of genes (*4*, *5*). Analogously, misexpression of strong transcriptional activators can cause precocious transcriptional activation. These conclusions are mainly based on the study of injected extrachromosomal DNA, and it therefore remains unclear to what extent the limited machinery model applies to endogenous genes.

The rapid cell cycles lacking G_1 and G_2 phases might constitute a third strategy that interferes with productive transcription during early cleavage stages (the "rapid cell cycle model"). DNA replication can interfere with transcription, and mitosis can lead to the abortion of nascent transcripts (*7*). Conversely, experimentally induced cell cycle lengthening can lead to premature transcription (*8*).

Although the excess repressor, limited machinery, and rapid cell cycle models can account for some aspects of MZT, they do not explain why several genes are already activated during early cleavage stages and why zygotic genome activation is a gradual and gene-specific process (*9*–*11*). These observations suggest that some of the mechanisms underlying zygotic genome activation remain to be discovered. Moreover, mammals activate zygotic transcription at very early cleavage stages (e.g., the mouse genome is activated at the two-cell stage) (*1*). It is conceivable that in mammals there might be sufficient time to assemble transcription complexes at early cleavage stages because the cell cycles are very long, but the exact mechanisms are elusive.

Whereas zygotic mRNAs are synthesized during embryogenesis, many maternal mRNAs are degraded. Degradation removes gene products that might interfere with later development. This regulated maternal mRNA destabilization is mediated by sequences in the 3′ untranslated region (3′ UTR) (*12*). Regulatory RNAs or proteins such as Smaug or EDEN-BP bind to these sequences and induce the deadenylation of target mRNAs, which are then prone to degradation by nucleases. Recent studies in zebrafish have identified the microRNA miR-430 as a potential link between zygotic genome activation and the decay of maternal mRNAs (*13*). MicroRNAs are short RNAs that bind to the 3′ UTR of target mRNAs to repress their translation and accelerate their decay. miR-430 targets several hundred maternally provided mRNAs by binding to complementary sites in their 3′ UTR and promoting their deadenylation. In the absence of miR-430 activity, these mRNAs accumulate and are thought to interfere with embryonic morphogenesis. miR-430 expression initiates at MZT, thus linking genome activation and maternal mRNA degradation.

In summary, multiple mechanisms regulate RNA synthesis and degradation during early embryogenesis. It remains unclear, however, whether most of the observed phenomena can be explained by a few key regulatory princi-

Department of Molecular and Cellular Biology, Harvard Stem Cell Institute, Center for Brain Science, Broad Institute, Harvard University, 16 Divinity Avenue, Room 1027, Cambridge, MA 02138, USA. E-mail: schier@fas.harvard.edu

ples, such as the nucleo-cytoplasmic ratio or microRNA-induced mRNA degradation. Future studies may also be relevant to the field of animal cloning. Cloning experiments rely on the reprogramming of donor nuclei by enucleated eggs. Thus, the milieu that silences the zygotic genome also reprograms transferred nuclei. Hence, understanding the mechanisms that underlie zygotic genome silencing will inform the design of reprogramming strategies (*4*).

References and Notes

1. P. H. O'Farrell, J. Stumpff, T. T. Su, *Curr. Biol.* **14**, R35 (2004).
2. J. Newport, M. Kirschner, *Cell* **30**, 675 (1982).
3. J. Newport, M. Kirschner, *Cell* **30**, 687 (1982).
4. N. Kikyo, A. P. Wolffe, *J. Cell Sci.* **113**, 11 (2000).
5. M. N. Prioleau, J. Huet, A. Sentenac, M. Mechali, *Cell* **77**, 439 (1994).
6. A. Ruzov *et al.*, *Development* **131**, 6185 (2004).
7. A. W. Shermoen, P. H. O'Farrell, *Cell* **67**, 303 (1991).
8. B. A. Edgar, G. Schubiger, *Cell* **44**, 871 (1986).
9. J. Yang, C. Tan, R. S. Darken, P. A. Wilson, P. S. Klein, *Development* **129**, 5743 (2002).
10. D. K. Pritchard, G. Schubiger, *Genes Dev.* **10**, 1131 (1996).
11. S. Mathavan *et al.*, *PLoS Genet.* **1**, 260 (2005).
12. W. Tadros, H. D. Lipshitz, *Dev. Dyn.* **232**, 593 (2005).
13. A. J. Giraldez *et al.*, *Science* **312**, 75 (2006).

14. I thank K. Eggan, N. Francis, D. Kimelman, M. Michael, S. Mango, P. Sabeti, G. Seydoux, and members of my lab for helpful discussions. Supported by grants from NIH, the Human Frontier Science Program, and the McKnight Endowment Fund for Neuroscience.

10.1126/science.1140693

REVIEW

Regulation of the Oocyte-to-Zygote Transition

Michael L. Stitzel[1,2] and Geraldine Seydoux[1]

Oocytes, the female germ cells, contain all the messenger RNAs necessary to start a new life but typically wait until fertilization to begin development. The transition from oocyte to fertilized egg (zygote) involves many changes, including protein synthesis, protein and RNA degradation, and organelle remodeling. These changes occur concurrently with the meiotic divisions that produce the haploid maternal genome. Accumulating evidence indicates that the cell-cycle regulators that control the meiotic divisions also regulate the many changes that accompany the oocyte-to-zygote transition. We suggest that the meiotic machinery functions as an internal pacemaker that propels oocytes toward embryogenesis.

Ex ovo omnia (Everything from an egg) (*1*).

How does an egg become "everything"? The journey begins with one of the most complex cell transformations in biology: remodeling of a fertilized oocyte into a totipotent zygote. Remarkably, this transition occurs in the absence of transcription and therefore depends on messenger RNAs (mRNAs) accumulated in the oocyte during oogenesis. Fully grown oocytes contain a dizzying array of RNA messages, corresponding to 20 to 45% of all mouse genes (*2*, *3*) and 55% of all *Drosophila* genes (*4*)! These transcripts guide oocytes during two makeovers on the way to becoming zygotes: oocyte maturation and egg activation. During oocyte maturation, extracellular signals stimulate oocytes arrested in prophase of meiosis I to enter meiotic M phase and initiate the meiotic divisions (*5*). Typically, oocytes are ovulated and become competent for fertilization before reaching a second arrest point (metaphase of meiosis II in mammals). Egg activation, triggered by sperm entry in many species, completes the transformation to zygote by signaling the completion of meiosis, the formation of pronuclei, and the first mitotic division (*6*). In this Review, we discuss the changes that accompany each of these transitions, addressing strategies of gene activation, gene inactivation, and organelle remodeling.

[1]Department of Molecular Biology and Genetics and Howard Hughes Medical Institute, Johns Hopkins School of Medicine, 725 North Wolfe Street, PCTB 706, Baltimore, MD 21205, USA. [2]Predoctoral Training Program in Human Genetics and Molecular Biology, Johns Hopkins School of Medicine, 725 North Wolfe Street, PCTB 706, Baltimore, MD 21205, USA.

In with the New...

Oocyte maturation requires the synthesis of new proteins. Interdependent translational activation events ensure that proteins are produced in the correct succession (*7*). For example, early during oocyte maturation in *Xenopus*, translation of the cyclin-dependent kinase (CDK)–binding protein RINGO/Spy activates maturation promoting factor (MPF; CDK1/cyclin B1 complex). Active MPF in turn stimulates the translation of proteins needed to maintain metaphase II arrest in the matured oocyte (Fig. 1). During egg activation, additional RNAs are recruited for translation. A study comparing matured oocytes and zygotes revealed dramatic differences in polysome-associated RNAs, with nearly one-third of transcripts (29%) showing differential translation between the two stages (*8*). Oocyte polysomes were enriched for transcripts encoding proteins implicated in cellular homeostasis, whereas zygotic polysomes were enriched for transcripts implicated in macromolecular biosynthesis.

How are oocyte mRNAs activated for translation? In many cases, activation depends on liberating mRNAs from complexes that block translation initiation (*7*, *9*). For example, in mouse, clam, and *Xenopus* oocytes, mRNAs that contain cytoplasmic polyadenylation elements (CPEs) in their 3′ untranslated region are stored with short poly-adenylated [poly(A)] tails and bound by a translation-repressing complex containing the CPE-binding protein (CPEB) and its partner, Maskin. Maskin binds the cap-binding protein eIF4E, preventing the recruitment of the translation initiation factor eIF4G. During oocyte maturation, phosphorylation of CPEB stimulates polyadenylation and recruitment of poly(A)-binding protein bound to eIF4G. Incoming eIF4G displaces Maskin from eIF4E, allowing formation of the initiation complex (*7*).

As first recognized in clam oocytes (*10*), translational activation of oocyte mRNAs is often linked to poly(A)-tail extension, but the two can also occur independently. For example, in *Drosophila* eggs, cyclin B mRNA is kept translationally silenced by the RNA binding protein Pumilio (*11*). During egg activation, the PAN GU kinase activates (by an unknown mechanism) cyclin B mRNA translation and poly(A) tail extension (*4*, *11*). In *pan gu* mutants, forced expression of poly(A) polymerase is sufficient to rescue polyadenylation of cyclin B but not translation (*4*). Depletion of Pumilio has the opposite effect: translation is restored, but polyadenylation is not (*11*). These observations suggest that both polyadenylation-independent and polyadenylation-dependent mechanisms activate translation in oocytes, and a challenge for the future will be to define the requirements for each mechanism. Another important question is the extent to which microRNAs contribute to translational repression in oocytes. A recent survey of nearly 1000 *Drosophila* oocyte proteins found only 4% with increased abundance in *Dicer* mutants, suggesting that microRNAs regulate only a minority of mRNAs in oocytes (*12*).

...And Out with the Old

Oocyte maturation and egg activation also stimulate mRNA degradation. Fifteen percent of transcripts are degraded during maturation in mice (*3*). Degradation is selective and preferentially removes transcripts required for prophase arrest and oocyte maturation (*3*). Further degradation occurs after fertilization to usher the transition to zygotic control (*2*, *9*, *13*). Mechanisms of RNA degradation and activation of zygotic transcription are discussed in an accompanying Review (*14*).

Proteins are also targeted for degradation during the oocyte-to-zygote transition. Components of the ubiquitin-proteasome pathway are well represented in the oocyte transcriptome (*2*), and several studies have reported examples of protein turnover in mouse (*15*–*17*), *Xenopus* (*18*), zebrafish (*19*), and

Caenorhabditis elegans (*20*) oocytes and/or early embryos. Protein degradation often serves to inactivate proteins that are needed early in the transition but that would be harmful later. For example, CPEB functions early in oocyte maturation (described above) but is partially degraded during meiosis I (*18*). Injection of a degradation-resistant form of CPEB in *Xenopus* oocytes interfered with translation of cyclin B1 and progression to meiosis II (*18*). Similarly in *C. elegans*, successful transition from meiosis to mitosis requires degradation of the microtubule-severing complex MEI-1/MEI-2 (*20*). MEI-1 and MEI-2 are required for meiosis but, if maintained during mitosis, interfere with growth of the first mitotic spindle. Protein degradation is also used to restrict proteins to specific areas of the egg. For example, in *Drosophila*, *C. elegans*, and zebrafish, germline-specific proteins are degraded from the somatic regions of the emerging embryo (*21*). In this respect, protein degradation may be viewed as a way to partially erase the germline program of the egg to promote totipotency in the zygote. Comprehensive proteomic approaches will be needed to reveal the extent of protein degradation during the oocyte-to-zygote transition and its contribution to oocyte remodeling.

Reshuffle What's There...

Changes during the oocyte-to-zygote transition are not restricted to proteins and RNAs but also affect cellular organelles. The meiotic divisions elicit many changes in the oocyte nucleus, but organelles in the cytoplasm and at the cell periphery are also affected. Redistribution of mitochondria and endoplasmic reticulum (ER) have been documented in several organisms. In *Xenopus*, redistribution of the ER-rich mitochondrial cloud to the vegetal cortex has been linked to localization of germline determinants (*22*). During oocyte maturation in *Xenopus* and mouse, ER-derived vesicles also align underneath the plasma membrane (*23*). This redistribution may facilitate propagation of Ca^{2+} waves at fertilization (see below) by moving Ca^{2+} stores closer to the site of sperm entry. After egg activation, cortical ER clusters are re-internalized (*24*). Perhaps the most dramatic rearrangement following fertilization is the rapid fusion of cortical granules with the plasma membrane to prevent polyspermy (*23*). A similar fusion event was recently described in *C. elegans* involving vesicles rich in caveolin (*25*).

...And Time It Just Right

What signals initiate these changes? Oocyte maturation typically is started by extracellular ligands (*23*). Egg activation, in contrast, depends on Ca^{2+} signaling inside the egg. In mammals, Ca^{2+} signaling may be initiated by a sperm-specific phospholipase C (PLC-ζ), which activates phosphoinositide signaling at fertilization to generate several Ca^{2+} waves (*6*). Remarkably, the egg appears to "count" each wave, with early responses (cortical granule exocytosis) requiring fewer oscillations than later ones (resumption of the second meiotic division) (*6*).

Several lines of evidence suggest that, after these initial triggers, the cell cycle machinery assumes control of subsequent events. For example, degradation of CPEB during meiosis I in *Xenopus* depends on phosphorylation by MPF (*18*). Similarly, internalization of ER granules during egg activation in mice depends on cell cycle resumption (*24*) (Fig. 1). In *C. elegans*, mutations that prevent the first meiotic division block MEI-1 degradation and caveolin vesicle fusion (*25*, *26*). Conversely, premature entry into M phase by removal of the MPF inhibitory kinase WEE-1 jumpstarts MEI-1 degradation in immature oocytes (*26*). The remarkable dependence of several aspects of the oocyte-to-zygote transition on meiotic progression suggests that the cell cycle machinery serves as an internal master timer that drives and coordinates the transition.

Egg quality is often cited as a crucial parameter for success in assisted reproductive technologies, yet the molecular processes that contribute to egg quality remain poorly defined (*27*). Increased understanding of the signaling and remodeling events that shape the oocyte-to-zygote transition will be critical to provide more definitive criteria for what constitutes a "healthy" egg. Already, the realization that the meiotic machinery drives many aspects of the transition raises questions about the practice of removing the meiosis II spindle from oocytes during cloning (*28*).

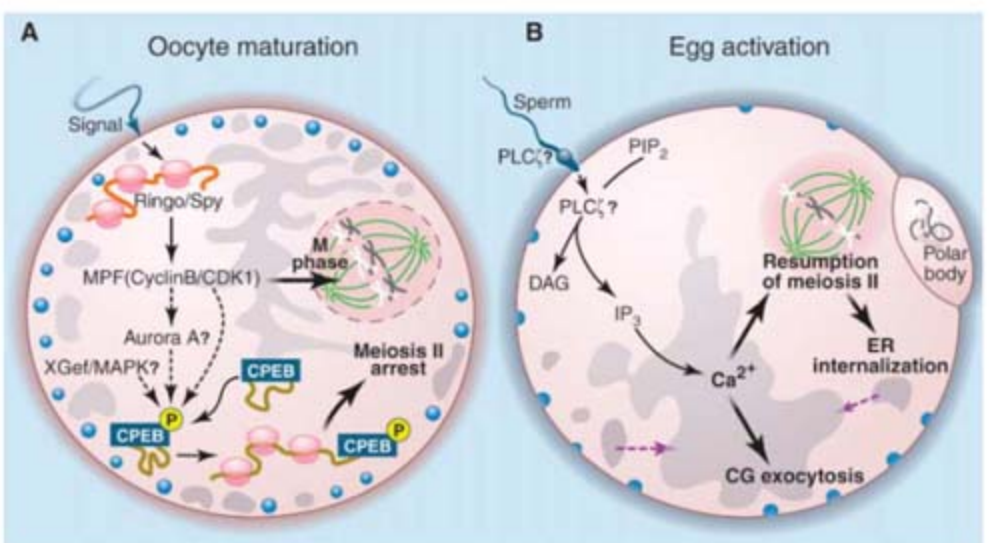

Fig. 1. Schematic of oocyte maturation and egg activation events in vertebrates. (**A**) An extracellular cue initiates oocyte maturation, stimulating the translation of specific mRNAs [for example, *Ringo/Spy* in *Xenopus*] leading to MPF activation. CPEB phosphorylation leads to translation of additional transcripts required for meiotic progression (*29*). ER-derived vesicles (gray) and cortical granules (blue) accumulate below the egg plasma membrane (Xgef, *Xenopus* guanine exchange factor; MAPK, mitogen-activated protein kinase). (**B**) Fertilization triggers egg activation in the matured oocyte. In mice, a sperm-specific phospholipase C isoform (PLC-ζ) has been proposed to be delivered into the oocyte at fertilization. Increased inositol 1,4,5-trisphosphate (IP_3) stimulates calcium (Ca^{2+}) release from the ER, which signals cortical granule exocytosis (blue) and meiosis II. Cell cycle resumption in turn drives internalization of cortical ER vesicles (purple arrows).

References and Notes

1. W. Harvey, *Disputations Touching the Generation of Animals*, G. Whitteridge, Transl. (Blackwell Scientific, London, 1981), p. xx.
2. A. V. Evsikov *et al.*, *Genes Dev.* **20**, 2713 (2006).
3. Q. T. Wang *et al.*, *Dev. Cell* **6**, 133 (2004).
4. W. Tadros *et al.*, *Dev. Cell* **12**, 143 (2007).
5. T. Kishimoto, *Curr. Opin. Cell Biol.* **15**, 654 (2003).
6. C. Malcuit, M. Kurokawa, R. A. Fissore, *J. Cell. Physiol.* **206**, 565 (2006).
7. S. Vasudevan, E. Seli, J. A. Steitz, *Genes Dev.* **20**, 138 (2006).
8. S. Potireddy, R. Vassena, B. G. Patel, K. E. Latham, *Dev. Biol.* **298**, 155 (2006).
9. W. Tadros, H. D. Lipshitz, *Dev. Dyn.* **232**, 593 (2005).
10. E. T. Rosenthal, T. R. Tansey, J. V. Ruderman, *J. Mol. Biol.* **166**, 309 (1983).
11. L. Vardy, T. L. Orr-Weaver, *Dev. Cell* **12**, 157 (2007).
12. K. Nakahara *et al.*, *Proc. Natl. Acad. Sci. U.S.A.* **102**, 12023 (2005).
13. T. Hamatani, M. G. Carter, A. A. Sharov, M. S. Ko, *Dev. Cell* **6**, 117 (2004).
14. A. F. Schier, *Science* **316**, 406 (2007).
15. N. Suzumori, K. H. Burns, W. Yan, M. M. Matzuk, *Proc. Natl. Acad. Sci. U.S.A.* **100**, 550 (2003).
16. A. M. Vitale *et al.*, *Mol. Reprod. Dev.* **74**, 608 (2006).
17. X. Wu *et al.*, *Nat. Genet.* **33**, 187 (2003).
18. R. Mendez, D. Barnard, J. D. Richter, *EMBO J.* **21**, 1833 (2002).
19. U. Wolke, G. Weidinger, M. Koprunner, E. Raz, *Curr. Biol.* **12**, 289 (2002).
20. B. Bowerman, T. Kurz, *Development* **133**, 773 (2006).
21. C. DeRenzo, G. Seydoux, *Trends Cell Biol.* **14**, 420 (2004).
22. M. Kloc, S. Bilinski, L. D. Etkin, *Curr. Top. Dev. Biol.* **59**, 1 (2004).
23. E. Voronina, G. M. Wessel, *Curr. Top. Dev. Biol.* **58**, 53 (2003).
24. G. FitzHarris, P. Marangos, J. Carroll, *Mol. Biol. Cell* **14**, 288 (2003).
25. K. Sato *et al.*, *Mol. Biol. Cell* **17**, 3085 (2006).
26. M. L. Stitzel, J. Pellettieri, G. Seydoux, *Curr. Biol.* **16**, 56 (2006).
27. R. M. Schultz, *Reproduction* **130**, 825 (2005).
28. S. Gao, K. E. Latham, *Cytogenet. Genome Res.* **105**, 279 (2004).
29. B. T. Keady, P. Kuo, S. E. Martinez, L. Yuan, L. E. Hake, *J. Cell Sci.* **120**, 1093 (2007).

30. We thank the Seydoux lab, A. Schier, and reviewers for helpful comments. The Seydoux lab is supported by the NIH and the Howard Hughes Medical Institute.

10.1126/science.1138236

REVIEW

Gametes from Embryonic Stem Cells: A Cup Half Empty or Half Full?

George Q. Daley

When first reported 4 years ago, gametogenesis from embryonic stem (ES) cells promised an accessible in vitro model to facilitate molecular analysis of the germ lineage. Formation of primordial germ cells is robust, but terminal gametogenesis remains inefficient and doubts about gamete function persist. Although useful for research, clinical use of ES cell–derived gametes appears a distant prospect.

Both human and mouse embryonic stem (ES) cells have pluripotency, the remarkable capacity to form all tissues in the body. When mouse ES cells are transplanted into early embryos, ES cells can sustain the entire somatic and germline development of a mouse. Although this proves that ES cells form gametes as part of the complex choreography of embryonic development, deriving gametes solely in vitro seems a daunting challenge. Gametes mature in a niche with specialized supportive cells and a highly regulated hormonal milieu, and it seems implausible that such a structure should self-assemble in vitro. How could the most specialized of cells—the egg and sperm—arise in a petri dish? A critical review of the literature shows that ES cells support the earliest stages of germ lineage formation in cell culture but do not robustly generate functional haploid gametes, making clinical applications in infertility untenable at this time. Nevertheless, the immense value to research that would follow from an in vitro system for gamete production, and the potential for applications in animal breeding and somatic cell reprogramming, makes it fruitful to consider where the field has been and where it is going. Is the cup half empty or half full?

Interest in gametogenesis from ES cells was motivated by a need for an inexhaustible supply of oocytes. Oocytes serve as the target cell for nuclear reprogramming by somatic cell nuclear transfer (SCNT), a method that can be used to derive ES cells from animals with specific genetic features or from specific human patients. SCNT-ES cells could be used to study disease or potentially to create rejection-proof tissues for therapy; however, a major bottleneck for human applications is a source of oocytes. If ES cells could be directed to generate oocytes, a major barrier to SCNT would be eliminated. This requires, however, that ES cells can be prodded to form oocytes that are mature enough to support effective reprogramming of the transferred somatic nucleus.

ES cells differentiate spontaneously in vitro unless cultured in leukemia inhibitory factor (LIF), a cytokine that maintains ES cell self-renewal. After LIF removal, ES cells can differentiate on the surface of the petri dish or aggregate to form 3-dimensional (3D) structures called embryoid bodies (EBs). To varying degrees, such 2D and 3D approaches yield disorganized tissue masses that loosely recapitulate the tissue transformations of the gastrulating embryo and harbor elements of the three primitive embryonic germ layers—ectoderm, endoderm, and mesoderm. Current efforts in numerous labs are aimed at defining which morphogens, cytokines, chemicals, and culture conditions can bias or enhance the formation of a specific tissue of interest. Despite these efforts, directed differentiation remains more hope than reality. Hence, most laboratories pursue a combined direction-selection approach; the cells are first prodded to differentiate with as much direction as possible, then the desired cells are removed from a heterogeneous culture using antibodies against target-cell surface antigens, or by virtue of reporter genes expressed from tissue-specific promoters.

Three independent laboratories originally reported the derivation of gametes from ES cells in vitro using direction-selection strategies (Fig. 1) (*1*–*3*). All three exploited markers or properties that distinguish germ cells from undifferentiated ES cells, a challenge given that germ cells share many features with ES cells (*4*). In the first case, Scholer and colleagues engineered a truncated promoter for Oct4, a gene central to pluripotency, to express green fluorescent protein (GFP) in germ cells (*5*). Scholer's group differentiated ES cells harboring the reporter gene in 2D cultures and detected prevalent GFP^+ cell clusters, suggestive of primordial germ cell formation. They collected

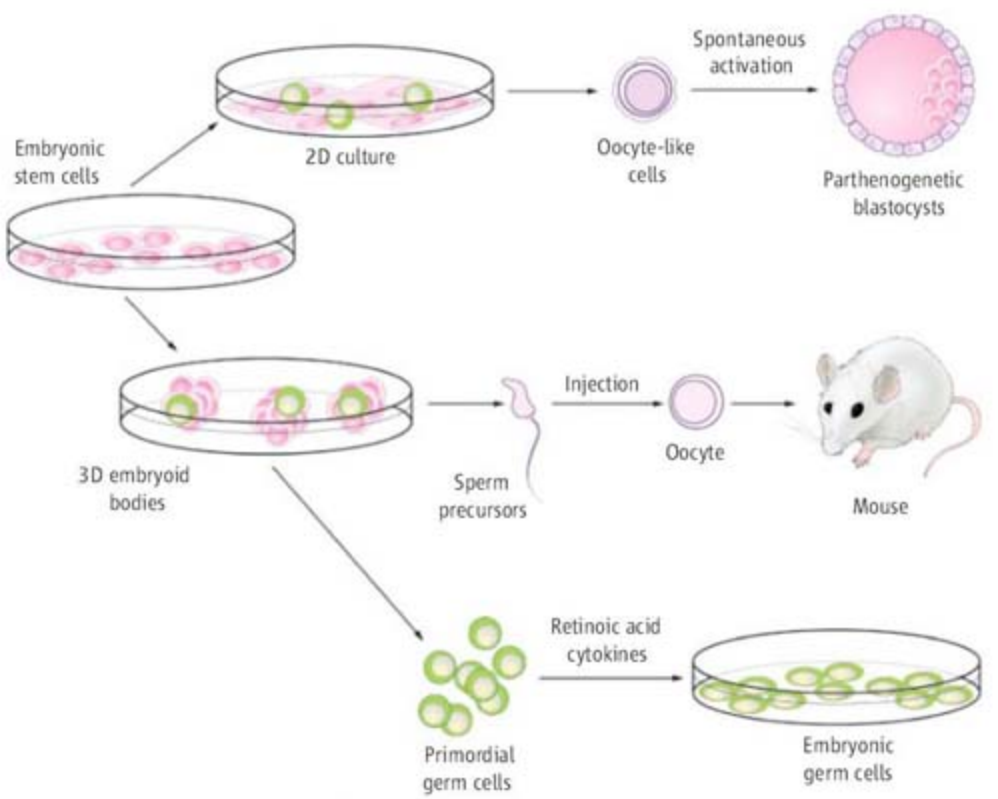

Fig. 1. In vitro gametogenesis from ES cells. (**Top**) A 2D culture yields oocyte-like cells and parthenogenetic blastocysts (*2*). (**Middle**) A male germ cell niche within EBs supports formation of primitive sperm (*1*, *3*, *13*). Oocyte injection with sperm precursors has been reported to generate offspring (*13*). (**Bottom**) Primordial germ cells can be isolated from EBs and cultured with retinoic acid and cytokines to generate embryonic germ cells (*1*).

Division of Pediatric Hematology/Oncology, Children's Hospital Boston; Department of Biological Chemistry and Molecular Pharmacology, Harvard Medical School; Division of Hematology, Brigham and Women's Hospital, Boston, MA; Harvard Stem Cell Institute, Cambridge, MA, USA. E-mail: george.daley@childrens.harvard.edu.

aggregates of GFP$^+$ cells, cultured them for a further several weeks, and observed a remarkable transformation: Complex multicellular structures developed that resembled ovarian follicles, and from these emerged oocyte-like cells surrounded by a zona pellucida–like coating. Extensive molecular, immunohistochemical, and ultrastructural data indicated that these cells were indeed oocytes. Even more surprising, cultures contained cystic structures that resembled blastocysts that the authors speculated arose from spontaneous parthenogenetic activation of the oocytes. Methods for oocyte formation from ES cells have not yet been widely exploited by the community, but Trounson's group has independently reported differentiation of ES cells into oocyte-like cells using testicular cell–conditioned medium, which presumably contains factors that stimulate both egg and sperm development (*6*). Although tantalizing, these results leave one wondering whether such ES-derived oocytes are functional. Can they be fertilized? Can they serve as recipients in nuclear transfer to support somatic cell reprogramming?

Two other laboratories reported deriving male gametes from ES cells differentiated into 3D EBs (*1*, *3*). Noce and colleagues exploited a reporter for the germ cell gene *vasa* and stimulated germ cell formation with bone morphogenetic protein-4 (BMP4). They isolated *vasa*-GFP$^+$ cells, mixed in tissue from embryonic gonads, and transplanted testes of germ cell–depleted mice. They found marker-positive cells in reconstituted seminiferous tubules, although no sperm function was documented (*3*). Follow-up studies from the same group found that media glucose concentration influences germ cell formation, suggesting that work remains to optimize differentiation (*7*). Although initially seeking oocyte development, our laboratory independently observed male gametogenesis from ES cells (*1*). We selected cells expressing the germ cell antigen SSEA-1 and treated them with retinoic acid, which induces germ cell proliferation. Then, using conditions established for isolating embryonic germ (EG) cells from embryos (*8*), we cultured EG-like cells that had erased their methylation marks at key imprinted gene loci, a diagnostic feature of primordial germ cells from the embryonic gonadal ridge. From EBs cultured for an additional 3 to 4 weeks, we used an antibody directed against primitive spermatocytes to isolate rare haploid cells that resembled round spermatids. When injected into oocytes, these cells generated diploid blastocysts, but never supported full mouse development.

These early reports all document robust formation of primordial germ cells, but limitations in achieving functional gametes. Using a germ cell–specific stella reporter, Surani's lab has independently confirmed formation of primordial germ cells from ES cells in vitro (*9*). In human ES cultures, germ cell–specific gene expression has been observed in an appropriate temporal sequence (*10*) and shown to be enhanced by incubation with bone morphogenetic proteins (*11*). Nonetheless, gametes have not yet been isolated from human cultures.

Primordial germ cells lack sexual dimorphism. Segregation of germ cell fates into oogonia or spermatagonia occurs within the developing tissues of the fetal gonad, and terminal gametogenesis requires tight hormonal control. The 2D ES culture condition employed by Scholer's group appears to stimulate oogenesis, whereas the 3D EB condition used by Noce's group and our own appears to favor spermatogenesis, for unclear reasons. Germ cell maturation appears to follow oogenesis by default, unless suppressed by male-specific factors like Müllerian inhibiting substance (MIS). Indeed, we detected MIS expression in our EBs, perhaps signaling the formation of a supportive germ cell niche for male gametogenesis (*1*).

The gold standard for gamete function is the production of offspring. All of the early studies lacked this crucial achievement, but Engel and colleagues recently reported success. Using a GFP reporter for Stra8 (stimulated by retinoic acid-8), a gene expressed in premeiotic germ cells, the Engel group differentiated the pluripotent F9 teratocarcinoma line for 2 months and identified GFP$^+$ cells, that when transplanted into germ cell–depleted testes, produced mature sperm. Although the sperm manifest structural abnormalities and reduced motility, they supported embryo formation after being injected into oocytes (*12*). Again, the lack of live offspring suggests that functional gametes were not formed. Even more remarkable, however, is their recent claim to have generated live mice from ES-derived gametes. In this case, the group sequentially selected Stra8-GFP$^+$ cells, followed by cells expressing a dsRed reporter driven by the protamine promoter, thus identifying cells at a later stage in spermiogenesis (*13*). Of 65 embryos formed when the protamine-dsRed$^+$ cells were injected into oocytes, 12 animals were born, and a few harbored the transgene by Southern blot analysis. Although these data are provocative, genome-wide polymorphism analysis would have been helpful to prove that these offspring carry a full haploid contribution from the ES-derived sperm.

Given the inefficiency of terminal gametogenesis from ES cells in vitro, and the paucity of data documenting reproductive function, employing ES cells as a source of gametes to treat infertility seems a distant prospect. For those who see the cup as half full, any gametogenesis is a marvel. Differentiation of ES cells into primordial germ cells appears robust and amenable to experimentation. ES cells thus provide an accessible tool to study genes that specify germ cells, the pathways that control germ cell migration, and the molecular machinery of imprint erasure that acts when germ cells arrive at the embryonic gonadal ridge. For those who view the cup as half empty, much work remains. Evidence of meiosis and terminal gametogenesis is lacking. It remains to be seen whether terminal spermiogenesis can occur in a petri dish and whether oogenesis can be optimized to provide a ready supply of oocytes for reprogramming studies. If additional laboratories replicate the remarkable achievement of living offspring from ES-derived gametes, then many new avenues for germ cell research are possible. Prospects for treating infertility become a more plausible prospect, and the cup will indeed seem more than half full.

References and Notes

1. N. Geijsen *et al.*, *Nature* **427**, 148 (2004).
2. K. Hubner *et al.*, *Science* **300**, 1251 (2003).
3. Y. Toyooka, N. Tsunekawa, R. Akasu, T. Noce, *Proc. Natl. Acad. Sci. U.S.A.* **100**, 11457 (2003).
4. T. P. Zwaka, J. A. Thomson, *Development* **132**, 227 (2005).
5. V. Nordhoff *et al.*, *Mamm. Genome* **12**, 309 (2001).
6. O. Lacham-Kaplan, H. Chy, A. Trounson, *Stem Cells* **24**, 266 (2006).
7. K. Mizuno *et al.*, *Mol. Reprod. Dev.* **73**, 437 (2006).
8. Y. Matsui, K. Zsebo, B. L. Hogan, *Cell* **70**, 841 (1992).
9. B. Payer *et al.*, *Genesis* **44**, 75 (2006).
10. A. T. Clark *et al.*, *Hum. Mol. Genet.* **13**, 727 (2004).
11. K. Kee, J. Gonsalves, A. T. Clark, R. Reijo Pera, *Stem Cells Dev.* **15**, 831 (2006).
12. K. Nayernia *et al.*, *Hum. Mol. Genet.* **13**, 1451 (2004).
13. K. Nayernia *et al.*, *Dev. Cell* **11**, 125 (2006).

14. G.D. is on the scientific advisory board of and holds equity in Viacell, which focuses on the use of human cells to treat disease, and MPM Capital, a venture capital firm investing in biotechnology and medical technology.

10.1126/science.1138772

Temperature Sex Reversal Implies Sex Gene Dosage in a Reptile

Alexander E. Quinn,[1]* Arthur Georges,[1] Stephen D. Sarre,[1] Fiorenzo Guarino,[1] Tariq Ezaz,[2] Jennifer A. Marshall Graves[2]

Sex is determined by genes on sex chromosomes in many vertebrates [genotypic sex determination (GSD)], but may also be determined by temperature during embryonic development [temperature-dependent sex determination (TSD)] (*1*). In reptiles, sex determination can involve GSD with XX and XY sex chromosomes (male heterogamety, as in mammals), GSD with ZZ and ZW sex chromosomes (female heterogamety, as in birds), or TSD (*1*, *2*). The distribution of TSD and GSD across reptiles suggests several independent evolutionary transitions in sex-determining mechanisms (*2*, *3*), but transitional forms have yet to be demonstrated. We show that high incubation temperatures reverse genotypic males (ZZ) to phenotypic females in the Australian central bearded dragon lizard (*Pogona vitticeps*), which, like birds, has GSD with female heterogamety (*4*). Temperature thus overrides gene(s) involved in male differentiation.

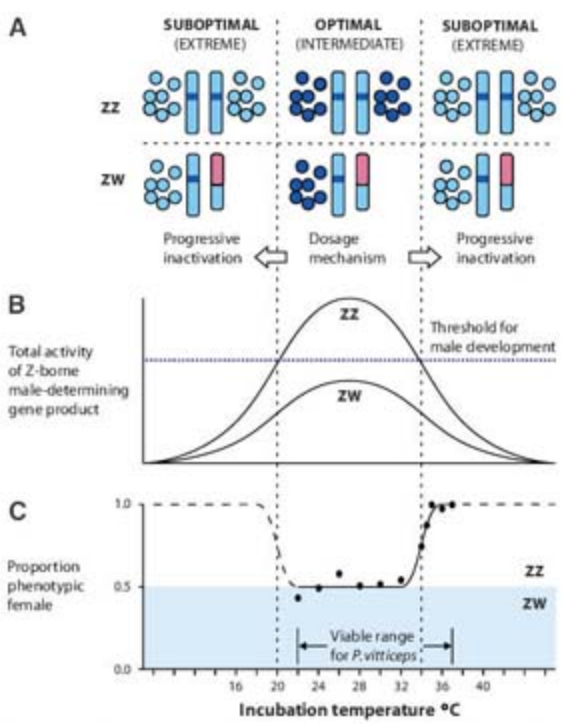

Fig. 1. Model for a ZZ dosage mechanism of sex determination in dragon lizards. (**A**) A Z-borne male-determining gene (dark blue line) that expresses a temperature-sensitive product (RNA or protein) is present in two copies in ZZ individuals but in only one copy in ZW individuals. At optimal (intermediate) incubation temperatures, the gene product is fully active (dark blue circles), but it is progressively inactivated at more extreme temperatures (light blue circles). (**B**) In ZW individuals, the total activity of the gene product is always half that of ZZ individuals. Activity exceeds a threshold level (dashed blue line) for male differentiation only within the optimal temperature range of ZZ individuals. At all other temperatures, female development proceeds. (**C**) Thus, the phenotypic sex ratio increases from 50% females at intermediate temperatures to 100% females at temperature extremes. Data points are for *P. vitticeps* (fig. S1).

We incubated eggs of *P. vitticeps* at constant temperatures between 20° and 37°C (*5*). No embryos survived to hatching at 20°C. Between 22° and 32°C, sex ratios did not differ significantly from 1:1, a response consistent with GSD (fig. S1A). However, between 34° and 37°C, there was an increasing female bias, suggesting that temperature was overriding genotypic sex in some males. Differential mortality cannot explain the deviation of the sex ratio from 1:1 at temperatures where survivorship allowed a test (at 34.5°, 35°, and 36°C), because the deviation remained significant even when all mortalities were conservatively scored as male (table S1).

We isolated a female-specific DNA marker for *P. vitticeps* by screening amplified fragment length polymorphisms (AFLPs) (*6*) to enable a test for sex reversal (*5*) (fig. S1B). To verify that the AFLP marker (designated Pv72W, GenBank accession no. ED982907) is specific to the W chromosome, we genotyped 15 juveniles and examined their metaphase chromosome spreads. There was 100% agreement between Pv72W genotype and karyotype as demonstrated by C banding (11 ZW and 4 ZZ).

Pv72W was used to identify genotypic sex of hatchlings from three clutches, each split between two incubation temperatures: a control treatment (28°C), which produced an unbiased phenotypic sex ratio, and a high-temperature treatment (34° or 36°C), which produced a strong female bias (table S2). Phenotypic sex was identified by hemipene eversion and examination of gonadal morphology. At 28°C, the phenotypic sex ratio was 1:1, compared with 2 males and 33 females at the high temperatures. All but one of the 30 lizards (97%) incubated at 28°C had concordant sex phenotype and genotype. However, only 18 of 35 animals (51%) from the high-temperature treatment were concordant. All discordant animals were genotypic males (ZZ) that developed as phenotypic females. Our data demonstrate that high incubation temperatures reverse sex (table S2). This finding extends a previous report of low-temperature sex reversal in a skink (*7*) by explicitly identifying discordance between genotype and phenotype and adds empirical support for the coexistence of TSD and GSD.

The W chromosome is thus unnecessary for female differentiation, which suggests that the molecular mechanism directing sex determination is the dosage of a gene on the Z chromosome rather than the presence of a female-determining gene on the W. That is, male differentiation requires two copies of a Z-borne gene, the expression or activity of which is sufficient for male development only at optimal temperatures (Fig. 1). We have demonstrated sex reversal at high temperatures; low-temperature sex reversal may be obscured by mortality below 22°C.

Selection for a wider range of thermosensitivity in species such as *P. vitticeps* could result in the evolution of TSD from GSD. Reversal of the ZZ genotype to the female phenotype at extreme temperatures will bias the phenotypic sex ratio toward females and drive down the frequency of the W chromosome under frequency-dependent selection. This could account for the pattern observed in many TSD reptiles, where both low and high temperatures produce 100% females, yet intermediate temperatures produce predominantly (occasionally 100%) males (*1*, *2*).

References and Notes

1. J. J. Bull, *Evolution of Sex Determining Mechanisms* (Benjamin/Cummings, Menlo Park, CA, 1983).
2. N. Valenzuela, V. A. Lance, Eds., *Temperature-Dependent Sex Determination in Vertebrates* (Smithsonian Institution, Washington, DC, 2004).
3. S. D. Sarre, A. Georges, A. Quinn, *Bioessays* **26**, 639 (2004).
4. T. Ezaz *et al.*, *Chromosome Res.* **13**, 763 (2005).
5. Materials and methods are available on *Science* Online.
6. P. Vos *et al.*, *Nucleic Acids Res.* **23**, 4407 (1995).
7. R. Shine, M. J. Elphick, S. Donnellan, *Ecol. Lett.* **5**, 486 (2002).
8. Supported by an Australian Research Council grant to S.D.S., A.G., and J.A.M.G. Experiments approved by the University of Canberra Committee for Ethics in Animal Experimentation.

Supporting Online Material

www.sciencemag.org/cgi/content/full/316/5823/411/DC1
Materials and Methods
Fig. S1
Tables S1 and S2

4 October 2006; accepted 19 January 2007
10.1126/science.1135925

[1]Institute for Applied Ecology, University of Canberra, ACT 2601, Australia. [2]Comparative Genomics Group, Research School of Biological Sciences, Australian National University, Canberra, ACT 0200, Australia.

*To whom correspondence should be addressed. E-mail: quinn@aerg.canberra.edu.au

The Amount of Recycled Crust in Sources of Mantle-Derived Melts

Alexander V. Sobolev,[1,2]* Albrecht W. Hofmann,[1] Dmitry V. Kuzmin,[1,3] Gregory M. Yaxley,[4] Nicholas T. Arndt,[5] Sun-Lin Chung,[6] Leonid V. Danyushevsky,[7] Tim Elliott,[8] Frederick A. Frey,[9] Michael O. Garcia,[10] Andrey A. Gurenko,[1] Vadim S. Kamenetsky,[7] Andrew C. Kerr,[11] Nadezhda A. Krivolutskaya,[2] Vladimir V. Matvienkov,[12] Igor K. Nikogosian,[13,14] Alexander Rocholl,[15] Ingvar A. Sigurdsson,[16] Nadezhda M. Sushchevskaya,[2] Mengist Teklay[17]

Plate tectonic processes introduce basaltic crust (as eclogite) into the peridotitic mantle. The proportions of these two sources in mantle melts are poorly understood. Silica-rich melts formed from eclogite react with peridotite, converting it to olivine-free pyroxenite. Partial melts of this hybrid pyroxenite are higher in nickel and silicon but poorer in manganese, calcium, and magnesium than melts of peridotite. Olivine phenocrysts' compositions record these differences and were used to quantify the contributions of pyroxenite-derived melts in mid-ocean ridge basalts (10 to 30%), ocean island and continental basalts (many >60%), and komatiites (20 to 30%). These results imply involvement of 2 to 20% (up to 28%) of recycled crust in mantle melting.

It is widely accepted that the heterogeneity of the convecting mantle observed in the composition of mantle-derived magmas is largely due to subduction and recycling of oceanic crust into the deep mantle (*1*, *2*). To understand the role of crustal material in creating compositional heterogeneities in the mantle and to evaluate the geodynamical consequences of this contribution, one must quantify the crustal input to the mantle sources of common, mantle-derived magmas in mid-oceanic ridges basalts (MORBs), ocean islands (OIBs), and large igneous provinces (LIPs). It is not possible to use incompatible element abundances in basalts to constrain the proportion of recycled component in the magma source because concentrations of these elements are also sensitive to the extent of melting. Similarly, the use of isotope ratios for making such quantitative estimates is compromised by the isotopic variability of subducted materials involved in the recycling process (*2*). We used an alternative approach based on a combination of major elements and compatible trace elements in parental melts, because these are more uniform in the mantle and are strongly controlled by the residual phases in equilibrium with partial melts (*3*–*5*).

Our method has its basis in the experimental and theoretical prediction that high-pressure ($P >$ 3.0 GPa) melting of typical recycled oceanic crust (in the form of eclogite with a separate SiO_2 phase) and reaction of this melt with peridotite produces olivine-free pyroxenite (*5*). We show that further melting of this hybrid lithology in the absence of residual olivine is more voluminous than the melting of peridotite (at a given pressure and temperature) and that pyroxenite-derived melts are characteristically enriched in Si and Ni but depleted in Mg, Ca, and Mn compared with their peridotite-derived counterparts. This difference arises because olivine principally controls the composition of melt produced in peridotite, whereas pyroxene mainly controls the composition of melt from olivine-free hybrid pyroxenite (*5*–*8*). Experimental data predict (*9*) that, as such pyroxenite-derived melts rise toward the surface, the decrease in pressure causes their saturation in olivine. This olivine is unusually Ni rich and Mn and Ca poor. With use of a new, large data set of high-precision analyses of olivine phenocrysts from OIBs, LIPs, MORBs, and komatiites, we show that hybrid pyroxenite is a common lithology in upwelling mantle and a major contributor to tholeiitic (silica-saturated) and transitional (moderately silica-undersaturated) magmas of OIBs and LIPs emplaced on thick oceanic or continental lithosphere.

Olivine data set. We use olivine phenocrysts as probes of parental melt composition, because olivine is the first phase to precipitate at low pressures in almost all mantle-derived magmas and because its forsterite content is an excellent measure of the degree of fractional crystallization allowing reconstruction of the parental melt composition.

Olivine phenocrysts were analyzed by electron microprobe using high probe currents and long counting times (*10*). This procedure routinely yields detection limits of around 6 to 15 parts per million (ppm) and errors (2 standard errors) of 15 to 30 ppm for trace elements (Ni, Ca, Mn, Cr, Co, and Al) and 0.01 mole percent (mol %) for forsterite content [defined as Fo = Mg/(Mg + Fe)], checked by repeated analysis of San Carlos olivine standard (*11*). In the following diagrams we use only high-precision data.

We have analyzed nearly 17,000 grains of olivine phenocrysts from 229 samples of tholeiitic to transitional compositions covering MORBs (40 samples) from Mid-Atlantic Ridge, East Pacific Rise, South-East Indian Ridge, and Knipovich Ridge; OIBs (138 samples) from Hawaiian Islands and Emperor Seamounts, Canary Islands, Reunion, Azores, and Iceland; LIPs (36 samples) from Ontong Java Plateau, Siberia, Emeishan, Karoo, Afar, and North Atlantic Province; komatiites and associated picrites (15 samples) from the Archean Abitibi greenstone belt in Canada and the Belingwe belt in Zimbabwe and South Africa; Proterozoic komatiitic basalts from Gilmour Island, Canada; and komatiites and picrites from Gorgona Island, Colombia. Most samples are picrites or olivine basalts containing large amounts of fresh, high-magnesium olivine phenocrysts. The samples are subdivided into four groups: (i) MORB; (ii) within plate magmas (WPM, magmas erupted far from plate boundaries) forming OIB emplaced over thin lithosphere (<70 km thick), WPM-THIN; (iii) WPM (OIB and LIP) emplaced over thick lithosphere (>70 km thick), WPM-THICK; and (iv) komatiites and associated magmas, KOMATIITES. Details of sample locations, references for sample descriptions, and their group correspondence are presented in table S2a.

The most-magnesian olivine compositions (defined by olivines phenocrysts with Fo within 1 mol % from a maximum Fo) for each specimen were averaged (table S2a) for the plots shown in Fig. 1. Individual olivine analyses are presented on fig. S4 and tables S2, e to f.

In addition to Mn and Ni concentrations, which strongly correlate with Fo (Fig. 1, A and

[1]Max Planck Institute (MPI) for Chemistry, Post Office Box 3060, 55020 Mainz, Germany. [2]Vernadsky Institute of Geochemistry and Analytical Chemistry, Russian Academy of Sciences, Kosygin Street 19, 119991 Moscow, Russia. [3]Institute of Geology and Mineralogy, Siberian Branch of Russian Academy of Sciences, Koptuyga prospekt 3, 630090 Novosibirsk, Russia. [4]Research School of Earth Sciences, Australian National University, Canberra, ACT 0200 Australia. [5]Laboratoire de Géodynamique des Chaînes Alpines, Université de Grenoble, 38401 Grenoble cedex, France. [6]Department of Geosciences, National Taiwan University, Post Office Box 13-318, Taipei 106, Taiwan. [7]Australian Research Council, Centre of Excellence in Ore Deposits and School of Earth Sciences, University of Tasmania, Private Bag 79, Hobart, Tasmania, 7001, Australia. [8]Department of Earth Sciences, Queen's Road, Wills Memorial Building, University of Bristol, Bristol BS8 1RJ, UK. [9]Department of Earth, Atmospheric, and Planetary Science, Massachusetts Institute of Technology (MIT), 77 Massachusetts Avenue, Cambridge, MA 02139, USA. [10]Department of Geology and Geophysics, University of Hawaii, 1680 East-West Road, Honolulu, HI 96822, USA. [11]School of Earth, Ocean and Planetary Sciences, Cardiff University, Main Building, Park Place, Cardiff CF10 3YE, UK. [12]P. P. Shirshov Institute of Oceanology of Russian Academy of Sciences, Nakhimovsky prospekt 36, 117997 Moscow, Russia. [13]Department of Petrology, Faculty of Geosciences Utrecht University, Budapestlaan 4, Utrecht, Netherlands. [14]Department of Petrology, Faculty of Earth and Life Sciences, Vrije Universiteit, De Boelelaan 1085, 1081 HV Amsterdam, Netherlands. [15]Department of Earth and Environmental Sciences, University Munich, 80333 Munich, Germany. [16]South Iceland Nature Centre, Strandvegur 50, Vestmannaeyjar, IS 900, Iceland. [17]Department of Earth Science, University of Asmara, Asmara, Eritrea.

*To whom correspondence should be addressed. E-mail: sobolev@geokhi.ru

C), we also plot Mn/Fe and Ni versus Mg/Fe ratios (Fig. 1, B and D). These ratios do not vary significantly with olivine fractionation (see model curves Frac 1 and Frac 2) but nevertheless range considerably (Fig. 1, B and D). Most olivine phenocrysts from MORBs and many from komatiites have Mn and Ni contents similar to those of peridotite-derived melts. In contrast, most olivines from the WPM-THICK group are significantly depleted in Mn and enriched in Ni. Their concentrations are not compatible with the melting products of common peridotites. The olivines from the WPM-THIN group have intermediate Mn and Ni contents.

Concentrations of Ca also provide some discrimination in spite of the greater overlap. Most olivines from the WPM-THICK group are too low in Ca to have precipitated from peridotite-derived melts (shown as experimental-based model compositions and fractionation trajectories, Fig. 1E).

Chromium is strongly controlled by garnet and spinel in peridotites and thus might be useful to decipher products of high-degree melting of peridotite, which leave residuals (restites) free of Cr-rich phases (*12*). Olivines from Archean komatiites have the highest Cr values and match compositions of olivines from a spinel- and garnet-free refractory restite (Fig. 1F). They could, therefore, be derived directly from high-degree melting of peridotite. In the other groups of olivines, Cr is markedly lower than expected in equilibrium with peridotite at high pressures (see experimental data on lherzolite melting, Fig. 1F). The lowest Cr contents are found in MORB olivines, indicative of residual Cr spinel.

Cobalt (Fig. 2A) shows nearly uniform correlation with Fo for all rock groups, with possibly only minor (around 5%) relative enrichment in WPM-THICK and WPM-THIN over MORB (estimated from group average Co/Fe of table S2a). Decoupling of Co and Ni yields Ni/Co ratios of many WPM-THICK olivines that are unusually high for the Earth mantle (Fig. 2B).

Mn/Fe is the parameter least dependent on olivine fractionation (as shown by the model fractionation curves in Fig. 3). Thus, it is diagnostic of parental magma compositional differences. There is a significant negative correlation of Ni/Mg versus Mn/Fe (linear correlation coefficient r is 0.66 for 238 samples) in spite of strong dependence of Ni/Mg on the degree of olivine fractionation (see fractionation trajectories in Fig. 3A). This correlation improves ($r = 0.88$ for 103 samples) for the subset of olivines with a narrower range of Fo contents (Fo89 to Fo91). MORB olivines are the lowest in Ni and highest in Mn, whereas olivines from the WPM-THICK group are the highest in Ni and lowest in Mn, with olivines from the WPM-THIN group being intermediate.

To minimize the effects of olivine fractionation, we show parameters Ni/(Fe/Mg) and Ca/Fe in Fig. 3, B and C. This procedure also reduces the scatter in the ordinate significantly, thus highlighting the differences between geodynamic settings.

Fate of recycled oceanic crust. In subduction at $P > 2.5$ GPa, the basaltic and gabbroic portions of the oceanic crust are transformed completely to eclogite (clinopyroxene and garnet) with a free SiO_2 phase (*13*–*15*). Unless silica has been

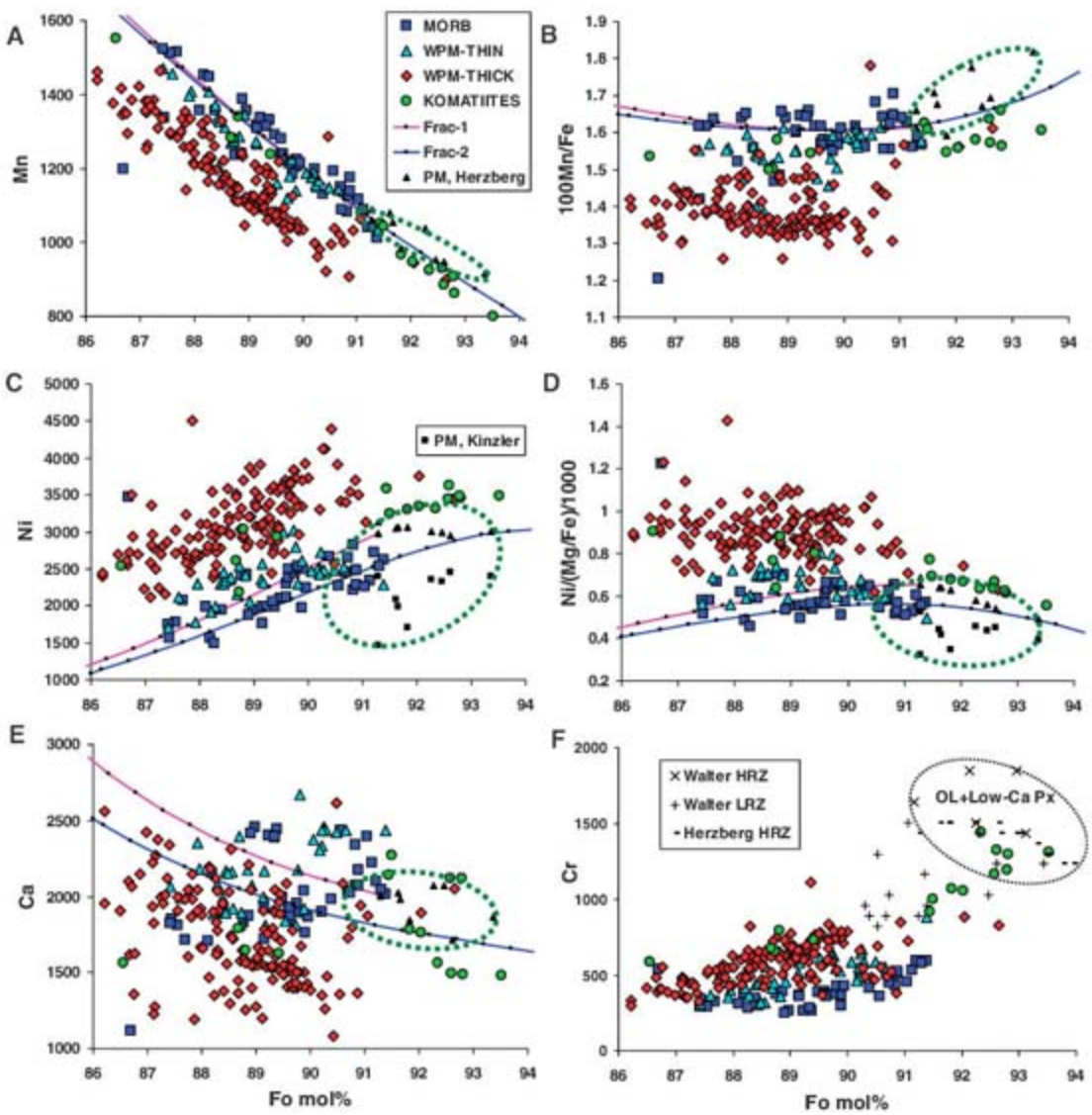

Fig. 1. (**A** to **F**) Average compositions of the most highly magnesian olivine phenocrysts in each sample. Concentrations and their ratios are given in ppm versus forsterite content of olivine in mol %. Olivine group names are as defined in text. PM, Herzberg indicates compositions of olivine in equilibrium at 0.1 MPa with melt originally generated at 3.0 to 5.0 GPa from fertile peridotite (*12*), calculated by Petrolog software (*41*) for oxygen fugacity corresponding to quartz-fayalite-magnetite (QFM) buffer using the Herzberg model (*4*), PM, Kinzler, olivine compositions similar to PM, Herzberg but with Ni calculated by using Ni partitioning between olivine and melt from Kinzler *et al.* (*28*). Frac 1 is the trend of olivine composition during fractional crystallization from a melt derived from fertile peridotite at 3 GPa and 1515°C (*12*). Fractionation of olivine modeled up to 20% for oxygen fugacity corresponding to QFM buffer using the Herzberg model (*4*). Frac 2 is similar to Frac 1 but calculated for 35% crystallization of melt derived at 4.0 GPa and 1630°C (*12*). Green ellipse indicates field of olivine compositions compatible with peridotitic source. In (F), HRZ, Herzberg stands for calculated compositions of olivine from spinel- and garnet-free harzburgite restite using (*4*); LHRZ, Walter and HRZ, Walter indicate experimental olivines from lherzolite- and garnet-free harzburgite residual assemblages, respectively, produced by high-pressure melting of fertile peridotite (*12*). Black ellipse marked "ol + low Ca-Px" indicates field of olivine compositions from refractory garnet- and spinel-free assemblage of olivine and low-Ca pyroxene.

removed during subduction (*16*), this combination will also be the relevant assemblage during recycling to the upper mantle (*17*).

In the ascending mantle (e.g., a mantle plume or upstream flow of convecting mantle), the silica-oversaturated eclogite starts melting at higher pressures than the peridotite and produces high silica melt (*18*, *19*). This melt reacts with olivine from peridotite, producing pyroxenes and garnet (*5*, *8*, *19*). Previous studies have envisioned that this reaction creates a refertilized peridotite enriched in pyroxene (*19*, *20*). This conclusion would predict variable mixing proportions of individual ingredients (eclogite-derived high-Si melt and peridotite) that are drastically different in composition. Melting such variable source compositions would create highly nonlinear correlations of $^{187}Os/^{188}Os$ and $^{87}Sr/^{86}Sr$ isotope ratios in the melts, and this is contradicted by the strongly linear correlations observed in Hawaiian basalts (*21*, *22*), which are thought to have a significant eclogite component (*3*, *5*).

However, it has been shown experimentally (*23*) and proposed on the basis of Korzinskii's theory (*24*) that, under conditions of local equilibrium, the reaction between high-Si eclogite-derived melt and peridotite produces an olivine-free lithology enriched in pyroxene (*5*). This fundamentally differs from a partial reaction (*19*, *20*) because it leads to a stable pyroxenite lithology (hybrid pyroxenite) generated by roughly fixed proportions of high-Si melt and peridotite [constrained by reaction stoichiometry between 40 and 60 weight % (wt %) of melt (*5*)] irrespective of the initial proportions of the reaction ingredients. Consequently, the hybrid pyroxenite has nearly uniform chemical and isotopic composition, thus constituting a single mixing endmember. Binary mixing of melts derived from peridotite and this pyroxenite leads to near-linear $^{87}Sr/^{86}Sr$ versus $^{87}Os/^{188}Os$ trends (*5*).

Other predicted geochemical consequences of replacement of olivine by pyroxene are a significant decrease of the bulk distribution coefficient between crystals and melt (K_d) for Ni

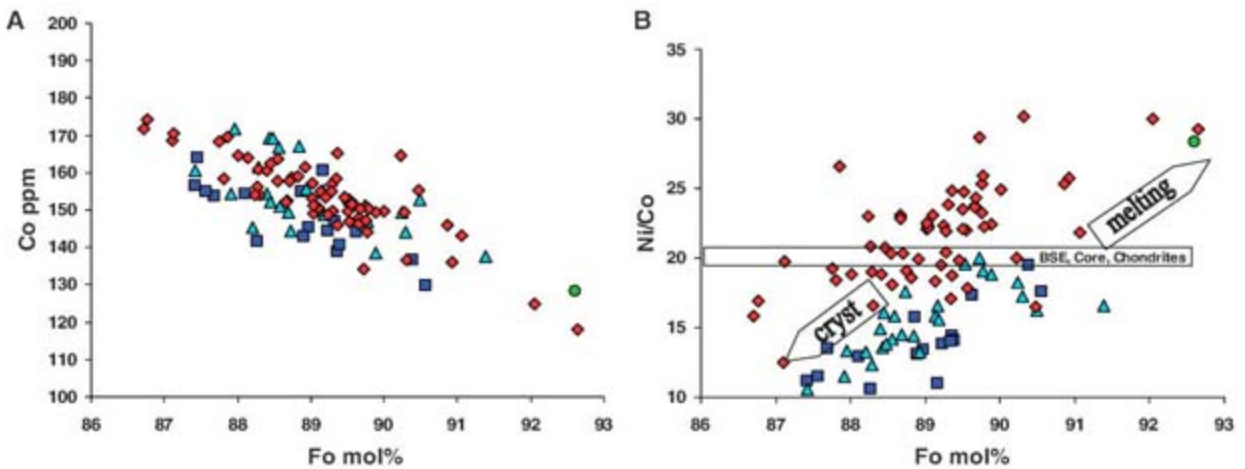

Fig. 2. (**A** and **B**) Cobalt and nickel to cobalt ratio versus Fo of average Mg-rich olivine phenocrysts. Pink band at Ni/Co 20 ± 1 represents estimated values for bulk silicate Earth (BSE), core, and chondrites (*39*). Arrows indicate trend of olivine compositions due to the mantle melting (melting) and magma crystallization (cryst). All other symbols are as on Fig. 1.

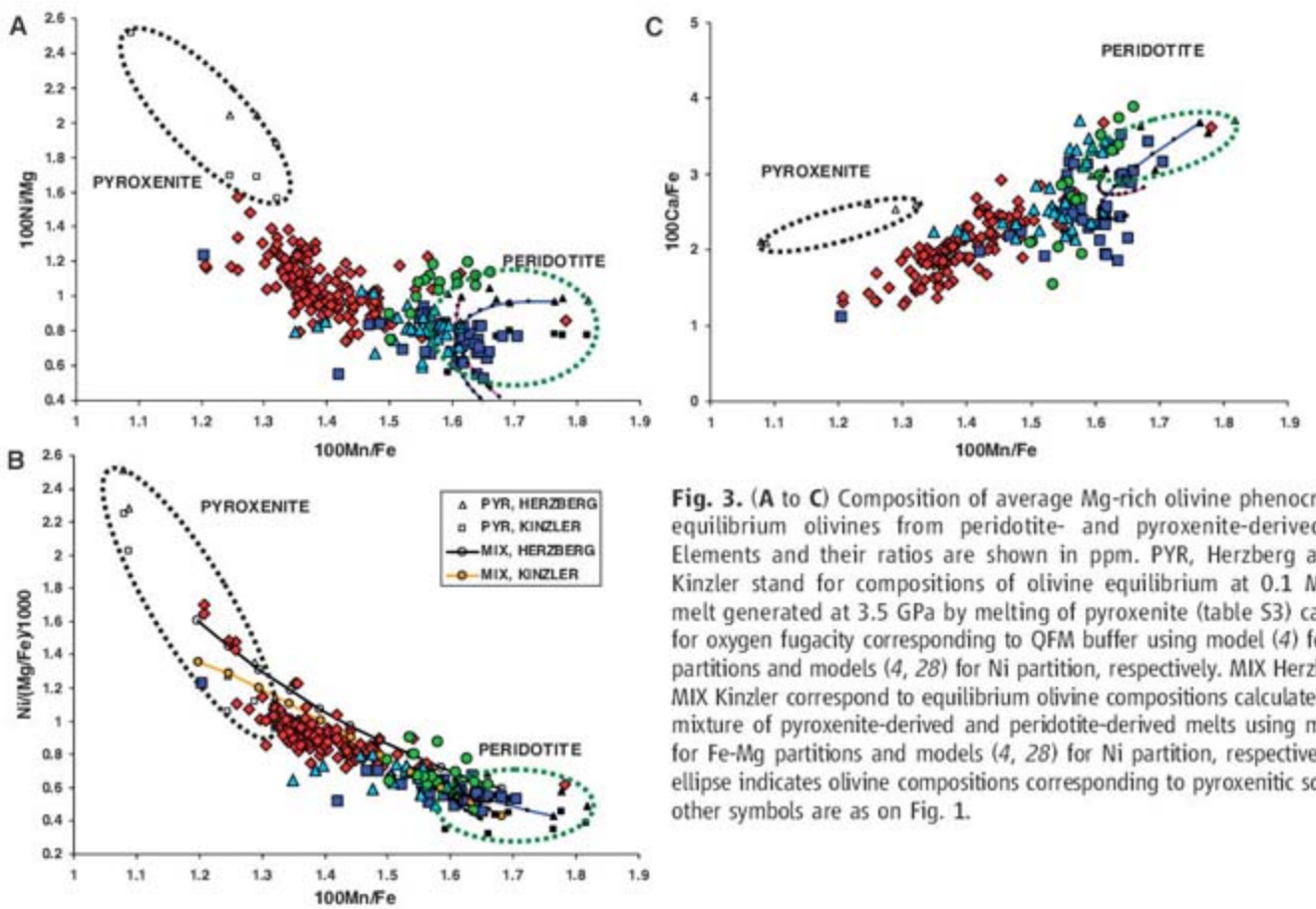

Fig. 3. (**A** to **C**) Composition of average Mg-rich olivine phenocrysts and equilibrium olivines from peridotite- and pyroxenite-derived melts. Elements and their ratios are shown in ppm. PYR, Herzberg and PYR, Kinzler stand for compositions of olivine equilibrium at 0.1 MPa with melt generated at 3.5 GPa by melting of pyroxenite (table S3) calculated for oxygen fugacity corresponding to QFM buffer using model (*4*) for Fe-Mg partitions and models (*4*, *28*) for Ni partition, respectively. MIX Herzberg and MIX Kinzler correspond to equilibrium olivine compositions calculated for the mixture of pyroxenite-derived and peridotite-derived melts using model (*4*) for Fe-Mg partitions and models (*4*, *28*) for Ni partition, respectively. Black ellipse indicates olivine compositions corresponding to pyroxenitic source. All other symbols are as on Fig. 1.

(*5*, *6*) and a decrease in the ratio of the bulk coefficients of Mn and Fe (*7*). These features occur because olivine is the major silicate phase in peridotite concentrating Ni and the only silicate phase in peridotite having K_d for Fe greater than K_d for Mn (*7*). The bulk K_d changes will increase Ni and lower the Mn/Fe ratio of pyroxenite-derived melt compared with peridotite-derived melts. In addition, melting of pyroxenite yields lower Ca compared with peridotite (*8*). Additional predicted differences are higher melt fractions for hybrid pyroxenite than peridotite and higher Si and lower Mg in pyroxenite-derived melt (*5*, *25*, *26*).

These predictions were tested by experimental melting of a model hybrid pyroxenite (*5*). Experiments were run at P = 3.5 GPa and temperatures between 1400° and 1570°C in a conventional 1.27-cm piston-cylinder apparatus at the Australian National University (*10*, *19*). These results, together with published experimental data for melting of peridotite (*12*), confirm the Ni and Mn relationships as well as melting rates predicted above (table S3 and fig. S5). From these data, we calculate equilibrium olivine compositions at low pressure (*4*, *27*, *28*) in order to compare them with the natural phenocryst data (Fig. 3). We used these results to estimate mixing proportions of melts derived from the two end-member sources for the olivine data sets representing different geodynamic settings. The end-member melt compositions were calculated from averaging experimental data on melting of pyroxenite and peridotite (*10*).

Quantitative estimates. We assumed mixtures (in 10% intervals) of the end-member melts (*10*) and calculated the composition of equilibrium olivines. The calculated mixing trajectories for the two different models for Ni partitioning are consistent with natural olivine data (Fig. 3B). The relation between Mn/Fe of modeled olivines and mixing proportions (*10*) was used to compute the amount of pyroxenite-derived component for individual samples (Fig. 4). Olivines from the WPM-THICK group of basalts yield an average of 61 ± 16% (standard deviation) pyroxenite-derived component, similar to results derived from Ni contents in Hawaiian melt inclusions and olivines only (*5*). The olivines from some continental LIPs (specific suits from Siberia and Karoo) indicate almost pure pyroxenitic sources. Corresponding results for the other groups are for WPM-THIN, 30 ± 13%; for Archean komatiites, 21 ± 10%; and for MORB, excluding one unusual sample from the Southern Atlantic (see below), 17 ± 12% [similar to predictions of (*25*)]. Because of the uncertainties involved in estimating the end-member compositions, the differences between groups are better constrained than the absolute numbers. Although MORBs contain the lowest proportion of pyroxenite-derived melt, the spread of MORB data is significant, and many samples do contain substantial amounts of pyroxenite-derived component [the extreme is the enriched in silica MORB sample from the Southern Atlantic (*29*) with 100% pyroxenite-derived component]. The calculations show that the Archean komatiites contain a significant amount of pyroxenitic component (maximum of 30% for samples from Canada and Belingwe), although the largest amount is in Proterozoic komatiitic basalts from Gilmour Island, Canada (up to almost 40%). From these calculations, an estimate of the amount of recycled oceanic crust (*10*) yields 4% for MORB, 11% for WPM-THIN group, 16% for WPM-THICK group, and around 13% for Archean komatiites. The highest estimate of the amount of recycled oceanic crust (*10*) yield Ontong Java high-Mg lavas: 13% to 28%.

Silica-undersaturated basalts. Most of the magmas analyzed in this study are silica saturated (tholeiites or transitional). Only a few samples are moderately silica-undersaturated alkali magmas (e.g., Azores and Afar). Our database is representative of the normal oceanic crust, several of the world's major suites of flood basalts (LIPs), several of the major modern mantle plumes (*30*), and some komatiites. The strongly silica-undersaturated associations not covered here include continental rift basalts, many smaller ocean islands consisting mostly of alkali lavas, and also some larger-flux plumes (*30*) such as Pitcairn, Tahiti, and Cape Verde islands. Why are such basalts that are highly enriched in incompatible elements, and therefore presumably generated by very low degrees of melting, nearly always undersaturated in silica? This observation appears to contradict our model; one would expect that silica-saturated melts generated from hybrid pyroxenites should be prevalent, especially at very low melt fractions. There are several possible explanations. (i) A volatile (mostly CO_2-) triggered melting of peridotite may be the dominant mechanism forming strongly silica-undersaturated alkaline magmas at temperatures lower than hybrid pyroxenite melts (*31*). (ii) Low-degree melts of silica-saturated eclogite may be retained in the source because of their high viscosity, thus preventing production of the hybrid pyroxenite (*5*). (iii) Melting of hybrid pyroxenite at the contact with peridotite may produce low-degree, silica-undersaturated melts at lower temperatures than melting of hybrid pyroxenite itself (*8*). (iv) Melting of bimineralic eclogites (no free silica phase) formed from silica-undersaturated recycled crust produces undersaturated alkaline magmas (*16*).

What controls the amount of pyroxenite-derived melt? By following the method outlined above, we estimated the proportions of melt derived from pyroxenite and peridotite for each parental magma. These proportions depend on several interrelated parameters, namely the thickness of lithosphere, the potential mantle temperature (T_p) (*32*), and the amount of recycled crust in the upwelling mantle (Fig. 5). Because at the same T_p pyroxenite melts at higher pressure than peridotite (*26*), a thick lithosphere (which imposes a high lower limit on the depth of melting) will suppress low-depth peridotite melting and therefore favor a high proportion of pyroxenite-derived melts (*33*, *34*). The extreme case is found in some continental flood basalts (specific suites of Siberia and Karoo at table S2a) where the amount of pyroxenite-derived melt is nearly 100%. In such a case, the amount of recycled material cannot be estimated because the peridotitic component contributes no melt. In contrast, a thin lithosphere (MORB, Iceland, Azores, and Detroit seamount) favors a higher proportion of peridotite-derived melt because of the increasing degree of melting of peridotite at shallower depths.

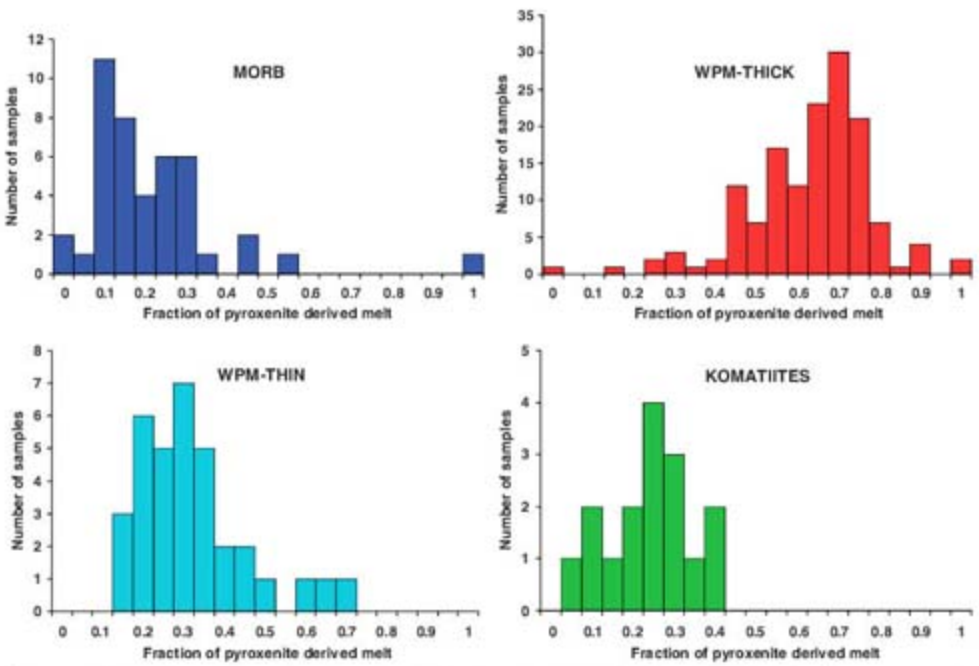

Fig. 4. Estimated amounts of pyroxenite-derived component in the parental melt for 229 samples of four different groups.

A high T_p is an important condition to maintain sufficient buoyancy of mantle plumes or any other upstream mantle flow, and this buoyancy limits the amount of dense eclogite that they can carry (*35*). Also, a high T_p affects mostly the proportion of peridotite-derived melt because fractional melting imposes a rather stringent upper limit to further melting at high melt fractions (*36*). High melt fractions are restricted to the eclogite and hybrid pyroxenite assemblages (*26*) (fig. S5). The peridotite assemblage produces lower melt fractions than pyroxenite (fig. S5) or eclogite (*19*, *25*) at any given temperature and pressure, and its actual extent of melting therefore depends strongly on the specific T_p.

Lastly, why are the proportions of recycled component lower beneath mid-ocean ridges than in thick-lithosphere settings? We suggest several explanations: (i) Relatively low amount of dense recycled component in MORBs is limited by their T_p, which is too low to carry more. (ii) For statistical reasons, plumes are more likely to encounter more-common thick lithosphere than less-common thin lithosphere and few plumes impinge directly on ridges, so we are forced to deal with very-small-number statistics. (iii) Detroit seamount represents one case where a (Hawaiian) plume has encountered thin lithosphere and where our results do indicate a high fraction of recycled crust, similar to those found on the island of Hawaii on the thick lithosphere. This amount is significantly higher than for Iceland, probably reflecting the effect of a higher T_p of the Hawaiian plume (*4*). (iv) The surface expression of a plume emplaced under thick lithosphere requires high T_p, which is necessary for carrying a significant amount of recycled crust (*35*), allowing melts to form at higher pressures than for ordinary peridotite (*5*, *25*, *26*), and melting a peridotite at higher pressures [e.g., komatiites (*37*)].

Heterogeneous versus homogeneous mantle. The model presented here assumes that the recycled crustal component was not fully mixed with peridotite during subduction and mantle convection and thus that the formation of the olivine-free hybrid lithology may take place. On the other hand, homogenization of crustal material within the peridotite mantle should create a range of ultramafic lithologies with variable amounts of olivine, similar to a model by Kelemen *et al.* (*20*). Under these circumstances, the major-element contents of partial melts will correspond to the eutectic-like composition, buffered by the peridotite assemblage, whereas the compatible trace elements (Ni and Mn) will be controlled by the bulk partition coefficients of this assemblage and thus by the amount of olivine and pyroxene present in the system. Therefore, the amount of recycled crust can still be estimated on the basis of these trace elements, but their abundances will no longer correlate with the buffered major elements (Si, Ca, and Al). For Hawaiian basalts, such correlations with Ni are present (*5*), which requires a strongly heterogeneous source.

Input from Earth's core? The Ni excess in mantle olivines from Siberian LIP (*38*) and the elevated Fe/Mn ratios in Hawaiian lavas (*7*) have been explained by input from Earth's core to the sources of mantle plumes. This suggestion is consistent with $^{186}Os/^{188}Os$ ratios for some Hawaiian and Gorgona lavas (*39*) but is contradicted by the fact that concentrations of highly siderofile (Pt) and chalcophile (Cu) elements reported for Hawaiian basalts are not affected by this process (*5*). Our olivine data provide strong arguments against any notable core contribution to Ni or Fe excess in the sources of mantle-derived magmas. Cobalt does not show significant excess in olivines (Fig. 2 and fig. S3) and is effectively decoupled from Ni. As a result, the Ni/Co ratio in most Ni-rich mantle plume olivines exceeds 30 at the typical mantle Fo range of 89 to 91 (Fig. 2). This is not expected from a core contribution, because Ni/Co ratios for both mantle and core are almost equal and close to the chondritic value of about 20 (*40*). In addition, Ca is significantly depleted in many high-Ni and low-Mn olivines from the WPM-THICK group, which cannot be explained by core contribution. Lastly, the olivines from Gorgona komatiites, which do show significant excess in ^{186}Os (*39*), do not indicate large anomalies in Ni and Mn/Fe, whereas Koolau lavas with the highest Ni excess and lowest Mn/Fe ratio in olivines do not show significant elevations in $^{186}Os/^{188}Os$ ratios (*39*). This suggests complete decoupling of these potentially strong indicators of core-mantle exchange.

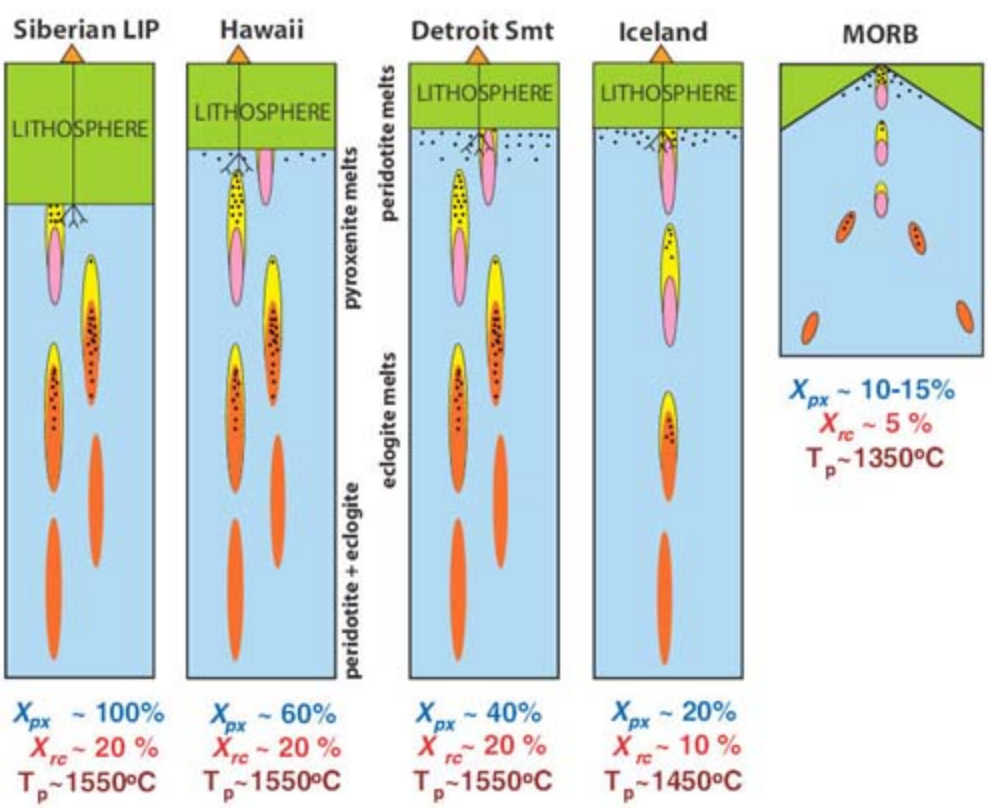

Fig. 5. Schematic model illustrating interplay between amount of recycled crust, thickness of lithosphere, and T_p. Blue, upwelling peridotitic mantle; red, recycled oceanic crust (eclogite with free SiO_2 phase); black dots, melting; yellow, reaction zones forming hybrid pyroxenite; pink, refractory restite after eclogite melting; and green, lithosphere. X_{px}, amount of pyroxenite derived melt in the mixture with peridotite-derived melt, and X_{rc}, amount of recycled oceanic crust in the peridotitic mantle (*42*).

References and Notes

1. A. W. Hofmann, W. M. White, *Earth Planet. Sci. Lett.* **57**, 421 (1982).
2. A. W. Hofmann, in *The Mantle and Core*, vol. 2 of *Treatise on Geochemistry*, H. D. Holland, K. K. Turekian, Eds. (Elsevier, Amsterdam, 2003), p. 61.
3. E. H. Hauri, *Nature* **382**, 415 (1996).
4. C. Herzberg, M. J. O'Hara, *J. Petrol.* **43**, 1857 (2002).
5. A. V. Sobolev, A. W. Hofmann, S. V. Sobolev, I. K. Nikogosian, *Nature* **434**, 590 (2005).
6. Ni was first proposed as a monitor for replacement of olivine by pyroxene in (*20*).
7. M. Humayun, L. P. Qin, M. D. Norman, *Science* **306**, 91 (2004).
8. C. Herzberg, *Nature* **444**, 605 (2006).
9. S. M. Eggins, *Contrib. Mineral. Petrol.* **110**, 387 (1992).
10. Materials and methods are available on *Science* Online.
11. E. J. Jarosevich, J. A. Nelen, J. A. Norberg, *Geostand Newsl.* **4**, 43 (1980).
12. M. J. Walter, *J. Petrol.* **39**, 29 (1998).
13. V. S. Sobolev, A. V. Sobolev, *Dokl. Akad. Nauk SSSR* **237**, 437 (1977).
14. T. Kogiso, M. M. Hirschmann, D. J. Frost, *Earth Planet. Sci. Lett.* **216**, 603 (2003).
15. T. Kogiso, M. M. Hirschmann, M. Pertermann, *J. Petrol.* **45**, 2407 (2004).
16. T. Kogiso, M. Hirschmann, *Earth Planet. Sci. Lett.* **249**, 188 (2006).
17. A. Yasuda, T. Fujii, K. Kurita, *J. Geophys. Res.* **99**, 9401 (1994).
18. A. E. Ringwood, D. H. Green, *Tectonophysics* **3**, 383 (1966).

19. G. M. Yaxley, D. H. Green, *Schweiz. Mineral. Petrogr. Mitt.* **78**, 243 (1998).
20. P. B. Kelemen, S. R. Hart, S. Bernstein, *Earth Planet. Sci. Lett.* **164**, 387 (1998).
21. E. H. Hauri, M. D. Kurz, *Earth Planet. Sci. Lett.* **153**, 21 (1997).
22. J. C. Lassiter, E. H. Hauri, *Earth Planet. Sci. Lett.* **164**, 483 (1998).
23. R. P. Rapp, N. Shimizu, M. D. Norman, G. S. Applegate, *Chem. Geol.* **160**, 335 (1999).
24. D. S. Korzhinskii, *Theory of Metasomatic Zoning* (Clarendon, Oxford, 1970).
25. M. M. Hirschmann, E. M. Stolper, *Contrib. Mineral. Petrol.* **124**, 185 (1996).
26. G. M. Yaxley, *Contrib. Mineral. Petrol.* **139**, 326 (2000).
27. P. Beattie, *Contrib. Mineral. Petrol.* **115**, 103 (1993).
28. R. J. Kinzler, T. L. Grove, S. I. Recca, *Geochim. Cosmochim. Acta* **54**, 1255 (1990).
29. V. S. Kamenetsky *et al.*, *Geology* **29**, 243 (2001).
30. N. H. Sleep, *Annu. Rev. Earth Planet. Sci.* **20**, 19 (1992).
31. G. H. Gudfinnsson, D. C. Presnall, *J. Petrol.* **46**, 1645 (2005).
32. D. McKenzie, M. J. Bickle, *J. Phys. Earth* **38**, 511 (1990).
33. J. P. Morgan, *Geochem. Geophys. Geosystems* **2**, 2000GC000049 (2001).
34. G. Ito, J. J. Mahoney, *Earth Planet. Sci. Lett.* **230**, 29 (2005).
35. M. Pertermann, M. M. Hirschmann, *J. Petrol.* **44**, 2173 (2003).
36. I. Kushiro, *Annu. Rev. Earth Planet. Sci.* **29**, 71 (2001).
37. N. Arndt, *J. Geophys. Res.* **108**, XX (2003).
38. I. D. Ryabchikov, *Dokl. Earth Sci.* **389**, 437 (2003).
39. A. D. Brandon, R. J. Walker, *Earth Planet. Sci. Lett.* **232**, 211 (2005).
40. W. F. McDonough, S. S. Sun, *Chem. Geol.* **120**, 223 (1995).
41. L. V. Danyushevsky, *J. Volcanol. Geotherm. Res.* **110**, 265 (2001).
42. D. McKenzie, M. J. Bickle, *J. Petrol.* **29**, 625 (1988).
43. We thank B. Schulz-Dobrick for supervising purchase and establishing electron microprobe facility in MPI; Hawaiian Scientific Drilling Project team, Koolau Scientific Drilling Project team, Ocean Drilling Program team, A. T. Anderson, E. A. Mathez, and N. Gitahi for providing samples; E. J. Jarosevich for supplying microprobe standards; A. Yasevich for sample preparations and N. Groschopf for maintaining the electron microprobe. The paper benefited from discussions with M. Hirschmann, P. Kelemen, C. Herzberg, B. McDonough, I. Ryabchikov, L. Kogarko, A. Kadik, E. Galimov, V. Batanova. Constructive reviews of C. Herzberg, and P. Kelemen improved the clarity of the manuscript. The study was supported by Wolfgang Paul Award of the Alexander von Humboldt Foundation, Germany, to A.V.S. Partial support from the following sources is also acknowledged: Russian Foundation for Basic Research (RFBR) grants 06-05-65234 and НШ-4264.2006.5 and Russian Academy of Sciences and Deutsche Forschungsgemeinschaft grant HO 1026/16-1 to A.V.S., RFBR grant 06-05-64651 to N.M.S., NSF grants EAR03-36874 to M.O.G. and EAR-0105557 to F.A.F., and Netherlands Research Center for Integrated Solid Earth Science grant 6.2.12 to I.K.N. This is School of Ocean and Earth Science and Technology, University of Hawaii, contribution no. 7104.

Supporting Online Material

www.sciencemag.org/cgi/content/full/1138113/DC1
SOM Text
Figs. S1 to S5
Tables S1 to S4
Data set

29 November 2006; accepted 16 March 2007
Published online 29 March 2007;
10.1126/science.1138113
Include this information when citing this paper.

Genes Required for Mitotic Spindle Assembly in *Drosophila* S2 Cells

Gohta Goshima,[1,3]* Roy Wollman,[2,3] Sarah S. Goodwin,[1] Nan Zhang,[1] Jonathan M. Scholey,[2] Ronald D. Vale,[1,3]† Nico Stuurman[1,3]

The formation of a metaphase spindle, a bipolar microtubule array with centrally aligned chromosomes, is a prerequisite for the faithful segregation of a cell's genetic material. Using a full-genome RNA interference screen of *Drosophila* S2 cells, we identified about 200 genes that contribute to spindle assembly, more than half of which were unexpected. The screen, in combination with a variety of secondary assays, led to new insights into how spindle microtubules are generated; how centrosomes are positioned; and how centrioles, centrosomes, and kinetochores are assembled.

The diamond-shaped mitotic spindle has become one of the most widely recognized images in biology, emblematic of life's propagation through cell division. In higher eukaryotes, the process of spindle formation begins after nuclear envelope breakdown (NEB) when microtubules (MTs), generated both from centrosomes and from the vicinity of chromatin, are organized into a bipolar array (*1*–*5*). Sister chromatids bind to MTs emanating from opposite poles, are aligned in the middle of the bipolar MT network, and then ultimately separate and move apart during anaphase. Failures early in mitosis result in the formation of an abnormal metaphase spindle, which can lead to mitotic delay and, potentially, chromosome missegregation during the ensuing anaphase.

To understand the mechanism of metaphase spindle assembly, it is critical to identify the proteins required for this process and then dissect how they function. Many mitotic proteins have been identified through genetic and RNAi screens (*6*–*10*), but the inventory is likely incomplete. Here, we present a genome-wide screen for mitotic spindle morphology in *Drosophila* S2 cells and the functional analysis of unexpected genes discovered through the screen.

Identification of genes involved in metaphase spindle formation by high-throughput microscopy. Because the percentage of S2 cells in mitosis is low (~1%), we conducted our RNAi screen in the presence of dsRNA (double-stranded RNA) to Cdc27 (a subunit of the anaphase-promoting complex) to delay anaphase and thereby increase the percentage of metaphase cells (~10% of the population). Thus, our screen was designed to investigate the assembly of the metaphase spindle, but not anaphase or cytokinesis. We also rescreened the final hits without Cdc27 RNAi–induced mitotic arrest. The majority (88%) showed identical phenotypes, although a few genes only manifest clear phenotypes under conditions of mitotic arrest (table S1).

Using our custom, full-genome (14,425 genes) *Drosophila* RNAi library (*11*), we treated S2 cells with dsRNA for 4 days, conditions that generally reduce protein levels by >80% (*12*, *13*). After dsRNA treatment, cells were fixed and stained for DNA, γ-tubulin, MT, and phosphohistone H3 (pH3) in 96 well plates, and about 40 sites per well were imaged by automated microscopy with a high numerical aperture air objective to obtain relatively high-resolution images of mitotic spindles (Fig. 1A). To reduce the complexity of this large amount of image data, a custom computer code was used to identify, crop, and arrange mitotic spindles into galleries, which were then blindly scored by an observer (Fig. 1B and fig. S1). In addition, computer algorithms measured eight parameters of spindle shape, as well as the intensity of γ-tubulin, cell number, and mitotic index (Fig. 1C) (*11*). More than 4,000,000 spindles were analyzed in this screen.

Before beginning this screen, we annotated 49 genes that produce mitotic defects in S2 cells (table S2). Of these 49 genes, 45 were identified as hits in the primary screen, indicating a high success rate of identifying mitotic phenotypes. However, our final list of genes should not be considered as a complete or universal inventory, because genes can be missed (particularly those with subtle phenotypes), and some phenotypes (or lack thereof) may be specific to S2 cells. False positives by off-target effects of dsRNA can occur in RNAi screens (*14*, *15*), so precautions were taken to minimize gene overlap in the dsRNA design, and all unexpected hits were confirmed with another dsRNA that had no overlap with the first dsRNA (*11*). To learn more about the functions of interesting genes,

[1]Howard Hughes Medical Institute and the Department of Cellular and Molecular Pharmacology, University of California, San Francisco, 600 16th Street, San Francisco, CA 94158, USA. [2]Department of Molecular and Cellular Biology, University of California, Davis, One Shields Avenue, 3203 Life Sciences, Davis, CA 95616, USA. [3]Physiology Course, Marine Biological Laboratory, 7 MBL Street, Woods Hole, MA 02543, USA.

*Present address: Institute for Advanced Research, Nagoya University, Furo-cho, Chikusa-ku, Nagoya, 464-8601, Japan. †To whom correspondence should be addressed. E-mail: vale@cmp.ucsf.edu

we determined protein localization by green fluorescence protein (GFP) tagging (38 genes, mostly tagged at both N and C termini to be certain of the localization pattern) (table S1 and figs. S3 to S7), analyzed RNAi phenotypes by live cell imaging, and/or examined the effect of gene knockdown on the localization of kinetochore or centrosome proteins.

Our screen identified ~150 unexpected or unknown genes that produced mitotic RNAi phenotypes, each of which was confirmed by 2 to 6 repeat experiments (Fig. 1D). In the following sections, we describe the roles of a subset of these genes in centrosome and γ-tubulin function, the shape and dynamics of the poles, and spindle size and chromosome alignment. The complete list of genes identified in the screen can be found in table S1 as well as our Web site, which also contains primary data on RNAi constructs, phenotypes, and protein localization (fig. S2 and http://rnai.ucsf.edu/mitospindlescreen).

Centrosomes and γ-tubulin localization. In preparation for mitosis, the centrioles duplicate, creating two γ-tubulin–containing centrosomes that nucleate MTs and ultimately become the poles of the mitotic spindle. However, centrioles are not needed for most cell divisions in flies, as MT nucleation around chromatin suffices for bipolar spindle formation (*13*, *16*, *17*). In our screen, depletion of proteins involved in centriole duplication would be expected to produce a mixture of anastral spindles (no γ-tubulin staining at the poles) and monastral bipolar spindles (only one pole with normal γ-tubulin staining), because centriole numbers only gradually diminished with dilution through successive cell cycles in a 4-day dsRNA treatment (Fig. 2A and fig. S3A).

Our screen identified several known proteins (Sak kinase, DSas-4, and Sas-6), as well as three previously unknown genes [anastral spindle phenotype (*Ana*)]. Consistent with their RNAi phenotype, GFP-Ana1 and -Ana2 colocalized during interphase and mitosis with the centriolar markers mRFP-Sas-6 (Fig. 2B and fig. S3C) and Sak and DSas-4 (fig. S3D). GFP-Ana1 was not detected at anastral spindle poles after Sak RNAi, and RNAi depletion of Ana1 resulted in a substantial decrease in GFP-Sas6 fluorescence from spindle poles, suggesting an important role in centriole formation (Fig. 2C). Thus, Ana1 and Ana2 (and possibly Ana3) may be core components of the centriole that are necessary for centriole duplication.

RNAi of the known genes Spd-2, Polo, centrosomin, Dgrip84, and Dgrip91 [these Dgrips make up the stable core (γTuSC) of the γ-tubulin ring complex (γTuRC)] decreased γ-tubulin staining at the pole without interfering with centriole marker localization (fig. S3, F and G). By examining the effects of RNAi of these genes on centrosomin and γ-tubulin localization, we suggest a molecular pathway leading to γ-tubulin localization at the spindle pole (Fig. 2G). We also found two previously unknown genes, Dgt1 and Dgt2 (dim γ-tubulin), that decreased spindle pole γ-tubulin staining without affecting centrosomin [a known γ-tubulin localization factor (*18*)]. RNAi of these genes also produced long spindles, a phenotype characteristic of γ-tubulin RNAi, thus further suggesting a role in γ-tubulin function.

In addition to centrosome localization, a subset of γ-tubulin localizes to the spindle (*16*, *19*), where it might contribute to MT nucleation within the spindle (*16*). Phosphorylation of a γTuRC subunit is required for spindle localization of γ-tubulin in mammalian cells (*19*), but otherwise, little is known about this population of spindle-localized γ-tubulin. In our screen, we identified genes that are needed to localize γ-tubulin to the spindle but not the pole (Fig. 2D and fig. S4A) (*11*). Among these are components of the γTuRC (Dgrip71, Dgrip75, Dgrip128, and Dgrip163). RNAi of several previously unknown genes (Dgt3 to Dgt6) also diminished γ-tubulin selectively within the spindle compared with the pole. Consistent with a role in targeting γ-tubulin to the spindle, GFP-tagged Dgt4, Dgt5, and Dgt6 localized uniformly on spindle MTs, with no enrichment at the centrosome; the spindle staining was lost upon MT depolymerization and was cell cycle dependent (no MT localization in interphase) (Fig. 2E and fig. S4B). High-throughput, automated imaging of living cells expressing mCherry-tubulin and H2B-GFP as well as high-resolution confocal imaging of MTs further revealed that RNAi of these Dgts reduced MT density inside the spindle, increased monopolar spindle formation, and caused chromosome/kinetochore misalignment and mitotic delay (Fig. 2F; and movie S1 of Dgt5 RNAi). Recently, γTuRC was implicated in the spindle-assembly checkpoint (SAC) signaling through binding Cdc20 and BubR1 (*20*), but our results suggest that the loss of proper kinetochore-MT interactions after removal of spindle-localized γTuRC may constitute the primary reason for failure to satisfy the SAC.

This study suggests two pathways for γ-tubulin localization in mitosis (Fig. 2G). At the spindle pole, a core set of proteins build centrioles (Ana1, Ana2, Sak, DSas-4, and Sas-6), which provide scaffolds for Spd-2, polo kinase, and centrosomin to recruit γ-tubulin through the γTuSC subunits. However, this pathway is dispensable for cell division in S2 cells. A second pathway involving a new set of proteins (Dgt3-6) and the outer γTuRC subunits recruit γ-tubulin to spindle MTs. Surprisingly, this site of γ-tubulin function is more important than the centrosome in building a normal-length bipolar spindle with properly aligned chromosomes.

The shape and dynamics of the poles. Mitotic spindles normally have two well-focused poles. In our screen, we identified a series of

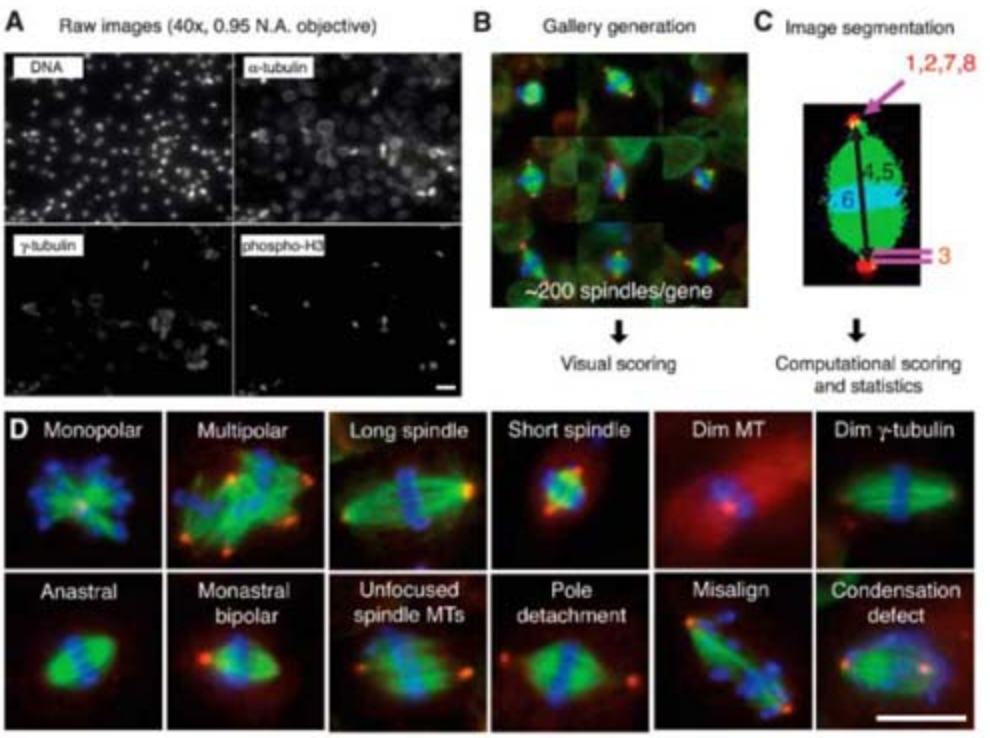

Fig. 1. An image-based, genome-wide RNAi screening of metaphase spindle morphology. (**A**) *Drosophila* S2 cells were treated with dsRNAs of 14,425 genes, along with Cdc27/Apc3 dsRNA, to accumulate metaphase cells. After 4 days, cells were transferred and adhered onto ConA-coated glass-bottom plates. Cells were immunostained for DNA, α-tubulin, γ-tubulin and pH3 and imaged by high-throughput automated microscopy. Scale bar, 20 μm. (**B**) Mitotic cells were automatically selected by a computer algorithm that detects pH3 staining. The selected ~200 mitotic cells (mostly metaphase) were displayed in a gallery for an observer to score phenotypes. (**C**) Phenotypes were also analyzed by computer after image segmentation (1, monopolar; 2, multipolar; 3, pole detachment; 4, long spindle; 5, short spindle; 6, misalignment; 7, large γ-tubulin area; 8, dim γ-tubulin) (*11*). (**D**) Twelve major phenotypes identified in the screen. Scale bar, 10 μm.

genes that affect the number or organization of spindle poles (table S1 and fig. S5). Unfocused kinetochore fibers (K-fibers), a rare phenotype, were obtained for RNAi of calmodulin (CaM), a broadly functioning calcium effector (Fig. 3A). By time-lapse imaging, CaM RNAi caused K-fiber detachment from centrosomes, a finding that mimicked observations for RNAi of Abnormal Spindle protein (Asp) (movie S2) (*21*). Like Asp, CaM localized at the minus ends of K fibers, even when these ends were disconnected from the centrosome by Ned/Dhc RNAi (Fig. 3B). Furthermore, CaM and Asp mutually depended upon one another for localization to the minus end of K fibers (fig S5F). Thus, Asp, which has multiple, predicted CaM-binding IQ motifs (*22*), requires CaM for its localization and function. Surprisingly, the specificity of the CaM RNAi phenotype suggests that CaM's main function during mitosis is serving as a cofactor in Asp-mediated pole-focusing.

An unexpected phenotype was increased numbers of monastral bipolar (but not anastral) spindles after RNAi of multiple proteasome subunits, the E2 ubiquitin conjugating enzyme UbcD6, the transcription factor Myb, and a Myb-interacting protein (Twit) (Fig. 3C). Proteasome RNAi showed other phenotypes, such as severe proliferation defects, but the monastral bipolar spindle phenotype was not characteristic of other RNAi treatments that reduced cell numbers. Moreover, RNAi of UbcD6 did not inhibit growth.

To better understand this phenotype, we scored the number of γ-tubulin–staining centrosomes in prophase to determine whether centrosome numbers were reduced (Fig. 3D). However, comparable (proteasome and UbcD6 RNAi) or higher [Myb and twit RNAi; see also (*23*)] numbers of prophase centrosomes were observed compared with control cells, suggesting that these RNAi treatments caused centrosome fusion after NEB to generate monastral bipolar spindles. To test this idea, we performed automated, live imaging of cells coexpressing γ-tubulin-GFP and mCherry-tubulin (Fig. 3E and movie S3). Myb RNAi cells initially formed normal bipolar (or occasionally multipolar) spindles after NEB. However, subsequently, one or more of the centrosomes detached from the poles and wandered toward the center [in contrast to dynein RNAi, which caused centrosome to detach and move away from the spindle (*24*)]. In some instances, centrosome fusion was observed, creating a monastral bipolar spindle as seen in fixed cells. This phenotype may reflect a direct action of Myb at the centrosome or could be mediated indirectly through its role in gene transcription. In contrast, RNAi of UbcD6 induced centrosome fusion shortly after NEB, generating monopolar spindles, which then converted into monastral bipolar spindles by chromatin-dependent MT generation.

Thus, we observed two previously unreported phenotypes concerning centrosome dynamics. Loss of a ubiquitin-dependent proteolysis pathway induced excess centrosome fusion, and Myb complex depletion caused centrosomes to reposition toward the spindle interior (Fig. 3F).

Spindle size and chromosome alignment. In addition to identifying known regulators of S2 cell spindle length (*25*), the screen also identified several previously unknown genes that produced short-spindle RNAi phenotypes [short spindle (*Ssp*) genes], and three of these localized to mitotic spindles (Fig. 4A, table S1, fig. S6). Depletion of one of these proteins [CG33130 (termed Ssp4)] caused pronounced MT severing in interphase cells (Fig. 4B and movie S4), a surprising effect because severing is rarely observed in untreated cells. The severed MTs often continued to grow at their plus ends and depolymerize at their minus ends, causing them to treadmill through the cytoplasm (*26*). Thus, Ssp4 regulates MT severing, and the shorter-spindle phenotype might be due to enhanced MT severing and depolymerization at the poles.

Our screen also identified genes involved in chromosome alignment (table S1, fig. S7, and movie S5). Chromosome misalignment frequently coincided with an increase in spindle length (table S1), consistent with a model in which defective chromosome-MT interactions result in an imbalance of forces acting upon the spindle (*25*). Five genes with severe-misalignment RNAi phenotypes encode proteins that localized at the kinetochore, and two (CG18156 and CG5148) also localized at centromeres in interphase nuclei (Fig. 4C and fig. S7, B and C). These five genes

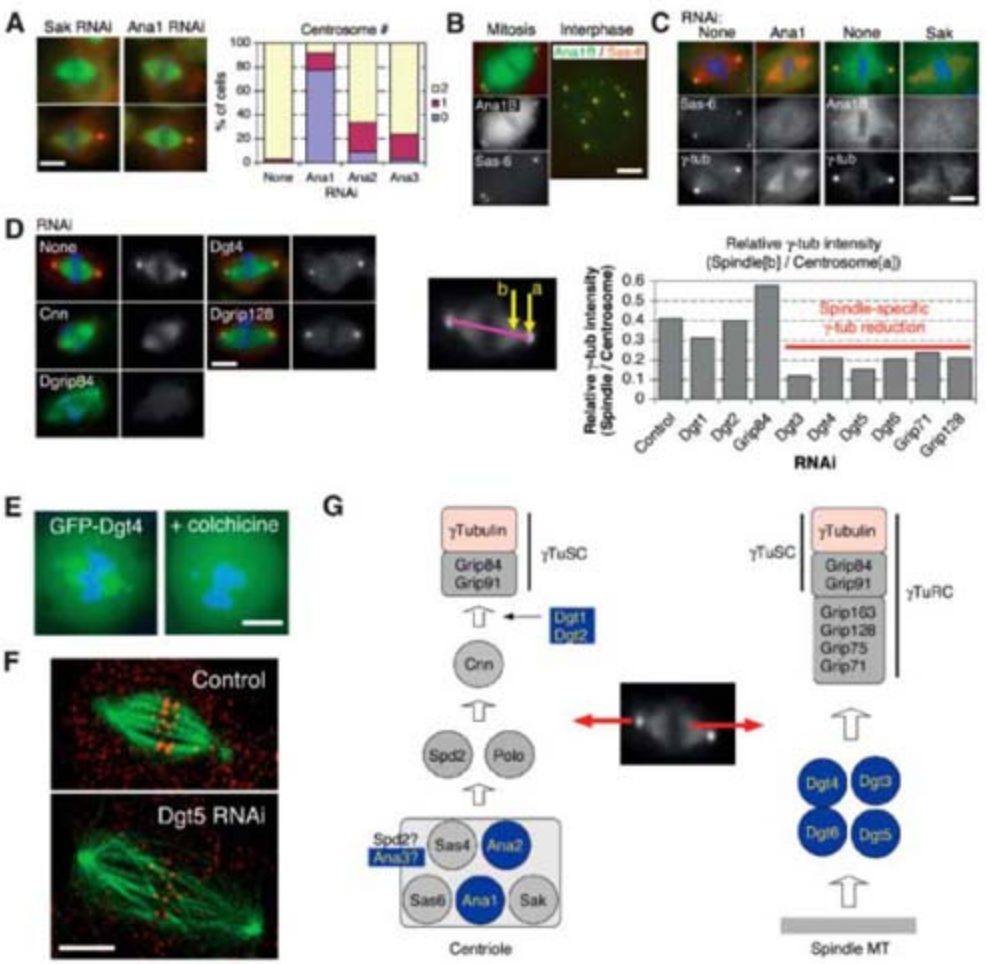

Fig. 2. Genes required for localizing γ-tubulin to the centrosome and the spindle. (**A**) (Left) Anastral as well as monastral bipolar spindles were observed after RNAi to Sak or three previously unknown Ana genes (the latter two shown in fig. S3). (Right) Centrosome number was counted for bipolar spindles after four rounds of RNAi treatment. (**B**) Ana1 (isoform B) was colocalized with the centriole marker mRFP-Sas-6. (**C**) Ana1 RNAi caused the loss of GFP-Sas-6 from the pole region of anastral spindles, whereas SAK RNAi interfered with GFP-Ana1B localization to poles. (**D**) (Left) Various dim γ-tubulin RNAi phenotypes. The γ-tubulin signal is reduced at the centrosome alone (Cnn), at both the centrosome and spindle (Dgrip84), or only at the spindle (Dgt4 and Dgrip128). (Right) Intensity at centrosome (a) and spindle region (b) was measured, and the relative intensity was calculated (*11*). (**E**) Spindle localization of GFP-Dgt4 is lost after colchicine-induced MT depolymerization. (**F**) RNAi of Dgt5 (as well as other genes required for spindle localization of γ-tubulin) produces long spindles with low MT density and misaligned chromosomes. Shown is a maximum intensity projection of four optical slices obtained at 0.25-μm intervals by spinning-disk confocal microscope. Red, antibody to CENP-A; green, MT. Scale bar, 5 μm. (**G**) Model for recruitment pathway of γ-tubulin to the centrosome and spindle MTs. Previously unknown or unexpected genes are highlighted in blue in this and other figures.

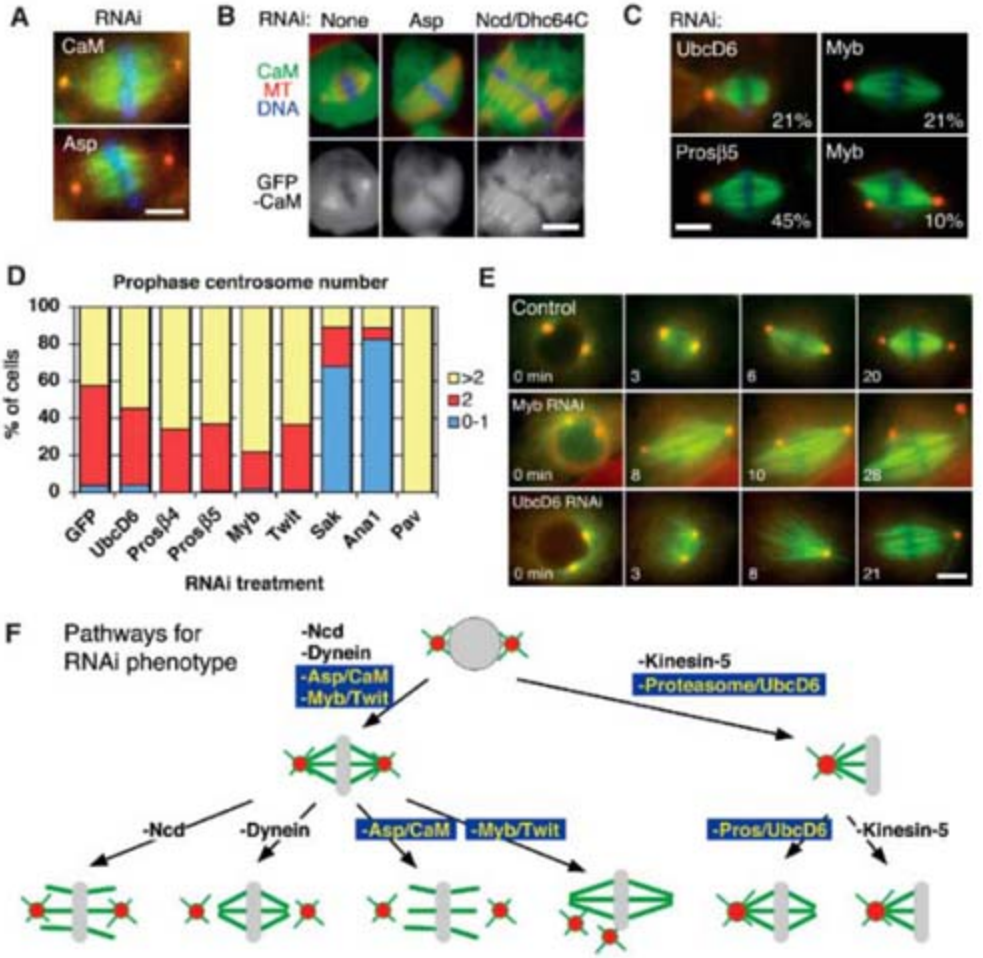

Fig. 3. Genes required for centrosome separation and association to spindle poles. (**A**) Identical kinetochore-fiber unfocusing and centrosome-detachment phenotypes were observed after Asp and calmodulin (CaM) RNAi. See movie S2. (**B**) GFP-CaM was localized at spindle poles in an Asp-dependent manner, but was still detected at unfocused poles induced by Ncd/Dhc64C RNAi. (**C**) Monastral bipolar spindles produced by UbcD6, proteasome subunit β5, or Myb RNAi (percentage of cells with phenotype indicated; 3% to 8% for untreated cells). Centrosome detachment also was detected after Myb RNAi. (**D**) At prophase, most proteosome (Prosβ4 and Prosβ5), UbcD6, Myb, and Twit RNAi cells ($n > 65$) had >1 centrosome; Sak, Ana1 (centriole duplication), and Pav (cytokinesis) served as control RNAis that decrease or increase centrosome numbers. (**E**) Time-lapse imaging of γ-tubulin-GFP (red) and mCherry-tubulin (green) from prophase to metaphase shows bipolar spindle formation, and then centrosome detachment after Myb RNAi (80%) ($n = 20$), and immediate centrosome fusion after NEB for UbcD6 RNAi (25%) ($n = 20$). See movie S3. Scale bars, 5 μm. (**F**) Models for various spindle-pole phenotypes in response to various protein depletions.

were unannotated at the time of our screen, but sequence alignments performed by our group and others (*27*) identified CG9938, CG8902, and CG18156 as fly homologs of Ndc80/Hec1, Nuf2, and Mis12, respectively.

Two genes, CG5148 [chromosome alignment defect (*Cal1*)] and CG7242 (*Cal2*) did not display sequence similarity to known kinetochore proteins. To understand how these proteins are integrated and function in the molecular assembly pathway of the *Drosophila* kinetochore, we investigated the localization dependency of the kinetochore proteins using GFP fusion proteins and RNAi. RNAi of Cal2 affected mitotic localization of Ndc80 and Nuf2, but not the constitutive centromere proteins Cal1, Mis12, and CENP-A/Cid, similar to results for Spc25 RNAi in HeLa cells (*28*). Thus, Cal2 [a 26-kD protein with known two-hybrid interaction with Ndc80 (*29*)] may be *Drosophila* Spc25. RNAi of Cal1, on the other hand, affected localization of all markers tested (Fig. 4D; and fig. S7, D to F). Different from other systems (*30*), centromere localizations of CENP-A, CENP-C, and Cal1 were mutually dependent, because RNAi depletion of any single protein disrupted or diminished the localization of the other two. Thus, S2 cell inner kinetochore formation may involve a coassembly process of CENP-A, -C, and the previously unknown protein Cal1 (Fig. 4D). Once these core proteins are assembled, Mis12 and the Ndc80 outer kinetochore complex are recruited in a linear pathway, similar to that described for *C. elegans* embryos (*31*).

Several known genes, including transcription factors (Spt), chromatin-binding proteins (Dmt/Dalmatian), and signaling proteins [target of rapamycin (TOR)–associated protein (Raptor) and the GTPase RheB], also produced unexpected RNAi chromosome misalignment phenotypes (table S1). The misalignment effects of Raptor and RheB RNAi, as well as those produced by the TOR inhibitor rapamycin (fig. S7H), were only observed with Cdc27 arrest. RNAi of numerous spliceosome components also caused chromosome misalignment. Although this finding is largely unexpected, mutations in splicing factors cause missegregation of mini-chromosomes in yeast (*32*). RNA splicing might regulate proteins involved in kinetochore structure or generate RNAs that have structural roles within the spindle (*33*). Thus, chromatin structure, RNA, and signaling pathways can influence chromosome alignment, although the mechanisms of these effects remain to be understood at a molecular level.

Conclusion. This morphological screen of the *Drosophila* mitotic spindle was made possible by computer-assisted identification of mitotic cells for visual scoring and quantitative computational image analysis. However, the resultant ~200-gene RNAi "hit" list, by itself, was insufficient to gain new insight into spindle formation. A suite of secondary assays was needed to decipher the site of action and mechanism of previously unknown proteins, as well as to develop an integrated understanding of how these proteins work together.

In addition to implicating many unexpected genes, this study has revealed unanticipated processes involved in spindle assembly. For example, the identification of Dgt proteins led to the finding that the activity of γ-tubulin within the spindle is more critical for spindle architecture and chromosome alignment than its better-known function at the centrosome. We also uncovered unanticipated RNAi phenotypes, such as excessive centrosome fusion (UbcD6 RNAi), centrosome detachment and motion within the spindle (Myb RNAi), and activation of MT severing (Ssp4 RNAi). Interfering with general cellular machines also gave rise to distinct spindle defects such as those seen with the proteasome (monastral bipolar spindles), RNA polymerase II (long spindles), and the spliceosome (chromosome misalignment). This work also provides a systematic analysis of the assembly of *Drosophila* centrosomes and inner kinetochores, ordering several proteins into these pathways. Many of the molecules and pathways described in this study are likely to be conserved in human cells. Therefore, the alterations in centrosome function and chromosome alignment observed in this screen may provide insight into how these commonly observed defects arise in human cancers (*34*–*36*).

References and Notes

1. T. J. Mitchison, E. D. Salmon, *Nat. Cell Biol.* **3**, E17 (2001).
2. J. R. McIntosh, E. L. Grishchuk, R. R. West, *Annu. Rev. Cell Dev. Biol.* **18**, 193 (2002).
3. C. L. Rieder, A. Khodjakov, *Science* **300**, 91 (2003).

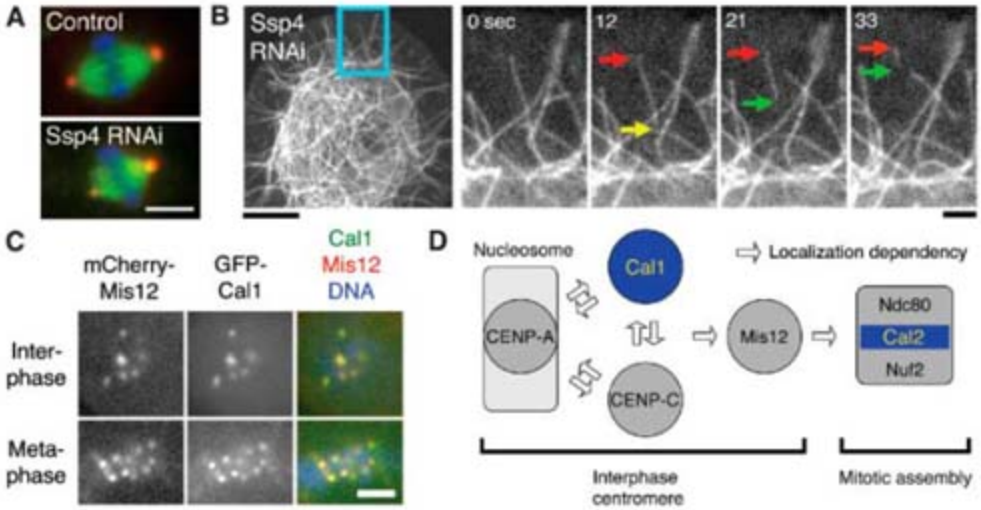

Fig. 4. Regulation of spindle length and chromosome alignment. (**A**) Spindle length was altered after RNAi depletion of the novel protein Ssp4. Scale bar, 5 μm. (**B**) MT severing (yellow arrow) frequently occurred after Ssp4 RNAi. Severed MTs often showed treadmilling behavior (red and green arrows) and then disappeared. Scale bars, 10 μm (left), 2 μm (right). See also movie S4. (**C**) Previously unknown Cal1 protein localizes to the centromere (marked by mCherry-Mis12). (Localization data for other proteins are in fig. S7). Scale bar, 2 μm. (**D**) Model for kinetochore assembly in S2 cells based on protein localization and RNAi. (Data are in fig. S7, D to F).

4. S. Gadde, R. Heald, *Curr. Biol.* **14**, R797 (2004).
5. J. M. Scholey, I. Brust-Mascher, A. Mogilner, *Nature* **422**, 746 (2003).
6. M. Yanagida, *Trends Cell Biol.* **8**, 144 (1998).
7. K. F. Doheny *et al.*, *Cell* **73**, 761 (1993).
8. K. Nasmyth, *Science* **297**, 559 (2002).
9. M. Bettencourt-Dias *et al.*, *Nature* **432**, 980 (2004).
10. B. Sonnichsen *et al.*, *Nature* **434**, 462 (2005).
11. Materials and methods are available as supporting material on *Science* Online.
12. S. L. Rogers, U. Wiedemann, N. Stuurman, R. D. Vale, *J. Cell Biol.* **162**, 1079 (2003).
13. G. Goshima, R. D. Vale, *J. Cell Biol.* **162**, 1003 (2003).
14. Y. Ma, A. Creanga, L. Lum, P. A. Beachy, *Nature* **443**, 359 (2006).
15. M. M. Kulkarni *et al.*, *Nat. Methods* **3**, 833 (2006).
16. N. M. Mahoney, G. Goshima, A. D. Douglass, R. D. Vale, *Curr. Biol.* **16**, 564 (2006).
17. R. Basto *et al.*, *Cell* **125**, 1375 (2006).
18. K. Li, T. C. Kaufman, *Cell* **85**, 585 (1996).
19. J. Luders, U. K. Patel, T. Stearns, *Nat. Cell Biol.* **8**, 137 (2006).
20. H. Muller, M. L. Fogeron, V. Lehmann, H. Lehrach, B. M. Lange, *Science* **314**, 654 (2006).
21. S. Morales-Mulia, J. M. Scholey, *Mol. Biol. Cell* **16**, 3176 (2005).
22. R. D. Saunders, M. C. Avides, T. Howard, C. Gonzalez, D. M. Glover, *J. Cell Biol.* **137**, 881 (1997).
23. S. M. Fung, G. Ramsay, A. L. Katzen, *Development* **129**, 347 (2002).
24. H. Maiato, C. L. Rieder, A. Khodjakov, *J. Cell Biol.* **167**, 831 (2004).
25. G. Goshima, R. Wollman, N. Stuurman, J. M. Scholey, R. D. Vale, *Curr. Biol.* **15**, 1979 (2005).
26. V. I. Rodionov, G. G. Borisy, *Science* **275**, 215 (1997).
27. P. Meraldi, A. D. McAinsh, E. Rheinbay, P. K. Sorger, *Genome Biol.* **7**, R23 (2006).
28. R. Bharadwaj, W. Qi, H. Yu, *J. Biol. Chem.* **279**, 13076 (2004).
29. L. Giot *et al.*, *Science* **302**, 1727 (2003).
30. G. K. Chan, S. T. Liu, T. J. Yen, *Trends Cell Biol.* **15**, 589 (2005).
31. A. Desai *et al.*, *Genes Dev.* **17**, 2421 (2003).
32. K. Takahashi, H. Yamada, M. Yanagida, *Mol. Biol. Cell* **5**, 1145 (1994).
33. M. D. Blower, M. Nachury, R. Heald, K. Weis, *Cell* **121**, 223 (2005).
34. Z. Storchova, D. Pellman, *Nat. Rev. Mol. Cell Biol.* **5**, 45 (2004).
35. E. A. Nigg, *Nat. Rev. Cancer* **2**, 815 (2002).
36. K. W. Yuen, B. Montpetit, P. Hieter, *Curr. Opin. Cell Biol.* **17**, 576 (2005).

37. We thank K. Pollard for valuable suggestions on statistics; Y. Guo, I. Vasenkova, and R. De Breuil for help in dsRNA synthesis at Open Biosystems Inc.; I. Cheeseman for advice on homology searches; A. Straight for sharing data in advance of publication; and S. Henikoff, M. Bettencourt-Dias, D. Glover, T. Kaufman, D. Agard, R. Tsien, and E. Griffis for reagents. G.G. received support from the Human Frontier Science Program and R.W. from a University of California GREAT Training Grant. We thank the Sandler Foundation (UCSF) for support.

Supporting Online Material

www.sciencemag.org/cgi/content/full/1141314/DC1
Materials and Methods
Figs. S1 to S7
Tables S1 and S2
References
Movies S1 to S5
Web site S1

14 February 2007; accepted 23 March 2007
Published online 5 April 2007;
10.1126/science.1141314
Include this information when citing this paper.

An Evolutionarily Conserved Mechanism Delimiting SHR Movement Defines a Single Layer of Endodermis in Plants

Hongchang Cui,[1] Mitchell P. Levesque,[1]*† Teva Vernoux,[1]*‡ Jee W. Jung,[1] Alice J. Paquette,[1] Kimberly L. Gallagher,[1]§ Jean Y. Wang,[1] Ikram Blilou,[2] Ben Scheres,[2] Philip N. Benfey[1]‖

Intercellular protein movement plays a critical role in animal and plant development. SHORTROOT (SHR) is a moving transcription factor essential for endodermis specification in the *Arabidopsis* root. Unlike diffusible animal morphogens, which form a gradient across multiple cell layers, SHR movement is limited to essentially one cell layer. However, the molecular mechanism is unknown. We show that SCARECROW (SCR) blocks SHR movement by sequestering it into the nucleus through protein-protein interaction and a safeguard mechanism that relies on a SHR/SCR-dependent positive feedback loop for *SCR* transcription. Our studies with *SHR* and *SCR* homologs from rice suggest that this mechanism is evolutionarily conserved, providing a plausible explanation why nearly all plants have a single layer of endodermis.

Stem cell renewal and patterned differentiation of their progeny are fundamental processes in the development of multicellular organisms. The root of *Arabidopsis thaliana* is particularly suitable to study these processes, because it has a simple and stereotyped cellular organization (fig. S1) (*1*). SHR and SCR are key regulators of root radial patterning (*2*, *3*) and stem cell maintenance (*4*). In *shr* and *scr* mutants, the cortex/endodermis initial (CEI) cell, which normally gives rise to two files of ground-tissue cells (an inner layer of endodermis and an outer layer of cortex), produces only a single cell layer (fig. S1) (*2*, *3*, *5*). SHR is a transcription factor (*6*) expressed in the stele that moves into the adjacent cell layer where it controls *SCR* transcription and endodermis specification (*6*). By contrast, the SCR protein is absent from the stele, is predominantly expressed in the endodermis, the CEI cell,

[1]Department of Biology and Institute for Genome Sciences and Policy, Duke University, Durham, NC 27708, USA. [2]Department of Molecular Genetics, Utrecht University, Padualaan 8, 3584CH Utrecht, Netherlands.

*These authors contributed equally to this work.
†Present address: Max Planck Institute for Developmental Biology, Department of Genetics and Genomics, Spemannstrasse 35/III, D-72076 Tübingen, Germany.
‡Present address: Reproduction et Développement des Plantes Laboratory, Unité Mixte de Recherche 5667, Ecole Normale Supérieure de Lyon, 46, Alleé d'Italie, 69364 Lyon Cedex 07, France.
§Present address: Department of Biology, University of Pennsylvania, Philadelphia, PA 19104, USA.
‖To whom correspondence should be addressed. E-mail: philip.benfey@duke.edu

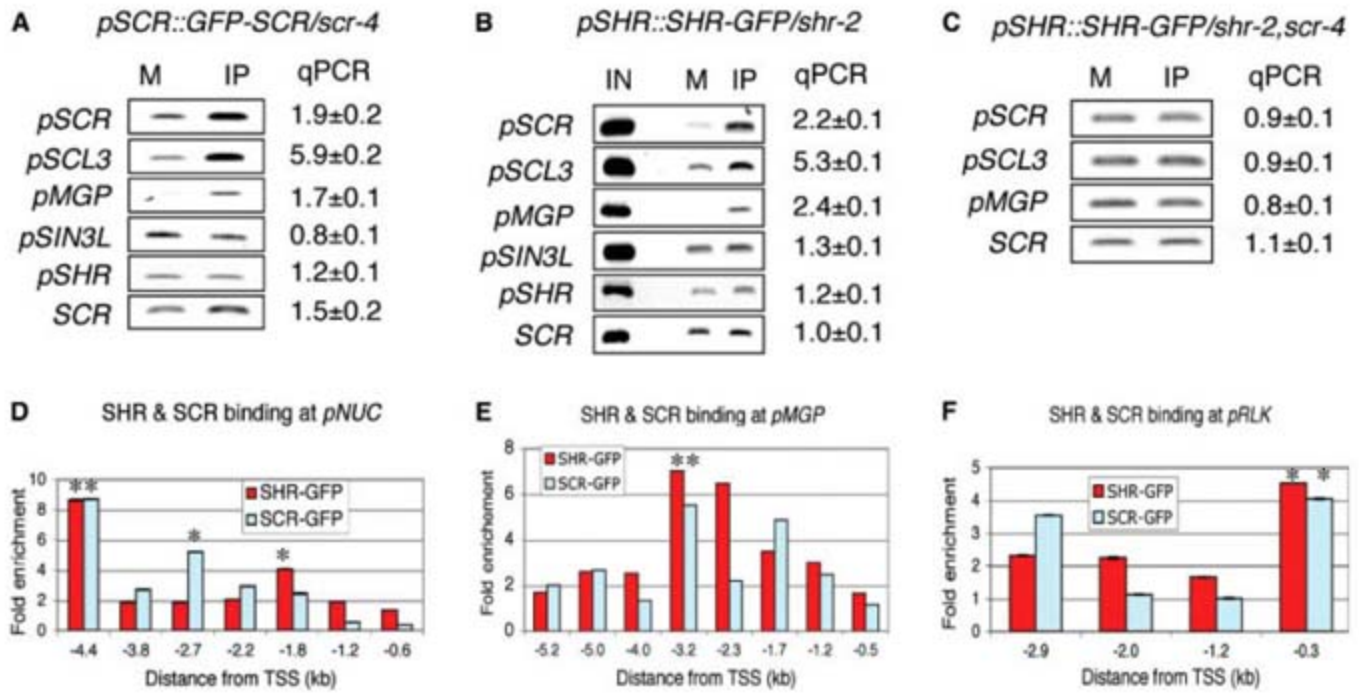

Fig. 1. SCR binds its own promoter and other SHR targets. (**A** and **B**) ChIP-PCR assay with the use of an antibody to GFP, showing binding by GFP-SCR and SHR-GFP to the promoters of *SCR*, *MGP*, and *SCL3*. Fold enrichment values in all panels, from (A) to (F), as determined by quantitative real-time PCR (QPCR), are means ± SE from technical replicates. *pSHR*, *SHR* promoter; *SCR*, *SCR* coding sequence; IN, input DNA; M, Mock ChIP. (**C**) SHR-GFP binding to some of its targets is abolished in *scr* mutant background. (**D** to **F**) SHR-GFP and GFP-SCR bind to the promoters of *NUC* (D), *MGP* (E), and *RLK* (F), as revealed by promoter scanning. The asterisks mark the positions of putative binding sites.

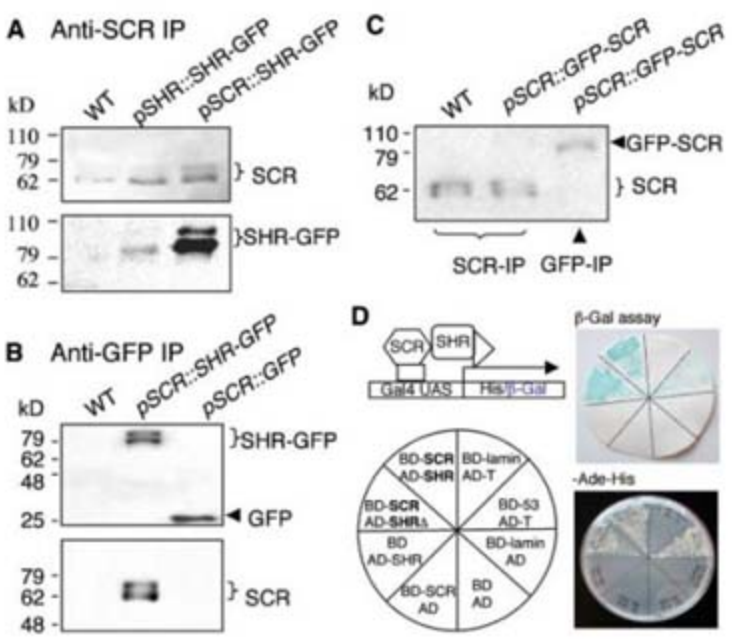

Fig. 2. SCR and SHR directly interact. (**A**) SHR-GFP is detected in SCR immunoprecipitates (SCR-IP). (**B**) SCR is coimmunoprecipitated with SHR-GFP. (**C**) SCR does not coimmunoprecipitate with GFP-SCR (GFP-IP). The SCR-IP assay shows that SCR is expressed in the transgenic plants expressing GFP-SCR. (**D**) Yeast two-hybrid assay showing direct interaction between SHR and SCR. AD-SHRΔ, which lacks the N-terminal 120 amino acids of SHR, still interacts with SCR. β-Gal, β-galactosidase; Gal4 UAS, Ga14 binding sites; BD, Ga14 DNA binding domain; AD, Ga14 activation domain; BD-53 and AD-T as a pair are used as a positive control, whereas the BD-lamin and AD-T pair is a negative control. BD-53, fusion between BD and the p53 protein; BD-lamin; fusion between BD and lamin; AD-T, fusion between AD and the T protein.

and the quiescent center (QC), and is required for the asymmetric cell division that gives rise to the cortex and endodermis (*3*, *7*). SHR protein does not move beyond a single layer comprising the endodermis, CEI cell, and QC. This is in sharp contrast to moving signal proteins in animals (*8*). Endodermis and cortex in the root are derived from the same initial cells through asymmetric cell divisions. Notably, although the number of cortex cell layers varies considerably, nearly all plant species examined so far have only one layer of endodermis, suggesting an evolutionarily conserved mechanism to form this single cell layer. SCR has been found to play a role in restricting SHR movement (*9*, *10*), but the underlying mechanism has remained unclear.

Positive feedback control of *SCR* transcription. SHR and SCR belong to the GRAS family of transcription factors (*11*). In both animals and plants, transcriptional regulation is known to play a key role in development (*12*, *13*). To elucidate the mechanism by which SHR and SCR control root radial patterning, we therefore first dissected their transcriptional circuits. Previously, it has been shown that SHR directly controls *SCR* transcription (*14*). However, there was also indication for SCR autoregulation (*9*). Using a chromatin immunoprecipitation–polymerase chain reaction (ChIP-PCR) assay (*15*), we found that SCR binds to its own promoter (Fig. 1A and fig. S2) but not to the promoters of *SHR* and a *SIN3*-like gene (*At5g15020*), which does not appear to be regulated by SHR (*14*). By reverse transcription PCR (RT-PCR), we confirmed the previous finding that *SCR* expression is reduced in both the *shr* and *scr* backgrounds (*9*) (fig. S2). Our results thus demonstrated that *SCR* is controlled by a SHR/SCR-dependent positive feedback loop.

SHR and SCR are functionally interdependent. Recently, we identified a number of additional putative direct targets of SHR (*14*). To determine whether these are also direct targets of SCR, we assayed binding by ChIP-PCR. Our initial results showed that SCR binds to the promoters of *MAGPIE* (*MGP*) and *SCR-LIKE 3* (*SCL3*) (Fig. 1A and fig. S3), which are also bound by SHR (Fig. 1B and fig. S3). We then checked SHR and SCR binding to other putative direct SHR targets by promoter scanning (*15*) (Fig. 1 and fig. S4). We found that SHR and SCR both clearly bind to the promoters of *NUTCRACKER* (*NUC*), a receptor-like kinase (RLK), and *MGP* (Fig. 1, D to F). Their binding

Table 1. Expression levels of SHR direct targets in *shr* and *scr* mutants, relative to WT, as measured by whole-genome Affymetrix ATH1 microarray. FC, fold change (reduction).

	shr (FC)	*P* value	*scr* (FC)	*P* value
NUC	2.8	6.4×10^{-27}	1.6	9.2×10^{-5}
MGP	2.5	3.7×10^{-19}	1.5	1.7×10^{-3}
SCR	2.5	5.0×10^{-8}	4.0	4.3×10^{-7}
Br6ox2	1.9	7.4×10^{-23}	1.8	3.0×10^{-4}
RLK	1.4	2.8×10^{-5}	1.4	3.8×10^{-1}
SCL3	1.3	6.3×10^{-3}	1.4	7.6×10^{-2}
Tropinone reductase (TRI)	1.2	2.7×10^{-1}	1.2	7.0×10^{-1}
SNEEZY (SNE)	1.0	6.6×10^{-1}	0.8	5.9×10^{-5}

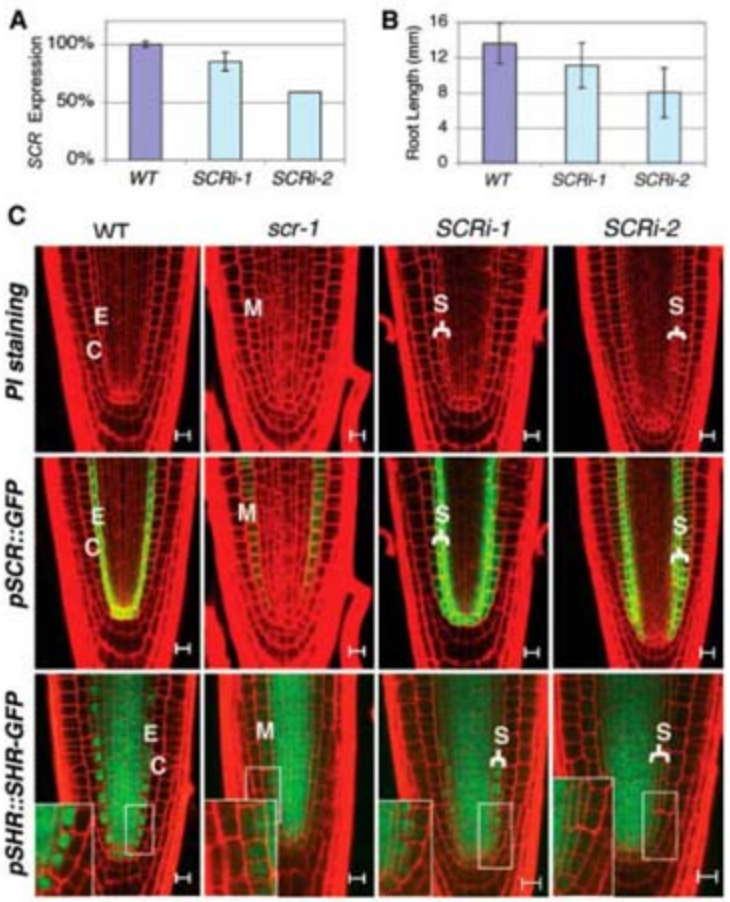

Fig. 3. SCR determines SHR subcellular localization and its range of movement. (**A**) *SCR* transcript levels in two independent *SCR* RNAi lines (*SCRi-1* and *SCRi-2*), relative to that in WT, as determined by RT-QPCR. (**B**) Root lengths of the *SCR* RNAi lines and WT 6 days after germination. Error bars in (A) and (B) indicate SD. (**C**) Confocal images of 6-day-old roots of WT, *scr-1*, *SCRi-1*, and *SCRi-2* seedlings, showing their structure [propidium iodide (PI) staining], an endodermal marker expression (*pSCR::GFP*), and SHR-GFP localization (*pSHR::SHR-GFP*). The insets in the bottom panels are enlarged images of the framed areas. C, cortex; E, endodermis; M, mutant cell layer; S, supernumerary cell layers. Scale bars, 10 μm.

sites on the *NUC* and *MGP* promoters were located in regions relatively far upstream of the translation start sites (TSS) (Fig. 2, D and E), which explains why we were unable to confirm *NUC* as a direct SHR target by ChIP-PCR using PCR primers that amplify more proximal sequences (*14*). Notably, most binding sites for SHR and SCR at these promoters appear to coincide.

The observation that SHR and SCR bind to a common set of genes suggests functional interdependence between these two transcriptional regulators. We therefore examined SHR binding to some of its targets in an *scr* background. In the absence of SCR, SHR binding to these targets is abolished (Fig. 1C). Expression levels of all these genes are reduced in the *shr* and *scr* mutants (fig. S2), indicating that SCR is required for SHR to regulate these genes. To determine the extent of overlap between SHR and SCR targets, we performed genome-wide expression analysis in *shr* and *scr* mutants. Nearly all putative direct SHR targets that we previously identified (*14*) show significant reduction in their expression in both mutant backgrounds (Table 1). Moreover, a large portion of SHR indirect targets also showed reduced expression in the *scr* background (table S1).

SHR and SCR proteins directly interact. Functional interdependence between SHR and SCR could be achieved through their cooperative binding to the same promoter or through direct interaction. To determine whether SHR and SCR form a complex, we performed coimmunoprecipitation. Reciprocal pull-down experiments showed that SCR and SHR are in a complex (Fig. 2, A and B). In yeast cells, SHR and SCR interact directly (Fig. 2D), and the central domain spanning the two leucine heptad repeats and the VHIID (Val-His-Ile-Ile-Asp) motif is responsible for this interaction (fig. S5). However, SCR does not appear to interact with itself (Fig. 2C). The finding that SCR physically interacts with SHR provides a molecular basis for their functional interdependence. However, clearly not all aspects of SHR activity rely on interaction with SCR, because the mutant ground-tissue layer in *scr* still expresses endodermal markers that are not detected in the *shr* mutant background. One hypothesis is that the SHR/SCR complex controls some aspects of SHR function, such as asymmetric cell division, QC specification, and stem cell maintenance, whereas complexes formed between SHR and other proteins fulfill other aspects of SHR function, particularly endodermis specification.

SCR affects SHR subcellular localization and movement. As the SHR protein with a strong nuclear localization signal is no longer capable of moving (*7*), the finding that SHR and SCR directly interact suggests that one role for SCR might be to sequester SHR into the nucleus, thus preventing its movement. Indeed, the fusion protein between green fluorescent protein (GFP) and SHR (SHR-GFP) becomes largely cytoplasmic in the mutant cell layer of *scr* (*scr-1* in Fig. 3C) (*10*), in contrast to its exclusive nuclear localization in the endodermis of wild-type (WT) roots (Fig. 3C). However, because of the low amount of SHR-GFP in the mutant cell layer, it is unclear whether SHR moves out of the mutant layer into the epidermis.

A large pool of SCR would be required to completely block SHR movement. The positive feedback loop for SCR transcription could provide such a mechanism (*16*). To test this hypothesis, we examined the effect of reduction in SCR expression on SHR movement using an RNA interference (RNAi) construct. We reasoned that, if SCR levels were reduced below a threshold level, some SHR protein might be able to move into the presumptive cortex where it would activate *SCR* transcription and endodermis specification. Asymmetric cell division would also occur, giving rise to an additional layer of ground tissue. This process could be repeated until free-moving SHR was exhausted. In support of our hypothesis, plants from the RNAi transgenic lines that we generated produced multiple layers of cells. Two lines that have different levels of *SCR* transcript were further examined (Fig. 3A). As shown in Fig. 3C, the extra cell layers in both lines express the endodermal marker *pSCR::GFP*, and SHR-GFP expressed in the stele is also present in these supernumerary cell layers. Notably, SHR-GFP is detected in both daughter cells of the CEI cell, whereas its levels appear to decrease in the outer cell layer after each additional cell division (Fig. 3C, insets). Moreover, the number of supernumerary cell layers is inversely correlated with the level of *SCR* transcript in the two independent transgenic lines. Furthermore, SHR-GFP is primarily nuclear-

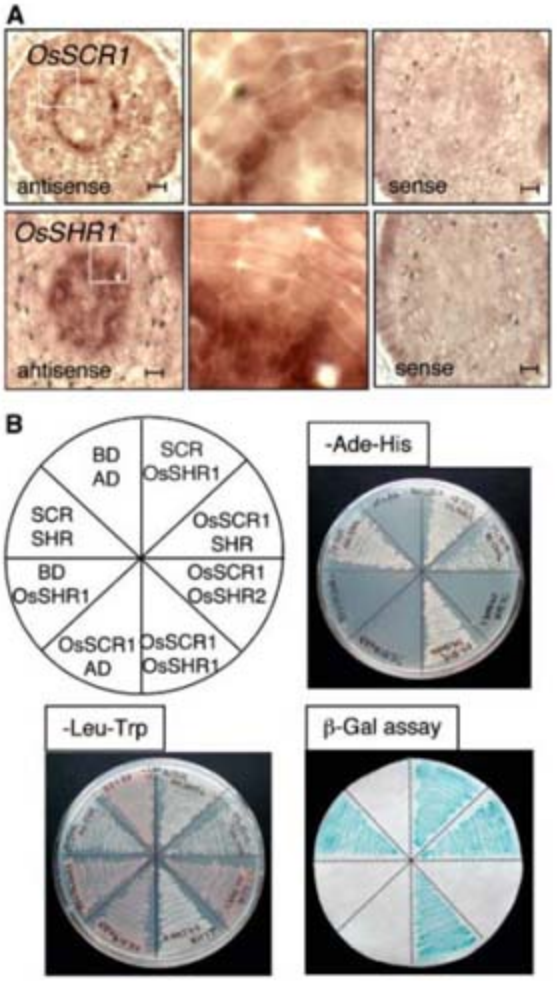

Fig. 4. Analysis of *SHR* and *SCR* homologs from rice. (**A**) In situ hybridization showing the expression patterns of *OsSCR1* and *OsSHR1* in rice root. The framed areas in the left panels are shown at a higher magnification (middle panels). Scale bars, 20 μm. (**B**) Yeast two-hybrid assay examining the interaction between OsSHR1 or OsSHR2 with OsSCR1, as well as their interaction with SHR and SCR. Ade, adenine.

localized in the supernumerary layers of *SCRi-1*, the weaker RNAi line, but is largely cytoplasm-localized in *SCRi-2*, the stronger RNAi line (Fig. 3C). The two lines also showed reduced root length that correlates with the strength of RNAi (*P* values are 2.9×10^{-5} and 2.8×10^{-13}, respectively; Student's *t* test, $n = 39$ roots), although the QC, CEI, and other initials appear normal (Fig. 3, A and B). These results demonstrate the critical role of the positive feedback mechanism for SCR in restricting SHR movement, root radial patterning, and root growth.

Our results support a mechanism by which SCR tightly restricts SHR movement, as described below. On the one hand, SCR sequesters SHR into the nucleus through protein complex formation, making SHR incapable of further movement. On the other hand, the SHR/SCR-dependent positive feedback loop for *SCR* transcription ensures no free-moving SHR can escape from the endodermis by driving a rapid buildup of SCR that does not self-interact but rather preferentially interacts with SHR. This mechanism would require a basal level of SCR expression to initiate the feedback loop. Notably, a substantial level of *SCR* mRNA is still detectable in both the *shr* and *scr* backgrounds, and its specific radial expression pattern is largely unaltered. This SHR/SCR-independent basal *SCR* transcription may be one of the key factors defining the boundary for SHR movement.

The model that we propose for SCR to restrict SHR movement could also account for the fact that different cell fates are rapidly acquired by the progeny of the daughter cells of the CEI cell (*9*). After this asymmetric cell division, the concentration of the SHR/SCR complex will remain high in the inner cell of the endodermal lineage driven by a sustained supply of SHR from the stele, which activates the SCR feedback loop. This high concentration of the SHR/SCR complex would maintain the expression of SCR as well as other downstream patterning genes. By contrast, the SHR/SCR concentration in the other cell of the cortex lineage would drop rapidly, resulting from the inability of SHR to move beyond the endodermis coupled with protein turnover and the dilution accompanying cell division. Indeed, although SCR is detected in both cells immediately after the asymmetric cell division, *SCR* and other endodermal markers are only expressed in the endodermis soon thereafter (*9*).

Interaction and expression of SHR and SCR homologs in rice. The observations that nearly all plants examined so far have only a single layer of endodermis (even though the number of cortex layers can be highly variable) and that *SCR* orthologs are exclusively expressed in the endodermis (*17*–*19*) suggest that the mechanism described above is likely to be evolutionarily conserved. However, the only *SHR* homolog cloned so far, which is claimed to be the closest *SHR* homolog from rice, shows an expression pattern that is distinct from *SHR* in *Arabidopsis* (*19*), thus casting doubt on this hypothesis.

Database searches revealed that there are, in fact, two close rice homologs for both *SHR* (*Os03g31750* and *Os07g39820*) and *SCR* (*Os11g03110* and *Os12g02870*). We named the more similar SHR and SCR homologs OsSHR1 (*Os07g39820*) and OsSCR1 (*Os11g03110*) and the more dissimilar ones OsSHR2 (*Os03g31750*) and OsSCR2 (*Os12g02870*), respectively (table S2).

The rice genes that were previously reported as homologs of *SHR* and *SCR* are *OsSHR2* and *OsSCR1* (*19*). We therefore cloned *OsSHR1* and analyzed its expression in rice roots by in situ hybridization. As shown in Fig. 4A, *OsSHR1* and *OsSCR1* are both expressed in tissues analogous to those of their counterparts in *Arabidopsis*. OsSCR1 and OsSHR1 interact in yeast as strongly as *Arabidopsis* SHR and SCR do (Fig. 4B). They also interact equally well with SHR and SCR, but no interaction was observed between OsSHR2 and OsSCR1 (Fig. 4B). These results strongly suggest that *OsSHR1* and *OsSCR1* are functional homologs of *SHR* and *SCR* in rice. They further suggest that the functional relationship between SHR and SCR, as well as their role in radial patterning in higher plants, is evolutionarily conserved.

Proteins that move as signaling molecules play a critical role in both animal and plant development (*8*, *20*, *21*). Although the list of transcription factors that are able to move is growing (*22*–*28*), little is known about the mechanisms regulating intercellular movement. Decapentaplegic (Dpp), for example, a well-characterized example from animals, moves passively by diffusion and forms a gradient across multiple layers of cells as a result of unregulated binding to and internalization by its receptors located on the surface of the cells that it passes through (*8*, *29*). By contrast, both SHR movement and its range of action are actively regulated, and the mechanism that we have uncovered in this study is quite distinct from those previously described. Although some aspects of this mechanism have been reported for other proteins, this is the first example where both protein-protein interaction and transcriptional control are involved to achieve tight control of protein movement. This difference may extend to other moving plant proteins and indicate a fundamental difference between plant and animal signaling during development.

References and Notes

1. L. Dolan *et al.*, *Development* **119**, 71 (1993).
2. Y. Helariutta *et al.*, *Cell* **101**, 555 (2000).
3. L. Di Laurenzio *et al.*, *Cell* **86**, 423 (1996).
4. S. Sabatini, R. Heidstra, M. Wildwater, B. Scheres, *Genes Dev.* **17**, 354 (2003).
5. B. Scheres *et al.*, *Development* **121**, 53 (1995).
6. K. Nakajima, G. Sena, T. Nawy, P. N. Benfey, *Nature* **413**, 307 (2001).
7. K. L. Gallagher, A. J. Paquette, K. Nakajima, P. N. Benfey, *Curr. Biol.* **14**, 1847 (2004).

8. T. Y. Belenkaya *et al.*, *Cell* **119**, 231 (2004).
9. R. Heidstra, D. Welch, B. Scheres, *Genes Dev.* **18**, 1964 (2004).
10. G. Sena, J. W. Jung, P. N. Benfey, *Development* **131**, 2817 (2004).
11. L. D. Pysh, J. W. Wysocka-Diller, C. Camilleri, D. Bouchez, P. N. Benfey, *Plant J.* **18**, 111 (1999).
12. M. Levine, E. H. Davidson, *Proc. Natl. Acad. Sci. U.S.A.* **102**, 4936 (2005).
13. P. N. Benfey, D. Weigel, *Plant Physiol.* **125**, 109 (2001).
14. M. P. Levesque *et al.*, *PLoS Biol.* **4**, e143 (2006).
15. Materials and methods are available as supporting material on *Science* Online.
16. H. Kitano, *Nat. Rev. Genet.* **5**, 826 (2004).
17. N. Sassa, Y. Matsushita, T. Nakamura, H. Nyunoya, *Plant Cell Physiol.* **42**, 385 (2001).
18. J. Lim *et al.*, *Plant Cell* **12**, 1307 (2000).
19. N. Kamiya, J. Itoh, A. Morikami, Y. Nagato, M. Matsuoka, *Plant J.* **36**, 45 (2003).
20. M. Strigini, *J. Neurobiol.* **64**, 324 (2005).
21. K. L. Gallagher, P. N. Benfey, *Genes Dev.* **19**, 189 (2005).
22. J. Y. Lee *et al.*, *Science* **299**, 392 (2003).
23. J. Y. Lee *et al.*, *Proc. Natl. Acad. Sci. U.S.A.* **103**, 6055 (2006).
24. T. Kurata *et al.*, *Development* **132**, 5387 (2005).
25. X. Wu *et al.*, *Development* **130**, 3735 (2003).
26. D. Rogulja, K. D. Irvine, *Cell* **123**, 449 (2005).
27. J. Y. Kim, Z. Yuan, M. Cilia, Z. Khalfan-Jagani, D. Jackson, *Proc. Natl. Acad. Sci. U.S.A.* **99**, 4103 (2002).
28. C. Weinl *et al.*, *Plant Cell* **17**, 1704 (2005).
29. Y. C. Wang, E. L. Ferguson, *Nature* **434**, 229 (2005).
30. We thank X. Dong (Duke University) for the *p35S::GFP* plants, and D. McClay, Z.-M. Pei, R. Heidstra, and members of the Benfey Laboratory for critical reading of the manuscript and helpful comments. We acknowledge fellowship support from the Human Frontiers Science Program and the European Molecular Biology Organization (for T.V.), NIH (for A.J.P.), and NSF (for M.P.L.). This work was supported by a grant to P.N.B. from NIH (RO1-GM043778).

Supporting Online Material

www.sciencemag.org/cgi/content/full/316/5823/421/DC1
Materials and Methods
Figs. S1 to S5
Tables S1 to S3
References

4 January 2007; accepted 6 March 2007
10.1126/science.1139531

REPORTS

Nonequilibrium Phase Transitions in Cuprates Observed by Ultrafast Electron Crystallography

Nuh Gedik,[1] Ding-Shyue Yang,[1] Gennady Logvenov,[2] Ivan Bozovic,[2] Ahmed H. Zewail[1]*

Nonequilibrium phase transitions, which are defined by the formation of macroscopic transient domains, are optically dark and cannot be observed through conventional temperature- or pressure-change studies. We have directly determined the structural dynamics of such a nonequilibrium phase transition in a cuprate superconductor. Ultrafast electron crystallography with the use of a tilted optical geometry technique afforded the necessary atomic-scale spatial and temporal resolutions. The observed transient behavior displays a notable "structural isosbestic" point and a threshold effect for the dependence of *c*-axis expansion (Δc) on fluence (F), with $\Delta c/F = 0.02$ angstrom/(millijoule per square centimeter). This threshold for photon doping occurs at ~0.12 photons per copper site, which is unexpectedly close to the density (per site) of chemically doped carriers needed to induce superconductivity.

The physical and chemical properties of materials can be altered as a result of the generation of metastable structures (*1*), electronic and/or structural modifications (*2*, *3*), and phase transitions (*4*). For the latter, much of the work has been done on solids at equilibrium, namely when temperature or pressure becomes the variable of change. In contrast, transient structures of nonequilibrium phases, which are formed by collective interactions, are elusive and less studied because they are inaccessible to conventional studies of the equilibrium state. Initiated by photons, the structural changes underlying such transitions involve charge redistribution and lattice relaxation, culminating in a process termed a photoinduced phase transition (*5*–*7*). In order to understand the nature of these optically dark phases, it is important to observe the structural changes with the use of time-resolved methods, especially those that use ultrafast electron microscopy (*8*–*10*), electron diffraction (*10*–*12*), and x-ray absorption and diffraction (*13*–*17*). Here, the direct observation of the nonequilibrium structural phase transition in superconducting cuprates is reported.

We have previously established ultrafast electron crystallography (UEC) (*10*) as a method for studying surfaces and nanometer-scale materials with atomic-scale resolutions. Our apparatus integrates a femtosecond laser system into an ultrahigh vacuum (UHV) assembly of three chambers (Fig. 1A). In this technique, the output of a Ti:sapphire femtosecond laser (with a pulse width of 120 fs) is split into two beams: an 800-nm pulse used to excite the sample and a 266-nm pulse (generated by frequency tripling) used to produce an electron packet via the photoelectric effect. The electrons are then accelerated at 30 kV, resulting in a de Broglie wavelength of $\lambda = 0.07$ Å. The diffraction patterns of these electrons from the sample are recorded on a charge-coupled device (CCD) camera with single-electron sensitivity. The time delay between the initiating laser pulse and electron probe packet is controlled by changing the optical path length between the two pulses. Diffraction patterns at different delay times (diffraction frames) provide a movie of structural change, with atomic-scale spatial and ultrashort temporal resolutions (*10*, *18*).

The material that we chose to study is oxygen-doped $La_2CuO_{4+\delta}$; although the undoped material is an antiferromagnetic Mott insulator, doping confers superconductivity below the critical temperature (T_c) and metallic properties at room temperature. Thin films were grown on a $LaSrAlO_4$ substrate by means of an atomic-layer molecular beam epitaxy system (*19*). The films under study were characterized during growth by reflection high-energy electron diffraction and ex situ by atomic force microscopy (AFM), x-ray diffraction (XRD), and measurements of resistivity and magnetic susceptibility as a function of temperature (*20*).

In order to observe lower-order Bragg diffractions from the material, the incident angle of electrons ($\theta/2$) is set typically between ~1° and 2°. Because the speed of electrons is about one-third that of light, a large group-velocity mismatch occurs between the laser pulse and the electron packet. Moreover, the electron beam has, at this angle of incidence, a large footprint on the surface of the material: in this case, the (001) planes with the *c* axis defining the surface normal direction. We have implemented a wavefront tilting scheme,

[1]Physical Biology Center for Ultrafast Science and Technology, California Institute of Technology (Caltech), Pasadena, CA 91125, USA. [2]Brookhaven National Laboratory (BNL), Upton, NY 11973–5000, USA.

*To whom correspondence should be addressed. E-mail: zewail@caltech.edu

so that the laser pulse arrives at every point on the sample precisely at the same time as the electron packet. All experiments reported here used this "tilted geometry" to achieve the necessary time resolution and sensitivity (*18*). To tune the temperature and incidence angle (for rocking curve measurements), we mounted the sample on a metallic holder that was coupled to a cryostat capable of reaching 10 K, which in turn was placed on a goniometer with an angular precision of 0.005°. The fluence at the specimen was measured by imaging the beam profile and measuring the Gaussian spot size.

In Fig. 1B, the static diffraction pattern obtained at room temperature with UEC is shown with no excitation. From the observed Bragg spots in s space, where $s = (4\pi/\lambda)\sin(\theta/2)$, we indexed the pattern using the tetragonal unit cell of the cuprate $La_2CuO_{4+\delta}$. Analysis of the diffraction patterns for different zone axes gives lattice constants of $a = b = 3.76$ Å and $c = 13.1 \pm 0.1$ Å, which are in agreement with the XRD measurements that we made on the same film ($a = b = 3.755$ Å and $c = 13.20$ Å). The error range in the determination of the absolute values of the lattice constants comes from the uncertainty in determining the sample-to-camera distance. However, relative changes can be measured with much better accuracy, reaching below 0.01 Å [accuracy can be increased to 0.001 Å by a fitting procedure (*21*)].

Structural dynamics of the material were obtained by recording the diffraction frames at different times, before and after the arrival of the optical excitation pulse. In Fig. 1, C and D, two representative diffraction-difference patterns are shown. These difference patterns display the changes induced by the initiation pulse; they are frames obtained at the specified times and referenced, by subtraction, to a frame at negative time (i.e., before optical excitation). At 1.55 eV, the femtosecond pulse excites the material only because the substrate is transparent to the 800-nm light; the penetration depth of the laser pulse in the material is 143 nm (*22*), which far exceeds that of the probing electron pulse (~10 nm). Therefore, the observed structural dynamics can only originate from the cuprate film.

After the femtosecond initial excitation, the observed Bragg spots shift downward (along the c direction), indicating an increase in the c-axis lattice constant. For other Bragg spots, the shift (Δs in s space) scales correctly with the order of diffraction. For example, the shift of the (008) spot is 80% of that of the (0 0 10) spot, in accord with the relationship $\Delta c/c = -\Delta s/s$. (We measured no change in the position of the direct electron beam on the CCD camera.) The observed changes are on three different time scales, characterized by time constants of 5 and 27 ps for the formation of the transient phase and 307 ps for structural recovery (Figs. 2 and 3).

The change with time is striking. In Fig. 2A, we plot the vertical profiles of the (0 0 10) Bragg spot along the c direction at different times. At negative times, the Bragg peak is centered at an s value corresponding to the equilibrium c value of the lattice: $s = 10\,|c^*| = 4.80$ Å^{-1}, where $|c^*| = 2\pi/c = 0.480$ Å^{-1}. The structure at positive times evolves first in a few picoseconds and then changes in tens of picoseconds; for example, at 120 ps after the excitation, the peak becomes centered at a lower value ($s = 4.70$ Å^{-1}), corresponding to a huge increase (~2.5%) in the c-axis lattice constant. We studied the material behavior at three different temperatures: 20, 100, and 300 K.

The unexpected feature of Fig. 2 is that, before restructuring, all of these curves obtained at different times cross at a single point: $s = 4.76$ Å^{-1} at the fluence used of 20.6 mJ/cm^2. What was expected, as observed in previous UEC studies (*10*, *21*, *23*), was that the peak would shift continuously while the intensity decreased with time. Neither behavior is observed at the high signal-to-noise level achieved (Figs. 2 and 3). Thus, this intensity sharing, with a common crossing point, indicates a structural transition from the initial phase to a new one. Such a crossing behavior in spectroscopy would be termed the isosbestic point, corresponding to the spectral position where two interconverting species have equal absorbance; regardless of the populations of the two states, the total

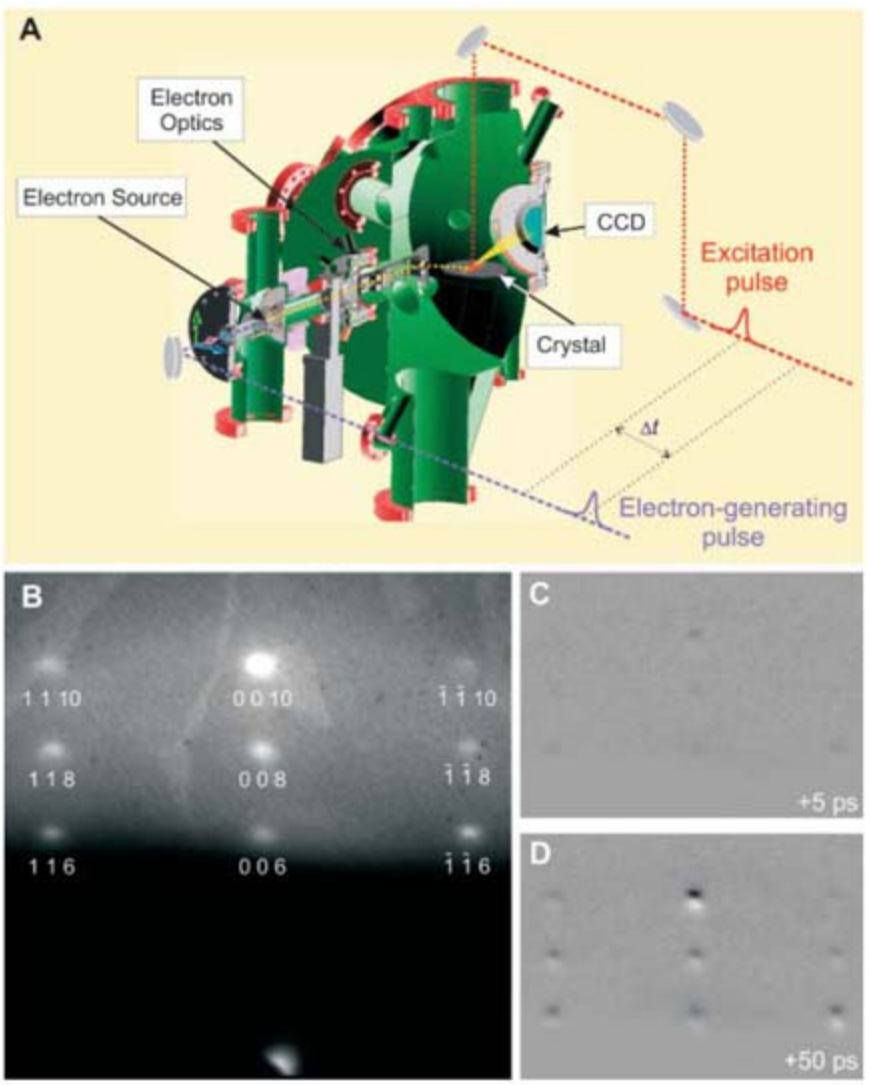

Fig. 1. Diffraction UHV chamber for UEC and diffraction patterns. (**A**) A cross-sectional view, with paths of the optical excitation and electron-generating beams (colored dashed lines), is shown along with electron optics and the CCD camera for detection. Δt is the delay time between the two pulses. The temporal resolution is maintained by the tilted optical geometry. The probing depth of electrons is ~10 nm. The laser pulse is cylindrically focused into an area of 240 μm by 3 mm (full width at half maximum), and the electron beam has a diameter of ~200 μm. (**B**) Diffraction pattern of $La_2CuO_{4+\delta}$ obtained at equilibrium. The pattern is transmission-like, and the spots are indexed with the use of the tetragonal unit cell. (**C** and **D**) Diffraction-difference images at +5 and +50 ps, respectively.

absorption at the isosbestic point does not change.

For the structural dynamics studied, we are observing the interconversion between two structures with different *c*-axis lattice constants, and, for this reason, we term this point the structural isosbestic point. At this particular *s* value, the two structures involved are diffracting equally (*24*), and their coexistence is evidenced in the temporal changes. This behavior of interconversion is clearly illustrated in Fig. 2B, where we display, as a function of time, the depletion of the initial structure and the growth of the transient-phase structure. The data, acquired over the same time delays as those of Fig. 2A (middle), were obtained by referencing all frames to the diffraction profile of the equilibrium structure at negative time. In the inset of Fig. 2B, the actual diffraction profile of the (0 0 10) Bragg spot is shown at two different times, −10 and +130 ps, with each profile fitted to a Voigt-type function.

The decay of the initial structure and the formation of the new structure are quantified by integrating the intensity underneath the (0 0 10) diffraction curves. For the diffraction data obtained in Fig. 2B, the green line in Fig. 3A is the total integrated intensity divided by two. The fact that it is not changing with time rules out the involvement of intensity-depletion processes, such as those described by the Debye-Waller mechanism; in that case, the mean vibrational displacement of the atoms would have increased and caused a decrease in diffraction intensity, contrary to what is observed. Moreover, because the linear expansion coefficient is $\alpha_l \leq 1.0 \times 10^{-5}$ K^{-1} (*25*), a 2.5% increase in the lattice constant would correspond to an unphysical 2500 K rise in the lattice temperature. The black and red curves are the total integrated intensity to the right and left of the crossing point in Fig. 2B, respectively. They reflect the population change of the initial structure and that of the new one. The population of the initial structure (black curve in Fig. 3A) decays with a time constant of 27 ps, describing the growth of the transient phase.

The restructuring at longer times is depicted by Δc as a function of time in Fig. 3B. The dashed line near time zero represents an average value of c for the structures that are present. With no crossing, the value of Δc decreases and reaches an asymptote at ~1 ns. This restructuring after the phase transition can be described by an exponential decay with a time constant of 307 ps with an offset of about 0.04 Å. Accordingly, even after 1 ns, the restructuring is incomplete, and, for complete equilibration, a much longer time scale is required. Some contribution from a temperature rise induced by the laser pulse may be present; the 1-ms delay between pulses is sufficient for the cooling of the sample.

Another notable feature of this structural phase transition is its dependence on the fluence of the initiating pulse. The maximum lattice constant change, $\Delta c_{max} = c(130\ \text{ps}) - c(-85\ \text{ps})$, is shown in Fig. 4, A (for the profiles at three typical fluences) and B (for all the fluences studied). We observe a threshold at 5 mJ/cm^2, below which no structural change can be detected. Above this fluence value, the basic picture described above—a crossing point at initial times and continuous restructuring at long times—is robust (Fig. 4A). The time scales do not change either. However, the lattice constant c of the transient-phase structure changes with the laser fluence (F) [i.e., $\Delta c = p\,(F - F_{th})$, where the slope p = 0.02 Å/(mJ/cm^2) and F_{th} is the threshold fluence].

From the results of structures and dynamics observed in the cuprate superconductor, we suggest the following simple model. At 1.55 eV, the excitation pulse induces a charge transfer (Fig. 3C) from oxygen (O^{2-}) to copper (Cu^{2+}) in the *a*-*b* copper-oxygen planes (*26*). With the lattice relaxation being involved,

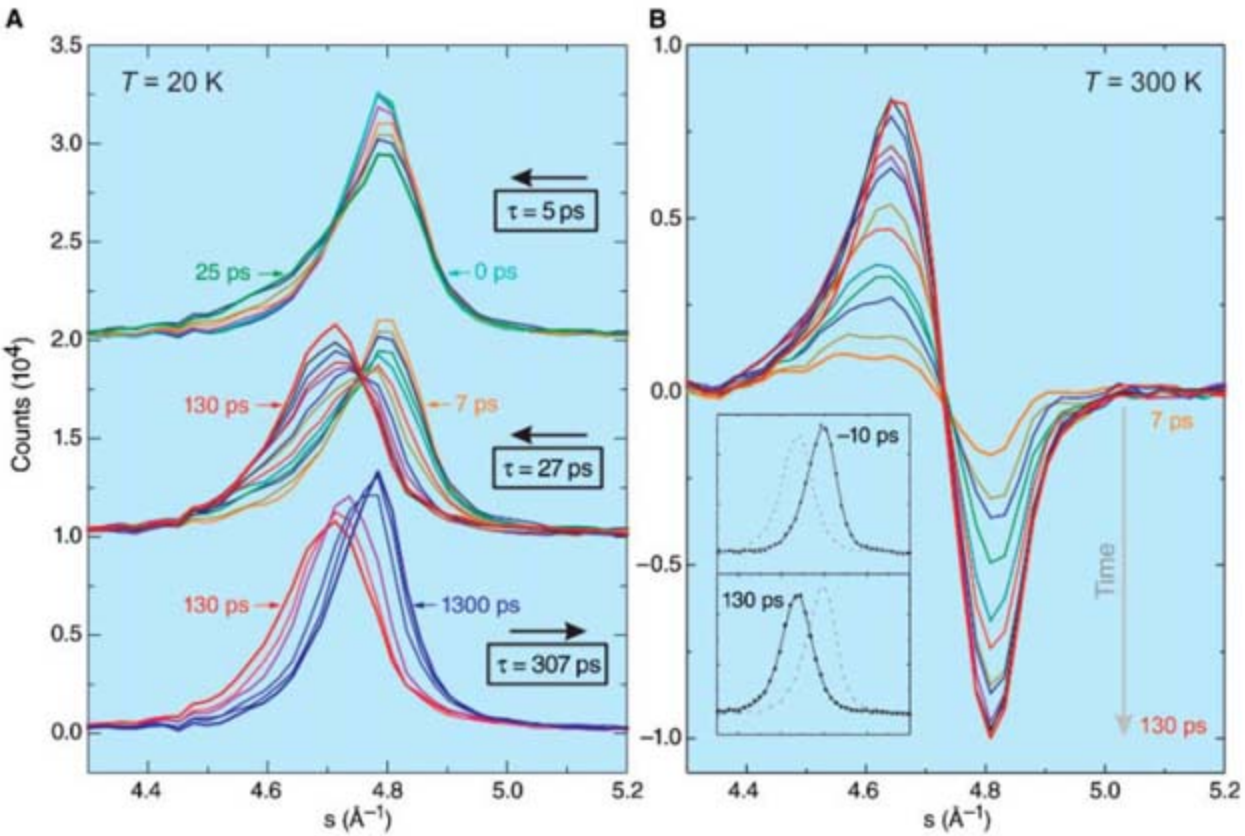

Fig. 2. Diffraction evolution with time. (**A**) Profiles of the (0 0 10) Bragg spot along the *c*-axis direction at different times. The fluence is 20.6 mJ/cm^2, and the temperature is 20 K. A small background (determined experimentally from a nearby diffuse region on the CCD) was subtracted. Similar diffraction results were obtained at room temperature and at T ~ 100 K. Three distinct behaviors are shown: between 0 and 25 ps [top; time (t) = −34, −11, 0, 1, 7, 13, 19, and 25 ps]; between 7 and 130 ps (middle; t = 7, 13, 19, 25, 34, 43, 52, 61, 70, 79, 88, 101, and 130 ps), there is a prominent structural isosbestic point at s = 4.76 Å^{-1}; and on a much longer time scale (bottom; t = 130, 191, 266, 516, 816, and 1300 ps), the restructuring back to the ground state is observed. For the recovery, the curves continuously shift to higher s values (shorter c) without crossing. The black arrows indicate the direction of temporal evolution for the formation and restructuring of the transient phase. (**B**) Difference profiles of the (0 0 10) Bragg spot along the *c*-axis direction at different times, referenced to the negative time frame. The fluence is 20.6 mJ/cm^2, and the temperature is 300 K. The structural isosbestic point is clearly seen near zero intensity, and the depletion of the initial structure and the growth of the transient structure are apparent. The inset shows the Voigt-type function fit for the diffraction intensity profiles at two different times: −10 and +130 ps.

the excitation is shared microscopically (exciton-type), and finally a transition to a transient phase is made (macroscopic domain). This transient phase requires a three-dimensional lattice ordering. The net charge distribution in the transient phase results in the weakening of interplanar Coulomb attractions, leading to expansion along the c axis. The behavior is nonlinear in that when the number of transformed sites is below a critical value, the macroscopic transition is not sustainable. The threshold, which has also been observed in organic crystals (*7*), reflects this need for cooperativity at the macroscopic scale. The crystal domain is at least 20 nm^2 (from the apparent peak width Δs_w, which gives the minimum coherence length); the maximum is determined by the 800-nm wavelength used. Symmetry breaking is not evident because charge transfer is in a plane perpendicular to the c-axis expansion, whereas, in (*7*), charge separation is along the axis of expansion.

At any fluence above the threshold, the interconversion is between two phases (isosbestic point). In order to account for the large magnitude of the expansion and its dependence on the fluence, a uniform charge distribution was considered, after the in-plane charge transfer from oxygen to copper. In the domains of the transient phase, the charges on copper and oxygen become $Q(\mathrm{Cu}) = 2 - \delta_p$ and $Q(\mathrm{O}) = -2 + \delta_p/2$, respectively, where δ_p is the transferred fractional charge determined by the number of photons absorbed per copper site; the changes refer to the copper-oxygen planes with the valence of all the other atoms remaining the same. The ionic cohesion energy $U(r_1, ..., r_N, \delta_p)$, where r_i ($i = 1, ..., N$) are the coordinates of the atoms in the unit cell, was then calculated as the sum of the Madelung energy and the core repulsion energy; the latter was modeled as the sum of binary repulsion terms in the standard Born-Meier form of $A_j \exp(-r_j/d_{BM})$, where the index j enumerates the relevant nearest-neighbor pairs (O-O, Cu-O, and La-O), and A and d_{BM} are the pair-wise atomic constants (*27*). For the equilibrium structure ($\delta_p = 0$), the parameters were optimized to match the experimentally determined equilibrium distances and the known lattice elastic constants. For a given fluence (equivalent to δ_p), the cohesive energy $U(r_1, ..., r_N, \delta_p)$ was then calculated to determine

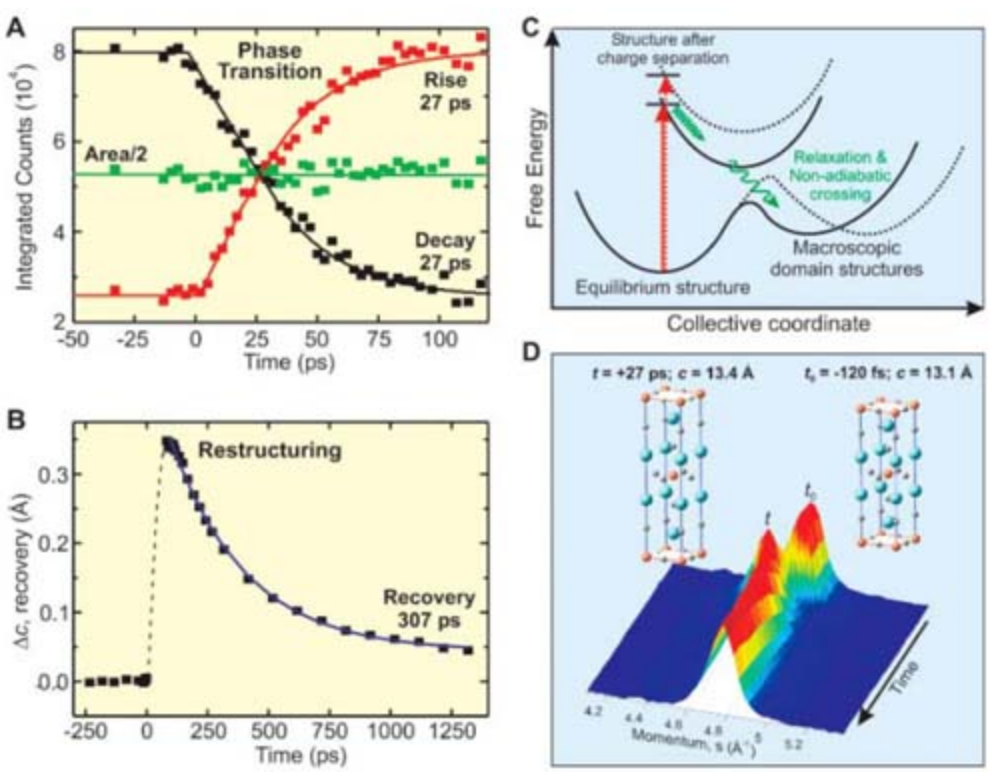

Fig. 3. Time scales and trajectories of structural changes. (**A**) Integrated intensity decay (black squares) and rise (red squares) of the structural isosbestic behavior shown in Fig. 2B. The green squares show, at given times, the total integrated intensity divided by two. The average of the black and red squares yields the green squares. The lines are a guide to the eyes. The intensity decay and rise give a time constant of 27 ps; the initial 5-ps range is not included. (**B**) Recovery of the c-axis lattice constant change (black squares). The dashed line indicates an average c-axis lattice spacing in the phase-transition region where more than one state is involved. The blue curve is a fit to an exponential decay with a time constant of 307 ps and a constant offset of 0.04 Å. (**C**) Free-energy curves. The initial charge-transfer excitation leads, after lattice relaxation and nonadiabatic crossing (*5*–*7*), to the new structure, in this case with the charge being transferred from oxygen to copper. Further increase in the energy of the charge-transfer subsystem results in displacement of the curves (dotted curves) (*28*). Red arrows indicate excitation, and green arrows indicate the relaxation and nonadiabatic processes. (**D**) The temporal evolution of the (0 0 10) Bragg diffraction in the s-t space is shown as a three-dimensional plot (bottom). The initial structure of $La_2CuO_{4+\delta}$ before time zero (t_0) is shown in the top right corner [copper (red spheres), oxygen (gray spheres), and lanthanum (blue spheres)]. After the phase transition, the new structure is indicated with a higher c-axis lattice constant (top left corner). The change is exaggerated for illustrative purposes. As restructuring takes place, the positions of the Bragg diffraction spots move continuously toward the equilibrium s values on a slower time scale.

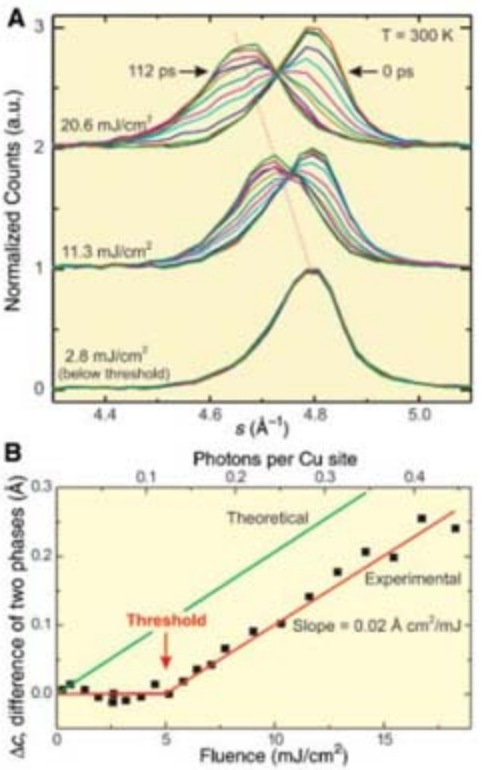

Fig. 4. Threshold behavior and fluence dependence. (**A**) Typical diffraction profiles at three fluences: 2.8 (below threshold), 11.3, and 20.6 mJ/cm^2 (above threshold). The profile for the equilibrium phase remains at the same s value, whereas that for the transient phase shifts toward a lower s value as the fluence increases. The structural isosbestic point is robust. The dashed line indicates the diffraction peak position for the new phase as the fluence increases. All peaks are normalized to the t = 0 peak maximum at each fluence; the displacement for different fluences is in arbitrary units (a.u.). (**B**) The difference of the c-axis lattice constant between the two phases, $\Delta c_{max} = c(130\ \mathrm{ps}) - c(-85\ \mathrm{ps})$, as a function of fluence. The horizontal axis on the top shows the number of photons absorbed per copper site as calculated with the use of the linear absorption coefficient. There is a clear threshold at 5 mJ/cm^2. Above the threshold, Δc increases linearly with fluence, with a slope of 0.02 Å/(mJ/cm^2) (red line). The theoretical calculations (green line) yield a slope that is in good agreement with that obtained from the experimental data.

the new crystal configuration by minimizing the potential energy. The calculations give the observed magnitude for the change along the *c* axis and the linear dependence on fluence, as shown by the green line in Fig. 4B. This agreement of the slope confirms the role of charge distribution in the formation of the transient phase. A full dynamical theory must consider such distributions as the system evolves in time. Electron transfer theory predicts that an increase in free energy will lead to a shift of the potential (*28*) and to a further increase of the expansion (Fig. 3C).

The dynamical nature of the energy landscape is determined by these changes in the electronic distribution and by the nuclear motions. For other materials exhibiting neutral-to-charged domain transitions, Nasu (*5*) has elucidated the origin of local and global minima, which are reminiscent of macromolecular structures (*29*–*31*), on the ground-state potential surface. More than one local minimum state may exist as a result of nonadiabatic "covalent-ionic" interactions (*32*) between the two potentials involved (*5*, *6*). The multidimensional nature of the landscape requires consideration of dynamical trajectories and possible bifurcation (*33*), in this case with the *c*-axis changes defining a unique coordinate (*34*). Figure 3D depicts the observed trajectories in momentum-time space and the two structures, only with *c*-axis expansions (*35*).

Unlike the phase formation dynamics, the recovery is a continuous process of shrinking in the *c*-axis value without crossing. In other words, after the femtosecond initial excitation and charge separation, the photoinduced phase transition can only recover toward the equilibrium structure by charge recombination and lattice relaxation [Fig. 3C and (*5*–*7*)]. For electron transfer processes (*28*), the recombination occurs on a much longer time scale than that of the charge transfer. For the cuprate, the time scale is more than an order of magnitude longer than the formation time of the transient phase. Optical phonons may be involved, but when the temperature was lowered from T = 300 to 100 or 20 K, we observed essentially the same recovery time. These observations suggest the involvement of lattice (acoustic) phonons, because the Debye temperature for this material is 163 K (*36*). The observed decay time of 307 ps is very close to the lifetime (300 ps) of coherent acoustic waves observed in the same material (*37*).

Finally, the meaning of the threshold value for the cuprate is addressed. What was not expected was the absolute value of the threshold in relation to charge distribution. Knowing the value of the threshold (5 mJ/cm^2) and the absorption coefficient at 800 nm ($\alpha = 7 \times 10^4$ cm^{-1}) (*22*), we obtained a value close to 0.12 photons per copper site. For the doped material used, the fractional charge on a copper site is 0.16 at the optimal doping level for superconductivity. The implication of this similarity is that chemical and light-induced carrier doping may be related. If general, this implication is important for the prospect of light-mediated control. When cuprates are doped chemically, the optical conductivity shows that the spectral weight of the charge-transfer gap is transferred into the intragap region (Mott transition); the photoinduced optical reflectivity and absorption display a similar behavior (*26*, *38*).

The combined atomic-scale spatial and ultrafast temporal resolutions of UEC enabled the direct observation of structural nonequilibrium phase transitions in nanometer-scale materials. The macroscopic transient structures are undetectable by optical probes with wavelengths longer than lattice spacings; the time scales of optical response and structural changes are also very different. For the cuprate studied, the observed phase transition is the result of electronic charge redistribution and lattice collective interactions that form domains. The similarity of the apparent threshold for photon doping and the chemical doping required for superconductivity may have its origin in the nature of the photoinduced inverse Mott transition (*39*). With UEC, it is now possible to explore these phenomena for different chemical and photon dopings and in materials of varying structures.

References and Notes

1. S. Ramdas *et al.*, *Nature* **284**, 153 (1980).
2. J. M. Thomas, *Philos. Trans. R. Soc. London Ser. A* **277**, 251 (1974).
3. N. Bloembergen, in *Laser Ablation: Mechanisms and Applications II*, J. C. Miller, D. B. Geohegan, Eds. (American Institute of Physics Conference Proceedings 288, Woodbury, New York, 1994), pp. 3–10.
4. R. W. Cahn, P. Haasen, E. J. Kramer, Eds., *Materials Science and Technology: A Comprehensive Treatment* (VCH, New York, 1991), vol. 5.
5. K. Nasu, Ed., *Photoinduced Phase Transition* (World Scientific, Hackensack, NJ, 2004) and references therein.
6. M. Kuwata-Gonokami, S. Koshihara, Eds., *J. Phys. Soc. Jpn.* **75**, 011001–011008 (2006).
7. E. Collet *et al.*, *Science* **300**, 612 (2003).
8. M. S. Grinolds, V. A. Lobastov, J. Weissenrieder, A. H. Zewail, *Proc. Natl. Acad. Sci. U.S.A.* **103**, 18427 (2006).
9. J. M. Thomas, *Angew. Chem. Int. Ed.* **44**, 5563 (2005).
10. A. H. Zewail, *Annu. Rev. Phys. Chem.* **57**, 65 (2006) and references therein.
11. X. Zou, in *Electron Crystallography: Novel Approaches for Structure Determination of Nanosized Materials*, T. E. Weirich, J. L. Lábár, X. Zou, Eds. (Springer, Dordrecht, Netherlands, 2006).
12. B. J. Siwick, J. R. Dwyer, R. E. Jordan, R. J. D. Miller, *Science* **302**, 1382 (2003).
13. C. Bressler, M. Chergui, *Chem. Rev.* **104**, 1781 (2004).
14. A. Rousse, C. Rischel, J.-C. Gauthier, *Rev. Mod. Phys.* **73**, 17 (2001).
15. D. von der Linde, K. Sokolowski-Tinten, J. Bialkowski, *Appl. Surf. Sci.* **109-110**, 1 (1997).
16. M. Bargheer, N. Zhavoronkov, M. Woerner, T. Elsaesser, *Chem. Phys. Chem.* **7**, 783 (2006).
17. A. Cavalleri, M. Rini, R. W. Schoenlein, *J. Phys. Soc. Jpn.* **75**, 011004 (2006).
18. P. Baum, A. H. Zewail, *Proc. Natl. Acad. Sci. U.S.A.* **103**, 16105 (2006).
19. I. Bozovic, *IEEE Trans. Appl. Supercond.* **11**, 2686 (2001).
20. For the single-crystal films, AFM shows atomically smooth surfaces (root mean square roughness values in the 0.3- to 0.6-nm range). In few films, we observed some surface roughness, in the form of some islands with a typical width of 50 to 200 nm, small enough for transmission electron diffraction to be observed (*40*). The islands were verified to have the same crystal structure and conductivity as those of the single crystal, as evidenced by measurements of the lattice constants and by electrostatic force microscopy, respectively. One such film, with a thickness of 52 nm and $T_c \sim 32$ K was chosen for the present study.
21. D.-S. Yang, N. Gedik, A. H. Zewail, *J. Phys. Chem. C* **111**, 4889 (2007).
22. M. Suzuki, *Phys. Rev. B* **39**, 2312 (1989).
23. C.-Y. Ruan, V. A. Lobastov, F. Vigliotti, S. Chen, A. H. Zewail, *Science* **304**, 80 (2004).
24. We have considered the influence of the time-independent instrumental response function. For the case of two interconverting structures with Gaussian intensity profiles, it can be shown that instrumental broadening only modifies the widths, but structural isosbestic points remain robust.
25. J. D. Yu, Y. Inaguma, M. Itoh, M. Oguni, T. Kyômen, *Phys. Rev. B* **54**, 7455 (1996).
26. D. N. Basov, T. Timusk, *Rev. Mod. Phys.* **77**, 721 (2005).
27. B. Piveteau, C. Noguera, *Phys. Rev. B* **43**, 493 (1991).
28. R. A. Marcus, *Angew. Chem. Int. Ed. Engl.* **32**, 1111 (1993).
29. P. F. McMillan, D. C. Clary, *Philos. Trans. R. Soc. London Ser. A* **363**, 311 (2005).
30. P. G. Wolynes, J. N. Onuchic, D. Thirumalai, *Science* **267**, 1619 (1995).
31. C. M. Dobson, *Nature* **426**, 884 (2003).
32. A. Mokhtari, P. Cong, J. L. Herek, A. H. Zewail, *Nature* **348**, 225 (1990).
33. K. B. Møller, A. H. Zewail, *Chem. Phys. Lett.* **295**, 1 (1998).
34. The disparity in yield for the 5- and 27-ps time regimes may suggest that the dynamics involve bifurcation with two types of trajectories: those that are direct and lead to a large *c*-axis structural change (low yield) and those that concurrently involve expansion and lattice relaxation (high yield) (*33*).
35. The anisotropy of expansion has been addressed in detail in (*21*). In this case, the sample is free to expand along the surface normal direction, whereas in *a*-*b* planes, the laser-excited region is constrained by the surrounding unexcited region. Moreover, for in-plane charge transfer, the Coulomb repulsion is mainly interplanar, which results in a substantial expansion along the *c* axis with essentially no lattice change in the *a*-*b* planes.
36. K. Kumagai *et al.*, *Phys. Rev. Lett.* **60**, 724 (1988).
37. I. Bozovic *et al.*, *Phys. Rev. B* **69**, 132503 (2004).
38. J. D. Perkins, R. J. Birgeneau, J. M. Graybeal, M. A. Kastner, D. S. Kleinberg, *Phys. Rev. B* **58**, 9390 (1998).
39. A. Pergament, A. Morak, *J. Phys. A Math. Gen.* **39**, 4619 (2006).
40. Z. L. Wang, *Reflection Electron Microscopy and Spectroscopy for Surface Science* (Cambridge Univ. Press, Cambridge, 1996).

41. This work was supported at Caltech by the Gordon and Betty Moore Foundation and NSF and at BNL by the U.S. Department of Energy (contract number MA-509-MACA). We thank P. Baum in the UEC laboratory and P. Cao in J. Heath's group at Caltech for AFM imaging; V. Butko, C. Deville-Cavelin, and L. Howald at BNL for XRD, AFM, and transport measurements; and Z. Radovic and N. Bozovic at BNL for the cohesive energy calculations.

14 December 2006; accepted 19 March 2007
10.1126/science.1138834

Negative Refraction at Visible Frequencies

Henri J. Lezec,[1,2]*† Jennifer A. Dionne,[1]* Harry A. Atwater[1]

Nanofabricated photonic materials offer opportunities for crafting the propagation and dispersion of light in matter. We demonstrate an experimental realization of a two-dimensional negative-index material in the blue-green region of the visible spectrum, substantiated by direct geometric visualization of negative refraction. Negative indices were achieved with the use of an ultrathin Au-Si_3N_4-Ag waveguide sustaining a surface plasmon polariton mode with antiparallel group and phase velocities. All-angle negative refraction was observed at the interface between this bimetal waveguide and a conventional Ag-Si_3N_4-Ag slot waveguide. The results may enable the development of practical negative-index optical designs in the visible regime.

When a beam of light enters a material from vacuum or air at non-normal incidence, it undergoes refraction—a change in its direction of propagation. The angle of refraction depends on the absolute value of the refractive index of the medium, according to Snell's law. For all naturally occurring substances, the beam is deflected to the opposite side of the interface normal, and the refractive index is taken to be positive.

In 1968, Veselago studied a theoretical material with simultaneously negative electric permittivity ε and magnetic permeability μ, and predicted that it would have a negative index of refraction n (*1*). Light crossing the boundary between such a medium and one with a positive refractive index would refract to the same side of the normal. Such a deflection, termed negative refraction, was predicted to lead to a variety of enabling applications, most notably subwavelength focusing with resolution well below the diffraction limit (*2*).

Considerable research has been devoted to developing artificial electromagnetic media with negative n resulting from negative ε and μ (*3*, *4*). Such media, known as negative-index materials (NIMs), were first implemented at microwave frequencies on the order of 10 GHz by means of periodic assemblies of millimeter-scale split-ring resonators and wires (*5*, *6*). Negative values of μ and ε were simultaneously achieved via, respectively, the resonant capacitive-inductive response of the split-rings (*7*) and the effective plasma response of the wire lattice determined by mutual inductance (*8*). All-angle negative refraction in two dimensions was then demonstrated by direct observation of plane-wave refraction through prism-shaped segments of such assemblies (*5*, *6*).

Efforts are now directed toward scaling down NIMs for operation at optical frequencies (*9*, *10*). So far, structures have been limited to one (*11*–*14*) or a few (*15*) layers of discrete resonator elements. Transmission and reflection spectra measured with out-of-plane illumination enable retrieval of ε, μ, and n (*16*); in this manner, negative indices were inferred at infrared frequencies (*11*–*13*, *15*) and recently at the red end of the visible spectrum (*14*). However, because the thickness of such NIMs is substantially smaller than the free-space wavelength, the interaction volume with the incident radiation presumably remains too small to induce angular deviations of light with sufficient amplitude to provide direct evidence of negative refraction.

Here, we demonstrate a planar NIM at visible frequencies. It is based on the proposal that a suitably designed metal-insulator-metal (MIM) waveguide can act as a two-dimensional NIM characterized by an effective ε and μ that are both negative when averaged over the thickness of the waveguide (*17*–*21*). The negative response arises from the in-plane isotropic dispersion properties of a transverse magnetic (TM) mode involving coupled surface plasmon polaritons (SPPs) at each metal-dielectric interface. For frequencies above the surface plasmon resonance frequency ω_{SP}, but below the bulk plasmon frequency ω_P, the dispersion curve exhibits negative slope leading to antiparallel group and phase velocities, meaning that the energy and phase fronts propagate in opposite directions. Such a mode then behaves as if it had a negative index of refraction (*22*). If it is the only sustained mode, this index can be considered to be equivalent to the effective index of refraction of the two-dimensional medium itself.

In this experiment, we used two MIM waveguides cascaded in series to directly visualize negative refraction. The first waveguide is designed to sustain propagation of only a single negative-index mode over a broad subset of the visible frequency range. The second waveguide is tailored to sustain propagation of only positive-index modes over the same range. Structures are fabricated by applying a sequence of thermal evaporation and focused ion beam milling steps to both sides of a suspended Si_3N_4 membrane.

Figure 1A illustrates the dispersion properties of a planar Ag-Si_3N_4-Ag waveguide with dielectric core thickness t = 500 nm. Modal properties were calculated via numerical solution of Maxwell's equations assuming perfect coupling between each metal-dielectric interface (*23*, *24*). The waveguide sustains a number of TM modes (*25*), each identified with the closest related mode of a parallel-plate waveguide with perfect metal surfaces (*26*). Most modes lie to the left of the light line $\omega = ck_0/n_d$, where n_d is the refractive index of the core and $k_0 = 2\pi/\lambda_0$. These "photonic" modes are characterized by a propagation constant $\beta < n_d k_0$. In addition, an SPP mode characterized by $\beta > n_d k_0$ and corresponding to degenerate, cutoff-free TM_0 and TM_1 modes is present to the right of the light line. Over the entire visible range (400 nm < λ_0 < 700 nm), all allowed modes obey the condition $d\omega/d\beta \geq 0$, corresponding to a positive refractive index of light in the waveguide.

As the dielectric core thickness t is reduced, the cutoff energy of each photonic mode increases. For t = 50 nm, a single allowed mode remains in the visible range: the TM_0 SPP mode [the TM_1 SPP mode of Fig. 1A is completely attenuated by absorption (*24*)]. The dispersion curve of this mode (Fig. 1B, gray curve) exhibits a negative slope ($d\omega/d\beta < 0$) and hence negative-index behavior over the ultraviolet frequency range $\omega_{SP}^{Ag\text{-}Si_3N_4} < \omega < \omega_P^{Ag}$ (where $\omega_{SP}^{Ag\text{-}Si_3N_4}$ and ω_P^{Ag} are the resonant frequencies of the Ag-Si_3N_4 surface plasmon and the Ag bulk plas-

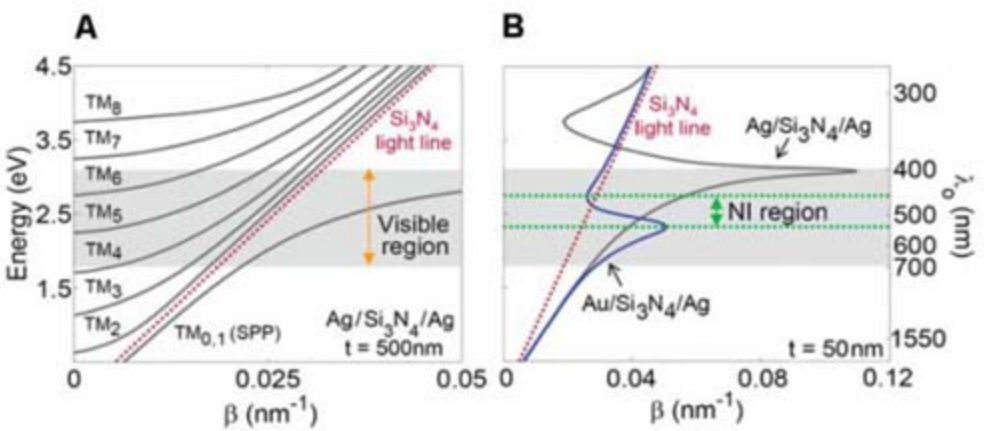

Fig. 1. Implementation of positive- and negative-index MIM waveguides. (**A**) Calculated dispersion curves for an Ag-Si_3N_4-Ag waveguide with a dielectric core thickness t = 500 nm. (**B**) Calculated dispersion curves for Ag-Si_3N_4-Ag and Au-Si_3N_4-Ag waveguides with t = 50 nm.

[1]Thomas J. Watson Laboratory of Applied Physics, California Institute of Technology, Pasadena, CA 91125, USA. [2]Centre National de la Recherche Scientifique, 3 rue Michel-Ange, 75794 Paris Cedex 16, France.

*These authors contributed equally to this work.
†To whom correspondence should be addressed. E-mail: lezec@caltech.edu

mon, respectively). By swapping Ag with Au in one of the cladding layers, this region of negative slope can be shifted to the interval 470 nm < λ_0 < 530 nm, well within the visible (Fig. 1B, blue curve). Calculated losses for the resulting negative-index mode in this Au-Si_3N_4-Ag waveguide indicate a characteristic power attenuation distance of ~50 nm, as well as an average figure of merit FOM = |Re(n)/Im(n)| ~4. This FOM appears somewhat higher than those summarized (*9*, *10*) for recent resonator-based negative-index metamaterials operating at the onset between the visible and infrared regimes (where quoted FOMs range from 3 at λ_0 = 1.4 μm to 0.5 at λ_0 = 780 nm).

Figure 2A displays a cross section of the experimental device used to demonstrate negative refraction. An Au-Si_3N_4-Ag waveguide (W1) with a thin dielectric core (t_1 = 50 nm) is positioned between two identical Ag-Si_3N_4-Ag waveguides (W2) with thick dielectric cores (t_2 = 500 nm). The 100-nm thicknesses of the Ag and Au cladding layers are substantially larger than the mode skin depth (*27*). In addition, a 200-nm-thick layer of Al is deposited on each side of the waveguide to ensure complete opacity of the respective top and bottom cladding layers. Slits of subwavelength width (w = 400 nm) couple light into and out of the waveguide (*28*). The input slit is illuminated at normal incidence with TM-polarized laser light (*H*-field parallel to the slit). The output slit is imaged using a 50× objective coupled to a liquid nitrogen–cooled charge-coupled device camera.

Direct characterization of positive or negative refraction is achieved by shaping W1 into a prism in the plane of propagation (Fig. 2B). A guided mode is first launched in W2 via the input slit. This mode impinges at normal incidence on the leading edge of the prism, where it excites a SPP mode that propagates through W1 with effective index n_1. The SPP mode in turn impinges on the slanted interface between W1 and W2, at angle φ_1. The mode is then refracted at an angle φ_2 into a guided mode of W2 with effective index n_2. We estimate φ_2 from the projected position of the mode on the output slit and use Snell's law (*22*) to determine the ratio $n_1/n_2 = \sin(\varphi_2)/\sin(\varphi_1)$.

Refraction results obtained at wavelengths λ_0 = 685 nm and 514 nm are illustrated in Fig. 3. These two wavelengths fall, respectively, in the calculated positive- and negative-index regions of W1 (Fig. 1B).

Figure 3A evaluates waveguide transmission through W2 in the absence of a prism. At both wavelengths, a clear image of the input slit is projected onto the output slit, consistent with previous observations of low lateral mode divergence within MIM waveguides (*28*).

Figure 3B illustrates the effect of introducing two symmetric prisms of W1 into W2. The diagonal edges of both prisms are parallel and form an angle of 7° with respect to the wavefront launched by the input slit. Vertical displacement of the incident beam is proportional to the angle

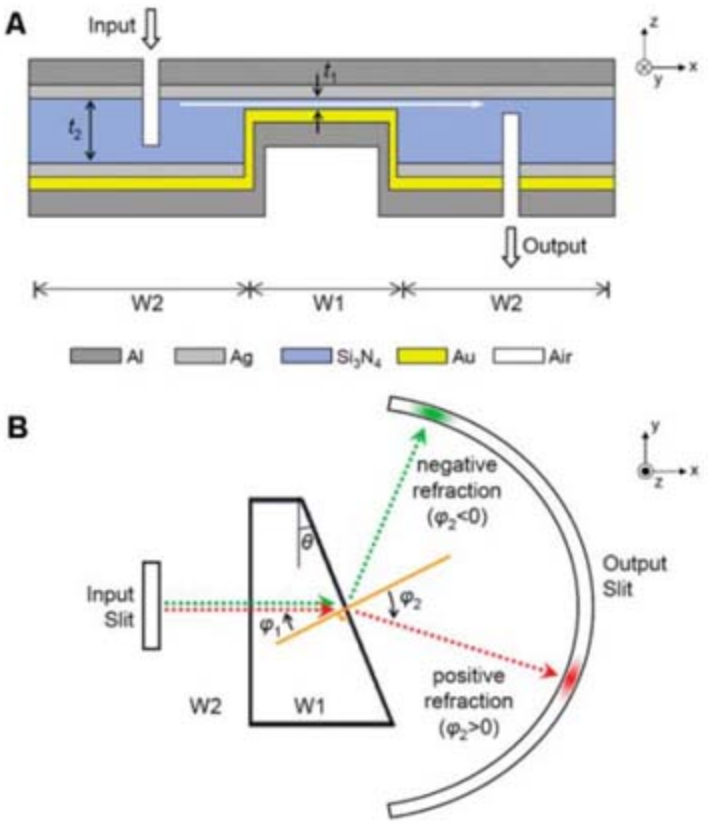

Fig. 2. Schematic diagram of structure fabricated to demonstrate in-plane negative refraction. A prism-shaped segment of Au-Si_3N_4-Ag waveguide with variable dielectric core thickness t_1 and edge angle θ ("W1") is embedded in an Ag-Si_3N_4-Ag waveguide of fixed core thickness t_2 = 500 nm ("W2"). Two slits extending into the waveguide core (nominal width w = 400 nm) are used to excite and intercept, respectively, a guided electromagnetic mode. (**A**) Cross section showing path of light through structure (white arrows). (**B**) Corresponding plan view showing hypothetical path of guided mode at two different frequencies illustrating, respectively, positive refraction (red arrow) and negative refraction (green arrow).

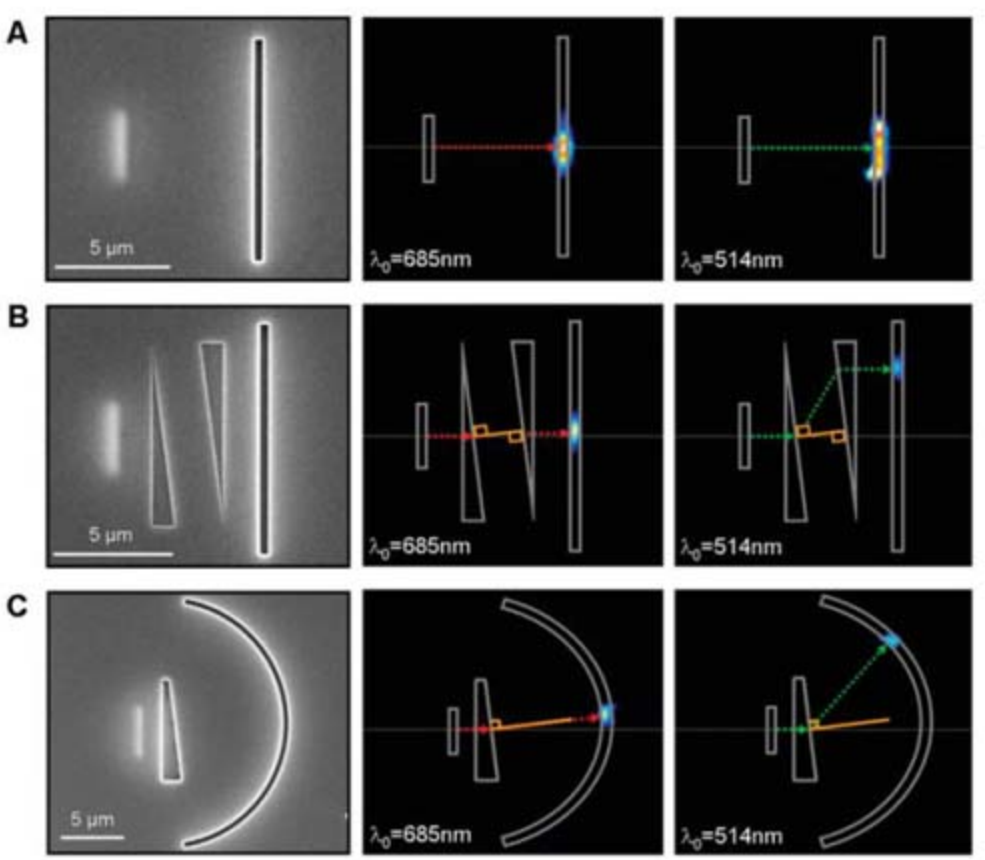

Fig. 3. Direct visualization of in-plane negative refraction. Three waveguide configurations are explored: (**A**) W2 alone, (**B**) two prisms of W1 (t_1 = 50 nm, θ = 7°) embedded in W2, and (**C**) one prism of W1 (t_1 = 50 nm, θ = 7°) embedded in W2. Left column: Scanning electron micrograph image of output side. Input slit position is revealed by electron transparency. Center and right columns: Optical microscope image of output side, given input-side illumination at λ_0 = 685 nm and 514 nm, respectively.

of refraction at the first angled interface, φ_2. The double-prism configuration corrects for differences in the optical path length, ensuring that the mode experiences uniform absorption during its transit from input slit to output slit. At λ_0 = 685 nm, the observed output-spot position indicates positive refraction at both slanted interfaces between W1 and W2, with an angle $\varphi_2 = +0.1°$. In contrast, at λ_0 = 514 nm, the output-spot position indicates negative refraction between W1 and W2, with an angle $\varphi_2 = -51°$. Given the prism angle $\varphi_1 = \theta = 7°$, Snell's law yields an index ratio $n_1/n_2 = +0.01$ and -6.26 at λ_0 = 685 nm and 514 nm, respectively.

Similar trends are observed when a single prism of W1 is placed in the path of the guided mode in W2 (Fig. 3C). The straight output slit of Fig. 3B is replaced with a semicircular slit to ensure that the refracted mode intersects the slit at normal incidence for any refraction angle. At λ_0 = 685 nm, the position of the output spot indicates positive refraction at the interface between W1 and W2, with an angle $\varphi_2 = +0.1°$. When λ_0 is reduced to 514 nm, the output-spot position shifts, indicating negative refraction at the interface between W1 and W2, with an angle $\varphi_2 = -43.7°$. Given the incident angle $\varphi_1 = 7°$, Snell's law yields an index ratio $n_1/n_2 = +0.01$ and -5.57 at λ_0 = 685 nm and 514 nm, respectively. These values are in good agreement with those measured using the double-prism configuration of Fig. 3B.

To derive the mode index of the thin Au-Si_3N_4-Ag waveguide, n_1, it is necessary to determine the mode index of the surrounding thicker Ag-Si_3N_4-Ag waveguide, n_2. To circumvent the difficulty of estimating n_2 theoretically, given the prediction of multimodal dispersion properties for W2 (Fig. 1A), we measured n_2 directly by an interferometric technique (*22*). At λ_0 = 514 nm, we obtained $n_2 = 0.82$, which implies effective refractive indices for the Au-Si_3N_4-Ag waveguides of Fig. 3 that are both large and negative: $n_1 = -4.6$ and -5.1 for Fig. 3, B and C, respectively. At λ_0 = 685 nm, we measured $n_2 = 0.75$, yielding a very small positive index $n_1 = 0.01$ in both cases. The effective index n_1 of a number of prisms with different angles θ and dielectric core thicknesses t_1 is summarized in Fig. 4A; data are tabulated for closely spaced free-space wavelengths spanning the predicted negative-index region. In particular, the relative invariance of n_1 as a function of θ confirms that our structures indeed obey all-angle in-plane refraction according to Snell's law (*22*). Finally, we plotted the full set of refraction data $n_1(\lambda)$ as $\lambda(\beta)$, yielding the dispersion behavior of the guided mode in the prism (Fig. 4B); the dispersion curve clearly presents a negative slope for λ_0 between 476 and 514 nm, in good agreement with calculations.

Using specially tailored metal-insulator-metal waveguides, we have realized a planar material with an effective negative refractive index in the blue-green region of the visible spectrum. Isotropic negative refraction in two dimensions is directly observed; in resonator-based metamaterials, such a measurement has so far been achieved only in the microwave regime. Nonresonant negative-index behavior is achieved over a broad ~50-nm ($\sim\lambda_0/10$) wavelength range, which can in principle be further extended by increasing the dielectric constant of the waveguide core. The structure is straightforward to fabricate because its performance depends only on the plasmonic properties of two smooth metal-dielectric interfaces and a single critical dimension adjusted to ensure monomode behavior: the thickness of a silicon nitride film. The approach appears promising for straightforward two-dimensional implementation of theoretically predicted negative refraction–based devices, such as a perfect lens capable of nonquasistatic, far-field focusing with subwavelength resolution (*2*). In addition, the inherent simplicity of the structure hints at its potential as a building block for future artificial media capable of all-angle negative refraction in three dimensions (*18*, *19*).

Fig. 4. Measured mode index (**A**) and mode dispersion (**B**) of Au-Si_3N_4-Ag prisms with various values of t_1 and θ, for frequencies spanning the negative-index region. The calculated dispersion curves for limiting cases t = 150 nm and t = 50 nm are also included.

A

	Single Prism (▲)			Double Prism (▲▼)	
t_1 (nm) →	150	150	75	50	50
λ_0(nm) ↓	□	■	▲	○	●
514	-3.79	-3.85	-4.65	-4.57	-5.14
501	-2.49	-2.52	-2.72		
496	-1.82	-1.81	-2.02		
488	-1.84	-1.71	-2.09		
476	-1.07	-1.18	-1.38		
	θ=5°		θ=7°		

B

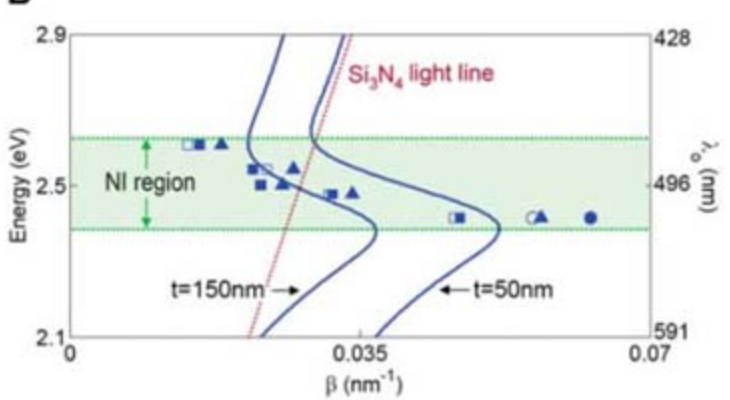

References and Notes

1. V. G. Veselago, *Sov. Phys. Usp.* **10**, 509 (1968).
2. J. B. Pendry, *Phys. Rev. Lett.* **85**, 3966 (2000).
3. S. A. Ramakrishna, *Rep. Prog. Phys.* **68**, 449 (2005).
4. C. M. Soukoulis, M. Kafesaki, E. N. Economou, *Adv. Mater.* **18**, 1941 (2006).
5. R. A. Shelby, D. R. Smith, S. Schultz, *Science* **292**, 77 (2001).
6. A. A. Houck, J. B. Brock, I. L. Chuang, *Phys. Rev. Lett.* **90**, 137401 (2003).
7. J. B. Pendry, A. J. Holden, D. J. Robbins, W. J. Stewart, *IEEE Trans. Microw. Theory Tech.* **47**, 2075 (1999).
8. J. B. Pendry, A. J. Holden, W. J. Stewart, I. Youngs, *Phys. Rev. Lett.* **76**, 4773 (1996).
9. V. Shalaev, *Nat. Photonics* **1**, 41 (2007).
10. C. M. Soukoulis, S. Linden, M. Wegener, *Science* **315**, 47 (2007).
11. S. Zhang *et al.*, *Phys. Rev. Lett.* **95**, 137404 (2005).
12. V. M. Shalaev, *Opt. Lett.* **30**, 3356 (2005).
13. G. Dolling, C. Enkrich, M. Wegener, C. M. Soukoulis, S. Linden, *Science* **312**, 892 (2006).
14. G. Dolling, M. Wegener, C. M. Soukoulis, S. Linden, *Opt. Lett.* **32**, 53 (2007).
15. G. Dolling, M. Wegener, S. Linden, *Opt. Lett.* **32**, 551 (2007).
16. D. R. Smith, S. Schultz, P. Markos, C. M. Soukoulis, *Phys. Rev. B* **65**, 195104 (2002).
17. P. Tournois, V. Laude, *Opt. Commun.* **137**, 41 (1997).
18. G. Shvets, *Physica B* **338**, 338 (2003).
19. G. Shvets, *Phys. Rev. B* **67**, 035109 (2003).
20. A. Alu, N. Engheta, *J. Opt. Soc. Am. B* **23**, 571 (2006).
21. H. Shin, S. H. Fan, *Phys. Rev. Lett.* **96**, 073907 (2006).
22. See supporting material on *Science* Online.
23. J. A. Dionne, L. A. Sweatlock, H. A. Atwater, A. Polman, *Phys. Rev. B* **72**, 075405 (2005).
24. J. A. Dionne, L. A. Sweatlock, H. A. Atwater, A. Polman, *Phys. Rev. B* **73**, 035407 (2006).
25. Transverse electric (TE) modes also exist but are not excited given the incident polarization.
26. K. Y. Kim, Y. K. Cho, H. S. Tae, J. H. Lee, *Opt. Express* **14**, 320330 (2006).
27. For 470 nm < λ_0 < 530 nm, calculated skin depths in the Ag and Au layers do not exceed 21.5 nm and 30.0 nm, respectively.
28. J. A. Dionne, H. J. Lezec, H. A. Atwater, *Nano Lett.* **6**, 1928 (2006).

29. Supported by a National Defense Science and Engineering Graduate Fellowship administered by the Army Research Office (J.A.D.) and by the Air Force Office of Scientific Research under Plasmon Multidisciplinary University Research Initiative FA9550-04-1-0434. We thank L. Sweatlock, D. Pacifici, R. Walters, B. Kayes, N. Vu, G. Derose, and A. Scherer for engaging discussions and technical assistance.

Supporting Online Material

www.sciencemag.org/cgi/content/full/1139266/DC1
SOM Text
Figs. S1 and S2
References

26 December 2006; accepted 12 March 2007
Published online 22 March 2007;
10.1126/science.1139266
Include this information when citing this paper.

Creep-Resistant, Al_2O_3-Forming Austenitic Stainless Steels

Y. Yamamoto,* M. P. Brady, Z. P. Lu, P. J. Maziasz, C. T. Liu, B. A. Pint, K. L. More, H. M. Meyer, E. A. Payzant

A family of inexpensive, Al_2O_3-forming, high–creep strength austenitic stainless steels has been developed. The alloys are based on Fe-20Ni-14Cr-2.5Al weight percent, with strengthening achieved through nanodispersions of NbC. These alloys offer the potential to substantially increase the operating temperatures of structural components and can be used under the aggressive oxidizing conditions encountered in energy-conversion systems. Protective Al_2O_3 scale formation was achieved with smaller amounts of aluminum in austenitic alloys than previously used, provided that the titanium and vanadium alloying additions frequently used for strengthening were eliminated. The smaller amounts of aluminum permitted stabilization of the austenitic matrix structure and made it possible to obtain excellent creep resistance. Creep-rupture lifetime exceeding 2000 hours at 750°C and 100 megapascals in air, and resistance to oxidation in air with 10% water vapor at 650° and 800°C, were demonstrated.

One key to reducing emissions and increasing efficiencies in energy-conversion systems is the development of new structural materials with higher-temperature capability (*1*, *2*). Areas of need range from thin metal foil for use in turbine recuperators to high-pressure steam tubing in fossil-fired ultrasupercritical steam plants. The dilemma is that higher operating temperatures shorten component lifetime by increasing the rates of degradation phenomena such as time-dependent deformation (creep) and oxidation, which result in loss of structural integrity and, ultimately, failure. The challenge is to improve both high-temperature creep strength and oxidation resistance, and yet achieve it at affordable cost for industrial use. There have been major advances in high-temperature alloy classes, ranging from oxide dispersion strengthened (ODS) alloys, intermetallic alloys, and Ni-base superalloys. However, all of these are either prohibitively expensive or have yet to exhibit the desired combination of mechanical properties, oxidation resistance, and manufacturability needed to make them viable for widespread use as heat-resistant components in energy-conversion systems.

Face-centered-cubic (fcc) austenitic stainless steels are the primary material of construction for high-temperature use (>600° to 650°C) in these applications (*3*), owing to their combination of relatively good high-temperature creep strength and oxidation resistance at a relatively low cost (about 10 to 20% that of Ni-base alloys). Notable gains have been made in recent years in improving the creep strength of austenitic steels through control of dispersions of MC carbides and carbonitrides (where M is Nb, Ti, or V) and related phases at the nanoscale (*3*, *4*). State-of-the-art alloys currently offer good creep strength up to ~750° to 850°C. However, from an oxidation standpoint, this can also be well above their practical temperature limit, particularly in operating environments that also contain water vapor or aggressive sulfur- and carbon-containing gas species, because of inherent limitations (*5*) of the Cr_2O_3-base protective scales formed on these alloys. Resistance to water vapor is crucial, because it is found in virtually all combustion environments. However, the Cr_2O_3 protective scales formed on austenitic stainless steels are substantially compromised by water vapor due to the formation of volatile Cr oxy-hydroxide species (*5*–*7*), which then results in accelerated oxidation kinetics and unacceptable material loss rates in service.

Alumina-base protective scales exhibit parabolic growth-rate constants that are an order of magnitude lower than those of Cr_2O_3-base scales and are virtually immune to water-vapor effects in the 600° to 850°C range of interest (*5*–*7*). Alumina is also more thermodynamically stable in oxygen than Cr_2O_3 and offers far superior protection in many industrially relevant environments. A number of attempts have been made over the past 30 years to create Al_2O_3-forming, Fe-base austenitic stainless steels for use as high-temperature structural alloys [e.g., (*7*–*12*)], but none has succeeded. The metallurgical intractability can be fundamentally traced to the very strong body-centered cubic (bcc)–stabilizing effects of Al on Fe. The concentrations of Al typically used to achieve Al_2O_3 scale formation [4 to 5 weight percent (wt %)] stabilizes the weak bcc ferritic phase at the expense of the parent face-centered cubic (fcc) austenitic matrix, resulting in loss of creep strength. (The bcc polymorph of Fe exhibits poor creep strength above ~500° to 600°C.) Efforts worldwide have, therefore, focused instead on development of coatings and/or aluminizing surface treatments [e.g., (*13*, *14*)], which can improve oxidation resistance but also add cost and processing difficulties and have reliability and compatibility issues due to interdiffusion with the substrate austenitic alloys.

The HTUPS (high-temperature ultrafine-precipitation-strengthened steel) family of austenitic alloys (*15*) was chosen as a starting point for exploring alloy behavior. A typical composition is Fe-14Cr-16Ni-2.5Mo-2Mn wt % base with additions of B, C, Nb, P, Ti, and V to form stable nanoscale precipitates for strengthening at elevated temperatures (Table 1). These alloys exhibit among the highest creep strengths reported for austenitic stainless-steel alloys, with creep resistance approaching that of far more expensive Ni-base, Cr_2O_3-forming alloys such as alloy 617 up to temperatures of ~700° to 750°C. However, they were developed for advanced nuclear reactor environments where gas-metal oxidation was less of a concern, and their oxidation resistance is relatively poor, even in dry air.

Table 1. Alloy compositions obtained by chemical quantitative analyses.

Elements	Compositions (wt %)				
	HTUPS* (*15*)	HTUPS 1	HTUPS 2	HTUPS 3	HTUPS 4
Fe	64.27	60.25	57.73	56.58	57.78
Ni	16	19.97	20.00	19.98	19.95
Cr	14	14.15	14.20	14.21	14.19
Al	–	–	2.40	3.67	2.48
Si	0.15	0.15	0.15	0.10	0.15
Mn	2	1.95	1.95	1.92	1.95
Mo	2.5	2.47	2.46	2.46	2.46
Nb	0.15	0.14	0.14	0.14	0.86
Ti	0.3	0.28	0.31	0.31	–
V	0.5	0.49	0.50	0.49	–
C	0.08	0.068	0.076	0.079	0.075
B	0.01	0.007	0.011	0.011	0.01
P	0.04	0.042	0.044	0.04	0.043
Remarks	Base alloy composition (nominal)	W: 0.01 wt % S: 30 ppm O: 70 ppm N: 170 ppm	S: 50 ppm O: 30 ppm N: 40 ppm	S: 50 ppm O: 20 ppm N: 30 ppm	Cu: 0.01 wt % S: 30 ppm O: 20 ppm N: 50 ppm

*HTUPS nominal baseline composition. HTUPS 1, 2, 3, and 4 are the modified alloys of the present work.

Materials Science and Technology Division Oak Ridge National Laboratory Oak Ridge, TN 37831–6115, USA.

*To whom correspondence should be addressed. E-mail: bradymp@ornl.gov

Recently, we explored a different alloy-development strategy by using Laves-phase precipitates to strengthen the austenitic stainless-steel alloys modified by Al, and we found that Al levels of only 2.4 and 3.8 wt % were sufficient to form Al_2O_3-base scales at 700° to 800°C in air with 10% water vapor, but these alloys did not show sufficient high-temperature creep strength (*16*, *17*). Kvernes *et al.* (*18*) also reported that as little as 1 wt % Al was enough to impart Al_2O_3 scale formation in the presence of water vapor at 650°C in bcc FeCrAl alloys, whereas 4 wt % Al was needed at 980°C. In general, Al_2O_3-forming MCrAl and related alloys (M is Co, Fe, or Ni) have required 4 to 5 wt % Al to provide a sufficient Al reservoir to maintain Al_2O_3 scale formation under long-term, very high-temperature conditions (>>10,000 hours, >900°C) for use as protective coatings or low-load applications such as heating elements (*5*). A similar Al content was also used in the development of Al_2O_3-forming stainless-steel alloys (*7*–*12*).

Three alloys were initially studied. HTUPS 1 was a control alloy with a 20 wt % level of Ni to stabilize the fcc austenite structure, but with no Al addition. We added 2.4 wt % Al to make HTUPS 2 and 3.8 wt % Al to make HTUPS 3. Analyzed compositions are shown in Table 1. The alloys were arc-cast, solution-treated, and thermomechanically processed at 1200°C to produce a grain size of ~100 μm, and then 10% cold rolled to introduce dislocations to enhance precipitate nucleation. The HTUPS-type alloys rely on dislocations associated with cold work to act as heterogeneous nucleation sites for stable, nanoscale MC carbide precipitates (M is Nb, Ti, or V), which are then the source of the excellent high-temperature creep strength of these alloys (*15*). Plate tensile specimens with 0.5 mm by 3.2 mm by 12.7 mm at the gage portion were prepared by electro-discharge machining, polished with SiC paper to a 600-grit surface finish, and then creep-rupture tested at 750° to 850°C and 70 to 170 MPa in air.

Creep curves at 750°C and 100 MPa in air for HTUPS 1, 2, and 3 are shown in Fig. 1. This is a very demanding creep-test condition, under which conventional austenitic alloys such as type 347 stainless-steel alloys (Fe-18Cr-11Ni-2Mn wt % base) rupture in less than ~100 to 300 hours. State-of-the-art austenitic stainless-steel alloys such as NF709 (Fe-25Ni-20Cr-1.5Mo-1Mn wt % base) can exhibit creep-rupture lives from ~2000 to 6000 hours under these conditions. The control HTUPS 1 alloy exhibited a low creep rate, consistent with the reported behavior for this class of alloys. This indicated that the increase in Ni level to 20 wt % did not adversely affect creep behavior. The HTUPS 2 also exhibited a low creep rate, indicating tolerance for 2.4 wt % Al. However, the HTUPS 3 alloy with 3.8 wt % Al ruptured after ~700 hours.

At the 2.4 wt % Al level of addition to the HTUPS base alloy, a Ni level of 20 wt % was sufficient to maintain the stability of the austenitic phase structure, and excellent creep resistance was obtained. In the ~3.7 to 3.8 wt % Al-containing HTUPS 3 alloy, ~4 volume % of the weak bcc delta-ferrite phase (with an open lattice structure) was present in the microstructure after solution treatment at 1200°C due to the bcc-stabilizing effect of Al. On exposure at 750° and 800°C, these delta-ferrite bcc regions transformed to coarse sigma-phase particles, with ~9 volume % sigma phase evident after 72 hours at 800°C (Fig. 2B, inset). Such micrometer-scale sigma-phase regions are also locally devoid of the NbC-strengthening precipitates. Further, the sigma phase is itself brittle and then acts as a preferential site for crack initiation. These factors result in the compromised creep resistance of HTUPS 3 and similar Fe-base austenitic alloys with higher amounts of Al.

Backscattered electron cross-section micrographs of HTUPS 2 and 3 steels after 72 hours' oxidation at 800°C in air are shown in Fig. 2. Neither the 2.4 nor the 3.8 wt % level of Al addition was sufficient to impart Al_2O_3 scale formation. Rather, the Al was internally oxidized, and the external scale consisted of faster-growing, nonprotective mixed Fe and Cr oxide phases. This result was surprising given that developmental Fe_2Nb (Laves phase)–precipitated Fe-20Ni-15Cr wt % base alloys formed a protective Al_2O_3 scale at levels of 2.4 wt % Al (*16*, *17*). These alloys were of composition similar to that of HTUPS 2 and 3, but without the small additions of Ti or V (~0.3 and 0.5 wt %, respectively; Table 1). We therefore designed the HTUPS 4 alloy (*19*), which contained 2.4 wt % Al but without Ti or V additions, and the amount of Nb was increased to compensate for the absence of Ti and V (Table 1). Despite the absence of Ti and V, the HTUPS 4 alloys still exhibited excellent creep resistance at 750°C and 100 MPa in air, albeit with a moderately lower creep-rupture life than that of HTUPS 2. Further, as shown in Fig. 2C, oxidation for 72 hours at 800°C in air resulted in the formation of a continuous, external Al_2O_3-base scale. Alloying additions of 0.3Ti and 0.5V wt % were then added to an alumina-forming Fe_2Nb Laves phase–precipitated alloy (*16*, *17*) of base composition Fe-21Ni-14Cr-1.7Nb-2.5Al wt %. These additions resulted in poor oxidation resistance similar to that shown in Fig. 2, A and B.

The observed microstructural features of internal alumina precipitates in the near-surface regions of the oxidized HTUPS alloys 2 and 3 fit well within the phenomenological framework established by Wagner (*20*) governing the transition from internal oxidation to external (protective) scale formation. According to Wagner, the

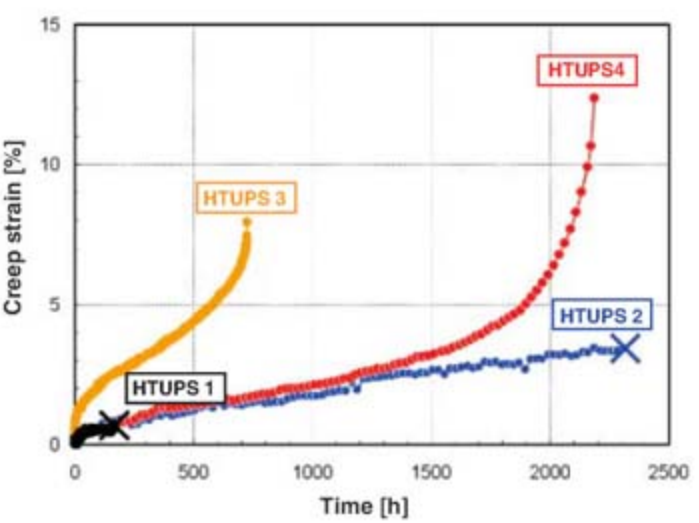

Fig. 1. Creep curves of HTUPS series tested at 750°C and 100 MPa in air. The creep testing of HTUPS 1 and 2 was stopped after 170 hours and 2300 hours, respectively, because of their relatively poor oxidation resistance and concerns about the possible influences of oxidation products on the thin-section specimens used to assess creep-rupture life.

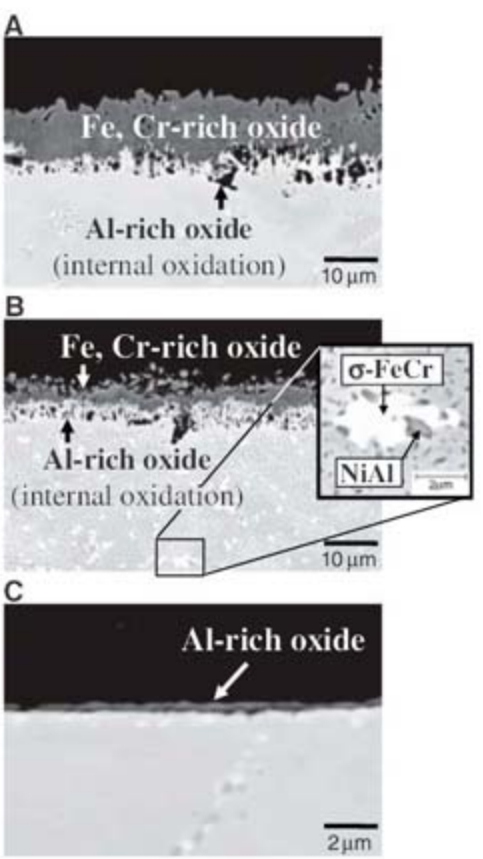

Fig. 2. Backscatter electron images after 72 hours of oxidation at 800°C in air. (**A**) HTUPS 2, (**B**) HTUPS 3, and (**C**) HTUPS 4.

critical level of an alloying addition needed for external scale formation (in this case Al) can be described by a flux criteria based on a competition between inward oxygen permeation and outward Al diffusion. Alloying additions that increase oxygen permeability or decrease Al diffusivity would raise the amount of Al needed for protective alumina scale formation. Given the high thermodynamic stability of Ti and V with oxygen, moderately greater than that of Nb, additions of Ti and V may be expected to promote an increased tendency for internal oxidation because of increased oxygen permeability, consistent with our results. Modification of the oxidation kinetics resulting from doping of the initially formed oxide scales by V or Ti could also play a contributory role.

Many high-temperature austenitic stainless steels and related alloys do feature additions of Ti and/or V to obtain good high-temperature creep strength, through precipitation of carbides and related phases. Other high-temperature austenitic alloys also contain high levels of nitrogen, which can react with added Al, resulting in poor creep behavior (*21*). This accounts for the inability of such stainless steels to form protective Al_2O_3 scales at the lower levels of Al needed to maintain the stability of the fcc austenitic structure.

To better assess oxidation resistance, we exposed ~1-mm-thick samples of HTUPS 4 at 650° and 800°C in air with 10% water vapor, an environment that is extremely aggressive to conventional Cr_2O_3-forming alloys (*7*). Low specific-mass gains, consistent with the slow oxidation kinetics of protective Al_2O_3 scale formation, were observed over the course of 10 100-hour cycles (1000 hours total time at temperature) (Fig. 3A). By comparison, ~100-μm-thick gas-turbine recuperator foil of NF709 (Fe-25Ni-20Cr base), a state-of-the-art Cr_2O_3-forming austenitic stainless alloy, showed moderately higher specific-mass gains than HTUPS 4 (Fig. 3A). However, the mass-change data for NF709 (*22*, *23*) reflect both the balance of oxygen uptake to form chromia and mass loss from volatilization of the chromia, such that the mass-change curve underrepresented the actual rate of oxidation and Cr consumption. At 800°C in air with 10% water vapor, NF709 foil suffers from volatility-driven Cr_2O_3 scale breakdown and extensive Fe-oxide nodule formation after only 5000 to 7000 hours of exposure, depending on foil thickness (*23*). Even at 700°C in air with 10% water vapor, NF709 alloy foil exhibits the onset of Fe-oxide nodule formation after ~10,000 hours (*23*). The desired durability for these applications is 40,000 to 100,000 hours. The available data indicate that alumina scale–forming alloys are not adversely affected in air with water vapor at these temperatures, owing to the high stability of Al_2O_3 in water vapor (*6*, *7*).

A bright-field transmission electron micrograph (TEM) cross-sectional image of the scale formed on HTUPS 4 after 1000 hours at 800°C in air with 10% water vapor is shown in Fig. 3B. The scale consisted of a 40- to 50-nm inner region of columnar α-Al_2O_3 (width 75 to 100 nm) adjacent to the alloy and an overlying 60- to 100-nm-thick, fine-grained (<20 nm) intermixed layer of transition Al_2O_3 + Cr_2O_3 + porosity. In some scale regions, a 0.05- to 0.5-μm columnar-grained surface layer of intermixed Al-Cr-Fe-O + Al-Cr-Mn-Fe-O–rich phase was also observed, as were occasional nodules 1 to 5 μm thick containing some Nb-rich oxide regions. Auger electron spectroscopy profiling indicated that the oxide scale was Al-rich, with generally less than 10 atomic % total combined Cr, Fe, and Si. The observed oxide-scale microstructure is consistent with the measured oxidation kinetics, which indicated relatively high mass gain during the first few hundred hours of exposure (when the mixed oxides were forming), followed by a transition to slow, protective oxidation kinetics when the α-Al_2O_3 layer developed.

Figure 4 shows the microstructure of HTUPS 4 after creep-rupture failure following 2200 hours at 750°C and 100 MPa. The grain boundaries in the alloy matrix were decorated with intermetallic Fe_2Nb Laves and NiAl phases, as well as some coarse NbC (Fig. 4A). Precipitation of NiAl is consistent with previous studies of Al-modified stainless steels (*9*). The Fe_2Nb Laves phase and coarse NbC regions suggest that the amount of Nb was too high, such that this alloy can be designed to further optimize its performance. The coarse intergranular Laves phase, NiAl, and NbC precipitates likely did not contribute appreciably to the creep resistance because they were generally on the order of micrometers, as compared to the nanoscale intragranular precipitate size achieved with NbC. Despite these grain-boundary phases, ductility at rupture exceeded 13%. Uniform nanodispersions consistent with NbC carbides (~10 nm in diameter) were observed throughout the microstructure (Fig. 4B), with extensive dislocation pinning, indicating that these were the source of the excellent creep-rupture resistance shown by this alloy.

Figure 5 shows a Larson Miller parameter plot (i.e., stress versus time-temperature parameter for creep rupture) for HTUPS 4 tested between 750° to 850°C and 70 to 170 MPa relative to current high-temperature alloys. The creep-rupture resistance was comparable to the levels exhibited by state-of-the-art austenitic alloys such as NF709 (Fe-25Ni-20Cr-1.5Mo-1Mn wt % base) and in the range of performance achieved by the Ni-base alloy 617 (Ni-22Cr-13Co-9Mo-1Al wt % base), but with the advantages of Al_2O_3 scale formation rather than Cr_2O_3 for long-term durability and higher operating temperature under aggressive oxidizing conditions. The material cost of the HTUPS 4 and related alloys should be moderately lower than that of NF709 and be considerably lower than that of alloy 617, owing to lower amounts of expensive Co, Cr, Mo, and Ni. An initial weldability assessment of HTUPS 4 via a gas tungsten arc weld pass also

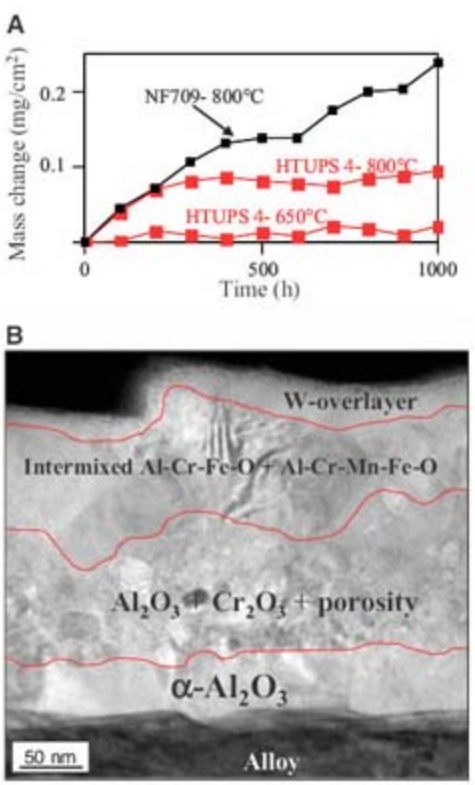

Fig. 3. (**A**) Oxidation kinetics in air with 10% water vapor (10 to 100 hours cycles) [NF709 data from (*22*, *23*)]. (**B**) TEM bright-field cross section of scale formed on HTUPS 4 after 1000 hours at 800°C in air with 10% water vapor.

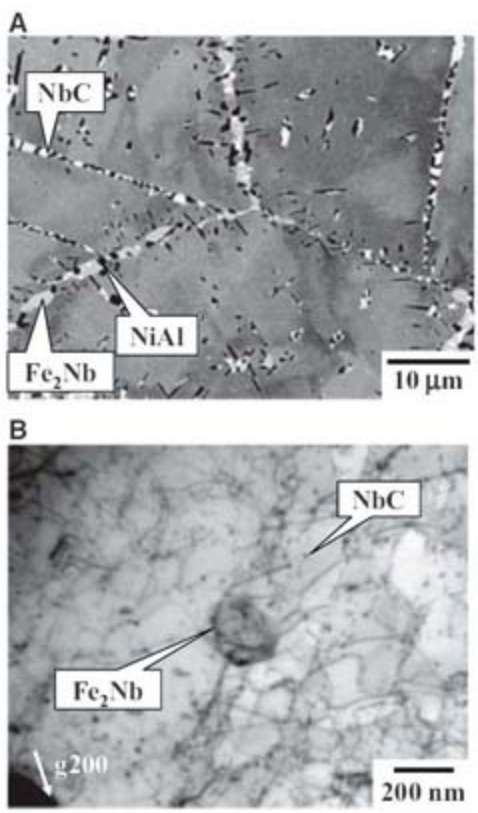

Fig. 4. Microstructure of HTUPS 4 after creep testing for 2200 hours at 750°C and 100 MPa. (**A**) Backscatter electron image and (**B**) TEM bright-field image.

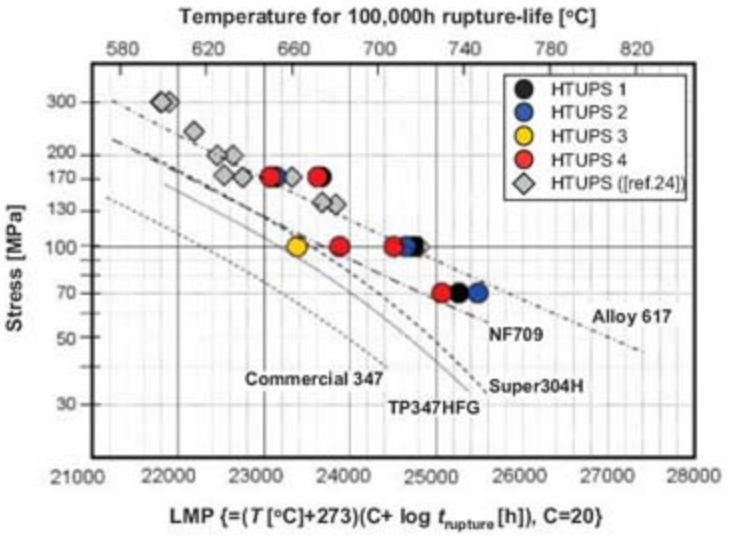

Fig. 5. Larson Miller Parameter (LMP) of HTUPS series plotted as a function of stress, together with those of some benchmark commercial high-temperature austenitic stainless steels and the Ni-base alloy 617 (*24*–*26*). The LMP scales with both creep-rupture time and test temperature.

indicated amenability to joining by conventional welding techniques, which is a key requirement for many applications.

The finding that low amounts of Al are sufficient to form Al_2O_3 scales on stable fcc austenitic stainless steels if Ti and V additions are eliminated (or minimized) also holds great promise for modifying other existing families of high-temperature alloys for Al_2O_3 scale formation, not just the HTUPS family. Creep-resistant, Al_2O_3-forming austenitic stainless steels will enable higher operating temperatures and greater durability in a range of energy-conversion system applications, as well as in the chemical and process industries.

References and Notes

1. R. Viswanathan, W. Bakker, *J. Mat. Eng. Per.* **10**, 81 (2001).
2. R. Viswanathan, W. Bakker, *J. Mat. Eng. Per.* **10**, 96 (2001).
3. T. Sourmail, *Mat. Sci. Technol.* **17**, 1 (2001).
4. M. Taneike, F. Abe, K. Sawada, *Nature* **424**, 294 (2003).
5. P. Kofstad, Ed., *High Temperature Corrosion* (Elsevier, London, 1988).
6. E. J. Opila, *Mater. Sci. Forum* **461-464**, 765 (2004).
7. B. A. Pint, R. Peraldi, P. J. Maziasz, *Mater. Sci. Forum* **461-464**, 815 (2004).
8. V. Ramakrishnan, J. A. McGurty, N. Jayaraman, *Oxid. Met.* **30**, 185 (1988).
9. D. Satyanarayana, G. Malakondaiah, D. Sarma, *Mater. Sci. Eng. A* **323**, 119 (2002).
10. T. Fujioka, M. Kinugasa, S. Iizumi, S. Teshima, I. Shimizu, U.S. Patent 3,989,514 (1976).
11. J. A. McGurty, U.S. Patent 4,086,085 (1978).
12. J. C. Pivin *et al.*, *Corros. Sci.* **20**, 351 (1980).
13. N. V. Bangaru, R. C. Krutenat, *J. Vac. Sci. B* **2**, 806 (1984).
14. Y. Zhang *et al.*, *Surf. Coat. Technol.* **188-189**, 35 (2004).
15. P. J. Maziasz, *J. Met.* **41**, 14 (1989).
16. M. P. Brady, C. T. Liu, Y. Yamamoto, Z. P. Lu, H. Meyer, "Multi-Phase High Temperature Alloys: Exploration of Laves Phase Strengthening of Steels," Proceedings of the 19th Annual Conference on Fossil Energy Materials, Knoxville, TN, 9 to 11 May 2005; available at www.ornl.gov/sci/fossil/.
17. Y. Yamamoto, Z. P. Lu, M. P. Brady, C. T. Liu, P. F. Tortorelli, "Multi-Phase High Temperature Alloys: Exploration of Laves Phase Strengthening of Steels," Proceedings of the 20th Annual Conference on Fossil Energy Materials, Knoxville, TN, 12 to 14 June 2006; available at www.ornl.gov/sci/fossil/.
18. I. Kvernes, M. Oliverire, P. Kofstad, *Corros. Sci.* **17**, 237 (1977).
19. M. P. Brady *et al.*, "Oxidation Resistant, High Creep Strength Austenitic Stainless Steel," U.S. Patent Disclosure (4 January 2007).
20. C. Wagner, *Z. Elektrochem.* **63**, 772 (1959).
21. J. P. Shingledecker, P. J. Maziasz, N. D. Evans, M. J. Pollard, in *Creep Deformation and Fracture, Design, and Life Extension*, R. S. Mishra, J. C. Earthman, S. V. Raj, R. Viswanathan, Eds. (TMS, Warrendale, PA), pp. 129–138.
22. B. A. Pint, *J. Eng. Gas Turbines Power* **128**, 370 (2006).
23. D. J. Young, B. A. Pint, *Oxid. Met.* **66**, 3/4, 137 (2006).
24. R. W. Swindeman, P. J. Maziasz, E. Bolling, J. F. King, "Evolution of advanced austenitic alloys relative to alloy design criteria for steam service: Part 1–Lean stainless steels" (Oak Ridge National Laboratory Rep. ORNL-6629/P1, Oak Ridge, TN, 1990).
25. J. P. Shingledecker, P. J. Maziasz, N. D. Evans, M. J. Pollard, in *Creep and Fracture in High Temperature Components—Design and Life Assessment Issues* (Destech, Lancaster, PA, 2005), pp. 99–109.
26. Allegheny Ludlum, *Technical Data Blue Sheet, Stainless Steels, types 321, 347 and 348* (ATI Allegheny Ludlum Corp., Pittsburgh, PA, 2003); www.alleghenyludlum.com.

27. We thank J. Shingledecker, P. Tortorelli, and E. George for helpful comments on this manuscript. This work was funded by the U.S. Department of Energy (DOE), Fossil Energy Advanced Research Materials Program. Additional funding and collaboration with the U.S. DOE Distributed Energy Program and the Division of Materials Sciences and Engineering, Office of Basic Energy Sciences, are also acknowledged. The SHaRE User Facility at Oak Ridge National Laboratory, sponsored by the U.S. DOE, Office of Basic Energy Sciences, Division of Scientific User Facilities, is also acknowledged. Oak Ridge National Laboratory is managed by UT-Battelle, LLC, for the U.S. DOE under contract DE-AC05-00OR22725.

17 November 2006; accepted 1 March 2007
10.1126/science.1137711

Synthesis of Ultra-Incompressible Superhard Rhenium Diboride at Ambient Pressure

Hsiu-Ying Chung,[1,2]* Michelle B. Weinberger,[1]* Jonathan B. Levine,[1] Abby Kavner,[3] Jenn-Ming Yang,[2] Sarah H. Tolbert,[1]† Richard B. Kaner[1,2]†

The quest to create superhard materials rarely strays from the use of high-pressure synthetic methods, which typically require gigapascals of applied pressure. We report that rhenium diboride (ReB_2), synthesized in bulk quantities via arc-melting under ambient pressure, rivals materials produced with high-pressure methods. Microindentation measurements on ReB_2 indicated an average hardness of 48 gigapascals under an applied load of 0.49 newton, and scratch marks left on a diamond surface confirmed its superhard nature. Its incompressibility along the *c* axis was equal in magnitude to the linear incompressibility of diamond. In situ high-pressure x-ray diffraction measurements yielded a bulk modulus of 360 gigapascals, and radial diffraction indicated that ReB_2 is able to support a remarkably high differential stress. This combination of properties suggests that this material may find applications in cutting when the formation of carbides prevents the use of traditional materials such as diamond.

The design of superhard materials is motivated by a need for robust, chemically diverse compounds for industrial applications ranging from abrasives and cutting tools to scratch-resistant coatings. Although diamond, with the highest known hardness (70 to 100 GPa), has traditionally been used to fulfill many of these needs, there are limits to its applicability. For example, diamond is not used to cut steel and other ferrous metals because of the detrimental formation of iron carbide during high-speed machining. Therefore, there is a need for synthetic materials that can be used in place of diamond. Cubic boron nitride (BN), the second hardest material (45 to 50 GPa), is used to cut steel because iron borides and nitrides are much less stable. However, cubic BN must be synthesized under extreme pressures (>5 GPa) and temperatures (>1500°C), making it expensive (*1*). Two other compounds that have been synthesized recently, B_6O (*2*) and cubic BC_2N

[1]Department of Chemistry and Biochemistry and the California NanoSystems Institute, University of California, Los Angeles, CA 90095–1569, USA. [2]Department of Materials Science and Engineering, University of California, Los Angeles, CA 90095–1595, USA. [3]Department of Earth and Space Sciences, University of California, Los Angeles, CA 90095-1567, USA.

*These authors contributed equally to this work.
†To whom correspondence should be addressed. E-mail: tolbert@chem.ucla.edu (S.H.T.); kaner@chem.ucla.edu (R.B.K.)

(*3*), rival the hardness of cubic BN. However, their syntheses also require extreme pressures, exceeding 5 GPa for B_6O and 18 GPa for BC_2N.

Our approach to creating ultra-incompressible superhard materials has been to optimize two design parameters: high valence-electron density and bond covalency (*4*, *5*). High electron densities can be found among the later transition metals, whereas small first-row main-group elements, such as B, C, and N, form the strongest covalent bonds (*6*). Among the transition metals, Os has the highest valence-electron density (0.572 electrons/Å^3) and a reported bulk modulus between 395 and 462 GPa (*7*–*9*) that rivals that of diamond (442 GPa) (*10*, *11*). However, unlike diamond, the hardness of Os metal is only 4 GPa. This can be explained by the nondirectional metallic bonding in Os versus the short, highly covalent, directional bonds formed by sp^3 hybridized C atoms in diamond. The strength and directionality of covalent bonds limit the creation and propagation of defects, which in turn causes diamond to resist plastic deformation, resulting in diamond's exceptional hardness. By optimizing covalent bonding and valence-electron density, we recently succeeded in designing, synthesizing, and characterizing an ultra-incompressible hard material, OsB_2 (*4*). In searching for even harder materials, we looked closely at the elements surrounding Os in the periodic table. Re, which lies directly to the left of Os, has a slightly lower valence-electron density (0.4761 electrons/Å^3) that produces a similar bulk modulus of 360 GPa (*12*). Despite being highly incompressible, the hardness of Re metal is also low, between 1.3 and 3.2 GPa, because of its delocalized nondirectional metallic bonding (*13*, *14*). Incorporating B into the interstitial sites of Re to form ReB_2 requires only a 5% expansion of the Re lattice. This results in the shortest metal-metal bonds of any known transition-metal diboride (*15*). In contrast, the Os lattice expands by approximately 10% upon the incorporation of B atoms to form OsB_2 and undergoes a distortion to an orthorhombic phase. Applying our design criteria, ReB_2 is thus considered to be the most likely candidate for improving on the mechanical properties of OsB_2.

ReB_2 has the highest B:Re ratio among the known Re_xB_y phases—Re_3B, Re_7B_3, and ReB_2 (*16*)—and therefore contains the greatest degree of covalent bonding. The structure of ReB_2 consists of alternating layers of hexagonal close-packed Re and puckered hexagonal networks of B (Fig. 1). The result is a compound that is layered perpendicular to the *c* axis along the (00*l*) planes. Recent theoretical calculations have shown that there are strong covalent B-B and Os-B bonds in OsB_2 (*17*–*20*). By analogy, ReB_2 should contain similar covalent B-B and Re-B bonds, with the Re-B bonds in ReB_2 expected to be shorter and stronger than those in OsB_2 because of the minimal lattice expansion.

ReB_2 was synthesized under ambient conditions via three methods, each of which may potentially be scaled up (supporting online text). First, a solid-state metathesis reaction was carried out between the metal trichloride and MgB_2, because this process has been used to produce many transition-metal diborides, including OsB_2 (*4*, *21*). Without excess B, however, this process forms multiple boride phases. Second, Re and B powders were mixed together, pressed into a pellet, and then liquefied with 80 amps of current in an Ar atmosphere. The result was a solid metallic ingot of ReB_2 that could be used for hardness testing. In the third method, stoichiometric quantities of Re and B powder were sealed in a quartz tube under vacuum and heated for 5 days at 1000°C. Powder x-ray diffraction, performed on a crushed portion of both the arc-melted ingot and the polycrystalline powder produced from the elements, confirmed the synthesis of phase-pure ReB_2 (fig. S1). These materials were then examined by microindentation and in situ high-pressure x-ray diffraction techniques.

To determine the Vickers hardness (H_V) of ReB_2, microindentation experiments were performed using a square pyramidal-shaped diamond indenter tip lowered onto a polished ingot with a known amount of force. When the indenter was removed, the area of the indent, indicating the extent of the plastic deformation of the sample, was measured. From this area and the applied load *P*, H_V was determined using Eq. 1

$$H_V = 1854.4\ P/d^2 \qquad (1)$$

where *d* is the arithmetic mean of the two diagonals of the indent.

Five indentations were made at varying loads on each of 10 grains of ReB_2. As the load was decreased from 4.9 to 0.49 N, the average hardness increased from 30.1 ± 1.3 to 48.0 ± 5.6 GPa, with a maximum measured hardness of 55.5 GPa under 0.49 N of load (Fig. 2A), which is comparable to the hardness of cubic BN under an equivalent load (*2*). The observed inverse relationship of applied load to hardness has been extensively documented in many different types of materials. This phenomenon is referred to as the indentation size effect. Although many factors may contribute to this effect, it is most frequently attributed to strain gradient plasticity in microindentation experiments (*22*). The superhard nature of ReB_2 was corroborated by a scratch test in which a piece of ReB_2 ingot was used to scratch a polished face of natural diamond parallel to the (100) plane (Fig. 2B).

The covalent bonding that results in high hardness values can also contribute to the elastic incompressibility (bulk modulus) of a material. To further explore the contribution of covalent bonding as well as the possible correlation between valence-electron density and bulk elastic

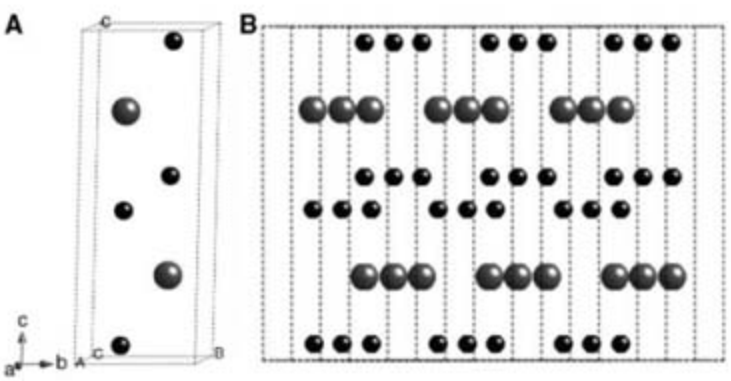

Fig. 1. The small dark spheres represent B atoms and the large light spheres represent Re. The structure is hexagonal with a = 2.9 Å and c = 7.478 Å. (**A**) A single unit cell. (**B**) Multiple unit cells demonstrating the layered structure viewed perpendicular to the $(3\bar{1}0)$ plane of ReB_2.

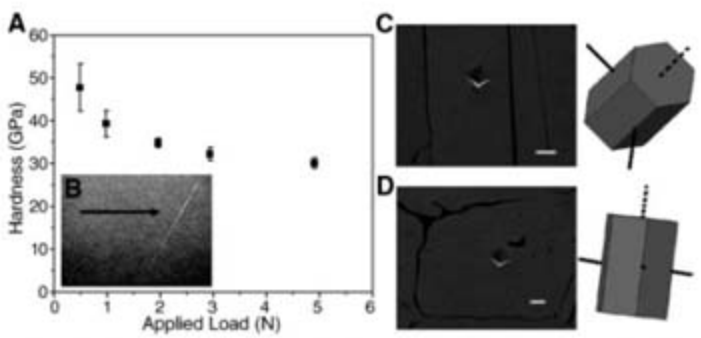

Fig. 2. (**A**) H_V of ReB_2 plotted as a function of applied load measured at room temperature, using a four-sided pyramidal diamond indenter tip. The average hardness increases from 30 to 48 GPa as the applied load decreases from 4.9 to 0.49 N (error bars = ±1SD). (**B**) An ingot of ReB_2 creates a scratch on the surface of a natural diamond parallel to the (100) plane. (**C**) Scanning electron microscope image of a diamond indentation under an applied load of 4.9 N in a ReB_2 grain yields a measured hardness of 31 GPa. The three-dimensional graphic at right corresponds to the crystallographic orientation of the indented grain. The dashed line is the *c* axis, and the solid lines lie parallel to the *a* and *b* directions. (**D**) Indentation on a grain with an orientation different from that in Fig. 2C (see graphic at right) produces a hardness of 27 GPa, consistent with the anisotropy of the hexagonal crystal structure of ReB_2. Scale bar in (C) and (D), 15 μm.

properties, data on the elastic volume compressibility of ReB_2 were collected via in situ high-pressure x-ray diffraction studies. Samples were compressed quasi-hydrostatically up to 30 GPa in a diamond anvil cell, and in situ diffraction data were collected under pressure. From the diffraction data, the fractional volume at increasing pressures was calculated. Fitting the pressure/volume (P versus V/V_0) data with a third-order Birch-Murnaghan equation of state, the bulk modulus of ReB_2 was determined to be 360 GPa when B_o' (derivative of the zero-pressure bulk modulus with respect to pressure) was fixed at the canonical value of 4. This high bulk modulus is in agreement with our understanding of the correlation between valence-electron density and incompressibility (*4*, *6*).

In addition to bulk volume compressibility, the high-pressure diffraction data also revealed an anisotropy in the compressibility of the two different lattice directions of hexagonal ReB_2 (Fig. 3). As seen in Fig. 3, the *c* axis is substantially less compressible than the *a* axis, and this *c* axis value is very similar to the analogous linear compressibility of diamond. This anisotropy results from greater electron density, and therefore greater electronic repulsions, along the *c* axis.

We sought to further elucidate the mechanical anisotropy among the crystallographic planes in ReB_2 through high-pressure radial diffraction experiments (*23*). These experiments differ from the conventional isotropic diamond anvil cell experiments described above. Here the material, held in place by a Be gasket, is intentionally subjected to nonhydrostatic pressures in a diamond anvil cell. The sample stress state can be divided into hydrostatic and deviatoric components. Hydrostatic compression of the sample results in elastic volume compression following the material's $P(V)$ equation of state. The deviatoric component is more complex, resulting from a combination of the applied-stress state and the sample mechanical response. To understand these plastic deformations, we consider the stress state inside the pressure cell. The direction of maximum stress is along the loading axis of the diamond anvil cell (σ_1), and the minimum stress direction is assumed to be cylindrically symmetric in the plane of the gasket (σ_3). The difference between these two stresses is the differential stress, t, which, if high enough, is capable of producing plastic deformation. Such high t values can be defined by the von Mises yield criterion (Eq. 2)

$$t = \sigma_1 - \sigma_3 \leq 2\tau = \sigma_y \qquad (2)$$

where τ is the shear strength and σ_y is the yield strength (*23*). Therefore, an estimate of t, provides a lower-bound estimate of the material's σ_y.

The differential stress can be calculated from measurements of lattice strain in the maximum and minimum stress directions and from knowledge of the single-crystal elastic properties via linear elasticity (*24*, *25*). The absence of single-crystal elastic moduli data necessitates the application of isotropic lattice strain theory for the analysis of strength in ReB_2. In this approach, we apply the isotropic theory to each lattice plane individually. Although substantial differences in strength behavior among different lattice planes are an indication of elastic anisotropy, we find that for related systems, the full anisotropic analysis does not substantially change the conclusions that can be drawn from the data.

For isotropic materials, the differential stress can be calculated from the lattice strain data using Eqs. 3 and 4

$$t = 6G\langle(\varepsilon_{hydro} - \varepsilon_{90})\rangle \qquad (3)$$

$$\varepsilon_{hydro} = (2\varepsilon_{90} + \varepsilon_0)/3 \qquad (4)$$

where G is the aggregate shear modulus of the polycrystalline sample; ε_{hydro} is the hydrostatic strain; and ε_{90} and ε_0 are the strains at the minimum and maximum stress orientations, respectively. These strains, specific for each lattice plane, are determined directly from the positions of the peaks in the x-ray diffraction patterns.

The greater the difference in the strain between the minimum and maximum stress directions, the greater the material's ability to support the differential stress in that plane without plastic deformation. In this experiment, data were collected from 0 to 14 GPa (Fig. 4), where ReB_2 supports a lattice averaged differential stress of 6.4 to 12.9 GPa, the highest measured for any material at these pressures. Other superhard materials, such as cubic Si_3N_4, B_6O, and TiB_2, are able to support only between 5 and 10 GPa of differential stress at these pressures (*26*–*28*). The lattice plane anisotropy is determined by the elastic anisotropy and perhaps also plastic anisotropy. As seen in Fig. 4, the (110) plane of ReB_2 is the stiffest plane and is able to support a differential stress of 17 GPa at 14 GPa of pressure. In contrast, the (004) plane shows a substantially lower differential stress. The difference in each lattice plane's ability to support differential stress can be attributed to the layered crystal structure of ReB_2. The (004) plane, which is orthogonal to the *c* axis and therefore lies parallel to the layers of Re and B, is likely to be a slip plane and a location of stress release in the material at high pressures. Consequently, it is able to support less differential stress than the other planes studied. In contrast, the (110) plane, which is perpendicular to these slip planes, is able to support the largest differential stress. Finally, as expected, the (101) plane, which has a component both parallel and perpendicular to the *c* axis, has an intermediate value between the (110) and (004) planes.

Having observed that the different planes of ReB_2 are able to support varying amounts of stress in the conventional and radial geometry

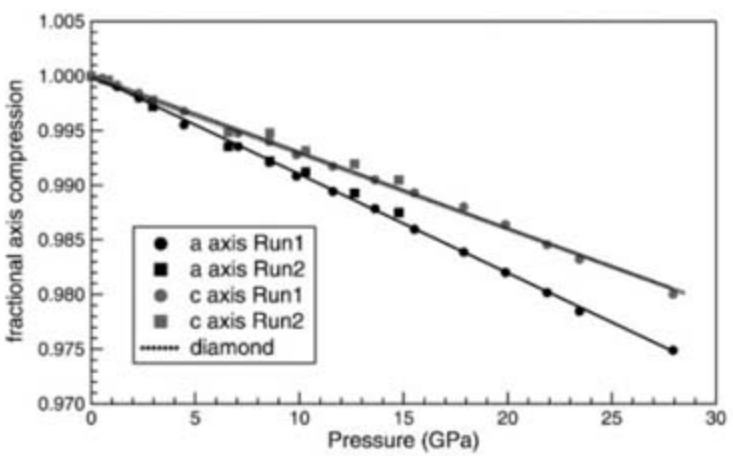

Fig. 3. There is substantial anisotropy in the compressibility of ReB_2. The *a* axis (black symbols) is more compressible than the *c* axis (gray symbols). The *c* axis of ReB_2 is as incompressible as the analogous axis of diamond (dashed line).

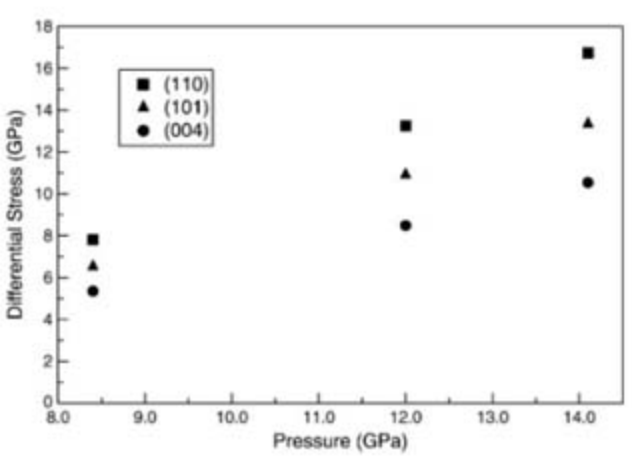

Fig. 4. When nonisotropic stress is applied to ReB_2, different planes support varying amounts of differential stress. The (110) plane (squares), which is orthogonal to the slip planes in ReB_2, exhibits the greatest ability to support differential stress, whereas the (004) plane (circles), which lies parallel to the slip planes, is able to support the least amount.

high-pressure experiments, we anticipated observing this effect in our hardness measurements as well. Indeed, Fig. 2A shows that there is a substantial difference between the highest and lowest measured hardness across grains of ReB_2 under the same load. This observed spread in hardness values at constant load can be attributed to the anisotropic structure of ReB_2, combined with our inability to control the crystallographic orientation of the tested grains. For example, under a load of 4.9 N, the highest measured hardness is 32.5 GPa and the lowest obtained value is 26.0 GPa.

We can begin to understand this variation in hardness by using electron backscattering diffraction to measure the orientations of the grains studied (Fig. 2, C and D). The results indicate that indentations parallel to the (00*l*) planes yielded the lowest average hardness, a value of 27 GPa. In contrast, indentations along directions that contained a larger component parallel to the *c* axis [that is, perpendicular to (00*l*)] resulted in measurements with an average hardness of 31 GPa, an increase of 15%. The dependence of hardness data on crystallographic orientation can be explained by the presence of the same slip planes described above. Furthermore, because similar anisotropic behavior is observed in the high-pressure data, we conclude that the radial diffraction study elucidates the plastic behavior of the material, giving an indication of the yield strength rather than merely measuring elastic behavior.

In our microindentation experiments to date, we have found no grains with pure (00*l*) orientation. As a result, our data demonstrate a minimum average hardness. It is likely that these planes parallel to (00*l*), which we were unable to directly measure, will have an even higher hardness and are responsible for scratching diamond (Fig. 2B).

References and Notes

1. P. F. McMillan, *Nat. Mater.* **1**, 19 (2002).
2. D. He *et al.*, *Appl. Phys. Lett.* **81**, 643 (2002).
3. V. L. Solozhenko, D. Andrault, G. Fiquet, M. Mezouar, D. C. Rubie, *Appl. Phys. Lett.* **78**, 1385 (2001).
4. R. W. Cumberland *et al.*, *J. Am. Chem. Soc.* **127**, 7264 (2005).
5. Incompressibility is the resistance to elastic volume compression and is reported as bulk modulus in units of gigapascals. Hardness is resistance to plastic deformation and is reported in units of force per unit area (in gigapascals).
6. R. B. Kaner, J. J. Gilman, S. H. Tolbert, *Science* **308**, 1268 (2005).
7. H. Cynn, J. E. Klepeis, C.-S. Yoo, D. A. Young, *Phys. Rev. Lett.* **88**, 135701 (2002).
8. F. Occelli *et al.*, *Phys. Rev. Lett.* **93**, 95502 (2004).
9. T. Kenichi, *Phys. Rev. B* **70**, 12101 (2004).
10. I. V. Aleksandrov, E. F. Goncharov, A. N. Zisman, S. M. Stishov, *Sov. Phys. JETP* **66**, 384 (1987).
11. H. J. McSkimin, W. L. Bond, *Phys. Rev.* **105**, 116 (1957).
12. M. H. Manghnani, K. Katahara, E. S. Fisher, *Phys. Rev. B* **9**, 1421 (1974).
13. C. A. Hampel, *Rare Metals Handbook* (Reinhold, London, 1961).
14. C. G. Fink, P. Deren, *Trans. Electro-chem. Soc.* **66**, 381 (1934).
15. A. Vegas, L. A. Martinez-Cruz, A. Ramos-Gallardo, A. Romero, *Z. Kristallogr.* **210**, 574 (1995).
16. S. La Placa, B. Post, *Acta Crystallogr.* **15**, 97 (1962).
17. Y. Z. Chen, H. J. Xiang, J. Yang, J. G. Hou, Q. Zhu, *Phys. Rev. B* **74**, 12102 (2006).
18. M. Hebbache, L. Stuparevic, D. Zivkovic, *Solid State Commun.* **139**, 227 (2006).
19. S. Chiodo, H. J. Gotsis, N. Russo, E. Sicilia, *Chem. Phys. Lett.* **425**, 311 (2006).
20. H. Gou *et al.*, *Appl. Phys. Lett.* **88**, 221904 (2006).
21. L. Rao, E. G. Gillan, R. B. Kaner, *J. Mater. Res.* **10**, 353 (1995).
22. H. Gao, Y. Huang, W. D. Nix, *Naturwissenschaften* **86**, 507 (1999).
23. A. L. Ruoff, *J. Appl. Phys.* **46**, 1389 (1975).
24. A. K. Singh, *J. Appl. Phys.* **73**, 4278 (1993).
25. A. K. Singh, C. Balasingh, H. K. Mao, R. J. Hemley, J. F. Shu, *J. Appl. Phys.* **83**, 7567 (1998).
26. B. Kiefer, S. R. Shieh, T. S. Duffy, T. Sekine, *Phys. Rev. B* **72**, 14102 (2005).
27. D. He, S. R. Shieh, T. S. Duffy, *Phys. Rev. B* **70**, 184121 (2004).
28. G. M. Amulele, M. H. Manghnani, M. J. Somayazulu, *J. Appl. Phys.* **99**, 23522 (2006).

29. This work was funded by NSF under grants DMR-0453121 (R.B.K.), EAR-0510914 (A.K.), and CMS-0307322 (S.H.T.), and an Integrative Graduate Education and Research Traineeship (J.B.L.). Use of the National Synchrotron Light Source, Brookhaven National Laboratory, and the Advanced Light Source, Lawrence Berkeley National Laboratory, were supported by the U.S. Department of Energy, Office of Basic Energy Science, under contracts DE-AC02-98CH10886 and DE-AC03-76SF00098, respectively. The authors thank S. Caldwell, S. Clark, R. Cumberland, S. Fakra, J. Gilman, J. Hu, M. Kunz, and A. Phan for their assistance with this research.

Supporting Online Material

www.sciencemag.org/cgi/content/full/316/5823/436/DC1
Materials and Methods
Fig. S1

26 December 2006; accepted 16 March 2007
10.1126/science.1139322

Facile Splitting of Hydrogen and Ammonia by Nucleophilic Activation at a Single Carbon Center

Guido D. Frey, Vincent Lavallo, Bruno Donnadieu, Wolfgang W. Schoeller,* Guy Bertrand*

In possessing a lone pair of electrons and an accessible vacant orbital, singlet carbenes resemble transition metal centers and thus could potentially mimic their chemical behavior. Although singlet di(amino)carbenes are inert toward dihydrogen, it is shown that more nucleophilic and electrophilic (alkyl)(amino)carbenes can activate H_2 under mild conditions, a reaction that has long been known for transition metals. However, in contrast to transition metals that act as electrophiles toward dihydrogen, these carbenes primarily behave as nucleophiles, creating a hydride-like hydrogen, which then attacks the positively polarized carbon center. This nucleophilic behavior allows these carbenes to activate NH_3 as well, a difficult task for transition metals because of the formation of Lewis acid-base adducts.

The activation of enthalpically strong small molecules such as molecular hydrogen (H_2) and ammonia (NH_3) has attracted considerable interest over the years. The first observation of H_2 splitting dates from the end of the 19th century, when Sabatier observed the formation of ethane in the addition of H_2 to ethylene over thin slivers of lightly heated reduced nickel (*1*). Since that time, most of the chemical and biological systems that have been found to split H_2 involve a transition metal center. Even for the so-called iron-sulfur cluster-free hydrogenase (Hmd), it has recently been shown that an iron center was of functional importance (*2*, *3*). The only nonmetallic systems reported to cleave H_2 under mild experimental conditions (*4*–*7*) are phosphine-borane species (*8*, *9*) and a stable digermyne (*10*).

In contrast to dihydrogen, ammonia usually forms simple Lewis acid-base adducts with transition metal complexes, as observed first by Werner in the late 19th century, because of the presence of a lone pair of electrons at nitrogen (*11*). Consequently, examples of NH_3 splitting are still very rare (*12*–*17*).

The activation of H-X and particularly H-H bonds requires that the pair of bonding electrons be perturbed in some way so as to form a chemically active species. The digermyne has substantial diradical character and therefore reacts through H atom abstraction from H_2, followed by recombination of the resultant radical pair (*10*). In contrast, the splitting of H_2 at a transition metal center results from the primary interaction of a vacant orbital at the metal and the σ-bonding orbital of H_2 (*18*–*22*) (Fig. 1). When concomitant back-donation from a filled *d* orbital to the anti-bonding σ* orbital of the bound H_2 is sufficiently strong, homolytic bond cleavage occurs. Otherwise, the acidic η^2-H_2 ligand undergoes proton transfer to another

UCR-CNRS Joint Research Chemistry Laboratory (UMI 2957), Department of Chemistry, University of California, Riverside, CA 92521–0403, USA.

*To whom correspondence should be addressed. E-mail: gbertran@mail.ucr.edu

metal-bound ligand. This latter type of process is often referred to as heterolytic cleavage and is also probably operative for phosphine-borane–containing species (*8*, *9*, *23*).

A singlet carbene has a vacant orbital and a filled nonbonding orbital (*24*, *25*) and in that respect resembles transition metal centers. Although the spatial disposition of a carbene's orbitals is not as ideally suited for interaction with hydrogen as that of a metal, we reasoned that sufficient overlap might still occur and thus enable activation of H_2 (Fig. 1).

Herein we report that stable, singlet, acyclic and cyclic (alkyl)(amino)carbenes **1** (*26*) and **2** (*27*) undergo a formal oxidative addition of H_2. Calculations predict that the transition state results from the primary interaction of the carbene's lone pair of electrons with an H_2 antibonding orbital; thus, the carbene acts as a base toward H_2, creating a hydridelike hydrogen that attacks the positively polarized carbon center. This hypothesis of a nucleophilic activation process is reinforced by observation of the reaction of **1** and **2** with NH_3. Because of the strong nucleophilic character of these carbenes, no "Werner-like" adducts can be formed, and hence N-H bond cleavage occurs smoothly.

It has already been shown that cyclic di(amino)carbenes (NHCs) (*28*, *29*) do not react with H_2 (*30*) nor with CO (*31*), whereas the latter adds to both acyclic and cyclic (alkyl)(amino)carbenes **1** and **2** (*32*). According to our calculations (*33*), the highest occupied molecular orbital (HOMO) and the singlet-triplet gap for the model mono(amino)carbenes (**1′**, **2′**, and **2″**) are slightly higher and significantly smaller in energy, respectively, than those of NHC **3′** and acyclic di(amino)carbene **4′** (Table 1). Consequently, carbenes **1** and **2** are slightly more nucleophilic, but considerably more electrophilic (*34*), than NHCs **3** and are therefore better candidates for transition metal–like behavior. This hypothesis was borne out upon bubbling H_2 through a solution of (alkyl)(amino)carbenes **1** and **2** at 35°C, because clean reactions occurred, and after purification adducts **5** and **6** were obtained in ~30% yield (*35*) as colorless crystals (Fig. 2A). All compounds were fully characterized by standard spectroscopic methods, including a single crystal x-ray diffraction study for **6a** (fig. S1) (*36*). We confirmed that cyclic bis(amino)carbene **3** (*37*) does not react with hydrogen under our experimental conditions and found that the acyclic version **4** (*38*) is similarly inert.

The calculated energy changes (ΔE) (Fig. 4, Table 1, and table S3) show that although the reactions of all carbenes with H_2 are exothermic, the reactions are significantly more favored for mono(amino)carbenes (**1′**, **2′**, and **2″**) than for di(amino)carbenes (**3′** and **4′**). More importantly, the activation energy is at least 40 kJ/mol lower in the case of the mono(amino)carbenes, which readily rationalizes our experimental results.

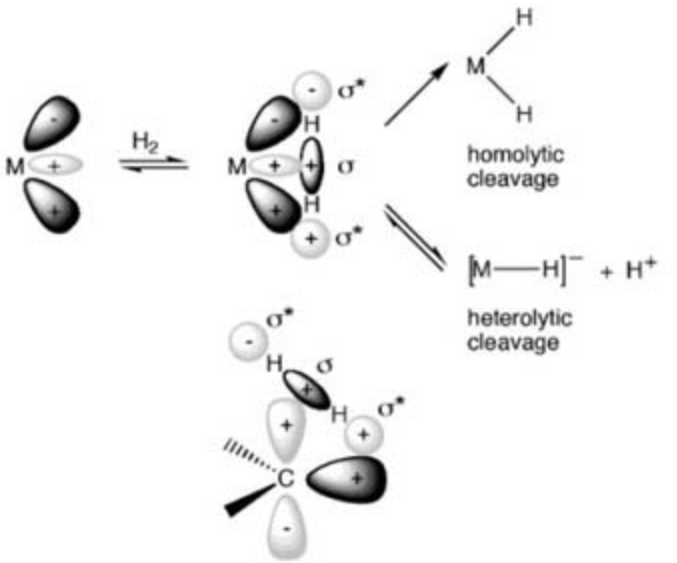

Fig. 1. Schematic representations of modes of activation of H_2 at a transition metal center (**top**) and a hypothetical extrapolation of a similar process at a carbene carbon (**bottom**); filled orbitals are in black, and vacant orbitals in gray.

Table 1. Calculated energy of the HOMO (E_{HOMO}) and singlet-triplet energy gap [$-(E_S - E_T)$] for the model carbenes shown in Fig. 4, as well as energy changes (ΔE) and activation energies ($\Delta E^{\ddagger}$) for their reactions with H_2 and NH_3 calculated at the B3LYP/6-311 g** level of theory.

	1′	2′	2″	3′	4′
E_{HOMO} (eV)	−5.0	−5.0	−4.9	−5.2	−5.1
$-(E_S - E_T)$ (kj/mol)	139.2	193.5	188.9	285.1	214.0
$\Delta E(H_2)$ (kj/mol)	−211.8	−189.4	−180.0	−106.3	−121.0
$\Delta E(H_2)^{\ddagger}$ (kj/mol)	93.0	99.1	108.3	150.0	147.8
$\Delta E(NH_3)$ (kj/mol)	−161.9	−139.3		−70.8	−73.4
$\Delta E(NH_3)^{\ddagger}$ (kj/mol)	87.4	94.5		141.3	137.5

For the addition of H_2 to model compound **2′**, we further calculated the geometric parameters of potential intermediate structures along the reaction pathway (Fig. 2B). According to the lowest energy simulated trajectory, the H_2 molecule approaches the carbene as depicted in Fig. 2B. In the transition state, the H-H bond distance (1.071 Å) is comparable to those found for purely σ-bonded H_2 transition metal complexes (1.0 to 1.2 Å) (compare with the bond distance in H_2 gas of 0.77 Å) (*20*). The H_2 molecule becomes polarized, and the positively charged H (+0.178) is already bonded to the carbon (1.206 Å), whereas the pseudohydridic H (–0.195) remains further away at a distance of 1.924 Å. The H-H bond then elongates further (1.388 Å), engendering greater hydridic character (–0.243) to one of the H atoms, which nonetheless remains distant from the carbon center (1.807 Å). Stereochemical inversion at the carbon center then allows the formation of the second C-H bond. This net process is a hybrid between a homolytic and heterolytic cleavage. However, in contrast to the electrophilic activation and proton transfer pathway favored by transition metal centers, carbenes act by initial nucleophilic activation, followed by hydride transfer.

Because H-H and N-H bond dissociation energies are comparable, the main obstacle for the activation of NH_3 by transition metals is the electrophilicity of the metal, which instead favors the formation of Werner-type amine complexes. Having observed the nucleophilic mode of activation of H_2 by mono(amino) carbenes **1** and **2**, we considered it likely that these carbenes would also activate the N-H bond of ammonia, although it is known that NHCs do not (*39*). Our calculations (Table 1 and table S4) predicted comparable reaction barriers to H_2 activation and a less favored, but still exothermic, driving force. Consistent with these computational results, both carbenes **1** and **2** rapidly react with liquid NH_3, even at –40°C, cleanly affording adducts **7** and **8**, respectively (Fig. 3A). The compounds were isolated in >90% yield, and compound **8b** was crystallographically characterized (Fig. 3B).

The mode of approach of NH_3 to **2′** is calculated to be very similar to that observed with H_2. In the transition state, one of the N-H bonds is very long (1.500 Å) and strongly polarized, with the positively charged H (+0.316) tightly bonded to the carbon (1.155 Å) and the pseudo-amide fragment (–1.042) remaining distant from the carbon center (2.314 Å). Importantly, the nitrogen lone pair is pointing away from the carbene vacant orbital, supporting the nucleophilic character of the activation process (Fig. 3B).

The results reported here show that stable singlet carbenes can mimic to some extent the behavior of transition metals. Like the latter, the electronic properties of carbene centers can be

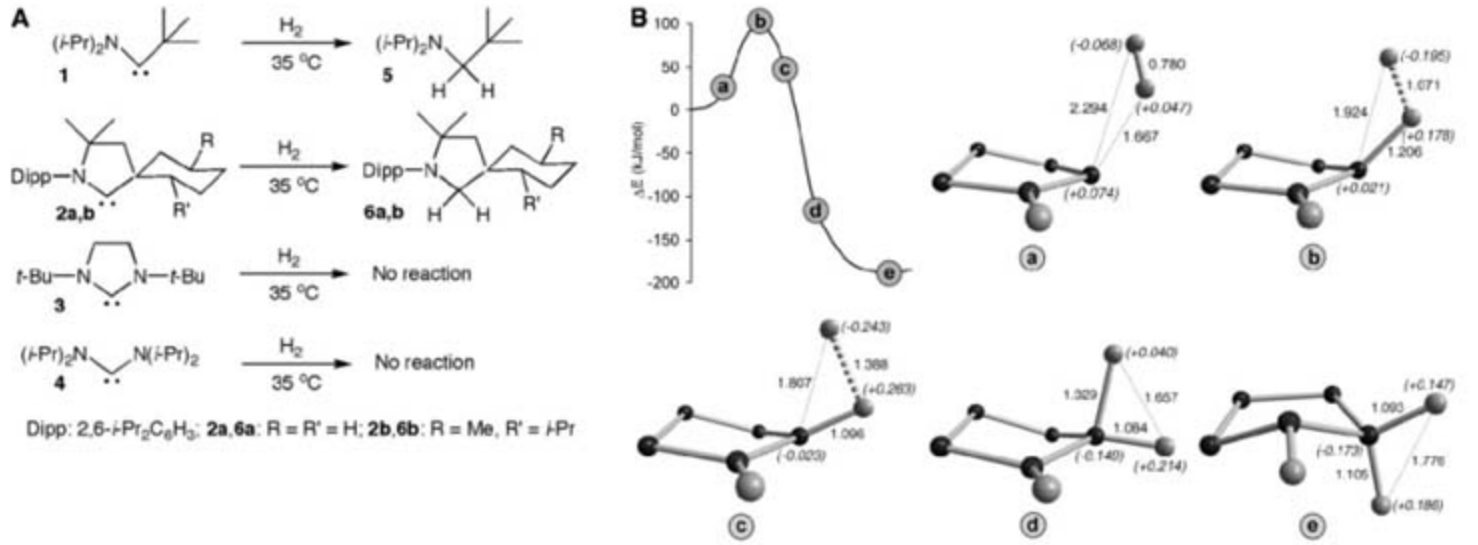

Fig. 2. (**A**) Under mild conditions, (alkyl)(amino)carbenes **1** and **2** activate H_2, whereas (diamino)carbenes **3** and **4** are inert. (**B**) Some structures along the reaction pathway of the insertion of carbene **2'** into H_2, calculated at the B3LYP/6-311 g** level of theory. Bond distances (Å) and charges (in parentheses) are given in the structure drawings, and relative energies are shown in the reaction coordinate diagram.

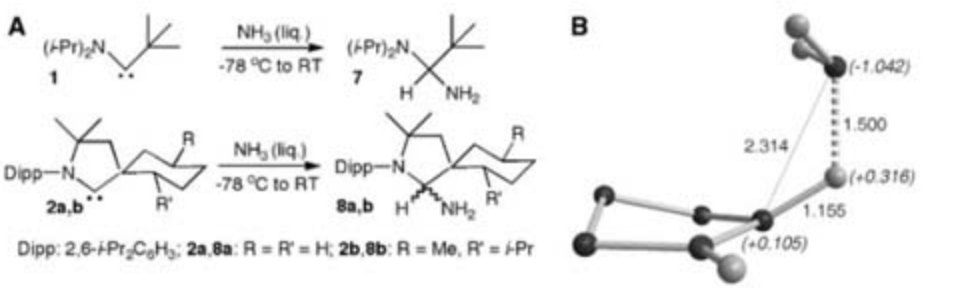

Fig. 3. (**A**) (Alkyl)(amino)carbenes **1** and **2** split ammonia at subzero temperatures. (**B**) Bond distances (Å) and charges (in parentheses) for the transition state of the reaction of NH_3 with carbene **2'**, calculated at the B3LYP/6-311 g** level of theory.

Fig. 4. Model carbenes used for the calculated values shown in Table 1.

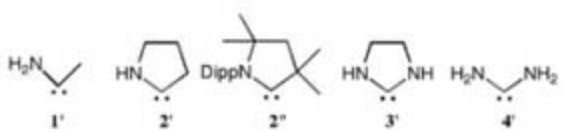

tuned by modifying the nature of the substituents, as shown by the differing reactivities of mono(amino)carbenes and diaminocarbenes with H_2 and NH_3. Moreover, the nucleophilic activation of NH_3, under very mild conditions, offers an alternative paradigm in the continuing search for catalytic systems capable of transforming ammonia efficiently into useful amino compounds.

References and Notes

1. P. Sabatier, *Ind. Eng. Chem.* **18**, 1005 (1926).
2. E. J. Lyon *et al.*, *Eur. J. Biochem.* **271**, 195 (2004).
3. O. Pilak *et al.*, *J. Mol. Biol.* **358**, 798 (2006).
4. A few species, which are only stable in matrices at 10 to 80 K, are also known to split H_2: subvalent group 13 species, (*5*) triplet carbenes (*6*), and the highly electrophilic singlet difluorovinylidene (*7*).
5. H.-J. Himmel, *J. Chem. Soc. Dalton Trans.* **2003**, 3639 (2003).
6. H. Tomioka, in *Reactive Intermediate Chemistry*, R. A. Moss, M. S. Platz, M. Jones Jr., Eds. (Wiley, New York, 2004), pp. 375–461.
7. C. Kötting, W. Sander, *J. Am. Chem. Soc.* **121**, 8891 (1999).
8. G. C. Welch, R. R. San Juan, J. D. Masuda, D. W. Stephan, *Science* **314**, 1124 (2006).
9. G. C. Welch, D. W. Stephan, *J. Am. Chem. Soc.* **129**, 1880 (2007).
10. G. H. Spikes, J. C. Fettinger, P. P. Power, *J. Am. Chem. Soc.* **127**, 12232 (2005).
11. A. Werner, *Z. Anorg. Chem.* **3**, 267 (1893).
12. Y. Nakajima, H. Kameo, H. Suzuki, *Angew. Chem. Int. Ed.* **45**, 950 (2006).
13. J. Zhao, A. S. Goldman, J. F. Hartwig, *Science* **307**, 1080 (2005).
14. E. G. Bryan, B. F. G. Johnson, K. Lewis, *J. Chem. Soc. Dalton Trans.* **1977**, 1328 (1977).
15. G. L. Hillhouse, J. E. Bercaw, *J. Am. Chem. Soc.* **106**, 5472 (1984).
16. A. L. Casalnuovo, J. C. Calabrese, D. Milstein, *Inorg. Chem.* **26**, 941 (1987).
17. M. M. B. Holl, P. T. Wolczanski, G. V. Duyne, *J. Am. Chem. Soc.* **112**, 7989 (1990).
18. G. J. Kubas, R. R. Ryan, B. I. Swanson, P. J. Vergamini, H. J. Wasserman, *J. Am. Chem. Soc.* **106**, 451 (1984).
19. G. J. Kubas, *Adv. Inorg. Chem.* **56**, 127 (2004).
20. G. J. Kubas, *J. Organomet. Chem.* **635**, 37 (2001).
21. G. S. McGrady, G. Guilera, *Chem. Soc. Rev.* **32**, 383 (2003).
22. R. H. Crabtree, *Acc. Chem. Res.* **23**, 95 (1990).
23. G. J. Kubas, *Science* **314**, 1096 (2006).
24. R. A. Moss, M. S. Platz, M. Jones Jr., Eds., *Reactive Intermediate Chemistry* (Wiley, New York, 2004).
25. D. Bourissou, O. Guerret, F. P. Gabbaï, G. Bertrand, *Chem. Rev.* **100**, 39 (2000).
26. V. Lavallo *et al.*, *J. Am. Chem. Soc.* **126**, 8670 (2004).
27. V. Lavallo, Y. Canac, C. Praesang, B. Donnadieu, G. Bertrand, *Angew. Chem. Int. Ed.* **44**, 5705 (2005).
28. A. J. Arduengo III, R. L. Harlow, M. Kline, *J. Am. Chem. Soc.* **113**, 361 (1991).
29. F. E. Hahn, *Angew. Chem. Int. Ed.* **45**, 1348 (2006).
30. M. K. Denk, J. M. Rodezno, S. Gupta, A. J. Lough, *J. Organomet. Chem.* **617–618**, 242 (2001).
31. D. A. Dixon, A. J. Arduengo III, K. D. Dobbs, D. V. Khasnis, *Tetrahedron Lett.* **36**, 645 (1995).
32. V. Lavallo, Y. Canac, B. Donnadieu, W. W. Schoeller, G. Bertrand, *Angew. Chem. Int. Ed.* **45**, 3488 (2006).
33. M. J. Frisch *et al.*, *Gaussian 03* (Gaussian, Wallingford, CT, revision C.02, 2004).
34. In a first approximation, the singlet-triplet energy gap parallels the HOMO-LUMO (lowest unoccupied molecular orbital) splitting.
35. Carbenes **1** and **2** are highly moisture sensitive, and the low yields observed are due to the presence of water in the H_2 gas, which gives rise to the H_2O-carbene adducts.
36. Preparation methods and spectroscopic data for compounds **5**, **6a**, **6b**, **7**, **8a**, and **8b** are available on *Science* Online.
37. A. J. Arduengo III *et al.*, *J. Am. Chem. Soc.* **116**, 6641 (1994).
38. R. W. Alder, P. R. Allen, M. Murray, A. G. Orpen, *Angew. Chem. Int. Ed. Engl.* **35**, 1121 (1996).
39. W. A. Herrmann, M. Elison, J. Fischer, C. Köcher, G. R. J. Artus, *Chem. Eur. J.* **2**, 772 (1996).

40. We are grateful to NSF (grant CHE 0518675) and RHODIA for financial support of this work, the University of Bielefeld for computer facilities, the Alexander von Humboldt Foundation for a fellowship (G.D.F.), and A. J. Arduengo for helpful discussions. Metrical data for the solid state structures of **6a** and **8b** are available free of charge from the Cambridge Crystallographic Data Centre under reference numbers CCDC-637184 and CCDC-637185, respectively.

Supporting Online Material

www.sciencemag.org/cgi/content/full/316/5823/439/DC1
Materials and Methods
Figs. S1 and S2
Tables S1 to S4
References and Notes

20 February 2007; accepted 13 March 2007
10.1126/science.1141474

The Variable Rotation Period of the Inner Region of Saturn's Plasma Disk

D. A. Gurnett,[1] A. M. Persoon,[1] W. S. Kurth,[1] J. B. Groene,[1] T. F. Averkamp,[1] M. K. Dougherty,[2] D. J. Southwood[2,3]

We show that the plasma and magnetic fields in the inner region of Saturn's plasma disk rotate in synchronism with the time-variable modulation period of Saturn's kilometric radio emission. This relation suggests that the radio modulation has its origins in the inner region of the plasma disk, most likely from a centrifugally driven convective instability and an associated plasma outflow that slowly slips in phase relative to Saturn's internal rotation. The slippage rate is determined by the electrodynamic coupling of the plasma disk to Saturn and by the drag force exerted by its interaction with the Enceladus neutral gas torus.

Because Saturn is a giant gaseous planet, its internal rotation period cannot be accurately determined from visual observations. Although it has been long accepted that the magnetic dipole axis of Saturn is aligned almost exactly with its rotational axis (*1*, *2*), various magnetospheric phenomena display rotational modulation effects near its nominal rotation period (*3*–*5*). Of these, the most thoroughly studied is Saturn kilometric radiation (SKR), which is an intense radio emission discovered during the 1980–1981 Voyager flybys of Saturn (*3*). The SKR modulation period was determined by Voyager to be 10 hours, 39 min, 24 ± 7s (*6*). This value is now the internationally accepted rotation period of Saturn (*7*). More recently, radio measurements from the Ulysses and Cassini spacecraft (*8*–*10*) have shown that the SKR modulation period varies by as much as 1% on time scales of years. Because of its large inertia, the internal rotation period cannot possibly have changed by such a large amount. How then is the SKR period related to the rotation period of the interior of Saturn? In this paper we show that the SKR modulation is directly linked to the rotational modulation of plasma and magnetic fields in the inner region of Saturn's plasma disk, near the moon Enceladus, which orbits Saturn at 3.95 Saturn radii (R_S) (1 Saturn radius = 60,268 km). We propose that the rotational modulation is caused by a centrifugally driven two-cell convective instability in the plasma disk that originates from its interaction with the neutral gas torus produced by Enceladus. This instability causes a rotating plasma outflow that imposes rotational control on other processes farther out in the magnetosphere, such as the generation of SKR.

Saturn's plasma disk, sometimes also called the plasma sheet or plasmasphere, is a dense corotating plasma with a north-south thickness of about 1 to 2 R_S that extends outward into the magnetosphere from near the outer edge of the A ring (*11*, *12*). The co-rotation is caused by electromagnetic forces imposed by currents that flow along the highly conducting magnetic field lines between the plasma disk and the upper atmosphere of Saturn. Most of the plasma in the plasma disk is believed to originate from ionization of a torus of neutral gas that is present near the orbit of Enceladus. This torus originates from geyserlike plumes of water on Enceladus that inject water vapor and ice particles into orbit around Saturn (*13*–*15*). Because of the rapid rotation of the plasma disk, the centrifugal force at these radial distances is substantially larger than Saturn's gravitational force. Interchange motions driven by the centrifugal force then act to transport the plasma outward into the magnetosphere. Because the plasma particles are constrained by electromagnetic forces to move approximately along magnetic field lines, the centrifugal force also acts to concentrate the plasma near the equatorial plane, thereby forming the disklike structure.

The data used in this study are from the Radio and Plasma Wave Science (RPWS) and Magnetometer (MAG) instruments on the Cassini spacecraft, which is in orbit around Saturn. In an earlier study (*16*) using electron density measurements from the RPWS, we noticed that in the vicinity of Enceladus' orbit, from about 3 to 5 R_S, the electron density is often quite different on the inbound and outbound portions of the same pass (Fig. 1). This variability was initially thought to be attributable to the spacecraft position relative to Enceladus, but further study showed that it was not so. Instead, using the time-variable SKR longitude system introduced by Kurth *et al.* (*17*), we found (Fig. 2) that the electron density in the inner region of the plasma disk has a nearly sinusoidal variation with SKR longitude and that this variation is in phase with a similar nearly sinusoidal variation in the azimuthal, B_φ, component of the magnetic field in the plasma disk. This relation strongly suggests that the plasma density and magnetic field in the inner region of the plasma disk have a rotational control that is directly linked to the time-variable period of the SKR modulation.

By itself, a sinusoidal longitude variation does not provide proof of rotational control, even though the longitude is measured relative to a rotating reference. To demonstrate rotational control, it is essential that measurements be made over a range of local times in order to confirm that the longitude is the controlling variable. Fortunately, the orbit of Cassini provides good local-time coverage and longitude coverage of both the magnetic field and the electron density (figs. S1 and S2). A simple test can then be performed to confirm rotational control. This test consists of plotting the measured quantities as a function of the longitude relative to some fixed direction, such as the Sun. This test shows that the amplitude of the modulation decreases and the spread of the data points relative to the best fit increases significantly (compare Fig. 2, B and C, with fig. S4, B and C), thereby providing convincing evidence that both the magnetic field and the

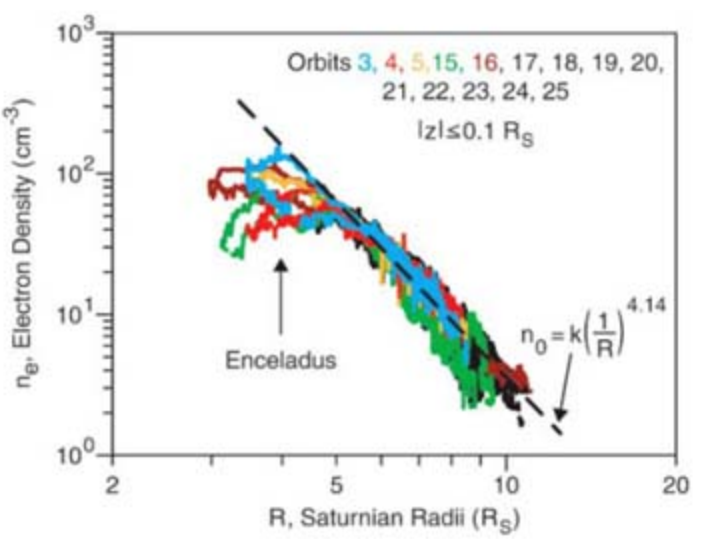

Fig. 1. The electron density n_e obtained from Cassini RPWS upper hybrid resonance measurements (*20*) for 14 equatorial orbits from 1 July 2004 to 1 July 2006. The dashed line is a power-law fit to the region beyond 5 R_S, and $k = 5.5 \times 10^4$ cm^{-3} $R_S^{4.14}$ is the constant in the power law. Only equatorial orbits with a north-south distance z from the equatorial plane less than 0.1 R_S were used in this study. There are large variations from the power-law fit in the region from 3 to 5 R_S. By following the colored line for a given orbit, one can see that the electron densities for the inbound and outbound portions of the same pass are often quite different. This hysteresis-like dependence on radial distance strongly suggests a longitudinal control.

[1]Department of Physics and Astronomy, University of Iowa, Iowa City, IA 52242, USA. [2]Blackett Laboratory, Imperial College, London SW7 2AZ, UK. [3]European Space Agency, 75738 Paris, France.

plasma density in the inner region of the plasma disk rotate at a rate that is synchronous with the time-variable SKR modulation. For other factors that could affect this interpretation, such as aliasing due to data gaps, and for an analysis of the slow long-term time variations in the rotation rate, see the supporting online material (SOM).

The occurrence of a large rotational modulation of the plasma and magnetic fields deep in the inner region of the magnetosphere that is phase-locked to the time-variable SKR modulation is surprising. Most of the rotational effects that have previously been reported occur much farther out in the magnetosphere. That the density modulation occurs near the orbit of Enceladus strongly suggests that the rotational effects observed farther out in the magnetosphere are driven by some rotational process that involves an interaction with the Enceladus neutral gas torus. This conclusion is consistent with the view that the general direction of energy flow should be outward, away from the source of the plasma and in the direction of the centrifugal force. In fact, this direction for the propagation of rotational disturbances has already been suggested and is the basis for the "camshaft" model proposed by Espinosa *et al.* (*4*). In this model, an unspecified rotating disturbance, the "cam," as in the camshaft of an engine, produces plasma and magnetic field disturbances that propagate outward into the magnetosphere. Here we propose that the newly discovered rotational density modulation in the inner region of the plasma disk acts as the cam that drives other rotationally modulated effects farther out in the magnetosphere. The main questions that remain are how are these rotational effects produced in the inner region of the magnetosphere, and how does the rotation rate relate to the internal rotation of Saturn?

Because there is presently no accepted mechanism for imposing a time-variable rotation rate from a source internal to Saturn, we proceed by exploring the possibility that the time variability arises entirely within the plasma disk. It is already widely accepted (*18*, *19*) that the rotation of the plasma disk is due to forces produced by field-aligned currents that link the plasma disk to Saturn (Fig. 3A). A very natural explanation for the time-variable rotation rate is then that the plasma disk slips at a time-variable rate relative to the upper atmosphere of Saturn, which is where the coupling to the planet takes place. The mechanism for driving this slippage could then be ionization and charge exchange in the neutral gas torus, both of which produce a drag force that opposes the rotation of the plasma disk. This process is called mass loading (*19*). In this model, the slippage rate is determined by the rate dm/dt (m, mass; t, time) at which mass is picked up by the plasma disk, and by the conductivity of the upper atmosphere, which controls the field-aligned currents that link the plasma disk to the planet. Because the ejection of mass from Enceladus probably has long-term variations that affect the density of the neutral gas torus, this model provides a ready explanation for the somewhat irregular long-term variations in the SKR modulation period (*9*). It is already known that the Enceladus neutral gas torus has variations on time scales of months (*20*), so variations on much longer time scales are highly likely. Another possible long-term effect that could cause changes in the rotation rate of the plasma disk is the seasonal variation of the solar inclination angle, which affects the conductivity of the upper atmosphere and thereby the coupling to the planet.

To proceed further, we must next explain how the density modulation is produced in the inner region of the plasma disk. A possible model is motivated by the two-cell convection mechanism suggested by Dessler *et al.* (*21*), which was originally proposed to explain rotational effects in the magnetosphere of Jupiter and was also suggested to apply to Saturn by Hill *et al.* (*22*). In our adaptation of this model (Fig. 3B), the two-cell convection pattern has its origin as a centrifugally driven instability in the plasma disk (*23*) near the orbit of Enceladus. Such convective instabilities are well known in laboratory plasma machines. As the plasma flows around the convection cycle (indicated by the closed streamlines in Fig. 3B), it picks up newly ionized plasma as it passes through the neutral gas torus (along the path from a to b in Fig. 3B), thereby increasing the plasma density. It is this density increase that accounts for the longitudinal density variations observed in the inner region of the plasma disk. The density increase also ensures that the centrifugal force, $F_c = nm\omega^2 R$, where n is the plasma number density, m is the molecular mass, ω is the rotation rate, and R is the radial distance, at point $F_c(2)$ is higher than at a symmetrically located point $F_c(1)$. It is this difference in the centrifugal forces that drives the convection. From the ionization rate given by Hansen *et al.* (*24*) for the neutral gas torus, 8.7×10^{-5} cm^{-3} s^{-1}, we estimate that it takes about a week to produce the observed ~50 cm^{-3} peak-to-peak density variation as the plasma flows through the neutral gas torus.

Most previous models of centrifugally driven convection suggest that the convective motions should be dominated by high-order, $m \gg 1$, azimuthal modes that evolve into fingerlike azimuthal structures (*25*, *26*). However, these models do not consider the process by which the plasma is produced. For an azimuthally symmetric plasma source, such as the Enceladus neutral gas torus, we believe that the lowest-order $m = 1$ (two-cell) mode should dominate, because this mode produces the longest path length through the source region, thereby giving the largest density increase and the largest growth rate for the instability. Because there is a continuous production of plasma from the torus, in a steady state there must be a corresponding outflow of plasma from the plasma disk into the outer re-

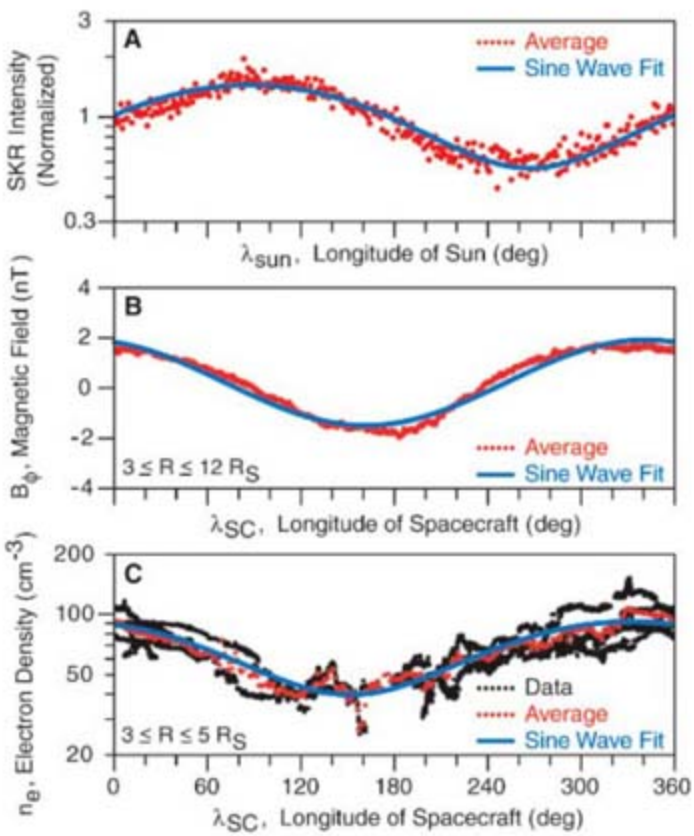

Fig. 2. (**A**) The normalized SKR intensity as a function of the longitude of the Sun, λ_{Sun}, using the time-variable SKR longitude system introduced by Kurth *et al.* (*17*). The longitude of the Sun is used in this plot because the SKR modulation is known to be a purely temporal variation (*29*), like a flashing light, not a rotating beacon. The characteristic nearly sinusoidal modulation of the SKR intensity is clearly apparent. (**B**) The average azimuthal B_ϕ component of the magnetic field in the plasma disk (3 to 12 R_S) as a function of the SKR longitude of the spacecraft λ_{SC}. λ_{SC} is used because we anticipated that the magnetic field would have a rotational control, as has been assumed by other authors (*4*). As can be seen, the magnetic field displays a very clear, nearly sinusoidal dependence on λ_{SC}. (**C**) The electron density as a function of λ_{SC}, where again we anticipated a possible rotational control. The radial distance range in this case has been limited to the inner region of the plasma disk (3 to 5 R_S), because this is the region where the electron density variations are the largest (Fig. 1). A very clear, nearly sinusoidal modulation is evident, with an amplitude variation of nearly a factor of 2 and a phase at the peak (λ_{SC} ~ 330°) that is almost the same as for the magnetic field.

gions of the magnetosphere. The two-cell convection would then cause a concentration of the outflowing plasma on the dense side of the convection pattern (Fig. 3B); that is, at an SKR longitude of $\lambda_{SC} \sim 330°$. As the convection pattern rotates, this outflow would produce perturbations that propagate far out into the magnetosphere, thereby acting as the cam that drives other rotationally modulated magnetospheric effects, such as the SKR. From the Voyager 1 and 2 radio observations (*27*), it is known that SKR is generated at relatively low altitudes along magnetic field lines that pass near the magnetopause on the late-morning side of the magnetosphere. As the perturbations from $\lambda_{SC} \sim 330°$ propagate outward, the associated magnetic field perturbations (fig. S3) develop a phase lag of about 149° to 195° by the time they reach the vicinity of the magnetopause at $R \sim 20\ R_S$. This phase lag, which has been previously studied by Espinosa *et al.* (*4*) and Cowley *et al.* (*28*), is almost exactly the right amount to explain the generation of SKR in the late morning at a local time of about 8 to 11 hours and a subsolar SKR longitude of $\lambda_{Sun} = 100°$. For a further discussion of the geometry involved and for comments on how the SKR might be generated as the outward-propagating disturbance from the cam interacts with the morning side of the magnetopause, see the SOM.

A potentially important feature of the convection pattern that needs to be explained is the close relation between the phase of the azimuthal magnetic field and the phase of plasma density modulation (Fig. 2, B and C). This relation is most likely related to the azimuthal torque required to oppose the change in the angular momentum of the plasma disk caused by the mass loading. Because both ionization and charge exchange are proportional to the plasma density, they both contribute to the mass loading. The current system that produces this torque and the resulting contribution to the B_φ magnetic field are then expected to be largest in the region of highest plasma density, which would explain why these two quantities are in phase. However, the relation between the magnetic field and the plasma density variations may be more subtle. If the current systems linking the plasma sheet to the northern and southern hemispheres are identical, then there would be no B_φ magnetic field component at the equator. The equatorial B_φ component would then have to be due to an asymmetry between northern and southern hemispheres. The asymmetry could be produced by the fact that the net dayside conductivity of the southern hemisphere of Saturn is currently higher than in the northern hemisphere, not only because high southerly latitudes are currently in sunlight but also because the rings are partially shadowing the northern hemisphere. This north-south difference in the illumination greatly increases the conductivity of the upper atmosphere in the southern hemisphere relative to that in the northern hemisphere. The immediate consequence of this difference is that interchange motion would be resisted more by the southern ionosphere (*23*). In the high-density sector where flux tubes would move out, the northern ionosphere has to transmit a poleward motion to the southern ionosphere and vice versa in the inward-moving sector. This asymmetry would require a significant transverse magnetic field component at the equator. A quarter-cycle lag is expected between outward motion and the peak bending inward of the field (that is, a peak negative value of the radial field perturbation, ΔB_r). Recalling the phase relation originally identified by Espinosa *et al.* (*4*) (that ΔB_r leads B_φ), one sees that the observed phase relation between B_φ and n_e (n_e, electron density) is consistent.

Because our model is based on a centrifugally driven instability in the plasma disk that acts as a camshaft, it does not necessarily require a rotating magnetic anomaly or any other rotating source internal to Saturn. Therefore, the internal rotation period of Saturn cannot be determined from the period of the SKR modulation. The only conclusion that can be drawn is that the internal rotation period must be less than the shortest SKR modulation period ever observed, which currently is slightly less than the period observed by Voyager (*9*). If some internal source with the correct time-variable rotation rate were to be eventually identified, it is clear that any new explanation would need to account for the rotating plasma density and magnetic fields reported in this paper, as well as their linkage to the time-variable SKR modulation rate.

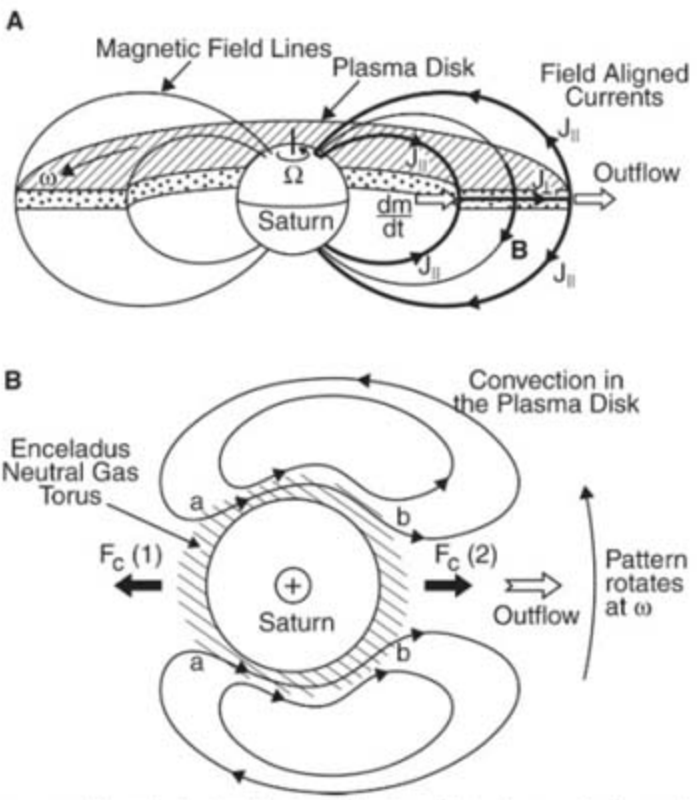

Fig. 3. (**A**), adapted from Hill (*18*), shows the mechanism by which the plasma disk is coupled to the upper atmosphere of Saturn via magnetic field–aligned currents, $\mathbf{J}_\parallel$. The field-aligned currents transfer angular momentum from the planet to the plasma disk via the $\mathbf{J}_\perp \times \mathbf{B}$ force exerted, where $\mathbf{J}_\perp$ is the component of current flowing perpendicular to the magnetic field **B**. This force opposes the drag force exerted on the disk as mass produced by ionization and charge exchange from the Enceladus gas torus is picked up by the rapidly rotating magnetic field. This drag force causes the plasma disk, which rotates at an angular rate ω, to slip slowly with respect to the rotation rate Ω of the upper atmosphere of Saturn. (**B**) The rotating two-cell plasma convection pattern that we propose to explain the longitudinal modulation of the plasma density and magnetic field in the inner region of the plasma disk. In this model, the two-cell convection pattern, shown as viewed from the north pole of Saturn, is driven by a centrifugal instability that arises from ionization of the neutral gas torus. As the plasma flows through the neutral gas torus from a to b, the density increases because of this ionization, causing the centrifugal force $F_c = nm\omega^2 R$ at $F_c(2)$ to be greater than at the symmetrical point $F_c(1)$ on the opposite side of the convection pattern. It is this difference in the centrifugal forces that drives the convection. A radial outflow of plasma in the "heavy" sector of the convection pattern then acts as the cam (*4*) that drives the rotational modulation of various phenomena in the outer magnetosphere, such as the SKR. The slippage rate, and therefore the SKR modulation period, are determined by the mass loading rate *dm/dt* from the neutral gas torus and by the coupling to the upper atmosphere, both of which are likely to have long-term variations.

References and Notes

1. E. J. Smith *et al.*, *Science* **207**, 407 (1980).
2. J. E. P. Connerney, L. Davis Jr., D. L. Chenette, in *Saturn*, T. Gehrels, M. S. Matthews, Eds. (Univ. of Arizona Press, Tucson, AZ, 1984), pp. 354–377.
3. J. W. Warwick *et al.*, *Science* **212**, 239 (1981).
4. S. A. Espinosa, D. J. Southwood, M. K. Dougherty, *J. Geophys. Res.* **108**, 1086 (2003).
5. G. Giampieri, M. K. Dougherty, E. J. Smith, C. T. Russell, *Nature* **441**, 62 (2006).
6. M. D. Desch, M. L. Kaiser, *Geophys. Res. Lett.* **8**, 253 (1981).
7. M. E. Davies *et al.*, *Cel. Mech. Dyn. Astron.* **63**, 127 (1996).
8. A. Lecacheux, P. Galopeau, M. Aubier, *Planetary Radio Emissions IV*, H. O. Rucker, S. J. Bauer, A. Lecacheux, Eds. (Austrian Academy of Sciences Press, Vienna, 1997).
9. P. H. M. Galopeau, A. Lecacheux, *J. Geophys. Res.* **105**, 13089 (2000).
10. D. A. Gurnett *et al.*, *Science* **307**, 1255 (2005).
11. D. T. Young *et al.*, *Science* **307**, 1262 (2005).
12. H. S. Bridge *et al.*, *Science* **212**, 217 (1981).
13. C. C. Porco *et al.*, *Science* **311**, 1393 (2006).
14. M. K. Dougherty *et al.*, *Science* **311**, 1406 (2006).
15. J. H. Waite Jr. *et al.*, *Science* **311**, 1419 (2006).

16. A. M. Persoon *et al.*, *Geophys. Res. Lett.* **32**, L23105 (2005).
17. W. S. Kurth, A. Lecacheux, T. F. Averkamp, J. B. Groene, D. A. Gurnett, *Geophys. Res. Lett.* **34**, L02201 (2007).
18. T. W. Hill, *J. Geophys. Res.* **84**, 6554 (1979).
19. A. Eviatar, R. L. McNutt Jr., G. L. Siscoe, J. D. Sullivan, *J. Geophys. Res.* **88**, 823 (1983).
20. L. W. Esposito *et al.*, *Science* **307**, 1251 (2005).
21. A. J. Dessler, R. R. Sandel, S. K. Atreya, *Planet. Space Sci.* **29**, 215 (1981).
22. T. W. Hill, A. J. Dessler, L. J. Maher, *J. Geophys. Res.* **86**, 9020 (1981).
23. D. J. Southwood, M. G. Kivelson, *J. Geophys. Res.* **94**, 299 (1989).
24. K. C. Hansen *et al.*, *Geophys. Res. Lett.* **32**, L20S06 (2005).
25. G. L. Siscoe, D. Summers, *J. Geophys. Res.* **86**, 8471 (1981).
26. Y. S. Yang, R. A. Wolf, R. W. Spiro, T. W. Hill, A. J. Dessler, *J. Geophys. Res.* **99**, 8755 (1994).
27. P. Zarka, *J. Geophys. Res.* **103**, 20, 159–20, 194 (1998).
28. S. W. H. Cowley *et al.*, *Geophys. Res. Lett.* **33**, L07104 (2006).
29. M. L. Kaiser *et al.*, in *Saturn*, T. Gehrels, M. S. Matthews, Eds. (Univ. of Arizona Press, Tucson, AZ, 1984), pp. 378–415.

30. The research at the University of Iowa was supported by NASA through contract 1279973 with the Jet Propulsion Laboratory.

Supporting Online Material

www.sciencemag.org/cgi/content/full/1138562/DC1
SOM Text
Figs. S1 to S8
References

7 December 2006; accepted 7 March 2007
Published online 22 March 2007;
10.1126/science.1138562
Include this information when citing this paper.

Strong Association of De Novo Copy Number Mutations with Autism

Jonathan Sebat,[1*] B. Lakshmi,[1] Dheeraj Malhotra,[1*] Jennifer Troge,[1*] Christa Lese-Martin,[2] Tom Walsh,[3] Boris Yamrom,[1] Seungtai Yoon,[1] Alex Krasnitz,[1] Jude Kendall,[1] Anthony Leotta,[1] Deepa Pai,[1] Ray Zhang,[1] Yoon-Ha Lee,[1] James Hicks,[1] Sarah J. Spence,[4] Annette T. Lee,[5] Kaija Puura,[6] Terho Lehtimäki,[7] David Ledbetter,[2] Peter K. Gregersen,[5] Joel Bregman,[8] James S. Sutcliffe,[9] Vaidehi Jobanputra,[10] Wendy Chung,[10] Dorothy Warburton,[10] Mary-Claire King,[3] David Skuse,[11] Daniel H. Geschwind,[12] T. Conrad Gilliam,[13] Kenny Ye,[14] Michael Wigler[1]†

We tested the hypothesis that de novo copy number variation (CNV) is associated with autism spectrum disorders (ASDs). We performed comparative genomic hybridization (CGH) on the genomic DNA of patients and unaffected subjects to detect copy number variants not present in their respective parents. Candidate genomic regions were validated by higher-resolution CGH, paternity testing, cytogenetics, fluorescence in situ hybridization, and microsatellite genotyping. Confirmed de novo CNVs were significantly associated with autism ($P = 0.0005$). Such CNVs were identified in 12 out of 118 (10%) of patients with sporadic autism, in 2 out of 77 (3%) of patients with an affected first-degree relative, and in 2 out of 196 (1%) of controls. Most de novo CNVs were smaller than microscopic resolution. Affected genomic regions were highly heterogeneous and included mutations of single genes. These findings establish de novo germline mutation as a more significant risk factor for ASD than previously recognized.

Autism spectrum disorders (ASDs) [Mendelian Inheritance in Man (MIM) 209850] are characterized by language impairments, social deficits, and repetitive behaviors. The onset of symptoms occurs by the age of 3 and usually requires extensive support for the lifetime of the afflicted. The prevalence of ASD is estimated to be 1 in 166 (*1*), making it a major burden to society.

Genetics plays a major role in the etiology of autism. The concordance rates in monozygotic twins are 70% for autism and 90% for ASD, whereas the concordance rates in dizygotic twins are 5% and 10%, respectively. Previous studies suggest autism displays a high degree of genetic heterogeneity. Efforts to map disease genes using linkage analysis have found evidence for autism loci on 20 different chromosomes. Regions implicated by multiple studies include 1p, 5q, 7q, 15q, 16p, 17q, 19p, and Xq (*2*). Moreover, microscopy studies have identified cytogenetic abnormalities in >5% of affected children, involving many different loci on all chromosomes (*3*). In some rare syndromic forms of autism, such as Rett syndrome (*4*) and tuberous sclerosis (*5*), mutations in a single gene have been identified. Otherwise, neither linkage nor cytogenetics has unambiguously identified specific genes involved.

Genetic heterogeneity poses a considerable challenge to traditional approaches for gene mapping (*6*). Some of these limitations are overcome by methods that rely on the direct detection of functional variants, which in most cases are de novo events. New array-based technologies can detect differences in DNA copy number at much higher resolution than cytogenetic methods (*7*) and, hence, might reveal spontaneous mutations that were previously unidentified. These techniques have shown an abundance of copy number variants (CNVs) in humans (*8*, *9*), and the same methods have been used to find de novo chromosome aberrations below the resolution of microscopy in children with mental retardation and dysmorphic features (*10*–*14*), including patients with syndromic forms of autism (*15*). Yet, the association of spontaneous CNVs in idiopathic autism has not been systematically investigated. Thus, a large-scale study of genome copy number variation in ASD was needed. We have performed high-resolution genomic microarray analysis on a sample of 264 families to determine the rate of de novo copy number mutation in unaffected and affected children.

Our study focused on a sample of 264 families, including 118 "simplex" families containing a single child with autism, 47 "multiplex" families with multiple affected siblings, and 99 control families with no diagnoses of autism. The majority of patients came from the Autism Genetic Resource Exchange (AGRE) and from the National Institute of Mental Health (NIMH) Center for Collaborative Genetic Studies of Mental Disorders. Additional families were obtained through the authors (T.C.G., J.S.S., J.B., and D.S). Efforts were made at all of the collecting sites to exclude cases of syndromic autism (i.e., those with severe mental retardation or other congenital anomalies) and to exclude known cytogenetic abnormalities. Identities of all subjects and their parents were coded so that analysis could be done blind to affected status while maintaining knowledge of

[1]Cold Spring Harbor Laboratory, 1 Bungtown Road, Cold Spring Harbor, NY 11724, USA. [2]Department of Human Genetics, Emory University School of Medicine, Atlanta, GA 30322, USA. [3]Department of Medicine and Genome Sciences, University of Washington, Seattle, WA 98195–7720, USA. [4]Pediatrics and Neurodevelopmental Psychiatry Branch, National Institute of Mental Health, National Institutes of Health, Bethesda, MD 20892–1255, USA. [5]Feinstein Institute for Medical Research, North Shore–Long Island Jewish Health System, Manhasset, NY 11030, USA. [6]Department of Child Psychiatry, University of Tampere, Medical School, Tampere, Finland. [7]Department of Clinical Chemistry, University Hospital of Tampere and University of Tampere, Medical School, Tampere, Finland. [8]Fay J. Lindner Center for Autism and Developmental Disorders, North Shore–Long Island Jewish Health System, 4300 Hempstead Turnpike, Bethpage, NY 11714, USA. [9]Center for Molecular Neuroscience, Vanderbilt University, Nashville, TN 37232–8548, USA. [10]Departments of Genetics and Development, and Pediatrics, Columbia University, New York, NY 10027, USA. [11]Behavioural and Brain Sciences Unit, Institute of Child Health, University College London, 30 Guilford Street, London WCIN 1EH, UK. [12]Interdepartmental Program in the Neurosciences, Program in Neurogenetics, Neurology Department, David Geffen School of Medicine, University of California at Los Angeles, Los Angeles, CA 90095–1769, USA. [13]Department of Human Genetics, The University of Chicago, 920 East 58th Street, Chicago, IL 60637, USA. [14]Department of Epidemiology and Population Health, Albert Einstein College of Medicine, Bronx, NY 10461, USA.

*These authors contributed equally to this work.
†To whom correspondence should be addressed. E-mail: sebat@cshl.edu (J.S.); wigler@cshl.edu (M.W.)

the parent-child relations. We performed whole-genome scans on all parents, patients, and unaffected children. Affected or unaffected siblings of many patients were included in the study as independent cases or controls, respectively; thus, the entire sample yielded a complete parent-child "trio" for each of 195 patients and 196 healthy individuals. (See supplementary methods and table S1 for more extensive details on the patient sample.)

We analyzed DNA samples, prepared from either whole blood or Epstein-Barr virus (EBV) immortalized B cells or both, collected from subjects and their biological parents. Genome scans were performed by ROMA, a form of comparative genomic hybridization described previously (*8*, *16*). We performed two-color assays by cohybridizing each sample to an oligonucleotide array, and we used a standard reference genome, SKN1, for comparison. Assays were performed in duplicate with dye-swap. The array consisted of 85,000 probes, providing a mean resolution of one probe every 35 kb. Log intensity ratios from duplicate scans were averaged, and normalized ratio data were segmented by a Hidden Markov Model to define CNVs relative to reference (*8*) (with minor modifications).

Detecting copy number variation from array data is an error-prone process, and so procedures were followed to ensure that events we detected in subjects were in fact de novo: not false-positive in the subject, and not false-negative in either biological parent. A flow chart of our procedure for finding and testing de novo mutations is depicted in Fig. 1. CNV regions detected in subjects were considered only if they involved at least three consecutive probes and had an overall likelihood measure >0.9 (*8*). Then, CNVs were disregarded if they were 60% similar in probe content to a variant detected in the set of all parents, where similarity between two CNVs is defined as (the number of common probes)/(the total number of probes in either CNV). This step was done in order to simultaneously filter out any CNVs present in the biological parents and to eliminate common polymorphic loci that would incorrectly appear to be de novo. The latter can occur, for example, when the parents and the reference are all heterozygous for a deletion and 0 or 2 copies are transmitted to the child. These two procedures greatly reduce the total number of candidates requiring validation.

We then further examined each candidate variant by a more careful assessment of the parents for the presence of the CNV, using a relaxed set of criteria for its presence (see legend to Fig. 2), to rule out false-negatives. If at that point the variant in the subject still appeared to be de novo, that is, present in the child but not in either parent, we tested parentage using multiple informative genetic markers. We then conducted additional validation of the suspect de novo lesion in parents and subjects, including Dpn II–ROMA using 390K arrays, CGH using Agilent 244K arrays, cytogenetics, and microsatellite genotyping. When de novo mutations were detected in DNA derived from an EBV-immortalized cell line, we sought to repeat analysis on DNA derived from an independent blood sample and found confirmation in 11 out of 12 available cases.

One example of the detection and confirmation of a de novo CNV is illustrated in Fig. 2. We detected a 1.1-Mb deletion of 20p13 in a child with the diagnosis of Asperger syndrome. This deletion involves ~27 genes, including the oxytocin gene *OXT*, a particularly noteworthy candidate in light of studies in humans and rodents that find evidence for the role of oxytocin in regulating social cognition (*17*, *18*). All validated de novo subject variants are listed in Table 1 with a description of each type of mutation, its methods of validation, genomic location, gene content, and information on the subject's affected status and family type (simplex, multiplex, or control). Additional details regarding these and other variants detected in this study are provided in table S2. Initially, we detected 19 de novo CNVs in 17 individuals. In one family, subsequent analysis of the parental chromosomes by fluorescence in situ hybridization (FISH) determined that the two de novo events detected (a duplication and deletion) were the result of an unbalanced translocation inherited from an unaffected father who carries the balanced reciprocal translocation. In conclusion, 17 CNVs were confirmed to be de novo in 16 individuals (Table 1), consisting of 14 patients and 2 controls. The majority of these mutations are novel, and only the largest of them (all CNVs >4 Mb in size) have been reported previously in the literature (*19*–*21*).

These data show that spontaneous copy number changes are more frequent in patients

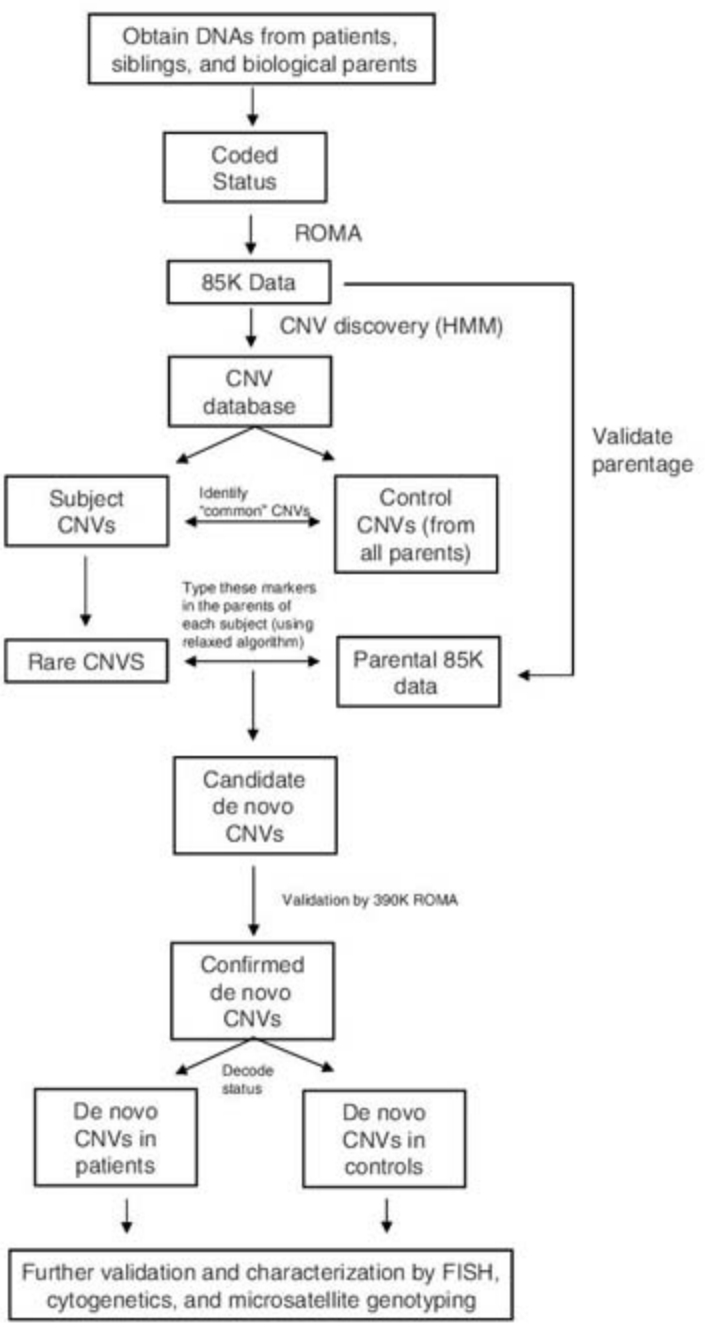

Fig. 1. Procedure for the detection of de novo CNVs. The flow diagram describes the step-by-step procedure for identifying regions of altered copy number that are present in a child and not in the biological parents.

with ASD (14 out of 195) than in unaffected individuals (2 out of 196), with an association that is statistically significant ($P = 0.0005$). The frequency of spontaneous mutation was 10% (12 out of 118) in our sample of sporadic cases and 3% (2 out of 77) in our sample of cases from multiplex families (Table 2). The frequency of spontaneous mutation in unaffected individuals was 1% (2 out of 196). Most mutations in persons with autism were deletions (12 out of 15); however, the two mutations detected in controls were both duplications.

The strong association of de novo CNVs with ASD is consistent with such mutations being a primary cause in most cases rather than merely contributory. A further line of evidence to support this claim is the higher proportion of females among cases with de novo mutations, where the genders of patients consisted of 9 males and 5 females (1.8:1) compared with 163 males and 32 females (5:1) in our overall sample. This reduced gender ratio suggests that de novo CNVs that are detectable by our method have increased penetrance and, thus, contribute to disease more equally in females and males.

A lower rate of de novo mutation in multiplex families is also consistent with a causal role for the mutations reported in this study. An alternative hypothesis is that de novo CNVs are associated with autism indirectly, the consequence of a "fragile-genome disorder" in which many lesions in addition to the ones we detected occur due to an unknown environmental or heritable factor. We regard this alternative as unlikely; first, because we would expect evidence for such a disorder to be present equally in multiplex or simplex families. Another observation that is inconsistent with this alternative hypothesis is that we do not see patients with copy number mutations littered throughout the genome. Instead, de novo CNVs typically involve a single mutational event.

Two of the patients mentioned in Table 1 have a formal diagnosis of Asperger syndrome, which suggests that spontaneous chromosomal imbalances are common across the whole spectrum of the disorder. We examined whether there were many cases of mental retardation [defined as having a nonverbal intelligence quotient (IQ) less than 70] among patients in whom we detected de novo mutations. Clinical data on 60 patients were obtained, and these data included five of the patients in Table 1. The average nonverbal IQ of five cases was 85 and the minimum was 70.

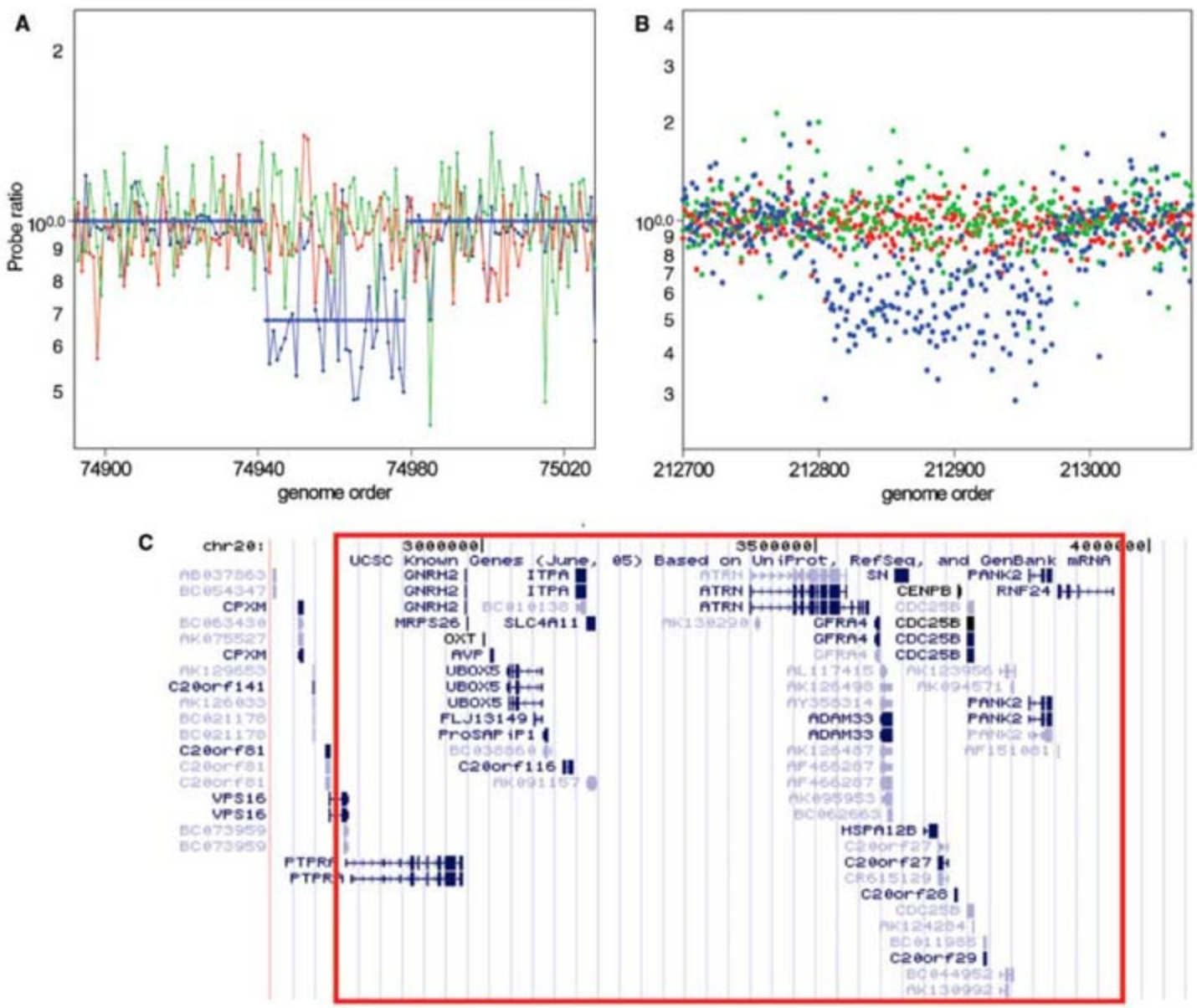

Fig. 2. Detection and validation of a spontaneous deletion in a patient with Asperger syndrome. CNVs were detected in patient scans using the standard HMM. Parents were ascertained and determined to have no change in copy number using an algorithm with relaxed criteria. These second detection criteria included (*1*) detection by an HMM with reduced stringency (false-positive expectation set at 1%), and median probe ratio ≤0.91 or ≥1.1. Probe ratio data are shown for the patient SK-135 (blue) and the mother (red) and father (green) for 85K ROMA (**A**) and 244K Agilent CGH (**B**) platforms. The map of annotated known genes was obtained from the UCSC Genome Browser, May 2004 assembly (*30*). The genomic region estimated to be deleted is shown in (**C**) outlined in red.

Table 1. Spontaneous CNVs detected by ROMA. A description of 17 de novo CNVs in 16 subjects is provided, along with the methods used for its validation. The number of unique RefSeq genes within each CNV region is indicated, and when the locus apparently encompasses only a single gene, the gene symbol is listed. Types of validation included (A) higher-resolution microarray scans by 390K ROMA or Agilent 244K CGH, (B) G-banded karyotype, (C) FISH, and (D) microsatellite genotyping. References are listed for four cases where similar de novo CNVs were previously reported in the literature.

Individual	Locus	Start position	Length	CN change	Family type	Diagnosis	Gender	Validation	# Genes	Single-gene targets	Ref.
63-144-2575 and 2667	2q24.2	162,212,720	99,252	Loss	Simplex	Autism	Female	A	1	SLC4A10	
61-2710-3	2q37.2-q37.3	236,414,455	6,286,648	Loss	Simplex	Autism	Male	A, B, D	50		(*19*)
Van69-258900	2q37.3	238,217,066	4,484,037	Loss	Simplex	Autism	Male	A, D	43		(*19*)
89-3507-1	3p14.2	60,746,033	101,507	Loss	Simplex	Autism	Male	A	1	FHIT	
63-562-6612	3p14.2	61,072,100	293,096	Gain	Simplex	Autism	Male	A	1	FHIT	
AU010604	6p23	13,997,280	1,264,651	Loss	Multiplex	Autism	Male	A, D	2		
	13q14.12-q14.13	44,199,441	1,943,737	Loss				A, D	13		
AU072203	7p21.1	15,160,118	151,880	Loss	Simplex	Autism	Male	A	1	FLJ16237	
AU032903	10q11.23-q21.2	50,562,149	10,916,362	Gain	Multiplex	Autism	Male	A, B	23		
60-3061-4	15q11-q13.33	18,526,971	12,229,800	Gain	Simplex	Autism	Male	A, B	30		(*21*)
AU077504	16p13.3	5,992,836	207,980	Loss	Simplex	Autism	Female	A, B, C, D	1	A2BP1	
CG2061	16p11.2	29,578,715	502,574	Loss	Simplex	Asperger's	Female	A, C, D	27		
71-259100	20p13	75,912	291,959	Loss	Simplex	Autism	Female	A, C, D	7		
SK-135-C	20p13	2,785,194	1,169,205	Loss	Simplex	Asperger's	Male	A, D	23		
89-3524-100	22q13.31-q13.33	45,144,027	4,321,856	Loss	Simplex	Autism	Female	A, B, C, D	30		(*20*)
NA10857	2p16.1	58,394,177	2,786,284	Gain	Control	Unaffected	Male	A	7		
AU070807	20p13-p12.3	111,824	5,316,286	Gain	Simplex	Unaffected	Female	A	69		

Table 2. Increased frequency of de novo CNVs in autism. The numbers of de novo events are listed for our autism sample and for each category of family separately (simplex, multiplex, and nonautism control). The difference between cases and controls was examined, and the statistical significance was determined using Pearson's chi-square test with simulated *P* value from 2000 replicates. The *P* value for the difference in frequency between cases from simplex and multiplex families was also determined.

Sample group	*n*	CNVs de novo	Ratio	*P* value	
				χ^2	Multiplex/simplex
Simplex autism	118	12	0.102	0.0005	0.043
Multiplex autism	77	2	0.026	0.59	
Simplex + multiplex	195	14	0.072	0.0035	
Controls	196	2	0.010		

Although this average was lower than the average for all patients (100), these data indicate that the de novo mutations identified in our study were not found generally in patients with mental retardation.

Because the difference in rate between autism and control is so marked, we can make a fair presumption that many of the lesions we observed contribute to the disorder. However, the observation of a de novo mutation in a single family is not sufficient evidence to prove that a mutation is causal, nor does it provide unequivocal evidence for the involvement of a specific gene in autism. When an individual gene candidate can be identified, because the mutation affects a single gene or a small number of functional candidates, a straightforward path to validation can be planned, involving sequencing and higher-resolution CNV analysis in additional samples. The principle is illustrated in the recent study by Durand *et al.* where an intensive survey of variation in a candidate gene, *SHANK3*, revealed multiple additional variants, including de novo and inherited mutations (*22*). *SHANK3* is one of the genes within the 4.3-MB deletion on chromosome 22q13 that we reported in Table 1, and this region is also a site of recurrent deletions in autism (*20*). Thus, an aggregate of deletions and coding variants that occurs in patients and not in controls can provide further evidence of a gene's role in disease once that candidate gene is identified by copy number mutation.

Some of the genes contained within the de novo CNVs we identified are good candidates for further study. A list of all RefSeq genes that overlap with the de novo mutations identified in this study is shown in table S3. Five of the de novo events we detected involved only a single gene and are worthy of mention. A spontaneous deletion was identified involving exons 2–8 of the putative sterol desaturase *FLJ16237*. Little is known about the function of *FLJ16237*, but its expression has been detected by in situ hybridization in the superior temporal gyrus of fetal brain (D.H.G.). In a pair of monozygotic twins concordant for autism, we detected a spontaneous deletion of exon 1 of the putative sodium bicarbonate cotransporter *SLC4A10*. Mutations of the related gene, *SLC4A4*, are associated with renal tubular acidosis and mental retardation (*23*). Other single-gene mutations were detected affecting ataxin 2–binding protein 1 (*A2BP1/FOX-1*) and the fragile histidine triad gene (*FHIT*) (Table 1). A2BP1 is known to interact with the SCA2, the gene for spinocerebellar ataxia type 2, and *A2BP1* mutations have been identified in mental retardation and epilepsy (*24*). We observed two independent spontaneous mutations of *FHIT*, a locus that is one of the most fragile sites in the human genome (*25*), but one of these was not detected in an extract of the original blood from which the cell line was derived.

All five single-gene mutations we detect involve unusually large genes, the smallest of which (*SLC4A10*) spans 359 kb of the genome. All four target genes rank among the top 3% of human genes by length. This is consistent with previous observations that large genes are frequently located within unstable regions of the genome (*26*). Our simulations, made by randomly permuting the location of our CNV regions, indicate that this result may simply reflect that large genes, by virtue of their size alone, are more likely to be affected by random rearrangements. Whatever the explanation, large genes do play prominent roles in spontaneous genetic disorders in humans, such as Duchenne muscular dystrophy (*27*), retinoblastoma (*28*), and neurofibromatosis (*29*); and the same could be true for autism.

These studies do not address the mechanisms by which structural mutations of genes contribute to autism. Changes in dosage or structure of genes within a lesion could have quantitative effects on gene function, including haploinsufficiency or altered transcription patterns. Alternatively, hemizygous deletion could result in total

loss of function if it is compounded by recessive mutation or monoallelic exclusion of the remaining allele. A genomic rearrangement may also disrupt regulatory elements that influence the expression of neighboring genes; thus, in some cases, a gene related to autism may lie adjacent to the deletion or duplication.

Our findings have implications for an understanding of the genetic basis for ASDs. An important feature of the de novo CNVs we report is that each is individually rare in the population of patients. None of the genomic variants we detected were observed more than twice in our sample, and most were seen but once. Although our sample size is small, these results suggest that lesions at many different loci can contribute to autism, a result consistent with the findings from cytogenetics, as well as consistent with the failure to find common heritable variants with a major effect on disease risk. Lack of recurrence may in fact reflect an underlying reality that autistic behavior can result from many different genetic defects. This would be consistent with the hypothesis that the common features of autism such as failure to develop social skills and repetitive and obsessive behavior may in fact be the consequence of a reaction to many different cognitive impairments, drawing their "commonality" from a normal but maladaptive programmed response of humans early in development to those diverse impairments.

We do not know the full contribution of spontaneous mutation to autism. Population studies divide autism into sporadic and familial or "multiplex." Our work provides clear evidence that these two classes are indeed genetically distinct. The rate of de novo mutation in multiplex families was significantly lower than for sporadic cases (Table 2, $P = 0.04$), as would be expected if there were two different genetic mechanisms contributing to risk: spontaneous mutation and inheritance, with the latter being more frequent in families that have multiple affected children.

The rate of spontaneous mutation that we detect in autism is an underestimate. Adding the known rate of cytogenetically visible abnormalities, the total frequency of de novo variation detectable in sporadic cases is ~15% at our current resolution. Because of the limited resolution of genome microarray scans, we expect that we fail to detect the vast majority of CNVs. Much smaller deletions or even point mutations can produce the same consequences as the larger, more easily detectable events. As technology for discovering spontaneous germline mutation in children improves, the proportion of autism cases with detectable events is bound to rise.

We can incorporate a high rate of spontaneous mutation in a genetic model that accounts for both sporadic and familial forms of the disease, based on new mutations that cause autism by haploinsufficiency but have incomplete penetrance, especially in females. Such individuals who escape the phenotypic consequences can then pass on the mutation in an apparently dominant fashion to their children. This model makes very clear predictions that can be tested in the short term.

Our findings highlight how methods for directly detecting CNVs genomewide provide a powerful alternative to traditional gene-mapping approaches for discovering genetic risk factors in autism and in other disorders of complex etiology. Improved technologies for mutation detection, such as high-throughput DNA sequencing and tiling-resolution oligonucleotide arrays, promise to improve our power to identify new mutations associated with disease.

References and Notes

1. E. Fombonne, *J. Clin. Psychiatry* **66** (suppl. 10), 3 (2005).
2. S. M. Klauck, *Eur. J. Hum. Genet.* **14**, 714 (2006).
3. J. A. Vorstman *et al.*, *Mol. Psychiatry* **11**, 1 (2006).
4. R. E. Amir *et al.*, *Nat. Genet.* **23**, 185 (1999).
5. European Chromosome 16 Tuberous Sclerosis Consortium, *Cell* **75**, 1305 (1993).
6. J. K. Pritchard, *Am. J. Hum. Genet.* **69**, 124 (2001).
7. L. Feuk, A. R. Carson, S. W. Scherer, *Nat. Rev. Genet.* **7**, 85 (2006).
8. J. Sebat *et al.*, *Science* **305**, 525 (2004).
9. A. J. Iafrate *et al.*, *Nat. Genet.* **36**, 949 (2004).
10. D. A. Koolen *et al.*, *Nat. Genet.* **38**, 999 (2006).
11. A. J. Sharp *et al.*, *Nat. Genet.* **38**, 1038 (2006).
12. C. Shaw-Smith *et al.*, *Nat. Genet.* **38**, 1032 (2006).
13. C. Shaw-Smith *et al.*, *J. Med. Genet.* **41**, 241 (2004).
14. L. E. Vissers *et al.*, *Am. J. Hum. Genet.* **73**, 1261 (2003).
15. M. L. Jacquemont *et al.*, *J. Med. Genet.* **43**, 843 (2006).
16. R. Lucito *et al.*, *Genome Res.* **13**, 2291 (2003).
17. J. N. Ferguson *et al.*, *Nat. Genet.* **25**, 284 (2000).
18. M. Kosfeld, M. Heinrichs, P. J. Zak, U. Fischbacher, E. Fehr, *Nature* **435**, 673 (2005).
19. M. Ghaziuddin, M. Burmeister, *J. Autism Dev. Disord.* **29**, 259 (1999).
20. M. A. Manning *et al.*, *Pediatrics* **114**, 451 (2004).
21. J. Veenstra-VanderWeele, E. H. Cook Jr., *Mol. Psychiatry* **9**, 819 (2004).
22. C. M. Durand *et al.*, *Nat. Genet.* **39**, 25 (2007).
23. T. Igarashi *et al.*, *J. Am. Soc. Nephrol.* **12**, 713 (2001).
24. K. Bhalla *et al.*, *J. Hum. Genet.* **49**, 308 (2004).
25. K. Huebner, C. M. Croce, *Nat. Rev. Cancer* **1**, 214 (2001).
26. D. I. Smith, Y. Zhu, S. McAvoy, R. Kuhn, *Cancer Lett.* **232**, 48 (2006).
27. S. M. Gospe Jr. *et al.*, *Neurology* **39**, 1277 (1989).
28. E. Orye, M. J. Delbeke, B. Vandenabeele, *Lancet* **2**, 1376 (1971).
29. D. Viskochil *et al.*, *Cell* **62**, 187 (1990).
30. W. J. Kent *et al.*, *Genome Res.* **12**, 996 (2002).

31. We wish to thank patients and families for their valuable contributions and the NIMH Center for Collaborative Genetic Studies of Mental Disorders, the Autism Genetic Resource Exchange (AGRE), the Centre d'Etude du Polymorphisme Humain (CEPH), and D. Levy for providing materials or data for the study. We are grateful to G. Fischbach, C. Lord, N. Heinz, E. Cook, L. Brzustowicz, J. and M. Simons, and L. Iakoucheva for helpful discussions throughout the study, and we thank C. Reed, P. Roccanova, J. Lloyd, V. Grubor, L. Rodgers, D. Esposito, L. Hufnagel, X. Zhao, E. Thorolfsdottir, K. A. Olafsdottir, and the staff of Lingen EHF for technical assistance. This work was supported by a grant from the Simons Foundation and by NIMH grant MH076431 to J.S., which reflects cofunding from Autism Speaks, Cure Autism Now, and the Southwestern Autism Research and Resource Center. Additional support was provided by NIMH grant MH61009 to J.S.S., grants to D.S. from Nancy Lurie Marks Family Foundation and the National Alliance for Autism Research (NAAR), and a grant to K.P. and T.L. from the University of Tampere Hospital Medical Fund. AGRE is a program of Cure Autism Now and is supported in part by NIMH grant MH64547 to D.H.G.

Supporting Online Material

www.sciencemag.org/cgi/content/full/1138659/DC1
Materials and Methods
Tables S1 to S3
References

11 December 2006; accepted 6 March 2007
Published online 15 March 2007;
10.1126/science.1138659
Include this information when citing this paper.

Raman-Assisted Crystallography Reveals End-On Peroxide Intermediates in a Nonheme Iron Enzyme

Gergely Katona,[1] Philippe Carpentier,[1] Vincent Nivière,[2] Patricia Amara,[1] Virgile Adam,[3] Jérémy Ohana,[1] Nikolay Tsanov,[1] Dominique Bourgeois[1,3]*

Iron-peroxide intermediates are central in the reaction cycle of many iron-containing biomolecules. We trapped iron(III)-(hydro)peroxo species in crystals of superoxide reductase (SOR), a nonheme mononuclear iron enzyme that scavenges superoxide radicals. X-ray diffraction data at 1.95 angstrom resolution and Raman spectra recorded in crystallo revealed iron-(hydro)peroxo intermediates with the (hydro)peroxo group bound end-on. The dynamic SOR active site promotes the formation of transient hydrogen bond networks, which presumably assist the cleavage of the iron-oxygen bond in order to release the reaction product, hydrogen peroxide.

The interaction of dioxygen with iron-containing proteins is important in many biological processes, including transport, metabolism, respiration, and cell protection. The reaction of oxygen or its reduced derivatives, superoxide and hydrogen peroxide, with iron enzymes often involves short-lived iron-peroxide intermediates along the reaction cycle (*1*, *2*). Heme-based peroxidases, catalases, and many oxygenases promote heterolytic cleavage of the peroxide oxygen-oxygen bond to form high-valence reactive iron-oxo species. In contrast, other iron enzymes, such as superoxide reductase (SOR) (*3*, *4*), are fine-tuned to cleave the iron-oxygen bond and avoid the formation of potentially harmful iron-oxo species. Although the

protein, the metal configuration, and the solvent environment have been shown to play a role, the mechanisms by which iron-peroxide intermediates are processed are not fully understood (*1*, *2*). Despite pioneering studies on heme proteins (*5*–*7*), structural data revealing peroxide species in nonheme mononuclear iron enzymes have remained scarce (*8*). We have developed an approach in which kinetic crystallography (*9*) was assisted by "in crystallo" Raman spectroscopy (*10*) to characterize (hydro)peroxo species in SOR. SOR is found in some air-sensitive bacteria and archaea and converts the toxic superoxide anion radical ($O_2^{\bullet-}$) into hydrogen peroxide (H_2O_2) via a one-electron reduction pathway: $O_2^{\bullet-} + 2H^+ + SOR(Fe^{2+}) \rightarrow H_2O_2 + SOR(Fe^{3+})$ (*3*, *4*, *11*). The SOR catalytic domain displays an immunoglobulin-like fold (*12*, *13*) encompassing an iron atom coordinated to four equatorial histidines and one axial cysteine, thus bearing structural resemblance to the ubiquitous cytochromes P450s. However, contrary to P450s, the ferrous enzyme is stable under atmospheric conditions, with a vacant, solvent-exposed, sixth coordination site where $O_2^{\bullet-}$ is thought to bind (*14*). Investigations of various SOR adducts (*12*, *14*, *15*), pulse-radiolysis studies (*16*–*18*), and resonance Raman spectroscopy experiments (*19*, *20*) have suggested an inner-sphere catalytic mechanism involving the formation of transient iron(III)-(hydro)peroxo species. As described for similar enzymes (*2*, *21*), protonation steps play a crucial role in governing the chemistry that occurs at the SOR active site (*11*, *16*, *17*). In SOR from the sulfate-reducing bacterium *Desulfoarculus baarsii* (*4*, *12*), a first iron(III)-peroxo intermediate has been proposed to be rapidly protonated (in ~100 μs), forming a more stable iron(III)-hydroperoxo species (*17*). A second protonation then occurs, possibly promoted by a water molecule (*22*), and yields the H_2O_2 product through a dissociative mechanism in which Glu^{47} ultimately binds to the oxidized enzyme (*13*, *17*). Thus, SOR avoids heterolytic cleavage of the O-O bond, preventing the formation of oxo-ferryl compounds. To date, the structure of the iron-peroxide species that can be accommodated within the SOR active site and the mechanism governing the decisive second protonation step have remained elusive (*11*). The structural data described below reveal a series of end-on iron(III)-(hydro)peroxo species involved in tight hydrogen bond networks (Fig. 1) and allow us to propose a mechanism for proton-assisted release of H_2O_2 in SOR.

[1]Institut de Biologie Structurale (IBS) Jean-Pierre Ebel, Commissariat à l'Energie Atomique (CEA), Centre National de la Recherche Scientifique (CNRS), Université Joseph Fourier, 41 rue Jules Horowitz, F-38027 Grenoble, France. [2]Laboratoire de Chimie et Biologie des Métaux, Institut de Recherches en Technologies et Sciences pour le Vivant, CEA, CNRS, Université J. Fourier, UMR 5249, 17 rue des Martyrs, 38054 Grenoble Cedex 9, France. [3]European Synchrotron Radiation Facility (ESRF), 6 rue Jules Horowitz, BP 220, 38043 Grenoble Cedex, France.

*To whom correspondence should be addressed. E-mail: dominique.bourgeois@ibs.fr

Table 1. Geometry of the active site. Fe distance from the His plane was defined by the coordinating N atoms of the equatorial histidines in Å. Increasing value indicates an iron position closer to Cys^{116}.

	WT-SOR	E114A-SOR reduced	E114A-SOR peroxide intermediates	DFT calculation
		Monomer A		
Fe-S (Å)	2.4	2.4	2.5	
Fe from His plane (Å)	0.4	0.4	0.3	
		Monomer B		
Fe-S (Å)	2.4	2.4	2.5	2.48
Fe-O1 (Å)			2.0	2.19
Fe-O1-O2 (°)			126	125
C_β-S-O1-O2 (°)			140	168
Fe from His plane (Å)	0.4	0.4	0.3	0.10
		Monomer C		
Fe-S (Å)	2.4	2.5	2.5	2.44
Fe-O1 (Å)			2.0	1.94
Fe-O1-O2 (°)			126	123
C_β-S-O1-O2 (°)			132	114
Fe from His plane (Å)	0.5	0.4	0.3	0.16
		Monomer D		
Fe-S (Å)	2.4	2.5	2.6	2.49
Fe-O1 (Å)			2.0	2.22
Fe-O1-O2 (°)			122	123
C_β-S-O1-O2 (°)			112	99
Fe from His plane (Å)	0.4	0.3	0.0	0.11

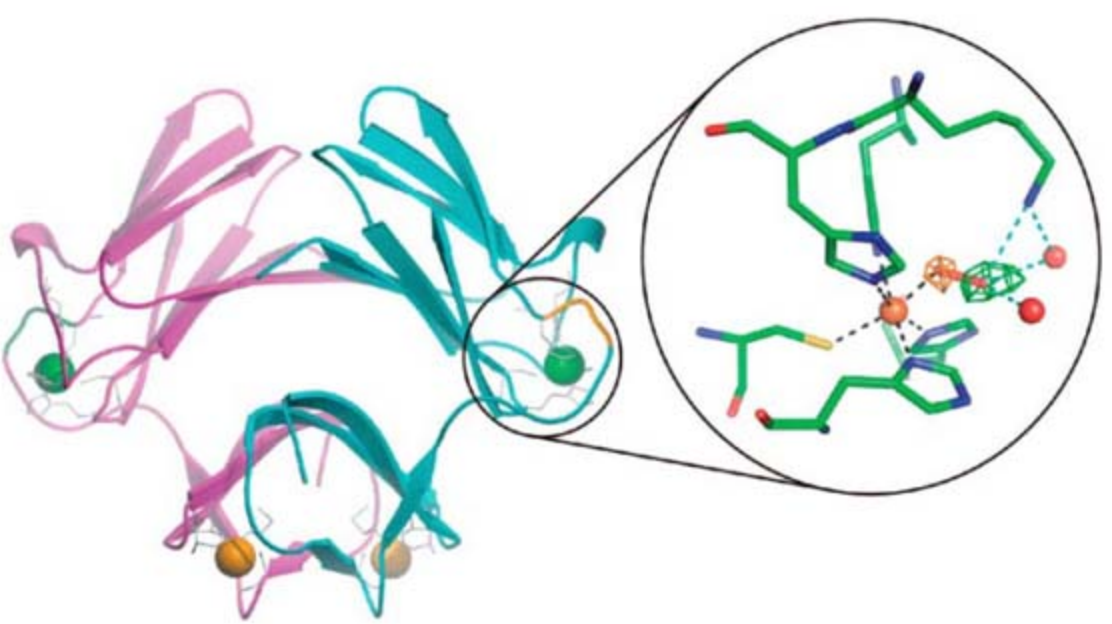

Fig. 1. Structural overview of SOR. The x-ray structure of the SOR-E114A homodimer in the native reduced state is shown as magenta (monomer A) and cyan (monomer B) ribbons with the exception of the LID loop (residues 45 to 49), which is colored in dark green and orange for monomers A and B, respectively. Reduced and oxidized iron atoms are shown as green and orange balls, respectively. (**Inset**) The active site of monomer B upon addition of H_2O_2. The residues coordinating the active iron (His^{49}, His^{69}, His^{75}, His^{119}, and Cys^{116}) as well as Lys^{48} are represented as sticks. The bound peroxide ligand is shown as a red stick. Water molecules are shown as red balls. In order to support the diatomic nature of the peroxide intermediate, simulated annealed $F_{obs} - F_{calc}$ maps omitting the distal or proximal oxygens of the O-O moiety, respectively, were calculated. The two maps are displayed in green (distal) and orange (proximal) at a contour level of 3.0σ.

Mononuclear iron-peroxide complexes are generally obtained by reacting iron(II) with excess H_2O_2 (*23*). However, to minimize Fenton-driven generation of toxic hydroxyl radicals, we first oxidized crystalline SOR with hexachloroiridate (IV) and then exposed it to H_2O_2 for 3 min before freezing (*24*). Because the isolation of iron(III)-peroxide complexes is hampered by their high reactivity, crystallographic data were collected with the mutant enzyme E114A (Glu^{114}→Ala^{114}), in which, as described for the E47A (Glu^{47}→Ala^{47}) variant (*19*, *20*), these intermediates are stabilized [Supporting Online Material (SOM) text]. Comparison of the native crystal structures of the wild-type and mutant enzymes revealed that the loss of the E114 side chain does not alter the overall enzyme structure (Table 1).

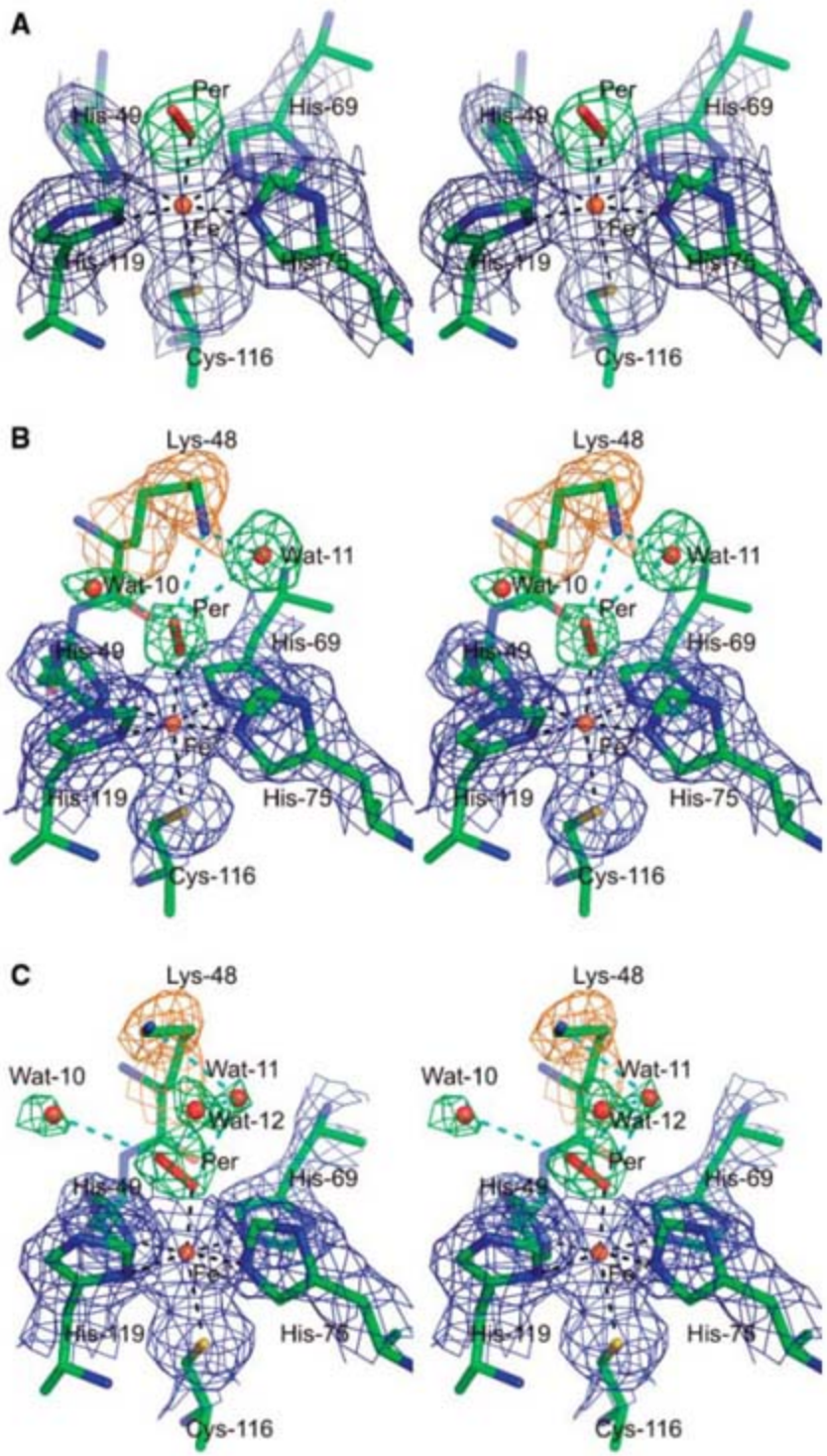

Fig. 2. Structure of the SOR-peroxide intermediates. Stereo views of the peroxide-bound SOR active sites in monomers C, B, and D are shown in (**A**), (**B**), and (**C**), respectively. Final $2F_{obs} - F_{calc}$ maps (blue, contoured at 1.0σ), simulated annealed $F_{obs} - F_{calc}$ maps omitting the peroxo moiety and associated water molecules (green, contoured at 4.5σ), and simulated annealed $F_{obs} - F_{calc}$ maps omitting only Lys^{48} (orange, contoured at 3.5σ) are shown, overlaid on the refined models of the SOR-peroxide intermediates. Hydrogen bonds and iron coordination are shown as blue and black dashed lines, respectively.

The asymmetric unit in SOR-E114A crystals contains four monomers, denoted A to D. Upon soaking with H_2O_2, diffraction data to 1.95 Å resolution (*24*) (table S1) revealed elongated features in the electron density maps that are consistent with the formation of end-on (η^1) peroxide species in monomers B, C, and D (Figs. 1 and 2), whereas monomer A did not react. To verify the chemical nature of the observed species, we developed a Raman spectrometer to analyze cryocooled crystals under conditions identical to those used for x-ray data collection (*24*, *25*) (fig. S1). Upon H_2O_2 treatment, two ^{18}O isotope–sensitive main bands at ~567 cm^{-1} and ~838 cm^{-1} appeared in the Raman spectra of SOR crystals (Fig. 3). Although these bands probably involve the coupling of a number of vibrational modes, they fall within the expected range for ν(Fe-OO(H)) and ν(O-O) frequencies of iron-peroxide species, respectively (*26*) (SOM text). Importantly, they are not specific to the crystalline phase, because they also appeared with solution samples similarly treated with hydrogen peroxide (SOM text). In addition, Raman spectra from crystals exposed to x-rays (*27*) showed the same signature as unexposed crystals, ruling out the possibility of substantial photo-alteration during data collection [it is known that the solvent-exposed SOR active site is sensitive to reduction by x-ray–induced photo-electrons (*12*)]. Overall, in crystallo Raman spectra strongly suggested the buildup of iron-peroxide species in the crystal. To assess the protonation state of these species, we performed density functional theory (DFT) calculations (SOM text) on model SOR active sites based on the x-ray structures determined in this work. In monomers B and D, these calculations favor high-spin η^1 hydroperoxo species that are protonated at the distal oxygen, consistent with pulse-radiolysis studies that suggested rapid protonation of the SOR iron-peroxo species even at the basic pH (pH = 9) used in our work (*17*). In monomer C, an η^1 species is also favored, but its protonation state cannot be firmly established.

Final x-ray models of SOR monomers B, C, and D show end-on iron(III)-peroxide species in three different configurations that all display the distal oxygen pointing toward His^{119} to accommodate steric constraints imposed by the protein matrix. Thus, the atoms $C_{\beta,Cys116}$-$S_{\gamma,Cys116}$-Fe-O-O are non-coplanar, resulting in nonoptimal π orbital overlap and contributing to weaken the iron-oxygen bond, as also suggested by the long Fe-O distances found in our DFT calculations (Table 1).

In SOR, a solvent-exposed flexible loop (residues 45 to 49, called "LID" thereafter) is located near the active site and includes Lys^{48}, an evolutionary conserved residue critical for efficient catalysis (*16*, *17*). The formation of iron-peroxide species modified the conformation of Lys^{48} relative to that in the native reduced state (SOM text). In monomer C, the hydroperoxo

moiety only interacts with the active iron, and the LID loop displays a "locked-open" conformation, possibly because of weak crystal lattice contacts (SOM text). This LID conformation prevents Lys[48] from interacting with the hydroperoxo moiety, leaving the side chain of this residue in a disordered state. In contrast, in monomer B, the LID loop is found "locked closed," and Lys[48] facilitates a tight hydrogen bond network around the distal oxygen of the peroxide moiety that also includes two water molecules (Wat[10] and Wat[11]) (Fig. 2). The positively charged amino group of Lys[48] (SOM text) attracts the peroxide ligand, presumably inducing a stretch of the $S_{\gamma,Cys116}$-Fe-O-O moiety that may further weaken the Fe-O bond. In monomer D, the side chain of Lys[48] slightly rotates away from the hydroperoxo moiety, and the two water molecules Wat[10] and Wat[11] are still observed, together with a third molecule (Wat[12]) that may play a stabilizing role. However, Wat[10] now forms a hydrogen bond with the amino group of Ala[45], whereas Wat[11] moves slightly toward the iron so that it interacts with both proximal and distal oxygen atoms of the hydroperoxo moiety. Wat[11] is therefore in a favorable position to donate a proton to the proximal oxygen atom, allowing the formation and release of hydrogen peroxide. This is a crucial step that differentiates SOR from heme enzymes where protonation occurs at the distal oxygen, liberating water and oxo-ferryl species (*2*). Simultaneously, a combination of subtle rearrangements of the iron-coordinating histidines shifts the iron into the plane defined by the four equatorial coordinating nitrogens (Table 1) (*28*). This conformation possibly facilitates access of Wat[11] to the metal and the proximal oxygen.

Our data highlight the dynamic behavior of the SOR active site en route to product formation (Fig. 4 and movie S1). Monomer C may be viewed as an early state along the reaction coordinate that precedes the conformational rearrangements leading to the protonation of the HOO^- adduct. We suggest that this state is sta-

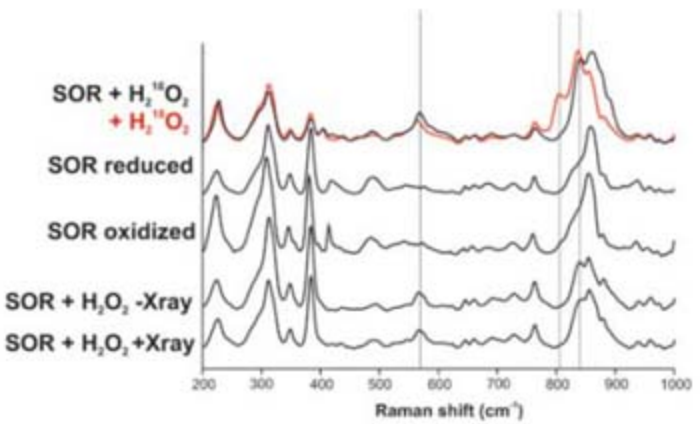

Fig. 3. Raman spectra of SOR crystals. After reaction with H_2O_2, the E114A SOR mutant reveals bands at ~567 cm^{-1} and ~838 cm^{-1}, which are isotopically shifted to ~563 cm^{-1} and ~802 cm^{-1} in the presence of $H_2{}^{18}O_2$ (vertical gray lines). Similar Raman bands and ^{18}O isotopic shifts are observed in solution experiments (fig. S2). E114A-SOR in the native reduced form does not exhibit these bands; neither do crystals oxidized by hexachloroiridate(IV). The peaks at ~567 cm^{-1} and ~838 cm^{-1} are not substantially affected by exposure to an x-ray dose of 3×10^5 Gy, which is about the same dose as used for data collection.

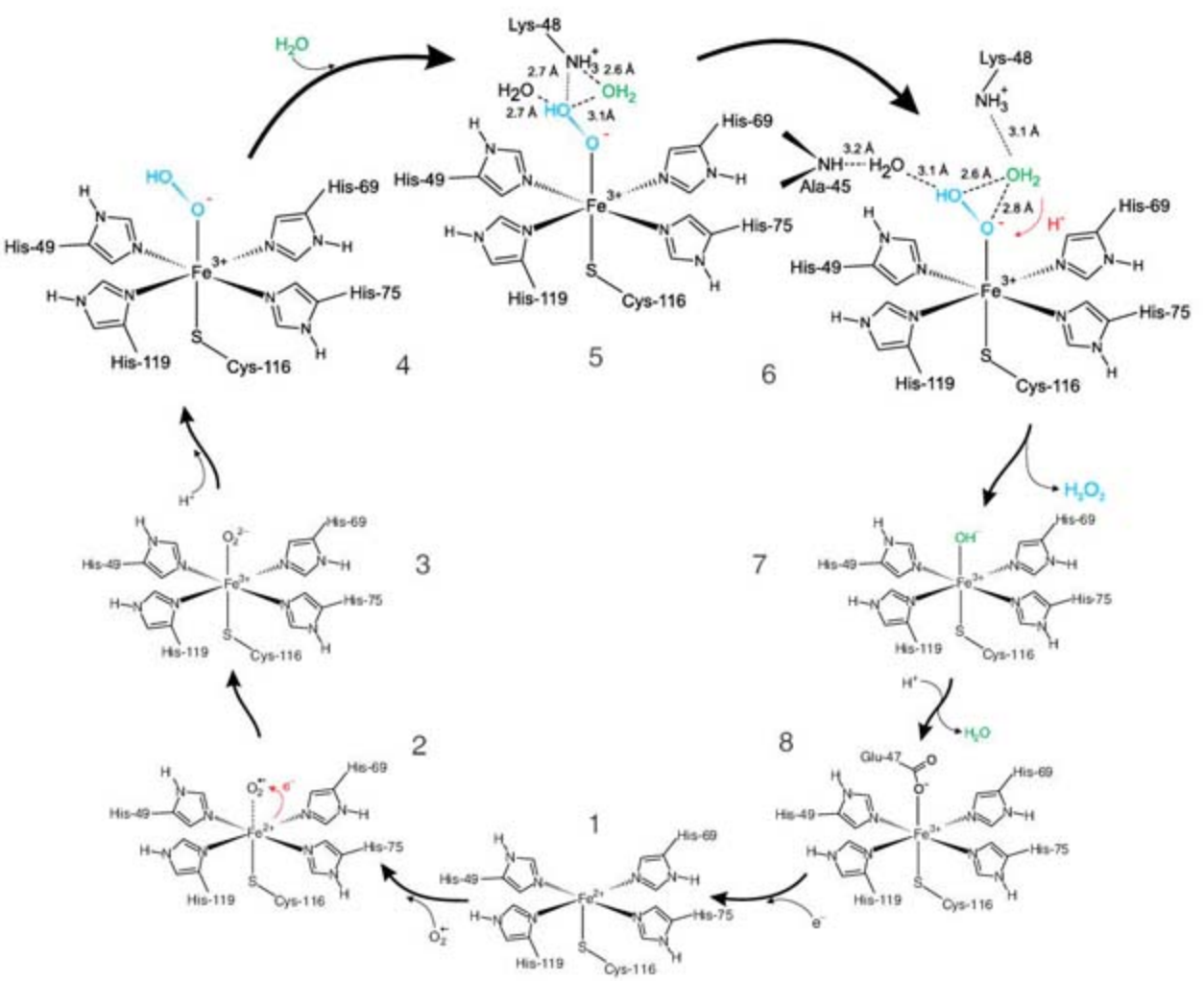

Fig. 4. Proposed mechanism of superoxide reduction by SOR. The proposed catalytic cycle begins with the reduced pentacoordinated active site (**1**). Superoxide binds (**2**) and gets reduced (red arrow) to an unprotonated peroxo species (**3**). Previous data suggested that this intermediate could correspond to a high-spin side-on peroxo-Fe^{3+} species (*19*, *20*) (SOM text). The first protonation step leads to the configuration observed in monomer C (**4**). Lys[48] and two water molecules are recruited (**5**), yielding the configuration observed in monomer B that subsequently rearranges to give the configuration of monomer D (**6**). At this point, protonation of the proximal oxygen atom (red arrow) is facilitated by the key water molecule Wat[11]. Hydrogen peroxide is formed and leaves the active site with the assistance of the hydroxide ion product (**7**). After a rearrangement of the LID loop, Glu[47] replaces the hydroxide ion (**8**). Lastly, the active site is regenerated to its reduced state (**1**) by an unknown external factor. Along the catalytic cycle, blue color indicates the (hydro)peroxo species.

bilized in the crystal because of the locked-open configuration of the LID loop. In contrast, monomers B and D reveal subsequent activated configurations, emphasizing the catalytic role of Lys^{48}. The observation of Wat^{11} in the immediate environment of the hydroperoxo species in these monomers strongly supports the hypothesis that this water molecule is the proton donor for product formation and release. We propose that Lys^{48} hydrogen bonds to Wat^{11} and imports it into the SOR active site in a motion promoted by electrostatic attraction of the positively charged amino group to the hydroperoxo ligand. Once anchored in the vicinity of the proximal oxygen, Wat^{11} becomes more acidic because of the interaction with the amino group of Lys^{48}. Protonation of the proximal oxygen is probably simultaneous with the cleavage of the iron-oxygen bond, and Wat^{11} may immediately replace the hydrogen peroxide product in the form of a hydroxide ion until Glu^{47} binds to the iron, as already suggested (*18*, *22*).

SOR illustrates the key role played by subtle protein motions in enzyme catalysis (*29*). In crystalline SOR, the flexible LID loop adopts various conformations, suggesting that there is little free energy difference between disordered (entropy-driven) states for this loop and ordered (enthalpy-driven) ones where Lys^{48} is stabilized by transient H-bonding networks. Our data are consistent with the idea of a breathing of the LID loop that serves to import catalytically competent water molecules into the SOR active site (*29*). In the crystal, local packing forces may slightly modify the thermodynamic energy balance, selecting different conformations in each monomer.

The structural observations described in this work are obviously not sufficient to entirely account for the specific reactivity of SOR toward breakage of the iron-oxygen bond. Finely tuned electron donation by the trans thiolate ligand (Cys^{116}) is expected to precisely adjust the strength of this bond (*11*). Furthermore, several lines of evidence indicate that the iron spin state greatly modulates the strength of the iron-oxygen and oxygen-oxygen bonds in iron(III)-peroxide complexes (*1*, *11*, *21*, *23*). Whereas many heme catalysts that promote cleavage of the O-O bond involve low-spin states of the iron, SOR (*19*, *20*, *30*) and the oxygen carrier di-iron hemerythrin (*31*) are unique in that they involve a high-spin ($S = 5/2$) iron state (*30*) (SOM text). Interestingly, SOR and hemerythrin share structural and spectroscopic properties: In oxy-hemerythrin, an end-on iron-peroxide species stabilized by a strong hydrogen bond is also observed (*31*). In addition, the Raman vibrations measured for SOR and oxy-hemerythrin are relatively similar and imply a weaker Fe-O bond and a stronger O-O bond when compared to low-spin iron-peroxide model compounds known to favor heterolytic cleavage of the O-O bond (*26*).

The data suggest a possible mechanism for hydrogen peroxide formation, highlighting the role of a key water molecule finely controlled by the enzyme dynamics. The revealed conformational transitions provide a strong basis for further computational and structural investigations of the mechanism of superoxide scavenging by SOR and may facilitate the design of biomimetic catalysts.

References and Notes

1. M. Costas, M. P. Mehn, M. P. Jensen, L. Que, *Chem. Rev.* **104**, 939 (2004).
2. I. G. Denisov, T. M. Makris, S. G. Sligar, I. Schlichting, *Chem. Rev.* **105**, 2253 (2005).
3. F. E. Jenney Jr., M. F. J. M. Verhagen, X. Cui, M. W. W. Adams, *Science* **286**, 306 (1999).
4. M. Lombard, D. Touati, M. Fontecave, V. Niviere, *J. Biol. Chem.* **275**, 27021 (2000).
5. G. I. Berglund *et al.*, *Nature* **417**, 463 (2002).
6. I. Schlichting *et al.*, *Science* **287**, 1615 (2000).
7. K. Kuhnel, E. Derat, J. Terner, S. Shaik, I. Schlichting, *Proc. Natl. Acad. Sci. U.S.A.* **104**, 99 (2007).
8. A. Karlsson *et al.*, *Science* **299**, 1039 (2003).
9. D. Bourgeois, A. Royant, *Curr. Opin. Struct. Biol.* **15**, 538 (2005).
10. P. R. Carey, J. Dong, *Biochemistry* **43**, 8885 (2004).
11. L. M. Brines, J. A. Kovacs, *Eur. J. Inorg. Chem.* **2007**, 29 (2007).
12. V. Adam, A. Royant, V. Niviere, F. P. Molina-Heredia, D. Bourgeois, *Structure* **12**, 1729 (2004).
13. A. P. Yeh, Y. Hu, F. E. Jenney Jr., M. W. Adams, D. C. Rees, *Biochemistry* **39**, 2499 (2000).
14. M. D. Clay *et al.*, *J. Am. Chem. Soc.* **124**, 788 (2002).
15. M. D. Clay *et al.*, *Biochemistry* **45**, 427 (2006).
16. J. P. Emerson, E. D. Coulter, D. E. Cabelli, R. S. Phillips, D. M. Kurtz Jr., *Biochemistry* **41**, 4348 (2002).
17. V. Niviere *et al.*, *Biochemistry* **43**, 808 (2004).
18. J. V. Rodrigues, I. A. Abreu, D. Cabelli, M. Teixeira, *Biochemistry* **45**, 9266 (2006).
19. C. Mathe *et al.*, *J. Am. Chem. Soc.* **124**, 4966 (2002).
20. C. Mathe, V. Niviere, C. Houee-Levin, T. A. Mattioli, *Biophys. Chem.* **119**, 38 (2006).
21. G. H. Loew, D. L. Harris, *Chem. Rev.* **100**, 407 (2000).
22. C. Mathe, V. Niviere, T. A. Mattioli, *J. Am. Chem. Soc.* **127**, 16436 (2005).
23. G. Roelfes *et al.*, *Inorg. Chem.* **42**, 2639 (2003).
24. Materials and methods are available as supporting material on *Science* Online.
25. Raman experiments were performed under nonresonant conditions, taking advantage of the large protein concentration found in crystals to enhance the signal-to-noise ratio. In this way, the crystals were sampled homogeneously, and potential light-induced damage or photochemistry that could develop under resonant conditions was avoided.
26. J.-J. Girerd, F. Banse, A. J. Simaan, in *Metal-Oxo and Metal-Peroxo Species in Catalytic Oxidations*, vol. 97 of *Structure and Bonding* (Springer, Berlin 2000), pp. 145–177.
27. A carefully controlled x-ray exposure was used to collect the diffraction data so that the dose absorbed by the crystal amounted to ~1% of the Henderson limit, i.e., $\sim 2.1 \times 10^5$ gray (Gy).
28. These rearrangements also bring the N_ε atom of His^{119} (the only histidine coordinating the iron through N_δ) to a close distance (3.5 Å) to the distal oxygen of the hydroperoxo moiety.
29. D. Tobi, I. Bahar, *Proc. Natl. Acad. Sci. U.S.A.* **102**, 18908 (2005).
30. M. R. Bukowski, H. L. Halfen, T. A. van den Berg, J. A. Halfen, L. Que, *Angew. Chem. Int. Ed.* **44**, 584 (2005).
31. T. C. Brunold, E. I. Solomon, *J. Am. Chem. Soc.* **121**, 8277 (1999).
32. Coordinates and structure factor amplitudes of the structures $SOR_{E114A,\ Fe(II)}$, $SOR_{E114A,\ Fe(II)}$-OOH and $SOR_{wt,\ Fe(II)}$ have been deposited in the RCSB Protein Data Bank with pdb codes 2ji2, 2ji3, and 2ji1, respectively.

The ESRF is acknowledged for continuous support of our methodological developments. We are grateful to the ESRF beamline staff at ID14-1, ID14-2, ID14-4, and ID29 for their expert assistance; T. Mattioli and C. Mathé for insightful discussions and for providing us with resonance Raman spectra on the E114A SOR mutant; C. Mathevon for help in sample preparation; M. F. Field and L. David for help with the pK_a calculations; J. C. Fontecilla for reading the manuscript; and H. Jouve and J.-P. Mahy for providing us with $H_2{}^{18}O_2$. G.K. acknowledges support by a European Molecular Biology Organization long-term fellowship, and D.B. acknowledges support by the Contrat de Plan Etat-Région and the Action Concertée Incitative programs from the French Ministry of Research. V.N. acknowledges support by the Toxicologie Nucléaire program from the CEA.

Supporting Online Material

www.sciencemag.org/cgi/content/full/316/5823/449/DC1
Materials and Methods
SOM Text
Figs. S1 to S3
Tables S1 to S5
References
Movie S1

15 December 2006; accepted 12 March 2007
10.1126/science.1138885

Crystal Structures of Fe^{2+} Dioxygenase Superoxo, Alkylperoxo, and Bound Product Intermediates

Elena G. Kovaleva and John D. Lipscomb*

We report the structures of three intermediates in the O_2 activation and insertion reactions of an extradiol ring-cleaving dioxygenase. A crystal of Fe^{2+}-containing homoprotocatechuate 2,3-dioxygenase was soaked in the slow substrate 4-nitrocatechol in a low O_2 atmosphere. The x-ray crystal structure shows that three different intermediates reside in different subunits of a single homotetrameric enzyme molecule. One of these is the key substrate-alkylperoxo-Fe^{2+} intermediate, which has been predicted, but not structurally characterized, in an oxygenase. The intermediates define the major chemical steps of the dioxygenase mechanism and point to a general mechanistic strategy for the diverse 2-His-1-carboxylate enzyme family.

Aerobic life is possible because O_2 must be activated before it will react rapidly with most biological molecules, which prevents indiscriminate oxidation. Oxygenase enzymes have evolved numerous chemical strategies to selectively effect this activation so that

the inherent oxidizing power of O_2 can be used productively (*1*, *2*). For example, in the nonheme Fe^{2+}–containing extradiol dioxygenase enzymes, which catalyze the pivotal ring-opening step in the aerobic, bacterial degradation pathways for many natural and manmade aromatic compounds (*3*), substrate binding facilitates oxygen binding and activation. The substrates for these enzymes are analogs of catechol (1,2-dihydroxybenzene), and they bind directly to the iron as a chelate by means of their adjacent hydroxyl functions (*4*, *5*). The substrate-binding reaction causes a change in the ligation state and electronic properties of the iron, so that O_2 can bind in an adjacent iron coordination site (*4*, *6*, *7*). O_2 activation and ring opening then occur without introduction of external reducing equivalents.

On the basis of spectroscopic studies of extradiol dioxygenases, we have proposed that the simultaneous binding of substrate and O_2 to the iron allows transfer of electron density such that the substrate gains cation radical character, while the O_2 becomes a nascent superoxide (Fig. 1, II) (*4*, *8*). Recombination of the incipient radicals would yield an alkylperoxo intermediate (III). A concerted Criegee rearrangement of this intermediate would result in O–O bond cleavage and insertion of one oxygen atom into the aromatic ring to form a lactone intermediate (IV), which would proceed to the ring-open product (V).

The x-ray crystal structures of several extradiol dioxygenases have shown that, as predicted, the substrate does chelate the iron, and this creates a vacant site in the iron coordination (*5*, *9*, *10*). The structures have also allowed the application of computationally based theoretical techniques, which has led to several new proposals for the mechanism of the O–O bond cleavage and ring-opening step(s) (*11*, *12*). However, all of these mechanisms posit the initial formation of an alkylperoxo intermediate, a species that has never been structurally characterized. Here, we have trapped this lynchpin species in a single crystal and structurally characterized it. The O_2 adduct precursor and the product complex successor to the alkylperoxo intermediate are remarkably found to be simultaneously present in different subunits of the enzyme in the same asymmetric unit, which allows these species to be structurally characterized as well.

Homoprotocatechuate 2,3-dioxygenase (2,3-HPCD) from *Brevibacterium fuscum* catalyzes the proximal extradiol ring cleavage of homoprotocatechuate (3,4-dihydroxyphenylacetate, HPCA) to form ring-opened 5-carboxymethyl-2-hydroxymuconic semialdehyde (*13*). In the original structural study of 2,3-HPCD and its complex with HPCA, a C-terminal deletion variant was used (*14*) to facilitate crystallization (*10*). The full-length enzyme was successfully crystallized only once, but the resulting low-resolution structure revealed that the C terminus forms a "lid" over the substrate-binding pocket (*10*). In the current study, conditions have been defined to allow reproducible crystallization of the full-length protein in a new space group ($P2_12_12$) (*15*). The structures of the new form (1.9 Å resolution) show numerous new intermolecular contacts (Fig. 2) that appear to influence the rates of the catalytic steps so that intermediates are stabilized, as described below.

Transient kinetic studies of 2,3-HPCD in solution have provided inroads into the detection of discrete intermediates in the catalytic cycle (*16*, *17*). The use of an alternative substrate, 4-nitrocatechol (4NC), slows the oxygen activation and insertion steps of the cycle (Fig. 1, I through V) and provides a chromophore that is sensitive to the hydroxyl substituent ionization state, protein environment, and ring cleavage. This approach allowed us to detect six reaction cycle steps before rate-limiting product release. Unfortunately, despite the decreased rates, the anticipated 4NC-Fe^{2+}-O_2 and alkylperoxo intermediates were not sufficiently long-lived to be observed directly. It has been reported that steps in the reaction cycle of an enzyme in a crystal often occur much more slowly than they would in solution (*18*). Accordingly, we show here that when the turnover of 4NC is initiated in a crystal of 2,3-HPCD, the key oxygen activation and reaction intermediates are stabilized (Fig. 3, A to C).

In subunit C (Fig. 3A), 4NC chelates the iron ($O2^{4NC}$-Fe = 2.2 Å, $O1^{4NC}$-Fe = 2.2 Å) (*19*) in sites opposite Fe^{2+} ligands His^{155} and His^{214}, respectively, and a diatomic molecule (see fig. S4), assigned as oxygen (*20*), occupies

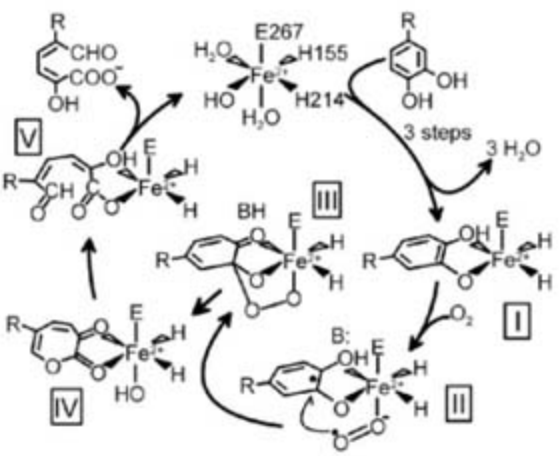

Fig. 1. Proposed reaction mechanism for extradiol ring-cleaving dioxygenases. R = $-CH_2COOH$ or $-NO_2$ (*32*). 4NC binds as the dianion.

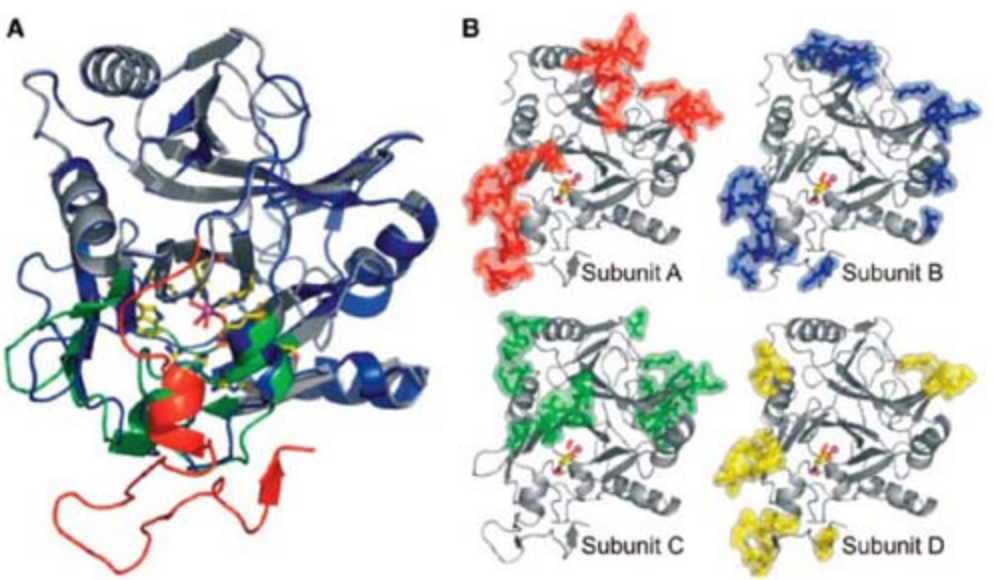

Fig. 2. (**A**) Overlay of monomeric subunit structures in the presence and absence of C terminus. Full-length enzyme (PDB code 2IG9) is shown in blue, and the C-terminal residues 323 to 362 are shown in red. C terminus truncated enzyme [PDB code 1F1X (*10*)] is shown in gray except for residues in the substrate-binding cleft that exhibit slight structural alterations in the absence of the C terminus, which are shown in green. Active site residues are shown as sticks, and mononuclear Fe center, solvent, and Cl^- are shown as purple, red, and blue spheres, respectively. (**B**) Crystal packing (intermolecular) contacts for subunits of the full-length homotetrameric enzyme 2,3-HPCD in $P2_12_12$ space group (PDB code 2IGA). Residues involved in contacts (<5Å) with symmetry-related molecules are shown as colored sticks and surfaces.

Department of Biochemistry, Molecular Biology, and Biophysics, University of Minnesota, Minneapolis, MN 55455, USA.

*To whom correspondence should be addressed. E-mail: lipsc001@umn.edu

the adjacent site opposite ligand Glu^{267}. The symmetrical, elliptical shape of the electron density of the diatomic molecule and the long distance between $C2^{4NC}$ and $O2^{O2}$ (2.4 Å) suggests that a bond between the 4NC and the bound oxygen has not yet formed. Two aspects of this structure are particularly noteworthy. First, the putative O_2 ligand is bound side-on ($O1^{O2}$-Fe = 2.5 Å and $O2^{O2}$-Fe = 2.4 Å) rather than the more commonly encountered end-on. Second, the plane of the 4NC ring is puckered rather than planar; this causes the $C2^{4NC}$ hydroxyl substituent to move far out of plane, which strengthens the hydrogen bond with Tyr^{257}. No deviation from a planar aromatic ring is observed for the anaerobic complex of 2,3-HPCD with substrate (*10*). The deviation at $C2^{4NC}$ from sp^2 toward sp^3 hybridization is consistent with electron transfer from 4NC to O_2 via the iron to give the ring cation-radical character and the O_2 superoxide character (see Fig. 1, II). Consequently, the superoxo state is assumed, and an O–O distance of 1.34Å was used during refinement (*21*).

The structures of subunits B and D (Fig. 3B) show that a bond has formed between $C2^{4NC}$ and $O2^{O2}$ (1.4 Å) to generate the alkylperoxo intermediate (see fig. S5). The ring of 4NC becomes more extensively puckered, and $C2^{4NC}$ assumes a full sp^3 hybridization, while both $O2^{4NC}$ and $O1^{4NC}$ remain coordinated to the iron (2.3 and 2.2 Å, respectively). During refinement of the alkylperoxo ligand, $C2^{4NC}$ was restrained to tetrahedral geometry (109.5°), and the O–O bond distance was refined to 1.5 Å (*22*). The bond between $O1^{O2}$ and the iron is retained (2.1 Å), but $O2^{O2}$ moves out of bonding distance (2.8 Å) in position to be transferred to the 4NC.

The structure in subunit A (Fig. 3C) shows that the aromatic ring of 4NC has been broken between the $C2^{4NC}$ and $C3^{4NC}$ carbons to form the ring-open product (see Fig. 1, V). The product remains bound to the iron via the carboxylate derived from the $C2^{4NC}$ carbon and the hydroxyl from the former $C1^{4NC}$ carbon. The newly formed carboxylate rotates to the optimal bonding orientation; this provides direct evidence for ring fissure. The open-ring structure allows rotation of the bonds that are not fixed by the iron-ligand structure. As a result, the electron density for two of the former ring carbons is not observed (see fig. S2) (*23*). The aldehyde and nitro substituents of the product interact strongly with the normal anion-binding pocket created by His^{248}, Arg^{243}, and Arg^{293} allowing electron density to be observed. However, the data do not allow the relative orientations of the aldehyde and nitro groups to be determined with certainty (fig. S3). The orientation shown in Fig. 3C causes the fewest bad contacts. Solvent occupies the iron-ligand position formerly occupied by oxygen, as it does in the structure of the resting enzyme after release of the product.

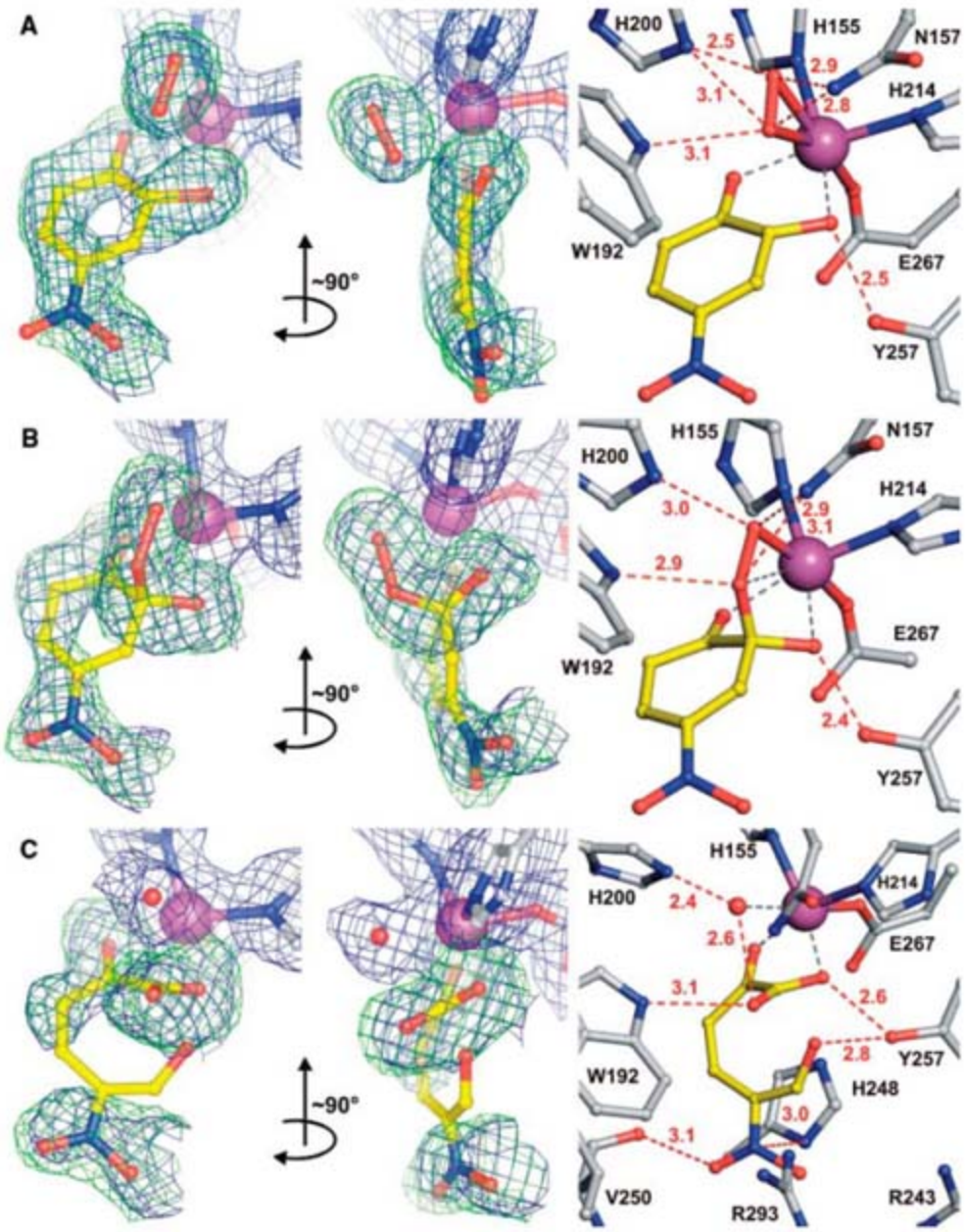

Fig. 3. Structures of reactive species trapped in the active sites of 2,3-HPCD during in crystallo reaction with 4NC and O_2 (PDB code 2IGA). (**A**) Ternary complex (subunit C) of enzyme with 4NC semiquinone and side-on bound dioxygen species. (**B**) Alkylperoxo intermediate complex [subunit D, similar structure observed in subunit B (not shown)]. (**C**) Complex with open-ring product (subunit A). The blue $2F_{obs} - F_{calc}$ maps are contoured at 1.0 σ (A, B) and 0.75 σ (C). The green $F_{obs} - F_{calc}$ ligand-omit maps were computed by removing ligands from the model and are contoured at +4 σ (A), 3.75 σ (B), and 3 σ (C). Atom color code: gray, carbon (enzyme residues); yellow, carbon (ligands); blue, nitrogen; red, oxygen; purple, iron. Red dashed lines show hydrogen-bonds (Å). Gray dashed lines indicate bonds or potential bonds to iron; distances are given in the text or in table S3. Additional views of the complexes are given in fig. S1.

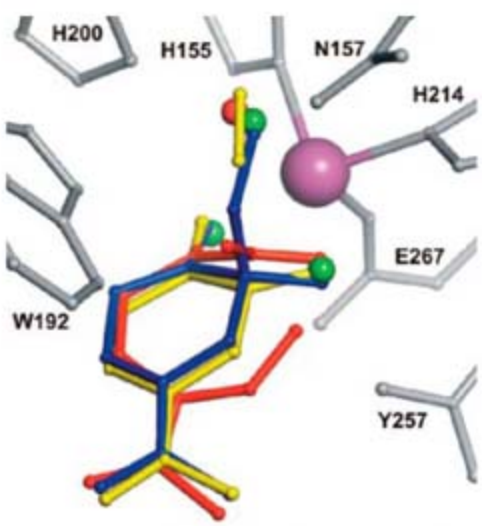

Fig. 4. Structure superposition of Fe-bound ligands observed at different steps of catalytic reaction: solvent in resting state (green), substrate and dioxygen (yellow, Fig. 3A), alkylperoxo intermediate (blue, Fig. 3B), ring-open product and solvent (red, Fig. 3C). Active site residues and Fe are shown in gray and purple, respectively.

Although the simultaneous presence of three different reaction cycle intermediates in a single enzyme with four independent active sites is not surprising, it was not anticipated that they could be independently observed in an x-ray crystal structure. If they occurred randomly in all of the active sites present in the crystal, only the (uninterpretable) average of all of the structures would be observed. This implies that, in the crystal, the reaction proceeds rapidly only as far as a specific intermediate in the active site located in a given region of the asymmetric unit. Similar observations have been made in a few other enzyme crystals (*24*). It is likely that the different reactivities of the 2,3-HPCD subunits can be attributed to crystal packing forces that cause minor structural differences (Fig. 2B). This is especially true at the interface between symmetry-related elements involving the residues surrounding the C-terminal lid that covers the active site cavity and alters the interaction of active site residues with the substrate (Fig. 2A). (For further information see table S2.)

The presence of product bound in the active site of one subunit shows that the enzyme in the crystal form used is active (see supporting online material). This suggests that the superoxo and alkylperoxo intermediates observed in the same crystal are relevant to the catalytic process. As such, they offer direct evidence for some of the most important aspects of the mechanistic hypothesis proposed previously (*4*, *8*, *17*). Specifically they show that: (i) the aromatic substrate and oxygen are bound to the iron simultaneously in adjacent sites; (ii) electron transfer occurs between these two substrates, giving rise to the puckered substrate ring; (iii) the attack on oxidized substrate occurs before O–O bond cleavage, apparently by the Fe^{2+}-superoxo species; (iv) the next cycle intermediate is not a dioxetane, as proposed in some early studies (*25*); and (v) the alkylperoxo intermediate that does form is located between the iron and the OH-bearing, C2 carbon of the aromatic substrate.

The observation of a side-on rather than an end-on oxy complex was not anticipated because we have shown in the past that the O_2 surrogate, NO, which can only form an end-on complex with iron, binds very strongly to the enzyme-substrate complex (*6*). Thus, there is sufficient room near the diatomic molecule–binding site for an end-on O_2 complex. Such a complex could lead to, or evolve from, the side-on complex observed. Hydrogen bonding interactions between the bound O_2 and the second sphere residues probably play important roles in stabilizing the unusual side-on binding orientation. In particular, His^{200} and Asn^{157} interact with dioxygen-derived atoms in both superoxo and alkylperoxo complexes (Fig. 3, A and B). The side-on binding orientation positions the oxygen adduct perfectly to react with the substrate at the correct ring carbon (Fig. 4).

It should be noted that the only other structurally characterized O_2 adduct among the mononuclear nonheme iron family also exhibits side-on binding (*26*). This species forms in the Rieske-type *cis*-diol forming naphthalene 1,2-dioxygenase (NDO) which differs in many structural and mechanistic respects from the ring-cleaving dioxygenase studied here (*27*, *28*). As for 2,3-HPCD, the side-on O_2 binding in NDO may be enforced by steric interactions, in that case, by close binding of the substrate and an asparagine residue. In NDO, two electrons (one from the Fe^{2+} and the other from a Rieske FeS cluster) are transferred to the O_2 in forming the side-on complex, resulting in a peroxo-Fe^{3+} species. The NDO complex O–O bond (1.47 Å) is as long or longer than that assumed here for the oxygen adduct, and it exhibits shorter bonds to Fe (1.99 and 1.74 Å), consistent with a greater degree of electron transfer to the oxygen and the consequent higher oxidation state of the iron.

The current studies provide experimental support for many aspects of recent computational investigations of the mechanism, but they also highlight a few inconsistencies. The side-on oxy complex was not predicted in the computational studies (*11*, *12*), which were influenced by the structure of the end-on nitrosyl complex (*7*). The alkylperoxo intermediate resembles the computed structures in bond lengths and orientations. In particular, it assumes the quasi-axial position relative to the substrate ring suggested by Bugg and Lin to direct extradiol rather than intradiol ring cleavage (*29*). As is pointed out in computational studies, hydrogen-bonding interactions and proton transfer to $O1^{O2}$ in the alkylperoxo intermediate are readily supported by the active site structure (Fig. 3, A and B) (see supporting online material for a discussion of the particularly strong hydrogen bonds). However, the current structural study shows that the proton donor is likely to be the ideally positioned His^{200} rather than the suggested water (not present) (*12*) or Glu^{267} (located on the other side of the iron) (*11*). This conclusion is in accord with kinetic studies of 2,3-HPCD His^{200} mutants that revealed a dramatic decrease in the rate constant for O–O bond cleavage in the absence of an in situ acid catalyst (*17*).

The extradiol dioxygenase is the archetypal member of the exceptionally broad class of Fe^{2+}-containing enzymes termed the 2-His-1-carboxylate facial triad family that catalyzes reactions ranging from aromatic biodegradation to the biosynthesis of antibiotics and the building blocks for mammalian connective tissue (*9*, *30*). Many of these enzymes activate O_2 during their catalytic cycle and bind substrates simultaneously to multiple Fe^{2+} ligand sites as described in the context of extradiol dioxygenases (*4*). A general mechanistic scenario for this enzyme class emerges from the structural studies presented here, in which the dual role of the iron is to juxtapose properly the organic substrate and O_2 and to facilitate electron transfer from the former to the latter. After this common initial oxygen activation step, a myriad of reactions can be envisioned.

References and Notes

1. B. J. Wallar, J. D. Lipscomb, *Chem. Rev.* **96**, 2625 (1996).
2. M. Costas, M. P. Mehn, M. P. Jensen, L. Que Jr., *Chem. Rev.* **104**, 939 (2004).
3. J. D. Lipscomb, A. M. Orville, *Met. Ions Biol. Syst.* **28**, 243 (1992).
4. D. M. Arciero, J. D. Lipscomb, *J. Biol. Chem.* **261**, 2170 (1986).
5. T. Senda *et al.*, *J. Mol. Biol.* **255**, 735 (1996).
6. D. M. Arciero, A. M. Orville, J. D. Lipscomb, *J. Biol. Chem.* **260**, 14035 (1985).
7. N. Sato *et al.*, *J. Mol. Biol.* **321**, 621 (2002).
8. L. Shu *et al.*, *Biochemistry* **34**, 6649 (1995).
9. S. Han, L. D. Eltis, K. N. Timmis, S. W. Muchmore, J. T. Bolin, *Science* **270**, 976 (1995).
10. M. W. Vetting, L. P. Wackett, L. Que Jr., J. D. Lipscomb, D. H. Ohlendorf, *J. Bacteriol.* **186**, 1945 (2004).
11. R. J. Deeth, T. D. H. Bugg, *J. Biol. Inorg. Chem.* **8**, 409 (2003).
12. P. E. M. Siegbahn, F. Haeffner, *J. Am. Chem. Soc.* **126**, 8919 (2004).
13. M. A. Miller, J. D. Lipscomb, *J. Biol. Chem.* **271**, 5524 (1996).
14. Visible residues out of a total of 365: C-terminal-deleted enzyme, 4-322 (PDB 1F1X); original full-length enzyme, 4-359 (PDB 1QO0); Form reported here, 4-362 (PDB 2IG9, 2IGA).
15. Materials and methods and structure statistics (table S1) are available as supporting material on *Science* online.
16. S. L. Groce, M. A. Miller-Rodeberg, J. D. Lipscomb, *Biochemistry* **43**, 15141 (2004).
17. S. L. Groce, J. D. Lipscomb, *Biochemistry* **44**, 7175 (2005).
18. J. Hajdu *et al.*, *Nat. Struct. Biol.* **7**, 1006 (2000).
19. Nomenclature: The superscript denotes the molecular origin of the atom. 4NC hydroxyl substituents are termed $O1^{4NC}$ and $O2^{4NC}$ on the basis of the carbon with which they are associated. O_2 atoms are termed $O1^{O2}$ and $O2^{O2}$, where O1 is that which remains bound to the iron in the alkylperoxo intermediate.
20. No diatomic molecule that can bind to Fe^{2+} other than O_2 is present in the crystallization medium. Attempts to fit the electron density without a diatomic molecule, with only a single atom, or with two solvents were unsuccessful (fig. S4).
21. At the current resolution (1.95 Å), diatomic bond lengths between 1.2 and 1.4 Å could be used to fit the electron density. Thus, the state of reduction of the bound O_2 could not be determined from the density alone.
22. Although no appropriate model complex for an Fe^{2+} alkylperoxo species has been reported, a Mn(II) chelate complex exhibits an O–O bond length of 1.411 Å, similar to that of free H_2O_2 (*31*).
23. The electron density is low for the three carbons closest to the nitro substituent supporting the presence of the more flexible, ring-open product in the active site. Product from 4NC was soaked into a crystal of 2,3-HPCD, and it assumed the same structure (fig. S2).
24. M. Hogg, S. S. Wallace, S. Doublie, *EMBO J.* **23**, 1483 (2004).
25. O. Hayaishi, H. Katagiri, S. Rothberg, *J. Am. Chem. Soc.* **77**, 5450 (1955).
26. A. Karlsson *et al.*, *Science* **299**, 1039 (2003).
27. M. D. Wolfe, J. V. Parales, D. T. Gibson, J. D. Lipscomb, *J. Biol. Chem.* **276**, 1945 (2001).
28. E. Carredano *et al.*, *J. Mol. Biol.* **296**, 701 (2000).
29. T. D. H. Bugg, G. Lin, *Chem. Commun.* 941 (2001).
30. E. L. Hegg, L. Que Jr., *Eur. J. Biochem.* **250**, 625 (1997).
31. H. Komatsuzaki *et al.*, *Inorg. Chem.* **37**, 6554 (1998).
32. Single-letter abbreviations for the amino acid residues are as follows: A, Ala; C, Cys; D, Asp; E, Glu; F, Phe; G, Gly; H, His; I, Ile; K, Lys; L, Leu; M, Met; N, Asn; P, Pro; Q, Gln; R, Arg; S, Ser; T, Thr; V, Val; W, Trp; and Y, Tyr.

33. The authors thank A. R. Pearson, B. J. Johnson, C. M. Wilmot, and D. H. Ohlendorf for their guidance and critical discussions during the course of this work, and J. C. Nix for technical assistance in data collection. This work was supported by National Institute of General Medical Sciences GM24689. We are grateful for beam time and assistance with x-ray data collection at the Lawrence Berkeley Laboratory Advanced Light Source (ALS), and for facilities and computer support from the Minnesota Supercomputing Institute. Coordinates have been deposited in the Protein Data Bank (PDB) [www.rcsb.org/pdb] as entries 2IG9 (full-length enzyme) and 2IGA (enzyme reacted with 4NC and O_2).

Supporting Online Material
www.sciencemag.org/cgi/content/full/316/5823/453/DC1
Materials and Methods
SOM Text
Figs. S1 to S5
Tables S1 to S3
References

5 September 2006; accepted 12 February 2007
10.1126/science.1134697

Neuronal Competition and Selection During Memory Formation

Jin-Hee Han,[1,2,3]* Steven A. Kushner,[4,5,6]* Adelaide P. Yiu,[1,3] Christy J. Cole,[1,2] Anna Matynia,[4] Robert A. Brown,[4] Rachael L. Neve,[7] John F. Guzowski,[8] Alcino J. Silva,[4] Sheena A. Josselyn[1,2,3]†

Competition between neurons is necessary for refining neural circuits during development and may be important for selecting the neurons that participate in encoding memories in the adult brain. To examine neuronal competition during memory formation, we conducted experiments with mice in which we manipulated the function of CREB (adenosine 3′,5′-monophosphate response element–binding protein) in subsets of neurons. Changes in CREB function influenced the probability that individual lateral amygdala neurons were recruited into a fear memory trace. Our results suggest a competitive model underlying memory formation, in which eligible neurons are selected to participate in a memory trace as a function of their relative CREB activity at the time of learning.

Competition is a fundamental property of many biological systems and creates selective pressure between individual elements. For example, competition between bilateral monocular neural inputs mediates ocular dominance plasticity (*1*, *2*). The transcription factor CREB (adenosine 3′,5′-monophosphate response element–binding protein) has been implicated in this competition in the developing brain (*3*, *4*). The finding that only a portion of eligible neurons participate in a given memory (*5*–*8*) suggests that competition between neurons may also underlie plasticity in adult brain.

Plasticity within the lateral amygdala (LA) is required for auditory conditioned-fear memories (*7*, *9*–*11*). Although ~70% of LA neurons receive the necessary sensory input, only one-quarter exhibit auditory fear conditioning–induced plasticity (*6*, *7*). We found that a similar proportion of LA cells show activated CREB (phosphorylation at Ser^{133}) after auditory fear conditioning (Fig. 1A), which suggests a role for CREB in determining which neurons are recruited into the fear memory trace. To examine this result, we manipulated CREB function in a similar portion of LA neurons by microinjecting replication-defective herpes simplex viral vectors expressing endogenous or dominant-negative CREB ($CREB^{WT}$ and $CREB^{S133A}$, respectively) fused with green fluorescent protein (GFP) (*12*).

To maximize the relative difference in CREB function between neurons, we first increased CREB levels in a subset of LA neurons in mutant mice that have reduced CREB function. Mice lacking the major isoforms of CREB (α and δ; CREB-deficient mice) show deficits in developmental and adult plasticity, including auditory fear memory (*13*, *14*) (Fig. 1B and fig. S1A). We microinjected $CREB^{WT}$ or control vector into the LA of CREB-deficient or wild-type littermate mice before fear conditioning and assessed memory (the percentage of time mice spent freezing during subsequent tone presentation) 24 hours later. Although $CREB^{WT}$ vector

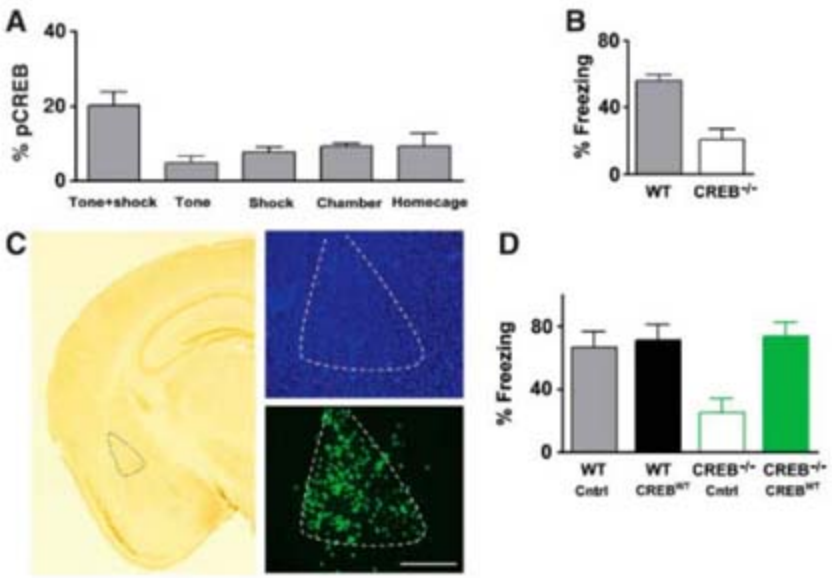

Fig. 1. Auditory fear conditioning activates CREB in ~20% of LA cells in wild-type (WT) mice; increasing CREB function in a similar portion of LA neurons rescues the fear memory deficit in CREB-deficient mice. (**A**) Percentages of LA cells expressing phosphorylated CREB after fear conditioning (tone + shock, $n = 6$) was higher than after control conditions [tone alone ($n = 4$), immediate shock ($n = 4$), exposure to chamber ($n = 4$), or homecage control ($n = 4$), $F(4,17) = 5.36$, $P < 0.05$]. Error bars in all figures represent SEM. (**B**) CREB-deficient ($CREB^{-/-}$) mice show impaired auditory fear memory [$F(1,20) = 24.23$, $P < 0.05$; WT $n = 12$, CREB-deficient $n = 10$]. (**C**) Left: Outline of the LA. Right: Roughly 20% of LA neurons expressed GFP after infusion of $CREB^{WT}$ vector [top, nuclei stained with 4′,6′-diamidino-2-phenylindole (DAPI); bottom, GFP]. Scale bar, 250 μm. (**D**) Microinjection of control vector (Cntrl; $n = 8$) or $CREB^{WT}$ vector ($n = 9$) did not change the high freezing in WT mice, whereas microinjection of $CREB^{WT}$ vector ($n = 9$), but not control vector ($n = 8$), into the LA of CREB-deficient mice rescued this memory deficit [Genotype × Vector $F(1,30) = 6.64$, $P < 0.05$].

[1]Program in Neurosciences and Mental Health, Hospital for Sick Children, 555 University Avenue, Toronto, Ontario M5G 1X8, Canada. [2]Department of Physiology, University of Toronto, Toronto, Ontario M5S 1A8, Canada. [3]Institute of Medical Sciences, University of Toronto, Toronto, Ontario M5S 1A8, Canada. [4]Departments of Neurobiology, Psychology, and Psychiatry, and Brain Research Institute, Gonda Building, 695 Young Drive South, University of California, Los Angeles, CA 90095, USA. [5]Department of Psychiatry, Columbia University, New York, NY 10032, USA. [6]New York State Psychiatric Institute, New York, NY 10032, USA. [7]Molecular Neurogenetics Laboratory, Department of Psychiatry, Harvard Medical School, McLean Hospital, Belmont, MA 02478, USA. [8]Neurobiology and Behavior, School of Biological Sciences, University of California, Irvine, CA 92697, USA.

*These authors contributed equally to this work.
†To whom correspondence should be addressed. E-mail: sheena.josselyn@sickkids.ca

infected only 18.0 ± 3.2% of LA neurons (Fig. 1C), the memory impairment in CREB-deficient mice was completely rescued: CREB-deficient mice infused with $CREB^{WT}$ vector froze at levels similar to those of wild-type mice infused with either $CREB^{WT}$ or control vector (Fig. 1D). Moreover, microinjecting $CREB^{WT}$ vector into the LA of CREB-deficient mice failed to rescue the memory impairment observed in a parallel-context fear-conditioning task (fig. S2) that also critically depends on intact hippocampal function (*15*). This finding indicates that infusing $CREB^{WT}$ vector into the LA does not simply increase freezing.

We next examined whether neurons containing $CREB^{WT}$ vector were disproportionately represented in the fear memory trace. To visualize the memory trace, we used the activity-dependent gene *Arc* (activity-regulated cytoskeleton-associated protein; also termed *Arg3.1*) (*8*). Neuronal activity induces a rapid but transient increase in *Arc* transcription, such that nuclear-localized *Arc* RNA serves as a molecular signature of a recently (5 to 15 min) active neuron (*8*). Five minutes after the fear memory test, we removed the brain and used fluorescence in situ hybridization to detect *Arc* RNA (*8*). Only neurons active in the preceding minutes (during the memory test) would have *Arc* RNA localized to the nucleus ("Arc^{+nuc}").

If relative CREB function influences the probability that individual LA neurons are selected to participate in the Arc^{+} memory trace, then neurons with elevated CREB function (with $CREB^{WT}$ vector) should be more likely than neighboring neurons (without $CREB^{WT}$ vector) to be Arc^{+} after the memory test. Indeed, in wild-type mice the probability of detecting Arc^{+} nuclei was higher by a factor of ~3 in neurons with $CREB^{WT}$ vector (64.1 ± 5.8%) than in their noninfected neighbors (19.5 ± 4.6%). In contrast, neurons containing control vector were no more likely to be Arc^{+} than their neighbors in either wild-type or CREB-deficient mice (Fig. 2, B and D). The preferential distribution of Arc^{+} nuclei in neurons with higher CREB function was also observed immediately after training (fig. S3). The bias in Arc^{+} distribution was even greater in CREB-deficient mice, where the probability of detecting Arc^{+} nuclei was higher by a factor of ~10 in neurons with $CREB^{WT}$ vector (69.6 ± 2.0%) than in their neighbors (6.9 ± 1.3%) (Fig. 2C).

Because the intense training (0.75-mA shock) used above induced ceiling levels of freezing in wild-type mice, we trained additional groups with a lower-intensity shock (0.4 mA) to examine

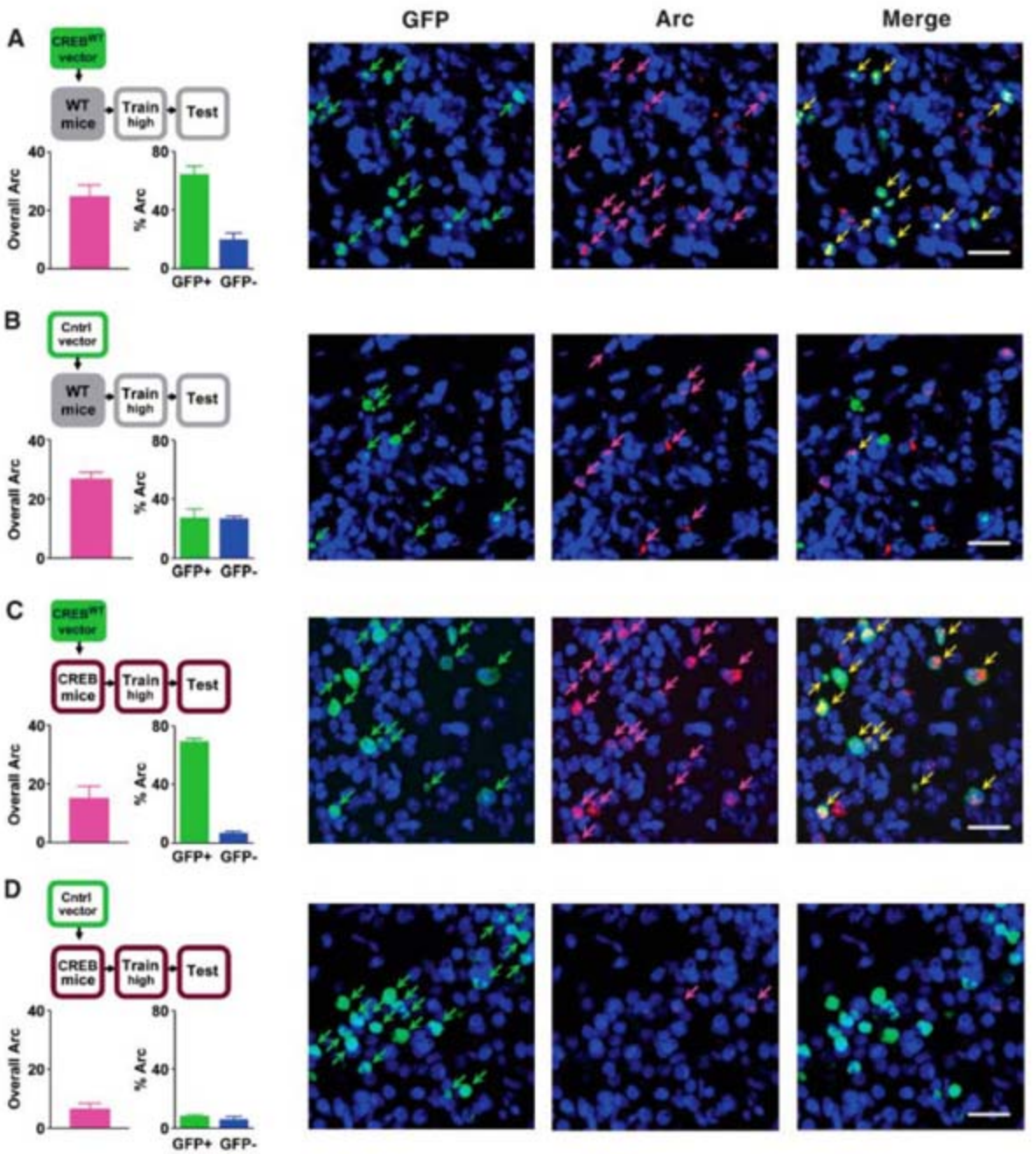

Fig. 2. Neurons with increased CREB function are more likely than their neighbors to be recruited to the fear memory trace. (**A**) Left: Proportion of LA neurons that were Arc^{+} (involved in the memory trace) in WT mice infused with $CREB^{WT}$ vector. Middle: Arc^{+} nuclei were more likely to be in neurons containing $CREB^{WT}$ vector (GFP^{+}) than in noninfected neighbors (GFP^{-}) [$F(1,4) = 23.31$, $P < 0.05$]. Right: Confocal images of LA. Blue, nuclei; green arrows, GFP^{+} (with $CREB^{WT}$ or control vector); pink arrows, Arc^{+} nuclei; yellow arrows, double-labeled neurons (GFP^{+} and Arc^{+}). (**B** and **D**) Arc^{+} nuclei were equally distributed in neurons with (GFP^{+}) and without (GFP^{-}) the control vector in WT (B) and CREB-deficient (D) mice ($Ps > 0.05$). (**C**) Arc^{+} nuclei were more likely to be in neurons with (GFP^{+}) than without (GFP^{-}) $CREB^{WT}$ vector in CREB-deficient mice [$F(1,2) = 373.42$, $P < 0.05$]. Scale bar, 50 μm.

the effects of increasing CREB function in wild-type mice. Increasing CREB function enhanced memory (Fig. 3A), consistent with results in flies (*16*), *Aplysia* (*17*), rats (*18*, *19*), and hamsters (*20*). Furthermore, the probability of detecting Arc^+ nuclei was higher by a factor of ~3 in neurons with $CREB^{WT}$ vector (65.8 ± 5.0%) than in neighboring neurons (21.9 ± 4.2%) (Fig. 3A and fig. S3), similar to the distribution of Arc observed in wild-type mice trained with a more intense protocol.

These imaging data could be simply explained if increasing CREB function directly induces *Arc* transcription. Previous findings do not support this idea (*21*), likely because the *Arc* promoter lacks a consensus CRE site (*22*). Nonetheless, to examine whether neurons with increased CREB function were more likely than their neighbors to be Arc^+ independent of fear conditioning, we microinjected $CREB^{WT}$ vector into the LA of wild-type mice that were not fear-conditioned. If increasing CREB function is sufficient to induce *Arc* expression, then neurons with $CREB^{WT}$ vector should be more likely than neighboring neurons to be Arc^+. However, the distribution of Arc^+ nuclei was similar in neurons with and without $CREB^{WT}$ vector in these home-cage mice (Fig. 3B). Because CREB may not be transcriptionally active under these conditions, we infused a vector encoding a constitutively active form of CREB [$CREB^{Y134F}$ (*23*)]. Again, neurons with increased CREB function (with $CREB^{Y134F}$ vector) were no more likely to be Arc^+ than their neighbors (Fig. 3C). Therefore, increasing CREB function in a subset of LA neurons in untrained mice does not affect the distribution of Arc, which highlights the importance of training and learning (fig. S4) in the preferential localization of Arc in neurons with increased CREB function.

Alternatively, neurons with increased CREB function may have a lower threshold for inducing *Arc* transcription that only becomes apparent in the fear memory test. We therefore microinjected wild-type mice with $CREB^{WT}$ vector 24 hours after training. Mice were tested 4 days after infusion and the distribution of Arc^+ was quantified. If the fear memory trace is consolidated in the LA within 24 hours after training (*24*, *25*), a preferential distribution of Arc in neurons with increased CREB function would not be expected. Although Arc^+ levels were comparable to those found in previous experiments in which wild-type mice were fear-conditioned (25.4 ± 4.0%), Arc was not preferentially localized in neurons with increased CREB function [$CREB^{WT}$ vector = 9.7 ± 1.6%, endogenous = 28.4 ± 3.7%, $F(1,4) = 27.58$, $P < 0.05$]. Together, these data suggest that increased CREB function enhances neuronal selection only during sufficiently salient learning.

We next investigated the effects of decreasing CREB function in a similar portion of LA neurons. We hypothesized that memory would be normal because the remaining neurons with intact CREB function would outcompete this subset for inclusion in the memory trace. Wild-type mice were microinjected with a vector expressing a dominant-negative form of CREB ($CREB^{S133A}$) before auditory fear training. Indeed, these mice showed normal memory (Fig. 3D). Consistent with this, the probability of detecting Arc^+ nuclei was lower by a factor of ~12 in neurons with $CREB^{S133A}$ vector (2.7 ± 0.6%) than in neurons without it (33.7 ± 0.9%) (Fig. 3D).

Together, these data provide evidence for neuronal selection during memory formation. The overall size of the Arc^+ fear memory trace was both consistent with electrophysiological estimates of the fear memory trace (*6*, *7*) and stable across experiments in fear-conditioned wild-type mice (Fig. 4A). That a constant proportion of LA neurons is recruited to the memory trace, regardless of CREB manipulation, suggests that the rules governing neuronal selection during memory formation are competitive rather than cell-autonomous. If neuronal selection were cell-autonomous, the size of the Arc^+ memory trace

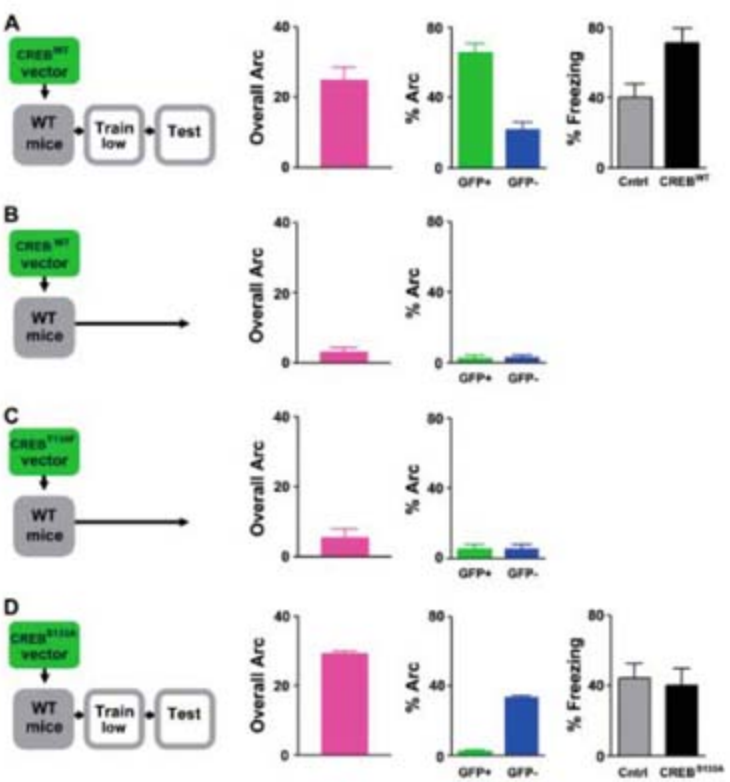

Fig. 3. Relative CREB function influences the recruitment of neurons into the memory trace. (**A**) Left: Proportion of Arc^+ LA neurons in WT mice with $CREB^{WT}$ vector. Middle: Arc^+ nuclei were more likely to be in neurons with $CREB^{WT}$ vector (GFP^+) than in noninfected (GFP^-) neurons [$F(1,3) = 23.62$, $P < 0.05$]. Right: $CREB^{WT}$ vector enhanced memory in WT mice trained with low-intensity shock [$F(1,11) = 7.31$, $P < 0.05$, control $n = 7$, $CREB^{WT}$ vector $n = 6$]. (**B** and **C**) Middle: Proportion of Arc^+ LA neurons in untrained WT mice with $CREB^{WT}$ (B) or constitutively active $CREB^{Y134F}$ (C) vector. Left: Neurons containing $CREB^{WT}$ (B) or constitutively active $CREB^{Y134F}$ (C) vector (GFP^+) were no more likely than noninfected neurons (GFP^-) to be Arc^+ in untrained mice ($P > 0.05$). (**D**) Neurons with decreased CREB function were less likely to be recruited to the memory trace. Left: Proportion of Arc^+ LA neurons. Middle: Arc^+ nuclei were less likely to be in neurons with $CREB^{S133A}$ vector (GFP^+) than in noninfected neurons (GFP^-) [$F(1,2) = 405.28$, $P < 0.05$]. Right: WT mice infused with $CREB^{S133A}$ vector show normal memory, even when trained with a lower-intensity shock [$F(1,13) = 2.08$, $P > 0.05$; control $n = 7$, $CREB^{S133A}$ $n = 8$].

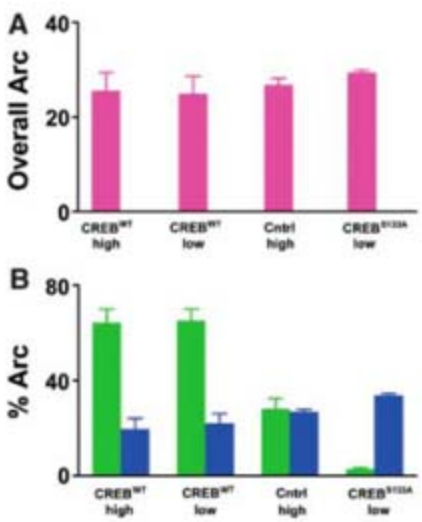

Fig. 4. Constant size of Arc^+ memory trace suggests competitive selection process. (**A**) Proportion of LA Arc^+ neurons did not differ in fear-conditioned WT mice, regardless of vector [$CREB^{WT}$, control, $CREB^{S133A}$] or training intensity [high (0.75-mA shock) or low (0.4-mA shock)] [$F(3,12) = 0.31$, $P < 0.05$]. (**B**) Distribution of Arc^+ varied according to CREB manipulation. First and second pairs of bars: Arc^+ nuclei were more likely to be in neurons with high CREB function (with $CREB^{WT}$ vector; GFP^+, green) than in noninfected neighbors (GFP^-, blue) in WT mice trained with high (first pair) or low (third pair) intensities. Third pair of bars: Arc^+ nuclei were equally distributed in neurons with (GFP^+, green) and without (GFP^-, blue) control vector. Fourth pair of bars: Arc^+ nuclei were less likely to be in neurons with decreased CREB function (with $CREB^{S133A}$ vector; GFP^+, green) relative to neighbors with intact CREB function (GFP^-, blue).

would vary according to CREB manipulation; $CREB^{WT}$ vector would induce a larger memory trace, whereas $CREB^{S133A}$ vector would induce a smaller one. Therefore, the finding that a fixed portion of winners emerge from a larger pool of eligible neurons suggests a competitive selection process. These studies reveal multiple aspects of this competition by advantaging ($CREB^{WT}$) and disadvantaging ($CREB^{S133A}$) subsets of neurons (Fig. 4B).

The precise mechanism by which CREB confers a competitive advantage to a neuron is unknown. Neurons infected with a vector expressing constitutively active CREB show facilitated long-term potentiation and an increased number of postsynaptically "silent" synapses relative to their noninfected neighbors (*26*). Silent synapses, containing *N*-methyl-D-aspartate (NMDA) receptors but not AMPA receptors, are highly plastic and may provide the necessary conditions for participation in new memory traces. Alternatively, CREB could increase neuronal excitability (*27*) and thus bias these neurons for selection into the memory trace. Nonetheless, our data show that in addition to being necessary for refining neural circuits during development, competition between neurons is fundamental to memory formation in the adult brain.

References and Notes

1. T. N. Wiesel, D. H. Hubel, *J. Neurophysiol.* **28**, 1029 (1965).
2. R. J. Cabelli, A. Hohn, C. J. Shatz, *Science* **267**, 1662 (1995).
3. T. A. Pham, S. Impey, D. R. Storm, M. P. Stryker, *Neuron* **22**, 63 (1999).
4. A. F. Mower, D. S. Liao, E. J. Nestler, R. L. Neve, A. S. Ramoa, *J. Neurosci.* **22**, 2237 (2002).
5. M. A. Wilson, B. L. McNaughton, *Science* **261**, 1055 (1993).
6. J. C. Repa *et al.*, *Nat. Neurosci.* **4**, 724 (2001).
7. S. Rumpel, J. LeDoux, A. Zador, R. Malinow, *Science* **308**, 83 (2005).
8. J. F. Guzowski, B. L. McNaughton, C. A. Barnes, P. F. Worley, *Nat. Neurosci.* **2**, 1120 (1999).
9. J. E. LeDoux, *Annu. Rev. Neurosci.* **23**, 155 (2000).
10. M. Davis, *Annu. Rev. Neurosci.* **15**, 353 (1992).
11. M. S. Fanselow, G. D. Gale, *Ann. N.Y. Acad. Sci.* **985**, 125 (2003).
12. M. Barrot *et al.*, *Proc. Natl. Acad. Sci. U.S.A.* **99**, 11435 (2002).
13. R. Bourtchuladze *et al.*, *Cell* **79**, 59 (1994).
14. T. A. Pham, J. L. Rubenstein, A. J. Silva, D. R. Storm, M. P. Stryker, *Neuron* **31**, 409 (2001).
15. R. M. Barrientos, R. C. O'Reilly, J. W. Rudy, *Behav. Brain Res.* **134**, 299 (2002).
16. J. C. Yin, M. Del Vecchio, H. Zhou, T. Tully, *Cell* **81**, 107 (1995).
17. D. Bartsch, A. Casadio, K. A. Karl, P. Serodio, E. R. Kandel, *Cell* **95**, 211 (1998).
18. S. A. Josselyn *et al.*, *J. Neurosci.* **21**, 2404 (2001).
19. T. L. Wallace, K. E. Stellitano, R. L. Neve, R. S. Duman, *Biol. Psychiatry* **56**, 151 (2004).
20. A. M. Jasnow, C. Shi, J. E. Israel, M. Davis, K. L. Huhman, *Behav. Neurosci.* **119**, 1125 (2005).
21. A. Barco *et al.*, *Neuron* **48**, 123 (2005).
22. R. Waltereit *et al.*, *J. Neurosci.* **21**, 5484 (2001).
23. K. Du, H. Asahara, U. S. Jhala, B. L. Wagner, M. Montminy, *Mol. Cell. Biol.* **20**, 4320 (2000).
24. K. Nader, G. E. Schafe, J. E. Le Doux, *Nature* **406**, 722 (2000).
25. S. Kida *et al.*, *Nat. Neurosci.* **5**, 348 (2002).
26. H. Marie, W. Morishita, X. Yu, N. Calakos, R. C. Malenka, *Neuron* **45**, 741 (2005).
27. Y. Dong *et al.*, *Nat. Neurosci.* **9**, 475 (2006).

28. Supported by Canadian Institutes of Health Research grant 480477 and Natural Sciences and Engineering Research Council of Canada grant RPGIN 250250 (S.A.J.), NIH grants AG13622 and P01HD33098 (A.J.S.), and Restracomp Fellowships (Hospital for Sick Children) (J.-H.H., A.P.Y., and C.J.C.). We thank E. J. Nestler and S. Kida for plasmids, A. DeCristofaro for technical assistance, M. Davis and P. W. Frankland for helpful discussions, and P. W. Frankland for comments on an earlier version of this manuscript.

Supporting Online Material

www.sciencemag.org/cgi/content/full/316/5823/457/DC1
Materials and Methods
SOM Text
Figs. S1 to S4
References

3 January 2007; accepted 20 March 2007
10.1126/science.1139438

Congratulations

to the AAAS Student Poster Winners!

AAAS Annual Meeting 15–19 February 2007

AAAS recognizes the winners of the 2007 Student Poster Competition at the AAAS Annual Meeting in San Francisco this past February. Their work in a variety of fields displayed originality and understanding that set them apart from their colleagues. First-place winners will receive cash prizes thanks to the generous support of Subaru.

PHOTOS: MICHAEL J. COLELLA

BRAIN AND BEHAVIOR

Winner: Shana R. Spindler, University of California, Los Angeles
Bazooka Localizes to Dendritic Branch Points in the Drosophila

Honorable Mention: Kameelah Abdullah and Desiree L. Salazar, University of California, Irvine
Delayed Transplantation of Human Central Nervous System Stem Cells Into Spinal Cord Contusion Injured NOD-Scid Mice

ENVIRONMENT AND ECOLOGY

Winner: Holmes Hummel, Stanford University
Policy Implications of Global Energy Scenarios for Climate Stabilization

Honorable Mention: Emily T. King, St. Mary's College of California
Transport Dynamics Associated with Surface Ozone Concentrations in Joshua Tree National Park

MATH, TECHNOLOGY, AND ENGINEERING

Winner: Manu Prakash, Massachusetts Institute of Technology
Microfluidic Bubble Logic

Honorable Mention: Dinesh G. Bansal, Georgia Institute of Technology
Design of a Precision Tribo-Tester for Studying Contact Transitions

MEDICINE AND PUBLIC HEALTH

Winner: Catherine Chen, Johns Hopkins University
Selectively Inhibiting MYC Oncogene Activation with Designed Peptides

Honorable Mention: Jorge L. Durand, Albert Einstein College of Medicine
A Novel Integration of MR Imaging and Raman Spectroscopy of Mouse Aortas

MOLECULAR AND CELLULAR

Winner: Sarah Piloto, University of California, Irvine
Requirements for an Ovo Orthologue in Neural Crest and Neural Tube Development

Honorable Mention: Shannon P. Fortin and Kelsey Drake, Arizona State University
Increased Fn14 Links to Glioma Cell Invastion and Poor Patient Outcome

PHYSICAL SCIENCES

Winner: Rodrigo Gonzalez, University of California, Los Angeles
Variations in Stability of Polynucleotide Hairpins Due to Stem-Loop Conformation

Honorable Mention: Dylan H. Rood, University of California, Santa Barbara and Lawrence Livermore National Laboratory
Changing Rates and Styles of Crustal Deformation at Timescales of 10 My to 10 Ky

SCIENCE AND SOCIETY

Winner: Lexyne L. McNealy, Northwestern University
Prosthetic Ankle Motion in Bilateral Transfemoral Amputees

Honorable Mention: Jean-François Sénéchal, Université Laval, Québec, Canada
Responsibility of Scientists: What Duties in the Struggle for Knowledge?

SOCIAL SCIENCES

Winner: Courtney Ficks, Lisa Doelger, and Karina R. Horowitz, Arizona State University; Whitney Guthrie, Pepperdine University
Child Psychopathology: Heritability and Parental Differential Treatment

Honorable Mention: David Bidwell and Rachael L. Shwom, Michigan State University
Deliberation Lite: How Does Feedback Influence Public Climate Change Policy?

►► Full abstracts can be viewed at www.aaasmeeting.org.

Keep an eye out for information about the 2008 AAAS Annual Meeting, 14–18 February in Boston.

For more details, visit
www.aaasmeeting.org

AAAS
ADVANCING SCIENCE, SERVING SOCIETY

EXIQON

Services also available

microRNA expression profiling
- using miRCURY™ LNA Arrays

Dear Researcher, we are happy to announce the launch of miRCURY™ LNA prespotted microarray slides and ready-to-spot probe sets for microRNA profiling for all organisms (vertebrates/invertebrates/plants/viruses) in miRBase 8.1. We have at least 92% coverage in miRBase 9.0.

Stay ahead of the field
- Most comprehensive probe set that contain proprietary miRPlus sequences not yet in miRBase

Increased discovery potential
- Cross species profile comparison possible
- Almost 1500 unique capture probes

Use less sample
- Works on 1 ug total RNA
- Highly sensitive LNA™ capture probes

Get reliable results
- Spike-In control probes for easy and improved normalizationprocedure and assessment of data quality and reproducibility
- Excellent discrimination of let-7 family members
- Tm normalized capture probes

Save time
- No miRNA enrichment required
- Fast 90 minutes miRNA labeling protocol

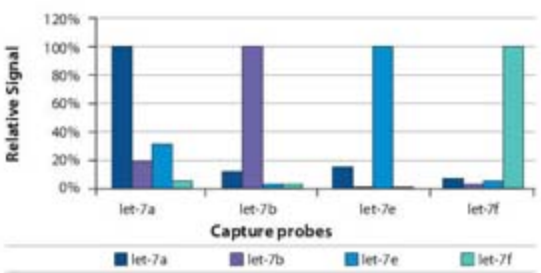

Discrimination of closely related miRNAs.

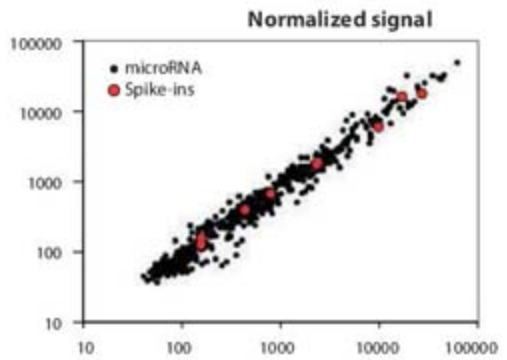

Spike-In capture probes allow assessment of reproducibility.

www.exiqon.com

Visit
www.exiqon.com/array
to learn more....

...or contact us for more info:

Phone:
US: 781 376 4150 / 888 miRCURY (EST)
Rest of world: +45 45 65 09 29 (GMT+1)

Email: support@exiqon.com

STEM CELLS:
BEYOND SOMATIC CELL NUCLEAR TRANSFER

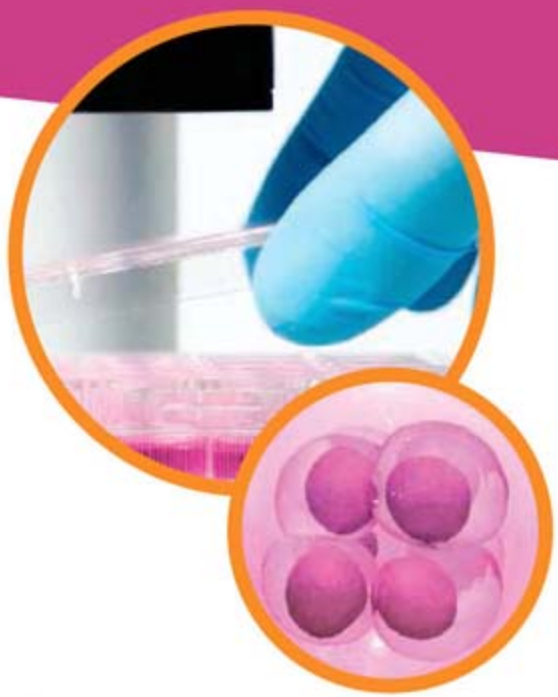

Despite the heated ethical and moral debate, research on embryonic stem cells has been forging ahead at breakneck speed. But before these cells make a dent in the clinic or in drug discovery, researchers must learn how to create cell lines from diseased individuals, so they can, for instance, learn how to stymie disease progression in others. Here we examine some of the recent scientific advances and look at where the technology pack leaders may take us in the future.
By Jeffrey M. Perkel

It's been 25 years since Martin Evans and Matthew Kaufman at the University of Cambridge and Gail Martin at the University of California, San Francisco independently launched the stem cell revolution with their establishment of murine embryonic stem cell lines, and the impact on biomedical research is undeniable.

As a research tool, embryonic stem cells – pluripotent progenitors, harvested from the inner cell mass of developing embryos, that can differentiate into any cell type in the body – "have revolutionized the way we do biomedical research," says George Daley, associate professor at **Children's Hospital Boston** and at the **Harvard Stem Cell Institute**. "Think of all the mouse models of cancer, of neurodegenerative and cardiovascular diseases that have really come about because of our ability to manipulate genes in murine embryonic stem cells."

But more than that, Daley says, researchers' ability to differentiate embryonic stem cells in a culture dish has made them interesting objects of study in their own right. "Those in vitro systems allow us to ask questions about tissue differentiation in a manner that previously was inaccessible," he says. Plus, he adds, the resulting elucidation of cellular lineages and how they emerge will provide a biological organizing principle akin to that gained from the sequencing of the human genome or chemistry's establishment of the periodic table of elements.

Yet many technical challenges remain, especially in humans. Precious little is known about the markers that distinguish one developmental lineage from another; about which cellular signals can induce differentiation in a controlled, robust, and predictable manner; and perhaps most important, about how to make embryonic stem cell lines from diseased individuals – a critical step for many therapeutic and drug-development applications.

Blast into the Past

Last August Shinya Yamanaka, professor of stem cell biology at the **Institute for Frontier Medical Sciences at Kyoto University**, demonstrated it was possible to deprogram murine somatic cells—specifically fibroblasts—into embryonic-like stem cells by expressing four genes: *c-myc*, *oct3/4*, *sox2*, and *klf4*.

According to Yamanaka, the proteins encoded by these genes—identified from a pool of 24 candidates—each serve a specific role: c-Myc opens tightly compacted chromatin, enabling the transcription factors oct3/4 and sox2 to bind to gene regulatory regions in the genome and restore pluripotency. klf4, he says, appears to fulfill two roles, both as a cofactor to oct3/4 and sox2, and as an apoptotic inhibitor.

Peter Mountford, president and CEO of **Stem Cell Sciences**, a stem cell research and development company in Edinburgh, UK, describes the findings as continued ›

> "Embryonic stem cells have revolutionized the way we do biomedical research."

Look for these **Upcoming** Articles

RNAi — June 1
Cell Signaling 2 — June 22
Microarray Technologies — August 24

Inclusion of companies in this article does not indicate endorsement by either AAAS or Science, *nor is it meant to imply that their products or services are superior to those of other companies.*

"In terms of cell therapy in general, it's likely some diseases will be treated by embryonic stem cells, and others by adult stem cells."

"potentially one of the most important breakthroughs and certainly one of the most extraordinary experiments in recent times."

Yamanaka says work is ongoing in his lab to migrate these findings to humans. Preliminary evidence suggests additional factors may be required, he says, but perhaps the biggest challenge to using this technique to make therapeutic patient-matched embryonic stem cells involves the gene-delivery technique itself.

"So far we can generate these embryonic stem cell–like cells only by using a retroviral system," Yamanaka explains. But retroviral vectors have been linked to leukemia in some gene therapy trials – a problem that is all the more acute because *c-myc*, at least, is a known oncogene. "Because of that, I think using the retroviral system is very, in a sense, dangerous," Yamanaka says.

Not implicated in Yamanaka's study was *nanog*, which like oct3/4 and sox2 is also a key transcriptional regulator in pluripotent cells. Kiminobu Sugaya, director of the **Stem Cell Laboratory at the University of Central Florida**, has presented data at meetings showing that adult mesenchymal stem cells—bone marrow–derived cells that are predestined to form connective tissues like bone and cartilage—can be dedifferentiated into embryonic-like stem cells by expression of *nanog*.

According to Kevin Eggan, assistant professor of molecular and cellular biology at **Harvard University**, others have shown that nuclear reprogramming during cell fusion can likewise be made more efficient by overexpression of *nanog* in mouse embryonic stem cells. "But that doesn't directly show that *nanog* is directly required for reprogramming in the sense that Yamanaka did," he cautions.

Sugaya's goal is to develop neural stem cell–based therapies for conditions like stroke and Alzheimer's disease. The process can work using fetal tissue-derived neural cells, he notes, "but the availability of these cells isn't so great." And in any event, such cells could provoke an immune response – hence, Sugaya's interest in autologous, adult stem cells.

Before they can be converted into neural tissue, however, the cells must relearn how to be embryonic. "We have to erase the memory, the commitment of the cells," Sugaya says. "Then we have to teach them what to become."

The Essence of ESC

When Sugaya talks of cellular memory, he is referring essentially to the epigenetic changes that occur as embryonic stem cells differentiate. All cells contain the same DNA, but embryonic stem cells express different genes to the more developmentally committed lineages. That change arises in part due to changes in gene methylation, changes which must be reset if the cells are to be restored to pluripotency.

A cell is called pluripotent if it can develop into any of the three germ layers of the body: endoderm, mesoderm, and ectoderm. Ectoderm gives rise to the skin, epidermis, and the nervous system; from mesoderm arises heart tissue, kidney, gonads, continued ›

Selected Embryonic Stem Cell Tools

Embryonic stem cells present a number of unique challenges that distinguish them from run-of-the-mill cultured cells. For one thing, embryonic stem cells traditionally are cultured either on a murine embryonic fibroblast feeder layer, or in media that have been conditioned by such cells. In addition, like many cultured cells, embryonic stem cells require "black-box" additives, such as fetal bovine serum.

Both of these components pose not only a potential contamination risk, but also a batch-to-batch consistency problem. Sera, for instance, can vary based on the animal's age, diet, sex, health, and reproductive status, among other factors, says Peter Mountford, president and CEO of Stem Cell Sciences. "You really have to get rid of any noncharacterized component. It must be like a chemical formula, so that every time you make it, it is exactly the same."

Mountford's company has developed media formulations, available through Millipore, for murine embryonic stem cell culture that require neither feeder cells nor serum; human media formulations that no longer require serum, but still require feeder cells, are also available.

Invitrogen also is developing so-called fully defined media formulations, part of the company's cradle-to-grave strategy for embryonic stem cell work, according to Joydeep Goswami, Invitrogen's vice president of stem cell and regenerative medicine division. Invitrogen plans to release in the third quarter of 2007 "the first feeder-free and serum-free defined culture media for human embryonic stem cells," Goswami says.

Cellartis is looking to modify culture procedures for industrial applications. Embryonic stem cells traditionally are passaged mechanically, by physically transferring undifferentiated colonies into fresh culture dishes. Such a process can be neither scaled nor automated easily. The company has developed a single-cell, enzyme-based dissociation method that can be used to maintain cells in culture flasks rather than in dishes, without enriching for chromosomal abnormalities.

"That means you can get more cells, more easily, and in an undifferentiated state," says Johan Hyllner, Cellartis's chief scientific officer. The enzyme at the heart of this approach is TrypLE, a recombinant trypsin from Invitrogen. Used to passage cells, trypsin typically is of porcine origin, but Invitrogen's reagent removes that animal-based component from the workflow.

BD Biosciences, a segment of Becton, Dickinson and Company, focuses on monitoring stem cell differentiation, or lack thereof. Embryonic stem cells can form any of the body's 220 or so different cell types, and each one expresses a unique, and largely undefined, set of intracellular and surface markers. The company offers several thousand antibodies for research use, but according to Robert Balderas, vice president of research and development, life science research reagents, there currently is no "perfect" marker or biosignature that defines the pluripotent stem cell, let alone its myriad descendents.

"There is a continual need for the identification of new proteins on these subsets of cells so that applications like fluorescence activated cell sorting can be used to better define, characterize, and isolate these cells," Balderas says.

blood cells and vessels, muscle, and connective tissue; and from endoderm comes the gut tube, plus all the principal organs that bud off of that, including the liver, pancreas, and lungs.

Adult stem cells, such as hematopoietic or neural stem cells, are not pluripotent, because they can yield only a limited number of different cell types: hematopoietic stem cells can create blood cells, for instance, but not skin.

According to Leonard Zon, the Grousbeck Professor of Pediatrics at **Harvard Medical School**, "We need to get better at turning embryonic stem cells into tissues more robustly, and that involves understanding how normal embryos make tissues and adapting those gene programs to the embryonic stem cells in culture." Researchers at **Novocell**, a stem cell engineering firm in San Diego, used precisely that approach in 2005 to coax embryonic stem cells to form definitive endoderm.

"I thought that was a breakthrough," says Johan Hyllner, chief scientific officer at **Cellartis**, a Swedish/Scottish company that uses human embryonic stems to derive both hepatocyte- and cardiomyocyte-like cells. "Endoderm was one of the trickier germ layers to grow. Ectoderm and mesoderm are somewhat easier to get, but true endoderm has been a challenge until this paper came out."

As Emmanuel Baetge, Novocell's chief scientific officer, puts it, the trick was to heed the lessons of cell biology. The three germ layers are established during gastrulation, occurring in the second to third week of human development. "We said, let's see if we can make human embryonic stem cells undergo a process like gastrulation to make definitive endoderm," Baetge explains.

The key was to force the cells to differentiate by both removing serum and the growth factors—fibroblast growth factor and insulin—and by adding a protein called activin. Activin is a member of the transforming growth factor (TGF)-ß family of signaling molecules, another member of which (Nodal) helps define germ layer fate during gastrulation.

Baetge and his team published a follow-up paper last year describing how to push the development even further, to create in four discrete steps fetal pancreatic islets – the insulin-producing cells that one day could be used as transplants for type 1 diabetics.

As with the first study, the key to this latest advance lay in the developmental biology literature, by knowing which factors to add, and in what order, says Baetge.

"If you want to work with stem cells, you need to apply developmental biology principles," he says. "They can provide a framework in which you should try to operate with these cells if you want to make defined lineages."

The Embryo with No Father

According to Eggan, Yamanaka's technique is one of three "ponies" in the race to develop patient-specific cell lines. The others are somatic cell nuclear transfer (SCNT), the technique used to clone Dolly the sheep, and cellular fusion, a technique in which a somatic cell is fused with an embryonic stem cell line, thereby sending the somatic cell back to its embryonic roots.

Each has pros and cons, says Eggan. Yamanaka's cells, for instance, "aren't really embryonic stem cells" – because they are neither completely reprogrammed nor express the full complement of embryonic genes. SCNT requires human eggs, which are hard to come by, while with cell fusion, "no one has figured out how to get rid of the embryonic chromosomes."

Daley at Harvard is working on yet another strategy: parthenogenesis. Literally meaning "virgin birth," parthenogenesis is a process in which an egg is tricked into thinking it has been fertilized and begins to develop into an embryo, without the contribution of a sperm. At the same time, the cell is prevented from completing the second round of meiosis that normally occurs, so that the cell ends up with a diploid chromosome content, all of which comes from the mother.

Ignoring the effects of crossing over, "it's like taking half a deck of cards and then photocopying them to give 52 cards," explains Michael West, president and CEO of **Advanced Cell Technology**, a stem cell company that also pursues parthenogenic stem cell lines.

According to Daley, parthenogenesis, which to date has only been achieved in mice, is more efficient than SCNT and requires fewer human eggs. In addition, the strategy could theoretically be used to create banks of HLA-matched cells for use in therapeutic applications.

That's because parthenogenic stem cell lines typically contain only half of the six HLA loci of a normal diploid cell. "It's a lot easier to match patients at three loci rather than six," says Daley.

There are, however, a few potential glitches in the system. First, parthenogenic embryos could have problems with imprinted genes. In addition, there exists a class of natural killer cells that recognize cells that don't express the full complement of an individual's MHC antigens. Daley suspects this will not be an issue for most tissue grafts, but could be a problem for blood tissue transplantation, which may require full HLA matches.

Despite these advances, all agree it could be a decade or more before embryonic stem cell–derived therapies arrive in the clinic. Those desiring more immediate benefits can look to the many adult stem cell–derived therapies winding their way through clinical trials right now.

In March, for instance, **Osiris Therapeutics** announced the results of a phase 3 clinical trial that used intravenous human mesenchymal stem cells for repair of cardiac tissue following heart attack. "In terms of cell therapy in general," says Harvard's Zon, "it's likely some diseases will be treated by embryonic stem cells, and others by adult stem cells. I think the science of each field informs each other, so it's important that both succeed."

Jeffrey Perkel is a freelance science writer based in Pocatello, Idaho.

Featured Participants

Advanced Cell Technology
www.advancedcell.com

BD Biosciences
www.bdbiosciences.com

Cellartis
www.cellartis.com

Children's Hospital Boston
www.childrenshospital.org

Harvard Medical School
www.hms.harvard.edu

Harvard Stem Cell Institute
www.hsci.harvard.edu

Harvard University
www.harvard.edu

Institute for Frontier Medical Sciences at Kyoto University
www.frontier.kyoto-u.ac.jp/eng/

Invitrogen
www.invitrogen.com

Novocell
www.novocell.com

Osiris Therapeutics
www.osiris.com

Stem Cell Laboratory at the University of Central Florida
sugaya.ucf.edu

Stem Cell Sciences
www.stemcellsciences.com

New Products

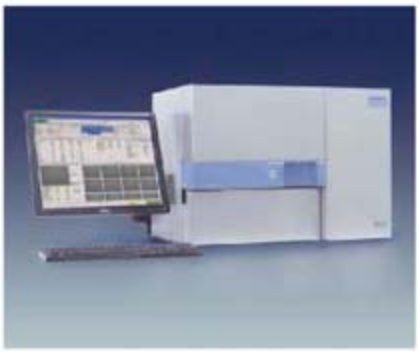

Cell Culture Analysis

The BioProfile FLEX analyzer provides fast, comprehensive analysis for cell culture processing. The automated system provides up to 16 cell culture attributes, including glucose, lactate, glutamine, ammonium, pCO_2, pO_2, pH, sodium, potassium, calcium, osmolality, cell density/viability, and phosphate or total proteins. This comprehensive test menu provides immediate access to the information required to optimize product quality and yield. The modular analyzer can be upgraded for use from research and development to manufacturing. It can be configured in combinations from one to four modules, building on the base chemistry/gas system with any combination of osmolality, cell density/viability, and phosphate or total protein modules. With its ability to consolidate the work of multiple analyzers into a single workstation, this analyzer requires only a 1 mL sample, to conserve cell culture mass and end product. The six-minute analysis saves as much as 30 minutes per sample over multiple instrument analyses. The system offers multiple sampling options, including individual sampling via a syringe/docking device, automated batch sampling using a 20-position sampling tray, and online automated sampling from up to four bioreactors.

Nova Biomedical
For information 781-647-3700
www.novabio.com

Automated Cell Culture

The CompacT SelecT is an automated cell culture and assay-ready plating system designed to meet the needs of medium-throughput laboratories. Compact robotics enables it to offer the capabilities of the established SelecT cell culture system with a lower capacity and smaller footprint, only slightly larger than a standard Class II safety cabinet. The role in drug discovery of cell-based assays necessitates a supply of many different cell lines, seven days a week at variable scales. CompacT SelecT automatically manages this entire process. CompacT SelecT grows and maintains cells from multiple cell lines in T175 flasks in a controlled environment (negative pressure laminar air flow), eliminating all possibility for cross-contamination. It counts and checks cell viability before dispensing the cells into plates ready for cell-based screening and assay development. It can hold up to 130 flasks in a temperature-controlled and carbon dioxide–controlled incubator, enabling the simultaneous culture of multiple cell lines, with media dispensed by 10 different pumps. Each flask can be processed with its own parameters. Output can be either as a harvested cell suspension or in 96-well or 384-well plates.

The Automation Partnership
For information +44 (0) 1763 227200
www.automationpartnership.com

Neural Stem Cells and Media Kit

The ENStem human neural progenitor stem cells come packaged with optimized growth media and substrates. Derived from National Institutes of Health-registered human embryonic stem cells, the cells provide a valuable tool for neural research in various areas, including Alzheimer's disease, spinal cord injury, and depression. A separate product, HEScGRO is an animal-component-free medium for human embryonic stem cell research. It has been shown to maintain human embryonic stem cells in their undifferentiated state. The medium is serum-free, ready-to-use, and complete. Media with animal-derived components are subject to wide variability and may contain factors that promote differentiation of human embryonic stem cells, as well as toxic proteins or immunogens.

Millipore
For information 800-548-7853
www.millipore.com

Multi-Lineage Progenitor Cells

Multi-Lineage Progenitor Cell (MLPC) clonal cell lines are karyotypically normal, multipotent progenitor cells obtained from post-partum human umbilical cord blood that have been expanded from a single cell. The MLPC has been analyzed for gene expression and been shown to be an early progenitor cell capable of extensive differentiation. The MLPC expresses a normal phenotype, thus providing a tool for developing better differentiation methods and cell delivery systems. Benefits of the cells are that they are clonal for highly repeatable experimentation, have an umbilical cord blood source so involve no ethical controversy, are genetically normal and stable (not immortalized), are highly characterized and multipotent, and have robust expansion capabilities without differentiating. Applications include disease modeling, in vitro toxicology modeling, compound screening, cellular therapy, studying developmental pathways, and providing an alternative to primary tissue culture.

BioE
For information 800-350-6466
www.bioe.com

Sample Storage at Room Temperature

A new room-temperature sample storage system eliminates the need for keeping biological samples cold or frozen. The system includes the SampleMatrix dry storage medium, SampleGard sample storage and transportation system, and SampleWare organizational and retrieval software. Together, these products allow biological samples to be stored, transported, and recovered at the bench without the need for cold storage. Liquid samples are added to the well or tube that comes preloaded with SampleMatix. This dissolvable polymer forms a protective seal around the sample as it dries, essentially shrink-wrapping the DNA, RNA, cell, protein, or blood sample. Samples are recovered by rehydrating for 15 minutes, and can be used immediately for transformation, polymerase chain reaction, transfection, sequencing, genotyping, or whole genome amplification without further purification. There is no loss due to freeze-thaw damage. The SampleGard system features a 96-well plate that comes preloaded with SampleMatrix medium, so it is ready to use in high-throughput applications.

Biomatrica
For information 858-550-0308
www.biomatrica.com

Neural Stem Cell Medium

Serum-free Stemline Neural Stem Cell Expansion Medium is optimized for expansion of human neural stem cells. Designed to support research in the area of neurodegenerative diseases such as amyotrophic lateral sclerosis, it has shown promising results in animal models. In order to be regulatory friendly, the formulation is entirely animal-component-free and ready-to-use, requiring only supplementation with an appropriate growth factor cocktail (which is not included). The elimination of serum reduces performance variability and safety risks. Neural stem cells cultured in this medium yield a healthy, high-density population of cells that maintain their differentiative capacity.

Sigma-Aldrich
For information 800-521-8956
www.sigma-aldrich.com

POSITIONS OPEN

POSTDOCTORAL OPPORTUNITIES
Translational Bioinformatics at Stanford University

The Laboratory of **Dr. Atul Butte** at Stanford Medical School is seeking highly motivated investigators to develop and study novel approaches in translational bioinformatics, or the application of analytic and interpretive methods to optimize the transformation of genome-scale data of many types into proactive, predictive, preventative, and participatory health. Postdoctoral Fellowships are fully funded for up to three years. Ideal candidates will have an M.D. and/or Ph.D. with a strong background in bioinformatics, computational biology, biostatistics, and genomics, and a great publication record. Strong problem-solving skills, creative thinking, and the ability to build new software tools as needed are required. Applicants must possess good communication skills and be fluent in both spoken and written English. A background in molecular biology or medicine or pharmacology will be a strong plus. Prior experience with genetic, microarray, drug, or clinical databases, XML, text-mining, knowledge representation, or parallel computing platforms is a plus. This exciting work will be guided by multidisciplinary collaborations with top scientists in stem cell, immunology, and transplantation research at Stanford. To apply, please send your curriculum vitae, a brief statement of research interests, and contact information for three references in one PDF document to **e-mail: butte-lab-jobs@lists.stanford.edu.**

POSTDOCTORAL POSITION
Program for Evolutionary Dynamics
Harvard University
Website: http://www.ped.fas.harvard.edu

The Program for Evolutionary Dynamics (PED) at Harvard University invites applications for an available Postdoctoral position in mathematical biology starting 2007-2008. Qualified applicants should have an accomplished doctoral record and a strong background in mathematical biology, including the dynamics of virus infections. In addition, applicants should have a desire to participate in collaborative, interdisciplinary work at the intersection of theoretical and experimental biology.

To apply, please send a statement of research interests, current curriculum vitae, and three letters of reference to: **Amy Ashbacher, Program for Evolutionary Dynamics, Harvard University, 1 Brattle Square, Suite 6, Cambridge, MA 02138-3758** or **e-mail: ashbach@fas.harvard.edu**

We strongly encourage applications from female and other underrepresented minority candidates. Harvard University is an Equal Opportunity Affirmative Action Educational Institution and Employer. Employment is contingent upon eligibility to work in the United States.

A **POSTDOCTORAL POSITION** is available for one year with possibility of extension for a self-motivated individual to study the role of steroid hormones on the expression of angiogenic growth factors in breast cancer. Prior experience in mammary gland biology, cell culture techniques, molecular biology and animal handling is important, and experience in using xenograft models is essential. The Laboratory is particularly interested in defining molecular switches that can be linked to hormone driven angiogenesis in endocrine dependent tissues. Please apply with names of three references to: **Dr. Salman Hyder, Dalton Cardiovascular Research Center, University of Missouri-Columbia (e-mail: hyders@missouri.edu).**

POSTDOCTORAL POSITION

A Postdoctoral position is available to study cell/molecular and biology of complications of diabetes mellitus and kidney development. Potential candidates must have documented experience in this area of research and in cell and molecular biology techniques. Please send curriculum vitae with references to: **Yashpal S. Kanwar, M.D., Ph.D., Northwestern University Medical School, 303 E. Chicago Avenue, Chicago, IL 60611 U.S.A. E-mail: ykanwar@northwestern.edu.**

POSITIONS OPEN

Henry Ford Health System and Vattikuti Urology Institute, first and foremost in urological excellence, offer a **POSTDOCTORAL FELLOW** position to study regulation of p53-induced apoptosis in prostate cancer cells with special emphasis on development of mechanism-based strategies for prostate cancer treatment. Recent graduates in molecular biology or biochemistry are encouraged to apply. Experience with handling laboratory animals will be a plus. Send your resume to: **Dr. J. Ghosh, Department of Urology, Henry Ford Health System, One Ford Place, Detroit, MI 48202. E-mail: jghosh1@hfhs.org, website: http:// www.henryford.org.**

POSTDOCTORAL POSITION
in Molecular Cytogenetics
Harvard Medical School

One to two-year Postdoctoral Fellowship positions are available at Harvard Medical School and Brigham and Women's Hospital in the area of Molecular Cytogenetics for individuals with a Ph.D. or M.D./Ph.D. degrees. Ongoing projects in the Laboratory include structural genomic variation (e.g. *Nat. Genet.* **36:** 949, 2004; *Nature* **444:** 444, 2006), zebrafish cytogenetic analyses (e.g. *Nat. Genet.* **34:** 59, 2003) and cancer biomarker studies (e.g. *Science* **310:** 644, 2005).

Exceptional candidates that have demonstrated research productivity and the ability to write proficiently for international, peer-reviewed journals should submit current curriculum vitae, a one-page statement of research experience, and the names of three individuals who can provide reference letters, to: **Charles Lee, Ph.D., Department of Pathology, Brigham and Women's Hospital, Harvard Medical School, 221 Longwood Avenue, EBRC 404A, Boston, MA 02115 U.S.A., e-mail: clee@rics.bwh.harvard.edu, website: http://www.chromosome.bwh.harvard.edu.**

Harvard Medical School and Brigham and Women's Hospital are Equal Opportunity/Affirmative Action Employers.

POSTDOCTORAL RESEARCH
Washington University School of Medicine

Positions are available immediately on NIH-funded projects at the level of **POSTDOCTORAL FELLOW/RESEARCH ASSOCIATE.** Successful candidates will use the latest techniques in molecular genetics to address important questions in (1) the regulation of apoptosis and the induction of immune tolerance; or (2) the role of the immune system in angiogenesis. Applicants must have a Ph.D., M.D., or equivalent and a strong background in immunology or related field. Applicants with additional experience in one or more of the following areas will be given top priority: molecular biology, biochemistry, cell biology, confocal microscopy, infectious diseases, cell death, vascular biology, protein chemistry. *Applicants must be fluent in English and eligible for U.S. employment.* Send curriculum vitae and names of three references to: **Thomas A. Ferguson, Ph.D. Washington University School of Medicine, 660 S. Euclid, P.O. Box 8096, St. Louis, MO 63110 (e-mail: ferglab@vision.wustl.edu).** *An Equal Opportunity/Affirmative Action Employer.*

POSTDOCTORAL POSITION
Brain Tumor Gene Therapy

Advanced retroviral vector development and engineering T cell effector (designer T cells) responses to develop therapeutics for human clinical trials in malignant glioma. Collaboration between **Dr. P. Sampath, M.D., Chief of Neurosurgery,** and **Dr. R. P. Junghans, Chief of Surgical Research** at the Roger Williams Medical Center, Boston University School of Medicine. Contact **Dr. Sampath** via **e-mail: pvassella@rwmc.org** with resume, research summary, and names of three references.

STONY BROOK

POSTDOCTORAL POSITIONS

The Research Foundation of Stony Brook University/SUNY anticipates the following postdoctoral positions being available between Spring and Fall 2007.

• BIOCHEMISTRY AND CELL BIOLOGY

Glycosylation of thrombospondin type 1 repeats. Robert Haltiwanger, WC-R-3998-07-04-S

Role of Hop1 phosphorylation in meiotic recombination in yeast. Nancy Hollingsworth, WC-R-3997-07-04-S

Role of RNA-protein interactions in bacterial pathogenesis. A. Wali Karzai, WC-R-3999-07-04-S

Developmental regulation of the secretory pathway during sporulation in yeast. Aaron Neiman, WC-R-3904-07-03-S

Structural biology of membrane proteins. Steven O. Smith, WC-R-4000-07-04-S

• CENTER FOR BIOTECHNOLOGY

In vitro wound healing assays with industry partners. Anil Dhundale, WC-R-4001-07-04-S

Drug discovery, toxicity and secondary efficacy assays with industry partners. Anil Dhundale, WC-R-4002-07-04-S

• CHEMISTRY

Ultrafiltration/nanofiltraton, water purification, polymer synthesis, polymer inorganic hybrids, polyoxometalates. Ben Chu, WC-R-4003-07-04-S

Flow-induced polymer crystallization, nanocomposites, ultrafiltration/nanofiltration using nanofiber technology. Benjamin Hsiao, WC-R-4004-07-04-S

Computational structural biology and biophysics. Carlos Simmerling, WC-R-3890-07-02-S

Geochemistry: Experimental Aqueous Geochemisty. Martin Schoonen, WC-R-3974-07-03-S

• MATERIAL SCIENCE AND ENGINEERING

Thermal spray materials processing, advanced coating technologies and associated application development. Sanjay Sampath, WC-R-4005-07-04-S

• MEDICINE

Biology/biochemistry of reactive oxygen/nitrogen species and oxidative stress. Basil Rigas, HS-R-4028-07-04-S

• MOLECULAR GENETICS AND MICROBIOLOGY

Regulation of STAT3 Signal Transduction. Nancy C. Reich, WC-R-4022-07-04-S

• NEUROSURGERY

Design/conduct experiments related to dynamics of pulsatile CSF flow. Mark Wagshul, HS-R-3901-07-03-S

• PHARMACOLOGY

Signal transduction, Lipid signaling and membrane trafficking. Guangwei Du, HS-R-4007-07-04-S

Molecular Carcinogenesis. Arthur P. Grollman, HS-R-4009-07-04-S

Functional Analysis of DNA Repair and Mutagenesis Proteins. Masaaki Moriya, HS-R-4006-07-04-S

Molecular Cellular Pharmacology; Molecular Toxicology; Structural Biology; Cell Biology; Animal Pharmacology. Jeffrey Pessin, HS-R-4008-07-04-S

• PHYSIOLOGY AND BIOPHYSICS

Single molecule structural biology of post-synaptic signal transduction proteins. Mark Bowen, WC-R-4010-07-04-S

• PSYCHOLOGY

Human and nonhuman operant and experimental economics research. Howard Rachlin, WC-R-4011-07-04-S

• RADIOLOGY

Improved Algorithms and Priors for ECT Reconstruction. Eugene Gindi, HR-R-3870-07-02-S

MedImaging informatics Lab, develop Virtual colonoscopy and conduct scientific experiments. Jerome Z. Liang, HS-R-3916-07-03-S

To apply online and for information, visit *www.postdocs.stonybrook.edu* or mail résumés to: Office of the President, Stony Brook University, Stony Brook, NY 11794-0701.

Stony Brook University/SUNY is an affirmative action/equal opportunity educator and employer.

Imagine being part of a team that makes a discovery.

POSTDOCTORAL POSITION

UMDNJ-School of Osteopathic Medicine currently has a Postdoctoral position available to study the role of cyclin C in stress signaling utilizing both yeast and mouse systems. The successful candidate will have a Ph. D (or equivalent) in Molecular Biology or a related field. Preference will be given to candidates with mouse cell culture/transgenic animal experience with a desire to learn yeast genetics. The laboratory is located on the Stratford Campus of the University of Medicine and Dentistry of New Jersey. Stratford is in southern New Jersey within easy commute by train or car to Center City Philadelphia.

Interested candidates should send a recent CV and summary of research to **Randy Strich, Ph. D or Katrina Cooper, Ph.D., UMDNJ–School of Osteopathic Medicine, 2 Medical Center Drive, Stratford, NJ, 08084 or email strichra@umdnj.edu.** UMDNJ is an AA/EOE, M/F/D/V.

UMDNJ SCHOOL OF OSTEOPATHIC MEDICINE
University of Medicine & Dentistry of New Jersey

What's your next career move?

- Job Postings
- Job Alerts
- Resume/CV Database
- Career Advice from Next Wave
- Career Forum

Get help from the experts.

ScienceCareers.org
We know science AAAS
www.sciencecareers.org

> "The ability to work well in a team is the No. 1 skill that industry employers look for."

Transferable Skills and Portable Careers

With academic jobs scarce, postdoctoral fellows must develop skills that will make them competitive for jobs beyond the university setting, but even those who go on to academic careers can benefit from learning the skill sets that industry demands. **By Christie Aschwanden**

Success in today's job market requires more than just solid lab skills and a stack of publications. Whether seeking tenure-track academic jobs, industry research positions, or nontraditional science careers, many job seekers are finding that a well-honed pipette thumb is not enough to land them an offer. "I don't know anyone who's gotten a job who spent their postdoc at the bench the whole time," says **Crystal Icenhour,** who was recently hired as vice president and director of research at IDX Labs, a startup in Charlottesville, Virginia.

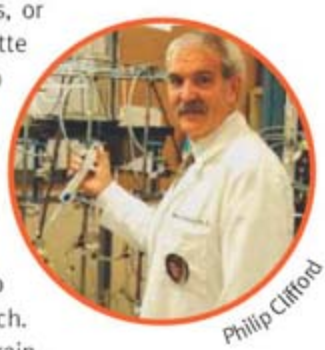

Philip Clifford

Postdocs must develop skills beyond the laboratory if they're to be competitive in the tightening job market, says Icenhour. Where nonacademic jobs once required skills that did not carry over to academia, that's not necessarily the case these days, says **Gregory Kopf,** who spent more than two decades at the University of Pennsylvania before moving to Wyeth Research. He has since returned to Penn as an adjunct professor. "When I first started in academia, the training skill sets were very different for industry and academia, but the lines are starting to become a lot more blurred," says Kopf. "Leadership, project management skills, the ability to develop goals and manage budgets and your lab—these are skills that are just as important for academia as for industry."

> "When you get to a postdoc, there are virtually no rules."

The ability to work well in a team is the No. 1 skill that industry employers look for, says **Neil Stahl,** senior vice president of research and development sciences at Regeneron Pharmaceuticals in Tarrytown, New York. "You have to be able to sort through issues and communicate effectively in a nonthreatening way."

Academic scientists also need team skills so they can work effectively on committees and form successful collaborations. Running a lab or working on a research team both demand strong interpersonal skills and diplomacy. "You have to be able to say the right things without antagonizing your colleagues, and that's a skill that many postdocs don't have," says **Chee-Keng Ng,** a principal research scientist at Wyeth Biopharma in Andover, Massachusetts. "We need people who can fit into the teamwork culture."

Whether the goal is to secure NIH funding or to sell the corporation on a novel idea, success hinges on the ability to communicate. "How you package and present your data matters, especially in a large company," says Ng. "You need to be able to communicate well, especially to people who aren't as expert as you. You have to be able to explain the science to the manag-

continued »

UPCOMING FEATURES

Biotech and Pharma — April 27

Focus on Diversity — May 11

Regional Focus: NC/Research Triangle — June 8

Careers for Postdoc Scientists

ing director on the project," says Stahl.

Project management is another skill in high demand. "In academia, you have to manage your research so you're competitive for the next funding round. In industry, you have very tight timelines, and you have to manage your project so you can meet those deadlines," says Kopf. Meeting project goals requires effective management of people and time, yet many postdocs don't recognize the importance of honing management skills until they start sending out their resumes, says **Philip Clifford,** associate dean for postdoctoral education at the Medical College of Wisconsin in Milwaukee.

"When you get to a postdoc, there are virtually no rules," Clifford says. Many postdocs lock themselves in the lab and hope that their toil will pay off in publications that lead to the job they want. "People feel that they need to do project after project and publish, publish, publish," Clifford says, but he suggested that they need to develop skills beyond the bench too, even if it means getting out of the lab.

Charting a Path

From the start, postdocs should identify the skills they need to make themselves marketable in their chosen career path so they can maximize their training, and the sooner the better, says Clifford. "We propose that people go through a self-assessment process to identify their own values, skills, and interests and then look at the potential universe of jobs that fit those," he says. ScienceCareers.org, a website offered by AAAS (American Association for the Advancement of Science) and books like Cynthia Robbins-Roth's *Alternative Careers in Science: Leaving the Ivory Tower* are good places to start. "Do some informational interviews with people in the career path you're interested in and find out what skills they use, then figure out what you need to do to get them," says Clifford. Some institutions employ career counselors that specialize in science. For instance, the Medical College of Wisconsin has hired a career adviser specifically to work with postdoctoral fellows and medical students.

Robert Tillman, postdoctoral program coordinator at New York University School of Medicine, advises budding scientists to create an individual development plan (IDP), through a process like the one developed by the FASEB Training and Careers Committee (opa.faseb.org/pdf/idp.pdf). Creating an IDP involves a four-step process to identify a well-suited career path and formulate a plan to achieve it. Tillman's institute has adopted IDPs as part of its postdoctoral handbook. "It's a way to focus my strengths and weaknesses in relation to my goals," Tillman says. "If I'm a postdoc and in four years I want to become faculty, what do I need to do to achieve that? How do I get there?" An IDP provides the roadmap for getting from a postdoc to a dream job.

Some postdocs expect that they will try for a tenure track research position and, if that doesn't work out, then they'll think about a plan B. But this type of approach sets postdocs up for failure, says Clifford. "Keeping your options open is exactly the wrong approach. You're not really doing the things that will direct you toward a specific career." There simply aren't enough tenure-track positions to go around, so postdocs should have an alternate plan in place from the start, Clifford says.

Many postdocs tell themselves that if they don't land a job at a top research institution, then they'll just apply for a teaching position. But that's a mistake, too, says Clifford, because teaching-oriented

"Keeping your options open is exactly the wrong approach. You're not really doing the things that will direct you toward a specific career." —Robert Tillman

Lisa Kozlowski

universities want people with proven teaching skills. "If your goal is to work at a teaching institution, you need to figure out how to get that experience," he says. Regardless of what career path you hope to follow, "you need to identify the skill sets that are necessary for that career option, and figure out how you're going to get those," says Clifford. Someone seeking a job in biotech, for instance, might consider a business course or even an MBA, he concludes.

Managing to Learn

Bench skills are just one component of a successful science career, yet they've long been the focus of graduate and postdoctoral training programs. "Whether you run your own academic lab or take a position at a company, learning how to manage people, projects, and budgets are necessary skills, but traditional graduate and postdoctoral training do not offer formalized courses in these topics," says **Garth Fowler,** outreach program manager for ScienceCareers.org. But that's changing as AAAS, ScienceCareers.org, and other organizations step in to fill the void with courses and workshops devoted to these topics.

In 2002 and 2005, the Burroughs Wellcome Fund and the Howard Hughes Medical Institute partnered on a course to teach laboratory management skills to postdocs and beginning faculty members. Though the course's focus stood squarely on the needs of the academic scientist, many of the skills taught, such as time management, project management, collaborations, and mentoring, carry over to nonacademic jobs as well. Organizers have turned the course into a book, *Making The Right Moves: A Practical Guide To Scientific Management For Postdocs And New Faculty* available for free from the HHMI website (www.hhmi.org/resources/labmanagement).

In 2005 organizers of the BWF/HHMI program put on a "train the trainers" course in an effort to encourage similar programs at institutions across the country. "They wanted to spread the wealth," says **Lisa Kozlowski,** assistant dean for postdoctoral affairs and recruitment at Thomas Jefferson University (TJU) in Philadelphia. Kozlowski attended the course and then, with support from AAAS and ScienceCareers.org, collaborated with three other Philadelphia-area institutions to develop a lab management course for postdocs from all four institutions.

A total of 55 postdocs enrolled in the Philadelphia Scientific Management Course, which is ongoing and split into four sessions spread over five months (www.tju.edu/JCGS/postdoc). Topics include leadership skills, time management, project continued »

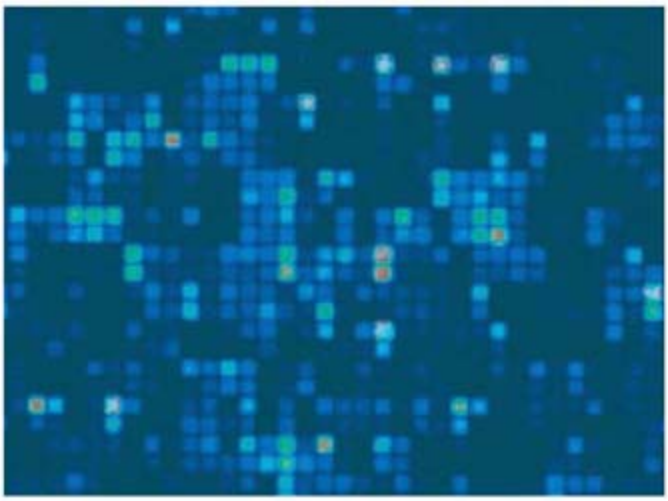

BECAUSE

Our CAUSE is Natasha and her rheumatoid arthritis.

For more than 30 years, Genentech has been at the forefront of the biotechnology industry, using human genetic information to develop novel medicines for serious and life-threatening diseases. Today, Genentech is among the world's leading biotech companies, with multiple therapies on the market for cancer and other unmet medical needs.

Please take this opportunity to learn about Genentech, where we believe that our employees are our most important asset.

Genentech is dedicated to fostering an environment that is inclusive and encourages diversity of thought, style, skills and perspective. Genentech is an equal opportunity employer.

To read commentary from current and past postdocs and for a listing of current postdoc opportunities, please visit **http://www.gene.com/gene/research/postdoctoral** and **www.gene.com/careers.**

Research a Postdoctoral position at Genentech's South San Francisco facility.

Genentech's Research Organization features world-renowned scientists who are some of the most prolific in their fields and in the industry. Genentech researchers have consistently published at a rate of 150+ papers per year and have secured over 6,100 current, non-expired patents worldwide (with 5,400 more pending). Genentech's Research Organization combines the best of the academic and corporate worlds, allowing researchers not only to pursue important scientific questions but also to watch an idea move from the laboratory into development and out into the clinic.

The Postdoctoral Program has become one of the strongest research assets at Genentech. In order to continue discovering, developing, manufacturing and commercializing biotherapeutics and small molecule therapies for significant unmet medical needs, Genentech depends on attracting and retaining top scientific talent, including promising postdoctoral fellows.

As a Genentech Postdoctoral Research Fellow working in either Research or Development Sciences, you would find yourself collaborating with world-class scientists both at the company and beyond Genentech's walls. Our fellowships typically last three years and offer the chance to do cutting-edge research in an inspired, purposeful and resource-rich environment. Throughout the program, you would be encouraged to present the progress and results of your work both internally and externally. As our many Postdoctoral Program alumni can attest, the program offers an unrivaled opportunity to put yourself at the forefront of science.

Our progressive Postdoctoral Research Fellows salary and benefits package includes full medical/dental/vision care, three weeks vacation, stock purchase plan and health club membership.

The following opportunities exist in our South San Francisco Headquarters:

Protein Chemistry, Req. 1000014182
Molecular Oncology, Req. 1000015084, 1000015279, 1000016828, 1000018325
Tissue Growth and Repair, Req. 1000016201
Tumor Biology/Angiogenesis, Req. 1000016822, 1000016884
Molecular Imaging, Req. 1000016254
Protein NMR Group, Req. 1000017874

In January 2007, Genentech was named to FORTUNE's list of the "100 Best Places to Work For" for the ninth consecutive year.

SCIENCE 2006 TOP EMPLOYER

Genentech
IN BUSINESS FOR LIFE

management, funding, mentoring, and landing a faculty position. **Vera Hintz,** a postdoc in TJU's department of dermatology, is attending the course and says it prodded her to look for opportunities to gain skills that will enhance her resume. When she looked at job ads, she saw that many wanted experience planning meetings, so she volunteered to help plan TJU's postdoctoral research symposiums. Hintz says the course has taught her to view her career as a project that she needs to manage, rather than just something that simply unfolds on its own.

Laboratory management courses like TJU's are becoming more common. Last November, the New York University School of Medicine, also with support from AAAS and ScienceCareers.org, put on a two-day workshop, Management Skills for Scientists, open to 25 people. "We wanted it small so it would be interactive," says Tillman of NYU. Postdoc **Marie-Hélène Delmotte** attended the course and says it helped her recognize that her lab skills alone might not be enough to land her the position she wants. "My resume is good but I realized that I need more to find a job. I need to know myself and know how to sell myself." Delmotte says the program helped her understand the importance of developing short-term and long-term goals for her career. Instead of focusing solely on her research, she is putting energy into mentoring, an effort that will pay off in a skill she can add to her resume.

The management course is just one way Tillman's institute is promoting career development. The school's office of learning and development offers courses on topics ranging from how to give an effective presentation to managing conflict and running meetings. Tillman says that NYU also helps about a half dozen of its postdocs enroll in a 16-week Fundamentals of the Biotech Industry course at the Center for Biotechnology, a state-funded center created to support the region's growing biotech industry.

"We use Lab Act to allow students to try out different solutions without putting anyone on the spot."

—John Galland

NYU's Fundamentals of the Biotech Industry Course

Acting the Part

Of all the laboratory management courses that have sprung up, perhaps the most innovative is the Laboratory Management Institute (LMI) at the University of California, Davis. The institute holds a three-week intensive program divided into five courses: leadership, management, best practices, mentoring, and innovation. Participants come from a wide range of disciplines and receive a certificate and 14 credit hours through the UC-Davis extension.

The program's hallmark, Lab Act, employs professional actors to play out the concepts explored in the course. Instructors discuss strategies for handling management issues, then actors play out scenarios that workshop attendees anonymously submit. Participants discuss what happened and work on new solutions that the actors then try out. "We're all about practicing," says LMI director **John Galland.** "We use Lab Act to allow students to try out different solutions without putting anyone on the spot."

In addition to the summer program, LMI offers a year-long program for postdocs. "I'm impressed at how effective it has been to watch the actors role play," says participant **Tamara Holst,** a postdoc at the Public Intellectual Property Resource for Agriculture. "It's almost uncanny how well the scenarios translate across different labs, and the way to defuse a situation is usually similar across the board."

American Associaton for the Advancement of Science
www.aaas.org

IDX Labs
www.idxlabs.com

Medical College of Wisconsin
www.mcw.edu

NYU School of Medicine, Sackler Institute of Graduate Biomedical Studies
www.med.nyu.edu/sackler

NYU School of Medicine, Skirball Institute of Biomolecular Medicine
www.saturn.med.nyu.edu

Public Intellectual Property Resource for Agriculture
www.pipra.org

Regeneron
www.regeneron.com

Thomas Jefferson University, Jefferson College of Graduate Studies
www.jefferson.edu/jcgs

University of California, Davis
www.ucdavis.edu

University of Pennsylvania
www.upenn.edu

Wyeth Biopharma
www.wyeth.com

Taking the Initiative

Formal programs like LMI's are not yet the norm, but even without them, motivated postdocs can find ways to develop useful and necessary additional job skills. Icenhour of IDX Labs made her resume stand out from the rest by getting involved in the postdoctoral associations at the Mayo Clinic in Rochester, Minnesota, and at Duke University where she did a second postdoc. She also joined the board of National Postdoctoral Association and credits this experience with teaching her the skills she needed to land her current job as vice president and director of research.

"My NPA experience really emboldened me," says Icenhour. "As a board member of NPA you're reviewing the employee handbook, revising budgets, and running committee meetings. The experience introduced me to a lot of the things I do in my daily work life now." Not every postdoc has the luxury of enrolling in an institute-sponsored program like LMI, but as Icenhour's experience illustrates, motivated postdocs can create their own opportunities to learn skills beyond the bench if only they would step out of the lab.

Christie Aschwanden is a freelance writer and editor living in western Colorado.

POSITIONS OPEN

CALIFORNIA INSTITUTE of TECHNOLOGY
Broad Fellows Program in Brain Circuitry

The California Institute of Technology is looking for a few outstanding scientists from any relevant backgrounds to study how networks of neurons give rise to perception, memory, emotion, and behavior. We encourage applications from individuals employing genetic manipulations in relevant animal model systems, electrophysiological recordings, functional imaging, and computational analyses and related tools. Broad Fellows are independent researchers who have recently received their Ph.D.s. They will receive internal funding for a group of up to three people (up to $150,000 in direct costs per year per Fellow). The initial appointment is for three years, with the possibility of renewal for two more years. Excellent salary ($70,000 per year) and benefits. Applications should include curriculum vitae, a statement of research plan, and three letters of recommendation. This material should be submitted online at **website: http://www.broadfellows.caltech.edu** or by **e-mail: heather@klab.caltech.edu** by May 1, 2007.

Caltech is an Equal Opportunity/Affirmative Action Employer. Women, minorities, veterans, and disabled persons are encouraged to apply.

Two **POSTDOCTORAL POSITIONS** available immediately to investigate G protein-coupled receptor function. Ongoing studies utilize molecular biological, biochemical, and biophysical approaches to address the mechanism of activation of the glycoprotein hormone receptors and receptor dimerization. Must have a Ph.D., M.D., or equivalent. Documented experience with molecular and cellular biological techniques and a background in cell signaling or reproductive endocrinology are preferred. Salary is competitive and commensurate with experience. These positions are being offered in the Laboratory of **Dr. Deborah L. Segaloff, Department of Molecular Physiology and Biophysics, the University of Iowa.** Please send curriculum vitae and names of three references by **e-mail: deborah-segaloff@uiowa.edu.** *The University of Iowa is an Equal Opportunity/Affirmative Action Employer. Applications from qualified women and minorities are encouraged.*

TWO POSTDOCTORAL POSITIONS
in Cellular Microbiology

Two Postdoctoral positions are available immediately to study molecular pathogenesis and cellular microbiology of the two intracellular bacteria *Legionella pneumophila* and *Francisella tularensis.* Priorities are given to individuals with expertise in cell biology or cellular microbiology. Send curriculum vitae and arrange for three references to be sent to: **Dr. Yousef Abu Kwaik, Department of Microbiology and Immunology, University of Louisville Health Sciences Center, Room 412A, Louisville, KY 40292. E-mail: abukwaik@louisville.edu.** *University of Louisville is an Equal Opportunity Employer.*

A **POSTDOCTORAL POSITION** is available immediately at the University of Massachusetts Medical School for a highly motivated scientist to explore functions of intracellular Ca2+ stores and Ca2+ syntillas in freshly isolated terminals of magnocellular and hippocampal neurons. Expertise in patch clamping is desirable and experience with molecular biology is a plus. We use both approaches combined with high-speed, high-resolution Ca2+ imaging which applicant can learn here. The main requirement is a keen interest in the questions being addressed. To apply, send curriculum vitae and three references to **Dr. John Walsh** via **e-mail: john.walsh@umassmed.edu.**

POSITIONS OPEN

NOVARTIS
NOVARTIS INSTITUTES FOR BIOMEDICAL RESEARCH

POSTDOCTORAL FELLOWSHIPS
Novartis Institutes for BioMedical Research (NIBR)
Think what's possible.

Would you like to contribute to innovative research with the goal of improving human health? Novartis Institutes for BioMedical Research (NIBR) has a variety of Postdoctoral positions in biology, chemistry, and computational sciences that provide excellent training in research and exposure to science in a pharmaceutical setting.

The NIBR Presidential Postdoctoral Fellowships provide talented scientists with the unique opportunity to conduct innovative, interdisciplinary research at one of our seven global sites (Basel, Switzerland; Cambridge, East Hanover, and Emeryville, United States; Horsham, United Kingdom; Tsukuba, Japan; Vienna, Austria). Presidential Fellows have a NIBR mentor and an academic mentor, and develop their projects in consultation with both mentors. Ph.D. students in the last year of their doctoral research, as well as postdoctoral fellows within three years of obtaining their Ph.D., are eligible to apply. Applications are accepted on a rolling basis, and Fellowships are for a maximum of three years. To apply, visit our webpage at **website: http://nibr.novartis.com/careers/Postdoc_fellowships/index.shtml.**

The NIBR Postdoctoral Fellowships support talented scientists on cutting-edge projects that originate within departments at NIBR. As they become available, the specific positions are posted with the eligibility requirements at **website: http://www.novartis.com/careers/job-search/brassring/index.shtml.**

Novartis is an Equal Opportunity Employer committed to embracing and leveraging diverse backgrounds. Minorities/females/persons with disabilities/veterans.

POSTDOCTORAL POSITION
Fox Chase Cancer Center
Philadelphia, Pennsylvania

A Postdoctoral position is available at the Fox Chase Cancer Center (Philadelphia, Pennsylvania) in a dynamic laboratory focused on understanding the pathogenesis of tuberous sclerosis complex. Our Laboratory uses biochemical approaches, cell biology, and yeast and *Drosophila* models **(website: http://www.fccc.edu/research/pid/henske).** Fox Chase is a National Cancer Insititute-designated comprehensive cancer center with 70 research laboratories and state-of-the-art core facilities. The Center's environment is highly interactive and collegial, and postdoctoral training is consistently ranked among the best in the country. Candidates should have a Ph.D. or M.D./Ph.D. and a strong background in cell and/or molecular biology. *Permanent U.S. residency is required.* Please send a cover letter briefly detailing your scientific experience and your interest in this position, together with curriculum vitae and contact information for three references to: **Dr. Elizabeth Petri Henske, Fox Chase Cancer Center, 333 Cottman Avenue, Philadelphia, PA 19111. E-mail: elizabeth.henske@fccc.edu.** *Fox Chase Cancer Center is an Equal Opportunity Employer.*

POSTDOCTORAL SCIENTIST, GENOMICS

Prognosys Biosciences is seeking exceptional, highly motivated individuals to help develop and apply innovative microarray-based technologies for genomics. We are a startup company where every person is a key employee. We offer an excellent benefits package, great opportunities for career development, and ownership in the company.

See **website: http://www.prognosysbio.com** for job openings and details.

Please e-mail your resume and cover letter to **e-mail: jobs@prognosysbio.com. Prognosys Biosciences, Incorporated, 505 Coast Boulevard South, Suite 310, La Jolla, CA 92037.** *Equal Opportunity Employer.*

POSITIONS OPEN

INSTITUT PASTEUR

POSTDOCTORAL FELLOWSHIPS
Institut Pasteur, Paris, France

Founded in 1887 by Louis Pasteur and located in the heart of Paris, the Institut Pasteur is a world-renowned private research organization. The Pasteur Foundation of New York is seeking outstanding Fellowship Applicants. Candidates may apply to any laboratory within ten departments: Cell Biology and Infection; Developmental Biology; Genomes and Genetics; Immunology; Infection and Epidemiology; Microbiology; Neuroscience; Parasitology and Mycology; Structural Biology and Chemistry; and Virology. See website for details.

Fellowship package is for a total of three years. *U.S. citizenship required.* This is a biannual call; next application deadline: September 7, 2007.

E-mail: pasteurus@aol.com.
Website: http://www.pasteurfoundation.org.

RESEARCH ASSOCIATE/POSTDOCTORAL FELLOWSHIP

A Postdoctoral position is available immediately in the Laboratory of **Dr. Rick Neubig** in the Department of Pharmacology, University of Michigan, Ann Arbor, to study the role of RGS proteins in adipose tissue function and carbohydrate metabolism in mouse models (*Mol. Cel. Biol.* **26:** 6870-9, 2006, and *Circ. Res.* **98:** 659-66, 2006). Highly motivated candidates are encouraged to apply. An M.D. and/or Ph.D. in an appropriate discipline is required. A strong background in signal transduction and experience with in vivo models is preferred. Qualified candidates should send a statement of research interest, curriculum vitae, and three references to **e-mail: rneubig@umich.edu** or **Richard Neubig, M.D., Ph.D., Department of Pharmacology, 1301 MSRB III, P.O. Box 0632, Ann Arbor, MI 48109.**

The University of Michigan is an Equal Opportunity/Affirmative Action Employer.

POSTDOCTORAL FELLOW

A Postdoctoral research position is available immediately for an individual interested in studying biochemistry of DNA helicases and polymerases. The projects include thermodynamic, kinetic, and structural studies of the enzymes in solution, using stopped-flow, rapid chemical quench, analytical ultracentrifugation, light scattering, fluorescence spectroscopy, and fluorescence titration methods. Candidates should hold a Ph.D. in chemistry, biochemistry, or related fields, and have some experience in enzyme kinetics and/or fluorescence spectroscopy. Please submit curriculum vitae and names of three references to: **Dr. Wlodeck Bujalowski, 301 University Boulevard, Department of Biochemistry and Molecular Biology, Route 1068, Galveston, TX 77555-1068; e-mail: wbujalow@utmb.edu, telephone: 409-772-1382.** *The University of Texas Medical Branch is an Equal Opportunity/Affirmative Action Employer.*

POSTDOCTORAL SCHOLAR
TWO POSTDOCTORAL POSITIONS
University of California, Berkeley

Positions are available after June 1, 2007, at the University of California, Berkeley, to conduct research on: (1) molecular function and regulation of secretory factors (including pref-1 and adipocyte-specific secretory factory/resistin) that control adipocyte differentiation, and novel adipocyte specific enzymes in triglyceride metabolism, (2) hormonal/nutritional regulation of lipogenic gene transcription. Ph.D must have been received within the last five years. Salary range: $32,304 to 36,732. Send curriculum vitae to **Dr. Hei Sook Sul (hsul@nature.berkeley.edu), Department Nutritional Sciences and Toxicology, University of California, Berkeley, CA 94720.**

Application deadline is June 1, 2007. The University of California is an Equal Opportunity, Affirmative Action Employer.

POSTDOCTORAL OPPORTUNITIES

NATIONAL RESEARCH COUNCIL
OF THE NATIONAL ACADEMIES

The Walter Reed Army Institute of Research will offer an NRC Research Associateship award for the study of pathogenic mechanisms of *Shigella* species for development of new vaccines. Tissue culture and animal models are used to assess the interface between mucosal pathogens and M cells using *Shigella* species as a model pathogen. Strategies for evaluating mucosal delivery and presentation of antigens are focused on novel *Shigella* subunit vaccine and adjuvant formulations with the goal of establishing correlates of immunity to mucosal pathogens, such as *Shigella*. Applicants should have a Ph.D. and a strong background in cell biology, immunology, and microbiology.

Prospective applicants should send CV, research interests, and names of three references to: edwin.oaks@na.amedd.army.mil.

Applications must be submitted online directly to the NRC. Instructions on how to apply are at:

www.national-academies.org/rap

Questions should be directed to: 202-334-2760
rap@nas.edu

THE NATIONAL ACADEMIES
Advisers to the Nation on Science, Engineering, and Medicine

Post Doctoral Opportunities

OMRF, a private, non profit research institute, provides state-of-the-art core facilities and a relaxed, interactive, yet rigorous research environment. OMRF is home to world-renowned scientists and numerous biomedical accomplishments. Research at OMRF focuses on the basic science of human disease: arthritis & immunology, cardiovascular biology, neuroscience and molecular/cellular biology.

In an era of new growth, we seek innovative and talented post doctoral applicants with the ability to independently develop projects and analyze experiments. Directly related experience not necessary. Completion of PhD within the last two years and first-author publication in internationally recognized journals preferred.

Join & enjoy:
- close scientific interactions & collaborations
- modern laboratories
- outstanding core facilities
- comprehensive benefits package
- low cost of living

Please visit www.OMRF.org for specific career opportunities & more information.

OMRF
Oklahoma Medical Research Foundation

EEO/DV/AA

POSITIONS OPEN

UNIVERSITY OF CALGARY
iseee
INSTITUTE for SUSTAINABLE ENERGY, ENVIRONMENT and ECONOMY

Executive Director

Creating a climate friendly energy system is one of the grand challenges of the new century. The ***Institute for Sustainable Energy, Environment and Economy*** at the University of Calgary was created to focus the efforts of some of the world's foremost thought leaders, scientists and corporate stakeholders in the field. The Institute provides leadership, co-ordination and support for sustainability research and practical progress. It champions solutions that are technically, economically and socially viable by encouraging researchers to be entrepreneurial oriented analysts and innovators.

The Institute is devoted to integrated, mission-oriented, multi-disciplinary research, education and innovation. ISEEE consolidates and builds upon the knowledge and expertise in six Faculties at the University of Calgary (Environmental Design, the Haskayne School of Business, Law, the Schulich School of Engineering, Science and Social Sciences). The University of Calgary, which is based in the heart of one of the world's energy capitals, has plans for a major facility that will provide classroom, research and teaching labs for faculty members and students associated with ISEEE-related projects and programs.

As Executive Director of ISEEE, your ability to unite the essential stakeholders in the creation of chains of sustainability will establish and distinguish the Institute as a unique international agent of research and mainstream change.

As it grows under your leadership, the ISEEE will continue to engage world-class, multi-disciplinary and mission-based education and research in the interest of advancing sustainable energy, the environment and the economy. In your position as Executive Director of the Institute, your ability to clarify goals, foster dialogue and influence the agenda will affect the global community.

With your academic credentials and professional experience ideally spanning academe and business, you will add passionate, collaborative and instantly credible leadership to the Institute. The stakes are high. The time is now. Develop the programs and partnerships. Grow the Institute. Lead with urgency and commitment as you attract the world's finest minds to the cause.

To explore this opportunity further, please forward your resume to our Calgary, Canada office: careers@hhsrb.ca or phone + (1) 403-410-6700. For further information on the Institute: www.iseee.ca

RAY & BERNDTSON
Global Leaders in Executive Search

St. Jude Children's Research Hospital
ALSAC · Danny Thomas, Founder
Finding cures. Saving children.

FACULTY POSITIONS

Department of Hematology

We are seeking laboratory-based faculty at the Assistant and/or Associate Member level with interests in erythropoiesis, hematopoietic stem cell biology, or other research programs in benign hematology. The Department currently consists of eight faculty members engaged in clinical and/or laboratory research in sickle cell disease, thalassemia, gene therapy for hematologic diseases, molecular hematopoiesis, and coagulation disorders. We are seeking interactive colleagues engaged either in basic or translational research who will complement these existing programs and who have documented potential or a proven track record for developing an outstanding laboratory research program. St. Jude offers a rich academic environment for hematology research that is supported by an NHLBI-funded Comprehensive Sickle Cell Center, an ongoing NHLBI-funded Program Project Grant in gene therapy for hemoglobinopathies, NHLBI-funded clinical and translational research protocols, and institutionally supported research. Numerous opportunities exist for interdisciplinary academic collaboration both within and outside of the Department for Hematology. Strong institutional support is in place for GMP manufacturing, clinical trials infrastructure, genetic research in animal models, pharmacogenomics, and bioinformatics. St. Jude offers competitive salaries and excellent benefit packages to faculty members.

Interested individuals should forward a letter with a statement of research interests and a CV to:

Brian Sorrentino, M.D.
Chair, Search Committee
Director, Experimental Hematology
St. Jude Children's Research Hospital
332 North Lauderdale
Memphis, TN 38105
E-mail: brian.sorrentino@stjude.org

St. Jude is an Equal Opportunity Employer and a Drug-Free Workplace. Candidates receiving offers of employment will be subject to pre-employment drug testing and background checks.

Positions @ NIH

THE NATIONAL INSTITUTES OF HEALTH

Department of Health and Human Services
National Institutes of Health
National Institute of General Medical Sciences
Cell Biology and Biophysics Division
HEALTH SCIENTIST ADMINISTRATOR

The National Institute of General Medical Sciences (NIGMS), a major research component of the National Institutes of Health (NIH) and the Department of Health and Human Services (DHHS), is seeking applications from exceptional scientists to serve as a **Health Scientist Administrator** in the **Cell Biology and Biophysics (CBB) Division**. This division supports major research grant programs in these fields, including the Protein Structure Initiative (PSI) -- a structural genomics research program. The Institute is seeking an individual with scientific, administrative, and leadership credentials who can manage and direct structural biology programs in this division and within the PSI. Information about the CBB and the PSI can be found at:
http://www.nigms.nih.gov/About/Overview/CBB.htm and
http://www.nigms.nih.gov/Initiatives/PSI.htm

Qualifications: The successful individual will possess a Ph.D., M.D. or equivalent degree in a field relevant to the position, have research experience in structural biology and biophysics and knowledge of and/or research experience in structural genomics or bioinformatics, leadership and managerial skills, and strong oral and written communication skills. Applicants must be U.S. citizens.

Salary: The current salary range is $93,822 - $121,967, depending on experience and accomplishments; a full Civil Service package of benefits (including retirement, health, life and long term care insurance, Thrift Savings Plan participation, etc.) is available. Recruitment incentive may be awarded and relocation expenses will be paid.

How to Apply: Position requirements and detailed application procedures are provided in vacancy announcements **NIGMS-07-181502-DE and NIGMS-07-181503-MP**, which can be obtained by accessing the NIGMS website at **http://www.nigms.nih.gov**. All applications and supplemental information must be received no later than **Friday, May 18, 2007**. For additional information, contact **Ms. Erin Bandak at (301) 594-2035**.

UPCOMING JOB OPPORTUNITIES

Department of Health and Human Services
National Institutes of Health (NIH)

National Institute of Dental and Craniofacial Research (NIDCR)

The Office of the Scientific Director (OSD), Division of Intramural Research (DIR), National Institute of Dental and Craniofacial Research (NIDCR) seeks a Deputy to the Scientific Director (Senior Investigator eligible or Senior Scientist, Cat.1). The mission of the DIR is to improve oral, dental and craniofacial health through research, research training, and the translation of discoveries to the public domain. The Division accomplishes this mission by: 1) performing distinctive basic and clinical research that emphasizes high quality and relevance to health; 2) training the next generation of researchers in its laboratories and clinic, and 3) translating the results of its research through publications and technology transfer.

The incumbent will serve as the Deputy Scientific Director for NIDCR with responsibility for management of a large scientific program and full delegation of authority to act for the Scientific Director, DIR, in matters related to the overall operation of the Institute's intramural research program. Specific responsibilities include aspects of administration that support and facilitate the DIR scientific mission. These may include, for example, coordinating reporting activities, assisting in budget preparation, preparation of the institute's Emergency Response Plan, overseeing renovations, serving as a liaison to the Executive Secretary to the Board of Scientific Counselors in preparation for reviews, reviewing and approving routine administrative actions and, when necessary, substituting for the Scientific Director in representing the NIDCR/DIR. The incumbent may be supported to carry out a focused independent research program, with associated effort being consistent with the duties of the Deputy Scientific Director. If the area of the individual's research expertise is appropriate, then (s)he may be involved in assisting in the planning and evaluation of the Division's research programs.

Applicants must have a DDS/DMD/MD/or Ph.D. degree and documented experience in leading an independent research program, as well as an interest and willingness to support the basic and clinical research programs of the NIDCR/DIR. In addition, they should have knowledge of all policies and procedures of the NIH intramural program. Applications from minorities, women and persons with disabilities are encouraged.

Applicants should submit a current CV, Bibliography and the names and contact information for three referees to: **Pamela McInnes, DDS, MSc.(Dent.), Search Committee Chairman, Director, CIBID, NIDCR, Bldg. 45, Room 4AN-12B, Bethesda, MD 20892-6402. Tel: 301-594-2419, Fax: 301-480-8319, Email: pmcinnes@nidcr.nih.gov.** Applications will be accepted until **May 4, 2007**. Salary commensurate with qualifications and experience. More detailed information about NIDCR can be obtained on our Home Page. Visit us at: **http://www.nidcr.nih.gov/Research/Intramural/**

WWW.NIH.GOV

Help Us Help Millions

Are you ready for an exciting career that could help improve millions of lives around the world?

Post-doctoral fellowship position

A post-doctoral fellowship position is available in the Molecular Viral Biology Section of the Laboratory of Infectious Diseases, Division of Intramural Research, National Institute of Allergy and Infectious Diseases (NIAID), NIH, Bethesda, MD. The laboratory's interests focus on:

(1) development of antibody-mediated prevention strategies against dengue and other insect-borne flaviviruses, including tick-borne encephalitis virus, West Nile encephalitis virus and Japanese encephalitis virus; and

(2) investigation of immuno-pathogenesis of dengue, especially, mechanisms of antibody-dependent enhancement (ADE) of dengue virus replication.

Research activities in the Section include: combinatorial antibody cloning by phage display to identify neutralizing monoclonal antibodies against each of these flaviviruses from infected chimpanzees or humans; molecular and immunological characterization of Fab fragments and humanized IgG antibodies; evaluation of antibody-mediated protection against challenge by dengue or other flaviviruses in animal models; and analysis of ADE of dengue virus replication in vitro and in monkeys.

This full-time position offers a unique opportunity to work on antibody projects that range from basic molecular biology, bacteriology, virology to immunology in infectious disease areas. Successful applicants must have less than three years of post-doctoral experience and a strong background in basic immunology, virology, and molecular biology.

To insure consideration for this position, please email your resume to Dr. Ching-Juh Lai at clai@niaid.nih.gov.

We invite you to explore our Institute and other available opportunities at **http://healthresearch.niaid.nih.gov/pdf**

Department of Health and Human Services
National Institutes of Health
National Institute of Allergy and Infectious Diseases *Proud to be Equal Opportunity Employers*

Department of Health and Human Services
National Institutes of Health
National Heart, Lung, and Blood Institute

Biochemistry and Biophysics Center
Postdoctoral Fellowship

The National Heart, Lung, and Blood Institute (NHLBI), Division of Intramural Research is recruiting a Postdoctoral Fellow to train in the Biochemistry and Biophysics Center under the mentorship of Dr. Rodney L. Levine. The research goal of his laboratory is the elucidation of the mechanisms by which oxidative signals and oxidative stress affect physiology and disease. The laboratory currently focuses on oxidative modification of specific proteins and the effect of that covalent modification on their susceptibility to degradation, especially by the proteasome. Additional information and references may be found on the NHLBI website at http://dir.nhlbi.nih.gov/staffpages/levinerl/index.asp

Candidates for this position must have a PhD or MD degree along with excellent training in biochemistry, molecular biology, or cell biology. The successful candidate will be provided stipend support commensurate with their experience. To apply, please submit via email your curriculum vitae, a statement of your future career goals, and the names and email addresses of three references:

Rodney L. Levine, MD, PhD, Senior Investigator, rlevine@nih.gov

DHHS and NIH are Equal Opportunity Employers.

Postdoctoral, Research and Clinical Fellowships at the National Institutes of Health

www.training.nih.gov/pdopenings

www.training.nih.gov/clinopenings

Train at the bench, the bedside, or both

Office of Intramural Training and Education
Bethesda, Maryland 20892-0240
800.445.8283

UMDNJ
NEW JERSEY MEDICAL SCHOOL
University of Medicine & Dentistry of New Jersey

Quantitative Neuroscience

The New Jersey Medical School seeks to fill a TENURE TRACK ASSISTANT PROFESSOR FACULTY POSITION. Applications for Associate and Full Professor rank will also be considered. Research should focus on interdisciplinary and quantitative approaches in any area of the neurosciences and complement existing research interests in molecular and cellular aspects of biochemistry, pharmacology and physiology. It is expected that more senior candidates will have achieved international recognition for their research accomplishments. Information about NJMS and its academic research departments is at: **http://njms.umdnj.edu**.

NJMS is investing heavily in a strong research infrastructure for basic and clinical neurosciences. Graduate training programs in this area are supported by the NIH and the Howard Hughes Medical Institute. This faculty position comes with a competitive salary, startup package and research facilities. NJMS is located in the University Heights area of Newark, adjacent to Rutgers University and the New Jersey Institute of Technology, and in close proximity to the extensive scientific and cultural amenities of New York City.

Review of applications will begin **May 15, 2007**. Applicants should send a cover letter, CV, research interests and future plans as a single Word or PDF e-mail attachment to **QNSfacsrch@umdnj.edu**. Please have three letters of reference sent as attachments to the same e-mail address, with hardcopies to: **QNS Faculty Search; c/o Office of the Dean; New Jersey Medical School; 185 South Orange Ave.; Newark, NJ 07101-1709**.

UMDNJ is an Affirmative Action/Equal Opportunity Employer, M/F/D/V and is a member of the University Health Systems of New Jersey.

U.S. Environmental Protection Agency
Office of Research and Development
National Exposure Research Laboratory (NERL)

Branch Chief (Supervisory Biologist/Supervisory Physical Scientist), GS-14/15

The U.S. Environmental Protection Agency is seeking qualified applicants for a Branch Chief position located in the National Exposure Research Laboratory (NERL), Environmental Sciences Division (ESD), Las Vegas, NV(**http://www.epa.gov/esd**). The incumbent of this position will serve as the Chief of the Landscape Ecology Branch and is expected to work both as a Supervisory Biologist/Supervisory Physical Scientist and to conduct research as a nationally and/or internationally recognized expert in his/her field of research related to the ESD's and NERL's mission. The incumbent will be responsible for the administrative management of the Branch, which conducts research in the field of landscape ecology and related disciplines, develops landscape assessment and characterization applications, and devises tools and methods for the solution of regional environmental problems, specifically regarding the vulnerability of ecosystems and watersheds to human-induced and natural stress. The incumbent serves as a first-line supervisor for a staff of about 20-25 researchers, technicians, and support staff located primarily in Las Vegas.

This is a permanent, full-time position requiring U.S. citizenship. Candidates must meet U.S. Office of Personnel Management qualification requirements including specific educational course work. Desirable applicants will have a degree in the areas of biology, landscape ecology or related biological and/or physical sciences disciplines. Salary ranges from $79,115 to $120,981 and is commensurate with qualifications. The selected candidate will be eligible for a full benefits package, including relocation, health insurance, life insurance, retirement, and vacation and sick leave.

HOW TO APPLY: This position will be advertised through the Federal Government's job web site: **http://www.usajobs.gov**. For additional information regarding the application process, please contact: **Ms. Barbara Howard** at **(800) 433-9633** or via email at **howard.barbara@epa.gov**.

The U.S. EPA is an Equal Opportunity Employer.

FULL TENURE TRACK FACULTY POSITION FOR A CANCER RESEARCH SCIENTIST

The Meharry Medical College/Vanderbilt-Ingram Cancer Center Partnership (MMC/VICC Partnership) is currently soliciting competitive applications for one cancer basic research scientist for a full tenure track faculty position at the level of either assistant or associate position at Meharry Medical College with a joint appointment at Vanderbilt-Ingram Cancer Comprehensive Center (VICC). The qualified candidate will also have either full or an associate membership status at the VICC. The candidate will be expected to develop and maintain a funded competitive cancer research. Initially, the position will be fully funded by the NCI's U54 Cancer Center Partnership Grant to the MMC/VICC Partnership, whose principal investigators are **Dr. Harold Moses**, Emeritus Director of VICC and **Dr. Samuel Evans Adunyah**, Chairman of Cancer Biology Division, Department of Biomedical Sciences at Meharry Medical College. Basic scientists (Ph.D. or M.D/Ph.D.) with cancer research interests in either prostate or breast cancer are encouraged to apply by **April 30, 2007**.

Please, send an electronic file on CD rom containing the following information to the address below.

- A letter which describes your interest in our position and your current position
- Research description and future research goals
- Current full CV
- References (at least 4)

Dr. Samuel Evans Adunyah
Chairman, Cancer Biology Division
Co-P.I., MMC/VICC Partnership
Cancer Biology Division
1005 D.B. Todd Blvd.
Nashville, TN 37208

Dr. Samuel Evans Adunyah can be reached at: **615/327-6345; Fax: 615/327-6440; e- mail: sadunyah@mmc.edu.**
OR
Send your materials by e-mail to: **Ms Ketia Barnes, MMC/VICC Cancer Partnership Program Coordinator, kbarnes@mmc.edu**.

Waseda Institute for Advanced Study

Call for Researchers

Waseda University recently established the Waseda Institute for Advanced Study (WIAS), to provide opportunities for younger researchers to exercise their capabilities to the full in a highly developed and flexible research environment. We are now issuing a call for researchers who wish to take up fixed-term appointments at the Institute to engage in research activity.

- Research Fields to be invited:
  Natural sciences
  Particularly welcome is research relevant to the following themes:
  Mathematics and information technology, nanotechnology and materials, robots and machines, physics, environment and construction, life-sciences and biotechnology, together with fields that synthesize these disciplines.
- Appointment Status:
  Visiting Professor*, Visiting Associate Professor*, Assistant Professor, Visiting Research Associate
  *As a rule, Visiting Professors and Visiting Associate Professors shall take charge of three year-long class units.
- Scheduled Starting Date of Appointment:
  October 1, 2007
- Duration:
  Three years
  Longer term appointments (four or five years) are available depending upon the results of performance reviews.

Applicants must have PhD or equivalent, or be expecting those degrees by October 1, 2007. Further details and application forms can be obtained from our website: **www.waseda.jp/wias**
Contact: **wias-info@list.waseda.jp**

Applications should be sent to the following address:
Waseda Institute for Advanced Study
attention: Faculty Hiring
1-6-1 Nishiwaseda, Shinjuku-ku,
Tokyo 169-8050, Japan

Closing Date: May 10, 2007

www.waseda.jp/wias

HOWARD HUGHES MEDICAL INSTITUTE

HHMI Investigator Competition

The Howard Hughes Medical Institute invites applications for investigator positions from scientists who have demonstrated originality and productivity in biomedical research and who show exceptional promise for future contributions.

Eligibility

- Ph.D. or M.D. (or the equivalent)
- Tenured or tenure-track position as an assistant professor or higher academic rank (or the equivalent) at an eligible U.S. institution
- Four to 10 years of experience since appointment as an assistant professor
- Principal investigator on one or more active national peer-reviewed research grants with a duration of at least three years

Application deadline: June 13, 2007

Application information:
www.hhmi.org/investigator2008/sci

HHMI investigators are among the most creative and promising biomedical scientists in the nation. They rigorously pursue significant biological questions, develop innovative research tools and methods, and lead their scientific fields into new areas of inquiry. Working to push the boundaries of fundamental knowledge and ultimately to improve human health, HHMI investigators forge links between basic biology and medicine.

The Institute seeks to appoint to its investigator program approximately 50 outstanding scientists. This competition will enable HHMI to strengthen its community of researchers and bring innovative approaches to the study of biological problems not only in the biomedical disciplines but also in adjacent fields, such as chemistry, physics and biophysics, biomedical engineering, and computational biology. Candidates should apply directly to HHMI; prior institutional endorsement is not part of the application process.

HHMI, a nonprofit medical research organization, plays a powerful role in advancing biomedical research and education in the United States. The investigator program rests on the conviction that scientists of exceptional talent, commitment, and imagination will make fundamental biological discoveries for the betterment of human health if they receive the resources, time, and freedom to pursue challenging questions. The Institute's investigators, selected through rigorous national competitions, include 11 Nobel Prize winners and 115 members of the National Academy of Sciences.

The Howard Hughes Medical Institute is an equal opportunity employer. Women and members of racial and ethnic groups traditionally underrepresented in the biomedical sciences are encouraged to apply.

HHMI
HOWARD HUGHES MEDICAL INSTITUTE

St. Jude Children's Research Hospital

ALSAC • Danny Thomas, Founder

Finding cures. Saving children.

FACULTY POSITION IN ZEBRAFISH DEVELOPMENTAL BIOLOGY

The Department of Chemical Biology and Therapeutics at St. Jude Children's Research Hospital invites applications for a faculty position at the level of ASSISTANT or ASSOCIATE MEMBER in zebrafish developmental biology. St. Jude Children's Research Hospital encourages translational research, and has laid out as a major strategic goal the development of novel chemotherapies for brain and solid tumors. We are specifically seeking applicants whose research program is or will be focused on the development of the nervous system, or other appropriate organ systems, and who have interest in developing robust collaborative research programs aimed at understanding the interactions between potential small molecule therapeutics and the developing organ systems. The successful applicant will have a demonstrated track record in developmental biology of zebrafish and either experience with or interest in establishing programs utilizing small molecules.

The Department of Chemical Biology and Therapeutics is a multidisciplinary, thematically integrated Department focused on the discovery and development of small molecules for perturbing cellular functions - particularly in systems relevant to pediatric oncology. Departmental faculty work in all areas of drug discovery including cheminformatics, high throughput chemistry, high throughput and high content screening, medicinal chemistry, and analytical chemistry. The department also houses a substantial infrastructure for the discovery and development of novel small molecules that affect biological systems.

Individuals will contribute to one or more existing and new programs at the institution, including the interdisciplinary research programs of Developmental Therapeutics for Solid Malignancies, Hematological Malignancies, Molecular Oncology, Neurobiology & Brain Tumor, Signal Transduction, or Chemical Biology.

St. Jude offers a very competitive package for these positions, including a generous start-up allowance with newly remodeled space and equipment; laboratory resources (as needed); and support positions. In addition, appointees have access to a range of institutional core facilities including protein and nucleic acid chemistry, microarray analysis, gene knockout and transgenic technologies, pharmacokinetics, and development of animal models.

Those interested in joining this multidisciplinary department should arrange to have their CV, a brief prospectus of research interests, and three letters of recommendation sent to:

R. Kip Guy, Ph. D., Chair
Department of Chemical Biology and Therapeutics
St. Jude Children's Research Hospital
322 North Lauderdale Street • Memphis, TN 38105

St. Jude is an Equal Opportunity Employer and a Drug-Free Workplace. Candidates receiving offers of employment will be subject to pre-employment drug testing and background checks.

Tenured Professor

CBR Institute for Biomedical Research & Harvard Medical School

As a part of CBRI's Longwood Consolidation and new building project, we are recruiting faculty at the level of full professor in partnership with the Department of Pathology at the Harvard Medical School. Successful candidates will be recognized world-wide for their accomplishments, and they will direct independent research laboratories at CBRI complementing and enhancing the efforts of our distinguished faculty.

Molecular Immunology/Stem Cell Biology - Pathology and CBRI

We are seeking candidates performing cutting-edge research to understand fundamental mechanisms in cellular or organismal biology. Areas of focus include cellular signaling, transcriptional regulation, cellular differentiation, development of organ systems, stem cell function, innate and adaptive immunity including NK cell biology, infectious diseases, cancer genetics and immunology, mathematical modeling of cellular processes using approaches spanning biochemistry and molecular biology, innovative microscopy, and mouse genetics.

Please forward a cover letter, curriculum vitae, a list of 10 key publications, a statement of present and future research interests and research funding. Please have four letters of reference sent directly to:

Frederick W. Alt
Scientific Director/Search Committees
CBR Institute for Biomedical Research
200 Longwood Avenue
Boston, MA 02115
CBRI-recruitment@cbrinstitute.org

CBRI and Harvard Medical School are affirmative action/equal opportunity employers. Women and minority candidates are encouraged to apply.

The CBR Institute for Biomedical Research

Harvard Medical School

Tenured Professor

CBR Institute for Biomedical Research & Harvard Medical School

We are recruiting faculty at the level of full professor in partnership with the Department of Biological Chemistry and Molecular Pharmacology (BCMP) at the Harvard Medical School (HMS). Successful candidates will be recognized world-wide for their accomplishments, and they will direct independent research at CBRI. We are seeking candidates who solve important biological questions such as how signals are transmitted in the extracellular and cytoplasmic environments. Areas of expertise include protein structure prediction, design of enzymes with recognition and cleavage of novel DNA sequences, and redesign of protein therapeutics and enzymes with the ability to make chemical compounds including novel antibodies.

Please forward a cover letter, curriculum vitae, reprints of key publications, and a statement of present and future research interests. Please have four letters of reference sent directly to:

Tomas Kirchhausen, Chair
Senior Search Committee
CBR Institute for Biomedical Research
200 Longwood Avenue
Boston, MA 02115
CBRI-recruitment@cbrinstitute.org

CBRI and Harvard Medical School are affirmative action/equal opportunity employers. Women and minority candidates are encouraged to apply

The CBR Institute for Biomedical Research

Harvard Medical School

UNIVERSITY OF DELAWARE

One of the oldest institutions of higher education in this country, the University of Delaware today combines tradition and innovation, offering students a rich heritage along with the latest in instructional and research technology. The University of Delaware is a Land-Grant, Sea-Grant, Urban-Grant and Space-Grant institution with its main campus in Newark, DE, located halfway between Washington, DC and NYC. Please visit our website at **www.udel.edu.**

Assistant Professor
Animal and Food Sciences

Tenure-track position in Toxicology available September 1, 2007.

REQUIREMENTS: Ph.D. with post-doctoral or equivalent experience in Toxicology, Biochemistry, Chemistry, Food Science, Molecular Biology, Mycology or another appropriate discipline. Ability to communicate effectively with academic, government, and industry colleagues and with students.

DUTIES: Position will be approximately 60% research and 40% teaching. Develop an active, extramurally funded, and contemporary research program focused on the chemical, analytical, molecular or genetic aspects of toxins in food or animal feed. Teach under-graduate/graduate courses in contemporary Food Chemistry and Food Analysis.

CONTACT: Send a letter of interest, curriculum vitae, a list of three to five references, and a brief description of research interests to Rolf D. Joerger, Search Committee Chair, Department of Animal and Food Sciences, 044 Townsend Hall, University of Delaware, Newark, DE 19716-2150 by June 15, 2007. The curriculum vitae and all application materials shall be shared with departmental faculty.

The UNIVERSITY OF DELAWARE is an Equal Opportunity Employer which encourages applications from Minority Group Members and Women.

Brain Science Institute RIKEN

RIKEN

Brain Science Institute

Laboratory Head / Unit Leader positions, Japan

New laboratories/ units will be established in the Intellectual Brain Functional Research Group, specifically aiming to understand fundamental brain mechanisms of emotional and social interactions among humans.

For further information:
http://www.brain.riken.jp/en/work/positions/20070328.html
Inquiries:
search25@brain.riken.jp
Closing date: **July 31, 2007 (receipt date)**

Does your next career step need direction?

There's only one place to go for career advice if you value the expertise of *Science* and the long experience of AAAS in supporting career advancement - ScienceCareers.org. The pages of *Science* and our website ScienceCareers.org offer:

- Thousands of job postings
- Career advice articles and tools
- Funding information
- Networking opportunities

www.sciencecareers.org

POSITIONS OPEN

ASSISTANT/ASSOCIATE RESEARCH PROFESSOR

The Cardiovascular Research Laboratory at Tulane University Health Sciences Center in New Orleans is seeking a full-time research scientist with considerable potential, expertise, and experience in tissue regeneration using adult stem cells.

Successful candidates will have a Ph.D. and/or M.D./Ph.D. degree and several years of postdoctoral trainings, knowledge, and expertise in all standard methods of molecular biology, cell culture, as well as interventional catheterization procedures in large animals. The academic appointment will be in the Department of Medicine as Director of Applied Cardiovascular Stem Cell Research leading multidisciplinary basic and applied stem cell research program in cooperation with the Department of Surgery and Medicine.

Prospective candidates should e-mail a letter of intent indicating research interest, curriculum vitae, and contact information for three references to: **Eckhard Alt, M.D., Ph.D., Professor of Medicine, Director of Cardiovascular Research. E-mail: ealtmd@aol.com.**

AQUATIC ECOLOGIST/LIMNOLOGIST. The Annis Water Resources Institute (AWRI) at Grand Valley State University seeks an Aquatic Ecologist/Limnologist. Candidate should have a Ph.D, postdoctoral experience, potential to develop and maintain a strong extramurally-funded research program, a demonstrated publication record, ability to teach graduate courses in field of expertise, and desire to work in a collaborative, interdisciplinary environment. We are especially interested in applicants working at the land-water interface, and who have expertise in the fields of coastal processes, landscape ecology, wetland ecology, molecular ecology, or aquatic biogeochemistry. This is a 12-month position with benefits. Review of applications will begin on June 1, 2007, and continue until the position is filled. Apply online (only) at **website: https://www.gvsujobs.org.** Further information about AWRI can be found at **website: http://www.gvsu.edu/wri.** For inquiries about the position, contact **Dr. Alan Steinman (e-mail: steinmaa@gvsu.edu).** *Grand Valley State University is an Affirmative Action/Equal Opportunity Institution.*

EVOLUTIONARY BIOLOGY
Carleton College

The Department of Biology invites applications for a temporary one-year position for the 2007-2008 academic year, 31 August 2007 to 15 June 2008. The full-time teaching responsibilities include an upper-level course in evolution, team teaching in the introductory biology sequence with laboratories, and an upper-level course with laboratory in an area of the applicant's expertise. Applicants should have Ph.D. degree or be near completion. Send a letter of application, curriculum vitae, a brief statement of teaching and research interests, and three letters of reference to: **Professor Matthew Rand, Department of Biology, Carleton College, Northfield, MN 55057-4025.** Review of applications will begin on 1 May 2007. *Carleton is an Affirmative Action/Equal Opportunity Employer. We are committed to developing our faculty to better reflect the diversity of our student body and American society. Women and members of minority groups are strongly encouraged to apply.*

FACULTY/GROUP LEADER POSITIONS are available at Institute for Nutritional Sciences, Chinese Academy of Sciences, Shanghai, China. The position offers an excellent opportunity to develop an individual research program that applies approaches of modern biology to solve nutrition related health issues. The Institute offers competitive salary, house benefit, startup package, and excellent research environment. Please submit resume, personal statement, and three recommendation letters to **Dr. Qiwei Zhai** at **e-mail: qwzhai@sibs.ac.cn.**

POSITIONS OPEN

ASSISTANT or ASSOCIATE DEAN for MANAGEMENT
The University of Texas Health Science Center at Houston Graduate School of Biomedical Sciences

Responsible for financial and personnel management, information systems, and institutional research for the University of Texas (UT) Graduate School of Biomedical Sciences at Houston **(website: http://gsbs.uth.tmc.edu)** which has 550 M.S. and Ph.D. students at the UT Health Science Center schools and the UT M.D. Anderson Cancer Center. Applicants must have five or more years of experience in higher education management, institutional research, or as a graduate school faculty member. Master's degree required but a Doctorate is preferred. Apply by e-mail to **e-mail: gsbs.mgmt.position@uth.tmc.edu.** Attach (1) a cover letter including a statement of interest and a brief description of relevant experience and qualifications, and (2) a resume or curriculum vitae. Starting date must be no later than September 1, 2007.

This is a security-sensitive position and thereby subject to Texas education code section 51.215. A background check will be required for the final candidate. The University of Texas Health Science Center at Houston is an Affirmative Action, Equal Opportunity Employer (minorities/females/persons with disabilities/veterans).

SENIOR SCIENTIST: PROCESS DEVELOPMENT/PROTEIN PRODUCTION

A Senior Scientist position is available immediately at Fraunhofer USA Center for Molecular Biotechnology (CMB) in Newark, Delaware, to lead a process development and protein production laboratory. The Center focuses on plant-based production of proteins for vaccine and therapeutic development. The successful candidate will be responsible for directing the development of processes for the purification of recombinant proteins from plant biomass. A key role will be to coordinate and implement scale-up of protein purification for pilot-scale production. The successful candidate will supervise a group of at least six laboratory personnel and will work closely with multi-functional groups within CMB and with outside partners. Applicants should be highly motivated, possess a Ph.D., and have a strong background in downstream processing and protein purification, preferably in an industrial setting. Experience in pilot and/or large-scale production of recombinant proteins is an advantage and applicants should have supervisory experience. Interested candidates should e-mail their curriculum vitae to **e-mail: personnel@fraunhofer-cmb.org.**

Fraunhofer USA offers competitive salaries and benefit packages and is an Equal Opportunity Employer.

DIRECTOR, CENTER for INDUSTRIAL and MEDICAL ULTRASOUND
University of Washington Applied Physics Laboratory

The University of Washington's Applied Physics Laboratory (UW-APL) is seeking a dynamic and visionary leader to direct the Center for Industrial and Medical Ultrasound (CIMU). This interdisciplinary organization of approximately 45 scientists, staff, physicians, and students has a mission to foster intra and extramural research collaborations; develop industrial and medical ultrasound technology; form industrial partnerships; and educate and train students and technical professionals working in the fields of industrial and medical ultrasound. CIMU is one of eight departments at APL, a leader in the basic and applied physics of sound. Active areas of research in CIMU include but are not limited to: image-guided ultrasound therapy, diagnostic ultrasound, shock wave therapy, sonoluminescence, sonochemistry, nonlinear acoustics, and ultrasound-mediated drug delivery; candidates pursuing research programs in these or related areas are especially desirable. To apply go to **website: http://www.washington.edu/admin/hr/jobs/,** staff jobs, external candidates requisition number 31343.

POSITIONS OPEN

DEPARTMENT of REPRODUCTIVE BIOLOGY
Case Western Reserve University, Cleveland, Ohio

Applications are invited for a **SENIOR RESEARCH ASSOCIATE** position for a project of early detection and treatment of epithelial cancers. The position offered is for one to three years. The candidate must have earned M.D., Ph.D. (biology, physiology, biochemistry, or molecular biology) or both, with proven postdoctoral fellowship expertise and track record in pathology. The candidate is required to be fluent in molecular biology and biochemical techniques, including RNA and DNA research; regular and advanced protein techniques (e.g. imaging, immunostaining, immunofluorescence, chemiluminescence and enzyme-linked immunosorbent assay); expertise in techniques involving the use of antibodies; as well as routine cell culturing techniques including handling of human cells and tissues, and handling and experimentation of rodent animals. Applicants with documented expertise in nanotechnology methods will have priority. The candidate will design, conduct, and analyze experiments in the above fields; will coordinate and supervise lower-ranking technicians in the Laboratory; and is expected to write laboratory protocols and procedures, drafts of research papers and grant applications. Required is also fluency in the use of computer facilities and the internet, and the ability to use existing data modalities (libraries, electronic sources, et cetera). The candidate will be in charge of the administrative aspects of running a busy laboratory, including interaction with other scientists from within and outside of the Institution. Work will be conducted in an excellent environment with state-of-the-art facilities.

Please send curriculum vitae, a description of research accomplishments, and the names of three references to: **George Gorodeski, M.D., Ph.D., Department of Obstetrics and Gynecology, University Hospitals of Cleveland, 11100 Euclid Avenue, Cleveland, OH 44106.** *An Affirmative Action/Equal Opportunity Employer.*

TISSUE CORE MANAGER

University of California San Francisco (UCSF) Comprehensive Cancer Center seeks experienced Core Leader to act as the Manager of the Tissue Core facility, dedicated to collecting, banking, and processing mouse and human tissue. These include fresh, frozen, and paraffin embedded tissues and processing services encompassing the whole spectrum of histology services and DNA/RNA extraction. Manage the daily Core functions and provide technological direction into future areas of service. Strong communication and organizational skills, management and teaching experience, and high degree of technical expertise required, as well as knowledge of tissue handling, mouse pathology and necropsy, biosafety protocols, and patient consent requirements. Supervise laboratory personnel, determine experimental design for users, and possess general knowledge of pathology and histology protocols. Advanced degree in biological sciences and/or a related clinical license and background in tissue handling and biological research required. Salary scale for Academic Coordinator I/II commensurate with experience. Please send a letter of interest, curriculum vitae, and names/contact information for three references to: **Tissue Core M2914, Human Resources, University of California San Francisco Comprehensive Cancer Center, 1600 Divisadero Street, P.O. Box 1297, San Francisco, CA 94143-1297.** *UCSF seeks candidates whose experience, teaching, research, or community service has prepared them to contribute to our commitment to diversity and excellence. UCSF is an Affirmative Action/Equal Opportunity Employer. The University undertakes affirmative action to assure equal employment opportunity for underutilized minorities and women, for persons with disabilities, and for covered veterans. All qualified applicants are encouraged to apply, including minorities and women.*

POSITIONS OPEN

SCRIPPS FLORIDA
The Scripps Research Institute

FACULTY POSITIONS
Department of Molecular Therapeutics

The Scripps Research Institute, Scripps Florida, is seeking outstanding applicants for Tenure-Track Faculty positions in the newly formed Department of Molecular Therapeutics. The Department focuses on chemical biology approach to dissecting signaling pathways and transcriptional programs, using state-of-the-art multidisciplinary technology and methodology and a variety of model systems for target identification, validation, and preclinical studies.

The Department of Molecular Therapeutics currently consists of two faculty members, **Dr. Patrick R. Griffin** (nuclear receptor signaling and proteomics, prevention and therapeutic approaches to metabolic disorders) and **Dr. Philip LoGrasso** (kinases and neurodegeneration). Dr. Griffin also oversees the Translational Research Institute at Scripps Florida, which consists of discovery biology, high throughput screening and lead identification, medicinal chemistry, pharmacology, chemical informatics, and drug metabolism and pharmacogenetics.

The Department is seeking highly qualified and interactive investigators who will bring and initiate creative therapeutic targets and programs that can take advantage of the unique high throughput core facilities of the Scripps Research Institute, Scripps Florida, including genomics, cell-based screening, proteomics, X-ray crystallography, informatics and lead optimization.

Appointments are available at the **ASSOCIATE and FULL PROFESSOR** levels. Scripps Florida offers very attractive startup packages, unique core services, and the outstanding intellectual environment of the Scripps Research Institute for fostering top-tier basic and translational research. Interested candidates should submit their curriculum vitae, a synopsis of their past research accomplishments and of their current and proposed research programs, along with complete contact information for at least four professional references, to:

Dr. Patrick R. Griffin
Chairman, Department of Molecular Therapeutics
c/o Mary Krosky
The Scripps Research Institute, Scripps Florida
5353 Parkside Drive, RF-1
Jupiter, FL 33458

The Department of Clinical Investigation (DCI) at Tripler Army Medical Center, Hawaii, invites applications to fill two **RESEARCH SCIENTIST STAFF** positions. Doctoral degree in biomedical field of research required. The scientist selected will be expected to establish an independent translational research program that is competitive for extramural funding. The scientist will mentor physicians in residency and fellowship training and keep a self-sustained line of research amenable to the inclusion of co-investigator physicians. Competitive applicants will be able to provide general guidance to trainees in a wide variety of clinical specialties in graduate medical education programs as well as allied health profession programs. Evidence of previous work in areas of translational research, undergraduate and graduate level instruction, and/or mentoring, and familiarity with statistical analyses desired. Salary is commensurate with experience and accomplishments, and a full civil service package of benefits (including retirement, health, life, and long-term care insurance, Thrift Savings Plan Participation) is available. Interested candidates should submit their resume at the following **website: http://www.cpol.army.mil** by 31 May 2007. If you have any questions, please call the **DCI Secretary** at **telephone: 808-433-6709.**

POSITIONS OPEN

NUTRITIONAL BIOCHEMISTRY and METABOLISM
The Ohio State University

The Department of Human Nutrition invites applications for three to four tenure-track positions at **ANY LEVEL** of appointment. Appointment at the Assistant Professor level requires postdoctoral experience, publications in well-established journals and evident potential to develop a nationally competitive research program focused on nutrient metabolism or dietary regulation of signaling processes. Appointments at senior levels require established, well-funded research programs. We are particularly interested in investigators who are exploring physiological, biochemical and molecular aspects of nutrient metabolism and disease processes modulated by diet, as well as investigators who complement existing strengths in the Department and the interdisciplinary nutrition program on campus. Experience in multidisciplinary approaches and collaborations addressing metabolic and chronic diseases, molecular nutrition, genomic/proteomic studies of diet-mediated regulation of metabolism, and integrative research involving human-clinical studies, animal models, and molecular mechanisms enhance competitiveness. Successful applicants will contribute to graduate and undergraduate teaching. Competitive salary, benefits, and startup will be provided. The Ohio State University was recently ranked third nationally as one of the best places to work in academia by *The Scientist* magazine and the city of Columbus has been ranked by *Money* magazine as one of the top ten cities in the country for general quality of life. Our College aspires to diversify our faculty and encourages applications from individuals in underrepresented groups (e.g., women, African Americans, Latinos, and Native Americans).

Applicants should submit cover letter, curriculum vitae, statements of research accomplishments and plans and teaching philosophy, and names and contact information for three references to: **Search Committee, Department of Human Nutrition, The Ohio State University, 1787 Neil Avenue, Columbus, OH 43210.** Screening of applications will begin May 15, 2007. *Equal Employment Opportunity/Affirmative Action Employer.*

CHIEF SCIENTIST

The Arizona Cancer Center invites applications for the position of Chief Scientist, Arizona Cancer Center. The Arizona Cancer Center (AZCC) is a National Cancer Institute-designated comprehensive cancer center which is celebrating its 30th anniversary. The Center, which was designated by the Arizona state legislature as the official Cancer Institute for the state of Arizona, is home to major programs in basic, translational, and clinical research, research education, and multidisciplinary, subspecialized cancer patient care. Research activities at the AZCC include developmental therapeutics, prevention and control, gastrointestinal cancer, cancer imaging, cancer biology and genetics. The scientist who fills this position will have an independent research program supported by extramural funding in basic and/or translational research and will have administrative responsibilities relating to leading and developing basic and translational research programs as well as mentoring junior faculty investigators. This position is supported in part by an endowment to the AZCC and offers a multimillion dollar startup package. For a full description of duties and qualifications, see our posting at **website: http://www.hr.arizona.edu.**

To apply, please visit our **website: http://www.uacareertrack.com,** link to our online application system and follow the instructions. Job number is 37338. Review of materials has begun and will continue until the position is filled. *The University of Arizona is an Equal Employment Opportunity/Affirmative Action Employer. Minorities/women/persons with disabilities/veterans.*

POSITIONS OPEN

FACULTY POSITION
Michigan Technological University
Forest Ecology

The School of Forest Resources and Environmental Science at Michigan Technological University (**website: http://forest.mtu.edu**) invites applications for a tenure-track faculty position in the area of forest ecology at the level of **ASSOCIATE or FULL PROFESSOR.** Candidates must possess a Ph.D. in a relevant field (e.g. forest ecology, forest ecosystems, or community dynamics addressing current issues relating to forest trees or forest ecosystems). A demonstrated record of research excellence is required. Responsibilities will include teaching in the applicant's area of expertise, and development of a vigorous, extramurally funded research program supporting Master's and doctoral students. For additional information, see **website: http://forest.mtu.edu/faculty/openings/index.html.** To apply, send curriculum vitae (with complete grants and contracts lists), publication list with selected reprints, and names of three references to: **Forest Ecology Search Committee, c/o Dr. David F. Karnosky, Chair, School of Forest Resources and Environmental Science, 1400 Townsend Drive, Houghton, MI 49931-1295.** Review of applications will begin on May 1, 2007, and will continue until the position is filled. Questions may be directed to **Dr. David F. Karnosky** at **e-mail: karnosky@mtu.edu.** *Michigan Technological University is an Equal Opportunity Education Institution/Equal Opportunity Employer.*

MOLECULAR and CELLULAR BIOLOGISTS
Center for Molecular Medicine

The newly established Center for Molecular Medicine at China Medical University Hospital at Taichung, Taiwan, is seeking Molecular and Cellular Biologists for up to ten tenure-track faculty with demonstrated excellence in (1) basic science research-receptor trafficking and nuclear/cytoplasmic import/export in cancer development; (2) translational research-cancer-targeted therapy and oral DNA vaccine. In addition, applicants with expertise in stem cell biology, proteomic approaches or animal model to elucidate the molecular mechanisms that cause cancer are also encouraged to apply. Applicants must have a doctoral degree with postdoctoral experience. Multiple Postdoctoral Fellowships are also available. Those who received a Ph.D. degree and are interested in the above-mentioned fields are encouraged to apply. Interested applicants should send a letter and curriculum vitae to: **Professor Mien-Chie Hung, Chair, Search Committee, Center for Molecular Medicine, China Medical University Hospital.** Mailing address: **Department of Molecular and Cellular Oncology, The University of Texas M.D. Anderson Cancer Center, 1515 Holcombe Boulevard, Houston, TX 77030. E-mail: mhung@mdanderson.org.**

RESEARCH PROFESSOR

The Medical Genetics Research Center at State University of New York Upstate Medical University seeks to fill a tenure-track **ASSISTANT or ASSOCIATE PROFESSOR** position for an individual to promote research involving the discovery or characterization of causative genes and pathophysiological mechanisms in transgenic in rodent models of disease. The position requires expertise in QTL mapping. The selected individual will be expected to develop an independent research program and also to provide assistance to other faculty. The position requires a Ph.D. in a relevant discipline (e.g., biology, biochemistry, physiology, genetics, psychology, zoology). Candidates should send their curriculum vitae and a letter describing research interests to: **Stephen V. Faraone, Ph.D., Director, Medical Genetics Research, State University of New York Upstate Medical University, 750 East Adams Street, Syracuse, NY 13210** or e-mail the same to **e-mail: genetics@upstate.edu.**

POSITIONS OPEN

ASSISTANT PROFESSOR
Molecular Parasitology
Louisiana State University
Department of Veterinary Science

An Assistant Professor position is available in the area of molecular parasitology. The major focus of the position will be to establish a nationally recognized and externally funded research program which will lead to improvement of existing or development of new control strategies for helminth parasites of livestock. The candidate must develop and obtain research grants while conducting original and innovative research. Applicant should have a D.V.M. and/or Ph.D., postdoctoral experience, and evidence of research accomplishments. Preference given to those creative, energetic investigators with research programs in molecular helminthology; however, individuals with a broad background in parasitology with experience in the genetic, molecular, cellular, and biochemical aspects of the discipline are encouraged to apply. The Louisiana State University (LSU) AgCenter offers a diverse and highly collaborative research environment with state-of-the-art equipment available. In addition, the Department of Veterinary Science has close ties to the LSU School of Veterinary Medicine. Interested applicants should submit a letter of application which includes a statement of research goals and curriculum vitae with three references to:

Dr. Thomas R. Klei
Chair of the Search Committee
Louisiana State University Department of Veterinary Science
111 Dalrymple Building
Baton Rouge, LA 70803
Telephone: 225-578-9727, fax: 225-578-4890
E-mail: klei@vetmed.lsu.edu

LSU Agricultural Center is a statewide campus of the LSU System and provides equal opportunities in programs and employment. An Equal Opportunity/Affirmative Action Employer.

CELL/MOLECULAR or MICROBIOLOGIST. One-year position to teach parts of the introductory biology sequence, a nonmajors course in her/his area of expertise, and an upper-level course in biology, preferably in microbiology or cell biology.

Postdoctoral research and/or teaching experience preferred. See description at **website: http://www.ohio5.org/faculty.htm** or contact **Dr. Dean Fraga, Chair, Department of Biology** at **telephone: 330-263-2557** or **e-mail: dfraga@wooster.edu.** *The College of Wooster is an Affirmative Action/Equal Opportunity Employer.*

POSTDOCTORAL OPPORTUNITIES

POSTDOCTORAL POSITION, ORGANIC CHEMISTRY (mainland United States only), **the University of Texas (UT), Austin.** Position available immediately to investigate organic dye interactions with cellulose for electronic paper applications (recent Ph.D. in organic chemistry required). Working knowledge of organic dye synthesis procedures and chemical processing equipment used in an organic chemistry laboratory. Experience with polymer modification and organic synthesis scale-up. Contact **e-mail: rmbrown@mail.utexas.edu** with resume/curriculum vitae and names of three references. *UT Austin is an Equal Opportunity Employer.*

POSTDOCTORAL POSITION immediately available to study the tumorigenesis of childhood solid tumors. Applicant must have Ph.D. and/or M.D. degree. Experience in molecular biology and animal studies is essential. Send curriculum vitae and three references to: **Dr. Lingtao Wu, Department of Pathology, MS 103, Childrens Hospital Los Angeles/University of Southern California Keck School of Medicine, 4650 Sunset Boulevard, Los Angeles, CA 90027. E-mail: lingtaow@usc.edu.**

POSITIONS OPEN

FACULTY POSITIONS
ASSISTANT/ASSOCIATE PROFESSORS of PHARMACOLOGY
Creighton University School of Medicine

The newly expanded Department of Pharmacology in the Creighton University School of Medicine invites applications for two tenure-track faculty positions at the Assistant or Associate Professor level beginning in the fall of 2007, or thereafter. We seek outstanding scientists with a Ph.D., M.D., or equivalent degree in pharmacology or a related area. We are interested in candidates who will establish an active, independent, extramurally funded research program and participate in professional and graduate student teaching. While the candidate's interests should complement the research strengths of the Department and the school, the excellence of the candidate is more important than his/her research focus. Program strengths within the Pharmacology Department include G protein-coupled receptors, receptor gene expression, signal transduction, ion channel modulation and drug discovery, in the context of the cardiovascular system, nervous system, exocrine glands and cancer. **Website: http://www2.creighton.edu/medschool/medicine/departments/pharmacology/.** These are new positions associated with the renovation and expansion of the Pharmacology Department.

The School of Medicine is one of nine schools or colleges, including professional schools of business, law, nursing, dentistry, pharmacy, and health professions, and a graduate school, within Creighton University. Founded in 1878, Creighton University is a Catholic, Jesuit institution with an enrollment of approximately 6,725 students. Creighton University is consistently ranked as one of the finest comprehensive universities in the nation by *U.S. News and World Report.*

Applicants should submit curriculum vitae, a brief statement of research plans, and a list of three references to: **Dr. Peter Abel, Search Committee Chair, Department of Pharmacology, Creighton University School of Medicine, 2500 California Plaza, Omaha, NE 68178. E-mail: pabel@creighton.edu.** Applications received by June 30, 2007, are assured full consideration.

Women and minority candidates are encouraged to apply. Creighton University is an Equal Opportunity, Affirmative Action Employer.

WILLIAM JEWELL COLLEGE. Visiting **ASSISTANT PROFESSOR of BIOLOGY.** Two positions open (plant ecology; genetics). Both are two-year, full-time, nontenure track, effective fall 2007. Qualifications: Ph.D. or all-but-dissertation in the biological sciences, teaching experience and record of teaching and scholarship. Please see our full job posting at **website: http:// www.jewell.edu** for a complete job description and instructions about submitting an application.

MARKET PLACE

New Products, Services, and Solutions

Reuse. Recycle. Restore.

Restore™ Western Blot Stripping Buffers efficiently strip your antibody and let you recycle your Western blots

Highlights:

- No need to rerun gels; reprobe the membrane using the same target sample
- Provides more efficient removal than "home-brew" buffers
- Does not damage target protein after stripping and reprobing
- Odor-free
- Less expensive than competing stripping buffers

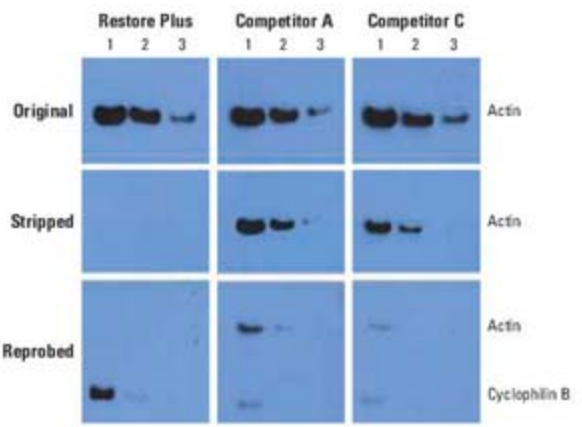

Reprobing with different antibodies.
HeLa cell lysate was probed for actin and detected with Pierce ECL Substrate (Original panel). Blots were then stripped with either Restore Plus Stripping Buffer or competitive stripping buffers (Stripped panel). The blots were then re-blocked and reprobed for cyclophilin B and detected with Pierce ECL Substrate (Reprobed panel).

Learn more today.

Visit www.piercenet.com/restore3, email Pierce.CS@thermofisher.com or call 800-874-3723 or 815-968-0747.

Thermo SCIENTIFIC

just add water

Biomātrica™

THE BIOSTABILITY COMPANY

www.biomatrica.com